INDIAN JOURNAL OF PHYSICS

VOL. XV

AND

PROCEEDINGS

OF THE

Indian Association for the Cultivation of Science Vol. XXIV

(Published in Collaboration with the Indian Physical Society)

BOARD OF EDITORS

M N. SAHA, D.SC., F.R.S., I. R. RAO, PH.D., D.SC.,
S. K. MITRA, D.SC.

P. N. GHOSH, PH.D., SC.D., *Secretary*.

(With Fifteen Plates)

PRINTED AT THE CALCUTTA UNIVERSITY PRESS, 48, HAZRA ROAD, CALCUTTA.
BY BHUPENDRALAL BANERJEE AND PUBLISHED BY THE SECRETARY,
INDIAN ASSOCIATION FOR THE CULTIVATION OF SCIENCE,
210, Bowbazar Street, Calcutta.
1941

Price Rs. 12 or £1-2-6

CONTENTS OF VOL. XV

PART I

PAGE

1. Dynamics of the Pianoforte String and the Hammer, Part VI (Displacement after Impact)—By M. Ghosh 1
2. Dynamics of the Pianoforte String and the Hammer, Part VII (Energy of the String)—By M. Ghosh 13
3. The Motion of Gases in the Sun's Atmosphere, Part II—On the Westward tilt of Prominence—By A. K. Das and B. G. Narayan ... 17
4. Structure of the Electronic Bands of the OD Molecule, Part I—By M. G. Sastry and K. R. Rao 27
5. On the Effect of Mercury Vapour on the Continuous Spectrum of Hydrogen excited by Canal Rays of Hydrogen—By V. T Chiplonkar ... 53
6. A Note on the Use of a few Baking Shellac Varnishes for Coating Graphite-on-glass Resistances in the Laboratory—By G. N. Bhattacharya 59
7. On the Dielectric Constants of Ionised Gases at Medium Radio Frequency—By S. R. Khastgir and C. Choudhury 63
8. Thermodynamic Functions for Two Dimensional Quantum Statistics—By B. N. Singh 73

PART II

9. The Motion of Gases in the Sun's Atmosphere, Part III—On the Stratification of the Solar Envelope—By A. K. Das 79
10. Structure of the Electronic Bands of the OD Molecule—Part II—By M. G. Sastry 95
11. Magnetic Susceptibility of Two Dimensional Free Electron Gas—By B. N. Sinha 103
12. On Nuclear Scattering—By K. C. Kar 113
13. Circumzenithal Arc Tangential to a Corona of 46°—By B. L. Mathur 123
14. On the Radial Limitation of the Solar Magnetic Field—By Bibha Mazumdar 131

The Use of Photographic Plates as an Aid to Cosmic Ray Investigations—By D. M. Bose 145

PART III

PAGE

15. Measurement of Acoustical Impedances—By (Miss) Chandrakanta ... 161
16. Determination of Dipole Moment in Solution—By G. R. Paranjpe and D. J. Davar 173
17. Electrolytic Dissociation in Nitric Acid as studied by Raman Effect—By N. Rajeswara Rao 185
18. Friction between a Liquid Surface and a Solid not wetted by It—By D. S. Subrahmanyam 191
19. On a Theoretical Estimate of an Upper Limit of Steller Diameter—By N. R. Sen 209
20. On Some Thermodynamic Properties of a Mixture of Gas and Radiation—By N. R. Sen 219
21. The Calculation of arg $\Gamma(ia+1)$—By J. G. Beckerley 229
22. Allotropes of Tellurium by X-ray Diffraction Method—By H. Bose and B. B. Ray 233

PART IV

23. A Rapid Method for Calculating the Least Squares Solution of a Polynomial of Degree not exceeding the Fifth—By S. M. Kerawala ... 241
24. Investigation of Tellurium and Arsenic Sulphide in the Colloidal State—By H. N. Bose 277
25. Measurement of the Angle of Incidence at the Ground of Downcoming Short-waves from the Ionosphere—Chaman Lal 289
26. The Short Wave Condenser Field—By B. Swaminathan 307

PART V

27. Theory of the Variation of the Resistance of a Thermionic Valve with Frequency—By S. R. Khastgir 317
28. Propagation of Supersonic Waves in Liquid Mixtures and Intermolecular Forces—By Ram Parshad 323
29. Formula Connecting Self-Reciprocal Functions—By Brij Mohan ... 337
30. On the High-Frequency Conductivity and Effective Dielectric Constant of Electronic Medium in a (High-Vacuum) Thermionic Valve—R. G. Basak 343

PAGE

31. Raman Effect in Deutero-Nitric Acid—By Dr. G. B. Banerjee and B. Mishra 359

32. Electrical Interference to Radio Broadcast Reception—By S. P. Chakravarti and N. L. Dutt 365

33. A Study of Allotropes of Selenium by the X-Ray Diffraction Method—By K. Das Gupta, S. R. Das and B. B. Ray 389

PART VI

34. X-Ray Study of Selenium in the Liquid and Colloidal State—By K. Das Gupta and S. R. Das 401

35. Diffraction Pattern of Sulphuric Acid at Different Concentrations—By H. N. Bose 411

36. Vibrograph used as a Viscometer—By T. Tirunarayanachar ... 417

37. The Optical Hygrometer and its Working—By L. D. Mahajan ... 425

38. The Secondary K-absorption Spectra of Ferric Oxide in Solid and in Colloidal Solution—By S. Sen 433

39. Studies in Antenna Resistance and Reactance—By S. R. Khastgir ... 437

40. Application of the Theory of Random Scattering on the Intensity Variations of the Down-coming Wireless Waves over Long Transmission Paths—By M. M. Sen Gupta 447

41. Structure of the Electronic Bands of the OD Molecule, Part III—By M. G. Sastry 455

AUTHOR INDEX

Author	Subject	Page
Banerjee, G. B., and Mishra, B. ...	Raman Effect in Deutero-Nitric Acid	359
Basak, R. G. ...	On the High-Frequency Conductivity and Effective Dielectric Constant of Electronic Medium in a (High-Vacuum) Thermionic Valve	343
Beckerley, J. G.	The Calculation of arg. $\Gamma(ia+1)$ ...	229
Bhattacharya, G. N.	A Note on the Use of a few Baking Shellac Varnishes for Coating Graphite-on-glass Resistances in the Laboratory ...	59
Bose, D. M. ...	The Use of Photographic Plates as an Aid to Cosmic Ray Investigations ...	145
Bose, H. N. ...	Investigation of Tellurium and Arsenic Sulphide in the Colloidal State	277
	Diffraction Pattern of Sulphuric Acid at Different Concentrations	411
Bose, H. N., and Ray, B. B.	Allotropes of Tellurium by X-Ray Diffraction Method	233
Chakravarti, S. P., and Dutt, N. L.	Electrical Interference to Radio Broadcast Reception	365
(Miss) Chandrakanta ...	Measurement of Acoustical Impedances ...	161
Chiplonkar, V. T. ...	On the Effect of Mercury Vapour on the Continuous Spectrum of Hydrogen excited by Canal Rays of Hydrogen ...	53
Choudhury, C., and Khastgir, S. R.	See Khastgir, S. R.	
Das, A. K., and Narayan, B. G.	The Motion of Gases in the Sun's Atmosphere, Part II—On the Westward tilt of Prominence	17
Das, A. K. ...	The Motion of Gases in the Sun's Atmosphere, Part III—On the Stratification of the Solar Envelope	79
Das Gupta, K., and Das, S. R. ...	X-Ray Study of Selenium in the Liquid and Colloidal State	401
Das Gupta, K., Das, S. R., and Ray, B. B.	A Study of Allotropes of Selenium by the X-Ray Diffraction Method	389

AUTHOR	SUBJECT	PAGE
Das, S. R., and Das Gupta, K.	See Das Gupta, K.	
Davar, D. J., and Paranjpe, G. R.	See Paranjpe, G. R.	
Dutt, N. L., and Chakravarti, S. P.	See Chakravarti, S. P.	
Ghosh, M. ...	Dynamics of the Pianoforte String and the Hammer, Part VI (Displacement after Impact)	1
	Dynamics of the Pianoforte String and the Hammer, Part VII (Energy of the String)	13
Kar, K. C. ...	On Nuclear Scattering ...	113
Kerawala, S. M. ...	A Rapid Method for Calculating the Least Squares Solution of a Polynomial of Degree not exceeding the Fifth. ...	241
Khastgir, S. R. ...	Theory of the Variation of the Resistance of a Thermionic Valve with frequency ...	317
	Studies in Antenna Resistance and Reactance	437
Khastgir, S. R., and Choudhury, C.	On the Dielectric Constants of Ionised Gases at Medium Radio Frequency	63
Lal, Chaman ...	Measurement of the Angle of Incidence at the Ground of Downcoming Short-waves from the Ionosphere	289
Mahajan, L. D. ...	The Optical Hygrometer and its Working ...	425
Majumdar, Bibha ...	On the Radial Limitation of the Solar Magnetic Field	131
Mathur, B. L. ...	Circumzenithal Arc Tangential to a Corona of 46°	123
Mishra, B., and Banerjee, G. B.	See Banerjee, G. B.	
Mohan, Brij ...	Formula Connecting Self-Reciprocal Functions	337
Narayan, B. G., and Das, A. K.	See Das, A. K.	
Paranjpe, G. R., and Davar, D. J.	Determination of Dipole Moment in Solution...	173
Parshad, Ram ...	Propagation of Supersonic Waves in Liquid Mixtures and Intermolecular Forces ...	323
Rao, K. R., and Sastry, M. G.	See Sastry, M. G.	
Rao, N. Rajeswara ...	Electrolytic Dissociation in Nitric Acid as studied by Raman Effect	185

AUTHOR	SUBJECT	PAGE
Ray, B. B., and Bose, H. N.	See Bose, H. N.	
Sastry, M. G., and Rao, K. R.	Structure of the Electronic Bands of the OD Molecule, Part I	27
Sastry, M. G.	Structure of the Electronic Bands of the OD Molecule, Parts II and III	95, 455
Sen, N. R.	On a Theoretical Estimate of an Upper Limit of Stellar Diameter	200
	On Some Thermodynamic Properties of a Mixture of Gas and Radiation	210
Sen Gupta, M. M.	Application of the Theory of Random Scattering on the Intensity Radiations of the Downcoming Wireless Waves over Long Transmission Paths	447
Sen, S.	The Secondary K-absorption Spectra of Ferric Oxide in Solid and in Colloidal Solution	433
Singh, B. N.	Thermodynamic Functions for Two-Dimensional Quantum Statistics	73
	Magnetic Susceptibility of Two-Dimensional Free Electron Gas	103
Subrahmanyam, D. S.	Friction between a Liquid Surface and a Solid not wetted by It	191
Swaminathan, B.	The Short Wave Condenser Field	307
Tirunarayanchar, T.	Vibrograph used as a Viscometer	417

SUBJECT INDEX

Subject	Author	Page
Acoustical Impedances, Measurement of	(Miss) Chandrakanta ...	161
Allotropes of Selenium by the X-Ray Diffraction Method, A Study of	K. Das Gupta, S. R. Das, and B. B. Ray	389
Allotropes of Tellurium by X-Ray Diffraction Method	H. Bose, and B. B. Ray ...	233
Antenna Resistance and Reactance, Studies in	S. R. Khastgir ...	437
arg $\Gamma(ia+1)$, The Calculation of	J. G. Beckerley ...	229
Baking Shellac Varnishes for Coating Graphite-on-glass Resistances in the Laboratory, A Note on the Use of a few	G. N. Bhattacharya ...	59
Circumzenithal Arc Tangential to a Corona of 46°	B. L. Mathur ...	123
Condenser Field, The Short Wave	B. Swaminathan ...	307
Continuous Spectrum of Hydrogen excited by Canal Rays of Hydrogen, On the Effect of Mercury Vapour on	V. T. Chiplonkar ...	53
Cosmic Ray Investigations, The Use of Photographic Plates as an Aid to	D. M. Bose ...	145
Dielectric Constants of Ionised Gases at Medium Radio Frequency, On the	S. R. Khastgir, and C. Choudhury	63
Diffraction Pattern of Sulphuric Acid at Different Concentrations	H. N. Bose ...	411
Dipole Moment in Solution, Determination of	G. R. Paranjpe and D. J. Davar	173
Downcoming Short-waves from the Ionosphere, Measurement of the Angle of Incidence at the Ground of	Chaman Lal ...	289
Electrolytic Dissociation in Nitric Acid as studied by Raman Effect	N. Rajeswara Rao ...	185
Electronic Bands of the OD Molecule, Structure of the, Part I	M. G. Sastry and K. R. Rao	27

Subject	Author	Page
Electronic Bands of the OD Molecule, Structure of the, Parts II and III	M. G. Sastry	95, 455
Friction between a Liquid Surface and a Solid not wetted by It.	D. S. Subrahmanyam ...	191
Gases in the Sun's Atmosphere, The Motion of, Part II	A. K. Das, and B. G. Narayan	17
Gases in the Sun's Atmosphere, The Motion of, Part III	A. K. Das ...	79
High-Frequency Conductivity and Effective Dielectric Constant of Electronic Medium in a (High-vacuum) Thermionic Valve	R. G. Basak ...	343
Intensity Variations of the Downcoming Wireless Waves over Long Transmission Paths, Application of the Theory of Random Scattering on the	M. M. Sen Gupta ...	447
K-absorption Spectra of Ferric Oxide in Solid and in Colloidal Solution, The Secondary	S. Sen ...	433
Least Squares Solution of a Polynomial of Degree not exceeding the Fifth, A Rapid Method for Calculating the	S. M. Kerawala ...	241
Magnetic Susceptibility of Two-Dimensional Free Electron Gas	B. N. Singh ...	103
Nuclear Scattering, On	K. C. Kar ...	113
Optical Hygrometer and its Working, The	L. D. Mahajan ...	425
Pianoforte String and the Hammer, Dynamics of the, Parts VI and VII	M. Ghosh	1, 13
Radio Broadcast Reception, Electrical Interference to	S. P. Chakravarti, and N. L. Dutt	365
Raman Effect in Deutero-Nitric Acid	G. B. Banerjee, and B. Mishra	359
Resistance of a Thermionic Valve with Frequency, Theory of the Variation of the	S. R. Khastgir ...	317
Self-Reciprocal Functions, Formula Connecting	Brij Mohan ...	337
Solar Magnetic Field, On the Radial Limitation of the	Bibha Majumdar ...	131

SUBJECT	AUTHOR		PAGE
Stellar Diameter, On a Theoretical Estimate of an Upper Limit of	N. R. Sen	...	209
Supersonic Waves in Liquid Mixtures and Intermolecular Forces, Propagation of	Ram Parshad	...	323
Tellurium and Arsenic Sulphide in the Colloidal State, Investigation of	H. Bose	...	277
Thermodynamic Functions for Two-Dimensional Quantum Statistics	B. N. Singh	...	73
Thermodynamic Properties of a Mixture of Gas and Radiation, On Some	N. R. Sen	...	219
Vibrograph used as a Viscometer	T. Tirunarayanachar	...	417
X-Ray Study of Selenium in the Liquid and Colloidal State	K. Das Gupta, and S. R. Das		401

DYNAMICS OF THE PIANOFORTE STRING AND THE HAMMER

PART VI (DISPLACEMENT AFTER IMPACT)

BY MOHINIMOHAN GHOSH
Burdwan Raj College, Bengal

(*Received for publication, June 20, 1940*)

ABSTRACT. The expression for the displacement of any point of a finite string excited by impact of a hammer, hard and elastic, is deduced from the general theory developed previously. An easy method for numerical computation is also given. The theoretical and the experimental values of the displacement, at different times, are compared graphically for typical cases when a string of 600 cms. length is struck and observed at distances, 120 cms., 290 cms. and 300 cms. from one of the fixed ends. The theoretical and the experimental values of the fundamental are also compared. The agreement in each case between the theory and the experiment is found excellent.

INTRODUCTION

In Part III the dynamics of the struck string [1] of *finite length* has been worked out for hard and elastic hammer. The displacement at any point of the string *during impact* has also been worked out. In the above paper, the theoretical time-displacement curve of a given point on the shorter segment has been drawn for different cases. They are compared with those obtained experimentally. The agreement is found to be exact as the form and number of kinks are, as found from experiment.

In this paper we derive the corresponding expressions for the displacement after impact. The variations with time are compared graphically with those obtained experimentally.

The symbols used here are same as used before.[1]

During impact the hammer presses against the string at the struck-point. As soon as the hammer leaves the string just after contact, *i.e.*, at $t=\Phi$, the string straightens out. As so, a new disturbance originates at the struck-point and moves in both the directions. Let the disturbance originating at $x=a$ be denoted by $F(t)$. It moves as $F\left(t+\frac{x_1}{c}\right)$ and $F\left(t-\frac{x_1}{c}\right)$ in opposite directions. Those disturbances that were developed during impact will also continue to travel along the string. Thus the displacements at different points during impact are

$$y_a = f_1(t) + \sum_1^n [f_{n+1} - f_n]\{(t-n\theta_1)+(t-n\theta_2)\} + 2[f_3 - 2f_2 + f_1](t-\Theta)$$

$$+\sum_1^n [(n+2).f_{n+3} - (3n+4).f_{n+2} + (3n+2).f_{n+1} - nf_n]\{(t-\Theta-n\theta_1)+(t-\Theta-n\theta_2)\}$$

$$+2[3f_5 - 9f_4 + 10f_3 - 5f_2 + f_1](t-2\Theta) \; ; \qquad \ldots \quad (52)$$

$$y_1 = f_1(t+\frac{x_1}{c}) + \sum_1^n f_{n+1}(t+\frac{x_1}{c}-n\theta_1) - \sum_1^n f_n(t-\frac{x_1}{c}-n\theta_2) + \sum_1^n [f_{n+1}-f_n](t+\frac{x_1}{c}-n\theta_2)$$

$$+[f_2 - f_1]\{(t+\frac{x_1}{c}-\Theta)-(t-\frac{x_1}{c}-\Theta)\} + 2[f_3 - 2f_2 + f_1](t+\frac{x_1}{c}-\Theta)$$

$$+[2f_3 - 3f_2 + f_1]\{(t+\frac{x_1}{c}-\Theta-\theta_1)-(t-\frac{x_1}{c}-\Theta-\theta_1)\}$$

$$+\sum_1^n [(n+2).f_{n+3} - (3n+4).f_{n+2} + (3n+2).f_{n+1} - n.f_n]\{(t+\frac{x_1}{c}-\Theta-n\theta_1)$$

$$+(t+\frac{x_1}{c}-\Theta-n\theta_2)\}$$

$$+\sum_1^n [(n+2)f_{n+3} - (2n+3).f_{n+2} + (n+1).f_{n+1}]$$

$$\{(t+\frac{x_1}{c}-\Theta-\overline{n+1}\theta_1)-(t-\frac{x_1}{c}-\Theta-\overline{n+1}\theta_1)\}$$

$$+\sum_1^n [f_{n+2} - f_{n+1}]\{(t+\frac{x_1}{c}-\Theta-n\theta_2)-(t-\frac{x_1}{c}-\Theta-n\theta_2)\}$$

$$+[3f_4 - 6f_3 + 4f_2 - f_1]\{(t+\frac{x_1}{c}-2\Theta)-(t-\frac{x_1}{c}-2\Theta)\}$$

$$+2[3f_5 - 9f_4 + 10f_3 - 5f_2 + f_1](t+\frac{x_1}{c}-2\Theta) \; ; \qquad \ldots \quad (64.1)$$

y_2 = Read $-x_1$ for $+x_1$, θ_1 for θ_2, and θ_2 for θ_1, in eq. (64.1). ... (64.2)

At any time $t > \Phi$

$y_a = F(t) + y_a$ in eq. (52), ... (97)

$y_1 = F(t+\frac{x_1}{c}) + y_1$,, (64.1), ... (98)

$y_2 = F(t-\frac{x_1}{c}) + y_2$,, (64.2), ... (99)

subject to the condition that y_a and $\left(\dfrac{\partial y}{\partial x}\right)_{x=a}$ are continuous at $t=\Phi$. If the above conditions are not satisfied, there will be discontinuous change in the displacement, which is not the case. Now, the above conditions will help us to evaluate $F(t)$, $F(t+\frac{x_1}{c})$ and $F(t-\frac{x_1}{c})$. The first condition gives

$$F(\Phi)=0 \qquad \ldots \qquad (100)$$

and the second condition gives, at $t=\Phi$,

$$\left(\frac{\partial y_1}{\partial x}\right)_{x=a}=\left(\frac{\partial y_2}{\partial x}\right)_{x=a} \qquad \ldots \qquad (101)$$

with the help of eqs. (98) and (99).

Eq. (101) gives

$$\begin{aligned}-F(t)={}&f'_1(t)+\sum_1^n f'_{n+1}\{(t-n\theta_1)+(t-n\theta_2)\}+2[f'_2-f'_1](t-\Theta)+2[f'_3-2f'_2\\&+f'_1](t-\Theta)+[2f'_3-3f'_2+f'_1]\{(t-\Theta-\theta_1)+(t-\Theta-\theta_2)\}\\&+\sum_1^n[(n+2)f'_{n+3}-(3n+4)f'_{n+2}+(3n+2)f'_{n+1}-nf'_n]\{(t-\Theta-n\theta_1)\\&+(t-\Theta-n\theta_2)\}+\sum_1^n[(n+2)f_{n+3}-(2n+3)f_{n+2}\\&+(n+1)f_{n+1}]\{(t-\Theta-\overline{n+1}\theta_1)+(t-\Theta-\overline{n+1}\theta_2)\}\\&+\sum_1^n[f'_{n+2}-f'_{n+1}]\{(t-\Theta-n\theta_1)+(t-\Theta-n\theta_2)\}\\&+2[3f'_4-6f'_3+4f'_2-f'_1](t-2\Theta)\\&+[6f'_5-18f'_4+20f'_3-10f'_2+2f'_1](t-2\Theta). \qquad \ldots \qquad (102)\end{aligned}$$

On integration,

$$\begin{aligned}C-F(t)={}&f_1(t)+\sum_1^n f_{n+1}\{(t-n\theta_1)+(t-n\theta_2)\}+2[f_3-f_2](t-\Theta)\\&+[2f_3-3f_2+f_1]\ \{(t-\Theta-\theta_1)+(t-\Theta-\theta_2)\},\\&+\sum_1^n[(n+2)f_{n+3}-(3n+4)f_{n+2}+(3n+2)f_{n+1}-nf_n]\{(t-\Theta-n\theta_1)\\&+(t-\Theta-n\theta_2)\}+[(n+2)f_{n+3}-(2n+3)f_{n+2}+(n+1)f_{n+'1}]\\&\{(t-\Theta-\overline{n+1}\theta_1)+(t-\Theta-\overline{n+1}\theta_2)\}\\&+\sum_1^n[f_{n+2}-f_{n+1}]\{(t-\Theta-n\theta_1)+(t-\Theta-n\theta_2)\}\\&+2[3f_5-6f_4+4f_3-f_2](t-2\Theta). \qquad \ldots \qquad (103)\end{aligned}$$

As $F(\Phi)=0$, so,

$$C=f_1(\Phi)+\sum_1^n f_{n+1}\{(\Phi-n\theta_1)+(\Phi-n\theta_2)\}+2[f_3-f_2](\Phi-\Theta)$$

$$+[2f_3-3f_2+f_1]\{(\Phi-\Theta-\theta_1)+(\Phi-\Theta-\theta_2)\}$$

$$+\sum_1^n[(n+2)f_{n+3}-(3n+4)f_{n+2}+(3n+2)f_{n+1}-nf_n]\{(\Phi-\Theta-n\theta_1)$$

$$+(\Phi-\Theta-n\theta_2)\}+[(n+2)f_{n+3}-(2n+3)f_{n+2}+(n+1)f_{n+1}]$$

$$\{(\Phi-\Theta-\overline{n+1}\,\theta_1)+(\Phi-\Theta-\overline{n+1}\,\theta_2)\}$$

$$+\sum_1^n[f_{n+2}-f_{n+1}]\{(\Phi-\Theta-n\theta_1)+(\Phi-\Theta-n\theta_2)\}$$

$$+2[3f_5-6f_4+4f_3-f_2](\Phi-2\Theta), \qquad \dots \quad (104)$$

where C is the constant of integration. Thus $F(t)$ is known.

The eqs. (97), (98) and (99), with the help of eqs. (103) and (104), become

$$y_a=C-\Bigg[\sum_1^n f_n\{(t-n\theta_1)+(t-n\theta_2)\}+2[f_2-f_1](t-\Theta)+[2f_3-3f_2+f_1]\{(t-\Theta-\theta_1)$$

$$+(t-\Theta-\theta_2)\}$$

$$+\sum_1^n[(n+2)f_{n+3}-(2n+3)f_{n+2}+(n+1)f_{n+1}]\{(t-\Theta-\overline{n+1}\,\theta_1)$$

$$+(t-\Theta-\overline{n+1}\theta_2)\}$$

$$+\sum_1^n[f_{n+2}-f_{n+1}]\{(t-\Theta-n\theta_1)+(t-\Theta-n\theta_2)\}$$

$$+2[3f_4-6f_3+4f_2-f_1](t-2\Theta)\Bigg], \qquad \dots \quad (105)$$

$$[y_1, y_2]=C-[\sum_1^n f_n\{(t-\frac{x_1}{c}-n\theta_1)+(t+\frac{x_1}{c}-n\theta_2)\}+[f_2-f_1]\{(t+\frac{x_1}{c}-\Theta)$$

$$+(t-\frac{x_1}{c}-\Theta)\}$$

$$+[2f_3-3f_2+f_1]\{(t-\frac{x_1}{c}-\Theta-\theta_1)+(t+\frac{x_1}{c}-\Theta-\theta_2)\}$$

$$+\sum_1^n[(n+2)f_{n+3}-(2n+3)f_{n+2}+(n+1)f_{n+1}]$$

$$\{(t+\frac{x_1}{c}-\Theta-\overline{n+1}\;\theta_2)+(t-\frac{x_1}{c}-\Theta-\overline{n+1}\;\theta_1)\}$$

$$+\sum_1^n [f_{n+2}-f_{n+1}]\{(t+\frac{x_1}{c}-\Theta-n\theta_1)+(t-\frac{x_1}{c}-\Theta-n\theta_2)\}$$

$$+[3f_4-6f_3+4f_2-f_1]\ \{(t+\frac{x_1}{c}-2\Theta)+(t-\frac{x_1}{c}-2\Theta)\}]. \qquad \dots \quad (105{\cdot}1)$$

The expression for y and y_2 are found to be *identical*, as they should be *after impact*. They depend only upon the position of the observed point x.

As the disturbances $F(t\pm\frac{x_1}{c})$ originate at $t=\Phi$, it is evident that the distance traversed by the disturbances at any instant t, measured from the beginning of impact on either side of the point $x=a$, *i.e.*, $x_1=0$, is $c\ (t-\Phi)$, so beyond this distance eqs. (64) will hold good. As soon as the impact terminates, any disturbance of the type $f_{n+1}(t-\zeta)$ ceases to be generated, and as these pulses which are generated during impact move away from the struck-point $x=a$, they are followed by a constant displacement C. It is then obvious that, for all values of $t>\Phi$, $f_{n+1}(t-\zeta)=f_{n+1}\ (\Phi-\zeta)$, as $f_{n+1}(t-\zeta)$ will only appear at any point at time t, obtained by equating the corresponding argument $(t-\zeta)=0$. In order to know the functions existing after impact, we are to retain only those, for which $(\Phi-\zeta)>0$. These disturbances are successively reflected from the two ends of the string.

In order to draw time-displacement diagram for any point of the string after impact, we prepare a table of all functions brought into existence during the impact and their successive reflections as shown below.

$$f_1(t+\frac{x_1}{c}), \qquad : \qquad f_1(t-\frac{x_1}{c}),$$

$$-f_1(t-\frac{x_1}{c}-\theta_1), \qquad : \qquad -f_1(t+\frac{x_1}{c}-\theta_2),$$

$$+f_1(t+\frac{x_1}{c}-\Theta), \qquad : \qquad +f_1(t-\frac{x_1}{c}-\Theta),$$

$$-f_1(t-\frac{x_1}{c}-\Theta-\theta_1), \qquad : \qquad -f_1(t+\frac{x_1}{c}-\Theta-\theta_2),$$

$$+f_1(t+\frac{x_1}{c}-2\Theta). \qquad : \qquad +f_1(t-\frac{x_1}{c}-2\Theta).$$

... ...

$$f_2(t+\frac{x_1}{c}-\theta_1), \qquad : \qquad f_2(t-\frac{x_1}{c}-\theta_1),$$

$$-f_2(t-\frac{x_1}{c}-2\theta_1), \qquad : \qquad -f_2(t+\frac{x_1}{c}-\Theta),$$

$$\begin{array}{lcl}
+f_2(t+\frac{x_1}{c}-\Theta-\theta_1), & \vdots & +f_2(t-\frac{x_1}{c}-\Theta-\theta_1), \\[2ex]
-f_2(t-\frac{x_1}{c}-\Theta-2\theta_1), & \vdots & -f_2(t+\frac{x_1}{c}-2\Theta), \\[2ex]
+f_2(t+\frac{x_1}{c}-2\Theta-\theta_1). & \vdots & +f_2(t-\frac{x_1}{c}-2\Theta-\theta_2). \\[2ex]
\cdots \quad \cdots & \cdots & \cdots \quad \cdots \\[2ex]
f_2(t+\frac{x_1}{c}-\theta_2), & \vdots & f_2(t-\frac{x_1}{c}-\theta_2), \\[2ex]
-f_2(t-\frac{x_1}{c}-\Theta), & \vdots & -f_2(t\pm\frac{x_1}{c}-2\Theta_2), \\[2ex]
+f_2(t+\frac{x_1}{c}-\Theta-\theta_2), & \vdots & +f_2(t-\frac{x_1}{c}-\Theta-\theta_2) \\[2ex]
-f_2(t-\frac{x_1}{c}-2\Theta), & \vdots & -f_2(t+\frac{x_1}{c}-\Theta-2\theta_2), \\[2ex]
+f_2(t+\frac{x_1}{c}-2\Theta-\theta_2). & \vdots & +f_2(t-\frac{x_1}{c}-2\Theta-\theta_2). \\[2ex]
\cdots \quad \cdots & \cdots & \cdots \quad \cdots
\end{array}$$

Similarly for f_3, f_4, etc.

In this way the table up to the last disturbance generated during impact can be built up.

In order to calculate the displacement at any instant t, the values of the arguments of each of the above functions representing disturbances, are to be examined. If $t-\zeta>\Phi$ then $t-\zeta$ is replaced by $\Phi-\zeta$. If, however, $t-\zeta<0$ the corresponding functions are rejected. The method will hold good to all cases including hard as well as elastic hammer and also for any 'mass-ratio'. Hence the method is perfectly general.

Some numerical examples will make it clear. The datas are supplied by M. Ghosh.[2] For $l=600$ cms. $\rho=0\cdot05$ gm./cm., $m=21\cdot21$ gms., $T=38$ kgm. wts., $a=120$ cms., the observed value of $c\Phi$ is 645 cms. The corresponding calculated value[1] (*vide* fig. 2, part IV) is found 625 cms. From the above values of $c\Phi$, it is found that $3\theta_1>\Phi>2\theta_1$, as $6a$ ($=720$ cm.) is less than $2b$ ($=920$ cms.), no disturbance after being reflected from the remoter end overtakes the hammer before it leaves the string. Hence just at the end of impact (the hammer being still in contact), we have,

$$y_a=f_1(t)+f_2(t-\theta_1)+f_3(t-2\theta_1)-f_1(t-\theta_1)-f_2(t-2\theta_1), \qquad \ldots \quad (106)$$

$$[y_1, y_2] = f_1\left(t \pm \frac{x_1}{c}\right) + f_2\left(t \pm \frac{x_1}{c} - \theta_1\right) + f_3\left(t \pm \frac{x_1}{c} - 2\theta_1\right)$$

$$- f_1\left(t - \frac{x_1}{c} - \theta_1\right) - f_2\left(t - \frac{x_1}{c} - 2\theta_1\right), \quad \ldots \quad (106.1)$$

and just after impact,

$$y_a = C - f_1(t - \theta_1) - f_2(t - 2\theta_1), \quad \ldots \quad (106.2)$$

$$y_1 = y_2 = C - f_1\left(t - \frac{x_1}{c} - \theta_1\right) - f_2\left(t - \frac{x_1}{c} - 2\theta_1\right), \quad \ldots \quad (106.3)$$

where,

$$C = f_1(\Phi) + f_2(\Phi - \theta_1) + f_3(\Phi - 2\theta_1). \quad \ldots \quad (106{\cdot}4)$$

At $t = \Phi = \frac{625}{c}$, we have,

$$y_a = f_1\left(\frac{625}{c}\right) + f_2\left(\frac{385}{c}\right) + f_3\left(\frac{145}{c}\right) - f_1\left(\frac{385}{c}\right) - f_2\left(\frac{145}{c}\right)$$

$$= \frac{v}{ac}\left[-e^{-a625} + e^{-a385}(1 + 385a) - e^{-a145}\frac{(145a)^2}{2\,!}\right] = {\cdot}039 \text{ cm.} \quad \ldots \quad (107)$$

where a stands for $\frac{2p}{m}$.

Again, at $t = \Phi + \Theta = \frac{1825}{c}$, as $c\Theta = 1200$ cms., we have for the following values of the disturbances after successive reflections,

$$\begin{tikzcd}
 & -f_1\left(\frac{1585}{c}\right), \arrow[r, "x=l"] & +f_1\left(\frac{625}{c}\right), \arrow[r, "x=0"] & -f_1\left(\frac{385}{c}\right) \\
f_1\left(\frac{1825}{c}\right) \arrow[ur, "\text{At } x=0"] \arrow[dr, "\text{At } x=l"'] \arrow[r, phantom, "\text{Reflected}"] & & & \\
 & -f_1\left(\frac{865}{c}\right), \arrow[r, "x=0"] & +f_1\left(\frac{625}{c}\right). &
\end{tikzcd}$$

This gives, for the net effect,

$$f_1\left(\frac{625}{c}\right) - f_1\left(\frac{385}{c}\right)$$

as any value of the argument greater than $\frac{625}{c}$ is replaced by $\frac{625}{c}$. Similarly for f_2,

$$\begin{tikzcd}
 & {-f_2\left(\frac{1345}{c}\right)} \arrow[r, "x=l"] & {+f_2\left(\frac{385}{c}\right),} \arrow[r, "x=0"] & {-f_2\left(\frac{145}{c}\right)} \\
{f_2\left(\frac{1585}{c}\right)} \arrow[ur, "\text{At } x=0"] \arrow[dr, "\text{At } x=l"'] & \text{Reflected} & & \\
 & {-f_2\left(\frac{625}{c}\right),} \arrow[r, "x=0"] & {-f_2\left(\frac{385}{c}\right)} &
\end{tikzcd}$$

$$=f_2\left(\frac{385}{c}\right)-f_2\left(\frac{145}{c}\right)$$

as greater values of arguments are always replaced by $\frac{385}{c}$. And for f_3,

$$\begin{tikzcd}
 & {-f_3\left(\frac{1105}{c}\right)} \arrow[r, "x=l"] & {+f_3\left(\frac{145}{c}\right)} \\
{f_3\ \frac{1345}{c}} \arrow[ur, "\text{At } x=0"] \arrow[dr, "\text{At } x=l"'] & \text{Refleted} & \\
 & {-f_3\left(\frac{385}{c}\right)} \arrow[r, "x=0"] & {+f_8\left(\frac{155}{c}\right)}
\end{tikzcd} \Bigg\} = f_3\ \frac{145}{c}$$

as greater values of arguments are replaced by $\frac{145}{c}$. Hence we have

$$y_a=f_1\left(\frac{625}{c}\right)+f_2\left(\frac{385}{c}\right)+f_3\left(\frac{145}{c}\right)-f_1\left(\frac{385}{c}\right)-f_2\left(\frac{145}{c}\right)=\cdot 039\text{ cm.} \quad \ldots \quad (108)$$

Thus we find that the values of y_a at $t=\Phi$ given by eq. (107) and at $t=\Phi+\Theta$ given by eq. (108) are identical. Similarly at $t=\Phi+2\Theta$ will have the same value as above. Thus it is conclusively proved that *the motion is periodic*, the period being the natural period of the string, $\frac{2l}{c}$ $(=\Theta)$. The displacement at any time $t>\Phi$ is calculated in the same way.

When the hammer strikes at $a=290$ cms., *i.e.*, $b=310$ cms., we have for the displacement at $t=\Phi=\frac{830}{c}$ sec. or at $t=\Phi+\Theta=\frac{2030}{c}$ sec.

$$y_a=f_1\left(\frac{830}{c}\right)-f_1\left(\frac{250}{c}\right)-f_1\left(\frac{210}{c}\right)+f_2\left(\frac{250}{c}\right)+f_2\left(\frac{210}{c}\right). \quad \ldots \quad (109)$$

Here reflections from both ends overtake the hammer at different time. The displacements at points other than the struck-point are calculated following similar procedure.

When the hammer strikes at mid-point, *i.e.*, $a=b=300$ cms., we have at

$$t=\Phi=\frac{812}{c}\text{ sec.}$$

$$y_a = f_1\left(\frac{812}{c}\right) + 2f_2\left(\frac{212}{c}\right) - 2f_1\left(\frac{212}{c}\right). \qquad \ldots \quad (110)$$

Here the reflections from both ends overtake the hammer at the same instant.

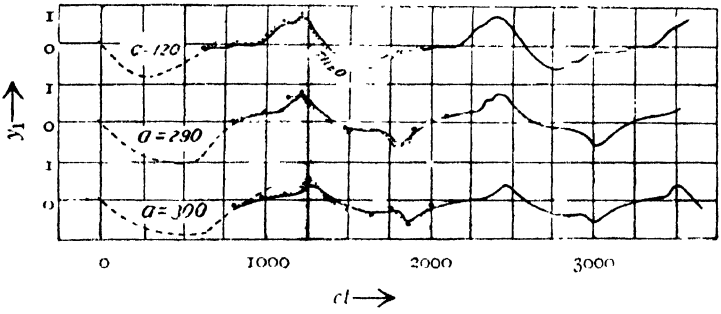

Experimental curve—continuous
Theoretical curve—broken line

FIGURE 1

The experimental photographic curves of these points are projected upon a squared paper by the help of an epidiascope. Owing to the definite width of the string, the vibration form, traced out by the surface of the string in contact with the hammer, is only drawn upon the paper. The time-displacement curves, as calculated from the theory, are superimposed upon the observed curves with the same unit of length. These curves are shown in fig. 1. They are found to be almost identical. Thus there is very good agreement between the theory and the experiment.

In order to study the tone quality, the time-displacement curves of the mid-point, excited by the impact at different points of the string, measured from one of the fixed ends, are analysed as was done by George.[3] But to calculate the corresponding theoretical values, the magnitude of the corresponding duration of contact should be calculated. This, however, is a lengthy process. In order to minimise this trouble of calculation and at the same time to test the theory in this direction systematically, the original time-displacement shadow-graph of different struck-point just after impact of an inelastic hammer are projected under the same optical magnification over a squared paper fixed upon a wall by the help of the epidiascope. The altitude of the curve, at twelve equidistant points on the time axis, of each projected shadow-graph, is measured. Then the amplitude of the fundamental is worked out following Taylor's[4] scheme.

The symbols to be used are same as in previous papers.

The general expression for the pressure as obtained before (Part III) is

$$-\mathrm{P} = 2\rho c\Big[f'_1(t) + \sum_1^n f'_{n+1}\{(t-n\theta_1)+(i-n\theta_2)\} + \{2f'_3 - 2f'_2\}(t-\Theta)$$

$$+\sum_1^n\{(n+2)f'_{n+3} - 2(n+1)f'_{n+2} + nf'_{n+1}\}\{t-\Theta-n\theta_1) + (t-\Theta-n\theta_2)\}$$

$$+\Sigma\{6f'_5 - 12f'_4 + 8f'_3 - 2f'_2\}(t-2\Theta), \qquad \dots \quad (56)$$

where, for inelastic hammer,

$$f'_{n+1}(t) = v_0 e^{-qt}\left[1 - {}^n\mathrm{C}_1 . qt + {}^n\mathrm{C}_2 . \frac{(qt)^2}{2\,!} - + - \dots + (-)^n . \frac{(qt)^n}{n\,!}\right. \qquad (56.1)$$

and

$$q = -\frac{2\rho c}{m}.$$

The respective functions in eq. (56) will appear at

$$t=0,\ \theta_1,\ 2\theta_1 \dots n\theta_1,\ \theta_2,\ 2\theta_2 \dots n\theta_2,\ \Theta+\theta_1,$$

$$\Theta+2\theta_1 \dots \Theta+n\theta_1,\ \Theta+\theta_2,\ \Theta+2\theta_2 \dots \Theta+n\theta_2. \text{ etc.},$$

which are obtained by equating the arguments of the functions to zero.

From the expression of the displacement at struck-point given by eq. (52), Part III, we get, after differentiating with respect to time,

$$\frac{y'_a}{v_0} = \frac{1}{v_0}\Big[f'_1(t) + \sum_1^n\{f'_{n+1} - f'_n\}\{(t-n\theta_1)+(t-n\theta_2)\}$$

$$+\{2f'_3 - 4f'_2 + 2f'_1\}(t-\Theta)$$

$$+\sum_1^n\{(n+2)f'_{n+3} - (3n+4)f'_{n+2} + (3n+2)f'_{n+1} - nf'_n\}$$

$$\{t-\Theta-n\theta_1) + (t-\Theta-n\theta_2)\}$$

$$+\{6f'_5 - 18f'_4 + 20f'_3 - 10f'_2 + 2f'_1\}(t-2\Theta)\Big], \qquad \dots \quad (111)$$

$$= \frac{v}{v_0}, \text{ for } t=\Phi. \qquad \dots \quad (112)$$

Eq. (111) gives the ratio of the velocity of the inelastic hammer at any time t during impact to the initial velocity v_0. The variable time t is evidently replaced by the duration of impact when we require the ratio of the velocity v of the hammer at the instant of separation to the initial velocity v_0.

The ratio of the loss of energy $\frac{1}{2}mv^2 - \frac{1}{2}mv_0^2$ to the initial energy $\frac{1}{2}mv_0^2$ is given by

$$\left.1 - \frac{v^2}{v_0^2}\right) \qquad \dots \quad (113)$$

which is easily calculated with the help of eq. (111), when the magnitude of the duration of impact is known.

The duration of impact, for a given struck-point, is the lowest positive root other than zero, obtained by solving for the point, $P = 0$. The expressions for the duration of impact, for different struck-points and 'mass-ratio' are already worked out in part IV. Here, of course, for the sake of simplicity we shall follow graphical method. We find that the expressions for the pressure exerted by the hammer eq. (56), and the ratio of the velocities, eq. (111), are the sum of different f''s which appear at different times.

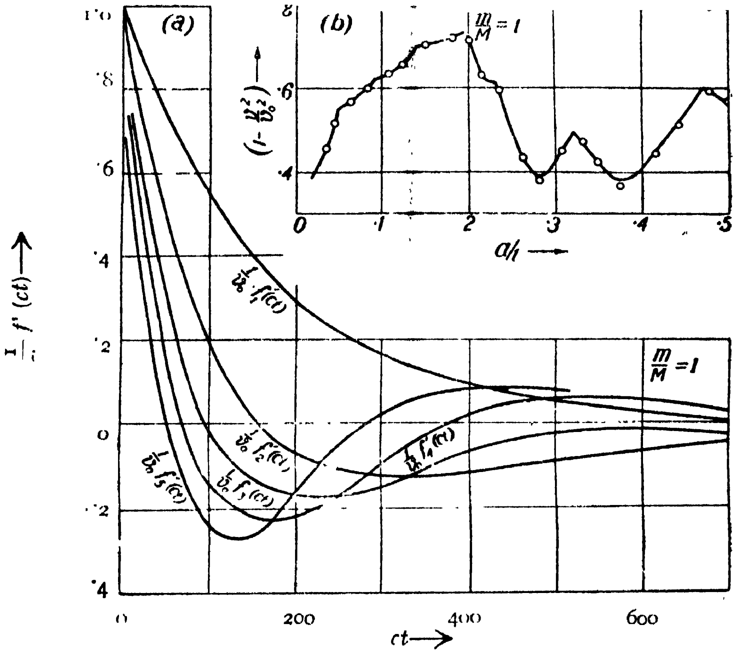

FIGURE 1

In order to simplify calculation of the duration of impact and the energy loss for a given 'mass ratio,' some of the functions f'_1, f'_2, f'_3, f'_4, etc., for different values of the 'mass-ratio' are graphically represented against the time axis over a big squared paper. The same are represented in figure (1*a*) and (2*a*) for $\frac{m}{M}$ is equal to 1 and 3 respectively. The duration of impact for a given striking point is graphically calculated with the help of (56). Here the functions appear at different times. The magnitude of each function for any argument is obtained from the graphs, in fig. (1*a*) or (2*a*). The functions actually appearing during impact are also detected as the pressure-time curves are drawn. Next we retain those appearing functions, in eq. (111) where we put the magnitude of Φ for t, and the arguments are calculated. The magnitude of these functions for the given argument is found from the graph similar to fig. (1*a*) or (2*a*), and the energy loss is calculated.

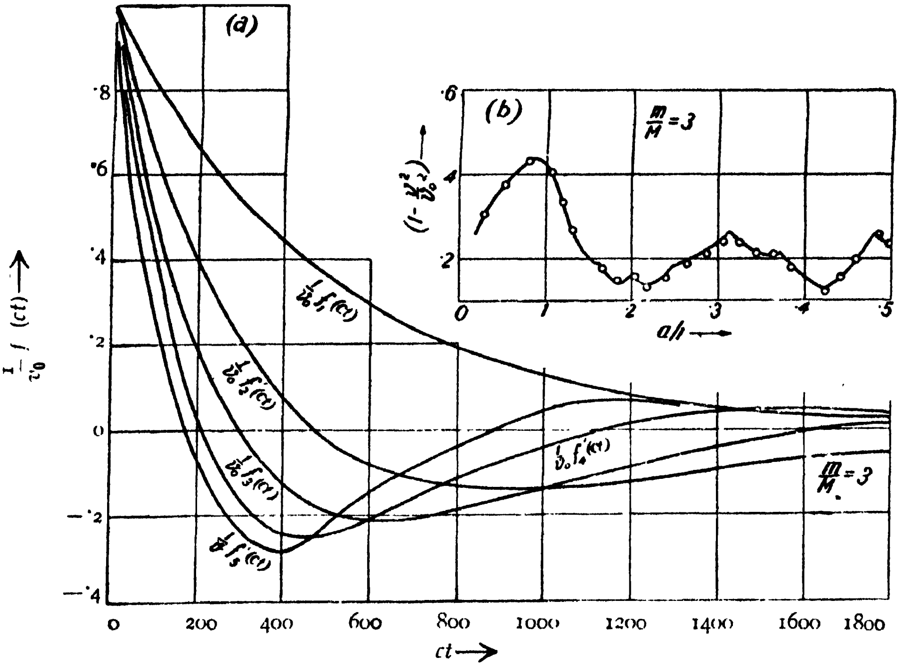

FIGURE 2

In this way the ratio $\left(1-\frac{v^2}{v_0^2}\right)$ of the loss of energy to the initial energy or given struck-points are calculated. They are represented by dots over the experimental curves given by George and Beckett.[3] Figures (1*b*) and (2*b*) correspond to two different hammers. They are of 'mass-ratio' $\frac{m}{M}=1$ and 3 respectively. The agreement between the theory and experiment is excellent. Here graphical representation of all the functions occurring when the struck-point is small, considerably—simplifies the labour involved in the calculation for a given 'mass-ratio.' The value of a given function before or after any reflection from one end or the other will only depend upon the nature of the corresponding arguments, so it is directly determined from the graph in fig. (1*a*) or (2*a*).

My best thanks are due to Professor K. C. Kar, D.Sc., of Presidency College, Calcutta, for the interest he took in the work.

PHYSICAL LABORATORY,
BURDWAN RAJ COLLEGE,
BURDWAN.

REFERENCES

[1] Ghosh, M., *Ind. Jour Phy.*, **12**, 317, (1938) Part I, **12**, 437, (1938) Part II; **13**, 277, (1939), Part III; **14**, 475 (1940) Part IV; **14**, 489 (1940) Part V; **15**, 1 (1941) Part VI.

[2] Das, P., *Ind. Jour. Phy.*, **1**, 437 (1927).

[3] George, W. H., and Beckett, H. E., *Proc. Roy. Soc.*, **114**, 111 (1927).

THE MOTION OF GASES IN THE SUN'S ATMOSPHERE

PART II. ON THE WESTWARD TILT OF PROMINENCES

By A. K. DAS

AND

B. G. NARAYAN

(*Received for publication, September 10, 1940*)

ABSTRACT. From measurements of 1346 absorption markings the authors find that prominences are rarely perpendicular to the sun's surface. The majority of prominences have a tilt towards the west of the vertical, although there are cases of eastward tilt and no tilt. The average tilt found, by proper weighting, from all the measurements is 8°W. An explanation of the origin of the tilt has been offered; and on the basis of this explanation it has been suggested that most stable prominences probably originate in the deep interior of the sun.

In recent years the geometrical aspect of the appearance of solar prominences during their passage across the disc has received a considerable measure of attention from T. Royds and his collaborators at Kodaikanal and from L. d'Azambuja and his co-workers at Meudon, and several useful observational facts have emerged from their investigations. One interesting conclusion brought out by these researches is that there is a marked dissymmetry in the behaviour of prominences projected on the sun's disc in regard to the two halves of the disc separated by the central meridian. From a statistical study of the measures of areas of the absorption markings (or filaments, as they are sometimes called) photographed in H_α light and lying parallel to the meridians at different heliographic latitudes M. Salaruddin[1] found that the areas at eastern longitudes were less than those at the corresponding western longitudes. At the same time he appears to have noted that the areas of absorption markings attained their minimum values at the central meridian. There is, however, an inherent contradiction between these two conclusions which becomes rather evident when one considers his interpretation of the first conclusion concerning the dissymmetry between the eastern and western areas. Salaruddin attempts to explain this dissymmetry by the tentative suggestion that it may be due to most of the filaments measured to the west being growing ones. This interpretation is obviously unconvincing in view of the artificiality of the supposition upon which it is based. There is no objection against assuming that some prominences may be continuously growing and others continuously decaying during their passage from the east limb to the west limb, so that in the average of a large number of cases the eastern and western areas at corresponding longitudes would be equalised and the minimum of area would necessarily occur at the central meridian. But there appears to be no admissible reason for supposing that prominences prefer to grow or decay only when they happen to be on the one side of the central meridian or the other ; in fact such a supposition would be contrary to the law of chance. From these considerations it seems clear that if there is a true inequality between the eastern and the western areas of filaments, then the minimum of area should occur at some longitude different from the central meridian. Indeed it is difficult to accept with equal confidence both the conclusions of Salaruddin referred to above. We have, however, verified by a personal discussion with him that his second conclusion is not intended to be regarded as the result of exact measurements; for the main purpose of his paper he did not require to determine the exact longitude at which the area of an absorption marking became minimum.

If one makes a careful determination of the longitude at which the area of a dark marking becomes minimum, one definitely finds that this longitude, in the vast majority of cases, does not coincide with the central meridian: Mme. M. d'Azambuja-Roumens[2] has found this in her measurement of 171 selected markings and we have arrived at the same conclusion after examining upwards of 1300 filaments which have been studied for the purposes of the present investigation. From the above-mentioned work Roumens concludes that the majority of absorption markings present their minimum area at some longitude to the east of the central meridian and derives a weighted average value of 10°E for this longitude. This result is obviously of the same nature as the dissymmetry referred to above which manifests itself in the increase of the western areas over the eastern areas at corresponding longitudes. In fact Roumens has offered for both these observations a very plausible explanation based on the hypothesis that prominences have a systematic westward tilt or inclination to the vertical at the points where they stand on the sun's surface, so that the average value of 10° found for the eastern longitude at which dark markings present their minimum area or breadth signifies that the average tilt of prominences is 10° towards the west.* It is to be noted, however, that this hypothesis involves a departure from the commonly accepted picture of a prominence. Usually a prominence is regarded as a thin flame (its height and breadth being considerably greater than its depth) resembling a fish-tail in shape and standing with its plane normal to the sun's surface. Since the assumption of the westward tilt is a notable departure from the accepted view about prominences one would naturally like to be certain that such a departure is really necessary and inevitable.

---

* As will be evident from the next two paragraphs this conclusion is to be regarded as provisional for the time being, for it depends upon whether the markings measured by Roumens were parallel to the meridians or inclined to them.

In a recent paper M. Waldmeier [3] has contended that it is quite unnecessary to make the assumption that prominences are systematically inclined towards the west of the vertical and that it is perfectly possible to account for the above-mentioned observation of Roumens from considerations of simple spherical trigonometry. Waldmeier's argument is briefly as follows : A prominence is a thin flame standing with its plane normal to the surface of the sun, *i.e.*, it has no tilt to the vertical. At the equator the corresponding filament makes an angle of 90° with the parallels of latitude, but at higher latitudes this angle progressively decreases towards the pole as is well known from observation. Let ϕ be the heliographic latitude at which the filament occurs, θ its inclination to the parallels of latitude and d the longitude (counted from the central meridian) at which the filament appears at its narrowest. Then from Fig. 1 it is easily seen that d is that longitude at which the length of the filament, prolonged if necessary, would pass through the centre of the disc and in this position the following relation must hold among the quantities d. ϕ and θ :

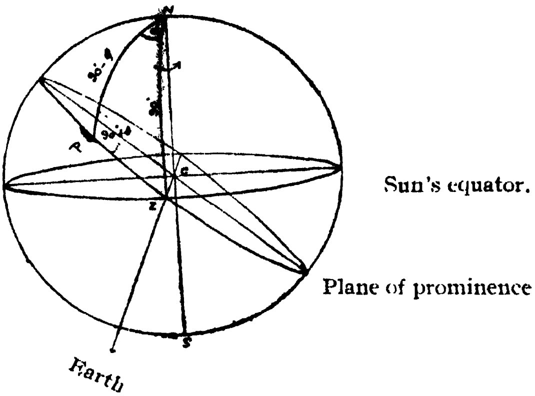

FIGURE 1

$$\tan d = \sin \phi / \tan \theta.$$

Now Roumens says in her note that she has used almost entirely filaments of the equatorial belt so that the average latitude of the filaments examined by her may be taken to be about 20°. Then, using the average value of θ obtained from observational data for latitude 20°, one obtains from the above furmula $d = 13°$, which is in excellent agreement with the average value (*viz.*, 10°) of the west tilt derived by Roumens. So far as the geometrical considerations are concerned there can be no doubt that Waldmeier is correct, but the present writers could not feel sure that he is right in assuming that the filaments measured by Roumens really had the average inclination to the parallels of latitude appropriate to latitude 20°, for in her short note in the *Comptes Rendus* sufficient details are not given.

Our doubt was further accentuated by the fact observed by Salaruddin that the western areas of filaments were larger than the eastern areas, although the filaments studied by him were parallel to the meridians. This dissymmetry can, by no means, be explained by Waldmeier's formula. The problem, therefore, appeared to us to be well worth re-examining.

Although generally filaments at the equator are parallel to the meridians and at higher latitudes the inclination of filaments to the meridians increases with the latitude, it is a fact of common observation that quite a number of filaments at latitudes higher than the equator do have little or no inclination to the meridians. Accordingly there appear to be two ways of determining the average tilt of prominences, if such tilt really exists. One way is to select for measurement only filaments parallel to the meridians and determine the longitudes at which they appear at their narrowest ; in this case naturally Waldmeier's geometrical considerations are automatically eliminated, but this method has the disadvantage that one has rather a small number of filaments to work with. The alternative way is to select filaments, which are definitely not parallel to the meridians ; by this method of selection one can obtain a very large number of filaments for measurement, so that one can expect to arrive at a much more reliable average value of the tilt if it exists. It must be noted, however, that in this second method one has to make proper allowances for the effect to be expected from the geometrical considerations set forth by Waldmeier. This will be clear from Fig. 2 in which we have illustrated the variations in the appearance of two types of filaments during their passage from the east limb to the west. The upper half of the diagram shows the successive aspects of a filament inclined to the meridians as it traverses the disc ; and the lower half represents the sequence of aspects of a filament parallel to the meridians. It is assumed that the prominences corresponding to the filaments represented in the diagram have no tilt to the vertical. It is clear that the filament parallel to the meridians attains its minimum breadth at the central meridian, while the filament inclined to the meridians appears narrowest at an eastern longi-

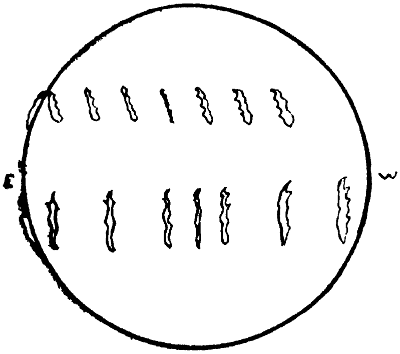

Successive aspects of prominences
when they traverse the disc

FIGURE 2

tude where its length points towards the centre of the disc. If, however, the filaments have a tilt towards the west, then the meridional filament should appear narrowest when it is at some eastern longitude instead of the central meridian ; while the inclined filament should be narrowest at some longitude further east of the position shown in Fig. 2. In the case of the meridional filament obviously the tilt is numerically equal to the longitude at which it appears narrowest ; but for the inclined filament the tilt is numerically equal to the difference between the longitude at which it is actually found to be narrowest and the longitude d calculated from the formula $\tan d = \sin \phi / \tan \theta$ by using the appropriate values of ϕ and θ obtained by actual measurement of the filament concerned.

In the present work filaments appreciably inclined to the meridians have been exclusively used. For the purpose of selecting suitable filaments we examined the daily disc spectroheliograms in H_α light and sun charts for about 10 years out of the records of the Kodaikanal Observatory and selected 1346 filaments. Only stable markings were selected for measurement so as to eliminate the uncertainties due to the variation of areas on account of dissipation of parts of markings. The selection was made from a preliminary examination of the bromide prints of photographs. The positives on paper were preferred to the original negatives primarily for the reason that the greatest depth of an absorption marking is better seen as a dark ridge on a positive than as a white marking on a negative; the line of greatest absorption is very helpful in finding the least area or breadth. But there was also the idea of avoiding the risk of damage involved in handling a large number of negatives on glass which form the permanent records of the observatory. After the preliminary examination, the variation of areas of markings, from the east limb to the west limb or until their disappearance, was carefully followed. A little consideration shows that the breadth of a filament must be least when the line of sight lies in the plane of the prominence, which is responsible for the formation of the filament ; and in this position the dark ridge of great absorption lies symmetrically to the wings. This criterion was found to be a dependable guide in finding the longitude at which a filament appeared narrowest. No great difficulty was experienced in choosing the photograph on which a particular marking appeared to have its least breadth. Photographs were thus chosen and then checked with reference to the sketches of markings on the sun charts which are prepared as a routine at this observatory. If the position of a marking showing the minimum breadth appeared on a photograph, then the longitude was measured accurately by means of a glass reseau which had latitudes and longitudes marked on a scale appropriate to the photograph. But photographs are available only at intervals of a day and consequently more often than not it happens that the position of minimum area of a marking occurs at a time which falls within the interval between the times at which photographs are taken on successive days. In such cases the most probable longitudes of markings were estimated by judging whether the minimum areas occurred nearer one day or the other and applying suitable corrections to the longitudes as measured from the photographs. This method of interpolation necessarily introduces a certain amount of uncertainty ; and as the variation due to the sun's rotation is about 13° per day the maximum error involved in any individual estimation may be ± 3°. The measurement of the latitudes of markings could be done with less uncertainty, the procedure followed being in accordance with the usual practice in solar statistics. If a marking was found to lie across a zone of 5° of latitude, the mean of the zone was marked against the marking. If the marking was shorter than a zone, the latitude of the midpoint to the nearest degree was taken as the latitude of the marking. If a marking was long and lay across several zones of latitude, then each portion of the marking lying across a zone was considered to be an individual marking and the mean of the zone noted against each. The inclinations to the parallels of latitude were measured, as is usually done, when the markings were at the central meridian or near it, so that the vitiating influence of the curvature of the sun's surface was eliminated. The values of the inclination, thus obtained, were noted against the markings to the nearest 5°. As it was found difficult to measure the inclinations of markings above latitude 45°, most of the markings chosen were below that latitude.

The observations were arranged in groups according to ranges of latitude and inclinations. The means (λ_m) of individual observations in each group were worked out and are given together with the number of observations in every group in Table I. The calculated values of d according to Waldmeier's formula for different values of ϕ and θ are given in Table II. In Table III are given the residual values ($\lambda_m - d$) which are the tilts of the markings. Of the 1346 markings measured for this work, 64 indicated no tilt, 237 indicated eastward tilt and 1045 indicated westward tilt ; that is, 78% of the filaments examined showed the existence of a westward tilt. The residual values in Table III vary from group to group both in sign and magnitude. In order to get an idea of the average tilt a general weighted mean of all the group values was worked out by giving appropriate weights according to the number of observations in every group. The weighted mean value thus obtained is $+8°\cdot 2$ with a probable error of $\pm 0°\cdot 96$. From the foregoing results it is evident that the majority of prominences do not stand perpendicularly to the sun's surface; they have a predominantly westward tilt, the average value of which is 8°W.

By the time all the computational work in connection with the present paper was completed Waldmeier[4] published a short note in which he admits that Mme. d'Azambuja-Roumens's conclusion regarding the existence of a westward tilt is correct in view of certain facts which she has communicated to him in private correspondence and also in view of what she has said in a second, somewhat more detailed, paper[5] which was not known to him when he criticised her conclusion. This second paper of Mme. d'Azambuja-Roumens had

TABLE I

θ / φ	15°	20°	25°	30°	35°	40°	45°	50°	55°	60°	65°	70°	75°	80°
	λ_m	λ_m	λ_m	λ_m	λ_m	λ_m	λ_m	λ_m	λ_m	λ_m	λ_m	λ_m	λ_m	λ_m
	0	0	0	0	0	0	0	0	0	0	0	0	0	0
0°-5°	— (-)	18 (7)	28 (3)	27 (4)	14 (3)	25 (13)	30 (5)	16 (9)	20 (4)	22 (6)	37 (4)	23 (7)	36 (1)	10 (2)
5°-10°	26 (2)	12 (4)	9 (3)	26 (6)	24 (5)	23 (13)	12 (6)	20 (17)	24 (5)	25 (5)	22 (1)	23 (6)	26 (2)	30 (1)
10°-15°	7 (1)	25 (1)	17 (5)	22 (11)	15 (13)	21 (24)	20 (17)	18 (25)	19 (10)	25 (20)	22 (8)	23 (12)	7 (2)	— (-)
15°-20°	7 (3)	16 (6)	23 (6)	20 (10)	27 (17)	22 (26)	20 (23)	22 (38)	20 (15)	27 (24)	27 (6)	26 (12)	28 (5)	23 (4)
20°-25°	13 (2)	37 (5)	27 (10)	20 (16)	17 (14)	28 (31)	24 (34)	24 (44)	22 (26)	28 (41)	34 (14)	31 (12)	30 (3)	34 (3)
25°-30°	— (-)	28 (3)	29 (7)	31 (14)	22 (16)	30 (28)	25 (35)	32 (38)	30 (18)	35 (37)	33 (12)	32 (20)	34 (9)	23 (2)
30°-35°	65 (1)	40 (6)	34 (5)	31 (8)	35 (12)	31 (33)	28 (27)	43 (17)	31 (21)	33 (24)	35 (9)	38 (10)	30 (3)	42 (1)
35°-40°	50 (1)	36 (3)	41 (2)	50 (7)	30 (3)	37 (14)	34 (15)	44 (10)	35 (5)	37 (18)	36 (8)	40 (8)	50 (2)	35 (1)
40°-45°	— (-)	30 (4)	36 (3)	39 (3)	45 (1)	47 (7)	39 (7)	36 (7)	— (-)	41 (12)	37 (3)	39 (5)	— (-)	— (-)
45°-50°	— (-)	60 (1)	— (-)	26 (2)	50 (3)	— (-)	— (-)	52 (4)	25 (1)	53 (5)	37 (2)	40 (1)	— (-)	— (-)
50°-55°	— (-)	— (-)	— (-)	— (-)	— (-)	— (-)	25 (1)	55 (2)	— (-)	70 (1)	— (-)	— (-)	— (-)	— (-)
55°-60°	— (-)	40 (1)	— (-)	— (-)	— (-)	— (-)	35 (1)	— (-)	— (-)	— (-)	— (-)	— (-)	— (-)	— (-)

Figures in brackets represent the number of observations

TABLE II

θ	15°	20°	25°	30°	35°	40°	45°	50°	55°	60°	65°	70°	75°	80°
φ	d	d	d	d	d	d	d	d	d	d	d	d	d	d
	0	0	0	0	0	0	0	0	0	0	0	0	0	0
0°- 5°	9	6	5	4	3	3	3	2	2	1	1	1	1	1
5°-10°	26	20	16	13	11	9	7	6	5	4	4	3	2	2
10°-15°	39	31	25	21	17	14	12	10	8	6	5	4	3	2
15°-20°	48	40	33	27	23	20	17	14	12	10	8	6	5	3
20°-25°	55	46	39	34	29	25	21	18	14	12	10	8	6	4
25°-30°	60	52	45	38	34	29	25	21	18	15	12	10	7	5
30°-35°	63	56	49	42	38	33	28	24	21	17	14	11	8	5
35°-40°	66	59	53	46	40	36	31	27	23	19	16	12	9	6
40°-45°	68	62	55	49	44	39	34	30	25	21	17	14	10	7
45°-50°	70	64	58	52	46	41	36	32	27	23	19	16	11	7
50°-55°	—	—	—	—	—	—	39	35	—	25	21	16	—	—
55°-60°	—	67	—	—	—	—	40	—	—	—	—	—	—	—

TABLE III

θ / Φ	15°	20°	25°	30°	35°	40°	45°	50°	55°	60°	65°	70°	75°	80°
	λ_m-d	λ_m-d	λ_m-d	λ_m-d	λ_m-d	λ_m-d	λ_m-d	λ_m-d	λ_m-d	λ_m-d	λ_m-d	λ_m-d	λ_m-d	λ_m-d
	0	0	0	0	0	0	0	0	0	0	0	0	0	0
0°-5°	—	+12	+23	+23	+11	+22	+27	+14	+18	+21	+36	+22	+35	+9
5°-10°	0	−8	−7	+13	+13	+14	+5	+14	+19	+21	+18	+20	+24	+28
10°-15°	−32	−6	−8	+1	−2	+7	+8	+8	+11	+19	+17	+19	+4	—
15°-20°	−41	−24	−10	−7	+4	+2	+3	+8	+8	+17	+19	+20	+23	+20
20°-25°	−42	−9	−12	−14	−12	+3	+13	+6	+8	+66	+24	+23	+24	+30
25°-30°	—	−24	−16	−7	−12	+1	0	+11	+12	+20	+21	+22	+24	+18
30°-35°	+2	−16	−15	−11	−3	−2	0	+19	+10	+16	+21	+27	+22	+37
35°-40°	−16	−23	−12	+4	−10	+1	+3	+13	+12	+18	+20	+28	+41	+29
40°-45°	-	−32	−19	−10	+1	+8	+5	+6	—	+20	+20	+25	—	—
45°-50°	—	−4	—	−26	+4	—	—	+20	−2	+30	+18	+24	—	—
50°-55°	—	—	—	—	—	—	−14	+20	—	+45	—	—	—	—
55°-60°	—	−27	—	—	—	—	−5	-	—	—	—	—	—	—

also escaped our notice ; but we have now read this paper and have not found in it any clear indication as to whether she has used meridional markings or markings inclined to the meridians in her determination of the west tilt of prominences. The second paper is, as far as we can see, an elaboration of her shorter note in certain respects, but her method of determining the tilt is precisely the same as we have described earlier in the present paper. Consequently, if she has used mainly filaments inclined to the meridians for her work, then her average value of 10°W for the tilt must be substantially in error, for her method does not make allowances for the geometrical effect pointed out by Waldmeier. But since our value of 8° W agrees closely with her determination we are led to the conclusion that she must have used mostly filaments parallel to the meridians, so that the geometrical effect was practically eliminated. The fact that Mme. d'Azambuja-Roumens's value is slightly higher than ours is probably due to her having used some inclined filaments as well without, however, applying necessary corrections for the geometrical effect. Combining Mme. d'Azambuja-Roumens's and our results we may, therefore, conclude that filaments both of the meridional and inclined types show that prominences have a predominantly westward tilt to the vertical.

As the foregoing paragraphs have shown, it is not difficult to establish from observational material the prevalence of a westward tilt in prominences, but it is not so easy to discern with certainty the cause of this phenomenon. One of the explanations so far available of the genesis of the tilt is due to Mme. d'Azambuja-Roumens who discovered it. She bases her tentative explanation on the assumption that the top of a prominence rotates from east to west with a higher angular velocity than the bottom of the prominence. We find, however, very little conclusive evidence in support of this hypothesis. A comparison of all available determinations of the angular velocity of rotation, made from the variation of the positions of sunspots, faculae, filaments, prominences, etc., indicates practically the same velocity of rotation at the heights corresponding to these phenomena ; and even if one claims that there is a tendency for the angular velocity to increase with altitude, there is scarcely any reason for concluding that the rate of increase with altitude is anything but extremely small. This being the case, an average tilt of 8°W would require several days to come into existence through the mechanism envisaged by d'Azambuja-Roumens, and the life of those prominences which show tilts of the order of 30° would have to be much longer than is warranted by observation. It must be mentioned, however, that the determinations of the east-west velocity in the upper parts of prominences made by J. Evershed[6] from the Doppler displacements of the H and K lines have given angular velocities at least 1° per day higher than the angular velocity determined from sunspots. Some other observers also have obtained like results from similar spectroscopic measurements. This may at first sight suggest that the top of a prominence moves much faster than its bottom, and this seems to be the reason for d'Azambuja-Roumens's assumption. But a difference in angular velocity of the order of 1° per day between the top and the base of a prominence would cause a rapid increase in the tilt and therefore a rapid change in the shape of the prominence and the corresponding filament; such rapid changes are, however, not observed in the quiescent prominences and absorption markings which exhibit a remarkable stability of shape. The virtual equality of the angular velocities at the sunspot and prominence levels as derived from the above-mentioned non-spectroscopic determinations and the observed stability of the shape of quiescent prominences and filaments appear to be clear evidence against d'Azambuja-Roumens's hypothesis; there is also no special reason for thinking that the spectroscopic measurements referred to above give the velocity of the bodily movement of the tops of prominences. In fact, the discrepancy between the angular velocity derived from the non-spectroscopic observation of filaments and the angular velocity determined from spectroscopic measurements of prominences may be regarded as an indication that the two methods measure two velocities quite distinct from each other. The non-spectroscopic method gives the apparent bodily movement of spots, filaments, etc., while the spectoscopic method applied to prominences determines the east-west velocity of the constituent atoms resulting from the internal motions of the prominences. The existence of internal motion in prominences is well known and there is little doubt that stable prominences are continually renewed from below. It seems probable that this internal motion is not random and that the atoms describe a cyclic trajectory in a plane more or less inclined to the meridians, so that atoms go up along one arm of the cycle steadily curving westwards until the trajectory becomes horizontal at the top and then descend back to the surface of the sun along the other arm of the cycle. There is good dynamical reason for such cyclic motion which is even necessary for maintaining the shape of stable prominences On this view the high velocity obtained from spectroscopic mersurements on the upper part of a prominence is the east-west velocity of the radiating atoms in the upper, more or less horizontal, part of their cyclic path, the translatory movement of the prominence being negligible in comparison.

In view of the difficulties pointed out in the above discussion the mechanism suggested by Mme. d'Azambuja-Roumens in order to explain the observed westward tilt of prominences cannot be regarded as satisfactory. The only other explanation of this phenomenon, so far as we are aware, has been given by one of us in a previous paper.[7] In that paper the dynamics of a particle ejected from the interior of the sun, where the angular velocity is much higher than at the surface, has been investigated and it has been shown from the equations of motion that the trajectory of such a particle will be inclined towards the west of the vertical at the point of the sun's surface at which the particle emerges into the coronal atmosphere, provided that the particle was initially projected in a radial direction. It has also been shown that the amount of deflection from the vertical to be expected from theoretical considerations is, on the average, of the same order as the average west tilt derived from observational data by d'Azambuja-Roumens and by us. Without going into further details, which will be found in the afore-mentioned paper, we may, however, mention that this explanation is free from the objections that can be raised against d'Azambuja-Roumens's explanation. The eastward tilt observed in some prominences also follows in a natural way from the equations of motion if the particle starts in a radial direction from some layer of the sun where the angular velocity is the same as the angular velocity observed at the surface; this eastward tilt is, however, very difficult to understand from the mechanism proposed by d'Azambuja-Roumens or from the hypothesis (advocated by some workers) of the existence of permanent east-west currents beyond the chromosphere. The occurrence of no tilt in a few prominences probably indicates that sometimes particles are ejected with an initial bias towards the east or west of the radial direction and this bias is compensated by the deflection to be expected from the equations of motion. But since the majority of prominences have a westward tilt, one may probably conclude, according to the mechanism advocated in the present paper, that stable prominences are generally formed by gases initially ejected in a radial direction from the deep interior of the sun.

SOLAR PHYSICS OBSERVATORY,
KODAIKANAL.

REFERENCES

[1] M. Salaruddin, *K.O.B.*, Vol. IV, No. 96, p 293.
[2] M. Roumens, *C.R.*, TOME 261, p. 127, 1935.
[3] M. Waldmier, *Astr. Mitt. Zurich.*, NO. 138, p. 482, 1939.
[4] M. Waldmeier, *Astr. Mitt. Zurich*, NO. 139, p. 508, 1940.
[5] M d'Azambuja-Roumens, *L'Astronomie*, Vol. 50, p. 505, 1956.
[6] J. Evershed, *M.N.R.A.S.*, Vol. 95, p. 503, 1935.
[7] A. K. Das, *Ind. Jour. Phys.*, 14, 369, 1940.

4

STRUCTURE OF THE ELECTRONIC BANDS OF THE OD MOLECULE.—PART I

By M. G. SASTRY

AND

K. R. RAO

Andhra University, Waltair

(*Received for publication, September 17, 1940*)

Plate I

ABSTRACT. Bands due to the OD molecule have been obtained free from any trace of the OH bands, by photographing discharges through vapour of heavy water of a very high degree of purity. Measurements on the plate between λ2800 and λ3060 have led to the rotational structure of the (1, 0), (2, 1) and (3, 2) bands.

Using Hill and Van Vleck's energy formula for the doublet electronic states the rotational constants have been evaluated.

The calculated positions of the null lines have enabled the determination of the vibrational constants of the OD molecule and the mass-ratio of the Hydrogen isotopes.

INTRODUCTION

In the course of a general investigation on the emission bands of heavy water, the authors have obtained the electronic band system $^2\Sigma^+ \longrightarrow {}^2\Pi_{\text{inv.}}$ of the OD molecule in the region λ3600 to λ2400, perfectly free from any trace of the bands of the OH molecule.

OH and OD form an interesting pair of isotopic molecules and a detailed study of the structure of the OD bands is considered to be of great importance as it yields valuable information on the electronic isotopic displacements as well as the effect of isotopes on the spin-doubling, and Λ-type doubling of molecular rotational levels. These considerations have been referred to in a short letter by Johnston (1934), but the detailed observations have not been published so far. Shaw and Gibbs (1934) also appear to have carried out work on the OD bands corresponding to λ3064 and λ3122 of OH. However, the only work published till now in detail is due to Ishaq (1937) and (1939), who obtained the rotational structure of the three bands λλ2708, 2736 and 3065. It is the purpose of the present paper to describe the rotational structure of the (1, 0), (2, 1) and (3, 2) bands which lie in the region between λ2800 and λ3060. The structure of the remaining bands in the regions λ3400* and λ2500 will be dealt with in a subsequent communication. (M. G. Sastry, Current Science, **9**, 368, 1940).

---

* The structure of these has been reported by Ishaq (Current Science, **9**, 275, 1940) as the present paper is being prepared.

EXPERIMENTAL

The bands were excited by sending uncondensed discharges from a ¼K-w transformer through vapour of pure heavy water contained in a pyrex tube of the usual H type, the central portion having a bore of about 1 cm. Preliminary attempts showed that with a tube of this bore the continuous background, which otherwise obliterates the faint lines, was very considerably reduced. The heavy water was supplied by the Imperial Chemical Industries, Ltd., and reported to be 98·6% pure. A continuous evacuation of the tube was found necessary as otherwise, due to increase of the vapour pressure, the discharge ceased to pass. The pale bluish violet discharge obtained under the conditions was so intense that photographs could be obtained even with a five-minute exposure, with a Hilger Large Quartz Littrow (E. 1) which was the main instrument used in the present work. With a slit width of less than 0·01 m/m and an exposure of 4 hours, the lines obtained were very sharp and permitted accurate measurement, using Iron Arc standards. Attempts are being made to obtain photographs of these and the other bands above λ3000 in the higher orders of a 10 ft. concave grating.

Plate I is an enlargement of the bands in the region λ2800 to λ3070, showing their rotational structure described in the succeeding sections.

APPLICATION OF THE COMBINATION PRINCIPLE

The assignment of the lines recorded in Table (10) at the end and the Fortrat diagrams (not shown here) of the several branches of the bands reveal that the bands λλ2872, 2916 and 2963 possess the same general structure as the bands λλ2708, 2756 and 3065 identified previously by Ishaq and characteristic of the electronic transition $^2\Sigma \longrightarrow {}^2\Pi_{\text{inv}}$. The application of the combination principle completes the identification and affords a check on the assignment of the quantum numbers. The expression for the wave numbers of the lines constituting the six main branches corresponding to the above electronic transition are

$$R_1(K) = F'_1(K+1) - F''_{1d}(K)$$
$$Q_1(K) = F'_1(K) - F''_{1c}(K)$$
$$P_1(K) = F'_1(K-1) - F''_{1d}(K)$$

together with similar expressions for the branches $R_2(K)$, $Q_2(K)$ and $P_2(K)$. The following combination relations are hence easily obtained.

$$R_1(K) - P_1(K) = F'_1(K+1) - F'_1(K-1) = \Delta_2F'_1(K) \qquad \dots \quad (1)$$
$$R_2(K) - P_2(K) = F'_2(K+1) - F'_2(K-1) = \Delta_2F'_2(K) \qquad \dots \quad (2)$$

The difference between the quantities $\Delta_2F'_1(K)$ and $\Delta_2F'_2(K)$ is a measure of the spin doubling in the upper $^2\Sigma^+$ state. In the present work, however, as the satellite branches have not been identified, the above difference is ignored and the upper rotational levels are treated as single.

The lower state $^2\Pi$ gives rise to four series of terms due to spin and Λ-type doubling. For the spin component $^2\Pi_{1\frac{1}{2}}$ state (F''_1 levels) we have

$$R_1(K)-Q_1(K+1)=F''_{1c}(K+1)-F''_{1d}(K) \qquad \ldots \quad (3)$$

$$Q_1(K)-P_1(K+1)=F''_{1d}(K+1)-F''_{1c}(K). \qquad \ldots \quad (4)$$

Subtracting, we get

$$\begin{aligned}[R_1(K)-Q_1(K+1)]-[Q_1(K)-P_1(K+1)]\\ =[F''_{1c}(K+1)-F''_{1d}(K+1)]+[F''_{1c}(K)-F''_{1d}(K)]\\ =\Delta\nu''_{cd}(K+1)+\Delta\nu''_{cd}(K)\\ =2\Delta\nu''_{cd}(K+\tfrac{1}{2}).\end{aligned} \qquad \ldots \quad (5)$$

The combination defect therefore leads to a mean value of the Λ-doubling in the levels K + 1 and K. A similar expression holds for the Λ-doubling in the other spin component $^2\Pi_{\frac{1}{2}}$ (F''_2 levels) state of the molecule. In the absence of the satellite branches, the above data constitute the only information that can be obtained of the Λ-doubling in the $^2\Pi$ states.

Table (1) :—$R \cdot (K)-P_1(K)=\Delta_2F'_1(K)$

K	2872 (1, 0)	2916 (2, 1)	2963 (3, 2)	2708 (2, 0)	2756 (3, 1)
1	52.6	51.1 b	47.9 b	—	48.1
2	87.6 b	83.5	81.4 b	83.9	80.3 b
3	121.4 b	117.1 b	114.2 b	118.0 b	113.6 b
4	156.1 b	150.8 b	144.5 b	150.6 b	144.6 b
5	191.1 b	184.4 b	177.4 b	183.8 b	176.7 b
6	225.7 b	215.9 b	208.8 b	217.2 b	208.8
7	259.8 b	249.1	240.1 b	250.0	240.0
8	293.4 b	282.1 b	272.2 b	282.9 b	271.4
9	327.4	315.2	302.8 b	315.4	302.8
10	360.8	347.5	333.6	347.1 b	333.6
11	394.[illegible]	379.3 b	364.9	379.4	364.8 b
12	427.2	411.0	394.1	410.7 b	394.5 b
13	459.8	442.5	424.0 b	441.8	424.6
14	492.4 b	474.1 b	—	473.4	454.2
15	523.7 b	504.2	—	503.2 b	483.5
16	556.0	534.3	—	533.6	—
17	586.8 b	563.9 b	—	563.1	—
18	616.6	594.4	—	593.3	—
19	647.5 b	—	—	621.7	—
20	676.0 b	—	—	650.6 b	—
21	706.1	—	—	677.7	—
22	734.0	—	—	—	—
23	762.5	—	—	—	—
24	790.1 b	—	—	—	—
25	816.4 b	—	—	—	—
26	841.8 b	—	—	—	—

b in this and all the subsequent tables indicates that the difference is obtained from blended lines.

TABLE (2) :—$R_2(K) - P_2(K) = \Delta_2F'_2(K)$

K	2872 (1, 0)	2916 (2, 1)	2963 (3, 2)	2708 (2, 0)	2756 (3, 1)
1	52.3 b	—	52.6	—	—
2	85.8 b	83.3 b	81.9	84.1	79.7 b
3	121.4	119.4 b	114.7	117.7 b	112.0 b
4	156.8 b	150.3 b	144.5 b	150.6	144.0 b
5	190.7 b	183.1 b	176.4 b	183.5 b	176.0 b
6	224.9 b	216.7 b	208.1 b	216.4	208.5 b
7	259.2 b	249.2 b	239.2 b	249.9 b	240.1 b
8	293.2	282.6 b	271.3 b	282.3	271.5 b
9	327.4 b	315.1 b	302.6 b	314.3	302.6 b
10	360.6 b	346.4 b	333.4 b	346.7	333.5 b
11	393.8 b	378.2 b	363.1	379.4 b	364.4 b
12	426.8 b	—	—	410.7	395.6 b
13	459.9 b	—	—	442.1	424.1 b
14	491.9 b	—	—	473.0 b	455.8 b

Tables (1) and (2) give the values of $\Delta_2F'(K)$ for the bands analysed by the authors together with the corresponding values for the bands identified by Ishaq (1937). The agreement between the respective rotational term differences indicate that λλ2916 and 2708 have a common upper vibrational state $v'=2$ and that λ2963 and λ2756 have the common value $v'=3$. The structure of λ2872 gives the rotational characteristics associated with the vibrational state $v'=1$, which have not been previously identified.

Tables (3), (4) and (5) represent the combination differences shown in equations (3) and (4) for the two spin component levels in each of the bands identified. A comparison of these values with Ishaq's data indicate a common lower vibrational level $v''=0$ for the bands λλ2872, 2708 and 3065, and $v''=1$ for λλ2916 and 2756. The data recorded for λ2963 represent values for $v''=2$ which are newly obtained in the present work. The fourth and seventh columns in each of the three tables show the "mean Λ-doubling" for various values of K, referred to in equation (5).

TABLE (3) :—λ2872

K	$R_1(K)$ — $Q_1(K+1)$	$Q_1(K)$ — $P_1(K+1)$	Mean Λ Doubling	$R_2(K)$ — $Q_2(K+1)$	$Q_2(K)$ — $P_2(K+1)$	Mean Λ Doubling
1	46.8	46.6	−0.1	32.2 b	30.9 b	−0.7
2	65.0	64.5 b	−0.3	51.4 b	52.3 b	0.5
3	83.8	83.7 b	−0.1	72.6 b	73·1 b	0.3
4	102.4 b	102.1	−0.2	93.6 b	93.4 b	−0.1
5	121.8 b	121.2	−0.3	113.9 b	114.2	0.2
6	141.0 b	140.1 b	−0.5	133.8 b	133.5 b	−0.2
7	160.4 b	159.0	−0.7	153.3 b	153.6	0.2
8	178.9	177.8 b	−0.6	173.1 b	174.1	0.5
9	198.1	196.5	−0.8	193.5 b	193.3	−0.1
10	216.7 b	215.0 b	−0.9	212.4 b	212.1	−0.2
11	236.1 b	233.9 b	−1.1	231.9 b	231.5	−0.2
12	255.4	251.6	−1.9	251.2 b	250.4	−0.4
13	274.1 b	269.6 b	−2.4	270.1	268.2 b	−1.0
14	293.2 b	286.6	−3.3	289.1 b	287.8	−0.7
15	311.9 b	305.6 b	−3.2	—	305.5 b	—
16	331.1	323.6	−3.8		323.3 b	—
17	347.9 b	339.4 b	−4.3	—	340.9 b	—
18	365.7	357.7	−4.0		359.0 b	—
19	384.1	374.3 b	−4.9	—	375.9	—
20	400.6 b	391.1 b	−4.8		392.1 b	—
21	418.9	407.5	−5.7	—	409.0	—
22	435.8	424.3	−5.8	—	426.4 b	—
23	452.3	440.2	−6.1	—	441.5 b	—
24	468.7	455.6 b	−6.6	—	457.7	—
25	485.4	470.1 b	−7.7	—	472.5 b	—
26	502.1	482.7 b	−9.7	—	487.7 b	—
27	—	—	—	—	502.6 b	—
28	—	—	—	—	517.4 b	—
29	—	—	—	—	531.2 b	—
30	—	—	—	—	544.9 b	—
31	—	—	—	—	558.4 b	—

TABLE (4) :—λ2916

K	$R_1(K)$ — $Q_1(K+1)$	$Q_1(K)$ — $P_1(K+1)$	Mean Λ Doubling	$R_2(K)$ — $Q_2(K+1)$	$Q_2(K)$ — $P_2(K+1)$	Mean Λ Doubling
1	46.3 b	45.4 b	−0.5	—	28.9 b	—
2	63.0	62.6	−0.2	50.5	51.3 b	04
3	83.2 b	81.4	−0.9	72.0	71.4 b	−0.3
4	99.9 b	99.0 b	−0.5	90.0 b	91.3 b	0.7
5	118.3 b	118.2 b	−0.1	110.2 b	111.1 b	0.5
6	135.8 b	136.3	+0.3	129.8 b	129.3 b	−0.3
7	154.9 b	154.5 b	−0.2	148.9 b	149.7 b	0.4
8	174.0 b	172.4	−0.8	169.0 b	169.3 b	0.2
9	193.1 b	190.6 b	−1 3	187.5 b	187 1 b	−0.2
10	211.8	208.6	−1.6	205.5 b	206.3 b	0,4
11	229.9 b	226.6	−1.7	224.4 b	225.0	0.3
12	247.9	244.9	−1.5	—	243.7	—
13	266.3	262.7	−1.8	—	261.8	—
14	284.9	279.8 b	−2.6	—	279.5 b	—
15	303.0	297.0	−3.0	—	297.0 b	—
16	320.5 b	313.3 b	−3.6	—	313 7 b	—
17	338.2	330.5 b	−3 9	—	331.3 b	—
18	357.2 b	347.8 b	−4.7	—	348 3 b	—
19	—	364.1 b	—	—	364.7	—
20	—	379.5	—	—	381.4 b	—
21	—	395.5 b	—	—	397.2	—
22	—	411.3 b	—	—	412.9 b	—
23	—	427.2 b	—	—	427.5	—
24	—	441.4 b	—	—	442.9 b	—
25	—	454.9 b	—	—	457.5	—

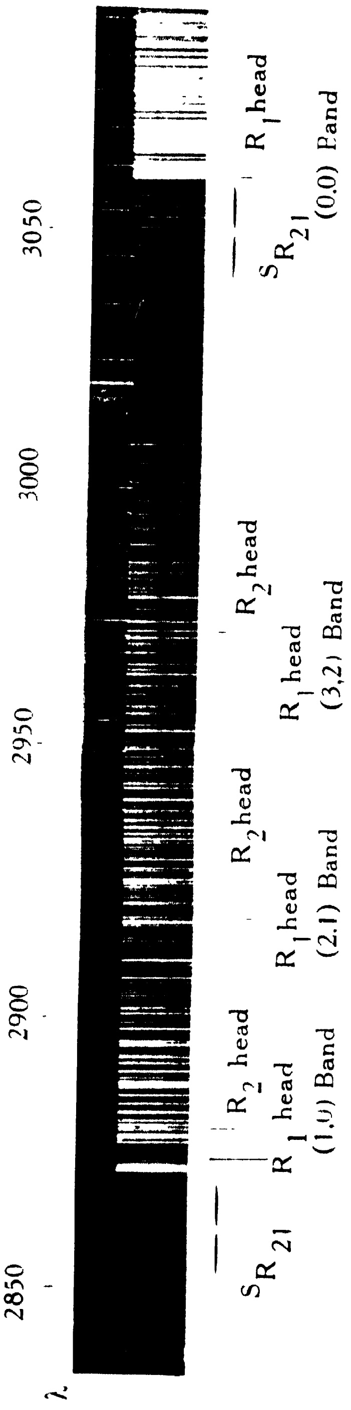

Structure of the OD bands of heavy water between λ 2800– λ 3060.

TABLE (5) :—λ2963

K	$R_1(K)$ — $Q_1(K+1)$	$Q_1(K)$ — $P_1(K+1)$	Mean Λ Doubling	$R_2(K)$ — $Q_2(K+1)$	$Q_2(K)$ — $P_2(K+1)$	Mean Λ Doubling
1	43.8 b	44·1	0.2	—	—	—
2	62.3 b	61·7	−0.3	49.4 b	48.0 b	−0.7
3	80.8 b	78·8	−1.0	70.1 b	70 1 b	0.0
4	96.8 b	96·6 b	−0.1	87.5 b	88,9	0.7
5	115.6 b	115·4	−0.1	106.8 b	107.4	0,3
6	133.3 b	133·2 b	−0.1	125.8 b	126.1 b	0.2
7	150.9 b	150·5 b	−0.2	144.2	145.5 b	0.7
8	169.6	167·5 b	−1.1	163.8 b	164.7 b	0.5
9	187.9 b	185·3	−1.3	180.9 b	182.8 b	1.0
10	205.9 b	202·9 b	−1.5	199.6 b	199.8 b	0.1
11	223.7	220·2	−1.8	—	217.7 b	—
12	240.2	237 2	−1 5	—	236.6	—
13	258.5 b	254·4 b	−2.1	—	255.7 b	—
14	—	271·7 b	—	—	275.1 b	—
15	—	287·6 b	—	—	294.3 b	—
16	—	304·5	—	—	—	—
17	—	320·7 b	—	—	—	—

ROTATIONAL CONSTANTS

The bands considered in this investigation are due to the electronic transition from the upper state $^2\Sigma^+$ to the ground-level $^2\Pi$ which is inverted, the magnitude of the ratio A/B being large and negative. For the initial level, the value of Λ being zero, S is not coupled to the internuclear axis and Hund's case (*b*) must obtain. The expression for the rotational energy may be written down as

$$F'(K) = B'_v K(K+1) + D'_v K^2(K+1)^2 + \ldots \qquad \ldots \quad (6)$$

in which the smal term $\frac{1}{2}\gamma[J(J+1) - K(K+1) - S(S+1)]$ representing case (*b*) spin doubling is omitted. From (6) and the equations for the R, Q and P branches quoted earlier, we can obtain the relation,

$$R_1(K) - P_1(K) \cong R_2(K) - P_2(K)$$

$$= \Delta_2 F'_1(K) = (4K+2)[B'_v + 2D'_v(K^2+K+1)] \qquad (7)$$

For the ${}^2\Pi$ states representing any stage of coupling between Hund's case (*a*) and case (*b*) Hill and Van Vleck (1928) have derived a general expression for the rotational and coupling energies from which, according to Johnston, Dawson and Waker (1933) the following expression is derived :—

$$\Delta_2F''_{12}(K)=4B''_v(K+\tfrac{1}{2})+\frac{2B''^2}{A\Lambda}+8D''_v[(K+\tfrac{1}{2})^3+(K+\tfrac{1}{2})]+\ldots \qquad (8)$$

$\Delta_2F''_{12}(K)$ represents the mean of $\Delta_2F''_1(K)$ and $\Delta_2F''_2(K)$ which are approximately given by the rotational term differences

$[R_1(K-1)-P_1(K+1)]$ and $[R_2(K-1)-P_2(K+1)]$, respectively,

if the relatively small values of the Λ-type doublet differences are neglected.

Equations (7) and (8) can be employed as usual to determine the values of both the rotational constants B and D in the upper and lower electronic states. This has been done and the results have been reported in our preliminary notes—Rao and Sastry (1940). However, as the magnitude of D is small (of the order of 10^{-4}) and the dispersion of the spectrograph employed is not large enough for the purpose, it is preferred to assume the values of D which can be calculated by the aid of the equation

$$D_v^{(OD)}=\rho^4.D_e^{(OH)}+\rho^5.\beta^{(OH)}.(v+\tfrac{1}{2})$$

ρ being the mass ratio of the hydrogen isotopes. The constants for the OH molecule are adopted from the work of Johnston, Dawson and Walker (1933). For the purpose of the above equation ρ^2 is assumed to be 0.5300, taking values determined by Aston (1935) $H^1=1.0081$ and $H^2=2.0148$. The values of D calculated in the above manner for the various vibrational states and those of B afterwards obtained from equations (7) and (8) and the observed rotational term differences are set forth in Table (6).

TABLE (6) :—Rotational Constants in cms.$^{-1}$

Vibrational State	$-D$ (Calc.) $\times 10^3$	B
$v'=1$	0·569	8·723
$v'=2$	0·560	8·389
$v'=3$	0·551	8·074
$v''=0$	0·549	9·927
$v''=1$	0·538	9·577
$v''=2$	0·528	9·408

THE SPIN COUPLING CONSTANT

The constant A in the rotational energy function represents the magnetic coupling energy of the doublet II states and is equal to the separations of the double P, Q and R branches when extrapolated to their origins. The value may be obtained graphically from the observed doublet separations. Alternatively, as done by Ishaq (1937), the rotational energy function may be simplified to the form

$$\left\{\frac{A}{B}-2\right\}^2=\frac{[F_1(J)-F_2(J)]^2}{B_v^2}-4[(J+\tfrac{1}{2})^2-1]$$

where $[F_1(J)-F_2(J)]$ is approximately equal to the rotational term differences $R_1(J)-Q_2(J)$ or $Q_1(J)-P_2(J)$. The values of A found for various values of J for the three bands are shown in Table (7).

TABLE (7) :—Values of A (cms.$^{-1}$)

J	2872	2916	2963
$1\frac{1}{2}$	−138.8	−139.7	−139.9
$2\frac{1}{2}$	−138.9	−139.3	−139.0
$3\frac{1}{2}$	−139.1	−139.6	−139.7
$4\frac{1}{2}$	−138.5	−138.9	−139.1
$5\frac{1}{2}$	−139.4	−140.3	−139.8
$6\frac{1}{2}$	−139.3	−139.2	−138.8
$7\frac{1}{2}$	−138.9	−139.6	−138.0
$8\frac{1}{2}$	−138.0	−140.8	−139.1
Mean value	−138.6	−139.6	−139.2

TABLE (8) :—Comparison of the values of A

$v' \backslash v''$	0	1	2
0	−139.5	—	—
1	−138.6	—	—
2	−139.1	−139.6	—
3	—	−140.0	−139.2

It might be expected that the value of A, the factor representing the magnetic coupling energy, varies with or depends upon the vibrational state of the molecule, particularly when there is a perturbation in any of the levels such as has been found in the Red CN band system for $v'=6$ and 7 by Jenkins, Roots and Mulliken (1932). No such variation, however, can be definitely postulated from the above table and if it is real, it appears to be of relatively small magnitude.

VIBRATIONAL CONSTANTS

An accurate estimate of the vibrational constants can be made only when the band origins or null lines are calculated. The wave-numbers ν_0 of the null lines may be estimated as Johnston, Dawson and Walker (1933) have done for the OH bands, from the equation

$$\nu_0 = F'_1(1) + F''_1{}^*(1) - F'_1(0)$$

for the ${}^2\Pi_{\frac{3}{2}}$ branches of the various bands where

$$F''_1{}^*(K) = F''_1(K) - F''_1(K-\tfrac{1}{2})$$

and $$F'_1(K) = B'(K+\tfrac{1}{2})^2 + D'(K+\tfrac{1}{2})^4.$$

Table (9) gives the values thus obtained. The values for the (0, 0), (2, 0) and (3, 1) bands are calculated from Ishaq's data.

TABLE (9) :—Null lines of the ${}^2\Pi_{\frac{3}{2}}$ branches of the OD bands

v'/v''	0	(2632·7)	1	(2544·2)	2
0	32542.3		—		—
	2215.0				
1	34757·3		—		—
	2112.1				
2	36869.4		34236.7		—
			2008.0		
2	–		36244.7		33700.5

The vibrational constants derived from the differences in Table (9) are

$\omega'_e = 2319.1$ $\omega''_e = 2721.2$

$x'_e\omega'_e = 51.75$ $x''_e\omega''_e = 44.25$

The above values of ω_e give the mass ratio of the hydrogen isotopes as

$$\rho = \frac{\omega'_e\ (OD)}{\omega'_e\ (OH)} = 0.7283$$

and $$\rho = \frac{\omega''_e\ (OD)}{\omega''_e\ (OH)} = 0.7286$$

which agrees fairly with the value 0.7281 calculated directly from the isotopic masses by Aston (1935).

A catalogue of all the observed lines is given in the following Table (10) which records the wave-numbers, visual estimates of the intensities and assignments of the lines, ascribed to the several branches of the three bands λλ2872, 2916 and 2963.

ν (Vae)	Int.	Classification						
		2872						
		$^SR_{21}$	R_1	Q_1	P_1	R_2	Q_2	P_2
35001.6	(0)	12	—	—	—	—	—	—
34997.8	(0)	11	—	—	—	—	—	—
34993.3	(0)	10	—	—	—	—	—	—
34984.6	(0)	9	—	—	—	—	—	—
34974.8	(1)	8	—	—	—	—	—	—
34962.6	(1)	7	—	—	—	—	—	—
34948.3	(1)	6	—	—	—	—	—	—
34931.4	(1)	5	—	—	—	—	—	—
34912.6	(1)	4	—	—	—	—	—	—
34892.3	(1)	3	—	—	—	—	—	—
34871.3	(1)	2	—	—	—	—	—	—
34847.9	(0)	1	—	—	—	—	—	—
34811.2	(10)	—	5, 6	—	—	—	—	—
34809.1	(10)	—	4, 7	—	—	—	—	—
34806.0	(3)	—	3	—	—	—	—	—
34804.6	(3)	—	8	—	—	—	—	—
34801.7	(3)	—	2	—	—	—	—	—
34798.3	(3)	—	9	—	—	—	—	—
34795.9	(3)	—	1	—	—	—	—	—
34790.0	(4)	—	10	—	—	—	—	—
34779.2	(4)	—	11	—	—	—	—	—
34766.6	(4)	—	12	—	—	—	—	—
34760.7	(4)	—	—	1	—	—	—	—
34751.3	(3)	—	13	—	—	—	—	—
34749.1	(5)	—	—	2	—	—	—	—
34743.4	(3)	—	—	—	1	—	—	—

ν (Vac)	Int.	Classification					
		2872					
		R_1	Q_1	P_1	R_2	Q_2	P_2
34739.8	(1)	—	—	—	8	—	—
34738.8	(4)	—	—	—	7, 9	—	—
34736.7	(5)	—	3	—	—	—	—
34734.0	(4)	14	—	—	6, 10	—	—
34727.0	(5)	—	—	—	5, 11	—	—
34722.2	(6)	—	4	—	—	—	—
34716.9	(4)	—	—	—	4, 12	—	—
34714.1	(4)	15	—	2	—	—	—
34706.7	(6)	—	5	—	—	—	—
34704.6	(2)	—	—	—	13	—	—
34702.3	(2)	—	—	—	3	—	—
34691.2	(2)	16	—	—	—	—	—
34689.4	(8)	—	6	—	14	—	—
34684.6	(4)	—	—	3	2	—	—
34670.2	(9)	—	7	—	—	—	—
34665.4	(3)	17	—	—	1	—	—
34653.0	(3)	—	—	4	—	—	—
34648.7	(8)	—	8	—	—	—	—
34637.3	(3)	18	—	—	—	—	—
34633.2	(5)	—	—	—	—	2, 3	—
34629.7	(4)	—	—	—	—	1, 4	—
34625.7	(5)	—	9	—	—	—	—
34623.3	(4)	—	—	—	—	5	—
34620.1	(5)	—	—	5	—	—	—
34613.1	(7)	—	—	—	—	6	1
34607.3	(4)	19	—	—	—	—	—
34600.2	(10)	—	10	—	—	7	—

ν (Vac)	Int.	Classification					
		2872					
		R_1	Q_1	P_1	R_2	Q_2	P_2
34598.8	(1)	—	—	—	—	—	2
34585·5	(8)	—	—	6	—	8	—
34580.9	(4)	—	—	—	—	—	3
34573·3	(6)	20	11	—	—	—	—
34570.8	(2)	—	—	—	—	—	—
34566·7	(5)	—	—	—	—	9	—
34560.1	(5)	—	—	—	—	—	4
34549·3	(4)	—	—	7	—	—	—
34545 3	(4)	—	—	—	—	10	—
34543·1	(4)	—	12	—	—	—	—
34538.2	(3)	21	—	—	—	—	—
34536·3	(4)	—	—	—	—	—	5
34521 6	(5)	—	—	—	—	11	—
34513 0	(1)	—	—	—	—	—	—
34511.2	(8)	—	13	8	—	—	—
34509.1	(3)	—	—	—	—	—	6
34506.0	(0)	—	—	—	—	—	—
34503 2	(3)	—	—	—	—	—	—
34499.2	(3)	22	—	—	—	—	—
34495·1	(6)	—	—	—	—	12	—
34479·6	(5)	—	—	—	—	—	7
34476.9	(5)	—	14	—	—	—	—
34470.9	(4)	—	—	9	—	—	—
34465·7	(8)	—	—	—	—	13	—
34457·5	(2)	23	—	—	—	—	—
34446.6	(3)	—	—	—	—	—	8

ν (Vac)	Int.	Classification					
		2872					
		R_1	Q_1	P_1	R_2	Q_2	P_2
34440.8	(4)	—	15	—	—	—	—
34434·5	(3)	—	—	—	—	14	—
34429·2	(3)	—	—	10	—	—	—
34424.9	(2)	—	—	—	—	—	—
34423.2	(1)	—	—	—	—	—	—
34413·3	(1)	24	—	—	—	—	—
34411·4	(4)	—	—	—	—	—	9
34402·2	(6)	—	16	—	—	—	—
34400.3	(6)	—	—	—	—	15	—
34385.2	(4)	—	—	11	—	—	—
34381.1	(2)	—	—	—	—	—	—
34375·1	(1)	—	—	—	—	—	—
34373·4	(4)	—	—	—	—	—	10
34366.0	(3)	25	—	—	—	—	—
34363·3	(5)	—	—	—	—	16	—
34360.1	(5)	—	17	—	—	—	—
34339.4	(4)	—	—	12	—	—	—
34334.4	(3)	—	—	—	—	—	—
34333.2	(3)	—	—	—	—	—	11
34325·7	(1)	—	—	—	—	—	—
34324·0	(6)	—	—	—	—	17	—
34319·7	(0)	—	—	—	—	—	—
34317·5	(7)	—	18	—	—	—	—
34316.3	(2)	26	—	—	—	—	—
34293·7	(0)	—	—	—	—	—	—
34291.5	(3)	—	—	13	—	—	—
34290·1	(2)	—	—	—	—	—	12

ν (Vac)	Int.	Classification								
		2872						2916		
		R_1	Q_1	P_1	R_2	Q_2	P_2	R_1	Q_1	P_1
34287.4	(1)	—	—	—	—	—	—	—	—	—
34284.7	(7)	—	—	—	—	—	—	4, 5	—	—
34282.5	(7)	—	—	—	—	18	—	3, 6	—	—
34279.2	(3)	—	—	—	—	—	—	7	—	—
34278.3	(3)	—	—	—	—	—	—	2	—	—
34274.3	(3)	—	—	—	—	—	—	1, 8	—	—
34271.6	(5)	—	19	—	—	—	—	—	—	—
34267.1	(3)	—	—	—	—	—	—	9	—	—
34262.2	(2)	—	—	—	—	—	—	—	—	—
34257.2	(3)	—	—	—	—	—	—	10	—	—
34246.6	(0)	—	—	—	—	—	—	—	—	—
34244.7	(4)	—	—	—	—	—	13	11	—	—
34241.6	(3)	—	—	14	—	—	—	—	—	—
34240.2	(3)	—	—	—	—	—	—	—	1	—
34237.6	(4)	—	—	—	—	19	—	—	—	—
34232.4	(2)	—	—	—	—	—	—	—	—	—
34229.8	(3)	—	—	—	—	—	—	12	—	—
34228.0	(4)	—	—	—	—	—	—	—	2	—
34223.2	(7)	—	20	—	—	—	—	—	—	1
34215.3	(6)	—	—	—	—	—	—	—	3	—
34212.4	(2)	—	—	—	—	—	—	13	—	—

(Vac)	Int.	Classification											
		2872						2916					
		R_1	Q_1	P_1	R_2	Q_2	P_2	R_1	Q_1	P_1	R_2	Q_2	P_2
34209.0	(5)	—	—	—	—	—	—	—	—	—	7, 8	—	—
34205·9	(5)	—	—	—	—	—	—	—	—	—	6, 9	—	—
34199·3	(7)	—	—	—	—	—	—	—	4	—	5, 10	—	—
34197·5	(2)	—	—	—	—	—	14	—	—	—	—	—	—
34194.8	(2)	—	—	—	—	—	—	—	—	2	—	—	—
34193·3	(1)	—	—	—	—	—	—	14	—	—	—	—	—
34190·3	(9)	—	—	15	—	20	—	—	—	—	4, 11	—	—
34184·4	(6)	—	—	—	—	—	—	—	5	—	—	—	—
34179·5	(2)	—	—	—	—	—	—	—	—	—	3	—	—
34176.7	(2)	—	—	—	—	—	—	—	—	—	—	—	—
34172·7	(4)	—	21	—	—	—		—		—		—	—
34170.5	(3)	—	—	—	—	—	—	15	—	—	—	—	—
34166.4	(4)	—	—	—	—	—	—	—	6	—	—	—	—
34165·4	(4)	—	—	—	—	—	—	—	—	3	—	—	—
34161.9	(2)	—	—	—	—	—	—	—	—	—	2	—	—
34146·7	(9)	—	—	—	—	—	15	—	7	—	—	—	—
34145·7	(9)	—	—	—	—	—	—	16	—	—	—	—	—
34140.9	(5)	—	—	—	—	21	—	—	—	—	—	—	—
34135·2	(3)	—	—	16	—	—	—	—	—	—	—	—	—
34133·9	(3)	—	—	—	—	—	—	—	—	4	—	—	—
34127.1	(3)	—	—	—	—	—	—	—	—	—	—	—	—
34124·3	(4)	—	—	—	—	—	—	—	8	—	—	—	—
34121.8	(0)	—	—	—	—	—	—	—	—	—	—	—	—
34119·3	(4)	—	22	—	—	—	—	—	—	—	—	—	—
34118 1	(3)	—	—	—	—	—	—	17	—	—	—	—	—
34114.1	(0)	—	—	—	—	—	—	—	—	—	—	—	—
34111.4	(5)	—	—	—	—	—	—	—	—	—	—	2, 3	—
34107·5	(4)	—	—	—	—	—	—	—	—	—	—	1, 4	—

ν (Vac)	Int.	Classification											
		2872						2916					
		R_1	Q_1	P_1	R_2	Q_2	P_2	R_1	Q_1	P_1	R_2	Q_2	P_2
34103.6	(3)	—	—	—	—	—	—	—	—	—	—	—	—
34100.3	(9)	—	—	—	—	—	—	—	9	5	—	5	—
34094.8	(3)	—	—	—	—	—	16	—	—	—	—	—	1
34089.1	(10)	—	—	—	—	22	—	18	—	—	—	6	—
34083.7	(2)	—	—	—	—	—	—	—	—	—	—	—	—
34078.6	(4)	—	—	17	—	—	—	—	—	—	—	—	2
34076.1	(3)	—	—	—	—	—	—	—	—	—	—	7	—
34074.0	(3)	—	—	—	—	—	—	—	10	—	—	—	—
34066.6	(4)	—	—	—	—	—	—	—	—	6	—	—	—
34063.4	(4)	—	23	—	—	—	—	—	—	—	—	—	—
34060.1	(6)	—	—	—	—	—	—	—	—	—	—	8	3
34054.5	(3)	—	—	—	—	—	—	—	—	—	—	—	—
34048.5	(2)	—	—	—	—	—	—	—	—	—	—	—	—
34045.4	(5)	—	—	—	—	—	—	—	11	—	—	—	—
34041.6	(0)	—	—	—	—	—	—	—	—	—	—	—	—
34040.0	(9)	—	—	—	—	—	17	—	—	—	—	9	4
34033.7	(4)	—	—	—	—	23	—	—	—	—	—	—	—
34030.1	(3)	—	—	—	—	—	—	—	—	7	—	—	—
34020.7	(3)	—	—	18	—	—	—	—	—	—	—	—	—
34018.4	(5)	—	—	—	—	—	—	—	—	—	—	10	—
34016.2	(2)	—	—	—	—	—	—	—	—	—	—	—	5
34014.8	(3)	—	—	—	—	—	—	—	12	—	—	—	—
34005.2	(5)	—	24	—	—	—	—	—	—	—	—	—	—
33993.8	(4)	—	—	—	—	—	—	—	—	—	—	11	—
33992.2	(4)	—	—	—	—	—	—	—	—	8	—	—	—
33989.2	(4)	—	—	—	—	—	—	—	—	—	—	—	6
33983.1	(3)	—	—	—	—	—	18	—	—	—	—	—	—
33981.9	(8)	—	—	—	—	—	—	—	13	—	—	—	—

ν (Vac)	Int.	Classification											
		2872						2916					
		R_1	Q_1	P_1	R_2	Q_2	P_2	R_1	Q_1	P_1	R_2	Q_2	P_2
33979.1	(1)	—	—	—	—	—	—	—	—	—	—	—	—
33976.2	(5)	—	—	—	—	24	—	—	—	—	—	—	—
33967.7	(0)	—	—	—	—	—	—	—	—	—	—	—	—
33965.9	(5)	—	—	—	—	—	—	—	—	—	—	12	—
33959.8	(6)	—	—	19	—	—	—	—	—	—	—	—	7
33951.9	(3)	—	—	—	—	—	—	—	—	9	—	—	—
33949.0	(2)	—	—	—	—	—	—	—	—	—	—	—	—
33946.1	(4)	—	—	—	—	—	—	—	14	—	—	—	—
33944.6	(4)	—	25	—	—	—	—	—	—	—	—	—	—
33937.5	(2)	—	—	—	—	—	—	—	—	—	—	—	—
33935.5	(5)	—	—	—	—	—	—	—	—	—	—	13	—
33927.5	(1)	—	—	—	—	—	—	—	—	—	—	—	—
33926.4	(3)	—	—	—	—	—	—	—	—	—	—	—	8
33923.5	(3)	—	—	—	—	—	19	—	—	—	—	—	—
33920.7	(1)	—	—	—	—	—	—	—	—	—	—	—	—
33918.2	(0)	—	—	—	—	—	—	—	—	—	—	—	—
33915.7	(4)	—	—	—	—	25	—	—	—	—	—	—	—
33909.7	(2)	—	—	—	—	—	—	—	—	10	—	—	—
33908.4	(5)	—	—	—	—	—	—	—	15	—	—	—	—
33902.7	(4)	—	—	—	—	—	—	—	—	—	—	14	—
33897.3	(3)	—	—	20	—	—	—	—	—	—	—	—	—
33892.6	(1)	—	—	—	—	—	—	—	—	—	—	—	—
33890.8	(5)	—	—	—	—	—	—	—	—	—	—	—	9
33880.6	(4)	—	26	—	—	—	—	—	—	—	—	—	—
33877.1	(2)	—	—	—	—	—	—	—	—	—	—	—	—
33867.5	(8)	—	—	—	—	—	—	—	16	—	—	15	—
33865.4	(4)	—	—	—	—	—	—	—	—	11	—	—	—
33861.7	(3)	—	—	—	—	—	20	—	—	—	—	—	—

ν (Vac)	Int.	Classification											
		2872						2916					
		R_1	Q_1	P_1	R_2	Q_2	P_2	R_1	Q_1	P_1	R_2	Q_2	P_2
33859.3	(1)	—	—	—	—	—	—	—	—	—	—	—	—
33852.9	(8)	—	—	—	—	26	—	—	—	—	—	—	10
33848.6	(2)	—	—	—	—	—	—	—	—	—	—	—	—
3845.2	(1)	—	—	—	—	—	—	—	—	—	—	—	—
33832.1	(5)	—	—	21	—	—	—	—	—	—	—	—	—
33828.6	(5)	—	—	—	—	—	—	—	—	—	—	16	—
33825.2	(5)	—	—	—	—	—	—	—	17	—	—	—	—
33818.8	(5)	—	—	—	—	—	—	—	—	12	—	—	—
33814.2	(5)	—	27	—	—	—	—	—	—	—	—	—	—
33812.1	(5)	—	—	—	—	—	—	—	—	—	—	—	11
33800.5	(2)	—	—	—	—	—	—	—	—	—	—	—	—
33798.2	(3)	—	—	—	—	—	21	—	—	—	—	—	—
33794.7	(1)	—	—	—	—	—	—	—	—	—	—	—	—
33789.7	(0)	—	—	—	—	—	—	—	—	—	—	—	—
33787.6	(6)	—	—	—	—	27	—	—	—	—	—	17	—
33779.9	(4)	—	—	—	—	—	—	—	18	—	—	—	—
33773.3	(1)	—	—	—	—	—	—	—	—	—	—	—	—
33769.9	(3)	—	—	—	—	—	—	—	—	13	—	—	—
33768.8	(3)	—	—	—	—	—	—	—	—	—	—	—	12
33765.2	(2)	—	—	22	—	—	—	—	—	—	—	—	—
33761.8	(1)	—	—	—	—	—	—	—	—	—	—	—	—
33758.8	(0)	—	—	—	—	—	—	—	—	—	—	—	—
33745.4	(3)	—	28	—	—	—	—	—	—	—	—	—	—

ν (Vac)	Int.	Classification													
		2872				2916				2963					
		Q_1	P_1	Q_2	P_2	Q_1	P_1	Q_2	P_2	R_1	Q_1	P_1	R_2	Q_2	P_2
33743.5	(6)	—	—	—	—	—	—	18	—	3, 4, 5	—	—	—	—	—
33740.1	(2)	—	—	—	—	—	—	—	—	2, 6	—	—	—	—	—
33734.8	(3)	—	—	—	—	—	—	—	—	1, 7	—	—	—	—	—
33731.9	(6)	—	—	—	22	19	—	—	—	—	—	—	—	—	—
33728.5	(2)	—	—	—	—	—	—	—	—	8	—	—	—	—	—
33722.2	(3)	—	—	—	—	—	—	—	13	—	—	—	—	—	—
33719.4	(5)	—	—	28	—	—	14	—	—	9	—	—	—	—	—
33708.9	(0)	—	—	—	—	—	—	—	—	—	—	—	—	—	—
33707.2	(1)	—	—	—	—	—	—	—	—	10	—	—	—	—	—
33702.8	(3)	—	—	—	—	—	—	—	—	—	1	—	—	—	—
33699.0	(0)	—	—	—	—	—	—	—	—	—	—	—	—	—	—
33696.8	(3)	—	—	—	—	—	—	19	—	—	—	—	—	—	—
33695.0	(3)	—	23	—	—	—	—	—	—	—	—	—	—	—	—
33693.3	(0)	—	—	—	—	—	—	—	—	11	—	—	—	—	—
33691.0	(3)	—	—	—	—	—	—	—	—	—	2	—	—	—	—
33686.9	(2)	—	—	—	—	—	—	—	—	—	—	1	—	—	—
33681.1	(3)	—	—	—	—	20	—	—	—	—	—	—	—	—	—
33677.8	(3)	—	—	—	—	—	—	—	—	—	3	—	—	—	—
33675.2	(0)	—	—	—	—	—	—	—	—	12	—	—	—	—	—
33673.7	(5)	29	—	—	—	—	—	—	14	—	—	—	—	—	—
33666.3	(3)	—	—	—	—	—	15	—	—	—	—	—	—	—	—
33662.7	(7)	—	—	—	23	—	—	—	—	—	4	—	7	—	—
33661.4	(2)	—	—	—	—	—	—	—	—	—	—	—	6, 8	—	—
33658.7	(1)	—	—	—	—	—	—	—	—	—	—	2	—	—	—
33656.4	(3)	—	—	—	—	—	—	—	—	13	—	—	5, 9	—	—
33648.2	(8)	—	—	29	—	—	—	20	—	—	—	—	4, 10	—	—
33646.7	(3)	—	—	—	—	—	—	—	—	—	5	—	—	—	—
33639.0	(2)	—	—	—	—	—	—	—	—	—	—	—	3	—	—

ν (Vac)	Int.	Classification													
		2872				2916				2963					
		Q_1	P_1	Q_2	P_2	Q_1	P_1	Q_2	P_2	R_1	Q_1	P_1	R_2	Q_2	P_2
33637.8	(1)	—	—	—	—	—	—	—	—	—	—	—	11	—	—
33629.3	(2)	—	—	—	—	—	—	—	—	—	—	3	—	—	—
33627.9	(6)	—	—	—	—	21	—	—	—	—	6	—	—	—	—
33623.2	(7)	—	24	—	—	—	—	—	15	—	—	—	2	—	—
33611.4	(4)	—	—	—	—	—	16	—	—	—	—	—	—	—	—
33606.8	(4)	—	—	—	—	—	—	—	—	—	7	—	1	—	—
33599.0	(5)	30	—	—	—	—	—	—	—	—	—	4	—	—	—
33595.9	(4)	—	—	—	—	—	—	21	—	—	—	—	—	—	—
33592.2	(4)	—	—	—	24	—	—	—	—	—	—	—	—	—	—
33588.6	(0)	—	—	—	—	—	—	—	—	—	—	—	—	—	—
33583.9	(6)	—	—	—	—	—	—	—	—	—	8	—	—	—	—
33573.8	(0)	—	—	30	—	—	—	—	—	—	—	—	—	3	—
33572.3	(3)	—	—	—	—	22	—	—	—	—	—	—	—	2	—
33570.5	(3)	—	—	—	—	—	—	—	16	—	—	—	—	1	—
33568.9	(3)	—	—	—	—	—	—	—	—	—		—	—	4	—
33566.1	(3)	—	—	—	—	—	—	—	—	—	—	5	—	—	—
33563.1	(0)	—		—	—	—		—	—	—	—	—	—	—	—
33560.7	(4)	—	—	—	—	—	—	—	—	—	—	—	—	5	—
33558.9	(4)	—	—		—		—	—	—	—	9	—	—	—	—
33554.2	(5)	—	—	—	—	—	17	—	—	—	—	—	—	—	1
33549.6	(7)	—	25	—	—	—	—	—	—	—	—	—	—	6	—
33541.3	(6)	—	—	—	—	—	—	22	—	—	—	—	—	—	2
33535.6	(5)	—	—	—	—	—	—	—	—	—	—	—	—	7	—
33533.6	(00)	—	—	—	—	—	—	—	—	—	—	—	—	—	—
33531.3	(7)	—	—	—	—	—	—	—	—	—	10	6	—	—	—
33525.7	(1)	—	—	—	—	—	—	—	—	—	—	—	—	—	—
33524.3	(3)	—	—	—	—	—	—	—	—	—	—	—	—	—	3
33521.7	(3)	31	—	—	—	—	—	—	—	—	—	—	—	—	—

ν (Vac)	Int.	Classification													
		2872				2916				2963					
		Q_1	P_1	Q_2	P_2	Q_1	P_1	Q_2	P_2	R_1	Q_1	P_1	R_2	Q_2	P_2
33518.5	(6)	—	—	—	25	—	—	—	—	—	—	—	—	8	—
33514.9	(5)	—	—	—	—	23	—	—	17	—	—	—	—	—	—
33503.7	(3)	—	—	—	—	—	—	—	—	—	—	—	—	—	4
33501.3	(3)	—	—	—	—	—	—	—	—	—	11	—		—	—
33497.6	(5)	—	—	31	—	—	—	—	—	—	—	—	—	9	—
33494.7	(4)	—	—	—	—	—	18	—	—	—	—	7	—	—	—
33484.0	(3)	—	—	—	—	—	—	23	—	—	—	—	—	—	—
33480.0	(3)	—	—	—	—	—	—	—	—	—	—	—	—	—	5
33474.5	(4)	—	26	—	—	—	—	—	—	—	—	—	—	10	—
33469.6	(3)	—	—	—	—	—	—	—	—	—	12	—	—	—	—
33462.3	(0)	—	—	—	—	—	—	—	—	—	—	—	—	—	—
33456.3	(6)	—	—	—	—	—	—	—	18	—	—	8	—	—	—
33453.3	(5)	—	—	—	—	24	—	—	—	—	—	—	—	—	6
33448.6	(3)	—	—	—	—	—	—	—	—	—	—	—	—	11	—
33443.2	(3)	—	—	—	26	—	—	—	—	—	—	—	—	—	—
33441.9	(3)	32	—	—	—	—	—	—	—	—	—	—	—	—	—
33435.0	(3)	—	—	—	—	—	—	—	—	—	13	—	—	—	—
33432.1	(2)	—	—	—	—	—	19	—	—	—	—	—	—	—	—
33423.5	(6)	—	—	—	—	—	—	24	—	—	—	—	—	—	7
33420.2	(3)	—	—	—	—	—	—	—	—	—	—	—	—	12	—
33417.5	(3)	—	—	32	—	—	—	—	—	—	—	—	—	—	—
33416.4	(3)	—	—	—	—	—	—	—	—	—	—	9	—	—	—
33397.9	(3)	—	27	—	—	—	—	—	—	—	14	—	—	—	—
33395.2	(5)	—	—	—	—	—	—	—	19	—	—	—	—	—	—
33390.1	(5)	—	—	—	—	—	—	—	—	—	—	—	—	13	8
33388.6	(2)	—	—	—	—	25	—	—	—	—	—	—	—	—	—
33373.6	(3)	—	—	—	—	—	—	—	—	—	—	10	—	—	—
33367.8	(4)	—	—	—	—	—	20	—	—	—	—	—	—	—	—

ν (Vac)	Int.	Classification													
		2872				2916				2963					
		Q_1	P_1	Q_2	P_2	Q_1	P_1	Q_2	P_2	R_1	Q_1	P_1	R_2	Q_2	P_2
33365.2	(4)	—	—	—	27	—	—	—	—	—	—	—	—	—	—
33361.0	(3)	—	—	—	—	—	—	25	—	—	—	—	—	—	—
33358.4	(4)	33	—	—	—	—	—	—	—	—	15	—	—	14	—
33353.8	(5)	—	—	—	—	—	—	—	—	—	—	—	—	—	9
33334.9	(3)	—	—	33	—	—	—	—	—	—	—	—	—	—	—
33332.1	(2)	—	—	—	—	—	—	—	20	—	—	—	—	—	—
33328.4	(2)	—	—	—	—	—	—	—	—	—	—	11	—	—	—
33323.2	(2)	—	—	—	—	—	—	—	—	—	—	—	—	15	—
33316.4	(5)	—	—	—	—	—	—	—	—	—	16	—	—	—	—
33314.8	(2)	—	—	—	—	—	—	—	—	—	—	—	—	—	10
33301.6	(3)	—	—	—	—	—	21	—	—	—	—	—	—	—	—
33295.1	(2)	—	—	—	—	—	—	26	—	—	—	—	—	—	—
33285.0	(2)	—	—	—	28	—	—	—	—	—	—	—	—	—	—
33281.1	(2)	—	—	—	—	—	—	—	—	—	—	12	—	—	—
33274.7	(2)	—	—	—	—	—	—	—	—	—	—	—	—	—	11
33273.5	(2)	34	—	—	—	—	—	—	—	—	—	—	—	—	—
33271.7	(2)	—	—	—	—	—	—	—	—	—	17	—	—	—	—
33266.8	(4)	—	—	—	—	—	—	—	21	—	—	—	—	—	—
33254.1	(2)	—	—	—	—	—	—	—	—	—	—	—	—	—	—
33249.1	(3)	—	—	34	—	—	—	—	—	—	—	—	—	—	—
33232.4	(4)	—	—	—	—	—	22	—	—	—	—	13	—	—	—
33230.9	(3)	—	—	—	—	—	—	—	—	—	—	—	—	—	12
33227.0	(2)	—	—	—	—	—	—	27	—	—	—	—	—	—	—
33224.4	(0)	—	—	—	—	—	—	—	—	—	18	—	—	—	—
33202.0	(2)	—	—	—	29	—	—	—	—	—	—	—	—	—	—
33198.7	(2)	—	—	—	—	—	—	—	22	—	—	—	—	—	—
33186.7	(0)	—	—	—	—	—	—	—	—	—	—	—	—	—	—
33183.6	(4)	—	—	—	—	—	—	—	—	—	—	—	—	—	13

ν (Vac)	Int.	Classification													
		2872				2916				2963					
		Q_1	P_1	Q_2	P_2	Q_1	P_1	Q_2	P_2	R_1	Q_1	P_1	R_2	Q_2	P_2
33180.6	(2)	—	—	—	—	—	—	—	—	—	—	14	—	—	—
33173.1	(0)	—	—	—	—	—	—	—	—	—	—	—	—	—	—
33161.0	(4)	—	—	35	—	—	23	—	—	—	—	—	—	—	—
33154.8	(2)	—	—	—	—	—	—	—	—	—	—	—	—	—	—
33145.1	(3)	—	—	—	—	—	—		—	—	—	—	—	—	—
33137.5	(0)	—	—	—	—	—	—	—	—	—	—	—	—	—	—
33134.4	(2)	—	—	—	—	—	—	—	—	—	—	—	—	—	14
33128.4	(2)	—	—	—	—	—	—	—	23	—	—	—	—	—	—
33126.2	(1)	—	—	—	—	—	—	—	—	—	—	15	—	—	—
33121.8	(0)	—	—	—	—	—	—	—	—	—	—	—	—	—	—
33117.0	(2)	—	—	—	30	—	—	—	—	—	—	—	—	—	—
33107.0	(0)	—	—	—	—	—	—	—	—	—	—	—	—	—	—
33091.4	(2)	—	—	—	—	—	—	—	—	—	—	—	—	—	—
33087.7	(2)	—	—	—	—	—	24	—	—	—	—	—	—	—	—
33083.3	(1)	—	—	—	—	—	—	—	—	—	—	—	—	—	15
33080.6	(0)	—	—	—	—	—	—	—	—	—	—	—	—	—	—
33070.8	(1)	—	—	—	—	—	—	—	—	—	—	16	—	—	—
33068.7	(2)	—	—	—	—	—	—	—	—	—	—	—	—	—	—
33056.5	(2)	—	—	—	—	—	—	—	24	—	—	—	—	—	—
33028.9	(2)	—	—	—	31	—	—	—	—	—	—	—	—	—	16
33018.3	(0)	—	—	—	—	—	—	—	—	—	—	—	—	—	—
33011.9	(2)	—	—	—	—	—	25	—	—	—	—	17	—	—	—
33003.1	(1)	—	—	—	—	—	—	—	—	—	—	—	—	—	—
32996.3	(1)	—	—	—	—	—	—	—	—	—	—	—	—	—	—
32980.6	(2)	—	—	—	—	—	—	—	25	—	—	—	—	—	—
32974.0	(2)	—	—	—	—	—	—	—	—	—	—	—	—	—	—
32971.4	(1)	—	—	—	—	—	—	—	—	—	—	—	—	—	17
32966.7	(2)	—	—	—	—	—	—	—	—	—	—	—	—	—	—

ν (Vac)	Int.	Classification													
		2872				2916				2963					
		Q_1	P_1	Q_2	P_2	Q_1	P_1	Q_2	P_2	R_1	Q_1	P_1	R_2	Q_2	P_2
32951.0	1)	—	—	—	—	—	—	—	—	—	—	18	—	—	—
32939.2	(2)	—	—	—	32	—	—	—	—	—	—	—	—	—	—
32933.7	(1)	—	—	—	—	—	26	—	—	—	—	—	—	—	—
32903.5	(2)	—	—	—	—	—	—	—	26	—	—	—	—	—	—
32898.4	(0)	—	—	—	—	—	—	—	—	—	—	—	—	—	—

SUMMARY

Bands due to the OD molecule have been obtained free from any trace of the OH bands by photographing discharges through vapour of heavy water of a very high degree of purity. Measurements on the plate between λ2800 and λ3060 have led to the rotational structure of the (1, 0), (2, 1) and (3, 2) bands.

Using Hill and Van Vleck's energy formula for the doublet electronic states, the rotational constants have been evaluated.

The calculated positions of the null lines have enabled the determination of the vibrational constants of the OD molecule and the mass ratio of the hydrogen isotopes.

The authors desire to express their very grateful thanks to Prof. A. Fowler, F.R.S., for his kind interest and encouragement.

REFERENCES

Johnston, *Phys. Rev.*, **45**, 79 (1934)

Johnston and Dawson, *Phys. Rev.*, **44**, 1031 (1933)

Shaw and Gibbs, *Phys. Rev.*, **45**, 124 (1934)

Ishaq, *Proc. Roy. Soc.*, A, **159**, 110 (1937); *Proc. Nat. Inst. Sc. Ind.*, **3**, 389 (1937) and **5**, 309 (1939)

Hill and Van Vleck, *Phys. Rev.*, **32**, 261 (1928)

Johnston, Dawson and Walker, *Phys. Rev.*, **43**, 478 (1933)

Aston, *Nature*, **135**, 541 (1938)

Jenkins, Roots and Mulliken, *Phys. Rev.*, **39**, 32 (1932)

Rao and Sastry, *Nature*, **145**, 778 (1940) and *Current Science* **9**, 172 (1940)

ON THE EFFECT OF MERCURY VAPOUR ON THE CONTINUOUS SPECTRUM OF HYDROGEN EXCITED BY CANAL RAYS OF HYDROGEN*

By V. T. CHIPLONKAR, M.Sc.
College of Science, Benares Hindu University

(*Received for publication, April 15, 1940*)

Plate II

ABSTRACT. It is shown that the presence of Mercury vapour in the discharge tube brings about a marked change in the relative intensity distribution of the continuous spectrum of Hydrogen, as excited by canal rays of hydrogen, in the observation chamber of a canal ray tube in its simple form. The effect is found to be more pronounced at higher operating voltages than at low. The bearing of this result on the known observations on the excitation of the continuous spectrum by canal rays is pointed out ; finally there is given a discussion of the possible explanations for the change brought about by the presence of mercury vapour.

INTRODUCTION

§ 1. There is a certain amount of evidence† to show that the continuous spectrum of Hydrogen, observed with the canal rays of Hydrogen, is in main identical with that obtained in the Geissler tube and is due to the excitation of the stationary molecules of Hydrogen by impact with the canal ray particles. The origin of the continuous spectrum in the Geissler tube has been generally ascribed to H_2 and according to the theory of Winans and Stueckelberg[1] is emitted as a result of a transition between the $1s\sigma, 2s\sigma : {}^3\Sigma_u$ and $1s\sigma, 2p\sigma : {}^3\Sigma_u$ states of the molecule. There appears to be a small but definite difference in the relative intensity distribution of the continuous spectrum as obtained with the canal rays and in the Geissler tube. The intensity in the region $\lambda 2500$Å in the case of the latter is much more accentuated than in the former. Another important finding† in the same connection is that this intensity distribution is independent of the energy of the exciting canal rays. The effect of Mercury vapour on the intensity distribution of the continuous spectrum obtained with the canal rays possesses a certain amount of interest on account of the fact that it is the foreign gas most likely to

---

* Communicated by the Indian Physical Society.

† *Vide* : A paper by the author " On the continuous spectrum of Hydrogen as excited by canal rays of Hydrogen " published elsewhere. This will be referred to as (I) in this paper.

ON THE EFFECT OF MERCURY VAPOUR ON THE CONTINUOUS SPECTRUM OF HYDROGEN EXCITED BY CANAL RAYS OF HYDROGEN*

By V. T. CHIPLONKAR, M.Sc.
College of Science, Benares Hindu University

(Received for publication, April 15, 1940)

Plate II

ABSTRACT. It is shown that the presence of Mercury vapour in the discharge tube brings about a marked change in the relative intensity distribution of the continuous spectrum of Hydrogen, as excited by canal rays of hydrogen, in the observation chamber of a canal ray tube in its simple form. The effect is found to be more pronounced at higher operating voltages than at low. The bearing of this result on the known observations on the excitation of the continuous spectrum by canal rays is pointed out ; finally there is given a discussion of the possible explanations for the change brought about by the presence of mercury vapour.

INTRODUCTION

§ 1. There is a certain amount of evidence† to show that the continuous spectrum of Hydrogen, observed with the canal rays of Hydrogen, is in main identical with that obtained in the Geissler tube and is due to the excitation of the stationary molecules of Hydrogen by impact with the canal ray particles. The origin of the continuous spectrum in the Geissler tube has been generally ascribed to H_2 and according to the theory of Winans and Stueckelberg[1] is emitted as a result of a transition between the $1s\sigma, 2s\sigma : {}^3\Sigma_u$ and $1s\sigma, 2p\sigma : {}^3\Sigma_u$ states of the molecule. There appears to be a small but definite difference in the relative intensity distribution of the continuous spectrum as obtained with the canal rays and in the Geissler tube. The intensity in the region λ2500Å in the case of the latter is much more accentuated than in the former. Another important finding† in the same connection is that this intensity distribution is independent of the energy of the exciting canal rays. The effect of Mercury vapour on the intensity distribution of the continuous spectrum obtained with the canal rays possesses a certain amount of interest on account of the fact that it is the foreign gas most likely to be present in the discharge space at the low pressures that obtain in the canal ray tube, unless specific precautions are taken to eliminate it. There is, therefore, the possibility that many of the apparently contradictory results obtained by different workers may in fact be due to the difference in the efficiencies of the experimental arrangements in preventing the diffusion of Mercury vapour into the discharge space. To quote a specific example, it is still obscure under what conditions the continuous spectrum in the canal rays observed by Stark[2] is obtained. It is, therefore, necessary to know the nature and the order of magnitude of the alterations produced in the intensity distribution of the continuous spectrum of Hydrogen by the presence of Mercury vapour for a satisfactory elucidation of the results obtained on its intensity distribution. The resonance line $\lambda 2537$ of the Mercury atom has got an excitation energy which nearly equals the dissociation energy of the Hydrogen molecule ; so that on general grounds we expect a weakening of the continuous spectrum as a whole relative to the Balmer lines as a result of the admixture with Mercury vapour. The minimum excitation potential of the continuous spectrum has been determined by Finkeinburg and Weizel[3] as 11.84 and the maximum as 13.8 volts. The excitation function of the continuum is, therefore, very narrow and sharply defined. The ionisation potential of Mercury atom[4] being less than this, the possibility of a change in the intensity distribution on account of collisions of the second kind is not probable. This does not, however, exclude the possibility of collisions of this type, involving Mercury atoms in stages of ionisation, higher than the second. An interaction involving molecules of Mercury[5] may be practically excluded both on account of the smaller available energy and the low probability for their occurrence at the pressures that obtain in the canal ray tube. It is well known that remarkable changes occur in the spectra of both atoms and molecules in the presence of foreign gases, resulting sometimes either in a general enhancement or reduction of intensity among lines and bands and sometimes in the production of lines and bands which under ordinary conditions are either absent or very weak. That fundamental changes in the intensity distribution of the continuous spectrum, obtained as a result of the addition of a foreign gas, are shown in a remarkable manner by the experiments of Smith.[6]

---

* Communicated by the Indian Physical Society.

† *Vide* : A paper by the author " On the continuous spectrum of Hydrogen as excited by canal rays of Hydrogen " published elsewhere. This will be referred to as (I) in this paper.

In these experiments, I have adopted the same plan of investigation as reported in (I). A study was made of the variation in the relative intensity distribution of the continuous spectrum, in the presence of Mercury vapour, with the energy of the exciting canal rays ; it was this aspect of the problem that had an immediate and a direct interest for the investigations described in (I).

EXPERIMENTAL

§2. The experimental arrangement used for this investigation is the same as that described in (I) except for the discharge tube and the connections in its neighbourhood. It was not necessary here, to have the elaborate system of liquid-air traps used in (I). For the sake of completeness, a brief description may be given of the experimental arrangement. The discharge tube was 3.5 cms. in diameter, with a cathode of moulded Aluminium 2.0 cms. in length provided with a canal 0.2 cms. in diameter. The anode which was of Aluminium was fixed in a side tube at a distance of about 16 cms. from the Cathode. Evacuation was obtained by means of a set of Mercury diffusion pumps of the Waran type backed by a Cenco Hyvac Oil pump. Liquid-air traps were used for preventing the diffusion of Mercury vapour from the pumps and manometers into the discharge tube. The gas Hydrogen was obtained electrolytically and was purified by passing over heated Magnesium and Copper filings. The method of gas-streaming was used. The H. T. was a half-wave rectified D. C. obtained from a transformer coupled with a Kenetron circuit. The anode was connected to the H. T., the cathode being earthed through a milliammeter. The spectra were taken with a small Hilger Quartz spectrograph, a cylindrical lens being used for focussing the image of the canal rays on the slit of the spectrograph. The observations given below were taken. A select number of these spectra were run on a recording Zeiss micro-photometer; the more important of the micro-photometer curves are shown in figs. (2-5).

For the purposes of the present investigation, it was not necessary to follow the absolute intensity distribution in the continuous spectra obtained under the different conditions. It was sufficient if differences in the relative intensities could be distinguished at any given point on the spectrum (compare : Finkelnburg[7]). So long, therefore, as the exposures were within the limit of saturation of the plate, which condition was kept true in these experiments, the density at any point became a measure of the intensity.

The experimental observations are the following : On Pl. 4, canal ray spectra were taken with canal ray energy of 4, 6, 8, 10 kV. respectively with a discharge current of 2.0 m.a. and a time of exposure of 2.5 hours. On Pl. 6, the first four observations give the canal ray spectra, for energies 4, 2, 8, 6 kV. with times of exposure of 3, 4, 2.5, 3.5 hours respectively with a discharge current of 2.0 m.a. The sixth observation again is a canal ray spectrum obtained with 1.0 kV. across the discharge tube and a time of exposure of 5 hours for a discharge current of 2.0 m.a. Observations 5, 7, 8, 9 give the Geissler tube spectra obtained under the same conditions (*cf.* I) for a discharge voltage of 1.0 kV. and a current of 0.5 m.a. with times of exposure of 0.5, 1, 2, 3 minutes respectively. Pl. 8 depicts the canal ray spectrum for operating voltages of 3, 2, 1.3 kV., with a discharge current of 2.0 m.a. exposed for 4, 4, 1/3 hours respectively.

RESULTS AND DISCUSSION

§3. *Results and Discussion.* In the spectra given herewith, the general absorption (due variously to the material of the spectrograph, air, the photographic emulsion) begins at about λ2300Å. The intensity distribution in the micro-photometer plates can be considered to be reliable only up to this limit. The diminution in the intensity of the continuous spectrum as a whole is well demonstrated by the order of magnitude of the times of exposure required for obtaining the spectra in the case of Hydrogen and in case where mercury is also present. In the former, exposures of the order of one hour sufficed (*cf.* I), whereas four to five hours were required for obtaining spectra of the same intensity in the latter case. It has been mentioned already that the atomic spectrum is expected to be relatively enhanced with respect to the molecular spectrum on account of the presence of Mercury vapour. There is the possibility, therefore, that the general background between λ3600-5000Å (approximately), in which region the lines of the Balmer series lie, may get accentuated in intensity because of the strong atomic lines. In order to avoid confusing the issues, we shall consider the intensity distribution of the continuous spectrum from about λ3600Å towards the short wavelength side (up to λ2300Å). For the sake of convenience the relative intensity distributions in the various spectra are compared with that obtained in the Geissler tube. Figures. 2, 3, 4 give the micro-photometer curves obtained with excitation by canal rays of energy 2, 3, 4, 6, 8, 10 kV. (*cf.* Pl. 8 and 4). The pressures used in these experiments were of the order of 10^{-2} cms. of Hg and less. The effect of Mercury vapour apparently begins to count only for the higher operating voltages of the order of 4 kV. or more. The variation in the relative intensity distribution curves for the low voltages (*viz.*, 2 and 3 kV.) is insignificant and the general shape of the curves approximates to that obtained in the Geissler tube. It has been shown in (I) that the intensity distribution curves in the case of the Geissler tube spectrum and the canal ray spectra are sensibly the same except for a small variation in the intensity of the region in the neighbourhood of λ2500Å. Spectra obtained with canal rays of energy of 4 kV. or more in the presence of Mercury vapour show a markedly more rapid fall in the intensity towards the short wavelength region. This departure from the usual distribution does not, however, show any regular dependence on the energy of the canal rays. Thus with 6 kV. energy canal rays the fall is more rapid than with 4 kV. energy. It is more rapid with 10 kV. than with 8 kV.; there is no difference on the other hand in the course of the intensity distribution obtained with canal rays of energy 4 and 8 kV.

In general, therefore, we can say that the presence of Mercury vapour affects appreciably the relative intensity distribution of the continuous spectrum, the effect being more pronounced at the higher voltages than at the lower ones. This has the net effect of bringing about an apparent variation in the intensity distribution of the continuum with the energy of the exciting canal rays. That there is no such effect has been shown in (I). It must be pointed out that the Mercury vapour being present only in traces in the discharge tube, it was not possible to control the quantity of the vapour present and thus maintain it constant. That it

Fig 1. (Pl. 4

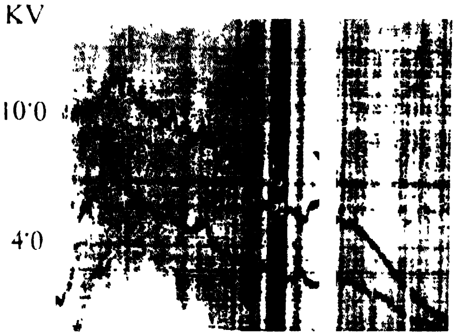

Fig. 2 (Pl. 4)

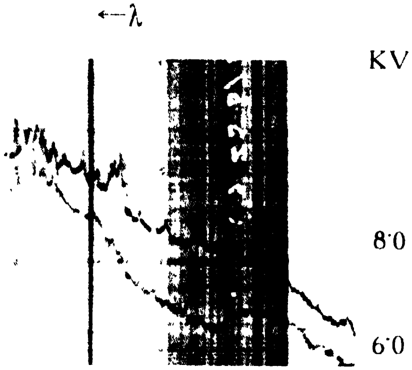

Fig. 3. (Pl 4)

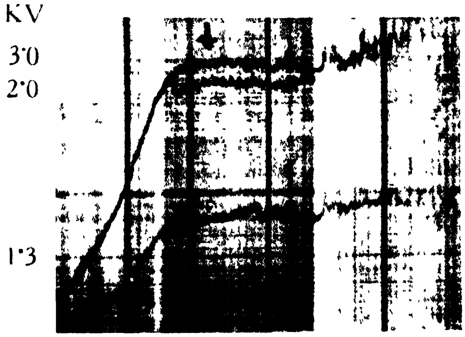

Fig. 4. (Pl. 8)

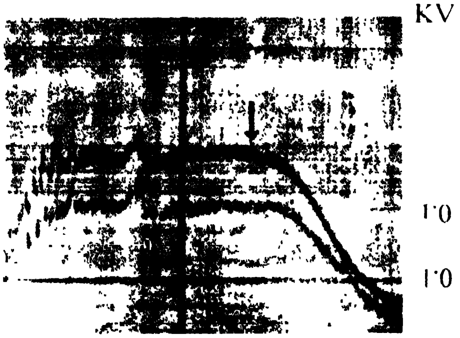

Fig. 5. (Pl. 6)

Figs. 1-4 Give the Spectra excited by Canal Rays of different energies.

Fig. 5 Gives the spectrum obtained in the Geissler tube.

The arrow in the figures indicates the position of the mercury line λ 2537Å

was present in appreciable amounts throughout the course of the experiment is shown by the continued presence of the $\lambda 2537$Å line with great intensity. It is likely that the amount of Mercury present in the vapour phase varied from experiment to experiment, for we naturally expect this amount to be relatively more at the lower pressures than at the higher ones.

It appears difficult to suggest a hypothesis for the explanation of the effects observed on account of the extremely large number of possibilities. Mercury in the molecular form, for example, possesses a large number of continua of its own (Finkelnburg[8]). Added to this, we have the possibility of the formation of the HgH molecules and a subsequent emission of its band spectrum (Jazewski[9]). It may be that the effects observed are of the type reported by Smith.[6] The possibility of collisions of second kind has already been pointed out. The experiments reported here make it clear that the presence of Mercury vapour is quite likely to vitiate results obtained on the intensity distribution of the continuum excited by the canal rays. The discrepancies in the results obtained by different workers may, therefore, well be due to such effects.

In the end, I offer my grateful thanks to Dr. S. S. Joshi for giving me the facilities for work and constant encouragement and to Dr. Asundi, with whose guidance the above work was carried out. To Dr. Ishaq, Chairman, Physics Department, Muslim University of Aligarh, I am indebted for facilities for the micro photometer work.

REFERENCES

[1] Winans and Stueckelberg, *Proc. Nat Acad. Sc. Amer.*, **14**, 867 (1928).

[2] Stark, Gorcke and Arndt, *Ann. d. Phys.*, **64**, 81 (1917).

[3] Finkelnburg and Weizel, *Zeits. f. Phys.* **68**, 577 (1931).

[4] Bacher and Goudsmit, " *Atomic Energy states* " *McGraw-Hill* (1932).

[5] H. Sponer, " *Molekulspektren* " *Julius Springer* (1936).

[6] Smith, *Phys. Rev.*, **49**, 345 (1936).

[7] Finkelnburg, " *Kontinuierliche Spektren* " *Eigenschaften und Struktur der Materie, Band XX*, 187 (1938).

[8] Finkelnburg, *ibid.*, 194-207.

[9] Jazewski, *J. de Physique et le Radium*, **9**, 278 (1928).

A NOTE ON THE USE OF BAKING SHELLAC VARNISHES FOR COATING GRAPHITE-ON-GLASS RESISTANCES IN THE LABORATORY

By G. N. BHATTACHARYA

Indian Lac Research Institute

(Received for publication, September 24, 1940)

ABSTRACT. Glyptal lacquer-coated high resistances made of graphite lines on pyrex glass rods have been successfully used in direct current amplifying circuits by a few workers. Similar resistances coated with a number of baking shellac varnishes have been examined by the writer of this note. The effect of keeping these resistances in atmospheres of different humidity has been studied and their values under varying voltages have been determined in order to see if they conform to Ohm's law. It has been found as a result of this investigation that varnishes composed of shellac and linseed oil fatty acids are generally very satisfactory for the purpose of coating these high resistances to protect them from atmospheric moisture.

D.C. Amplifying circuits are now being used for various purposes in communication engineering and other electrical laboratories, such as for the measurement of resistivities of dielectrics, for photo-electric currents, with ionisation chambers etc., but the success of such circuits depends mostly on the reliability of very high resistances of the order of 10^8 to 10^{12} ohms, which are generally used with special vacuum tubes known as electrometer tubes. A form of such a resistance enclosed in a glass tube to protect it from atmospheric moisture has been described by Brewer[1], but perhaps the most convenient form that can be easily made in any laboratory is that described by Curtiss[2]. He has used resistances made of graphite lines on Pyrex glass rods coated with glyptal lacquer. These have been found by Curtiss to give no more ' noise ' than the best commercial resistors in the market, to obey Ohm's law and not to be appreciably affected by changes of temperature or of humidity. He also tried several other kinds of lacquers for this purpose but without success.

Most of the insulating lacquers alter the value of such a resistance when applied to protect it from atmospheric moisture. This is probably not due to

Resistance coated with varnish composed of	Applied voltage	Deflection of galvanometer & calculated resistance					
		Humidity 30%		Humidity 60%		Humidity 90%	
		Defln. in mms.	Resistance in megohms	Defln. in mm.	Resistance in megohms	Defln. in mms.	Resistance in megohms
Shellac, glycerine and linseed oil and baked at 140°C for 3 hours.	2.0	22	337	23	322	25	297
	4.0	45	330	45	330	51	290
	12.2	136	332	138	328	150	301
	24.2	270	332	270	332	310	289
	48.0	540	329	550	323	610	289
Glyptol and baked at 120°C for 2 hours.	2.0	62	120	62	120	70	106
	4.0	120	123	122	121	138	107
	12.2	370	122	360	125	410	110
	24.2	730	123	730	123	830	107
	48.0	1440	123	1420	125	1650	108

From the above table it appears that shellac-linseed oil baking varnishes are generally the least affected by humidity and may therefore be very satisfactorily used for coating such high resistances in the laboratory. Either of the varnishes composed of shellac or methyl ester of aleuritic acid, meleic anhydride and linseed oil fatty acids is particularly suitable for the purpose. The aleuritic acid one is light golden in colour and gives almost a transparent film. For most purposes, however, the other lac varnishes as well as the glyptol varnish which have been shown in the table are also satisfactory.

ACKNOWLEDGMENT

I am indebted to Dr. H. K. Sen, the Director of this Institute for his kind interest in this work and also to Messrs. M. Venugopalan, Y. Sankaranarayanan and T. Bhowmick for kindly supplying me some of the samples of varnishes used in this investigation.

REFERENCES

[1] Brewer, A. K., *Rev. Sci. Inst.*, 1, 325, (1930)
[2] Curtiss, L. F., *Rev. Sci. Inst.*, 4, 679, (1933)
[3] Venugopalan, M. & Sen, H. K., *J. Soc. Chem. Ind.*, 57, 371, (1938)

ON THE DIELECTRIC CONSTANTS OF IONISED GASES AT MEDIUM RADIO-FREQUENCY *

By S. R. KHASTGIR, D.Sc.(Edin), Mem.I.R.E.

AND

C. CHOUDHURY, M.Sc.,

Dacca University

(Received for publication, September 24, 1940)

ABSTRACT. Measurements of the effective dielectric constants of ionized air and helium in the discharge tubes by the double-beat method yielded the following results for medium frequencies (1100 kc./sec. to 375 kc./sec.).

(1) When the frequency of the measuring field was fixed, the effective dielectric constant which was found slightly greater than unity increased proportionately with the increase of the discharge current except when the latter was large.

(2) When the discharge current was fixed, the effective dielectric constant decreased gradually with the increase of the wavelength of the measuring field.

The possibility of a resonance frequency of the ionized medium much higher than the frequency employed in this work has been indicated. Accepting such a resonance frequency it would be possible to explain both sets of results according to the classical dispersion formula.

INTRODUCTION

In the present investigation, measurements of the effective dielectric constants of ionised air and helium were undertaken for a frequency range from about 1100 Kc./sec. to about 375 Kc./sec.

Fräulein Szekely[1] was perhaps the only previous worker who carried out similar measurements on medium radio-frequencies. The method she followed was a resonance method with the experimental condenser inside the discharge tube. The effect of the conductivity and also that of the positive ionic sheath were likely to bring in complications in the correct evaluation of the effective dielectric constant of the ionized gas in these experiments. She obtained the values of the dielectric constants of ionized air *always* greater than unity.

In the present investigation external condenser plates were used touching the outer surface of the discharge tube. The discharge was a D. C. discharge with

---

* Communicated by the Indian Physical Society.

[1] Szekely, Ann. der Physik, 5, 3, p. 112 (1929).

the help of an induction coil. The conductivity correction was not therefore necessary. As before two sets of experiments were performed :

1. Variation of the effective dielectric constant of the ionized air and helium for various values of the discharge current for a definite frequency of the measuring field, and
2. Variation of the effective dielectric constant of the two ionized gases for various frequencies when the discharge current was kept fixed.

EXPERIMENTAL PROCEDURE AND DETAILS

The experimental condenser was made up of two cylindrical brass pieces placed round the outer surface of the discharge tube. This external condenser of capacity C_G was connected in parallel with the tuning condenser of capacity C of a suitable Hartley oscillator. The change in the effective capacity of the experimental condenser round the discharge tube when a discharge was passed through the latter was balanced by changing the capacity of an accurately calibrated small variable air condenser of capacity C_A in parallel with C_G and C, so that the total capacity ($C_G + C + C_A$) remained constant. The procedure was as follows : The high-frequency signal from the oscillator was received by an oscillator-detector valve-circuit which was exactly similar to the oscillator circuit. When the detector circuit was nearly in tune with the oscillator, the familar heterodyne whistle was heard in the telephones placed in the anode circuit of the detector. The audio-frequency voltage developed across the telephones was then amplified by a three-valve amplifier and fed into a loudspeaker which gave a loud musical note. On introducing into the same loudspeaker an audio-frequency current from an audio-oscillator capable of producing an intense note of fixed frequency, beats were heard by suitably adjusting the heterodyne frequency. A variable resistance was placed in series with the secondary coil of the audio-oscillator to match the intensity of the heterodyne whistle with that of the audio-frequency note. Adjustments of the variable vernier condenser C_A in the oscillator to produce no beats were then made successively ; *first* when there was no discharge through the discharge tube and *next* when a discharge was passed. In this way the change in the effective capacity of the experimental condenser on ionizing the gas inside it was accurately determined. In the first set of experiments where the frequency of the measuring field was kept fixed, the values of this change of capacity ΔC were determined for various values of the current through the discharge tube and in the second set where the discharge current was maintained at the same value, the values of ΔC were obtained for different frequencies of the measuring field. The actual values of the effective dielectric constant of the ionized gases could, however, be approximately calculated from a knowledge of the ratio of the observed change of the effective capacity of the experimental condenser to the actual capacity-value of the same. The diagram of the experimental arrangement is shown in figure 1.

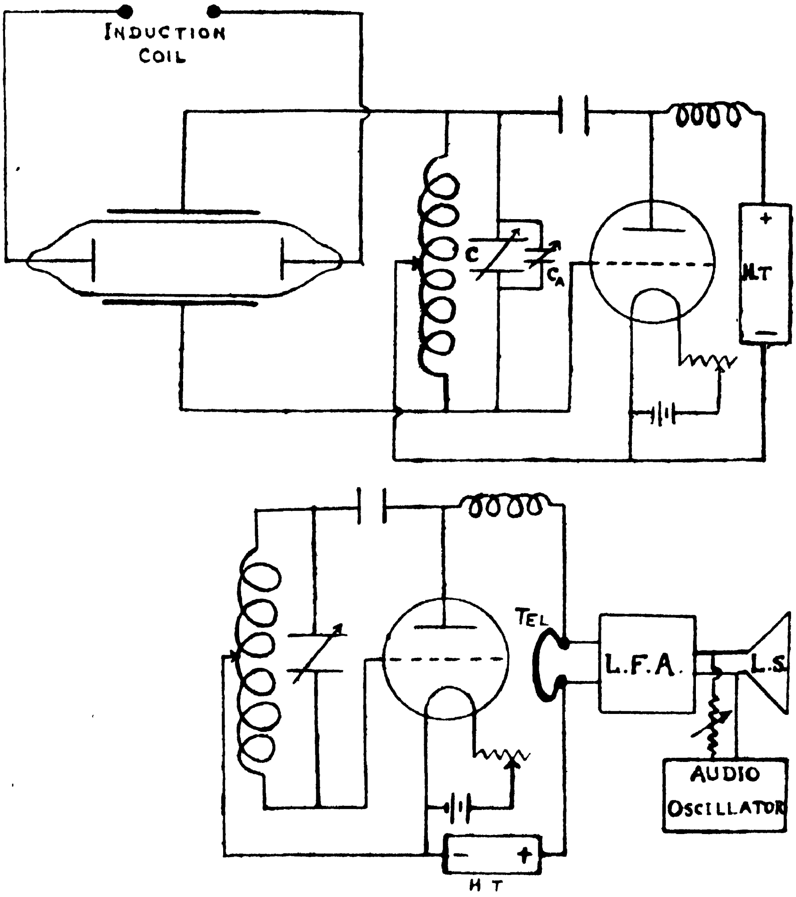

FIGURE 1

The tuning condenser C of the Hartley Oscillator and the vernier air condenser C_A were properly shielded.

TABLE I

Air discharge tube

Frequency 428.6 kc/sec. ($\lambda = 700$m) Capacity of the experimental condenser : 3·4$\mu\mu f$.

Discharge current (m.a.)	Increase in capacity ($\mu\mu f$)	Dielectric constant ϵ
.25	.05	1.015
.5	.10	1.029
.8	.10	1.047
1.2	.23	1.068
1.5	.26	1.076
1.8	.30	1.082

TABLE II

Helium discharge tube

Frequency 419.6 kc./sec. (λ=715m.)

Capacity of the experimental condenser: 8·5 $\mu\mu f$.

Discharge current (m.a.)	Increase in capacity ($\mu\mu f$)	Dielectric constant ϵ
.25	.053	1.0062
.75	.16	1.019
.8	.21	1.025
1.1	.27	1.032
1.4	.32	1.038

The latter was constructed out of a spherometer. A circular disc formed the fixed plate of this condenser and a similar circular disc placed vertically above and parallel to the former could be pushed by the central leg (which was cut short), when the graduated spherometer disc was given a right-handed turn. On giving a left-handed turn to the spherometer disc, the central leg would move up and the upper circular disc of the vernier condenser could be pulled up by a steel spring suitably fixed. Earthed guard-rings made up of thin brass foils were inserted round the two parallel discs. With two complete revolutions of the spherometer disc, the upper plate would be displaced vertically through 1 mm. and the capacity of the condenser was found to change by 10 $\mu\mu f$. The spherometer disc had a graduated scale with 50 big divisions so that a turn through one such division would mean a capacity-change of 0.1 $\mu\mu f$. Each big division was further divided into 5 smaller divisions. A turn through one small division would cause a change of 0.02 $\mu\mu f$ only.

EXPERIMENTAL RESULTS

(a) *Effective dielectric constant of the ionized gases for different discharge currents for a fixed frequency of the measuring field.*

The results of two typical sets of experiments, one with ionized air and the other with ionized helium are given in tables I & II. They are graphically shown in figure 2. The effective dielectric constant in either case was found slightly greater than unity, *i.e.*, there was an increase in the effective capacity of the experimental condenser on ionizing the gas inside. In the case of helium the discharge current ranged from .25 m.a. to 1.4 m.a. and there was an almost linear relation between the increase of effective capacity and the current passing through the discharge tube. In the case of air, the maximum discharge current was 1·8 m.a. and the increase in the effective capacity of the experimental condenser was found directly proportional to the discharge current up to about

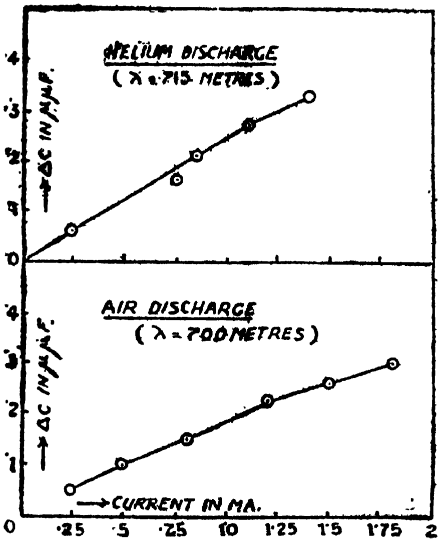

FIGURE 2

TABLE III

Air discharge tube

Capacity of the experimental condenser : 3·4 $\mu\mu f$

Discharge current : .2 m.a.			Discharge current : 1·15 m.a.		
Wavelength (metres)	Increase in capacity ($\mu\mu f$)	ϵ	Wavelength (metres)	Increase in capacity ($\mu\mu.f$)	ϵ
307	·10	1·0294	265	·43	1·126
420	·08	1·0235	310	·41	1·121
480	·07	1·0206	420	·37	1·109
592	·06	1·0177	505	·34	1·100
723	·04	1·0118	645	·30	1·088
825	·03	1·0088	720	·28	1·082
			827	·25	1·074

TABLE IV

Helium discharge tube

Capacity of the experimental condenser : 8·5 μμf

Discharge current : ·2 m.a.		Discharge current : ·75 m.a.	
Wavelength. (metres)	Increase in capacity. (μμf)	Wavelength. (metres)	Increase in capacity. (μμf)
265	.14	315	·40
337	.12	420	·31
433	.10	510	·26
501	.09	623	·22
623	.07	713	·10
781	.05	810	·09
827	.03		

1·25 m.a. beyond which ΔC was found to increase with the discharge current at a slower rate. We can therefore conclude that the effective dielectric constant of ionized air or helium in our experiments increased linearly with the discharge current except when the latter was large.

The wavelength of the measuring field in these experiments was about 700 metres (frequency : 426 kc.). On calculating the value of the effective dielectric constant it was found that the dielectric constant of ionized air varied from 1.015 to 1.082 as the discharge current was increased from .25 m.a. to 1.8 m.a. The calculated value of the effective dielectric constant of ionized helium was found to vary from 1.006 to 1.038 over a range of discharge current from .25 m.a. to 1.4 m.a.

(b) *Effective dielectric constants of the ionized gases for different frequencies of the measuring field for a definite ionization value*

The experimental results with air discharge tube for two different discharge currents are given in table III. They are illustrated in fig. 3 where the increase of capacity ΔC is plotted against wavelength of the measuring field for each set of observations. Similar results with the helium discharge tube for two different discharge currents are given in table IV. They are illustrated in figure 4.

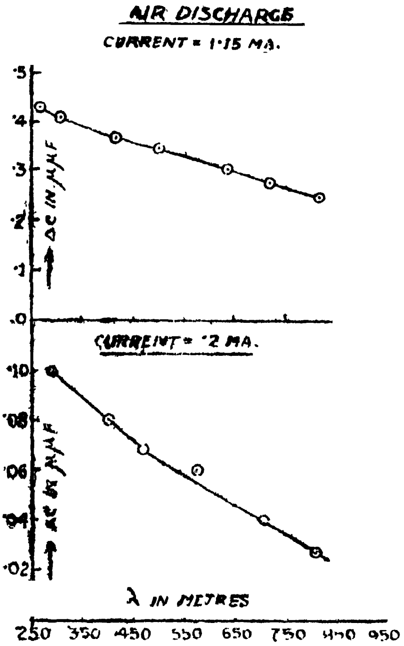

FIGURE 3

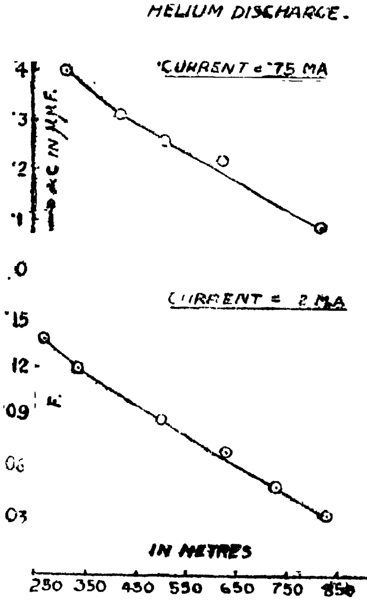

FIGURE 4

For both the ionized gases, the value of ΔC was found to decrease slowly and gradually with the increase of wavelength of the measuring field. This meant that the effective dielectric constant of the ionized gas (air or helium) also diminished slowly and gradually as the wavelength was increased.

It is significant that the effective dielectric constant of the ionized air and helium was *always* found to be slightly greater than unity for medium radio-frequencies. Test experiments were, however, performed with different air discharge tubes having different sizes of electrodes and in all cases the effective dielectric constant of the ionized air was found to be slightly greater than unity. Experiments with the same air discharge tube were also carried out in the ultra-high frequency range, keeping the discharge current at a small steady value and varying the wavelength of the measuring field over some range. For wavelengths smaller than about 9 metres, the effective dielectric constant of the ionized air was found to be definitely less than unity.

DISCUSSION OF THE EXPERIMENTAL RESULTS

It is considered unlikely that within the range of the discharge currents employed in this work, the effect of the positive ionic sheath on the inner surface of the discharge tube could be the explanation of the value of the dielectric constant being greater than unity in the case of medium radio frequencies. For the same discharge current and tube pressure the thickness of the ionic sheath would remain the same and if the value of the effective dielectric constant was found greater than unity for medium radio frequency, the result would be similar for ultra-high frequency also. For very small discharge currents, when the sheath effect would be negligible, it was, however, found that the value of the dielectric constant of the ionized air was definitely less than unity in the ultra-high frequency range, whereas for the same discharge current, under exactly similar conditions, the effective dielectric constant was found to be slightly greater than unity. This suggests the existence of a resonance frequency for the ionized medium much higher than the medium radio-frequencies employed in these experiments. Investigation to locate the resonance frequency is in progress.

It may be said that Gutton's quasi-elastic resonance and Tonk and Langmuir's plasma resonance would be both possible in the medium inside a discharge tube. On either view, the resonance frequency would be very much higher than the medium radio-frequencies we employed in this work. Accepting such a resonance frequency and neglecting the Lorentz term, the complex dielectric constant of the ionized gas would be given by

$$\epsilon' = 1 + \frac{4\pi N e^2/m}{(w_0^2 - w^2) - jwg}$$

where w = angular frequency of the measuring field
w_0 = resonance angular frequency higher than w
g = frictional constant = $m\nu$
ν = collision frequency
N = electron concentration
e = charge on an electron
m = mass of an electron.

Here in this formula w_0 is related to N. If the resonance is the quasi-elastic one of Gutton,

$$w_0^2 = \mathrm{A.N}_{4}^{3},$$

whereas for the plasma-electronic resonance of Tonks and Langmuir

$$w_0^2 = \mathrm{B.N.}^{*}$$

where A and B are constants.

Hence it can be seen from the expression for the dielectric constant that if the frequency w is fixed and the electron concentration is increased by increasing the discharge current, the dielectric constant would increase proportionately except for the higher currents. With higher currents however, N would be greater and consequently the resonance frequency w_0 would be higher. The dielectric constant ϵ would therefore assume smaller values than what the linear relationship between ϵ and N would demand. This is exactly what was observed.

---

* *i.e.*, N. $\lambda_0^2 = 1{\cdot}1 \times 10^{13}$ where λ_0 is the resonance wavelength.

Coming to the variation of the dielectric constant of the ionized gases with the frequency of the measuring field when the discharge current was kept constant, the experimental results would be explicable if a resonance frequency, much higher than the measuring frequency, is supposed to exist. According to the expression for the dielectric constant it is evident that the dielectric constant of either ionized gas which is greater than unity would slowly diminish as the frequency w is diminished or as the wavelength λ is increased.

ACKNOWLEDGEMENTS

Our sincere thanks are due to Prof. S. N. Bose, Head of the Physics Department, Dacca University, for all the facilities given during the progress of the work.

PHYSICS DEPARTMENT,
DACCA UNIVERSITY.

8

THERMODYNAMIC FUNCTIONS FOR TWO DIMENSIONAL QUANTUM STATISTICS*

By B. N. SINGH

(University of Delhi)

(*Received for publication, July 5, 1940*)

In recent years the Fermi-Dirac statistics applied to the case of electron gas has found numerous applications. The case in which the electron gas is restricted to two dimensions is also of interest in certain special cases. In the first part of the present paper the various thermodynamical functions for a ν-dimensional space for a gaseous assembly obeying Fermi-Dirac statistics or Bose-Einstein statistics have been evaluated in the usual familiar way,[1] and the values of these functions for a two dimensional space have been deduced as a special case. An application of the results has been made in a following paper[2] in deducing the magnetic susceptibility of a free electron gas when the electrons are confined to a plane.

1. We first determine the distribution laws for a ν-dimensional space. The wave function for an allowed state of a free particle in a space of 'volume' L^{ν} is

$$\psi = C \sin \frac{l_1 \pi x_1}{L} \sin \frac{l_2 \pi x_2}{L} \cdots\cdots\cdots \sin \frac{l_\nu \pi x_\nu}{L},$$

$$= C \prod_{\alpha=1}^{\alpha=\nu} \sin \frac{l_\alpha \pi x_\alpha}{L}, \qquad \ldots \quad (1)$$

where $$C = \left(\frac{2}{L}\right)^{\frac{\nu}{2}}.$$

The wavelength λ associated with a normal mode of vibration is given by

$$\frac{1}{\lambda} = \frac{l_\alpha}{2L},$$

and, therefore, $$p^2 = \Sigma \frac{h^2}{\lambda^2} = \frac{h^2}{4L^2} \Sigma\, l_\alpha^2,$$

where p is the momentum.

---

* Communicated by the Indian Physical Society

Now, taking account of relativistic mechanics,

since $$\frac{m\beta c}{\sqrt{1-\beta^2}}, \quad \text{and} \quad \epsilon = mc^2\left(\frac{1}{\sqrt{1-\beta^2}}-1\right),$$

we have $$\epsilon_0\Sigma(l_\alpha)^2 = \epsilon\left(\frac{\epsilon}{2mc^2}+1\right),$$

where $$\epsilon_0 = \frac{h^2}{8mL^2}.$$

The number of states $C_\nu(\epsilon)$ for which the energy is less than ϵ is equal to $2^{-\nu}$ times the volume of a sphere of radius $\{\Sigma(l_\alpha)^2\}^{\frac{1}{2}}$ and is given by

$$C_\nu(\epsilon) = \frac{\pi^{\frac{\nu}{2}}2^{-\nu}}{\Gamma\left(\frac{\nu}{2}+1\right)}\left\{\frac{\epsilon}{\epsilon_0}\left(\frac{\epsilon}{2mc^2}+1\right)\right\}^{\frac{\nu}{2}}. \qquad \dots (2)$$

Therefore $a_\nu(\epsilon)\,d\epsilon$, the number of states of energy lying between ϵ and $\epsilon+d\epsilon$, is given by

$$a_\nu(\epsilon)d\epsilon = gC'_\nu(\epsilon),$$

$$= 2g\left(\frac{\pi L^2}{h^2c^2}\right)^{\frac{\nu}{2}}\frac{1}{\Gamma\left(\frac{\nu}{2}\right)}(\epsilon+mc^2)(\epsilon^2+2mc^2\epsilon)^{\frac{\nu}{2}-1}, \qquad \dots (3)$$

g being the weight factor.

In the completely non-relativistic case $\left(\frac{mc^2}{kT}>>1\right)$, this reduces to

$$a_\nu(\epsilon)d\epsilon = \frac{g}{\Gamma\left(\frac{\nu}{2}\right)}\left(\frac{2\pi mL^2}{h^2}\right)^{\frac{\nu}{2}}\epsilon^{\frac{\nu}{2}-1}d\epsilon, \qquad \dots (4)$$

and in the completely relativistic case $\left(\frac{mc^2}{kT}<<1\right)$, we have

$$a_\nu(\epsilon)d\epsilon = \frac{2g}{\Gamma\left(\frac{\nu}{2}\right)}\left(\frac{\pi L^2}{h^2c^2}\right)^{\frac{\nu}{2}}\epsilon^{\nu-1}d\epsilon. \qquad \dots (5)$$

Equations (4) and (5) for the two limiting cases can be written as

$$a_\nu(\epsilon)d\epsilon = D\epsilon^{s-1}d\epsilon, \qquad \dots (6)$$

where, in the non-relativistic case,

$$s=\frac{\nu}{2}, \qquad D=\frac{g}{\Gamma(s)}\left(\frac{2\pi m L^2}{h^2}\right)^s, \qquad \dots (7)$$

and, in the relativistic case,

$$s=\nu, \qquad D=\frac{2g}{\Gamma\left(\frac{s}{2}\right)}\left(\frac{\pi L^2}{h^2c^2}\right)^{s/2}. \qquad \dots (8)$$

It is to be noted that for the three dimensional case s takes the values 3/2 and 3 in the non-relativistic and relativistic cases respectively. For the two dimensional case its values are 1 in the non-relativistic case and 2 in the relativistic case.

The distribution function $f(\epsilon)=\dfrac{1}{\frac{1}{A}e^{\epsilon/kT}+\beta}$ is not affected by the number of dimensions. $\beta=+1$ for Fermi-Dirac statistics and $\beta=-1$ for Bose-Einstein statistics. The number of particles, therefore, possessing energy in the range ϵ to $\epsilon+d\epsilon$ is given by

$$N(\epsilon)d\epsilon=\frac{D\epsilon^{s-1}}{\frac{1}{A}e^{\epsilon/kT}+\beta}\,d\epsilon. \qquad \dots (9)$$

2. We shall first consider the case of non-degeneracy.

In this case $A<<1$ and the distribution function is easily expanded as a series.

The total number N of the particles in the assembly is given by

$$N=\int_0^\infty N(\epsilon)d\epsilon=D(kT)^s\int_0^\infty\frac{u^{s-1}}{\frac{e^u}{A}+\beta}\,du \qquad \dots (10)$$

$$=D(kT)^sA\Gamma(s)\left\{1-\frac{\beta A}{2^s}+\frac{\beta^2A^2}{3^s}-\dots\right\}. \qquad \dots (11)$$

And, therefore, $$A_1\equiv\frac{N}{D(kT)^s\Gamma(s)}=\Sigma\frac{A^n}{n^s}(-\beta)^{n-1}. \qquad \dots (12)$$

The total energy of the assembly E is given by

$$E=\int_0^\infty\epsilon.N(\epsilon)d\epsilon=D(kT)^{s+1}\int_0^\infty\frac{u^s}{\frac{e^u}{A}+\beta}\,du, \qquad \dots (13)$$

$$=sNkT[1+a\beta A_1-b\beta^2A_1^2+c\beta^3A_1^3+\dots], \qquad \dots (14)$$

where $$a=\frac{1}{2^{s+1}}, \qquad b=\left(\frac{2}{3^{s+1}}-\frac{1}{4^s}\right), \qquad c=\frac{3}{4^{s+1}}+\frac{5}{2.8^s}-\frac{3}{6^s}.$$

From (12) and (14), we easily obtain, noting that $E = spV$, the general formulae for the non-degenerate case

$$\frac{G}{NkT} = \log A = \log A_1 + 2a\beta A_1 - \tfrac{3}{2}b\beta^2 A_1^2 + \tfrac{4}{3}c\beta^3 A_1^3 \ldots \qquad \ldots (15)$$

$$\frac{F}{NkT} = \frac{G - pV}{NkT} = \log A_1 - 1 + a\beta A_1 - \tfrac{1}{2}b\beta^2 A_1^2 + \tfrac{1}{3}c\beta^3 A_1^3 \ldots\ldots\ldots, \qquad \ldots (16)$$

and
$$\frac{S}{Nk} = \frac{E - F}{NkT} = (s+1) - \log A_1 + (s-1)a\beta A_1 - \frac{(2s-1)}{2}b\beta^2 A_1^2$$
$$+ \frac{3s-1}{3}c\beta^3 A_1^3 \ldots\ldots\ldots, \qquad \ldots (17)$$

where G, F and S are respectively the Thermodynamic Potential, Free Energy and Entropy of the assembly.

As a special case we write down the values of the above functions in the non-relativistic two-dimensional case.

We have
$$s = \frac{\nu}{2} = 1, \qquad D = \frac{g2\pi m L^2}{h^2},$$

and
$$A_1 = \frac{N}{DkT} = \frac{nh^2}{g2\pi m kT}, \qquad \ldots (18)$$

where n is the surface density. Also $a = \frac{1}{4}$, $b = \frac{-1}{36}$ and $c = 0$.

$$\frac{E}{NkT} = 1 + \beta\frac{A_1}{4} + \frac{1}{36}\beta^2 A_1^2 + \ldots\ldots\ldots, \qquad \ldots (19)$$

$$\frac{G}{NkT} = \log A_1 + \beta\frac{A_1}{2} + \frac{\beta^2 A_1^2}{24} + \ldots\ldots\ldots, \qquad \ldots (20)$$

$$\frac{F}{NkT} = \log A_1 - 1 + \frac{\beta A_1}{4} + \frac{\beta^2 A_1^2}{72} + \ldots\ldots\ldots, \qquad \ldots (21)$$

and
$$\frac{S}{Nk} = 2 - \log A_1 + \frac{\beta^2 A_1^2}{72} + \ldots\ldots\ldots \qquad \ldots (22)$$

We shall now take up the degenerate case.

In degeneracy the Fermi-Dirac and Bose-Einstein cases are considered separately. In Bose-Einstein statistics $A = 1$, $\beta = -1$ and equation (13), therefore, easily gives

$$E = \Gamma(s+1)D(kT)^{s+1}\zeta(s+1), \qquad \ldots (23)$$

$$G = 0, \qquad \ldots (24)$$

$$F = -\frac{E}{S} = -\Gamma(s)D(kT)^{s+1}\zeta(s+1), \qquad \ldots (25)$$

$$S = \frac{s+1}{s} \cdot \frac{E}{T} = (s+1)\Gamma(s)D(kT)^{s}k\,\zeta(s+1), \qquad \dots \quad (26)$$

$$C_L = \left(\frac{\partial E}{\partial T}\right)_L = (s+1)\frac{E}{T}, \qquad \dots \quad (27)$$

where C_L is the specific heat when the size of the space ("volume") occupied by the assembly remained fixed.

In the two-dimensional non-relativistic case these reduce to

$$E = \frac{g\,2\pi m L^2}{h^2}(kT)^2\zeta(2), \qquad \dots \quad (28)$$

$$G = 0, \qquad \dots \quad (29)$$

$$F = -E, \qquad \dots \quad (30)$$

$$S = \frac{2E}{T}, \qquad \dots \quad (31)$$

$$C_\sigma = \frac{2E}{T}, \qquad \dots \quad (32)$$

where C_σ denotes specific heat at constant area.

The degenerate case of the Fermi-Dirac statistics is characterised by $A >> 1$ and $\beta = +1$. The integrations are carried out by using Sommerfeld's formula according to which, for large A,

$$\int_0^\infty \frac{u^s\,du}{\frac{e^u}{A}+1} = \frac{u_0^{s+1}}{s+1}\left\{1 + \frac{\pi^2 s(s+1)}{6\,u_0^2} + \frac{7\pi^4(s+1)s(s-1)(s-2)}{360\,u_0^4}\dots\right. \qquad (33)$$

where $u_0 = \log A$. Equation (10) yields

$$N = D(kT)^s\frac{u_0^s}{s}\left\{1 + \frac{\pi^2(s-1)s}{6\,u_0^2} + \frac{7\pi^4}{360}\cdot\frac{s(s-1)(s-2)(s-3)}{u_0^4}\dots\right\}. \qquad \dots \quad (34)$$

And, defining A_1 by relation (12), we have

$u_0 = \log A =$

$$\{\Gamma(s+1)A_1\}^{1/s}\left\{1 - \frac{\pi^2(s-1)}{6\{\Gamma(s+1)A_1\}^{2/s}} - \frac{\pi^4}{720}\cdot\frac{(s-1)(4s^2-30s+54)}{\{\Gamma(s+1)A_1\}^{4/s}}\dots\right\}\dots \qquad (35)$$

Similarly, integrating equation (13) for large A, we have

$$E = \frac{s}{s+1}\,NkT\{\Gamma(s+1)A_1\}^{1/s}\left[1 + \frac{\pi^2(s+1)}{6\{\Gamma(s+1)A_1\}^{2/s}} - \dots\dots\dots\right], \dots \qquad (36)$$

from which we easily obtain

$$\frac{G}{NkT} = \{\Gamma(s+1)A_1\}^{1/s}\left\{1 - \frac{\pi^2}{6}\,\frac{(s-1)}{\{\Gamma(s+1)A_1\}^{2/s}}\dots\dots\dots\right\}, \qquad \dots \quad (37)$$

$$\frac{\mathrm{F}}{\mathrm{N}k\mathrm{T}}=\frac{s}{s+1}\{\Gamma(s+1)\mathrm{A}_1\}^{1/s}\left\{1-\frac{\pi^2}{6}\,\frac{s+1}{\{\Gamma(s+1)\mathrm{A}_1\}^{2/s}}\,\ldots\ldots\ldots\right\}, \tag{38}$$

$$\frac{\mathrm{S}}{\mathrm{N}k}=\frac{s}{3}\,\frac{\pi^2}{\{\Gamma(s+1)\mathrm{A}_1\}^{1/s}}\,, \quad \ldots \tag{39}$$

$$\mathrm{C}_{\mathrm{L}}=\frac{s}{3}\,\frac{\mathrm{N}k\pi^2}{\{\Gamma(s+1)\mathrm{A}_1\}^{1/s}}\,. \tag{40}$$

In the two dimensional case $s=1$ and the values obtained for the various thermodynamic functions are entered in Table I, where for the sake of comparison results for the three dimensional case are also shown.

My thanks are due to Dr. D. S. Kothari for his help and interest in this work.

TABLE I

	Two dimensional	Three dimensional
log A	(A_1+1)*	$\left(\frac{3\pi^{\frac{1}{2}}}{4}\right)^{\frac{2}{3}}\mathrm{A}_1^{\frac{2}{3}}\left\{1-\frac{\pi^{\frac{4}{3}}\,2^{\frac{2}{3}}}{3^{\frac{7}{3}}\,\mathrm{A}_1^{\frac{4}{3}}}\ldots\right\}$
$\frac{\mathrm{E}}{\mathrm{N}k\mathrm{T}}$	$\frac{\mathrm{A}_1}{2}\left\{1+\frac{\pi^2}{3\mathrm{A}_1^2}\ldots\right\}$	$\frac{3}{5}\left(\frac{3\pi^{\frac{1}{2}}}{4}\right)^{\frac{2}{3}}\mathrm{A}_1^{\frac{2}{3}}\left\{1+\frac{5\pi^{\frac{4}{3}}\,2^{\frac{2}{3}}}{3^{\frac{7}{3}}\,\mathrm{A}_1^{\frac{4}{3}}}\ldots\right\}$
$\frac{\mathrm{G}}{\mathrm{N}k\mathrm{T}}$	A_1+1	$\left(\frac{3\pi^{\frac{1}{2}}}{4}\right)^{\frac{2}{3}}\mathrm{A}_1^{\frac{2}{3}}\left\{1-\frac{\pi^{\frac{4}{3}}\,2^{\frac{2}{3}}}{3^{\frac{7}{3}}\,\mathrm{A}_1^{\frac{4}{3}}}\ldots\right\}$
$\frac{\mathrm{F}}{\mathrm{N}k\mathrm{T}}$	$\frac{\mathrm{A}_1}{2}\left\{1-\frac{\pi_2}{3\mathrm{A}_1^2}\ldots\right\}$	$\frac{3}{5}\left(\frac{3\pi^{\frac{1}{2}}}{4}\right)^{\frac{2}{3}}\mathrm{A}_1^{\frac{2}{3}}\left\{1-\frac{5\pi^{\frac{4}{3}}\,2^{\frac{2}{3}}}{3^{\frac{7}{3}}\,\mathrm{A}_1^{\frac{4}{3}}}\ldots\right\}$
$\frac{\mathrm{S}}{\mathrm{N}k}$	$\frac{1}{3}\,\frac{\pi^2}{\mathrm{A}_1}=\frac{\mathrm{C}_\sigma}{\mathrm{N}k}$	$\frac{\pi^2 mk\mathrm{T}}{h^2}\left(\frac{4\pi g}{3n}\right)^{\frac{2}{3}}=\frac{\mathrm{C_v}}{\mathrm{N}k}$

---

* In the case of two dimensions the equation can be integrated exactly and log A comes out equal to A_1+1. It may be noted that the series in Sommerfeld's integration formula for the degenerate case are correct to an order of $1/\mathrm{A}$.

REFERENCES

[1] Fowler & Guggenheim. "Statistical Thermodynamics," p. 239.

[2] "Magnetic Susceptibility of two dimensional electron gas."

THE MOTION OF GASES IN THE SUN'S ATMOSPHERE

PART III. ON THE STRATIFICATION OF THE SOLAR ENVELOPE

By A. K. DAS

(*Received for publication, November 18, 1940*)

ABSTRACT. In the introductory part of the paper the relative merits of existing theories of the solar chromosphere and their inadequacy to explain some of the salient facts of observation are discussed and the necessity for analysing the phenomena of the solar envelope from a different angle is emphasized. The dynamics of the motion of gases in the sun's atmosphere developed in an earlier paper is then used to evolve a mode of formation and maintenance of the different layers of the solar envelope. It is shown that this new process admits of quantitative treatment and yields heights of the reversing layer, the chromosphere and the quiescent prominences in good agreement with observation. The fact that all gases reach practically the same height in prominences, the increase of rotation speed with altitude in prominences, the fibrous structure of the chromosphere and several other facts of observation follow naturally from this process. The picture is however admittedly incomplete, but its success so far indicates that the dynamical principle on which it is based probably plays an important part in the phenomena of the solar envelope.

INTRODUCTION

The idea of selective radiation pressure advanced by Prof. M. N. Saha[1] in 1919 has been widely used for the interpretation of several astrophysical phenomena. Saha himself applied it to explain the occurrence, in the spectra of the early B-classes of stars, of the so-called "stationary" absorption lines H and K; he suggested that under the influence of selective radiation pressure singly ionised atoms of calcium were driven far away from these hot stars and formed a highly attenuated atmosphere which did not take part in the orbital motion of the stars, so that the stationary H and K lines were formed through the blanketing effect of this absorbing atmosphere of calcium vapour on the spectrum of the parent stars. This explanation must at present be regarded as superseded as the result of the long series of most careful observations made by Dr. J. S. Plaskett and his collaborators and in view of Sir A. S. Eddington's masterly theory of interstellar matter, both of which leave no reasonable doubt that diffuse matter containing calcium, sodium and perhaps most of the other elements present on the earth is uniformly distributed in interstellar space with a density of the order of 10^{-25} gm./cm.^{3}, except where local condensations form the diffuse nebulae. Nevertheless the idea of selective radiation pressure holds the field and has found numerous fruitful applications in recent astrophysical theories, notably those of the extended envelopes of Be stars and planetary nebulae. But the researches in which the most extensive and persistent use has been made of selective radiation pressure, in spite of considerable difficulties, are the theories of the solar chromosphere, which are mostly modifications of E. A. Milne's[2] theory of the calcium chromosphere, supported by light pressure. The mechanism of support of the CaII atom in Milne's theory is essentially the same as that indicated by Saha several years earlier, the principal feature of which is that the resonance line of CaII occurs in a part of the spectrum where the Sun radiates strongly, so that CaII atoms are subject to considerable radiation pressure which balances or sometimes even overbalances gravity. Milne has worked out the consequences of this idea at great length for the case of static equilibrium and has successfully accounted for the formation of a chromosphere of ionised calcium, of prominences of ionised calcium and for the occurrence of enormous velocities sometimes observed in eruptive prominences photographed in calcium light. Notwithstanding these successes, Milne's theory is confronted with considerable difficulties which have not so far been eliminated by the numerous attempts at modification and improvement made by S. R. Pike, J. Voltjer, S. Chandrasekhar[3] and others.

One of the principal difficulties of Milne's theory is that it cannot satisfactorily account for the permanent presence of hydrogen and helium in the chromosphere and in the prominences so long as the theory is based on the usual assumption that the intensity in the extreme ultraviolet solar spectrum follows a Planck law corresponding to a temperature of the order of 6000°K. The resonance lines of hydrogen are situated far outside the main region of the solar spectrum and in the case of helium the frequencies of the resonance lines are about twice as large as in the case of hydrogen; in fact, assuming that the Sun radiates as a black body at an effective temperature of 6000° K, the radiation pressure on hydrogen, according to Gurney, works out to be 10^5 times smaller than on singly ionised calcium and on helium 10^{13} times smaller. Yet it is a common fact of observation that all the three elements reach almost the same heights in the chromosphere and in the prominences. Besides, as D. H. Menzel[4] has pointed out, the quiescent type of equilibrium discussed by Milne is non-existent in the chromosphere. The evidence of eclipse observers shows that the chromosphere, like the corona, has a fibrous structure which is very different from that to be expected in an atmosphere approximately in hydrostatic equilibrium of the type tacitly assumed in Milne's theory. A formal possibility of escape from the discrepancy between the chromosphere of Milne's theory and the actual chromosphere has however been provided by Chandrasekhar, who has introduced a periodic space-term in the photospheric flux and has also taken account of the darkening towards the limb. Nevertheless Milne's theory in Chandrasekhar's modified form is far from being able to give a satisfactory explanation of some of the noteworthy features of the chromosphere, particularly the abundance of hydrogen. It seems fairly obvious that any theory which postulates the paramount importance of selective radiation pressure as a means of support for the chromospheric gases will be confronted with the extreme difficulty of explaining the existence of the major constituent, hydrogen, provided that the extreme ultraviolet spectrum of the Sun is taken to be identical with that of a black body at 6000°K. So forcibly has this difficulty impressed itself on some of the most eminent theoretical astrophysicists that S. Rosseland[5] says, "it may be wise to relax a little one's confidence in the significance of light pressure also as regards the distribution of calcium and allied elements in the chromosphere, pending the outcome of the case of hydrogen, helium and other elements with unfavourable resonance lines in the chromosphere and the prominences." He remarks further, "it is surely premature as yet to assert that we know enough about the stars to assert that light pressure is the only agency which can lead to the expulsion of particles. I think, it is fair to say that the evidence of solar observations, taken as a whole, is against this idea, and to such a degree that it fully justifies an attempt at the development of a non committal formal analysis of the solar phenomena from a wider point of view." Rosseland himself has worked out a theory in which an envelope is kept distended through the bombardment by corpuscular rays (electrons) emitted by a star; with the help of this theory he has been able to explain some of the characteristic features of the solar chromosphere and the corona without recourse to the idea of support by radiation pressure. This theory has many obvious advantages, but it has not yet reached the stage of development at which a final judgment can be formed about it. Another theory which does not depend at least explicitly on the idea of selective radiation pressure has been advanced by W. H. McCrea[6] according to whom the chromosphere is supported by "turbulent motion." But McCrea defines this turbulence in a way quite different from what is understood by this term in hydrodynamics and bases his theory on the obviously untenable idea that the particles taking part in the turbulent motion have a Maxwellian velocity of the order of 15 km./sec., but not the temperature corresponding to this velocity. In spite of the unsatisfactory character of McCrea's theory, turbulence ought to play a part in the mechanics of the chromosphere, just as it cannot be denied that selective radiation pressure must have its contribution in the complex phenomena of the solar envelope though perhaps not in the manner postulated by Milne. In the present state of our knowledge, as McCrea has remarked, "we cannot say even whether radiation pressure provides the normal means of chromospheric support, with hydrogen and helium occupying somewhat exceptional positions, or whether, on the other hand, normal chromospheric support comes from quite a different agency with a few gases like CaII and SrII showing additional peculiarities owing to their happening to be subject in addition to radiation pressure." In these circumstances the following attempt at exploring an alternative mode of formation of the solar envelope, somewhat different from those hitherto considered and yet incorporating some of their features, may not be entirely superfluous.

MECHANICS OF EJECTION OF SOLAR GASES

As mentioned in the foregoing section, the evidence of experienced eclipse observers is quite convincingly in favour of the view that the solar envelope is to be looked upon not as a true atmosphere like that of the earth but as composed of innumerable jets of glowing gases emanating from the body of the Sun. The appearance of the chromosphere is that of a tangle of interlacing trajectories which, though not so pronounced, is very similar to that of the corona; also the agglomeration of matter in the solar envelope is very many times more than what is to be expected on any simple hydrostatic theory. The chromosphere, the corona and the prominences would therefore seem to be due to a complex of dynamical phenomena in which there may be no static equilibrium. Indeed it seems most probable that there is no essential difference between the modes of occurrence of these varied phenomena, so that the division of the envelope into several strata may merely represent different degrees of the same underlying process. Whatever may be this underlying mechanism it must possess certain properties which are indicated by facts of observation. For instance, it must be capable of explaining why no essential differences of prominence structure are noted in photographs of prominences taken in not only the strong lines of hydrogen, helium, ionised calcium, ionised strontium and ionised titanium, but also in the lines of faint and medium intensities. This observation imposes an important requirement upon the mechanism of formation of prominences, namely, that the acceleration acting upon the various types of atoms must be at least approximately equal. This condition cannot be satisfied by selective radiation pressure so long as its effect is negligibly small on hydrogen; for it seems scarcely reasonable to expect that the most abundant constituent can be dragged along by the comparatively rare atoms of ionised calcium, etc., which may develop considerable velocities through selective light pressure.

The assumption that the Sun's spectrum in the extreme ultraviolet is exactly the same as that of a black body at 6000°K has however, as Saha[7] has recently argued, no unquestionable experimental or theoretical justification. In fact, Saha has urged that certain features of the night-sky spectrum and of the ionospheric phenomena require that the unobservable part of the ultraviolet spectrum of the Sun should consist of a faint continuous background on which are superposed intense emission lines of H, He^+, Fe^+ and other elements which are represented in the visible range by lines of the subordinate series. Should this hypothesis represent the actual spectrum of the Sun, the difficulties about the support of chromospheric and prominence gases against gravity would be considerably reduced. In fact, K. O. Kiepenheuer[8] has argued that the extreme ultraviolet spectrum of the Sun must be as postulated by Saha and that an exact compensation of gravity in the quiescent prominences and in the chromosphere actually takes place through selective radiation pressure arising out of the absorption of L_a radiation by the H-atoms which are by far the most abundant constituents of the solar envelope. It may be remarked in this connection that the emission lines in the extreme ultraviolet solar spectrum postulated in Saha's hypothesis arise through the mechanism of fluorescence in an attenuated atmosphere as suggested by Rosseland in a famous paper in 1926; if the compensation of gravity in the chromosphere takes place in the way suggested by Kiepenheuer then the mechanism of fluorescence must operate in some layer between the photosphere and the chromosphere. If this intermediate layer is identified with the reversing layer or some transition layer between the photosphere and the reversing layer, then in this layer the conditions of pressure (which according to St. John and Babcock's scheme is at least 10^{-2} atms. and probably much higher) would be unfavourable for the operation of Rosseland's process of fluorescence and consequently the chromosphere could not be effectively supported by selective radiation pressure acting on hydrogen. If, on the other hand, the pressure of the photospheric gases is less than 10^{-1} atm. and the mean presssure in the reversing layer is at most 10^{-4} atm. as concluded by Russell and Stewart, then the reversing layer, the chromosphere and the prominences may all be supported by selective radiation pressure acting on hydrogen, provided the Sun radiates in the way suggested by Saha. This mode of support of the solar envelope is apparently not entirely free from uncertainty. There is however an alternative; the Sun emits continuously high velocity electrons for which there is direct evidence; the bombardment of the atoms of the envelope by these electrons may compensate the effect of gravity on these atoms and may conceivably fulfil also the functions attributed to the absorption of L_a radiation. But, whatever the ultimate explanation may be, several facts of observation show that the effect of gravity on the solar envelope is completely or almost completely neutralised by some mechanism which at present remains obscure.

In almost all the current theories of the chromosphere, the atoms forming the chromosphere are assumed to have originated in the photosphere or just above it. But, if we accept the view that there is probably no essential difference between the processes underlying the formation of a prominence and of the chromosphere, then there is good reason for thinking that the chromospheric gases have their origin below the photosphere and probably in the deep interior of the Sun; for there is little doubt that the quiescent prominences originate in the interior of the Sun. In fact, starting from the generalised postulate that all the material of the solar envelope comes from the interior of the Sun, one can arrive at a way of visualising the complex phenomena of the solar envelope which seems to have distinct advantages over the pictures which form the basis of the current theories of the chromosphere. For this purpose we have first to consider the process through which a mass of material can be ejected from the interior and then the motion of this mass in the space above the photosphere.

According to the current theory of internal constitution, the temperatures within the stars are of the order of a few million degrees and at these temperatures the radiation consists of waves of about the same lengths as X-rays, while matter is broken up mostly into atomic neuclei and electrons. The conditions in the interior of stars are almost those of an ideal thermodynamical enclosure, so that all particles behave like black bodies and the radiation pressure is the same as the light pressure calculated from Maxwell's electromagnetic theory of light. Under equilibrium conditions at any point in the interior gravity is balanced by the combined effect of gas pressure and radiation pressure. This state of static equilibrium can be maintained also in a rotating star so long as the rotation is like that of a rigid body and the rate of generation of energy at every point of the interior depends only upon the density and the temperature in the way required by a well-known theorem due to H. v. Zeipel. But the theories of Jeans,[9] Eddington[10] and Rosseland[11] show that an actual star does not rotate like a rigid body; in fact it is generally accepted that the interior of a star rotates much faster then the surface and that the angular speed of rotation increases rapidly with the depth below the surface. According to Eddington an actual star does not obey v. Zeipel's theorem and this leads to local variations of temperature in the interior. Thus, from theoretical considerations, localised rises of temperature in the interior of the Sun are to be expected, but we can draw this inference also from the fact that on the Sun's surface sudden localised increases of temperature (eruptions) are often observed. It may be mentioned in this connection that Eddington has shown that the non-fulfilment of v. Zeipel's theorem results in the establishment of a system of internal circulatory currents; Rosseland has concluded that there is a possibility of these internal currents being periodically unstable. It seems likely therefore that the periodic variation of solar activity is intimately connected with the periodic instability of the internal currents. But the fairly common occurrence of eruptive phenomena on the Sun's surface may be regarded as indicating that internal disturbances do occur also frequently and quite irregularly.

Let us suppose that in a limited region of the Sun's interior the temperature rises suddenly to a value higher than the normal. This increase of temperature will give rise to increased radiation pressure and a consequent outflow of matter in a radial direction. Since the radiation pressure experienced by the constituent particles is due to the amount of the forward momentum of the radiation absorbed or scattered by the particles the velocity of ejection will depend upon the cross-sections and the weights of the particles as well as on the rate of recombination of the neuclei and electrons. In the absence of precise knowledge about these factors it is not possible to estimate with any certainty the initial velocity of ejection of the particles for a given increase of radiation. But without any calculations it can be safely concluded that at the pressure prevailing in the interior of the Sun there will be frequent collisions among the various types of particles resulting in a re-distribution of the acquired momenta and an eventual movement of the whole mass of matter affected by the disturbance. The velocity with which the mass of gases will move outwards towards the photosphere will of course depend upon the actual increase of radiation pressure and since the radiation pressure is proportional to the fourth power of the temperature it is likely that appreciable velocities will be acquired through comparatively small rises of temperature. The velocity with which a mass of gas thus ejected from the interior will emerge from the photosphere will, because of frictional resistance, be considerably less than the initial velocity which the mass started with. Outside the photosphere the frictional resistance will be small and we may ignore it as a rough approximation. If, in addition, gravity is neutralised by some such process as discussed earlier in this paper, then the magnitude of the velocity with which the mass of gas emerges from the photosphere will remain unchanged during the subsequent motion. Now, since the ejected mass originated in the interior of the Sun where the angular speed of rotation is much faster than at the surface, it will tend to rotate with a higher speed than the surface of the Sun. This brings us precisely to the hypothesis which forms the basis of the considerations set forth in Part I.[12] Recently I have come to know that an almost identical hypothesis was put forward in 1935 by Mr. J. Evershed[13] in order to explain the discrepancy between the angular motion of prominences derived by him from his measures of Doppler shift by the spectrographic method and the rotation speed derived from the times of successive meridian passages of prominences and dark markings.* For comparison I quote Mr. Evershed's hypothesis in his own words. "A possible explanation may now be suggested of the increasing angular speed with height above the photosphere, and of the decreasing speed with decreasing solar activity. This depends upon the fact, I believe fairly well established, that the gases above the photosphere do not form a true atmosphere to the Sun, but consist of innumerable jets of luminous gas projected radiallly outwards from beneath the photospheric level. If the interior of the Sun is rotating faster than the photosphere, and with uniform angular speed in all latitudes, then these jets will tend to retain the velocity of the interior regions, and the deeper the origin of a jet the more closely will its motion conform to the angular speed of the interior. The prominences coming from the deepest layers will give the greatest rotation speeds, and the most uniform angular motion. At times of intense solar activity the great prominences, streaming out at definite points in the photosphere, are probably ejected from greater depths than the smaller prominences seen at times of minimum activity." It is evident from the above quotation that the essential features of Mr. Evershed's hypothesis are the same as those of the hypothesis the dynamical consequences of which were worked out in Part I. From the results obtained in Part I it was evident that many of the major features of prominences and dark markings could be explained both qualitatively and quantitatively on the basis of the dynamical ideas developed there. From the details of the process of ejection of matter from the interior of the Sun just discussed and the equations of motion, as derived in Part I, of a mass of matter thus ejected in the space above the photosphere, it is clear that some of the peculiar features of the solar envelope discussed earlier in this paper bear a similarity to the peculiarities of the dynamical picture here presented.

---

* I am indebted to Messrs. P.R.C. Iyer and B. G. Narayan for drawing my attention to a paper by R. de Lury (Canada, R.A.S., November, 1939), which was received at the Kodaikanal Observatory a few months ago and in which the apparent slight increase of the rotation speed with altitude above the photosphere is explained by the hypothesis that the gases of the envelope originate in the interior of the Sun and retain the high angular speed of rotation of the interior. It is clear from the paper that the hypothesis is originally due to Mr. Evershed.

As shown in Part I, the motion of a mass of gas (ejected from the interior of the Sun) in the space outside the photosphere will be controlled by the dynamical equations—

$$\left.\begin{aligned} &\text{Equatorwards :} && m\frac{d^2x}{dt^2} = X \quad 2m(\omega'-\omega)v\sin\phi + m(\omega'-\omega)^2 R\sin\phi\cos\phi \\ &\text{Westwards :} && m\frac{d^2y}{dt^2} = Y + 2m(\omega'-\omega)(u\sin\phi + w\cos\phi) \\ &\text{Upwards :} && m\frac{d^2z}{dt^2} = Z - 2m(\omega'-\omega)v\cos\phi + m(\omega'-\omega)^2 R\cos^2\phi. \end{aligned}\right\} \qquad (12)$$

In these equations the positive x-axis points towards the equator, the positive y-axis towards the west and the positive z-axis points vertically upwards; u, v, w are the components of the velocity of the moving mass (m); X, Y, Z are components of the external forces including gravity, friction, etc.; R is the radius of the Sun, ϕ the heliographic latitude, ω the angular velocity at the surface of the Sun and ω' the higher angular velocity of the interior retained by the ejected mass of gas. If the mass, as it emerges from the photosphere, has only a velocity V directed vertically upwards and has no external forces acting on it, then the equations (12) can be written

$$\begin{aligned} \frac{}{dt^2} &= -2(\omega'-\omega)v\sin\phi + (\omega'-\omega)^2 R\sin\phi.\cos\phi \\ \frac{d^2y}{dt^2} &= \quad 2(\omega'-\omega)(u\sin\phi + w\cos\phi) \qquad\qquad (12{\cdot}1) \\ \frac{d^2z}{dt^2} &= -2(\omega'-\omega)v\cos\phi. \end{aligned}$$

Now from equations (12·1) it is clear, since at the initial moment $u=v=0$, $w=V$, that the velocity u arises out of the acceleration d^2x/dt^2 which must be of a smaller order than d^2y/dt^2 and d^2z/dt^2 and therefore we may also, as rough approximation, neglect u against w and v. The equations (12·1) may then be simplified into

$$\left.\begin{aligned} &\text{Equatorwards :} \quad \frac{d^2x}{dt^2} = 0 \\ &\text{Westwards :} \quad \frac{d^2y}{dt^2} = 2(\omega' - \omega)w \cos\phi \\ &\text{Upwards :} \quad \frac{d^2z}{dt^2} = -2(\omega' - \omega)v \cos\phi. \end{aligned}\right\} \quad \dots \quad (12{\cdot}2)$$

The second equation shows that if the particles of the gas mass have an *upward velocity*, they are acted upon by a *westward horizontal* acceleration which deflects them from their vertical path. On the other hand, if the particles have a *downward velocity* the path is deflected *eastward*. Similarly the third equation shows that if the particles have an *eastward velocity*, they are acted upon by an *upward deflective acceleration* and, conversely, a *westward velocity* gives rise to a *downward deflective acceleration*. It is to be noted that the deflective accelerations depend only on the velocity, so that if the particles started with the same initial velocity they would maintain their relative positions throughout the subsequent motion and the trajectories of the different particles would be identical. Under the combined action of the equations (12·2), a particle moving vertically upwards at the start will travel in a direction more and more inclined to the west of the vertical until the velocity becomes entirely horizontal and westward ; thereafter the particle will turn progressively downward and finally the velocity will become entirely horizontal but directed eastward so that the particle must rise again. In the idealised condition of absence of friction and other external forces the particle will go on moving indefinitely along a trajectory which will consist of a series of overlapping loops. In reality, however, the motion cannot be frictionless and it will also be complicated by the equatorward acceleration which will not be nil. The actual motion of gases in the solar envelope will be a three-dimensional spiral motion of great complexity and will resemble highly turbulent motion. Nevertheless our idealised equations of motion may be used for drawing general conclusions which should be reliable so far as the orders of magnitude are concerned.

DIVISION OF ENVELOPE INTO LAYERS

A glance at equations (12·2) shows that a particle describing a periodic trajectory in accordance with these equations reaches a maximum height (above the photosphere) which depends on the initial vertical velocity (V) at the moment of emergence from the photosphere and on ϕ and $\omega' - \omega$. For a given value of ϕ and of $\omega' - \omega$ therefore all particles emerging from the photosphere with a given vertical velocity will reach the same height and the natural upper boundary of the trajectories of all such particles will be a spherical surface situated at this height above the photosphere. It seems possible that in this way different boundary layers in the envelope may be formed by particles emerging with different ranges of velocity. In order to test this possibility quantitatively we have to calculate the maximum height reached by particles with a given velocity of emergence (V). Integrating the third of equations (12·2) with the initial conditions $t=0$, $w=\mathrm{V}$ and $v=0$, we have

$$z = -(\omega'-\omega)v\cos\phi\cdot t^2 + \mathrm{V}t.$$

Now, at the highest point of the trajectory $w=0$ and $v=\mathrm{V}$, so that the average value of v during the upward motion is $\frac{1}{2}\mathrm{V}$. Then the maximum height reached by a particle is given by

$$z_{\max} = -\tfrac{1}{2}(\omega'-\omega)\mathrm{V}.\cos\phi.t^2 + \mathrm{V}t. \qquad \ldots \quad (12{\cdot}3)$$

Similarly, integrating the second of equations (12·2) and remembering that the average value of w during the ascent is $\frac{1}{2}\mathrm{V}$, we get

$$y_{\max} = \tfrac{1}{2}(\omega'-\omega)\mathrm{V}.\cos\phi.t^2. \qquad \ldots \quad (12{\cdot}4)$$

Eliminating t from (12·3) with the help of (12·4), we have

$$z_{\max} = -y_{\max} + \sqrt{\frac{2y_{\max}.\mathrm{V}}{(\omega'-\omega)\cos\phi}}\,. \qquad \ldots \quad (12{\cdot}5)$$

Now, as in Part I, we identify $y_{\max}/z_{\max}$ as the tangent of the tilt of the trajectory from the vertical. Then $\tan\delta = y_{\max}/z_{\max}$. In Part II[14] we have shown that the average tilt (δ) of a prominence is of the order of 8° as determined from the measurement of a large number of dark markings. Assuming that this is generally valid, we put $y_{\max} = \tan 8^\circ.\ z_{\max} = 0.14\ z_{\max}$ in (12·5) and obtain

$$z_{\max} = 0{\cdot}216.\frac{\mathrm{V}}{(\omega'-\omega)\cos\phi}\,. \qquad \ldots \quad (12{\cdot}6)$$

If the particles are ejected from all depths of the interior, we may on the average put, as in Part I, for the equator ($\phi=0$) $\omega'=10\omega$, so that $\omega'-\omega = 2{\cdot}63\times 10^{-5}$ and we have

$$z_{\max} = 0{\cdot}082\times 10^{5}.\mathrm{V}. \qquad \ldots \quad (12{\cdot}7)$$

Now, if the reversing layer, the chromosphere and the stable prominences are formed in the purely dynamical way as contemplated in the present paper, then the values of $z_{\max}$ computed from (12·7) by using appropriate values of V derived from observation should agree with the observed heights of the prominences, the chromosphere and the reversing layer so far as the orders of magnitude are concerned. Unfortunately there is considerable uncertainty about the observed values of V. According to St. John[15] the iron lines, belonging to the lowest level, give an upward velocity of about 0.2 km./sec. We may take this as the value of V for the reversing layer. St. John also finds that the calcium vapour, to which the bright emission line K_2 is due, has an ascending motion over the general surface of the sun of 1.97 km./sec. in the mean. We use this as the value of V for the chromosphere. St. John's determinations are from spectrographic measurements of Doppler shifts and therefore possess a much higher degree of accuracy than the values of upward velocity available in the case of the prominences. According to Pettit[16] the commonest velocities observed in the internal motions of a typical stable prominence are 5-10 km./sec. We therefore take 7.5 km./sec. as the value of V in an average prominence of the stable type. Using these values of V we obtain from (12·7) the following values for the heights of the tops of the different layers above the photosphere :

Reversing Layer	...	1640 km.
Chromosphere	...	16150 km.
Average Prominence	...	61300 km.

It is to be noted in this connection that according to observational practice the height of a prominence is reckoned from a level about $10''$ above the photosphere and not from the photosphere. In order to compare with the observational height we have therefore to subtract about 8000 km. from the above calculated height of an average prominence. For ready comparison between the observational values and the values calculated above the following table has been prepared. The observed values of the heights of the reversing layer and the chromosphere are taken from St. John and Babcock's[17] scheme of the Sun's atmosphere and the observed height of a typical quiescent prominence is taken from Abetti—*The Sun*, 1938, p. 142.

Part of Envelope		Height (observed)	Height (calculated)
Reversing Layer	...	1500 km.	1640 km
Chromosphere	...	14000 km	16150 km.
Prominence	...	50000 km.	53300 km.

It is evident from the table that the agreement between observation and theory is very satisfactory indeed. Although, in view of the various approximations used in the calculations, one should not place excessive confidence in numerical agreements, yet it seems safe to conclude from the results obtained that the dynamical process considered in the present series of papers ought to play a fundamental part in the formation of the solar envelope. The corona has been purposely left out of our discussion as the equations (12) are valid so long as it is justified to neglect x, y and z against R (*cf.* Part 1). Although these equations ought to be applicable to the inner corona, they cannot have application in the mechanics of the outer corona which extends to several times the solar radius.

CONCLUSIONS

In the above calculations we have put on the average $\omega'-\omega=9\omega$ at the equator on the supposition that the particles are ejected from all depths in the interior; and by using values of V derived from observation we have found that the calculated heights of an average stable prominence, the chromosphere and the reversing layer agree with the observed heights. Now, from equation (12.6) we see that these heights are proportional to the ratio $V/(\omega'-\omega)$, so that we can always obtain the same heights for any arbitrary values of V provided we adjust the values of $\omega'-\omega$ suitably. But observational data show that only particular values of V occur in the quiescent prominences, the chromosphere and the reversing layer; and our calculations have shown that with these values of V we have to use a particular value of $\omega'-\omega$ at the equator, namely $\omega'-\omega=9\omega$ in order to obtain good agreement between the observed and calculated heights. From this we may draw the conclusion that the matter which mostly forms the quiescent prominences, the chromosphere and the reversing layer originates not at all depths but only at a particular depth at which the angular speed at the equator is such that the ejected matter has an angular speed about 10 times the angular speed of the photosphere. It may be noted that this depth roughly corresponds to the core which the sun is believed to possess. Thus, from the view-point here advocated, the core is the seat of the disturbances which lead to the ejection of matter from the interior of the Sun. This constitutes an important difference between our hypothesis and Mr. Evershed's hypothesis quoted earlier in this paper. While, according to Evershed, the increase of angular speed with height above the photosphere is to be explained by supposing that the gases constituting the higher levels of the envelope originate in the deeper levels of the interior (having higher angular speeds), according to our point of view the gases which form the different levels of the envelope originate in the same internal level (the core), but gases of the higher levels of the envelope have been ejected with greater velocities and therefore shew an apparent higher rotation speed. This would of course lead us to expect an increasing angular speed and also increasing heights of the prominences, the the chromosphere and the reversing layer with increasing solar activity; such variations appear actually to happen except in the case of the reversing layer for which there seems to be no observation available in this respect.

Our dynamical picture reduces the origins of the reversing layer, the chromosphere and the stable prominences to one and the same general process and brings out clearly the possibility that there is no fundamental difference between the modes of formation of these phenomena. According to this picture ordinary stable prominences are formed by gases ejected from limited regions of the Sun's interior and emerging from the photosphere with radial velocities ranging from 2 to 7.5 km./sec. roughly; such a prominence must be continually supplied with matter ejected from the disturbed region in the interior as long as the prominence lasts. The chromosphere and the reversing layer are formed by particles ejected from the interior and emerging from the photosphere with radial velocities ranging respectively from 0.2 to 2 km./sec. and from 0 to 0.2 km./sec. roughly ; as these layers are permanent features of the Sun, they have to be constantly supplied with matter from widespread and permanently active regions in the interior. According to this view there is no static equilibrium in the quiescent prominences, the chromosphere and in the reversing layer ; the equilibrium is dynamic. All these conclusions appear to harmonise with observational facts. Our picture is, however, far from being complete ; it will require much further development, particularly the part that concerns the interior of the Sun, before it can attempt to answer the questions as to why particles of definite ranges of velocity emerge from the photosphere and why the vertical density-gradient in the envelope is exponential ; but even as it stands at present it seems to point the way in which the answers to such questions are to be sought.

Before concluding we may mention an indefiniteness in our calculations which arises out of the uncertainty in the nature of the variation of the angular velocity (ω') with latitude in the interior of the Sun. There are two extreme ways in which ω' may vary with latitude : one is that ω' increases with latitude proportionally to $\sec^2\phi$ for which there is theoretical justification ; the other is that ω' decreases with increasing latitude in the same way as ω on the surface is observed to vary. In Part I the first type of variation of ω' was used in calculating the variation of the meridian inclination of dark markings with latitude and excellent agreement was obtained between the calculated and the observed values. If this type of variation of ω' is used in (12 6) above, then the heights of stable prominences, the chromosphere and the reversing layer should decrease with increasing latitude becoming zero at the pole. Observation however shows that there is no evidence of this kind of variation of height; in fact, the chromosphere appears to have practically the same height at all latitudes. If we use the second type of variation of ω' with latitude in (12·6), then it is evident that the heights of prominences, the chromosphere and the reversing layer would increase with increasing latitude becoming infinite at the pole, which is again contrary to observation. On this basis the calculated variation of the meridian inclination of dark markings will still show the same trend as the observed variation, but the agreement between the calculated and the observed curves will not be so good as before. The actual variation of ω' with latitude may however be something in between the two extreme types which will give a satisfactory agreement between observation and theory both as regards the latitude variation of meridian inclination of dark markings and the heights of prominences, the chromosphere and the reversing layer.

ADDENDUM

In calculating the heights of the reversing layer, the chromosphere and an average stable prominence we have taken $y_{\max}/z_{\max}$ to be equal to the tangent of the average tilt of the ascending part of the trajectory. Also in a stable prominence the gases are continually going up and dissipating at the top, so that what we see as a prominence is mainly the ascending portion with some of the top part of the trajectory; accordingly in evaluating $z_{\max}$ we have put $y_{\max}/z_{\max}$ equal to the tangent of the observed average tilt of stable prominences. This procedure may not be strictly correct, but it is not a bad approximation; besides it has the advantage that it indirectly takes account of the retarding effect of frictional resistance and incomplete compensation of gravity on the velocity of ejection (V). One may however evaluate $z_{\max}$ by first finding the general solution of equations (12·2) and then making allowances for the effect of retarding forces on V. As this procedure is more general and permits of the evaluation of z and y at any point of the trajectory, it seems desirable to include this also here. We put $2(\omega'-\omega)\cos\phi = b$ and write equations (12·2) as follows:

$$d^2z/dt^2 = -b.dy/dt \qquad \ldots \quad \text{(I)}$$

$$d^2y/dt^2 = b.dz/dt. \qquad \ldots \quad \text{(II)}$$

In order to solve these equations we put $p = dz/dt$; then we have

$$\begin{aligned} d^2y/dt^2 &= b.p\,; \\ dy/dt &= b.p.t, \text{ since for } t=0,\ dy/dt=0\,; \\ d^2z/dt^2 &= -b^2pt = dp/dt\,; \\ d^2p/dt^2 &= -b^2p\,. \qquad \ldots \quad \text{(III)} \end{aligned}$$

The general solution of (III) is

$$p = C_1 \sin bt + C_2 \cos bt,$$

where C_1 and C_2 are constants. Now $dz/dt = V$ when $t=0$; therefore $C_2 = V$, and $dz/dt = C_1 \sin bt + V.\cos bt$. ... (IV)

Integrating (IV) with the initial conditions $t=0$, $z=0$, we have

$$z = \frac{V}{b}.\sin bt + \frac{C_1}{b}.(1-\cos bt).$$

From (II) and (IV) we have with the initial conditions $t=0$, $y=0$, $dy/dt=0$

$$\begin{aligned} d^2y/dt^2 &= b(C_1 \sin bt + V \cos bt), \\ dy/dt &= -C_1 \cos bt + V \sin bt + C_1, \qquad \ldots \quad \text{(V)} \\ y &= C_1\left(t - \frac{\sin bt}{b}\right) + \frac{V}{b}\ (1-\cos bt). \end{aligned}$$

Evaluating C_1 in the usual way with the help of (V), (IV) and (I), we have $C_1 = 0$ and therefore finally we get

$$\left.\begin{aligned} z &= \frac{V}{b}\cdot \sin bt \\ y &= \frac{V}{b}\left(1-\cos bt\right) \end{aligned}\right\} \qquad \ldots \quad \text{(VI)}$$

Now z is maximum when $\sin bt$ is equal to 1; therefore we have

$$z_{max} = 0.5 \cdot \frac{V}{(\omega' - \omega)\cos\phi}. \qquad \ldots \quad \text{(VII)}$$

This is the same relation as (12.6) obtained previously except for the numerical factor. It is to be noted that the derivation of (VII) implies that V remains constant all along the trajectory so far as its magnitude is concerned. In reality however the magnitude of **V** will vary through the influence of retarding forces, but it is uncertain by what factor it is actually reduced. It is clear, however, that a factor of about 0.4 would make (VII) the same as (12·6). St. John (Ap. J., Vol. 32, p. 36, 1910) finds that towards the base of the chromosphere the velocity is about 2 km./sec. upwards and near the top of the chromosphere it is about 1 km./sec. downwards. This observation makes a factor of 0.4 entirely likely, so that by the alternative method of calculation considered here we would obtain the same heights for the reversing layer, the chromosphere and an average stable prominence as obtained previously. These heights would be the same at all latitudes if the latitude variation of ω' is such that $\omega' - \omega$ varies as $\sec\phi$, so that $(\omega' - \omega)\cos\phi$ is a constant.

Incidentally it is to be noted that the relations (VI) may be expected to have a bearing on the forms of active prominences and their movement towards apparent centres of attraction. I hope to discuss these questions in a later paper.

KODAIKANAL,
S. INDIA.

REFERENCES

[1] M. N. Saha, *Ap. J.*, September (1919).

[2] E. A. Milne, *M.N.R.A.S.*, **86**, 578 (1926), and later papers.

[3] S. Chandrasekhar, *M N.R.A.S.*, **94**, 14 and 726 (1933-34).

[4] D. H. Menzel, *Pub. Lick Observatory*, **17**, I (1931).

[5] S. Rosseland, *Pub Univ Observatory*, Oslo, **5** (1933); Theoretical Astrophysics, Oxford (1936).

[6] W. H. McCrea, *M.N R A S.*, **89**, 718 (1929) and **95**, 80 (1934).

[7] M. N. Saha, *Proc. Roy. Soc.* (*A*), **160**, 155 (1937).

[8] K O. Kiepenheuer, *Zeit F. Astroph.*, Bd **15**, S. **53** (1938).

[9] J. H. Jeans, *M N R.A.S*, **86**, 328 and 444 (1926).

[10] A. S. Eddington, *M.N.R A.S.*, **90**, 54 (1929).

[11] S. Rosseland, *Astrophysica Norvegica*, II, **3** (1936).

[12] A. K. Das, *Ind Journ. Physics*, **14**, V, 369-86 (1940).

[13] J. Evershed, *M N.R.A S.*, **95**, 507 (1935)

[14] A. K. Das and B G. Narayan, *Ind Journ Physics*, **15** 17 (1941).

[15] St. John, *Ap. J*, **32**, 36 (1910); also see Abetti—*The Sun*, 190 (1938) and Abbot, *The Sun*, 100-102 (1929).

[16] E. Pettit, *Ap. J.*, **76**, 42 (1932).

[17] St. John and Babcock, *Ap. J.*, **60**, 406 (1924).

STRUCTURE OF THE ELECTRONIC BANDS OF THE OD MOLECULE—PART II

By M. G. SASTRY
Andhra University, Waltair

(*Received for publication December 10, 1940*)

Plate III

ABSTRACT. In continuation of the work on the structure of the OD bands of heavy water, the (3,0) band at λ 2569 was photographed with a Hilger Quartz Spectrograph An exposure of about 5 hours was found necessary on account of the faintness of the band By an extrapolation of the existing data of the bands hitherto analysed, the rotational structure of this band was analysed. The values of the constants are found to be $B_3''=8{\cdot}13$, $B_0'=9{\cdot}94$ and the spin coupling constant $A=-139{\cdot}6$ cms^{-1}.

INTRODUCTION

In an earlier paper,[1] the rotational structure of some of the electronic bands of heavy water, due to the diatomic molecule OD, were reported. A scrutiny of the plates taken with long exposures revealed the existence of a faint band at about λ 2570, the region in which the (3,0) band of OD corresponding to the band λ 2447 of the OH molecule must be expected. An examination of the rotational structure of this band confirmed the above supposition. The present paper gives details of the study of this band, a preliminary report of which has appeared in *Current Science*, 1940, 9, 368.

EXPERIMENTAL

The experimental arrangement for the excitation of the bands was already described in Part I. The faintness of this band made it impracticable to use an instrument of high dispersion ; the band was therefore photographed with a Hilger medium Quartz spectrograph giving a dispersion of about 9 A.U. per mm. in the region λ 2570. With the time of exposure extending to about 5 hours, a picture of the band was obtained which could be conveniently measured, while the other bands were heavily over-exposed. The bands are reproduced in Plate I. The usual Iron Arc standards were adopted for the determination of the wavelengths. Due to the general faintness of the band and overlapping of the structure arising from the small dispersion of the instrument, the probable error in measurement is of the order of 0.1 to 0.2 A.U. Where the lines happened to be broad, the cross-wire was set in two or three positions—at the centre and at the edges. Such lines are indicated by asterisks in the list in Table I.

TABLE I

Int.	λ (obs.)	ν_{vac} (obs.)	ν_{vac} (calc.)	Classification					
				R_1	Q_1	P_1	R_2	Q_2	P_2
* 3	2569.1	38912	38913.6	2, 3	—	—	—	—	—
	69.4	908	909.7	1, 4	—	—	—	—	—
	69.6	904	903.8	5	—	—	—	—	—
2	70.1	896	895.5	6	—	—	—	—	—
3	71.2	880	882.7	7	—	—	—	—	—
			879.3	—	1	—	—	—	—
3	72.3	864	866.4	8	—	—	—	—	—
			865.4	—	2	—	—	—	—
			863.3	—	—	1	—	—	—
2	73.4	847	848.7	—	3	—	—	—	—
			847.1	9	—	—	—	—	—
3	74.4	831	832.9	—	—	2	—	—	—
			830.6	—	4	—	—	—	—
2	74.9	825	824.1	10	—	—	—	—	—
3	75.4	818	818.7	—	—	—	5, 6	—	—
			816.3	—	—	—	4	—	—
2	75.8	811	812.4	—	—	—	7	—	—
			809.2	—	—	—	3	—	—
3	76.3	803	806.4	—	5	—	—	—	—
			801.6	—	—	—	8	—	—
3	76.7	797	798.7	11	—	3	—	—	—
			796.9	—	—	—	2	—	—
2	77.5	786	786.8		—	—	9	—	—
3	77.9	779	781.6	—	6	—	—	—	—
			778.3	—	—	—	1	—	—
3	78.8	766	769.5	12	—	—	—	—	—
			768.1	—	—	—	10	—	—
			765.2	—	—	4	—	—	—

TABLE I (*contd.*)

Int.	λ (obs.)	ν_{vac} (obs.)	ν_{vac} (calc.)	Classification					
				R_1	Q_1	P_1	R_2	Q_2	P_2
3	2580.0	38748	38752.7	—	7	—	—	—	—
			748.7	—	—	—	—	1 2	—
			746.2	—	—	—	11	—	—
			744.7	—	—	—	—	3	—
2	80.8	735	737.3	—	—	—	—	4	—
			735.9	13	—	—	—	—	—
2	81.1	731	731.9	—	—	—	—	—	1
1	81.4	727	727.7	—	—	5	—	—	—
* 3	81.8	721	722.3	—	—	—	—	5	—
			721.8	—	8	—	—	—	—
	81.9	719	719.0	—	—	—	12	—	—
	82.0	717	716.2	—	—	—	—	—	2
2	82.9	704	704.8	—	—	—	—	6	—
2	83.7	692	694.7	—	—	—	—	—	3
			692.7	14	—	—	—	—	—
* 3	84.1	686	687.5	—	—	—	13	—	—
			686.9	—	9	—	—	—	—
			685.4	—	—	6	—	—	—
	84.4	682	682.4	—	—	—	—	7	—
2	85.1	671	71.9	—	—	—	—	—	4
2	86.1	656	657.0	15	—	—	—	8	—
2	86.7	648	652.8	—	—	—	14	—	—
			648.8	—	10	—	—	—	—
2	87.1	641	643.6	—	—	—	—	—	5
			641.8	—	—	7	—	—	—
2	88.1	627	626.6	—	—	—	—	9	—
2	89.4	607	613.9	—	—	—	15	—	—
			608.6	—	—	—	—	—	6
			607.2	—	11	—	—	—	—

TABLE I (*contd.*)

Int.	λ (obs.)	ν_{vac} (obs.)	ν_{vac} (calc.)	Classification					
				R_1	Q_1	P_1	R_2	Q_2	P_2
3	2590.3	38593	38594.2	—	—	8	—	—	—
			592.8	—	—	—	—	10	—
2	91.7	572	571.5	—	—	—	—	—	7
1	92.9	556	562.0	—	12	—	—	—	—
			554.6	—	—	—	—	11	—
1	93.8	541	544.0	—	—	9	—	—	—
1	94.6	530	529.4	—	—	—	—	—	8
1	95.8	512	512.8	—	13	—	—	—	—
			512.4	—	—	—	—	12	—
3	97.5	487	490.9	—	—	10	—	—	—
			483.8	—	—	—	—	—	9
2	99.0	465	467.8	—	—	—	—	13	—
			461.4	—	14	—	—	—	—
2	2601.1	433	434.9	—	—	—	—	—	10
			433.9	—	—	11	—	—	—
1	02.3	415	418.6	—	—	—	—	14	—
1	03.2	402	404.5	—	15	—	—	—	—
1	04.7	380	381.3	—	—	—	—	—	11
1	06.0	361	364.0	—	—	—	—	15	—
1	08.6	322	324.7	—	—	—	—	—	12
1	09.8	305	311.8	—	—	13	—	—	—
1	12.7	262	264.7	—	—	—	—	—	13
1	14.2	241	243.8	—	—	14	—	—	—
1	17.2	196	199.4	—	—	—	—	—	14
1	18.8	174	174.1	—	—	15	—	—	—

DISCUSSION AND RESULTS

As the rotational lines constituting the various branches of the band are not completely resolved, a method of extrapolation based on the previously known data is adopted to predict and identify the structure. Considering the bands[2] (2,0) (3,0) and (2,1), (3,1) the interval between the $Q_1(1)$ lines of the (2,0), (3,0) bands is approximately equal to that between the corresponding lines of the (2,1), (3,1) bands, this interval being approximately equal to the difference between the initial vibrational levels $v'=2$ and $v'=3$, determined from the equation

$$G(v') = \omega'(v'+\tfrac{1}{2}) + x'\omega'(v'+\tfrac{1}{2})^2 + \ldots\ldots$$

Hence the position of the initial line $Q_1(1)$ of the (3,0) band is predicted. The positions of the other lines of this and those of the other branches are similarly located. The data thus predicted with respect to all the branches are collected and compared with the observed values and a consistent scheme of the structure of the band is developed. Table I gives the details of the intensity, the wavelength and other data of all the measured lines. Columns (3) and (4) show the observed and calculated values and the last columns give their assignments.

A check on the identification of the band is afforded by comparison of the doublet separations of the bands having the same final level, *i.e.*, (0,0), (1,0), (2,0) and (3,0). As an illustration, the doublet separations

$$Q_1(K) - Q_2(K)$$

and

$$P_1(K) - P_2(K)$$

for the above bands are given in Table II, in which the data for the (3,0) band have been obtained from the assignments shown in Table I (Column 3, ν observed).

TABLE II

K	$Q_1(K)-Q_2(K)$				$P_1(K)-P_2(K)$			
	λ 3065 (0,0)	λ 2872 (1,0)	λ 2708 (2,0)	λ 2569 (3,0)	λ 3065 (0,0)	λ 2872 (1,0)	λ 2708 (2,0)	λ 2569 (3,0)
1	131.4	131.0	131.1	132	131.	130.3	131.8	133
2	116.0	115.9	116.0	116	116.8	115.3	115.8	114
3	103.7	103.5	103.5	99	103.4	103.7	102.9	105
4	92.3	92.5	92.4	96	92.9	92.9	92.8	95
5	83.5	83.4	83.0	82	84.1	83.8	83.6	86
6	75.8	76.3	75.7	75	77.0	76.4	76.4	79
7	69.1	70.0	68.8	66	70.0	69.7	66.7	69
8	63.6	63.2	63.3	65	64.3	64.6	64.3	63
9	58.7	59.0	58.7	59	59.9	59.5	59.3	54
10	54.6	54.9	54.7	55	56.0	55.8	55.7	54
11	50.9	51.7	50.9	51	52.3	52.0	52.6	53
12	47.7	48.0	47.8	44	49.3	49.3	49.6	—
13	45.0	45.5	44.9	47	46.7	46.8	46.7	43
14	42.8	42.4	42.6	—	44.4	44.1	44.2	45
15	40.5	40.5	40.4	41	42.4	43.6	—	—

A further check on the correctness of the assignments is obtained by the application of the combination relations shown below and already referred to in detail elsewhere.[1] It can be easily seen that

$$R_1(K)-P_1(K)=\triangle_2F'_1(K)$$
$$R_2(K)-P_2(K)=\triangle_2F'_2(K).$$

The difference between the values $\triangle_2F'_1(K)$ and $\triangle_2F'_2(K)$ may be ignored on account of the small spin-doubling in the upper $^2\Sigma^+$ state. Table III gives the values of $R_1(K)-P_1(K)$ and of $R_2(K)-P_2(K)$ for the (3,2), (3,1) and (3,0) bands.

TABLE III

Rotational term differences for the $^2\Sigma^+$ state

K	$R_1(K)-P_1(K)$			$R_2(K)-P_2(K)$		
	λ 2963 (3,2)	λ 2756 (3,1)	λ 2569 (3,0)	λ 2963 (3,2)	λ 2756 (3,1)	λ 2569 (3,0)
2	81.4	80.3	81	81.9	79.7	80
3	114.2	113.6	115	114.7	112.0	119
4	144.5	144.6	142	144.5	144.0	147
5	177.4	176.7	177	176.4	176.0	177
6	208.8	208.8	210	208.1	208.5	211
7	240.1	240.4	239	239.2	240.1	239
8	272.2	271.4	271	271.3	271.5	273
9	302.8	302.8	306	302.6	302.6	299
10	333.6	333.6	338	333.4	333.5	333
11	364.9	364.8	364	363.1	364.4	368
12	394.1	394.5	—	—	—	—
13	424.0	424.6	430	—	424.1	424
14	—	454.2	451	—	455.8	452
15	—	483.5	482	—	—	—

The table confirms that the band at λ 2569 corresponds to the initial level $v'=3$.

The combination relations involving the lower $^2\Pi$ state are contained in the equation,

$$R(K-1)-Q(K)=Q(K-1)-P(K).$$

It must be noted that the equation is only approximate, the difference between the two sides being a measure of the Λ-doubling in the rotational levels.

Tables IV and V show the values of the above differences. The values in columns (3) and (5) in these tables are obtained from the observed values of the lines in Table I. Columns 2 and 4 contain the values estimated from the bands (0,0), (1,0) and (2,0). The data indicate the correctness of the assignment of the band λ 2569 as arising from the final state $v''=0$

TABLE IV

K	$Q_1(K-1)-P_1(K)$		$R_1(K-1)-Q_1(K)$	
	Estimated mean for bands (0,0), (1,0), (2,0)	Observed for λ 2569 (3,0)	Estimated mean for bands (0,0), (1,0) (2.0)	Observed for λ 2569 (3,0).
2	46.6	49	46.2	44
3	65.0	67	65.0	65
4	83.7	81	84.1	81
5	102.1	104	102.9	105
6	120.9	117	122.0	125
7	140.0	138	141.2	148
8	158.0	155	160.2	159
9	177.6	180	179.3	178
10	196.1	199	198.4	199
11	214.8	215	217.2	218
12	233.2	-	236.5	241
13	251.3	251	255.3	254
14	269.5	271	274.1	270
15	287.0	291	293.0	290

TABLE V

K	$Q_2(K-1)-P_2(K)$		$R_2(K-1)-Q_2(K)$	
	Estimated mean for bands (0,0), (1,0), (2,0)	Observed for λ 2569 (3, 0)	Estimated mean for bands (0,0), (1,0), (2,0)	Observed for λ 2569 (3,0)
2	31.4	31	31.8	31
3	52.5	56	52.1	49
4	73.0	77	72.9	76
5	93.5	94	92.2	97
6	114.2	114	113.8	114
7	133.9	132	133.4	136
8	154.0	152	153.5	155
9	173.8	169	173.3	176
10	193.2	194	193.2	193
11	212.3	213	212.3	210
12	231.4	234	231.8	236
13	250.2	250	250.8	254
14	268.6	269	270.1	271
15	—		288.8	287

The final check consisted in estimating the values of the rotational constants B_3' and B_0'', the method of calculating them being that previously adopted by the author for the bands λλ 2872, 2916 and 2963. The values of these constants are found to be $B_3'=8.13$ and $B_0''=9.94$ cms.$^{-1}$. They are in good agreement with those observed previously, *i.e.*, $B_3'=8{\cdot}074$ from the (3,1) band and $B_0''=9.927$ from the (1,0) band. The spin-coupling constant is found to have a mean value -139.6 cms.$^{-1}$.

Table VI is an extension of that given in Part I showing the vibrational analysis of the OD-bands. For each band the calculated value of the null line is inserted in the table, the value for the (3,0) band being determined from the present data.

TABLE VI

Null lines of the OD-bands $^2\Sigma^+ - {}^2\Pi_{\frac{3}{2}}$

v' \ v''	0		1		2
0	ν 32542.29	—	—	—	—
	2215.9	—	—	—	—
1	34757·3	—	—	—	—
	2112.1	—	—	—	—
2	36869.4	2632.7	34236.7	—	—
	2007.7	—	2008.0	—	—
3	38877.1	2632.4	36244.7	2544.2	33700.5

The author desires to express his grateful thanks to Dr. K. R. Rao for his interest in the work and to the Andhra University for the award of a Fellowship.

REFERENCES

[1] M. G. Sastry and K. R. Rao, *Ind. J. Phys.*, **15**, 27 (1941).

[2] The data quoted in this paper for the bands (0,0), (2,0) and (3,1) are due to Ishaq, *Proc. Roy. Soc.*, **159**, 110 (1937) and *Proc. Nat. Inst. Sc. Ind.*, **3**, 389 (1937) and those for (1,0), (2,1) and (3,2) are due to the author and K. R. Rao, *ibid.*

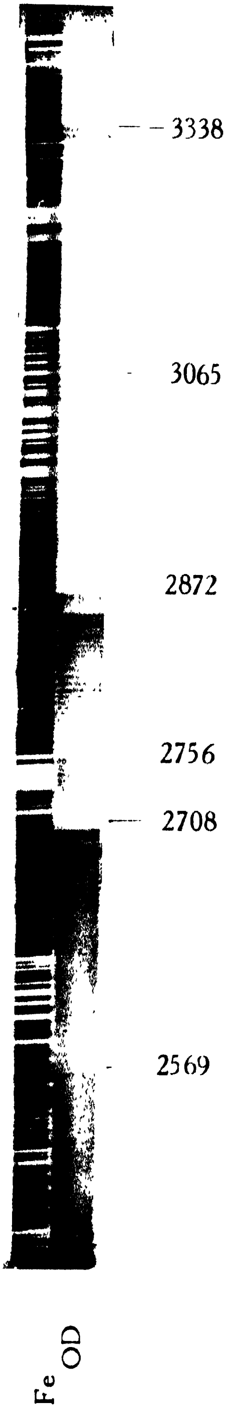
3338
3065
2872
2756
2708
2569
Fe
OD

MAGNETIC SUSCEPTIBILITY OF TWO DIMENSIONAL FREE ELECTRON GAS *

By B. N. SINGH
University of Delhi

(Received for publication, September, 1940)

ABSTRACT. The paramagnetic and diamagnetic susceptibilities of a two dimensional free electron gas have been calculated and the results compared with the susceptibilities of a three dimensional assembly.

The first application of Fermi-Dirac statistics was made by Pauli (1927) in discussing the paramagnetism of a free electron gas. It was shown by Landau[1] (1930) that on the basis of quantum mechanics there was also a diamagnetic contribution to the magnetic susceptibility, although on the basis of classical mechanics there should be no such effect. The paramagnetic effect arises due to the spin magnetic moment and the diamagnetic effect due to the quantization of the motion of the electron in a magnetic field. The temperature dependence of these effects has been investigated recently amongst others by Stoner[2] (1935). In the first part of the paper expressions for the paramagnetic susceptibility for the two dimensional case are obtained. The case of diamagnetism is discussed in section 2.

1. *Paramagnetism* :—In this section we shall consider the paramagnetism of a free electron gas and ignore the diamagnetism which is considered in the next section. When an external magnetic field H acts on the assembly of the electrons, the magnetic energy of an electron will have only two values—either $+H\mu$ if the spin is parallel to H, or $-H\mu$ if the spin is anti-parallel to H, where μ denotes the Bohr magneton and is given by

$$\mu = \frac{eh}{4\pi mc}. \qquad \ldots \quad (1)$$

The magnetic moment M produced by the magnetic field H can be determined as usual from F, the free energy, by the relation

$$M = -\left(\frac{\partial F}{\partial H}\right)_{T,V}, \qquad \ldots \quad (2)$$

---

* Communicated by the Indian Physical Society.

and we obtain, proceeding in the usual way, the result *

$$M_P = \frac{N\mu^2 H}{kT}\left[\frac{F'_{s-1}(\eta) + \frac{\beta_1^2}{6} F'''_{s-1}(\eta)\ldots}{F_{s-1}(\eta) + \frac{\beta_1^2}{2} F''_{s-1}(\eta)\ldots}\right] \qquad \ldots \quad (3)$$

where $$\beta_1 = \frac{\mu H}{kT}, \quad F_s(\eta) = \int_0^\infty \frac{u^s}{e^{u-\eta}+1}\, du. \qquad (4)$$

In the above expressions s has to be put equal to 3 for the three dimensional non-relativistic case, and equal to unity for the two dimensional non-relativistic case.

However, the magnetic moment can also be determined in a more straight forward way by using the Gibbs free energy instead of the Helmholtz free energy F, and this is equivalent to using the generalised form of Boltzmann's law. In the presence of the magnetic field, let N_+ denote the number of electrons in the assembly possessing spins parallel to H (magnetic moment opposite to H) and N_- possessing spins antiparallel to H, and let the difference between them be denoted by x, *i.e.*, $N_+ = N_- - x$. Then from a well-known theorem in thermodynamics† we have

$$\eta_+ - \eta_- = -\frac{2\mu H}{kT},$$

or $$\log A_+ - \log A_- = -\frac{2\mu H}{kT}, \quad i.e., \quad \frac{A_+}{A_-} = e^{\frac{-2\mu H}{kT}} \qquad \ldots \quad (5)$$

where A_+ and A_- are the distribution parameters (absolute activities) for the N_+ electrons and N_- electrons respectively, and are related to η of the equation above by the relation $\eta_+ = \log A_+$, $\eta_- = \log A_-$.

We first consider the non-degenerate case.

In non-degeneracy $\frac{2\mu H}{kT} << 1$, and the terms in equation (5) can be expanded in a series. We have, since $\beta = +1$, in Fermi-Dirac statistics, inverting the series in (12) A.‡

$$A_+ = A_{1+}[1 + a_1 A_{1+} + a_2 A_{1+}^2 + \ldots], \qquad \ldots \quad (6)$$

---

* Stoner (1935). Stoner's result is for the special case of $s = \frac{3}{2}$-(Non-relativistic 3 dimensional case).

† $\eta kT = kT \log A$ is called the chemical potential.

‡ (12) A refers to equation (12) of the paper on 'Thermodynamic functions for two dimensional quantum statistics.' 'A' attached to an equation number will have the same significance in the rest of the paper.

$$A_- = A_{1-}[1 + a_1 A_{1-} + a_2 A_{1-}^2 + \ldots], \tag{7}$$

where

$$_1 = \frac{1}{\ }, \; a_2 = \left(\frac{2}{4^s} - \frac{1}{3^s}\right),$$

$$A_{1+} = \frac{2N_+}{D(kT)^s \Gamma(s)} \tag{8*}$$

$$= \frac{N_+}{N} 2A_1 . \tag{9}$$

Similarly $$A_{1-} = \frac{N_-}{N} 2A_1$$

Therefore, $$\frac{A_+}{A_-} = \frac{N_+}{N_-}\left[1 + \left(\frac{N_+ - N_-}{N}\right) 2a_1 A_1 + \left(\frac{N_+^2 - N_-^2}{N^2}\right) 4a_2 A_1^2 + \left(\frac{N_-^2 - N_+ N_-}{N^2}\right) 4a_1^2 A_1^2 \ldots\ldots\right]. \tag{10}$$

But, $$N_+ = \frac{N}{2}\left[1 - \frac{x}{N}\right] \text{ and } N_- = \frac{N}{2}\left[1 + \frac{x}{N}\right].$$

Hence $$\frac{A_+}{A_-} = 1 - \frac{2x}{N}\left[1 + a_1 A_1 + (2a_2 - a_1^2) A_1^2 \ldots\right] \frac{2x^2}{N^2} - \frac{2x^3}{N^3} \tag{11}$$

$$= e^{\frac{-2\mu H}{kT}} = 1 - \frac{2\mu H}{kT} + \frac{2\mu^2 H^2}{k^2 T^2} - \frac{4}{3}\frac{\mu^3 H^3}{k^3 T^4} \ldots\ldots, \tag{12}$$

which gives, after a little algebra,

$$M = \mu x = \frac{\mu^2 HN}{kT}\left[1 - a_1 A_1 - 2(a_2 - a_1^2) A_1^2 - \frac{1}{3}\frac{\mu^2 H^2}{k^2 T^2} \ldots\ldots\right], \quad \ldots \tag{13}$$

since x is the number of Bohr magnetons contributing to the magnetism of the assembly. In non-relativistic non-degeneracy, therefore, substituting the values of a_1 and a_2 for $s = \frac{3}{2}$, corresponding to the three dimensional case,

$$M_3 = \frac{u^2 HN}{kT}\left[1 - \frac{A_1}{2^{3/2}} + \left(\frac{2}{3^{3/2}} - \frac{1}{4}\right) A_1^2 - \beta_1^2\right] \tag{14}$$

where $$\beta_1 = \frac{\mu H}{kT}.$$

---

* In three dimensions $s = 3/2$ and $D = 2\pi g \frac{(2m)^{3/2}}{h^3} V$,

and in two dimensions $s = 1$ and $D = 2\pi g \frac{m\sigma}{h^2}$

where σ represents the area, $g = 2$ for electrons.

The two asymptotic expressions (24) and (25) meet for $T=T_{02}$ and the expressions (26) and (27) meet for $T=T_{03}$.

It will be at once noticed that, for $T>T_{0\nu}$, the non-degenerate equation (24) and (26) will give a better approximation than (25) and (27). For $T<T_{0\nu}$, it is *vice versa*. $T_{0\nu}$ is called the degeneracy temperature. When $\nu=2$, *i.e.*, for the two dimensional case, we have from equation (22)

$$T_{02}=\frac{\epsilon_{02}}{k}=\frac{N}{Dk}=\frac{n^*h^2}{4\pi mk}, \qquad \ldots (29)$$

and, for the three dimensional case, T_{03} is given by

$$T_{03}=\frac{\epsilon_{03}}{ks}=\frac{h^2}{4mk}\,\frac{n^{\frac{2}{3}}}{\pi^{\frac{2}{3}}3^{\frac{1}{3}}}. \qquad \ldots (30)$$

Hence
$$\frac{T_{03}}{T_{02}}=\frac{n^{\frac{2}{3}}}{n^*}\left(\frac{\pi}{3}\right)^{\frac{1}{3}}, \qquad \ldots (31)$$

where T_{03} is the degeneracy temperature in three dimensions and T_{02} in two dimensions.

2. *Diamagnetism* :—We consider the case in which the electron gas is restricted to move in a plane, the magnetic field H being at right angles to this plane. The electrons move in circular orbits and the possible values of energy for any electron (excluding spin energy) are given by $\epsilon_l=2\mu H(l+\frac{1}{2})$, where l is any integer.

The number of states with the given quantum number l is determined in the following way. When the field is applied, the electrons group themselves into the nearest quantized energy level. The condition that this energy level has the quantum number l is that the energy $\frac{p^2}{2m}$ of the electrons in the absence of the field (p is the momentum of the electron in the plane) lies in the range

$$2\mu Hl\leq\frac{p^2}{2m}\leq 2\mu H(l+1).$$

And hence, if σ denotes the area of the plane containing the electrons, the corresponding area of phase space is $2\pi\sigma p\,dp=4\pi\sigma m\mu H$. Allowing the weight factor g for each h^2 of phase space, we have the number of states possible

$$=g.\frac{4\pi\sigma m\mu H}{h^2}=g.\frac{eH\sigma}{ch}. \qquad \ldots (32)$$

Therefore*, $$\Omega=\frac{-kTgeH\sigma}{ch}\sum_{l=0}^{l=\infty}\log\left\{1+e^{\eta-(l+\frac{1}{2})\frac{2\mu H}{kT}}\right\}.$$

---

* Stoner, *loc.cit.* Ω is the partition function.

Using Euler's formula $\sum_{l=a} f(l+\tfrac{1}{2}) = \int f(x)\,dx - \frac{1}{24}\, f'(x)^{\,b}$

we have, $$\Omega = -kTg\frac{eH\sigma}{ch}\left[\int_0^\infty \frac{2\beta_1 x}{e^{2\beta_1 x-\eta}+1}\,dx + \frac{\beta_1}{12}\left(\frac{1}{e^{-\eta}+1}\right.\right. \qquad (33)$$

where $\beta_1 = \frac{\mu H}{kT}$. Putting $2\beta_1 x = u$ and simplifying,

we have $$\Omega = -\frac{2\pi mg\sigma}{h^2}(kT)^2\left[F_1(\eta) - \frac{\beta_1^2}{6}\,\frac{1}{e^{-\eta}+1}\ \cdots\right]. \qquad \cdots\ (34)$$

Therefore, $$N = -\frac{1}{kT}\,\frac{\partial\Omega}{\partial\eta} = \frac{2\pi mg\sigma}{h^2}\,kTF_0(\eta), \qquad \cdots\ (35)$$

and $$M_D = -\frac{\partial\Omega}{\partial H} = \frac{2\pi mg\sigma}{3h^2}\mu^2 H\,\frac{1}{e^{-\eta}+1}$$

$$= -\frac{N}{3}\,\frac{\mu^2 H}{kT}\,\frac{1}{F_0(\eta)}\,\frac{1}{e^{-\eta}+1}. \qquad \cdots\ (36)$$

In non-degeneracy $\Lambda = e^\eta << 1$, $F_0(\eta) = A$, and therefore to a first order

$$M_D = -\frac{1}{3}\,\frac{N\mu^2 H}{kT}. \qquad \cdots\ (37)$$

In degeneracy $\eta >> 1$, $F_0(\eta) = \eta$ and to a first order

$$M'_D = -\frac{1}{3}\,\frac{N\mu^2 H}{kT\eta}. \qquad \cdots\ (38)$$

But from equation (22), for $\eta >> 1$,

$$\epsilon_{02} = \eta kT = \frac{Nh^2}{g.2\pi m\sigma},$$

and therefore, in degeneracy,

$$M'_D = -\frac{1}{3}\,\frac{g.2\pi m\sigma}{h^2}\mu^2 H. \qquad \cdots\ (39)$$

Hence the particle susceptibility for two dimensions is given by $\chi_2 = -\frac{1}{3}\,\frac{\mu^2}{kT}$ for the non-degenerate case and $\chi'_2 = -\frac{\mu^2}{3}.\frac{4\pi m}{h^2 n^*}$ for the degenerate case, where n^* is the number of electrons per unit area.

ON NUCLEAR SCATTERING

By K. C. KAR

(*Received for publication, August 15, 1940*)

ABSTRACT. The formula for the intensity of proton-proton scattering given by Kar and Basu (*Phil Mag.*, Vol. **29**, p. 200, 1940) is shown to be in better agreement with the second and improved experiment of Heydenburg, Tuve and Hafstad (*Phys. Rev.*, Vol. **56**, p. 1078, 1939). The formula was derived assuming the existence of a short range attractive force of neutron-proton type in addition to the Coulombian force of repulsion. The corresponding formula for the deuteron-deuteron scattering is deduced in the present paper assuming a short range repulsive force of the same type; and it is found to be in good agreement with the observations of Heydenburg and Roberts (*Phys. Rev*, Vol. **56**, p. 1092, 1939). Again, assuming a short range attractive force and neglecting the effect of exchange, a formula is derived for the intensity of scattering of deuteron by helium The agreement with the experiment of Heydenburg and Roberts is fairly satisfactory It is also shown that the correction for the relative motion of the scattering particle is not negligible in case of deuteron scattering by helium but may be neglected even at large angles in the case of proton scattering by helium. It is in agreement with the above experiment.

A. Proton-Proton Scattering

Recently the theory of proton-proton scattering has been developed by me.[1] The theory is based on the assumption that in addition to the Coulomb repulsive force there is a short range attractive force between the protons. The latter force is of the nature of the attractive force existing between a neutron and a proton. The formula thus derived for the departure (I/I_{MKB}) from Coulomb scattering, is

$$\frac{I}{I_{MKB}}=\frac{\operatorname{cosec}^4\theta+\sec^4\theta-\operatorname{cosec}^2\theta\sec^2\theta\left(1+\frac{Mv^2}{e^2}g\right)+\left(\frac{Mv^2}{e^2}g\right.}{\operatorname{cosec}^4\theta+\sec^4\theta-\operatorname{cosec}^2\theta\sec^2\theta}, \quad \ldots \quad (1)$$

where M, e, v have their usual meaning and g denotes the relative value of the scattering function due to the short range force, being taken independent of the scattering angle (θ) and the incident velocity (v) as in neutron-proton scattering.[2] It should be noted that g is independent of the angle and the velocity only for high-velocity bombardments. Consequently formula (1) is strictly valid in this region and is only approximately true at low velocity. Now, in the paper cited above[1] the theoretical values given by (1) have been compared with the experimental values of Heydenburg, Tuve and Hafstad.[3] The agreement has been fairly good for 900 k.v., 800 k.v. and 700 k.v. incident velocities. Recently they have repeated the experiment[4] more carefully and have found slight discrepancies. The incident velocities in their second experiment are 867 k.v., 776 k.v. and 670 k.v.

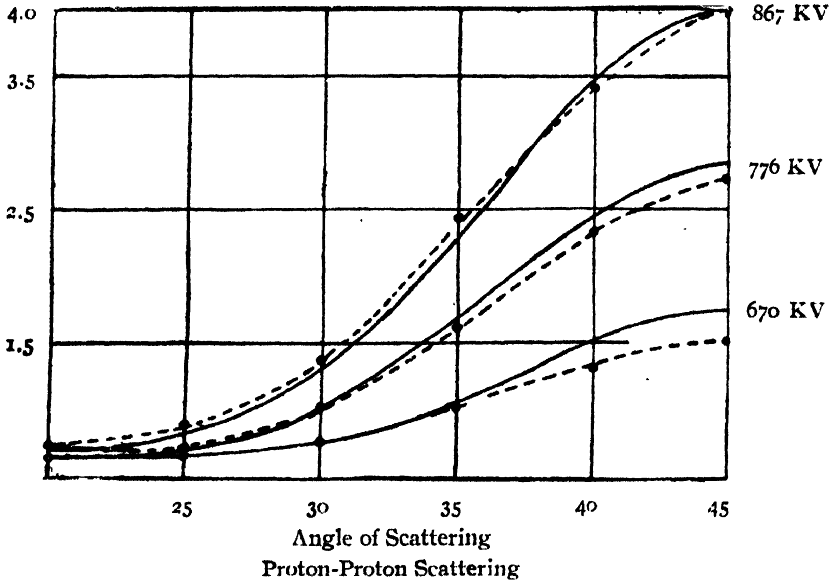

FIGURE 1

In Fig. 1, the values of I/I_{MKB} obtained from the second experiment of Heydenburg and others, for different angles of scattering are given by the dotted curves while the corresponding theoretical curves from (1) are drawn continuous. The agreement appears to be better than before. The fitting value of g at 45° for 867 k.v., which is used for theoretical calculations, is 4.949×10^{-13}.

B. *Deuteron-Deuteron Scattering*

The short range force in case of deuteron-deuteron interaction may be taken as before spherically symmetrical and independent of the incident velocity at least to a first approximation, although on account of the complexity in structure the field should have axial symmetry. Moreover, we have to suppose that in the present case, unlike the proton-proton and proton-neutron field, the short range force is *repulsive*. This appears to be supported by the observations of Heydenburg and Roberts who find that the ratio (I/I_{MKB}) of the observed value of the intensity to that given by the MKB-formula is greater than unity even at small angles.

Now remembering that the short range force is repulsive and the weights for anti-parallel and parallel spins are as 2:1, one obtains for deuteron-deuteron scattering, on proceeding exactly as in deriving (1),

$$\frac{I}{I_{MKB}} = \frac{\operatorname{cosec}^4\theta + \sec^4\theta + \frac{2}{3}\operatorname{cosec}^2\theta\sec^2\theta\left(1 + 4\frac{Mv^2}{e^2}g\right) + \frac{8}{3}\left(\frac{Mv^2}{e^2}g\right)^2}{\operatorname{cosec}^4\theta + \sec^4\theta + \frac{2}{3}\operatorname{cosec}^2\theta\sec^2\theta}$$

where it should be noted, g is taken to be spherically symmetrical as before. The experimental values of the ratio for different angles and for incident velocities 832 k.v., 720 k.v. and 614 k.v. are given by Heydenburg and Roberts. Their experimental curves are drawn dotted in Fig. 2. The corresponding theoretical curves from (2) are drawn continuous.

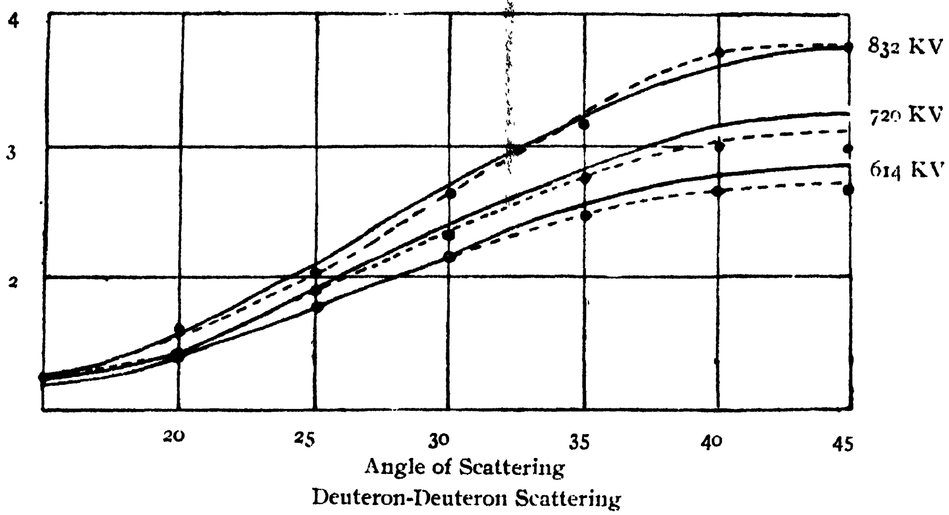

FIGURE 2

It appears from Fig. 2 that the agreement is fairly satisfactory. A better agreement, specially for low velocities, would have been desirable. The fitting value of g at 45° and for 832 k.v. incident velocity is found to be 1.605×10^{-13}.

C. *Deuteron-Helium Scattering*

Heydenburg and Roberts (*l.c.*) have also determined the intensity of scattering of deuteron by helium, and have given its values for different angles relative to the corresponding theoretical values calculated from Born-Rutherford formula. They have taken this ratio probably because they have thought that as there is no possibility of exchange, Born-Rutherford formula is applicable in this case if the force of interaction is Coulombian.

It is clear that as the scattered deuteron and the recoil helium are easily distinguishable, the effect of exchange need not be considered. However, one should not use Born-Rutherford formula because it does not take into account (1) the idea of critical approach found necessary in explaining electron scattering by atoms[6] and (2) the error due to neglecting the velocity of the scattering particle. In the following it is proposed to derive general formulae of scattering and critical approach for any two masses of the interacting particles in a Coulomb field. This enables us at once to estimate the order of the error involved in taking Born-Rutherford formula for deuteron-helium scattering.

Let us suppose that a particle of mass m_2 is at rest and that it is bombarded by a second particle of mass m_1 moving with velocity v. If we refer the motion to the centre of gravity of the combined system (*C*-system), it can be easily shown that the total energy of the particles in this system is $E=\frac{1}{2}\mu v^2$, where $\mu=\frac{m_1 m_2}{m_1+m_2}$. Thus we have for the wave equations in the *C*-system, without and within the potential field,

$$\Delta x+\frac{8\pi^2\mu}{h^2}Ex=0 \text{ (outside)}$$

$$\Delta x+\frac{8\pi^2\mu}{h^2}(E-V)x=0 \text{ (inside)},$$

where $$V=\frac{zz'e^2}{r},$$

ze and $z'e$ being the charges of the two interacting particles.

Now, Eqs. (3) and (4) are almost identical with the corresponding equations in electron scattering. The important difference is that here we have μ the effective mass in place of m the electronic mass of the previous case. Thus proceeding in the same way as before we obtain for the relative intensity of scattering at an angle ϕ

$$I=2\pi\left(\frac{zz'e^2}{2\mu v^2}\right)^2 \operatorname{cosec}^4\frac{\phi}{2}\cos^2 k'r_0 \sin\phi\, d\phi, \quad \ldots \quad (5)$$

where $$k'=\frac{4\pi\mu v}{h}\sin\frac{\phi}{2} \quad \ldots \quad (5{\cdot}1)$$

and $$r_0=1{\cdot}35\times\frac{zz'e^2}{\mu v^2}\left(\operatorname{cosec}\frac{\phi}{2}+1\right). \quad \ldots \quad (5{\cdot}2)$$

It should be noted that ϕ in eqs. (5)→(5.2) denotes the angle of scattering in the *C*-system. Thus in order to verify the above equation experimentally, it is necessary to correlate ϕ with θ the angle of scattering in the laboratory co-ordinates (R-system). We shall proceed to do it in the following:—

As already taken, m_1 is the mass of the incident particle bombarding with velocity v and m_2 the mass of the scattering particle being initially at rest. Thus the total energy in the R-system is $\frac{1}{2}m_1v^2$. Let v_1 and v_2 be the velocities of the two particles in *C*-system. Elementary considerations give

$$\left.\begin{aligned} v_1 &= \frac{m_2}{m_1+m_2}v \\ v_2 &= -\frac{m_1}{m_1+m_2}v \end{aligned}\right\} \qquad \dots (6)$$

as the velocities, and $\frac{1}{2}\mu v^2$ as the total energy in the *C*-System. Now, as $\frac{1}{2}m_1v^2-\frac{1}{2}\mu v^2$ is equal to the energy due to the motion of the centre of gravity of the system, we have, for the velocity of *c.g.*,

$$\frac{m_1}{m_1+m_2}v_1 \qquad \dots (6\cdot 1)$$

Again, in the *C*-system, the scattered particle has components of velocity

$$v_1\cos\phi=\frac{m_2}{m_1+m_2}v\cos\phi \qquad \dots (6\cdot 2)$$

parallel to the line of centres and

$$v_1\sin\phi=-\frac{m_2}{m_1+m_2}v\sin\phi \qquad \dots (6\cdot 3)$$

perpendicular to it. In R-system the perpendicular component is unaffected but from (6·1) the parallel component becomes

$$\frac{m_1+m_2\cos\phi}{m_1+m_2}v. \qquad \dots (6\cdot 4)$$

Thus taking the ratio of the components in R-system we obtain at once

$$\frac{m_2\sin\phi}{m_1+m_2\cos\phi}=\tan\theta. \qquad \dots (6\cdot 5)$$

where θ is the angle of scattering in R-system. After easy transformations we get from (6·5)

$$\phi=\theta+\sin^{-1}\left(\frac{m_1}{m}\sin\theta\right). \qquad \dots (6\cdot 6)$$

Hence,

$$\frac{\sin\phi\, d\phi}{\sin\theta\, d\theta}=2\frac{m_1}{m_2}\cos\theta+\frac{1+\left(\frac{m_1}{m_2}\right)^2\cos 2\theta}{\sqrt{1-\left(\frac{m_1}{m_2}\right)^2\sin^2\theta}}. \qquad \dots (6\cdot 7)$$

On using the relations (6·6) and (6·7) we get for the relative intensity scattering at angle θ, in laboratory co-ordinates,

$$I = 2\pi\left(\frac{zz'e^2}{2\mu v^2}\right)^2 \operatorname{cosec}^4\left\{\tfrac{1}{2}\theta+\tfrac{1}{2}\sin^{-1}\left(\frac{m_1}{m_2}\sin\theta\right)\right\}\cos^2 k'r_0$$

$$\times\left\{2\frac{m_1}{m_2}\cos\theta+\frac{1+\left(\frac{m_1}{m_2}\right)^2\cos 2\theta}{\sqrt{1-\left(\frac{m_1}{m_2}\right)^2\sin^2\theta}}\right\}, \quad \ldots \quad (7)$$

where

$$k'=\frac{4\pi\mu v}{h}\sin\left\{\tfrac{1}{2}\theta+\tfrac{1}{2}\sin^{-1}\left(\frac{m_1}{m_2}\sin\theta\right)\right\}, \quad \ldots \quad (7{\cdot}1)$$

and for the critical approach

$$r_0=1{\cdot}35\times\frac{zz'e^2}{\mu v^2}\left[\operatorname{cosec}\left\{\tfrac{1}{2}\theta+\tfrac{1}{2}\sin^{-1}\left(\frac{m_1}{m_2}\sin\theta\right)\right\}+1\right]. \quad \ldots \quad (7{\cdot}2)$$

Formulæ (7)→(7·2) are valid for interaction between *any two masses* under Coulomb field. However, some special cases of importance are worth considering.

Case I : If $m_2 >> m_1$, Eqs. (7)→(7·2) become

$$I=2\pi\left(\frac{zz'e^2}{2m_1v^2}\right)^2\operatorname{cosec}^4\frac{\theta}{2}\cos^2 k'r_0\sin\theta\,d\theta. \quad \ldots \quad (8)$$

$$k'=\frac{4\pi m_1 v}{h}\sin\theta \quad \ldots \quad (8{\cdot}1)$$

$$r_0=1{\cdot}35\times\frac{zz'e^2}{m_1v^2}\left[\operatorname{cosec}\frac{\theta}{2}+1\right]. \quad \ldots \quad (8{\cdot}2)$$

For bombardment by very high speed light particles $r_0 \to 0$ and $\cos k'r_0 \to 1$. Hence (8) reduces to the well-known Rutherford formula.

Case II : If $m_1=m_2=m$, $z'=z=1$; so $\mu=\frac{m}{2}$. Hence eqs. (7)→(7·2) become

$$I=2\pi\left(\frac{e^2}{mv^2}\right)^2\operatorname{cosec}^4\theta\cos^2 k'r_0{\cdot}4\cos\theta\sin\theta\,d\theta \quad \ldots \quad (9)$$

where

$$k'=\frac{2\pi mv}{h}\sin\theta \quad \ldots \quad (9{\cdot}1)$$

and

$$r_0=1{\cdot}35\times\frac{2e^2}{mv_2}(\operatorname{cosec}\theta+1). \quad \ldots \quad (9{\cdot}2)$$

Eq. (2) gives the relative intensity for proton-proton scattering without exchange. So it corresponds to an ideal case.

Case III : In case of scattering of deuteron by helium, we have $m_2 = 2m_1$ and $z = 1$, $z' = 2$. And so $\mu = \frac{2}{3}m_1$. Hence we have from eqs. (7)⟶(7·2)

$$I = 2\pi \cdot \frac{9}{4}\left(\frac{e^2}{m_1 v^2}\right)^2 \operatorname{cosec}^4\{\tfrac{1}{2}\theta + \tfrac{1}{2}\sin^{-1}(\tfrac{1}{2}\sin\theta)\}\cos^2 k' r_0$$

$$\times \left\{\cos\theta + \frac{1 + \frac{1}{4}\cos 2\theta}{\sqrt{1 - \frac{1}{4}\sin^2\theta}}\right\}\sin\theta\, d\theta \qquad \ldots \quad (10)$$

$$k' = \frac{\frac{8}{3}\pi m_1 v}{h}\sin\{\tfrac{1}{2}\theta + \tfrac{1}{2}\sin^{-1}(\tfrac{1}{2}\sin\theta)\} \qquad \ldots \quad (10{\cdot}1)$$

$$r_0 = 1{\cdot}35 \times \frac{3e^2}{m_1 v^2}\left[\operatorname{cosec}\{\tfrac{1}{2}\theta + \tfrac{1}{2}\sin^{-1}(\tfrac{1}{2}\sin\theta)\} + 1\right], \qquad \ldots \quad (10{\cdot}2)$$

where m_1 is the mass of deuteron.

Case IV : In case of scattering of helium by deuteron, we have $m_2 = \frac{1}{2}m_1$ and $z = 2$, $z' = 1$. And so $\mu = \frac{1}{3}m_1$. Hence we obtain from eqs. (7)⟶(7·2)

$$I = 2\pi \times 9\left(\frac{e^2}{m_1 v^2}\right)^2 \operatorname{cosec}^4\{\tfrac{1}{2}\theta + \tfrac{1}{2}\sin^{-1}(2\sin\theta)\}\cos^2 k' r_0$$

$$\times \left\{4\cos\theta + \frac{1 + 4\cos 2\theta}{\sqrt{1 - 4\sin^2\theta}}\right\}\sin\theta\, d\theta \qquad \ldots \quad (11)$$

$$k' = \frac{\frac{4}{3}\pi m_1 v}{h}\sin\{\tfrac{1}{2}\theta + \tfrac{1}{2}\sin^{-1}(2\sin\theta)\} \qquad \ldots \quad (11{\cdot}1)$$

$$r_0 = 1{\cdot}35 + \frac{6e^2}{m_1 v^2}\left[\operatorname{cosec}\{\tfrac{1}{2}\theta + \tfrac{1}{2}\sin^{-1}(2\sin\theta)\} + 1\right] \qquad \ldots \quad (11{\cdot}2)$$

where m_1 is the mass of helium. It is evident that in eqs. (11)⟶(11·2), $2\sin\theta$ must be less than 1. Thus $\sin\theta << 1$, *i.e.*, $\theta << 30°$. Hence the maximum angle at which helium may be scattered by deuteron is 30°. It may be noted that similar conclusion was arrived at by Rutherford and Darwin.

Let us return once again to deuteron scattering by helium. It is now clear that instead of taking after Heydenburg and Roberts (*l.c.*), the intensity relative to that given by Born-Rutherford formula one should rather take the ratio with the intensity given by (10). The error made in taking Born-Rutherford formula is obviously [*vide* (8) and (10)]

$$D_1 \,.\, D_2 \qquad \ldots \quad (12)$$

where D_1 and D_2, the corrections for relative motion and critical approach respectively, are given by

$$D_1 = \frac{4}{9}\cdot\frac{\operatorname{cosec}^4 \frac{1}{2}\theta}{\operatorname{cosec}^4\{\frac{1}{2}\theta + \frac{1}{2}\sin^{-1}(\frac{1}{2}\sin\theta)\}}\cdot\frac{1}{\cos\theta + \dfrac{1 + \frac{1}{2}\cos 2\theta}{\sqrt{1 - \frac{1}{4}\sin^2\theta}}} \qquad \ldots \quad (12{\cdot}1)$$

and

$$D_2 = \frac{\quad}{\cos^2 k' r_0} \tag{12·2}$$

in which k' and r_0 are given in (10·1) and (10·2). In columns (4) and (5) of Table I we give the values of D_1 and corrected I/I_0 for different angles of scattering. It should be noted that D_1 is independent of the incident velocity. The experimental values of Heydenburg and Roberts (*l.c.*) are given in column 3. It is evident that the correction is quite appreciable at large angles. The second correction D_2 for the critical approach varies from 5.95×10^2 at 20° to 2.29 at 75° for incident velocity 880 k.v. Thus it follows that at 20° Rutherford's formula gives a value (as $D_1 \sim 1$) 5.95×10^2 times greater than that given by (10).

TABLE I

Incident Volt	Angles of Scattering	$\dfrac{I\text{ (obs.)}}{I_0\text{ (Rutherford)}}$	D_1	$\dfrac{I\text{ (obs.)}}{I_0\text{ (corrected)}}$
880 k.v.	20	0.95 ± .006	1.002	0.952 ± .006
	25	1.08 ± .02	1.0025	1.083 ± .02
	30	1.25 ± .03	1.003	1.254 ± .03
	35	1.42 ± .03	1.004	1.426 ± .03
	40	1.49 ± .04	1.006	1.499 ± .04
	45	1.75 ± .05	1.009	1.766 ± .05
	55	2.44 ± .09	1.021	2.499 ± .05
	65	3.07 ± .15	1.043	3.202 ± .15
	75	4.37 ± .35	1.077	4.707 ± .35

It may be mentioned that if as in the previous cases the idea of taking the bounded solution be given up, the correction D_2 is dropped out and so formula (10) gives for the intensity nearly same values as are obtained from Rutherford's formula (*vide* Table I). However, it should be remembered that the bounded solution was found necessary in explaining electron scattering by atoms. Now it is evident from the last column in Table I that the ratio obtained is too high to be explained by the existence of Coulomb force alone. Let us, therefore, assume tentatively that there is in addition a short range attractive force having radial symmetry as in neutron-proton interaction. Now, because the effect of exchange need not be considered unlike the case of interaction between two similar particles, we find from (5), without taking bounded solution,

$$\frac{I}{I_0} \quad \frac{\mathrm{cosec}^4 \quad - 4\dfrac{\mu v^4}{zz'e^2}\, g\, \mathrm{cosec}^4 \quad \cos k' r_0 + 4\left(\dfrac{\mu v^2}{zz'e}\right.}{\mathrm{cosec}^4} \tag{13}$$

where I_0 is the intensity for Coulomb force only, ϕ is given in (6.6) and g has the same meaning as in (1) and (2). As in the present case $\mu=\frac{2}{3}m_1$ and $z=1$, $z'=2$, we have from (13), on substituting for k' and r_0 from (5·1) and (5·2),

$$\frac{I}{I_0}=\frac{\operatorname{cosec}^4\tfrac{1}{2}\phi-\frac{4}{3}\frac{m_1v^2}{e^2}g\operatorname{cosec}^2\tfrac{1}{2}\phi\cos\left\{1.35\times\frac{8\pi e^2}{hv}\left(1+\sin\frac{\phi}{2}\right)\right\}+\frac{4}{9}\left(\frac{m_1v^2}{e^2}g\right)^2}{\operatorname{cosec}^4\tfrac{1}{2}\phi}\qquad\ldots\quad(13\cdot1)$$

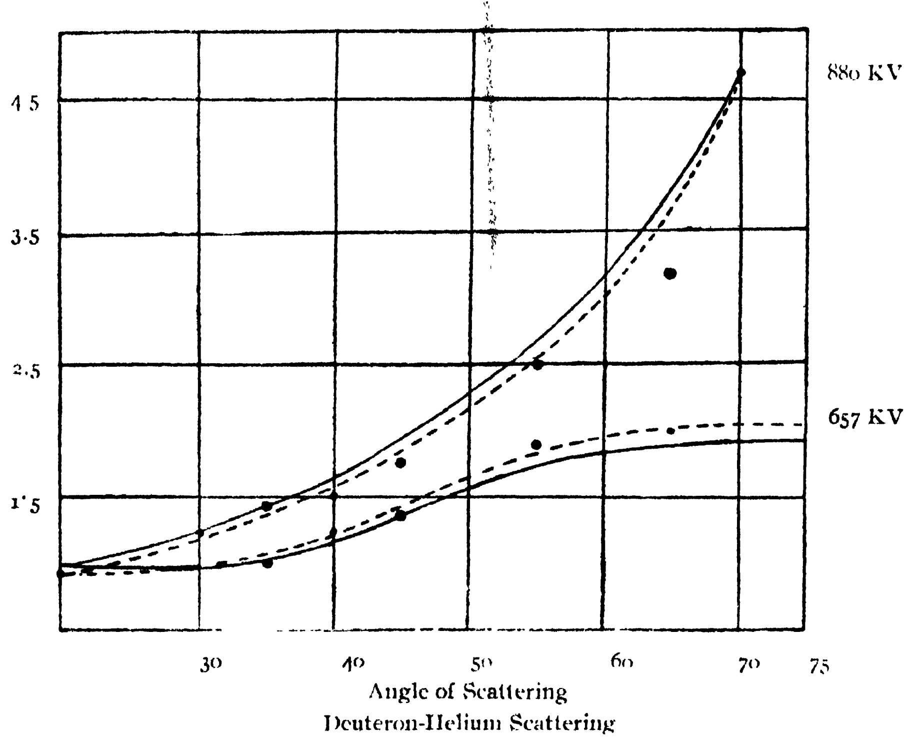

FIGURE 3

The theoretical values for different angles of scattering and for incident velocities 880 k.v. and 657 k.v. are obtained from (13.1), and the curves are drawn continuous in Fig. 3. The corresponding corrected experimental values (*vide* Table I, Column 5 for 880 k.v.) are given by the dotted curves. The agreement, it appears, is fairly satisfactory. The value of g used in the theoretical calculation is 2.701×10^{-13}. It is its fitting value at 75° for incident velocity 880 k.v.

D. Proton-Helium Scattering

In the case of scattering of proton by helium we have $m_2=4m_1$ and so $\mu=\frac{4}{5}m_1$ and $z=1$, $z'=2$. On substituting these values, the intensity and the critical approach are readily obtained from (7) and (7.2). The correction for the relative motion is also easily obtained, and we have

$$D_1 = \frac{16}{25} \cdot \frac{\operatorname{cosec}^4 \frac{1}{2}\theta}{\operatorname{cosec}^4 \{\frac{1}{2}\theta + \frac{1}{2}\sin^{-1}(\frac{1}{4}\sin\theta)\}} \cdot \frac{1}{\frac{1}{2}\cos\theta + \dfrac{1 + \frac{1}{16}\cos 2\theta}{\sqrt{1 - \frac{1}{16}\sin^2\theta}}} \cdot \qquad \ldots \quad (14)$$

From the above we find that for $\theta = 45°$, $D_1 = 1.001$. Thus the correction is negligible at least up to 45°. Consequently, Rutherford's formula (7) (after dropping the factor $\cos k'r_0$ for reasons explained before) should agree up to 45° angle of scattering. This is also supported by Heydenburg and Roberts (*l.c.*) who find that for angles of scattering between 20° and 45°, their observed intensities are very nearly equal to those given by Rutherford's formula. However, it should be noted that in using Rutherford's formula it is implicitly assumed that between proton and helium there is no short range force as in neutron-proton interaction. It is rather difficult to support this assumption in view of the fact that in all the previous cases we have already assumed the existence of such a force.

It appears to me that the above difficulties cannot be removed unless the question of bounded solution is settled. Further, we have supposed the short range force to be spherically symmetrical even for deuteron and helium. But for such complicated nuclei the force should have some axial symmetry. Attempts to improve upon the present theory on these lines will be made in future.

PHYSICAL LABORATORY,
PRESIDENCY COLLEGE, CALCUTTA.

REFERENCES

[1] K. C. Kar and D. Basu, *Phil. Mag.*, **29**, 200 (1940).

[2] K. C. Kar and D. Basu, *Phil. Mag*, **27**, 76 (1939).

[3] N. P. Heydenburg, M. A. Tuve and L. R Hafstad, *Phys. Rev.*, **50**, 806 (1936).

[4] N. P. Heydenburg, M. A. Tuve and L. R. Hafstad *Phys Rev*, **56**, 1078 (1939).

[5] N. P. Heydenburg and R. B. Roberts, *Phys. Rev.*, **56**, 1092 (1939).

[6] K. C. Kar, M. Ghosh and K. K. Mukherjee, *Phil. Mag*, **24**, 964 (1937); K. C. Kar, *ibid*, **24**, 971 (1937).

CIRCUMZENITHAL ARC TANGENTIAL TO A CORONA OF 46°

By S. B. L. MATHUR
Physics Department, Lucknow University

(*Received for publication, January 30, 1941*)

INTRODUCTION

The object of the present paper is, primarily, to describe a rather unusual optico-meteorological phenomenon, and, secondarily, to offer a probable explanation. It must, however, be made clear that, as no measuring instruments of any type were available at the time of the occurrence of the phenomenon, accurate observations could not be taken. The explanation here offered is, therefore, merely a qualitative one.

DESCRIPTION OF THE PHENOMENON

The phenomenon was noticed by the author, at Lucknow, on the 9th of September, 1939, between 4-45 p.m. and 5-5 p.m. It must, however, have been in existence sometime earlier than 4-45 p.m as another observer, Mr. Rahat Husain Rizavi, then a student of the B.Sc. class in this University, who very kindly lent to the author his notes taken at the moment of observation, recorded 4-20 p.m. as the time when he noticed the phenomenon.

It had rained earlier in the afternoon ; and the sky, which was full of cirro-cumulus clouds around the zenith and of a stretch of dark cloud, probably of the cumulo-nimbus type, in the west and in the south, was just clearing. The author is not quite sure of the exact variety of that cloud as the formation was rather complex. He, however, later on learnt from a meteorologist that there were widespread thunderstorms in the west United Provinces on that date. Hence it is concluded that in the complex formation there must have been a good deal of cirrus spreading from the top of cumulo-nimbus clouds.

Some distance down the zenith towards the west there was, what appeared to the eye, a brightly coloured arc with its centre at the zenith and curvature convex towards the sun (arc no. 1). The red or orange hue, which was outermost, *viz.*, towards the sun, was followed by yellowish green and then greenish blue in the interior. The length was short—about one quadrant ; and the plane

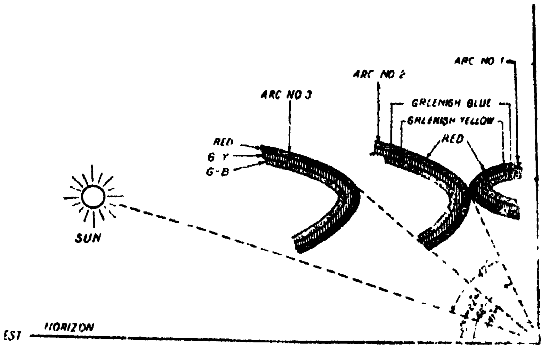

of the arc seemed to be horizontal—at any rate it was not sharply inclined to the horizontal with the summit higher than the ends.

Tangential to the above arc was another (arc no. 2). But this was concave to the sun with the red or orange hue outermost, *viz.*, away from the luminary, followed by yellowish green and then greenish blue in the interior. The reds of the two arcs overlapped each other at the summit thus forming a tangency. The hues were less bright, but the radius and length were much greater than those of the first arc.

Further down the west, there was a third arc with a still bigger length but so faint as to be seen with difficulty. The sequence of hues was the same as in arc no. 2.

One had to face the sun in the west to see the three arcs.

The author saw the phenomenon from a small courtyard measuring 15′ by 13′. Unfortunately, as no measuring instruments of any type were available at the moment the author had to content himself with recording the sequence of hues and fixing in his mind, as well as he could, the position of the three arcs in the sky with the help of the various details in the courtyard hoping to make angular measurements with the aid of stars occupying analogous altitudes later on. In the absence of instruments it was fortunate that the courtyard was rather small as the position of the arcs could be better fixed in it than in an open space where no reference points would have been available. But, the rainy season being not quite over, it took quite a long interval of time before the sky was found to be clear at nights and any stars were found to occupy analogous altitudes. However, observations were made on various dates and at different times of the night. But it is obvious that, as our eyes are not trained to judge angular distances in the region of the zenith and as measurements taken long after the event are liable to be vitiated for faults of the memory, the data collected cannot be expected to have any great accuracy. The following observations will show for themselves the extent to which they may be relied on.

MEASUREMENTS

The altitude of the sun at 4-45 p.m. on the 9th of September, 1939, was kindly calculated for the author by Prof. J. A. Strang, Head of the Mathematics Department, Lucknow University, as nearly 19 degrees.

The following table is given to show roughly the position of the three arcs in the sky. The angles were measured with a sextant.

Observations for the altitude of the									
Tangential arcs (1 & 2) at the place of contact					Arc no. 3				
	Date	Time	Name of the star	Altitude		Date	Time	Name of the star	Altitude
1	8.10.39	8-30 p m.	α-Delphinus	74°	1	5.11 39	8-0 p.m.	α-Aquilae	45°
2	8.10.39	8-31 p.m.	α-Aquilae	60°	2	11.11.39	4 20 a.m.	β-Orion	34°
3	5.11 39	10-40 p.m.	γ-Pegasus	70°	3	11.11.39	7-35 p.m.	α-Aquilae	45°
4	6.11.39	3-15 a m.	α-Taurus	67°	4	13 11.39	5-50 a m.	α-Orion	42°
5	6.11.39	6-40 p.m.	α-Aquilae	60°	5	21.11 39	7-25 p.m.	α-Aquilae	37°
6	8.11.39	9-55 p. m	α-Pegasus	62°					
7	11.11 39	5-5 p m.	γ-Gemini	67°					
			Mean	66°				Mean	41°

It will thus appear that, roughly, the distance of the arcs 1 & 2 from the sun was (66° – 19°) *viz.*, 47° and that of arc no. 3 was (41° – 19°) *viz.*, 22°.

DISCUSSION

It is obvious that, as the above observations were, at the best, very rough, they can scarcely serve as the basis of any conclusions. The author is, however, sure of the accuracy of his observations as regards the sequence of hues in the arcs as he took notes about this at the time of the occurrence of the phenomenon. As a matter of fact, the sequence of hues was the only aspect of the phenomenon about which he could be sure. Further, when difficulties were found in explaining the event, the author had the good fortune of having his observations in this respect corroborated by the independent evidence of Mr. Rizavi, who saw the phenomenon from a place about 3 miles to the north and recorded his observations at the time of the occurrence. Mr. Rizavi did not see arc no. 3 which at 4-45 p.m. was found to be very faint by the author. The explanation here offered is, therefore, entirely based on the sequence of the hues in the arcs.

(1) *Arc no. 1*

At first the author thought that the arc no. 1 was a rainbow of the 3rd or the 4th order, as it was visible on the same side as the sun. From the simple relations

$$\cos i = \sqrt{\frac{\mu^2 - 1}{n^2 + 2n}}$$

and

$$D = 2(i - r) + n(\pi - 2r)$$

it is easy to calculate that for the red H-line $\lambda = 6562.9$ A°, μ being equal to 1.3311, the angle D, of deviation, for $n = 3$ and $n = 4$ are $(2\pi - 42^\circ\ 30')$ and $(3\pi - 137^\circ\ 10')$ respectively. The deviated red rays will, therefore, make angles of 42°30′ and 42°50′ with the horizontal for the tertiary and quarternary rainbows respectively. Since the sequence of hues in the tertiary is the same as that in the primary, *viz.*, red outermost, the arc should be a tertiary rainbow. Further, the section made by the screen of water drops of the cone formed round the line joining the sun with the observer and having an angle of 42½° will be convex to the luminary—just the type of curvature found in the arc.

But there were two main reasons which went against the view that the arc was a rainbow. Firstly, the intensity of the hues was so strong as to be comparable to a primary bow, whereas, in a tertiary, the intensity should be extremely small. Indeed, although cases are on record when, under exceptionally favourable circumstances, tertiary, or even quarternary, rainbows have been seen,[1] some authors go so far as to say that "rainbows of order higher than the second are not to be seen in nature."[2] Secondly, the centre of the bow must lie on the line joining the observer to the sun so that the plane of the bow must be steeply inclined to the horizontal. The author is quite definite that the arc seemed to lie more or less in a horizontal plane and had its centre at, or near, the zenith.

As the arc was convex to the sun, the former could not have been a halo or a corona. But, all indications point to the conclusion that it was a circumzenithal arc.

A circumzenithal arc is an arc of 90°, having its centre at the zenith, and is seen at some 46°, or a little more, above the sun. It is said that it lasts only a few minutes, but during this time it is often so brilliantly coloured—red on the outside to violet inclusive—as to be mistaken for an exceptionally bright rainbow. It occurs most frequently when the altitude of the sun is about 20° and at times when the parhelia of 22° are conspicuous.

It will thus be seen that, apart from the absence of parhelia, the description of the circumzenithal arc tallies in all essential details so well with what was actually observed that one feels almost certain that arc no. 1 was a circumzenithal one. The presence of cirro-cumulus clouds, thus ensuring the existence of ice crystals necessary for the production of the arc, the inclination of 47° of the arc with the sun, the intensity and the sequence of the hues and, finally, the location of the centre at the zenith—all point to the same conclusion. Incidentally, it will be seen that the mean of the various values found for the distance of the arc from the sun, *viz*., 47°, appears to be wonderfully near the mark—a strange coincidence.

In passing, it may be added that circumzenithal arcs are formed when the principal axes of a large portion of ice crystals are practically vertical, *i.e.*, when the snow crystals are largely columnar with tabular caps, or more likely, perhaps, merely tabular. They have been explained by Bravais [3] as being due to refraction of light through snow crystals in still or steadily flowing air, when the crystals keep their principal axes substantially vertical. Since they are formed at an angle of 46° with the sun, they will be tangential to the 46° halo, if the latter also occurs at the time.

(2) *Arcs nos. 2 & 3*

Since arc no. 1 has been established to be a circumzenithal arc at a distance of 47° from the sun, the radius of the concave arc no. 2 must be 47°. This fact emerges from the observation that the two arcs were tangential to each other at the summit and is apart from the measurements which are, by no means, to be considered as accurate. The measurements, however, happen to confirm this conclusion, and one feels inclined to believe that the measurements made on the 3rd arc may not be very incorrect.

Arcs round the sun at angles of 46° and, presumably, 22° occurring in the presence of cirro-cumulus clouds have every chance of being the well-known halos of 46° and 22°. However, the colour sequence, *viz.*, red outermost, is definitely of the type that occurs mainly in diffraction and not in refraction phenomena. Further, it is well-known that, of the two, the 22° halo is the more intense, whereas the opposite was found to be the case—the arc nearer to the sun being scarcely visible. It is true that diffraction also may play a rôle in the formation of halos. Visser [4] has taken diffraction into account in an attempt to explain better the features of a halo, but, even then, the red hue occurs at the inner edge and not at the outer.

Hence, unless there is some particular process of refraction of light from snow crystals, which is hitherto not known, and, which produces halos of 46° and also of about 22°, with the colour sequence reversed, the arcs in question will have to be classed as coronas. On the other hand, coronas with such well-defined rings of large angles like 46° have never been known to occur. The only instance of large-radii corona known is that of Bishop's rings which were observed in 1883, and again in 1903, after the eruptions of Krakatoa and Mt. Pelee respectively, and had a radius of only 22° for the red hue. Iridescent clouds, which Simpson[5] and Brooks[6] hold to be portions of coronas, and are produced by the diffraction of light by water drops, have been found by the latter to occur at even 60° from the sun. But, the author did not notice any colour patches of which the arcs 2 and 3 could be considered as end fringes.

It will, perhaps, be of interest to derive the size of the diffracting particles for rings of size 46° and 22° respectively. As the intensity of the 46° arc was greater than that of the 22° one, it would be reasonable to postulate that the former was not merely a higher order corona of the latter. Hence, there must have been diffracting bodies of two different sizes present in the atmosphere.

Using the simple relation $\theta=\lambda/2a$ the size of the drops responsible for the 22° corona would be $1{\cdot}9\ \mu$ and of those producing the 46° one would be $0{\cdot}9\ \mu$. It will thus appear that the size of the diffracting body is about the same as that of the light waves themselves. It must, however, be said that the relation between the radius of the corona and the size of the diffracting body has not yet been satisfactorily worked out in the case of very small water drops

The author would like to thank Prof. J. A. Strang of the Lucknow University for kindly calculating the altitude of the sun, Mr. Rahat Husain Rizavi, B.Sc., for placing his records at the disposal of the author thus enabling him to confirm his observations about the colour sequence of the arcs at the time when he began to doubt their correctness, and Mr. R. K. Joardar, B.Sc., for drawing the diagram for this paper. A few other gentlemen also helped the author with their verbal reports, but, as they had not made any accurate records, their evidence was not of much value beyond corroborating some of the features of the two tangential arcs.

SUMMARY

A remarkable optico-meteorological phenomenon was seen in Lucknow on the 9th of September, 1939, between roughly 4 and 5 p.m. Although no measurements could be taken at the time, the author, from considerations of the intensity of the hues and their sequence in the two tangential arcs in the sky, concludes that he saw a circumzenithal arc tangential to a corona of 46°. Further, he found another arc further down in the west which was probably another corona of 22°. Although coronas of such large radii have not been known and radii of 46° and 22° are strongly suggestive of the well-known halos of those angles, the sequence of the hues is definitely in favour of two of the arcs being coronas and not halos. If the conclusions drawn are correct, this paper gives the first record of a circumzenithal arc being tangential to a corona and of the possibility of coronas of large sizes like 46°.

PHYSICS DEPARTMENT,
LUCKNOW UNIVERSITY.

REFERENCES

[1] Houston, *Treatise on Light,* 114 (1928); J. Neff Huyette, *Monthly Weather Review,* **32**, 325-6 (1904); Farwell, *Science,* **40**, 595 (1914).

[2] Glazebrook, *Dictionary of Applied Physics,* **3**, 526 (1923).

[3] Bravais, *Memoirs sur less halos, Journal de l' Ecole polytechnique,* 31 me cahier.

[4] Visser, *K Akad. Amsterdam Proc.,* **19** (1917), 1174-1196, **21** (1918), parts 1 & 2, 119-24.

[5] Simpson, *Quarterly J. Royal Met. Soc.,* **3[illegible]**, 291 (1912).

[6] Brooks, *Monthly Weather Review,* **53**, 49-58 (1925).

ON THE RADIAL LIMITATION OF THE SOLAR MAGNETIC FIELD

By BIBHA MAJUMDAR, M.A.

(*Received for publication, November 18, 1940*)

ABSTRACT. The Drift current, Dynamo and Diamagnetic theories of the radial limitation of the general magnetic field of the sun are discussed in the light of the present knowledge of Physics. In the first article a summary is given of the mathematical results, obtained in a previous paper of the authoress, for the behaviour of an electron in electric, magnetic and gravitational fields. In the second article the results are applied to analyse the drift current and dynamo theories of the radial limitation in a solar atmosphere of isothermal equilibrium under gravity. In the third article the diamagnetic theory of this limitation has been developed, the diamagnetism being now induced, not by the classical method of Schrödinger, but by the quantisation in the motion of the electrons in the magnetic field. It is concluded that according to none of these theories the magnetic field can be radially limited to the extent as found from the observations of Hale in 1913. Similar conclusions seem to follow from a study of the polarisation of non-uniform rotation of the sun in its magnetic field.

INTRODUCTION

One of the greatest triumphs of the application of the spectroscopic methods to Astrophysics is the discovery of the magnetic field of the sun. The study of the polarisation of the doublets of the absorption lines in sun-spots and its comparison with that of Zeeman effect led Hale,[1] in 1908, to the discovery of strong magnetic field of the sun-spots, the intensity of which in the case of large spots amounts to even as large as 4000 Gauss. The discovery gave a stimulus for the search of a general magnetic field of the sun and thanks to the untiring perseverance of Hale and his collaborators in Mount Wilson Observatory, who at last announced in 1913 that the sun possessed a general magnetic field much like that of the earth with the following principal properties:

(*i*) The magnetic axis of the sun, like that of the earth, was found to be not coincident with the axis of rotation but situated at a distance of 4° from it and revolving round it in a period of 31.5 days.

(*ii*) The magnetic field, though similar in some respects to that of a uniformly magnetised sphere, showed distinct deviations from it in the distribution of intensity with respect of latitude. Taking the sun to be a uniformly magnetised sphere, the polar intensity of the field has been estimated from the observations as derived from two different latitude zones (-10° to $+10^\circ$) and $\pm$ (10° to 45°) and the estimates are found to be very different, that from the equatorial regions being 1.84 times as great as that from higher latitude zones.

(*iii*) The magnetic field intensity was found to decrease rapidly outwards in the radial direction falling from 150 Gauss (after the correction of Rosseland) to an amount (perhaps 30 Gauss) too small to be measured between the base and top of the reversing layer. The decrease was estimated to take place in a height of about 300 Km.

Different theories have been put forward by Chapman[2] and Gunn[3] to explain the cause of the radial limitation of solar magnetic field. The methods of both are based on a consideration of the motions of the charged particles that exist in the solar atmosphere under the action of magnetic, electric and gravitational fields of the sun. In general, when a charged particle on the surface of the sun is subject to a horizontal and south to north magnetic field, the vertically downward gravitational field and the vertical electric (upwards for ions and downwards for electrons according to Pannekoek-Rosselands' Theory) field of the sun, as is really the case at the equator, it would describe a cycloidal path in a plane at right angles to the meridian plane together with its motion along the horizontal magnetic field. The motion may therefore be resolved into two parts: a translational motion which is in a direction perpendicular to both the fields and motion in a helix with its axis of spiralling along the magnetic field of the sun. The first part is known as drift current and has been considered in details by Chapman. He shows that, as a result of this drift, the charges of opposite signs separate out in opposite directions resulting in a net eastward current in the solar atmosphere which reduces the magnetic field rapidly outwards along the radius. According to Gunn, however, the limitation is brought about by the second part of the motion, namely the spiralling of the electrons round the magnetic field, which, he showed, would produce diamagnetism in the solar atmosphere and reduce the field in the required manner. Gunn's method is based on an idea which has been used by Schrödinger to explain the diamagnetism in metals. The electrons in a metal under the action of a magnetic field describe circular arcs in their free paths due to Lorentz force and this produces diamagnetism, as, according to classical electrodynamics, the electrons describing circles are equivalent to magnetic doublets whose axes are in a direction opposed to the applied magnetic force.

Though the results of Chapman and Gunn agreed fairly well with the observations of Hale, it was shown later on by Cowling[4] in two consecutive papers that such an agreement was really spurious. He showed that none of these explanations was tenable in an atmosphere of thermodynamic equilibrium, the effects of Chapman and Gunn when properly considered being cancelled out. Because of this failure Ferraro[5] made a fresh investigation of formulating the 'Dynamo' theory of the radial limitation. In this theory the eastward current, necessary for the limitation, is produced by the motion of the Sun's atmosphere in meridian planes across the radial component of the magnetic field, the motion being, as suggested by Bjerknes, from the poles to the equator with a back poleward current beneath. The theory was already considered by Chapman but the effect produced by this way was shown by him to be quite negligible. But Ferraro's investigation showed that an appreciable limitation of the field could be obtained if the mean velocity of the atmosphere along the meridian corresponded to the motion of sun-spots from latitude 45° to the equator in 11 years. It was supposed that such a motion of the solar atmosphere might result from the unequal heating of the poles and the equator but a calculation of Eddington[6] showed that velocity for this cause was far too small to be of importance.

Thus we find ourselves faced with a dilemma. The failure of the attempts to explain the radial limitation of the general magnetic field of the sun tends us to suspect the genuineness of the observational evidence for its existence.[7] Before we can definitely question about the existence of such a limitation it is desirable that a fresh theoretical investigation along the line of present developments in physics should be made to clarify the present position. It should be mentioned that there are some obscurities in Cowling's method of calculation. Further we know today that the diamagnetic effect considered by Gunn after Schrödinger's method is really spurious. It has been shown by Landau[8] and Darwin[9] that under the action of a magnetic field the motion of the electrons is no more continuous but descrete, or quantised as it is called and the change in energy induced by this quantisation is responsible for the observed diamagnetism in metals. The whole problem therefore requires a thorough revision on a more rigorous mathematical basis incorporating into it the new outlook about the behaviour of the electrons in a magnetic field. This will be attempted in the present paper. In the first part we shall summarise the mathematical results for the behaviour of an electron in electric, magnetic and gravitational fields. In the second part we discuss the results of Chapman in the light of our present theory. In the third part we develope the diamagnetic theory as the cause of the radial limitation, the diamagnetism being induced, as mentioned above, by the quantisation of the motion of the electrons in the magnetic field.

EXPRESSION FOR THE CURRENT DENSITY[10]

The current density, $\vec{I}$, *i.e.*, the total charge passing through unit area in unit time is defined by

$$\vec{I} = 2e\iiint \vec{v}\, f_1 d\kappa_x d\kappa_y d\kappa \qquad \ldots \quad (1)$$

where f_1, the change in the distribution function of the electron due to resultant action of the electric and magnetic fields on the one hand and the interaction between electrons and ions on the other hand is given by

$$f = f_0 + f_1 \qquad \dots \quad (2)$$

f and f_0 being the Fermi distribution functions in the presence and absence of the fields respectively.

f_1 is determined from the usual Maxwell-Boltzmann's equation

$$\frac{\partial f}{\partial t} + \frac{h}{m}\left(\vec{\kappa}\ \mathrm{grad}_{\vec{r}}\, f\right) + \frac{1}{h}\left(\vec{F}\ \mathrm{grad}_{\vec{k}}\, f\right) = -\frac{f_1}{\tau} \qquad \dots \quad (3)$$

$\vec{F}$ being the total Lorentz force acting on the electron.

Thus
$$\vec{F} = \vec{X} + \frac{e}{c}\left[\vec{v}\ \vec{H}\right] \qquad \dots \quad (4)$$

where the first term X includes all the forces, electrical, electrostatic, gravitational, etc., and the second one gives the force due to the magnetic field $\vec{H}$. $\vec{\kappa}$ is the wave vector, $\vec{v}$ is the velocity of the electron and τ is the time of relaxation.

Solving equation (3) for f_1 and substituting its value so obtained in (1) we obtain after some simplifications

$$I = KV + L\left[\vec{V}\ \vec{\omega}_L\right] + M\,\omega_L\left(\vec{\omega}_L\ \vec{V}\right) \qquad \dots \quad (5)$$

where
$$K = -\frac{2eh^2}{3m^2}\iiint \frac{\tau\dfrac{\partial f_0}{\partial \epsilon}\kappa^2 d\kappa_x d\kappa_y d\kappa_z}{1+\tau^2\omega_L^2} \qquad \dots \quad (6)$$

$$L = -\frac{2eh^2}{3m^2}\iiint \frac{\tau^2\dfrac{\partial f_0}{\partial \epsilon}\kappa^2 d\kappa_x d\kappa_y d\kappa_z}{1+\tau^2\omega_L^2} \qquad \dots \quad (7)$$

$$M = -\frac{2eh^2}{3m^2}\iiint \frac{\tau^3\dfrac{\partial f_0}{\partial \epsilon}\kappa^2 d\kappa_x d\kappa_y d\kappa_z}{1+\tau^2\omega_L^2} \qquad \dots \quad (8)$$

$$\vec{V} = \vec{X} - \frac{kT}{A}\ \mathrm{grad}_{r}\,A \qquad \dots \quad (9)$$

$$A = \frac{nh^3}{2(2\pi mkT)^{\frac{3}{2}}},\quad \omega_L = \frac{eH}{mc} \qquad \dots \quad (10)$$

n being the number of electrons per unit volume.

Before we discuss the theories of the limitation some remarks regarding the approximations to be used in our mathematical calculations for the evaluation of the integrals occurring in the current expression are necessary. It is to be particularly noted that the integrals (6), (7) and (8) can only be evaluated in the two limiting cases, namely when the electrons are or are not free to spiral between two collisions,

i.e., (*i*) $\tau\omega_L >> 1, \quad H >> H_0$ ... (11)

or (*ii*) $\tau\omega_L << 1, \quad H << H_0,$ ... (12)

H_0 being a limiting magnetic field defined by

$$H_0 = \frac{mc}{c\bar{\tau}}, \qquad \ldots (13)$$

where

$$\bar{\tau} = 1{,}89 \frac{T^{\frac{3}{2}}}{z^2 n^+ \bar{J}} \qquad \ldots (14)$$

$$\bar{J} = \log\ (t+1) - \frac{t}{t+1} \qquad \ldots (15)$$

$$t = 3{\cdot}3 \times 10^{13} \frac{T^2}{n'} \qquad \ldots (16)$$

and z = number of free electrons per atom, n' = number of ions per unit volume.

We have calculated in the following table the values of H_0 at the base and the top of the reversing layer. It shows that the spiralling of the electrons has already begun to be prominent even at the base of the reversing layer. We shall therefore use the approximation (11) in our present calculations. We have also added in the table the conductivities σ_1 and σ_2 ; σ_1 is the conductivity in the radial direction and σ_2 the conductivity in a direction at right angles to the meridian plane, which we call the transverse conductivity.

n^+ in c.c.	T in °K	H in Gauss	H_0 in Gauss	σ_1 in E.S.U.	σ_2 in E.S.U.
5×10^{13}	5500	150	56·6	$6{\cdot}1 \times 10^{12}$	$4{\cdot}8 \times 10^{12}$
$2{\cdot}5 \times 10^{12}$	5500	30	3·4	$4{\cdot}6 \times 10^{11}$	$1{\cdot}2 \times 10^{12}$

The first set of values corresponds roughly to conditions at the base of the reversing layer, whereas the second set gives the values at a height of 300 km. We have assumed thereby that the gas is singly ionised, *i.e.*, $z = 1$.

DRIFT CURRENT AND DYNAMO THEORIES OF RADIAL LIMITATION

Drift Current Theory: We specialise the problem. We take the current layer at the equator. The gas is assumed to be in isothermal equilibrium under gravity, the density changing exponentially with the height. If X-axis be taken vertically upwards and the Z-axis horizontal in the south-north direction, the Y-axis will be horizontal and eastward. The electric and magnetic fields will vary along the X-axis. We obtain the current in Y-direction, *i.e.*, the drift current as

$$I_y = -L\left(X - \frac{kT}{A}\,\frac{\partial A}{\partial x}\right)\omega_t \qquad \ldots \quad (17)$$

or we obtain

$$I_y = -\frac{LeH}{mc}\left(X - \frac{kT}{n}\,\frac{\partial n}{\partial x}\right) \qquad \ldots \quad (18)$$

where L is given by (7).

In X we must include, as mentioned before, gravitational as well as a vertical eloctrostatic field which is set up by the tendency of the light electrons to spread out farther in the vertical direction than the heavier ions; the drift due to electric field, as is evident from (18) and (7), being the same for the ion and the electron, no electric current will be produced and hence we shall leave this out of account from our present discussion. The electrostatic field developed on the sun's surface has been discussed by Pannekoek, Rosseland and Milne; it is of the order of 4370 Volts. The electrostatic field will be such that

$$eE = \tfrac{1}{2}(m_i - m_e)g. \qquad \ldots \quad (19)$$

This is upward on the positive ion, and downward on the electron; hence

$$X = -m_e g - \tfrac{1}{2}(m_i - m_e)g = -\tfrac{1}{2}(m_i + m_e)g. \qquad \ldots \quad (20)$$

The same force will also be acting on the ion.

(I) Now in the case of homogeneous atmosphere in which density is constant the expression (18) is reduced to

$$I_v = \frac{LeH}{2mc}(m_i + m_e)g \qquad \ldots \quad (21)$$

and further taking the time of relaxation to be constant, we obtain from (21) and (7), by putting

$$\tau = \frac{l}{v}, \quad R = \frac{mvc}{eH} \qquad \ldots \quad (22)$$

where l = mean free path and R is the radius of the spiralling,

$$I_y = \frac{l^2}{l^2 + R^2}\cdot\frac{nc}{2H}(m_i + m_e)g \qquad \ldots \quad (23)$$

which is exactly the Chapman's expression.

(II) But when the atmosphere is not homogeneous, we have

$$n^{+} = n = n_0 e^{-\frac{(m_i + m_e)}{2kT} gx} \qquad (24)$$

where n_0 is the number of particles at the base of the reversing layer.

Thus from (18), (20) and (24) we obtain $I_y = 0$, that is, there is no current in the eastward direction. Thus we see clearly that Chapman's drift current in eastward direction is completely masked by westward current produced by the inhomogeneity of the gas. Drift current theory therefore fails to give any limitation of the solar magnetic field.

Dynamo Theory : In Dynamo theory, as already mentioned, the requisite eastward current is produced by the motion of the gas in the solar atmosphere from pole to the equator in the meridian plane across the radial component (though very small, indeed) of the sun's magnetic field. The eastward current due to induced electromotive force is therefore given by

$$r_2{}^{v} H_r = {}^{r_2}v.{}^{r_0} H_\theta \cot\theta \qquad \ldots \quad (25)$$

where we have taken after Ferraro[5]

$$H_r = \frac{r_0}{r} H_\theta \cot\theta \qquad (26)$$

which is correct at least in order of magnitude and where θ is the colatitude of the region, r_0 is given by (29), v is the velocity of the gas in the meridian plane, H_r, H_θ are the radial and horizontal components of the field and σ_2 is the transverse conductivity.

Now since

$$\cdot \frac{c}{4\pi} \frac{\partial H_\theta}{\partial r} \qquad (27)$$

we obtain by neglecting the variation of r compared with a, the radius of the sun,

$$H_\theta = H_0 e^{-\frac{r}{r_0}}, \qquad (28)$$

where

$$r_0 = \left(\frac{ac^2 \tan\theta}{4\pi\sigma_2 v} \right)^{\frac{1}{2}} \qquad (29)$$

We now take $\theta \sim 45°$ and assume that the motion of the solar atmosphere in the meridian planes to be due to the unequal heating of the sun at the poles and the equator owing to the solar rotation. In this case the velocity v comes out of the order of 10^{-3} cm./sec. as shown by Eddington. Substituting these values of θ

and v and taking σ_2 from the table given before we find that the Dynamo theory becomes quite inadequate to explain the required limitation as observed.

REVISED DIAMAGNETIC THEORY OF RADIAL LIMITATION

Following the methods of Landau, Darwin, Peirls and others it can be proved that the motion of the electrons of an ionised atmosphere in the presence of a magnetic field becomes quantised and it is this quantisation which renders the medium diamagnetic, that is, equivalent to a distribution of intensity of magnetisation directed opposite to the original magnetic field at each point. As this quantisation effect is entirely a quantum mechanical phenomenon having no analogy in classical physics and the deduction of the formula for the intensity of magnetisation is fundamentally different from that of Schrödinger and Gunn, we prefer to give first a short derivation of the formula. The quantisation is due to the fact that the circular motion of the electron in a plane at right angles to the direction of the impressed magnetic field can be resolved into two harmonic motions vibrating at right angles, which can take up only descrete energy values in quantum mechanics.

Let the magnetic field H be parallel to the Z-axis. Then the motion of the electron will be composed of two parts—one linear along the Z-axis and the other circular, hence quantised, in the plane XY. The energy will, therefore, be given by

$$\epsilon = \epsilon_{trans} + \epsilon_{long} = (2n+1)\mu H + \frac{h^2 \kappa_z^2}{2m}, \qquad \ldots \quad (30)$$

where μ is the Bohr magneton $= \dfrac{eh}{4\pi mc}$ ... (31)

and n the quantum number.

To find the magnetism we must first calculate the energy of the system. Following the usual method of statistical mechanics, we have

$$N = \frac{2V}{h^3} \iiint f\, dp_x\, dp_y\, dp_z = 2V \iiint f\, d\kappa_x\, d\kappa_y\, d\kappa_z \qquad \ldots \quad (32)$$

with the transformations $\kappa_x = \kappa \cos \alpha$, $\kappa_y = \kappa \sin \alpha$,

we have
$$N = 4\pi V \iint f \kappa\, d\kappa\, d\kappa_z\,. \qquad \ldots \quad (33)$$

Now
$$\int \kappa\, d\kappa = \tfrac{1}{2}(\kappa_{n+1}^2 - \kappa_n^2) = \frac{2m\mu H}{h^2}\,. \qquad \ldots \quad (34)$$

Thus $$N=\frac{8\pi V m\mu H}{h^2}\sum_n\int f d\kappa_z$$

$$=\frac{8\pi V m\mu H}{h^2}A_H\sum_{n=0}^{\infty}\int_{-\infty}^{\infty}e^{-\frac{h^2}{2mkT}\kappa_z^2}d\kappa_z\,.\,e^{-\frac{(2n+1)\mu H}{kT}} \qquad \ldots \quad (35)$$

or, since $$\sum_{n=0}^{\infty}e^{-(2n+1)y}=\frac{1}{2\sinh y},$$

we obtain by integration

$$N=\frac{2V}{h^3}\frac{\mu H}{kT}(2\pi mkT)^{\frac{3}{2}}.\frac{A_H}{\sinh\frac{\mu H}{kT}}. \qquad \ldots \quad (36)$$

Or, since $$\frac{\mu H}{kT}<<1,$$

$$N=\frac{2V}{h^3}\cdot\frac{\mu H}{kT}(2\pi mkT)^{\frac{3}{2}}A_H\cdot\frac{kT}{\mu H}\left[1-\frac{1}{6}\left(\frac{\mu H}{kT}\right)^2\ldots\ldots\right]. \qquad \ldots \quad (37)$$

Or, introducing A, the value of A_H without the magnetic field, which is equal to

$$\frac{nh^3}{2(2\pi mkT)^{\frac{3}{2}}},$$

we obtain $$A_H=A\left[1+\frac{1}{6}\left(\frac{\mu H}{kT}\right)^2\right]. \qquad \ldots \quad (38)$$

The energy is now given by

$$E=\frac{8\pi V m\mu H}{h^2}\sum_{n=0}^{\infty}\int_{-\infty}^{\infty}f\epsilon_n d\kappa_z$$

$$=\frac{8\pi V m\mu H}{h^2}A_H\sum_{n=0}^{\infty}\int_{-\infty}^{\infty}\left\{(2n+1)\mu H+\frac{h^2}{2m}\kappa_z^2\right\}e^{-\left(\frac{h^2}{2mkT}\kappa_z^2+\frac{(2n+1)\mu H}{kT}\right)}d\kappa_z$$

or since $$\sum_{n=0}^{\infty}(2n+1)\mu H e^{-\frac{(2n+1)\mu H}{kT}}=\mu H\frac{\cosh\frac{\mu H}{kT}}{2\sinh^2\frac{\mu H}{kT}},$$

$$E=\frac{2V}{h^3}\frac{\mu H}{kT}.(2\pi mkT)^{\frac{3}{2}}.\frac{A_H}{\sinh\frac{\mu H}{kT}}\left\{\mu H\coth\frac{\mu H}{kT}+\frac{kT}{2}\right\}. \qquad \ldots \quad (39)$$

Expanding coth $\frac{\mu H}{kT}$ and sinh $\frac{\mu H}{kT}$ and substituting the value of A_H we obtain after some simplifications,

$$E = N\left(\tfrac{3}{2}kT + \frac{\mu^2 H^2}{3kT} + \ldots\right). \qquad \ldots \quad (40)$$

For H = 0, average energy is thus reduced to $E = \tfrac{3}{2}kT$.

The intensity of magnetisation due to the quantisation is, therefore, given by

$$I = -\frac{\partial E}{\partial H} = -\frac{2}{3}\cdot\frac{n\mu^2 H}{kT}. \qquad \ldots \quad (41)$$

Now, since at the equatorial regions where we chiefly confine our attention, H is approximately horizontal, the layer is everywhere tangentially magnetised and the potential at a point $P(R, \theta, \phi)$ due to the magnetised shell of radius r' will be given by

$$\Omega_p = dr' \iint I_{\theta'} \frac{\partial}{r'\partial\theta'}\left(\frac{1}{r}\right) r'^2 \sin\theta' d\theta' d\phi', \qquad \ldots \quad (42)$$

where r is the distance between P and any point $Q(r', \theta', \phi')$ on the shell. Thus

$$r^2 = R^2 + r'^2 - 2Rr'\cos\lambda, \qquad \ldots \quad (43)$$

where $\cos\lambda = \cos\theta\cos\theta' + \sin\theta\sin\theta'\cos(\phi - \phi')$.

Integrating partially we have from (42)

$$\Omega_p = -dr' \iint \frac{1}{r}\left[\frac{1}{r'\sin\theta'}\frac{\partial}{\partial\theta'}(I_{\theta'}\sin\theta')\right] r'^2 \sin\theta' d\theta' d\phi'$$

$$= dr' \iint \frac{\sigma}{r} r'^2 \sin\theta' d\theta' d\phi \qquad \ldots \quad (44)$$

where

$$\sigma = -\frac{1}{r'\sin\theta'}\frac{\partial}{\partial\theta'}(I_{\theta'}\sin\theta'). \qquad \ldots \quad (45)$$

The potential at P is thus equivalent to that due to a distribution of magnetic matter of surface density σ given by (45).

Since σ is a function of θ' only and not ϕ' it can be expanded in a series of zonal Harmonics.

Thus

$$\sigma = \sum_n \sigma_n P_n(\cos\theta'), \qquad \ldots \quad (46)$$

where σ_n is the coefficient of the zonal Harmonic of order n and given by

$$\sigma_n = \frac{2n+1}{2}\int_{-1}^{+1} P_n(\mu)\sigma(\mu)d\mu. \qquad \ldots \quad (47)$$

Also
$$\frac{1}{r} = \frac{1}{\sqrt{R^2 + r'^2 - 2Rr' \cos\lambda}}$$

$$= \sum_m \frac{R^m}{r'^{m+1}} P_m(\cos\lambda), \qquad \ldots \quad (48)$$

R being less than r', as P is an internal point.

Thus, $$\Omega_p = dr' \sum_m \sum_n \sigma_n \,.\, \frac{R^m}{r'^{m-1}} \iint P_n(\mu) P_m(\cos\lambda)\, d\mu\, d\phi' \qquad [\mu = \cos\theta']$$

$$= 4\pi dr' \sum_n \frac{\sigma_n}{2n+1} \,.\, \frac{R^n}{r'^{n-1}} P_n(\cos\theta). \qquad \ldots \quad (49)$$

The magnetic force F at P, which is equal to $\frac{1}{R}\frac{d\Omega}{d\theta}$ is thus given by

$$F = 4\pi dr' \sum_n \frac{\sigma_n}{2n+1} \frac{R^{n-1}}{r^n} \frac{dP_n(\cos\theta)}{d\theta} \qquad \ldots \quad (50)$$

As we are considering the regions very near to the spherical shell, R will be approximately equal to r' ; so that with the help of (47) we obtain

$$F = 2\pi dr' \sum_n \frac{dP_n(\cos\theta)}{d\theta} \int_{-1}^{+1} P_n(\mu)\sigma(\mu) d\mu \,. \qquad \ldots \quad (51)$$

Now in our special case when the value of σ is given by (45) with $I_{\theta'}$ taken from (41) the above expression becomes much simplified and we obtain at once

$$F = -\frac{16\pi}{9} \,.\, \frac{n\mu^2}{kT} H_\theta \frac{dr'}{r'} \,, \qquad \ldots \quad (52)$$

where $H_\theta = H_e \sin\theta$, H_e being the value of the magnetic field at the equator so that the change dH in H due to a layer of thickness dr' is

$$dH_\theta = -\frac{16\pi}{9} \frac{n\mu^2}{kT} H_\theta \frac{dr'}{r'} \,. \qquad \ldots \quad (53)$$

Since we may neglect the variation of r' compared with a, the radius of the sun, it follows from (53), when we remember

$$n = n_0 e^{-\frac{Mgr'}{kT}} \qquad \ldots \quad (54)$$

that $$\log \frac{H}{H_0} = -\frac{16\pi}{9} \,.\, \frac{n_0\mu^2}{aMg}\left(1 - e^{-\frac{Mgr}{kT}}\right). \qquad \ldots \quad (55)$$

Here M is the average mass of a particle in an atmosphere of Russel Mixture.

$$\text{When} \qquad \frac{Mgr}{kT} << 1, \qquad H = H_0 e^{-\frac{r}{r_0}} \qquad (56)$$

$$\text{and when} \qquad \frac{Mgr}{kT} >> 1, \qquad H = H_0 e^{-\frac{kT}{Mgr_0}} \qquad \ldots \quad (57)$$

where H_0 is the value of H at the base of the reversing layer and

$$r_0 = \frac{9kTa}{16\pi n_0 \mu^2} \,. \qquad \ldots \quad (58)$$

We, therefore, find that according to the Diamagnetic Theory, the Magnetic field first decreases exponentially with the height reaching a constant value when the height is large compared with $\frac{kT}{Mg} \backsim 100$ km. Though this result seems to be in accordance with the observations, a little calculation shows that the value of r_0 is so large as to produce no decrease at all of the magnetic field in the sun's atmosphere.

CONCLUSION

We are, therefore, led to conclude from the above considerations that none of these theories can be a proper explanation of the radial limitation of the solar magnetic field as observed by Hale in 1913. There is no *a priori* reason also why the Sun's field will have such a limitation when there is no such thing in the case of the Earth's magnetic field except that it decreases with height according to Schmidt's formula. Similar conclusions have also been reached by Ferraro[11] from a study of the polarisation of non-uniform rotation of the sun in its magnetic field. He has shown that for the polarisation to be set up the angular velocity of the sun should be constant over the surfaces traced out by revolving the magnetic lines of force around the magnetic axis and which would mean no limitation of the radial field. It may be noted in this connection that the recent investigation of Millikan and Neher[12] on the latitude distribution of cosmic ray intensity and its theoretical analysis by Epstein[13] show that the sun is surrounded by a magnetic field whose intensity at the polar region should be about 25 Gauss. It will be interesting if the cosmic ray investigations in this line can furnish an evidence for the existence of this radial limitation.

My thanks are due to Dr. D. M. Bose, the Director of the Institute for his kind interest and encouragement and to Dr. R. Majumdar for discussions.

Bose Research Institute,
Calcutta.

REFERENCES

[1] G. E. Hale, *Mount Wilson Contributions*, Nos. 50, 61, 71, 72, 118

[2] S. Chapman, *M. N.*, **89**, 59 (1928).

[3] R. Gunn, *Phys. Rev.*, **33**, 614 (1929).

[4] T. G. Cowling, *M. N.*, **90**, 140 (1929), *ibid*, **92**, 407 (1932).

[5] V. C. A. Ferraro, *M. N.*, **95**, 280 (1935).

[6] A. S. Eddington, *M. N.*, **90**, 54 (1929).

[7] V. C. A. Ferraro, *Observatory*, **61**, 241 (1938).

[8] L. Landau, *Zs. f. Phys.*, **64**, 629 (1930).

[9] C. G. Darwin, *Proc. Camb. Phil. Soc.*, **27** (1931).

[10] B. Majumdar, *Tras. Bose. Research. Inst.*, **14**, 17 (1938-1939).

[11] V. C. A. Ferraro, *M. N.*, **97**, 458 (1937).

[12] I. S Bowen, R. A. Millikan and H. V. Neher, *Phys. Rev.*, **53**, 855 (1938).

[13] P. S. Epstein, *Phys. Rev*, **53**, 862 (1938).

THE USE OF PHOTOGRAPHIC PLATES AS AN AID TO COSMIC RAY INVESTIGATIONS *

By D. M. BOSE

This is the second occasion on which I have the opportunity of addressing an annual meeting of the Indian Physical Society. The past year has been marked by an intensification of the war in Europe, by an increased effort made in this country to produce in larger measure the materials required for a successful prosecution of the war in the near East, and also to manufacture articles whose supply from Europe and America have been cut off as a result of the war. A Board of Scientific and Industrial Research has been created under the able and energetic directorship of Professor S. S. Bhatnagar. Sub-committees have been appointed to investigate and work out schemes of research for the production of technologically important articles. Researches in technical physics have been directed towards the production of optical glasses, scientific instruments, wireless goods and allied articles. This recent development of research in technical physics has again brought up to my mind the question once put to me by a friend of mine in Bombay in 1928, at the time when Sir C. V. Raman had made his epoch-making discovery of the effect associated with his name. The question put to me was that why Indians, who have made such fundamental discoveries in pure physics, were so tardy in working out technological inventions. It appears to me that the present time is suitable for a review of the development of the various sciences, pure and applied, in this country since the advent of the British, and of their applications to the welfare of this country. The whole problem could be reviewed from the standpoint which is so widespread at present in some of the western countries, that scientific development at any epoch takes place in response to the social requirements of the period. I had at first intended to take up this theme as the subject of my address before you to-day. Subsequently I discovered that the time at my disposal was not sufficient for a satisfactory investigation and an adequate presentation of the subject. I have therefore decided to present before you a short review of a subject which has been engaging my attention during the last two years, *viz.*, the use of photographic plates as a means of investigation of problems of nuclear physics and of cosmic rays, the stress being laid on investigations in the last-named subject.

*** Presidential address of Dr. D. M. Bose before the annual meeting of the Indian Physical Society held at Benares.**

As you are aware that the effects produced accidentally on photographic plates led to the discovery of X-rays by Röntgen and of radiations from uranium compounds by Becquerel. In those days photographic plates formed an indispensable adjunct in such investigations, but subsequent development of sensitive methods of measuring ionisation currents, the development of Wilson's cloud chamber and of the counter-tube arrangements by Geiger placed the photographic plate in the background. Recently the photagraphic plate has been found of great help in the study of nuclear disintegration and scattering investigations, and also in cosmic ray research. For the last type of work the photographic plate acts as an integrating Wilson's chamber, by means of which cosmic ray processes of very rare occurrence can be conveniently investigated.

As an introduction, I propose to give a short account of the constitution of the photographic emulsion, the action of light radiation in producing developable latent image, and the generally accepted theoretical interpretation of the known properties of the emulsion towards light radiation. The action of ionising particles in producing latent image in photographic emulsion has not yet been so thoroughly studied. With the growing importance of the photographic emulsions for such investigations, new types of plates are being placed in the market by Agfa, Kodak and specially by Ilford and Co. It is a pity that we have no firm manufacturing photographic emulsions in this country with whose co-operation it would have been possible for us to investigate the action of moving charged particles in producing latent images and also in making new emulsions to suit the changing requirements of research. For example, it has been found that the dye pina-kryptol yellow, which is a desensitiser of the action of light on photographic emulsions, increases the sensitivity of the latter to the detection of protons, and no explanation of this effect has yet been found.

A photographic emulsion consists of a suspension of tiny AgBr crystals with a small percentage of AgI in gelatine. In ordinary emulsions there are about 10^9 grains per cm.^{2} of plate area, and the average size of the grains vary from 0.1×10^{-8} cm.^{2} for slow speed positive emulsions to 1.0×11^{-8} cm.^{2} for fast negative emulsions. The grains are usually flat plates of triangular and hexagonal shape, and their thicknesses are about 1/10 of their diameters. It is found that the sensitiveness of the emulsion to light is increased by the presence of a minute quantity of Ag_2S in it, and it can be further increased by the process of ripening. It is supposed that on the surface of each AgBr grain is a sensitive spot containing either a small amount of Ag_2S or a minute silver speck formed during the process of ripening. The latent image is formed during the exposure to light by a sufficient number of silver atoms being deposited round this speck.

The mechanism by which the silver atoms are deposited is conceived according to the generally accepted theory of Gurney and Mott, as follows. Each quantum of light absorbed raises one of the attached electron in Br⁻ ions to the conduction level of the AgBr crystal, where it begins to migrate until it gets finally trapped on the sensitive spot on the grain. The accumulation of a few such electrons on the spot produces a strong local field in which some of the Ag^+ ions in the ionic AgBr crystal begin to migrate and get finally attached to the spot as neutral Ag atoms. A mechanism is also proposed according to which the Br^- ions released by the production of neutral Ag atoms can ultimately escape from the surface of the grain. As to the size of the latent image it is found that the number of light quanta required to be absorbed for their formation vary with the grains; on an average about 50 per cent of the grains become developable by the absorption of 50 light quanta by each. We conclude that the latent image in any grain of AgBr is a speck of silver containing at least 50 atoms.

It is found that these photographic emulsions also react to the action of ionising particles like α-particles, protons, deuterons and even electrons. The effects observed fall under two categories—(*i*) the density of blackening produced on photographic emulsions exposed normally to a corpuscular beam, in which the density-exposure relation for different kinds of charged particles are studied. Investigations have been made as to how far the Reciprocity law holds for irradiation by charged particle and (*ii*) the number of grains developed along the tracts of the charged particle in the emulsion. Two reports are available which summarise the results so far obtained, the first one by H. Wambacher, 'Action of corpuscular radiation on photographic emulsion,' *Zeit. f. Wiss. Phot.*, **38**, 38, 1939, the other is a report by T. R. Wilkins 'The response of photographic materials to Atomic particles,' *J. of App. Phy.*, **11**, 35, 1940.

The results obtained have been summarised by Wambacher as follows :—

1 X-ray quantum ($\lambda = 0.5$Å)—on an average develops one grain of AgBr (total number of Ag atoms released 1000)

1 α-particle from Ra ($6.10^6 eV$)—10-15 grains of AgBr (total number 50,000 Ag atoms)

6-8 β-particles (10^5-$10^6 eV$)—1 AgBr grain

1 electron ($10^4 eV$)—2 AgBr grains

10^4 positive-ray particles (800 eV)—one AgBr grain.

The most carefully investigated effect of corpuscular radiation on photographic emulsion has been with α-particles. Each α-particle produces on an average 2-3 thousand Ag atoms per AgBr particle struck, it thus, as experimentally proved, blackens every particle passed through by it.

The action of β-particles and positrons on photographic emulsion is not clearly known. Slow electrons (energy of order 10^4 eV) may ionise the AgBr grain on its path but owing to their small mass they are easily scattered and therefore do not form a linear deposit of blackened grains; further they give rise to fluorescent radiation, by collision both with the emulsion and its glass backing, which blackens the emulsion. On the other hand fast electrons (energy 10^5-10^6 *e*V) do not sufficiently ionise the AgBr grains so that their tracks cannot be made visible on photographic emulsions.

Fast protons produced by the recoil of α-particles with hydrogen have also been shown to produce definite ionisation tracks. These investigations are due to Taylor and to Blau and Wambacher, and as the latters' investigations have been the starting point of our own work, more attention will be given to it.

The technique of the method used to see the tracks of individual high energy particle like α-particle, deuteron or proton is as follows. The photographic plate exposed to the radiation is developed and examined under a high-power microscope. The quantities to be measured are the length of the tracks on the emulsion usually given in units of $\mu(10^{-4}$ cm.). It is found that the emulsions have a density of about 2.8, and one cm. of length of track in air is equivalent to about 7μ length in the emulsion. The other important factor to be noticed is the quantity known as mean grain distance (m.p.d.) along a track = $\frac{\text{length of the track in } \mu}{n-1}$, where n is the number of developed grains on the track. Both these quantities depend upon the charge and energy of the ionising particle.

The suitability of a photographic emulsion for this kind of work depends upon that

(*i*) the emulsion must be as fine-grained as possible so as to have the maximum number of developed grains along the track of an ionising particle;

(*ii*) it should be as free from background fog as possible, and the development should be so conducted as to minimise the production of such fogs. The effect of background fog is to prevent the clear discernment of the tracks of ionising particles, specially those in which the grain distance is large;

(*iii*) it is found that different types of emulsion are sensitive to one or more kinds of ionising particles, *e.g.*, Ilford R_1 plates only record tracks of α-particles, while the R_2 plates record in addition the tracks of slow protons. Blau found that certain emulsion like Imperial process plates when bathed in a solution of pinakryptol yellow (a desensitiser in ordinary photographic process) the tracks due to the passage of protons are greatly lengthened. Similar treatment of Ilford R_2 plate by Kuerti and Wilkins led to the proton tracks on them being increased by 8 or 9 times in length as that in untreated plates, and the tracks so obtained corresponded in full to the range of the proton in the emulsion. But the best results were obtained by Blau and Wambacher by using Ilford New Halftone plates, which for purpose of cosmic ray investigations were used with a film thickness of 70μ (ordinary R_2 plates have a thickness of 14μ).

The m.p.d. for different particles found with these plates are given below :

Particle	Blau & Wambacher m.p d.	Bose & Chowdhury
Particles from Th. C range 8.62 cm. in air	1.42 μ	1.8 μ
Proton range 5.8-29 cm	1.5 μ	2.6 μ
29-85 cm.	1.56 μ	

i.e., according to Blau and Wambacher, up to energies of 10 MeV the mean particle distance of α-particles and protons are independent of their energies. Our results are slightly different and may be attributed to some difference in the composition of the emulsion supplied to us. Such plates were exposed in their original packing at Hafelecker (230 m) and kept there for four months at the temperature 15° C In an area of .507 cm^2, when only tracks of length greater than 10 cm. air were counted. Blau and Wambacher found the number to be 85. They consisted of 29 tracks with lengths greater than 1 metre of air, one of length 6½ metres and another of 12 metres. The mean particle distance varied between 1.37μ and 5.7μ. It was improbable that with the exception of two with m.p.d less than 1.5μ they were due either to α-particles or β-particles or positrons.

The conclusion was drawn that they are due to fast protons. This conclusion tacitly implies that though, up to energies of 10 MeV, the mean grain distance of the proton tracks was a constant, for higher energies however the m.p.d- increased. The authors tried to build up an energy calibration curve on the line of Braggs Ionisation curve for these particles. For this curve use was made of the fact that along different portions of long tracks the grain distances were found to decrease continuously from one end of the track to the other, this direction of decrease would correspond to the direction of diminution of velocity of the ionising particle. This calibration curve was used to determine the energy of short-range tracks on the emulsion which had large values of m.p.d. It was shown that in many such tracks the direction of traversal of the ionising particle was inclined to the plane of the emulsion surface and so only a short range of the track was continued inside the emulsion. These tracks were assumed to be due to protons, which were supposed to be produced in the material of the emulsion by recoil from the fast primary neutrons in the cosmic rays. As will be reported later, our own investigations lead to the conclusion that the tracks with m.p.d. $> 3\mu$ are due mostly to mesotrons. In addition to these single tracks, 60 cases of nuclear disintegration were observed, giving rise to multiple star like tracks radiating from a centre (up to 12 in member). Out of 31 stars which were measured the energy of disintegration in four cases was 100 MeV, the emitted particles being assumed to be prtoons. Such emission of protons (with emission of an equal number at least of non-ionising neutrons) can take place according to the nuclear evaporation process (on the liquid drop model), If the particle has a range R(p) in the given medium

$$R=\frac{mc^2}{a}\left[\frac{2+\left(\frac{pc}{mc^2}\right)}{\sqrt{1+\left(\frac{pc}{mc^2}\right)^2}}-2\right]$$

where a is a constant of the medium.

For low values of p, $R=\frac{b}{Z'^2}\frac{E^{\frac{3}{2}}}{\sqrt{M}}$; if the energy E is expressed in MeV, and M the mass of the particle in proton unit, then for air $b=\frac{1}{3}$.

The average deflection θ of such a particle due to multiple scattering is given by $\theta=(19.5-3.1\log_{10} Z)^{\frac{1}{2}}e\frac{ZZ'c^2\sqrt{Nt}}{E}$.

In a Wilson chamber, for ionising particles of energy between 10^7-10^8 eV, the ionisation of a mesotron will be much stronger than that of an electron, and the mass of the former can be derived from any two of the following measurements, range (if the particle track ends inside the chamber), ionisation density, and curvature in a magnetic field.

Now let us consider the application of these formulas to the tracks of the ionising particle on photographic emulsions. According to Wambacher the composition of a silver bromide emulsion (probably Ilford Halftone) is as follows

H	C	N	O	S	Br	Ag
15,	9.6,	2.8,	3.5,	0.1,	1,	1

Its density is 2.89 and it has an average atomic number $Z=6.2$ and the number of atoms per c.c. comes out to be 1.4×10^{23}. From the ionisation loss formula, knowing the velocity and charge of the ionising particle, we can calculate the average number of ions produced per unit length. Assuming that the silver bromide crystallites are of uniform size, then theoretically it is possible to calculate the number of electrons produced in each grain; if this number is above the minimum number n_0 necessary to develop all the silver bromide grains, then all of them are developed (50 to 100 atoms of silver require to be deposited in grains of silver bromide by light in order that 50% of the grains may be developed). According to Blau, each α-particle on an average produce 2000-3000 silver atoms per AgBr particle struck, and therefore as found experimentally up to α-particle from Th C′ (energy 9.7 MeV), the mean particle distance remains constant and equal to the distance between the silver bromide crystals in the emulsion.

In the case of recoil proton tracks on Ilford Halftone emulsion, Blau and Wambacher find that up to a range of 100 cm. air, the m.p.d. is 1.54μ as against 1.4μ for α-particle. While from our own records we find that the m.p.d. increase from 1.8μ for α-particle to 2.6μ for protons. We find therefore for recoil protons even for ranges up to 60 cm. air, not all the silver halide grains along their tracts are affected. To account for this we suppose that if the average number of Ag atoms deposited per grain of AgBr by proton be $\bar{n}$ and it is less than n_0 the minimum number per grain required to develope it, than the probability that a grain is developed is $P(n_0)=\frac{\bar{n}_0^{\,n}\ e^{-n}}{n_0!}$; this integrated over the limits n_0 to ∞ and mutiplied by the number of AgBr grains per unit length of emulsion will give the number of grains which will be deposited per unit length of the track. There are many difficulties in the way of solving this problem; for one thing the size of the grains is not uniform, nor are they all at the same stage of ripeness, *i.e.*, different grains will require the deposition of different number of silver atoms to enable them to act as latent image.

Since it is not possible to deduce from the general ionisation formula, the relation between the charge and velocity of a particle and the number of silver grains deposited per unit length along its track in a photographic emulsion, we may proceed to attack the problem in a semi-empirical way as suggested by Helen & Wilkin. According to them due to the motion of charged particle, each of the grains receives an impulse $I=\int F dt \sim \frac{Z'e^2}{\rho^2}.\frac{1}{v}$ approximately, where ρ = the distance between the moving particle of charge $Z'e$, and an electron in the silver halide grain and v is its velocity. If this impulse is greater than a critical value I_0, then a sufficient number of electrons is set free in the grain to produce a latent image. Thus all the silver halide grains n within a volume $\pi\rho^2.1$ will be affected where $n \sim \pi\rho^2 \sim \frac{Z'e^2}{v}.\frac{1}{I_0}$. Using the formula giving the range of a charged particle as function of its mass energy and charge, it can be shown that if n_α, n_p and n_D are the number of silver grains developed per unit lengths of the tracks of α-particle, proton and deuteron of the same range,

then $\frac{n_\alpha}{n_p}=2$ while Helen & Wilkins find experimentally the value 1.7

and $\frac{n_D}{n_p}=1.25$,, ,, ,, 1.4

There is thus only a very approximate agreement with experimental results. According to this formula the number of grains, developed per unit length of a moving charged particle is proportional inversely to the velocity of the particle. This formula is not even approximately correct. If a proper correlation between the values of n and v for any kind of charged particle can be found, then the mass of that particle can be determined from it and from the multiple scattering suffered by the same particle traversing through a known length of the photographic emulsion. The multiple scattering is proportional inversely to the energy E of the particle.

· The importance of this result lies in the fact that many of the highly ionising tracks observed in Ilford Halftone plates exposed by us to cosmic radiation have been found to be curved. As will be shown just now, it has enabled us to decide that the particles responsible for them must have a mass lower than that of protons, and since fast electrons do not produce such tracks on photographic emulsions, these tracks must be due to mesotrons.

I shall next proceed to give an account of our own investigation on cosmic rays using the photographic plates as detectors. We have followed Taylor's procedure of keeping R_2 plates at high altitudes, half of each plate being treated with a solution of a salt of a heavy element like Uranium, Lead, Bismuth, Samarium, and Rubidium. Like Taylor we have obtained positive results of disintegration of Samarium nucleus under the action of some component of cosmic rays. No definite results could be obtained with Uranium, due to the large number of secondary particle tracks shown on the plates, resulting from the natural disintegration of the Uranium nucleus and of its products. The investigations with the other substances are being continued, no definite results have yet been obtained.

We have also in another series of investigations followed Blau and Wambacher in keeping untreated Ilford Halftone plates in paper cartons exposed to cosmic radiation. The plates are kept at three different elevations—Darjeeling (Mayapuri Research Station, elevation 7,000 ft.), Sandakphu (Dak Bungalow, 12,000 ft.) and Phari Jong Post-Office (14,500 ft.). These plates were kept vertically standing on their longside, under the following conditions (*i*) Darjeeling exposed to air, (*ii*) Sandakphu, exposed to air, kept under 20 cm. of water, under 5.5 cm. of lead, (*iii*) Phari Jong exposed to air, kept vertical and flat.

From the plates kept at Darjeeling and Sandakphu, information has been obtained on (*a*) the relative intensity of the track producing rays at these two places (*b*) the relative absorption in 20 cm. of water of the radiation at Sandakphu and in the air mass between Sandakphu and Darjeeling which has a mass of 140 gm./cm.^{2} (*c*) the possibility of production of doubly charged proton. According to Bhabha's theory the following reaction is possible: $P+P \rightarrow P^{++}+N$ and it can take place when a fast proton of energy greater than 35 MeV traverses 45 cm. of water.

The tracks which have been obtained on these plates consist of single and multiple tracks. The number of different kinds of tracks, obtained in the different plates is given in Table II. The last columns give the frequency of single, double, etc. tracts on the given plate areas.

TABLE II

Place	Time of Exp.	Area of plate	Track No.						
			$_{1}^{le}$	$_{2}^{le}$	$_{3}^{le}$	$_{4}^{le}$	$_{5}^{le}$	$_{6}^{le}$	$_{7}^{le}$
Sandakphu (air)	150 days	1.10 cm.^{2}	87	18	18	18	14	2	1
Sandakphu (water)	202 ,,	1.05	60	8	8	5	4		
Darjeeling (air)	150 ,,	1.00	20	5	19	10	3	2	one burst of 13 tracks

Many of these tracks are curved, and such curved tracks also form part of the multiple star tracks. We shall first confine our attention to the single tracks shown in the plates kept at Sandakphu under air and under 20 cm. of water. In Table III such tracks are collected, in the last column of which the energy of the particles as calculated from the multiple scattering formula of Williams is given. For comparison similar data for fast proton tracks are given under C. They are produced by the recoil of hydrogen atom in the photographic emulsion by fast neutrons produced by a tube containing Ra and filled with Be powder. Between the source and the photographic plate a block of 10 cm. lead was kept to cut off γ-rays.

TABLE III

A. Sandakphu (Air) Track No.	Total air length	m p.d.	No. of curved tracks	Total angle of scattering	Energy MeV
1-22	380 cm.	5.5	4	19°	1.91
23-45	356 cm.	4.2	9	57°	0.61
46-47	395 cm.	3.4	12	61°	0.61
78-87	107 cm.	2.7	2	12°	
B. Sandakphu (Water)					
1-43	411.0 cm.	4.2	9	55°	0.69
	128	2.4	2	16°	1.31
C. Recoil proton	1111 cm.	2.6μ	2 single scattered 1 slightly curved		

From the above table the following inferences can be made (i) if the tracks found on the plates exposed to cosmic ray were due to protons, then those with larger values of m.p.d. (*i e.* > 2.6μ of proton under C) should possess higher energies, and since the multiple scattering suffered by them are inversely proportional to their kinetic energies, they should be less scattered than the recoil protons shown in C. Actually they are more scattered, and since these particles cannot have less than one unit of charge, their mass must be less than that of proton. Further these tracks cannot be due to electrons, *they must therefore be due to mesotrons.* That is, the particles responsible for tracks with large m.p.d. obtained both by Blau and Wambacher and ourselves in Ilford Halftone plates are principally mesotrons and not protons. It is of further interest to note that the tracks with low m.p.d. on the cosmic ray plates (2.7-2.4μ) have large energies. This result can be satisfactorily explained on the assumption that the particles responsible for them contain a large proportion of protons, produced by recoil from neutrons contained in the cosmic rays

The next point we shall consider is the relative absorption of the primary cosmic radiation responsible for the production of the tracks in air and in water.

In Table IV is given the number of tracks observed in photographic plates kept at Sandakphu and at Darjeeling under different conditions. As a measure of the energy of the cosmic radiation responsible for the production of these tracks, we have taken simply the number of tracks recorded on unit area of the plate in a given time. This is permissible since if these tracks are due to mesotrons, their energy of creation is of the order 10^8 eV, which is very large compared to their kinetic energies. From this count we have excluded tracks in which the m.p.d. is less than 2μ as experience shows that such tracks are usually due to α-particle contamintaions.

TABLE IV

	Plates kept under	No. of tracks per cm²/100 days	No. of tracks absorbed in	Ratio of absorption
Sandakphu.	(i) air	165	20 gm. of water 98	
	(ii) 20 cm. water	67	140 gm./cm ² of air 61	1.6
Darjeeling	(iii) air	103		

We find that the rays responsible for the production of tracks on the photographic plates are more strongly absorbed in water than in air, *i.e.*, they are chiefly neutrons. This conclusion is supported by the observations of Heitler and his fellow workers who kept similar Halftone plates at Jungfraujoch (13,400ft) under different thicknesses of lead. The number of tracks observed on the plates was a maximum under 1.2 cm. of lead, and it slowly falls down near to its value in air, at under 12 cm. lead. They draw the conclusion that the responsible constituents of the cosmic ray consist of two portions, one easily absorbable and the other very little absorbable in lead, *i.e* , they consist partly of photons and partly of neutrons. Our own plates kept under lead were found fogged on developement and so could not be utilised. Reverting to our own results, we can calculate from the following considerations the relative energy loss of fast neutrons which are responsible for the creation of single and multiple mesotron showers in the given masses of air and water. A neutron, suffering an elastic collision with an atom of mass M, looses on an average 2/M of its kinetic energy, *i.e.*, it requires M/2 collision to produce the same loss of energy as collision with a hydrogen atom. On calculating the number of equivalent hydrogen-like collisions in the given masses of water and air, the ratio of hydrogen-like collisions comes out to be 1.7, which is very near to the observed value of 1.6.

The agreement between the two (if not accidental) can be made plausible on the following assumptions : (i) the rate of production of such high energy neutrons in the air mass between Sandakphu and Darjeeling are very few compared to the number present in the original beam (ii) the cross-section for elastic scattering is very large compared to that for mesotron production (iii) on an average they do not suffer more than one hydrogen-like collision in the given masses of air and water.

TABLE V

Pair Tracks No.	Total length	m.p.d.	No. of curved tracks	Total angle of scattering	Mean angle between pair
1-18	528 cm.	4 6 μ	8 (in one pair both tracks are curved)	42°	17°

In Table V data for 18 pair tracks found on the plate at Sandakphu under air is given. From the relation between track lengths m.p.d. and total angle of scattering, there can be no doubt that these pairs consist of mesotrons. The angle between the pairs vary from 6° to 35°, with a mean value of 17°. It is interesting to apply to these pairs the consideration used by Wentzel to limit the angular spread of pairs arising out of the interference of a wave packet of energy E scattered over an obstacle of linear dimension a

$$\theta \lesssim \frac{\lambda}{2\pi a} \lesssim \frac{hc}{2\pi a E} \; ; \text{ here } E = \text{total energy} \sim 2 \times 10^8 \text{ eV} \; ; \; \theta \simeq 17^\circ \; ;$$

the value of a comes out to be 2.07×10^{-13} cm. which is of the same order as the electron radius 2.8×10^{-13}. It is difficult to say whether any physical significance can be attached to this quantity.

Since in the other higher multiple tracks the m.p.d. of the tracks also vary between 6μ and 2.5μ, and some of them also appear curved, it is permitted to infer that they are all of mesotron character. The detailed examination of these multiple star tracks is being carried out.

The conclusion can be drawn from our investigation that by the interaction of one or more high-energy components of the cosmic radiation (principally neutrons) with atoms in the photographic emulsion multiple mesotron showers are produced. This conclusion appears to be important since, according to the classical theory of mesotron proposed recently by Bhabha and later taken up by Heitler, the scattering cross-section of mesotrons of energy 10^8 eV by proton or neutron is of the order 10^{-27} to 10^{-28} cm.^{2} This is in agreement with the meagre experimental data of J. G. Wilson ; there is no place however for mesotron shower production according to this theory. According to the theory developed by Heitler this cross section remains a constant over a large range of energy. In Bhabha's later developement of the theory of mesotron with a spin, however, the cross-section has a maximum in the region of energy 3.2×10^8 eV. Whether, the sudden increase of scattering cross-section in this region can lead to a process of multiple mesotron shower generation is not clear. A recent theory of Heisenberg appears to give a reasonable picture of multiple mesotron shower production due to impact of uncharged particles on protons and neutrons. It is also free from certain of the theoretical objection raised against the older quantum theory of scattering of mesotron. If the conclusions I have drawn from our photographic records are valid and are further verified by later investigations, then this method can produce experimental evidence of a type of interaction between matter and certain constituents of cosmic radiation, not readily available by other methods. The photographic plate is specially suited to record processes in which protons, mesotrons, α-particles are produced over comparatively low range of energy, *viz.*, in the region of 10^6 eV for α-particles and protons. For this region and for these types of particles the method is superior to the Wilson Chamber apparatus.

We have made a preliminary search for the existence of doubly charged protons, on the plate kept at Sandakphu under 20 cm. of water. As stated earlier, such particles are expected to be created when fast protons of energy greater than 3.5×10^7 eV traverse 45 cm. length of water. Our plate was kept exposed for 202 days and we looked for tracks with m.p.d. between 1.7μ to 2.0μ and of range greater than 10 cm. of air, which is the length of the highest energy particle tracks due to Th C$'$. In an area of 1.05 cm.^{2} no such track has been observed. The investigation is being further continued.

We can summarise the results which have been obtained from a study of cosmic radiation using Ilford Halftone plates as follows :

(*i*) Blau and Wambacher find long single tracks and star-like multiple tracks on such plates in which the m.p.d. vary from 1.37μ to 5.7μ. These tracks are assumed to be due to protons, produced in the case of single tracks by the recoil of protons in the emulsion with fast cosmic ray neutrons. The star-like tracks represent the products of nuclear explosions (presumably of the evaporation type), in which both protons and neutrons are emitted, and of which only the former are recorded.

(*ii*) Heitler and his co-workers only count the number of tracks which appear in such plates kept under different thicknesses of lead plates at Jungfraujoch. They conclude that the components of the cosmic ray responsible for the heavy-ionisation track are partly photons and partly neutrons.

(*iii*) Bose and Choudhury find from the multiple scattering of these tracks that they are principally due to mesotrons, whose energy lie in the range 10^5-10^6 eV. From the relative absorption in water and air the conclusion is drawn that the fast neutrons in the cosmic ray are principally responsible for the creation of mesotrons either singly or in a multiple process.

The data so far collected allow only qualitative conclusions to be drawn. It can be expected that accumulation of a larger amount of data will allow certain quantitative conclusions to be drawn (*i*) on the energy distribution and the relative proportions of photons, neutrons and other possible constituents in the cosmic ray which produce mesotrons by multiple processes of the type envisaged by Heisenberg, (*ii*) on the cross-section for single scattering and for shower production, (*iii*) on the existence of doubly charged protons and anti-protons which according to Bhabha can be created during interaction between protons and protons $P + P \longrightarrow P^{++} + N$ and between neutrons and neutrons $N + N \longrightarrow P^{-} + P^{+}$.

It is imperatively necessary that further investigations on the formation of latent images by the action of moving charged particles in photographic emulsions is undertaken. Without such investigations it will not be possible to make the photographic emulsion an instrument for accurate quantitative measurement in cosmic ray investigations.

Recently the mass of the particles producing curved tracks on the photographic emulsion has been determined. The theory of the method used as follows—if the unknown particle is mesotron, it is singly charged like the proton. and the assumption is made that both the proton and the mesotron will produce tracks on the emulsion with the same m.p.d , provided they start with the same velocities. Then the ratio of the kinetic energies of mesotron and proton with the same m.p.d. will be proportional to the masses of these two particles. The energy of the mesotron can be obtained from the multiple scattering in the emulsion using William's formula. That of the protons can be obtained from calibration curve connecting the K.E. of proton producing tracks on the emulsion, with the m.p.d. along the tracks. The calibration curve was found, up to energies of 10 Mev, to be a straight line, from which the K.E. of the protons corresponding to the m.p.d. found for cosmic ray particles can be obtained by extrapolation. The following values of the mass of the particles have been obtained in terms of electron mass mo, 173, 149, 158, 153, 167 with mean equal to (160.2 ±4.3) mo, which falls within the range of the best determination of the mesotron. It is expected that the introduction of certain corrections will increase the value of μ by ten per cent. The results have been communicated in a note sent recently to 'Nature.'

REFERENCES

Bhabha, *Proc. Ind. Acad. Sci.* A., **11**, 436 (1940).

Blau and Wambacher Wien, *Akad. Bau.*, IIA, **140**, 259, 469, 623 (1937).

Bose and Chowdhury, *Nature*, **146**, 894, (1940); 147, 240 (1941).

Gurney and Mott.

Heisenberg, *Zeit. f. Phys.*, **113**, 61 (1939).

Heitler and Ma, *Proc. Roy. Soc.*, **176A**, 368 (1940).

Heitler, et al, *Nature*, **146**, 65 (1940).

Taylor and Dhabolker, *Nature*, **141**, 472 (1938)

Wambacher, *Phys. Zeit.*, **39**, 888 (1939).

Wentzel, *Phys. Rev.*. **54**, 869 (1938).

Wilkins and Helen, *Phys. Rev.*, **54**, 783 (1938).

Williams, *Phys. Rev.*, **58**, 292 (1940).

Wilson, *Proc. Roy. Soc. A.*, **176**, 88 (1940).

MEASUREMENT OF ACOUSTICAL IMPEDANCES *

By (Miss) CHANDRA KANTA, M.Sc.

(Received for publication, February 4, 1941)

ABSTRACT. The present paper describes determination of *acoustical impedances* by measuring the electrical impedances of a speaker under different air loads. It is a continuation of the previous work. With a proper temperature control, very reliable results are obtained even for small acoustical impedances. Measurements of resistance, reactance and phase in the case of a reflecting surface of Treetax, Felt or simply a Helmholtz Resonator have been made at different frequencies. The variations are plotted graphically. Acoustical resistance of a Helmholtz Resonator, reactance and phase at different frequencies show fair agreement with the theory.

This paper is a continuation of previous work which has already been published.[1] The method is indirect but quite capable of measuring small acoustical impedances with repeatable results. The only defect is that it takes some time to complete one set of observations, otherwise quite consistent results are obtained with a little care and watchfulness. We have extended the method to the measurement of acoustical impedances of materials obtainable in small quantities and to Helmholtz resonators. Some results have been obtained in the case of artificial materials composed of a number of vaccine tubes. Since the experimental procedure is described in detail in the paper referred to above, we shall first discuss the theoretical background for the evaluation of the acoustical resistance and reactance and then the results.

Theory :—The electrical impedance Z_{ET} of a moving-coil receiver is given by

$$Z_{ET} = Z_{EW} + \frac{k^2}{Z_m + a^2 Z_1}$$

where Z_{EW} is the electrical impedance of the windings of the coil in the absence of vibration of the diaphragm. Z_m is the mechanical impedance of the vibrating system and Z_1 the air-load impedance. a is the area of the piston.

Writing $Z_m = R_p + jX_p,$

$$Z_{ET} = Z_{EW} + \frac{k^2}{R_p + jX_p + a^2 Z_1}. \qquad (1)$$

---

* Communicated by the Indian Physical Society.

From measurements at $X_{\mathrm{EL}} = 0$

$R_{\mathrm{EL}} = 3.2$ ohms

$l = 19.7$ cms.

Then $$R = \left(\frac{k^2}{R_{\mathrm{EL}}} - R_p\right)\frac{1}{aZ_0} = \frac{.91854}{3.2} - .1701 = .11694$$

and $$X = -\frac{X_p}{aZ_0} = -.6056.$$

Putting these values in equation (9) we get

$$A = .5756 \log \frac{(1+.117)^2 + .6056^2}{(1-.117)^2 + .6056^2} = .08545.$$

From the tables of hyperbolic functions

$$\tanh A = .08524.$$

Putting this value of tanh A in equation (8) we get

$$\tan C = \frac{.11694 - .08524}{-.6056 \times .08524} = -.6142.$$

$$\therefore \qquad C = -31^\circ.55.$$

But $$C = B + kl$$

or $$-31.55 = B + \frac{360}{30} \times 19.7$$

or $$\tan B = -\tan 87.95 = -28.0.$$

Radius of the piston tube $= 2.8$ cms.

$$\therefore \qquad a = \pi \times 2.8^2.$$

Now substituting all these values in equations (10) and (11) we get

$$Z_r = \frac{42}{\pi \times 2.8^2} \cdot \frac{.08545(1+28^2)}{1 + .08545^2 \times 28^2} = 1.703,$$

similarly $$Z_x = -7.074.$$

From equation (12)

$$kB = +535.9 - 360 = 175^\circ.9$$

and $$a = \operatorname{Antilog}\left(\frac{-2 \times .08524}{2.303}\right) = .9286.$$

In this way readings were taken for Treetax and Felt at different frequencies and Z_r, Z_x, α and phase change calculated. Tables I and II give the results.

TABLE I

Treetax

λ	Z_1	Z_2	α	$k\beta$
28.4	12.74	+ 9.55	.843	172.6
29.5	16.85	+ 2.49	.820	178.3
30.0	17.03	+ 7.07	.928	175.9
31.4	16.92	+29.60	.859	175.0
33.2	14.16	+10.31	.855	173.4
35.0	18.43	+ 3.41	.836	178.1
36.0	24.13	+ .67	.868	179.7

TABLE II

Felt

λ	Z_1	Z_2	α	$k\beta$
28.4	1.99	− 8.76	922	159.0
29.5	3.34	− 8.77	.905	160.6
30.0	1.76	− 7.83	.916	156.8
31.0	1.24	− 6.64	916	157.5
31.4	1.44	− 7.73	927	155.9
33.2	1.68	− 8.71	.932	158.6
35.0	3.39	−11.82	.928	164.8
36.0	1.79	− 9.54	.939	160.4

It can be seen that reflection coefficient varies with wavelength in both cases. It has maxima and minima at different wavelengths; for example, in the case of Treetax at $\lambda = 30$, the coefficient of reflection approaches a maxima, and then as the wavelength increases α falls down. Beyond $\lambda = 35$ it again starts increasing. Resistance also has maxima and minima as the wavelength of sound varies, but the change is more marked in the case of reactance. Figure I shows the results of Treetax graphically. It can be seen that there are marked minima and maxima in all cases and the curve of phase follows the resistance curve very closely. The phase goes on increasing with increasing wavelength, showing thereby that at lower frequency phase tends to 180°. It means that the material behaves like a perfect reflector at low frequency as far as phase is concerned.

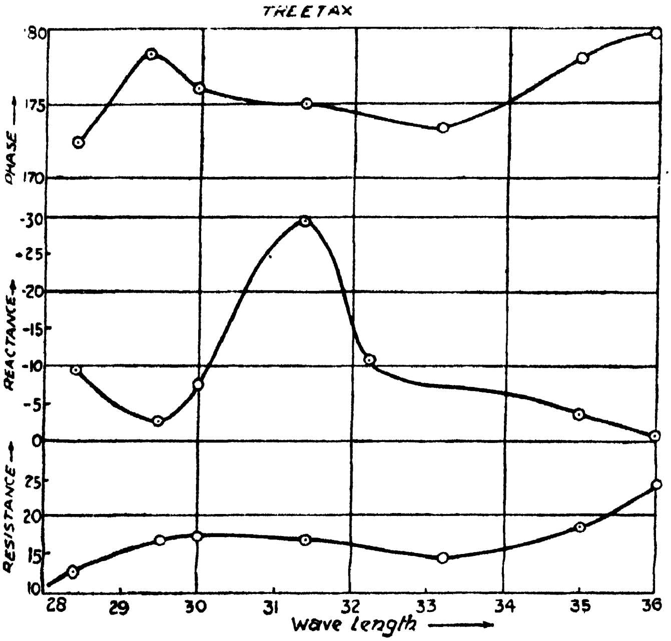

FIGURE 1

By comparing the two tables it can be seen that the reflection coefficients are smaller in the case of Treetax than Felt, but the changes are more pronounced in Treetax. Treetax is harder to touch than Felt, but it has greater resistance to sound waves than Felt. Mass per unit area is also greater in the case of Treetax. One more physical constant, namely, porosity has to be considered in discussing the question of impedance. The author proposes to find out the relation between porosity and resistance. Probably then it would be possible to correlate the coefficient of reflection with the various constants of the material.

Resonators :—Another type of acoustical system of which the acoustical impedance was determined is Helmholtz Resonator. A hole was bored at the centre of a piston disc and to this hole was attached a variable cylindrical chamber, so that the volume of the resonator could be altered. In the present set of experiments the holes were practically of the same size, the volume being adjusted for different frequencies. Below is given a typical calculation for the case of a resonator at $\lambda = 33.5$ cms.

The radius of the opening of the resonator = .27 cm.

Thickness of its neck = .36 cm.

$$k^2 = 1.2732\ aZ_0$$

$$R_p = .2122\ aZ_0$$

$$X_p = 1 \cdot 1343\ aZ_0$$

$$R_{EL} = .9 \text{ ohm.}$$

$$l = 10.95 \text{ cms.}$$

Now $$R=\frac{1}{aZ_0}\left(\frac{k^2}{R_{EL}}-R_p\right)=\frac{1.2732}{.9}-.2122=1.20247$$

$$X=-\frac{X_p}{aZ_0}=-1.1343.$$

Putting these values in equation (9)

$$A=.5756\log\frac{(1+1.2025)^2+1.1343^2}{(1-1.2025)^2+1.1343^2}=.3839.$$

From tables of hyperbolic functions

$$\tanh A=.36522.$$

Putting this value of tanh A in equation (8)

$$\tan C=\frac{1.20247-.36522}{-1.1343\times .3652}=-2.021$$

$$C=-63^\circ.7.$$

But $$C=B+kl$$

$$\therefore\quad -63.7=B+\frac{360}{33.5}\times 10.95$$

$$\therefore\quad B=-181.4$$

$$\tan B=-.0244.$$

Substituting these values of tanh A and $-\tan B$ and $a=\pi\times 2.8^2$ we get

$$Z_r=\frac{42}{\pi\times 2.8^2}\cdot\frac{.3652(1+.0244^2)}{1+.3652^2\times .0244^2}=.6227$$

$$Z_x=\frac{42}{\pi\times 2.8^2}\cdot\frac{(-.0244)(1-.3652^2)}{1+.3652^2\times .0244^2}=-.03604$$

$$-\tan\phi=\frac{Z_x}{Z_r}=-\frac{.03604}{.6227}=-.0079$$

$$\therefore\quad \phi=-3^\circ.3$$

$$\alpha=\text{Antilog}\left\{-\frac{2\times .3652}{2.303}\right\}=.4818.$$

In the case of resonators it may be noted that the terminal impedance Z_2 gives the impedance of a resonator since the impedance of the remaining piston is infinite. Hence $Z_2=Z_r+j\,Z_x$. The phase in this case is calculated from $\tan\phi=Z_x/Z_r$ where ϕ is the phase inside the resonator. Table III gives the result for five different resonators of equal orifice but different volumes.

TABLE III—*Resonators*

I

λ	28.4	28.5	29.2	31.0	34.0	36.0
Z_r	1.493	.958	1.188	1.328	1.392	1.276
Z_x	1.097	.439	− 2.288	− 5.797	−11.24	−18.66
a	.365	.325	641	.890	.963	.988
ϕ	36.3°	25°.0	−63.0	−77°.1	−83.°0	−86.°1

II

λ	28.2	29.5	30.0	31.0	32.0	34.0	36.0
Z_r	1.331	1.331	1.054	1.105	1.405	1.178	1.178
Z_x	4.166	1.672	.631	− .815	− 2.27	− 9.53	− 9.53
a	.812	.508	.357	.378	.602	.959	.959
ϕ	72°.3	51°.4	30°.9	−36°.4	−58°.2	−76°.3	−83°

III

λ	28.2	29.5	30.0	31.0	31.4	32.0	33.0	34.0
Z_r	1.226	1.332	1.318	.925	1.144	1.253	1.267	1.455
Z_x	5.546	2.805	2.117	1.148	.819	− 1.273	− 2.339	− 4.566
a	.887	.724	.591	.498	.369	.397	.634	.824
ϕ	77°.5	64°.6	58°.1	51°.1	35°.6	−38°.8	−61°.6	−72°.4

IV

λ	28.2	31.0	32.0	33.0	33 5	34.0	36.0
Z_r	1.311	1.247	1.117	.869	.623	1.017	1.409
Z_x	8.578	4.317	2.231	1.125	− .036	− 1.254	− 4.281
a	.944	.831	.646	.513	482	.493	.812
ϕ	81°.3	73°.9	63°.4	52°.4	− 3° 3	−51°.0	−71°.8

V

λ	32.0	33.0	34.0	34.5	35.0	36
Z_r	1.417	1.447	1.144	.856	.714	1.042
Z_x	4.946	4.146	2.353	1.433	.632	− 1.61
a	.848	.798	.656	.576	.513	.556
ϕ	74°.0	70°.7	63°.9	59°.1	41°.5	−57°.1

The increase of resistance beyond the resonance point is a general effect observed in all cases. At resonance frequency the resistance is minimum. According to the current theory of Helmholtz Resonator the impedance of a resonator is given by

$$Z = R_r + R_f + j\left(\frac{\omega}{k} - \frac{c^2}{\omega v}\right)$$

$$\therefore \quad Z_r = R_r + R_f$$

where R_r represents the radiation resistance given by

$$R_r = \frac{\rho c k^2}{2\pi}$$

and R_f represents the resistance due to friction and is given by

$$R_f = \frac{l\rho}{\pi r^3}\sqrt{2\nu\omega}.$$

Here r is the radius of the neck of the resonator.
l, the length of the neck
ρ, the density of air
ν, the kinematic viscosity of air
$k = 2\pi/\lambda$, where λ is the wavelength of sound
$\omega = 2\pi f$, f being the frequency of sound.

In the above case

$r = .27$ cm. $l = .36$ cm. $\lambda = 33.5$ cms. $f = 1037$ cycles/sec.

$$R_r = \frac{\rho\omega k}{2\pi} = \frac{2\pi f\rho}{\lambda} = \frac{2\pi \times .0013 \times 1037}{33.5} = .2528$$

$$R_f = \frac{l\rho}{\pi r^3}\sqrt{2\nu\omega} = \frac{.36 \times .0013}{\pi \times .27^3}\sqrt{\frac{4 \times .132 \times \pi \times 1037}{33.5}} = .3137$$

$$Z_r = R_r + R_f = .5665.$$

From the results it can be seen that the expected resistance at resonance is also of the same order. The increase of resistance beyond resonance is a general effect observed in all cases and cannot be attributed to experimental errors. Sivian[2] has pointed out that the internal resistance term R_i depends upon the magnitude of the particle velocity in the orifice, and it increases considerably with the particle velocity. Since the velocity amplitude is maximum at resonance frequency, it seems that the increase of the total resistance is due to 'end correction.' It can also be seen that the resistance does not go on increasing, but starts decreasing after reaching a certain limit. It is clear from the tables that the resistance term does not exceed 1.5 ohms in any case.

The reflection coefficient is also minimum at resonance, showing thereby that the absorption of sound is greatest at resonance. Theoretically also it can be seen that the value of α can never be zero but is minimum at resonance.

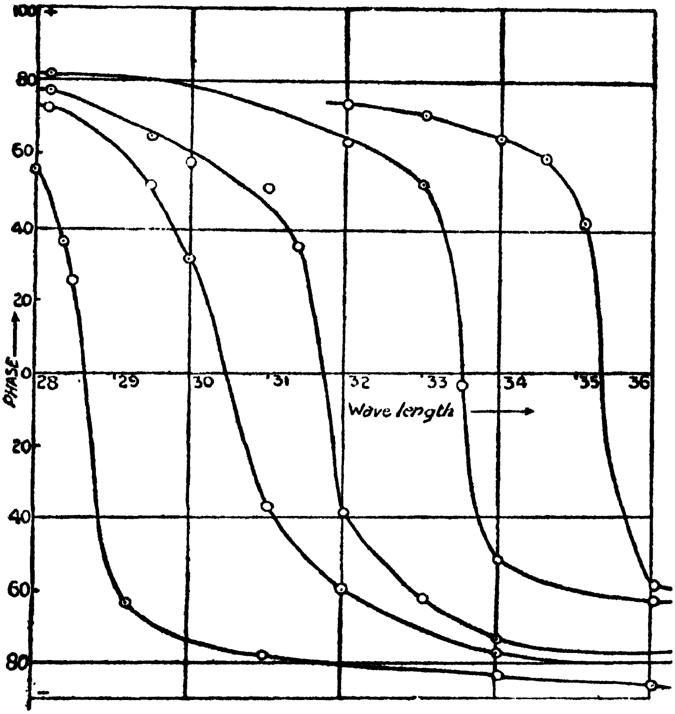

FIGURE 2

Figure 2 shows the variation of phase with wavelength. It can be observed that at resonance the phase becomes zero and, beyond it, it is negative. On both sides of resonance the phase does not go beyond 90° in any case. The change of phase is between +90° and −90° in every case.

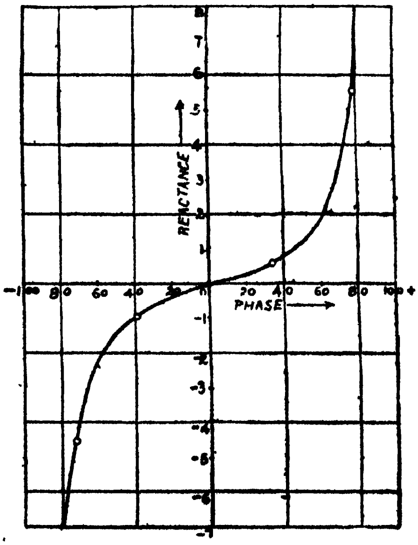

FIGURE 3

Figure 3 shows the relation between phase and reactance. It is found that the phase changes with reactance irrespective of the volume of the resonator. The reactance also becomes zero at resonance and then becomes negative which is entirely in agreement with theory. The curves for different resonators superimpose each other in this case.

PHYSICS DEPARTMENT,
ALLAHABAD.

REFERENCES

[1] C. Kanta, *Nat. Ins. of Sc.*, VI, 6716, 40.

[2] Sivian, *Jour. Acoustical Soc. America*, V, 46.

DETERMINATION OF DIPOLE MOMENT IN SOLUTION *

By G. R. PARANJPE

AND

D. J. DAVAR

(*Received for publication, March 1, 1941*)

ABSTRACT. The apparent electric moment of ortho-, meta- and para-nitrotoluene is measured in each of the solvents hexane, heptane, carbon tetrachloride, benzene, toluene, carbon disulphide and chloroform. The results are used to verify the empirical relations of Müller, Sugden and Jenkins, and the theories of Frank and Higasi, which connect the measured value of the electric moment with the value in the gaseous state. It is found that (1) the Sugden relation $P_2 = A + \frac{B}{\epsilon + 2}$ can be used for determining polarization at infinite dilution; (2) the empirical relation ${}_0P_2 = \alpha / \sqrt{\epsilon}$(solvent) represents the results as well as the relations of Sugden and Jenkins; (3) the idea of extrapolation to $\epsilon = 1$ for the gaseous state needs reconsideration since the values obtained from the relations of Sugden, Jenkins, Frank and the authors are widely different; (4) if a critical dielectric constant, which requires extrapolation to $\epsilon = 1.7$ for the gaseous state, is introduced as a hypothesis, there appears a general agreement between the values so derived from the relations of Sugden, Jenkins, Frank and the authors.

The apparent electric moment of ortho-, meta- and para-nitrotoluene was measured in each of the solvents hexane, heptane, carbon tetrachloride, benzene, toluene, carbon disulphide and chloroform at room temperature (30°C). These solvents cover a range of dielectric constant 1.878 to 4.795. Of them hexane, heptane, carbon tetrachloride, benzene and carbon disulphide may be regarded as non-polar, and toluene as slightly polar. Chloroform, which is decidedly polar, was selected to test the applicability of the empirical relations to polar solvents.

Hexane and heptane (both Kahlbaum) were kept over calcium chloride and distilled over phosphorus pentoxide.

Carbon tetrachloride (Merck) was distilled over phosphorus pentoxide.

Benzene (Kahlbaum—for analysis) was dried over sodium wire and fractionated.

Toluene (Kahlbaum) was dried over sodium wire and fractionated.

Carbon disulphide (Kahlbaum—for analysis) was distilled over phosphorus pentoxide.

Chloroform (Merck—anaesthetic) was distilled over phosphorus pentoxide.

Ortho- and meta-nitrotoluene (both Merck) were distilled.

Para-nitrotoluene (Merck) was recrystallised from benzene.

---

* Communicated by the Indian Physical Society.

In each case the solvent was distilled a few hours before using it and the use of stored samples was avoided. The values of the density, the refractive index and the dielectric constant are given in table I.

TABLE I

Substance	Density	Refractive Index	Dielectric Constant
Hexane	0.66680	1.3772	1.878
Heptane	0.71045	1.3972	1 942
Carbon tetrachloride	1 5756	1 4531	2.212
Benzene	0 86588	1 4932	2.262
Toluene	0 85404	1.4892	2.358
Carbon disulphide	1.2542	1.6200	2.648
Chloroform	1.4699	1.4389	4.795
o-nitrotoluene	1.1548	1.5422	...
m-nitrotoluene	1.1484	1.5424	. .

The apparatus and procedure were the same as employed in previous work[1].

The total molar polarization P_2 of a solute in a non-polar solvent is usually calculated from the Debye equation

$$P_2 = \frac{1}{f_2}\left[\frac{\epsilon-1}{\epsilon+2}\cdot\frac{M_1f_1+M_2f_2}{d}-\frac{\epsilon_1-1}{\epsilon_1+2}\,\frac{M_1}{d_1}\cdot f_1\right]$$

When P_2 varies with f_2, the polarization at infinite dilution ${}_{\infty}P_2$ is determined from the P_2—f_2 curves extrapolated to $f_2=0$. To avoid this graphical extrapolation, Hedestrand[2] has introduced the method of mathematical extrapolation which assumes a linear variation of the density and the dielectric constant of the solution with the mole-fraction of the solute at low concentrations. Thus $\epsilon=\epsilon_1(1+\alpha f_2)$ and $d=d_1(1+\beta f_2)$ ${}_{\infty}P_2=A\ (M_2-B\beta d_1)+C\alpha\epsilon_1$ where

$$A=\frac{\epsilon_1-1}{\epsilon_1+2}\,\frac{1}{d_1},\ B=\frac{M_1}{d_1}\quad\text{and}\quad C=\frac{3M_1}{d_1(\epsilon_1+2)^2}\ .$$

To avoid discrimination, polarization at infinite dilution was calculated using both the methods. The result is given in table II. The agreement between the two methods is good for ortho-nitrotoluene. For meta- and para-nitrotoluene the values exhibit differences. The disparity is more pronounced for para-nitrotoluene in the solvents hexane and heptane. Such differences might be attributed to the uncertainty involved in the extrapolation of the P_2—f_2 curves to $f_2=0$ wherever the curves are steep near $f_2=0$. Besides, $\alpha\epsilon_1$ and βd_1 do not always give constant values as might be expected from Hedestrand's assumption. In such cases graphical extrapolation of $\alpha\epsilon_1$ and βd_1 to $f_2=0$ has to be used, and the values are subject to the inaccuracies of graphical methods. Hence, it was thought desirable to calculate ${}_\infty P_2$ by a method which does not involve curvilinear extrapolation to $f_2=0$. Since the variation of ϵ and d with f_2 is not linear for some of the solutions, it was thought desirable to investigate the variation of ϵ and d with the weight fraction or the volume fraction of the solute. For this purpose solution of ortho-nitrotoluene in benzene, which does not show the linear variation of ϵ and d with f_2, was selected.

Le Fèvre [3] has used Hedestrand's method of mathematical extrapolation for calculating the specific polarization using weight fractions. Starting from the equation

$$p_2 = p_1 + \frac{1}{w_2}\left(\frac{\epsilon-1}{\epsilon+2}\,\frac{1}{d} - \frac{\epsilon_1-1}{\epsilon_1+2}\,\frac{1}{d_1}\right) \qquad \ldots \quad (1)$$

proposed by Sugden [4], Le Fèvre assumes that the variation of ϵ and d with w_2 (the weight fraction of the solute) is linear. Thus: $\epsilon=\epsilon_1(1+\alpha' w_2)$,

$$d=d_1\,(1+\beta' w_2) \text{ and } {}_\infty p_2 = p_1(1-\beta') + C\alpha'\epsilon_1,$$

where $$p_1 = \frac{\epsilon_1-1}{\epsilon_1+2}\,\frac{1}{d_1} \quad\text{and}\quad C = \frac{3}{d_1(\epsilon_1+2)^2}$$

When $\alpha'\epsilon_1$ and $\beta' d_1$ are calculated for *o*-nitrotoluene in benzene the values are not constant and graphical extrapolation is necessary. The specific polarization ${}_\infty p_2$ is 2.443 and the molar polarization ${}_\infty P_2 = M_2 p_2 = 335$ c.c.

Having failed so far in avoiding curvilinear extrapolation it was now thought necessary to develope other methods. It may be assumed that the variation of ϵ and d with V_2 (the volume fraction of the solute) is linear. Such an assumption is supported by the mixture law for densities and Silberstein's formula for the dielectric constant of mixtures. Thus $\epsilon=\epsilon_1(1+\alpha V_2)$ and $d=d_1(1+\beta V_2)$. Substituting for ϵ and d in the Sugden relation (1), we have

$$p_2 = p_1 + \frac{1}{w_2 d}\cdot\frac{V_2[3\alpha\epsilon_1 - \beta(\epsilon_1-1)\{\epsilon_1(1+\alpha V_2)+2\}]}{\{\epsilon_1(1+\alpha V_2)+2\}(\epsilon_1+2)}\,.$$

Putting $V_2 = \dfrac{w_2 d_1}{d_2 + w_2 d_1 - w_2 d_2}$ and proceeding to the limit when $V_2 \to 0$,

$$\begin{aligned} {}_\infty p_2 &= p_1 + \frac{1}{d_2}\cdot\frac{3\alpha\epsilon_1 - \beta(\epsilon_1-1)(\epsilon_1+2)}{(\epsilon_1+2)^2} \\ &= p_1(1-\beta d_1 K) + KL\alpha\epsilon_1 \end{aligned}$$

where $$p_1 = \frac{\epsilon_1-1}{\epsilon_1+2}\,\frac{1}{d_1}\,;\; K=\frac{1}{d_2} \text{ and } L=\frac{3}{(\epsilon_1+2)^2}\,.$$

Again $a\epsilon_1$ and $\beta\epsilon_2$ calculated for *o*-nitrotoluene in benzene are not constant and graphical extrapolation is necessary. The specific polarization $_\infty p_2$ is 2·432 and the molar polarization $_\infty P_2$ is 333 c.c.

In order to exhaust the possible methods of mathematical extrapolation to infinite dilution, the following method based on the volume polarization introduced by Van Arkel and Snoek [5] was attempted.

Starting from $p_2 = p_1 + \frac{1}{V_2}(p_{12} - p_1)$, where the volume polarization $p = \frac{\epsilon - 1}{\epsilon + 2}$, we assume $\epsilon = \epsilon_1(1 + aV_2)$. Substituting for ϵ,

$$p_2 = p_1 + \frac{1}{V_2}\left[\frac{\epsilon_1(1 + aV_2) - 1}{\epsilon_1(1 + aV_2) + 2} - \frac{\epsilon_1 - 1}{\epsilon_1 + 2}\right]$$

$$p_2 = p_1 + \frac{1}{V_2} \cdot \frac{3a\epsilon_1 V_2}{(\epsilon_1 + 2)\{\epsilon_1(1 + aV_2) + 2\}}.$$

Proceeding to the limit when $V_2 \rightarrow 0$

$$_\infty p_2 = p_1 + \frac{3a\epsilon_1}{(\epsilon_1 + 2)^2}.$$

It may be noted that this method reduces the mathematical calculations considerably. Taking the extrapolated value of $a\epsilon_1$, the polarization per c.c. $_\infty p_2 = 2.846$ and the molar polarization $_\infty P_2 = 338$ c.c.

The Sugden relation $P_2 = A + B\frac{\epsilon - 1}{\epsilon + 2}$ applied to a solute in one particular solvent at one temperature is found to hold for all the solutions investigated. According to Sugden [6] $A = a + {}_{ga}P_2$ and $B = {}_{ga}P_o$. From the solutions investigated this part of Sugden's relation cannot be substantiated. The values of A are different for the same solute in different solvents, the extreme variation being 6%. This may be due to the variation of a with the solvent. The slope B of the lines is not constant for the same solute in different solvents, the extreme variation being 11%. Similar variations of A and B have been noted by Jenkins.[7] Thus, while it is generally accepted that the Sugden relation is of the right form for a solute in one particular solvent at one temperature, "it is doubtful if the significance originally attached to A... and to B... can be substantiated either theoretically or from actual measurements." (Glasstone[8])

So far the Sugden relation has been used exclusively to calculate the polarization in the gaseous state. Taking advantage of the linearity of the relation it was thought desirable to use it to calculate the total molar polarization ($_\infty P_2$); this being the value of P_2 at $\frac{\epsilon_1 - 1}{\epsilon_1 + 2}$, where ϵ_1 is the dielectric constant of the pure solvent. Such a method has an obvious advantage over the usual method of curvilinear extrapolation using the P_2—f_2 curves. Since the relation is linear, $_\infty P_2$ can be calculated by mathematical computation using either the method of averages or least squares. $_\infty P_2$ calculated in this manner is given in table II. The values agree, wherever possible, with those obtained from graphical extrapolation and Hedestrand's method. On account of the mathematical procedure involved, the results obtained from the Sugden relation were used to calculate the electric moment.

TABLE II

Polarisation at infinite dilution by different methods

	Hexane	Heptane	Carbon tetrachloride	Benzene	Toluene	Carbon disulphide	Chloroform
o-nitrotoluene							
Graphical	342	363	334	330	319	295	224
Hedestrand's	343	365	333	333	316	293	225
Sugden's	346	354	334	330	317	302	224
m-nitrotoluene							
Graphical	429	441	395	411	385	375	266
Hedestrand's	417	432	391	418	389	372	261
Sugden's	420	428	404	412	388	365	264
p-nitrotoluene							
Graphical	493	503	442	452	443	415	306
Hedestrand's	484	473	435	462	444	408	298
Sugden's	486	469	443	454	434	412	302

For each of the solutions the electronic polarization P_{E_2} was sensibly constant. Hence the relation $P_{E_2} f_2$—f_2 represents a straight line whose slope is P_{E_2}. P_{E_2} was, therefore, calculated using least squares. The apparent electric moment was calculated from

$$\mu = 0.01273 \sqrt{(_\infty P_2 - P_{E_2})\,T} \text{ Debye.}$$

The values are given in table III.

TABLE II

Apparent electric moment of o-, m- and p-nitrotoluene

Solvent	ortho-	meta-	para-
Hexane	3.91	4.33	4.68
Heptane	3.94	4.38	4 60
Carbon tetrachloride	3.81	4.23	4.45
Benzene	3.79	4.29	4.52
Toluene	3.71	4 12	4.41
Carbon disulphide	3.61	4.01	4.29
Chloroform	3.01	3.32	3 59

Applying Müller's empirical relation

$$\frac{P_0 \text{ (solution)}}{P_0 \text{ (gas)}} = 1 - 0.075 \, (\epsilon_{\text{solvent}} - 1)^2$$

to the data in hand the following results were obtained.

TABLE IV

P_0(gas) and μ(gas) calculated from Müller's relation

	ortho-		meta-		para-	
	P_0 (gas)	μ (gas)	P_0 (gas)	μ (gas)	P_0 (gas)	μ (gas)
Hexane	330.1	4.03	405.4	4.46	474.4	4.83
Heptane	338.5	4 08	417.8	4 53	461.7	4 76
Carbon tetrachloride	332.7	4 04	410.2	4.49	454.0	4.72
Benzene	332.7	4.04	425.9	4.57	472 4	4.82
Toluene	324.9	4 00	406.1	4.47	459.6	4 75
Carbon disulphide	332.8	4.04	411.9	4.50	469.7	4.80

The agreement for all the solutes is fairly good.

The Sugden relation ${}_{\infty}P_2 = A + B \dfrac{\epsilon - 1}{\epsilon + 2}$, as applied to one solute in different solvents, was next considered. According to Sugden, the extrapolated value of ${}_{\infty}P_2$ at $\epsilon = 1$ should give the total polarization in the gaseous state augmented by a small constant, while the slope of the line should give the orientation polarization in the gaseous state. The graph showing ${}_{\infty}P_2$ against $\frac{\epsilon-1}{\epsilon+2}$ represents a straight line. The values of the intercept A and the slope B of the lines are:

ortho-nitrotoluene	A 454,	− B 420
meta-nitrotoluene	A 552,	− B 514
para-nitrotoluene	A 618,	− B 550

Jenkins' relation ${}_{\infty}P_2 = K_1 + \frac{K_2}{\epsilon}$ was next considered. The graph showing ${}_{\infty}P_2$ against $\frac{1}{\epsilon}$ was found to indicate the expected straight line. When the line was extrapolated to $\epsilon = 1$, to obtain the polarization in the gaseous state, the intercept was found to be too high. At this stage it was thought desirable to exclude the results directly read off from the graphs. Jenkins' relation may be written as ${}_{\infty}P_2\epsilon = K_1\epsilon + K_2$. The constants K_1 and K_2 were calculated using the method of averages. The values obtained were:

ortho-nitrotoluene	K_1	140,	K_2	416,	K_1+K_2	556
meta-nitrotoluene	K_1	157,	K_2	535,	K_1+K_2	692
para-nitrotoluene	K_1	193,	K_2	558,	K_1+K_2	751

K_1+K_2 given in the last column represents the value of the polarization in the gaseous state ($\epsilon = 1$).

Failing to get any correspondence between the values derived from the empirical relations of Müller, Sugden and Jenkins, it was thought desirable to investigate the relation between the polarization at infinite dilution ${}_{\infty}P_2$ and the dielectric constant ϵ of the solvent. It may be assumed that ${}_{\infty}P_2$ and ϵ are connected by a relation ${}_{\infty}P_2 = a\epsilon^b$.

Hence $\log {}_{\infty}P_2 = \log a + b \log \epsilon$.

The plot of $\log {}_{\infty}P_2$ against $\log \epsilon$ for solution in different solvents showed three parallel lines with an approximate slope −0.5. This furnishes an indication that the relation is the same for all the solutes. The graphical methods, however, are subject to personal error; hence the slope and the intercept were evaluated using least squares. This method has a further advantage; the correlation coefficient provides a test for the linearity of the relation which is assumed. The results are:

Solute	Intercept	Slope b	Correlation co-efficient
o-nitrotoluene	487	−0.4928	1−0.004
m-nitrotoluene	608	−0.5256	1−0.01
p-nitrotoluene	666	−0.5012	1−0.004

Thus for the substances investigated $_{\infty}P_2 = \frac{a}{\sqrt{\epsilon_{\text{solvent}}}}$

when $\epsilon = 1$, $_{\infty}P_2 = a$; and this may be regarded as the value for the gaseous state.

So far as the empirical relations are concerned it may be concluded that: (*i*) of the four empirical relations considered, Müller's relation gives the best agreement; (*ii*) the relations of Sugden, Jenkins and the authors are suitable to represent the results; (*iii*) extrapolation to $\epsilon = 1$ gives widely different values in the three instances where it is used. At this stage it is felt that there is good reason to suspect the validity of extrapolation to $\epsilon = 1$ for the gaseous state. The empirical relations have been derived from results obtained from measurements on solutions and as such must apply only so far as the liquid state is concerned. The region beyond the point representing the pure solvent is unexperimented on and to that extent unknown; there is no evidence to assume that the prolongation of the graphs in that region is valid.

Frank's relation $\frac{\mu(\text{sol.})}{\mu(\text{gas})} = 1 + (A_1 + A_2) - \frac{A_1 + A_2}{\epsilon}$ was then considered. The equation may be written in the form $\mu(\text{sol.}) = a + b/\epsilon$. The constants a and b were calculated applying the method of averages. Knowing these, the moment in the vapour state ($\epsilon = 1$) was calculated.

o-nitrotoluene	μ(gas) 5.31
m-nitrotoluene	μ(gas) 6.00
p-nitrotoluene	μ(gas) 6.17

These values are very high compared with those derived from Müller's relation. It may, however, be remarked that Frank's equation usually gives a high value on extrapolation to $\epsilon = 1$.

The applicability of Higasi's theories was next considered. In the absence of the values of the optical polarizabilities of ortho-, meta- and para-nitrotoluene, the size of the molecule was ascertained from X-ray data. It is now fairly well established that the benzene nucleus is similar, both in structure and in dimensions, to the plane ring of six carbon atoms, each of diameter 1.41 Å, previously known to exist in graphite.

Starting from this plane model, the dimensions of the molecules of ortho-, meta- and para-nitrotoluene were calculated taking the necessary data from Robertson[9] and James, King and Horrocks.[10] The electric moment might be taken to act along the diameter of the regular hexagon joining the centres of the C-atoms of the benzene ring. Since the moment of $-NO_2$ is -3.8 and of $-CH_3$ 0.4 (Williams[11]) it may be assumed that while locating the dipole only $-NO_2$ need be considered. Higasi[12] has assumed the dipole to be at the centre for the nitrobenzene molecule. Hence it was assumed that the dipole in ortho-, meta- and para-nitrotoluene is also at the centre of the molecule. Taking a to represent the length along the dipole axis and b to represent the width of the molecule, the ratio $a/b = K$ was calculated from the X-ray data. Thus

o-nitrotoluene	a 6.23,	b 4.98,	K 1 251,	A −0.059
m-nitrotoluene	a 6.23,	b 4.98,	K 1.251,	A −0.059
p-nitrotoluene	a 7.70,	b 4.23,	K 1.42,	A −0.142

Since K is greater than unity in each case, the value of A was calculated from $A = \frac{}{K^2-1}\left\{1-\frac{K}{\sqrt{K^2-1}}\log\left(K+\sqrt{K^2-1}\right)\right\}-\frac{1}{3}$. Using these values of A, μ(gas) was calculated from

$$\mu(\text{gas}) = \frac{\mu(\text{sol})}{1+3\frac{\epsilon-1}{\epsilon+2}A}.$$

Solvent	Ortho-	Meta-	Para-
Hexane	4·07	4·51	5·18
Heptane	4·11	4·57	5.12
Carbon tetrachloride	4·01	4·46	5·07
Benzene	4·00	4·53	5·17
Toluene	3·93	4·36	5·09
Carbon disulphide	3·85	4·28	5·05
Chloroform	3·34	3·68	4·71

The values calculated from Higasi's equations show a slight agreement with those derived from Müller's relation for ortho- and meta-nitrotoluene. For para-nitrotoluene the agreement is not good. Besides, the results for solution in chloroform do not fit into the set. Assuming that this difference is due to fixing the dipole at the centre of the molecule, instead of locating it at the contact of C and N atoms, the result for para-nitrotoluene was recalculated using $A = B_1 + A_2$.

$$B_1 = \frac{-c^2}{a_1^2-c^2}\left\{1-\frac{a_1}{\sqrt{c^2-a_1^2}}\sin^{-1}\frac{\sqrt{c^2-a_1^2}}{c}\right\}-\frac{1}{3}$$

$$A_2 = \frac{-c^2}{a_2^2-c^2}\left\{1-\frac{a_2}{\sqrt{a_2^2-c^2}}\log\frac{a_2+\sqrt{a_2^2-c^2}}{c}\right\}-\frac{1}{3}$$

$a_1 = 1.99$, $a_2 = 5.71$, $c = 2.11$ were calculated from X-ray data.

Recalculating μ(gas) for para-nitrotoluene the following result was obtained.

Solvent	μ(gas)
Hexane	5·32
Heptane	5·27
Carbon tetrachloride	5·25
Benzene	5·36
Toluene	5·28
Carbon disulphide	5·28
Chloroform	5·10

There is good agreement between the values for different solvents if we assume the dipole to be at the contact of C and N atoms; on the other hand, the difference between μ(gas) from Higasi's equation and from Müller's relation has increased. It is difficult to choose between the two sets of values since each set shows good inter-agreement and there is no extraneous determination of the moment in the gaseous state. It may, then, be concluded that while Higasi's equation gives in some cases values nearly the same as those given by Müller's relation, it is reduced to an approximation when the dimensions of the molecule are not known. Besides, exact location of the dipole in the molecule is uncertain in many cases, and to that extent are uncertain the results obtained from Higasi's theory.

It seems apparent that no agreement is possible between gas P_2 derived from different empirical relations so long as extrapolation is carried out to $\epsilon = 1$ for the gaseous state. The validity of extrapolation to $\epsilon = 1$ has already been questioned. Marsden and Moss[13] have shown that the dielectric constant of liquids and their saturated vapour are not identical at the critical temperature. In view of this discontinuity in the dielectric constant it seems reasonable to carry out extrapolation only up to transition from the liquid to the gaseous state.

Le Fèvre[14] has found that the dielectric constant of benzene, carbon tetrachloride, carbon disulphide and other liquids is nearly the same at the critical temperature of the respective liquids. This may be called the critical dielectric constant. Since the polarization of a non-polar substance does not vary with temperature, the critical dielectric constant can be calculated from

$$\frac{\epsilon_c - 1}{\epsilon_c + 2} \frac{1}{d_c} = \frac{\epsilon - 1}{\epsilon + 2} \frac{1}{d}$$

where the sub-index c denotes the values at critical temperature. The transition dielectric constant at temperature t°C may be calculated from $\epsilon_t = \epsilon_c + \frac{d\epsilon}{dt}(t - T_c)$. The transition dielectric canstant works out to be 1.60 for hexane, 1.64 for heptane, 1.81 for carbon tetrachloride and 1.86 for benzene at 30°C. Hence for one solute in different solvents extrapolation may be carried out to $\epsilon = 1.7$, (the mean).

When the relations of Sugden, Jenkins and the authors are each extrapolated to $\epsilon = 1.7$, there is a general unification in the values obtained from the different relations.

Substance	Müller c.c	Sugden c.c.	Authors c.c.	Jenkins c.c.
o-nitrotoluene	369	368	374	385
m-nitrotoluene	451	466	466	472
p-nitrotoluene	503	513	511	521

Table V gives the value of the electric moment in the gaseous state of ortho-, meta- and para-nitrotoluene as obtained from different methods. The values marked with asterisks are calculated using extrapolation to $\epsilon = 1.7$. The mean value of the moment in different solvents is taken for Müller's relation. The same is done for the values derived from Higasi's equation but the polar solvent chloroform is not taken into account.

TABLE V

	o-nitrotoluene	*m*-nitrotoluene	*p*-nitrotoluene
Müller	4.04	4.51	4.78
Sugden*	4.03	4.53	4.84
Authors*	4.07	4.58	4.82
Jenkins*	4.13	4.62	4.87
Frank*	4.15	4.64	4.86
Higasi	4.00	4.45	5.11

PHYSICS LABORATORY, ROYAL INSTITUTE OF SCIENCE,
BOMBAY

REFERENCES

1 Paranjpe and Davar, *Indian Journal of Physics*, **12**, 283 (1938).
2 Hedestrand, *Z. physikal Chem.*, **B 2**, 428 (1929).
3 Le Fèvre, *J.C.S.*, 1807 (1937).
4 Sugden, *Trans. Farad. Soc.*, **30**, 720 (1934).
5 Van Arkel, *Trans. Farad. Soc.*, **30**, 721 (1934).
6 Sugden, *Nature*, **133**, 415 (1934).
7 Jenkins, *J.C.S.*, 611 (1935).
8 Glasstone, *Annual Reports, Chem. Soc.*, 117 (1936).
9 Robertson, *Proc. Roy. Soc.*, **A 142**, 669 (1933).
10 James, King and Horrocks, *Proc. Roy. Soc.*, **A 153**, 241 (1936).
11 Williams, *Physik. Z.*, **30**, 391 (1929).
12 Higasi, *Scientific Papers of I.P.C.R.* (Tokyo), **28**, 286 (1936).
13 Marsden and Moss, *Canad. J. of Research*, **13**, sect. **B**, 296 (1935). (Abst. 1936, No. 835).
14 Le Fèvre, *Trans. Farad. Soc.*, **34**, 1131 (1938).

ELECTROLYTIC DISSOCIATION IN NITRIC ACID AS STUDIED BY RAMAN EFFECT*

By N. RAJESWARA RAO, M.Sc.

(Received for publication, March 1, 1941)

ABSTRACT. Electrolytic dissociation in nitric acid was studied by employing Raman Effect first by I. R. Rao. He studied the degrees of dissociation of the acid in different concentrations, relative to the highest concentration. In the present work, the absolute degree of dissociation of the acid is calculated by comparing the intensities of the Raman lines in the spectra of solutions of sodium nitrate and nitric acid of equal molal concentrations, assuming that sodium nitrate dissociates completely even in very concentrated solutions. The results indicate that in the lower concentrations, the increase of dissociation with dilution is very small, whereas in the concentrated solutions, it is rapid. This is explained as being due to the increase in the H-ions in the lower concentrations, which therefore favour the backward reaction.

$$HNO_3 \longrightarrow H^+ + NO_3'.$$

INTRODUCTION

It is first suggested by I. R. Rao[1,2] that Raman Effect can be employed to study the electrolytic dissociation in concentrated solutions of strong electrolytes and nitric acid was the first to be studied by him. On studying the Raman spectra of the acid in different concentrations, he observed two sets of lines one decreasing in intensity on diluting the acid and the other increasing in intensity up to a certain dilution. The latter set of lines are found in solutions of nitrates also. He concluded that the first set of lines, the strongest of which is of Raman frequency about 1300, are excited by the undissociated nitric acid molecules, and the latter, the strongest of which is of frequency 1050, are excited by the nitrate ion. On determining the intensities of the lines for solutions of different concentrations he determined the relative degree of dissociation of the acid in different concentrations.

In a previous communication,[3] the author, while reporting similar investigation in solutions of sulphuric acid, suggested that since the sulphates of alkaline elements can be assumed to be completely dissociated in solutions, a comparative study of the intensity of the Raman lines due to the sulphate ion in solutions of the sulphate, acid sulphate and sulphuric acid affords a method

Communicated by the Indian Physical Society.

of obtaining the value of absolute degree of dissociation of the acid in different concentrations. The present work is undertaken to make a similar study in nitric acid, as thus far no one has attempted to determine the absolute degree of dissociation of this substance by a study of its Raman effect.

EXPERIMENTAL

The experimental technique is the same as that employed in the case of sulphuric acid. The Raman spectra of sodium nitrate and nitric acid at different concentrations are taken to compare the intensity of the 1050 line excited by the NO_3' ion in the acid and the salt. Solutions of concentrations from 14.85N to 2.3N are worked with and are exposed for equal times. The intensities of the lines are measured in the usual manner by employing a Zeiss step-filter.

RESULTS

The intensities of the lines are tabulated in the table I.

TABLE I

Concentration (molal)	Intensity if equal exposures are given	No. of NO_3 ions	Percentage degree of dissociation
14.85	29.1	1.96	13.2
13.5	37.8	2.55	18.9
12.15	43.0	2.90	23.9
10.80	53.8	3.63	33.6
7.2	62.1	4.19	58.2
5.7	64.1	4.33	76.0
4.5	57.8	3.90	86.7
3.5	46.1	3.12	89.2
2.3	31.5	2.13	92.6

Since, in the solutions of sodium nitrate, the molecules are assumed to be completely dissociated, the number of NO_3' ions in that solution equals the total number of molecules. Therefore, on dividing the intensity of the 1050 line in the sodium nitrate solution by the total number of molecules of $NaNO_3$, the intensity of the Raman radiation due to each NO_3' ion "a" can be obtained. The intensities of the 1050 line in all the solutions are tabulated in column 2. Dividing these values of the intensities by "a" the number of NO_3' ions "n" in each of the solutions of the acid is obtained. Dividing this number by the total number of molecules of the acid the degree of dissociation α in each of the solutions is calculated and tabulated in column 4.

To have an idea of the nature of the variation of the electrolytic dissociation of nitric acid with dilution, the degree of dissociation is plotted against the concentration for the different solutions of the acid in figure 1. It is evident from the graph that, in the higher concentrations, the rate of dissociation is very large while in the lower concentrations it is less as is conspicuous from the smaller inclination of the curve to the dilution axis for these concentrations. A similar result was obtained in the case of solutions of sulphuric acid and it is explained as being due to the increased number of H-ions formed on dissociation, which favour the backward reaction in the equation in the case of smaller concentrations.

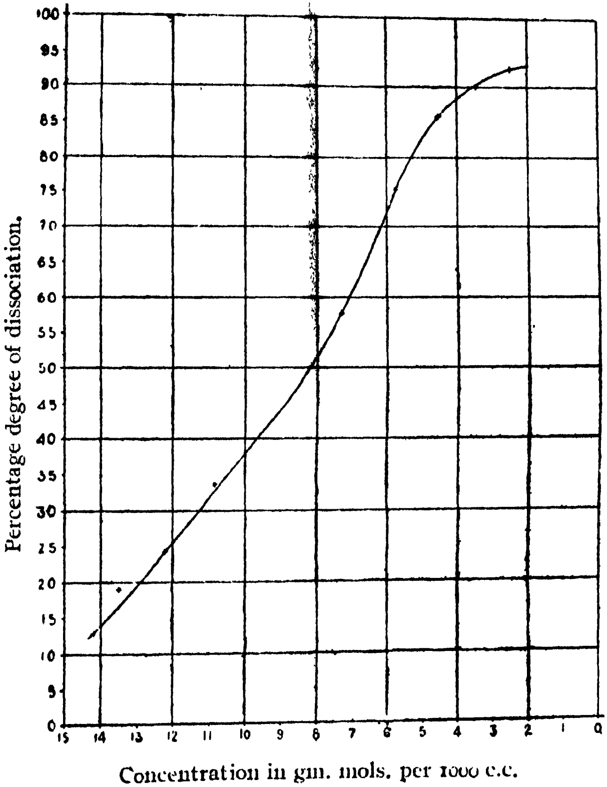

FIGURE 1

$$H_2SO_4 \rightleftharpoons HSO_4' + H^+.$$

It is quite likely that a similar explanation holds good in the case of nitric acid also. Due to the increase in the H-ions with dilution, the backward reaction in the equation

$$HNO_3 \rightleftharpoons NO_3' + H^+$$

is more favoured than the forward reaction.

In this connection, one point requires elucidation. It is assumed that sodium nitrate dissociates completely in solution, and the above calculation of the absolute degree of dissociation of the acid does not contemplate any polymerisation of the NO_3' ions. To test this point, solutions of sodium nitrate of concentrations 4.5N, 3.5N and 2.3N are taken and exposed for times proportional to dilution. The intensities of the 1050 line in solutions are measured and are found to be in the ratio 224.5 : 227.5 : 228.1. From the above values of the intensity, it is seen that they are nearly equal within the range of experimental error, and they confirm the assumption that sodium nitrate is completely dissociated at all concentrations and that there is no polymerisation of these ions.

But, Sidgwick [4,5], while studying the depression of freezing point of the solutions, finds that, on calculating the depressions on the assumption that the salts are completely dissociated, the values are too low. For example, with the solutions of alkaline nitrates all of the same concentration 3N, he found that, while the calculated value of the depression of the freezing point comes out to be as high as 12°.4C, the experimental values are between 6°.3C and 9°.0C except for lithium nitrate where it agrees with the calculated value. Agreeing that the laws of dilute solutions cannot be applied to concentrated solutions, Sidgwick opines that the abnormally low value must be due to some polymerisation of the NO_3' ions into N_2O_6, in the concentrated solutions. The values of the depression of the freezing point calculated on this assumption will be too low and he thinks that this may be due to the hydration of the anions, and the high value of the depression in the lithium nitrate solution may be due to the high capacity of the Li^+ ion to form a hydrate in virtue of its smallness and positive charge and the fact that it is the only alkaline nitrate that forms a hydrate in the solid form, adds strength to this view.

If, as is assumed by Sidgwick, it is true that NO_3' ions polymerise in solution, the method adopted in this work for the calculation of the absolute degree of dissociation of nitric acid is based on a wrong foundation. Supposing that there is a certain number of polymerised NO_3' ions in 4.5N solution, of sodium nitrate, and that when the concentration is reduced, a depolymerisation of some of the N_2O_6 molecules is to be expected as the polymerised molecules always do so on dilution. Also, 2 sets of Raman lines, one corresponding to N_2O_6 type of molecules and the other due to NO_3 type are to be expected as in the case of solutions of acetic acid where Koteswaram[6] found that there is one set of lines corresponding to polymerised molecules and another set corresponding to the single molecules, the former set of lines being more prominent in concentrated solutions and as the solution is diluted, they become feeble, while the latter set becomes strong.

We do not find a similar behaviour in the case of Raman lines of nitrate solutions, and therefore we may assume that no polymerised molecules exist.

But, by some chance, the radiations excited by both the types of molecules may happen to be identical, in which case, the intensity of the 1050 line increases in intensity as the dilution is increased due to increase in the number of NO_3 ions formed on depolymerisation. As is already pointed out, the intensity of 1050 line did not change with dilution, thereby indicating that there is no increase in the number of NO_3 ions. Therefore, it can be safely concluded that the NO_3 ions are not polymerised, and the calculation of the degree of dissociation of nitric acid given in table I, based on this assumption, is correct.

The smaller values for the lowering of the freezing points may be due to the lowering of the osmotic pressures of the solutions due to the inter-ionic forces, as explained by Debye and Huckel.

In conclusion, the author wishes to record his grateful thanks to Dr. I. Ramakrishna Rao under whose direction the present work is undertaken.

DEPARTMENT OF PHYSICS,
ANDHRA UNIVERSITY,
WALTAIR.

REFERENCES

[1] I. R. Rao, *Proc. Roy. Soc. (Lond.)*, **127**, 279 (1930)

[2] I. R. Rao, *Proc. Roy. Soc. (Amsterdam)*, **33**, 634 (1930).

[3] N. R. Rao, *Ind. Jour. Phys.*, **14**, 143 (1940).

[4] Sidgwick, *Electronic theory of Valency*, 197.

[5] Sidgwick and Ewbank, *J. C. S.*, **125**, 2273 (1924).

[6] Koteswaram, *Zeits. f. Physik*, **110**, 118 (1938).

FRICTION BETWEEN A LIQUID SURFACE AND A SOLID NOT WETTED BY IT

By D. S. SUBRAHMANYAM, M.A.

(Received for publication, March, 1931)

ABSTRACT. If the narrow uniform stem attached to an oscillating float is given a thin coating of paraffin wax, the oscillations are very quickly damped and the value of the logarithmic decrement increases as the amplitude decreases. The hypothesis is made that this is due to friction between the solid and the liquid, which is of the same nature as that between two solids in relative motion. Applying the analysis of vibrations damped by solid friction in addition to fluid friction to these oscillations, it has been possible to calculate the value F, of the limiting kinetic frictional force per cm. of the line of contact. The values obtained with three stems of diameters 0.246 cm., 0.296 cm and 0.360 cm. have been found to be practically uniform : 15.36, 14.86 and 15.42 dynes per cm. respectively It is also found that the value of this friction decreases at low velocities and that it is considerably reduced by contamination of the water surface. For rough surfaces it is found to be higher and, in addition, to show a rise in value as the velocity increases For palmitic acid F is found to be 17.02 dynes per cm., and for stearic acid 27.90 dynes per cm.

These experiments confirm the hypothesis made by Adam and Jessop, in regard to the hysterisis of contact angle, that it may be the effect of a frictional force, F, operating along the solid surface with equal intensity as the liquid advances or recedes.

INTRODUCTION

While working on the oscillations of a float for verifying Stokes' theory of a sphere oscillating in a liquid,[1] it was found that the damping was very high sometimes and the logarithmic decrement, λ, several times greater than the normal value (*vide* Tables 1 and 2). Another interesting observation was that the value of λ increased as the value of the amplitude of oscillation became smaller. This is possible if the resistance offered to the motion of the float is independent of its velocity like friction between two solid surfaces in relative motion. This additional damping, on investigation, was found to be due to the contamination of the stem, for after repeated cleaning and washing of the stem, the damping was reduced to the normal value. It thus became evident that if the surface of the stem is contaminated, the surface of water offers frictional resistance to motion across it. Contaminating the stem in a known manner—giving it a coating of paraffin wax, for example,—it should be

---

* Communicated by the Indian Physical Society.

possible to study this frictional resistance between the surface of water and paraffin wax. The present paper is the result of investigations made in this direction.

This resistance to the motion of solid across the surface of water has a bearing on the angle of contact. It is found in the determination of the latter that the angle is much larger usually if the liquid is advancing than it is receding. This difference between the advancing and receding angles is called the 'hysterisis' of the contact angle, and so far the cause of this hysterisis is considered to be obscure.[2] Adam and Jessop[3] attempted to formulate the hysterisis as the effect of a frictional force, F, operating along the surface with equal intensity when advancing and receding motions were just prevented. It can be easily shown that if γ_{LA} is the surface tension of the liquid, θ_R and θ_A are the receding and advancing angles respectively, $2F=\gamma_{LA}(\text{Cos}\,\theta_R-\text{Cos}\,\theta_A)$. They, however, consider the description to be 'formal' for 'it is difficult to see how there can be a permanent frictional resistance to the motion of a liquid over a solid.' An alternative explanation adopted by most writers is that the work of adhesion between the liquid and the solid surface is actually different for a dry surface and for one that has been wetted even for a short time. The results of the experiments reported here go to show that the hypothesis of friction between the liquid surface and the solid is able to account for the large damping observed in the oscillation of the float in a satisfactory manner. The hypothesis of Adam and Jessop may therefore be taken to be confirmed by these experiments and their description considered to be real and not merely formal.

THE OSCILLATING FLOAT

The experiment was conducted on similar lines to the previous experiment[1] on the verification of Stokes' theory. The hollow spherical body of the float of diameter about 6″ has a glass stem of diameter about 2.5 mm. and length about 25 cm. attached to it radially. The sphere is suitably loaded with lead shot so as to make the sphere go under water with a portion of the stem above the surface. At the top of the stem is attached a small pan in which weights are placed to make the float sink to the desired point on the stem which is about its middle. A millimetre scale of length 10 cm. is attached to the stem below the pan and the turning points of the float as it oscillates up and down are read with the help of a reading telescope from a distance of 1½ metres. The tank of water in which the float oscillates is oval in shape and is about 5′ × 3′ × 1½′. It is kept in a closed room from which draughts of air are excluded. The float is initially kept displaced upwards from its equilibrium position and the wire attached to the top pan clamped between two vertical jaws. Releasing the clamp made the jaws go apart, when the float went down and oscillated. This method of starting was found to be as satisfactory as the previous one in which the float was tied up by an unspun silk fibre and started to oscillate by burning it. The method has an advantage in that the setting in the required position can be obtained more easily and speedily.

Cleaning the water surface : Before observations were made the water in the tank was made to overflow and the surface blown over from one side by an electric fan. This rendered the surface of water clean.

The experiment was first conducted with a clean stem without a coating and the damping observed. Paraffin wax was dissolved in benzene and the solution then applied to the stem from top to bottom by means of a small brush previously cleaned in benzene to form a very thin layer. The experiment was repeated after the coating dried.

Below are given typical sets of observations of consecutive turning points taken (1) with the clean stem and (2) with the stem coated with paraffin wax :—

Mean diameter of the spherical body of the float : 7.71 cm.

Mean diameter of the stem : 0.246 cm.

Period of oscillation : 51.6 sec.

TABLE 1

(*With clean stem*)

Turning Points	Extent of Swing A	$\mathrm{Log}_{10}A$	$\mathrm{Log}_{10}A_n - \mathrm{Log}_{10}A_{n-1}$
13.38 cm.			
19.72	6.34 cm.	0.8021	
14.17	5.55	0.7443	0.0578
18.99	4.82	0.6830	0.0613
14.73	4.26	0.6294	0.0536
18.49	3.76	0.5752	0.0542
15.19	3.30	0.5185	0.0567
18.09	2.90	0.4624	0.0561
15.52	2.57	0.4099	0.0525
17.77	2.25	0.3522	0.0577

Mean of 4 similar observations : 0.0566 Mean Value : 0.0562

TABLE 2

(*With paraffin wax coating*)

Turning points	Extent of Swing A	$\mathrm{Log}_{10}A$	$\mathrm{Log}_{10}A_n - \mathrm{Log}_{10}A_{n-1}$
12.62 cm.	6.04 cm.	0.7810	0.1485
18.66	4.29	0.6325	0.1885
14.37	2.78	0.4440	0.2708
17.15	1.49	0.1732	0.5821
15.66	0.39	$\bar{1}.5911$	0.9890
S 16.05	0.04	$\bar{2}.6021$	0.0000
16.01	0.04	$\bar{2}.6021$	0.0000
16.05			
...	...	...	...
...	...	...	...

It is seen from this table that not only is the logarithmic decrement much higher than that observed with the clean stem but it also increases gradually as the amplitude decreases. This goes on until the stage marked S is reached when the amplitude becomes very small and the oscillations are observed through the telescope to continue for a time with much less damping. The oscillations thus appear to be divided into two series : the large oscillations with considerable damping and the small oscillations with much less damping. Further, it is found that the period of the large oscillations is very nearly the same as that observed with the clean stem, 51·6 sec. in the above case, while the period of the small oscillations is much less, only about 18 sec. The cause for these small oscillations is not quite clear. They may be due to the circulation set up in the water by the oscillation of the float which does not stop by the time the oscillations proper of the float die out, which happens in a short interval of time in this case on account of friction. However, since this is a minute effect and its nature has not been understood, the small oscillations will be omitted from the present study and the considerable damping of the large oscillations taken up for investigation.

Starting with an extent of swing equal to 6·04 cm. the large oscillations come to an end after 5 semi-oscillations. This large damping together with the fact that the damping is proportionately greater at smaller amplitudes suggests that the resisting force responsible for this may be constant in magnitude, reversing its sign at the end of every semi-oscillation, as in the case of friction between two solid surfaces. This hypothesis may be tested by applying the results obtained for oscillations damped by solid friction to these large oscillations.

ANALYTICAL STUDY OF VIBRATIONS DAMPED BY SOLID FRICTION IN ADDITION TO FLUID FRICTION

The values of the logarithmic decrement λ of the float with a clean stem are found to be constant (*vide* Table I), which shows that the surrounding fluid offers a resistance which is proportional to its velocity. With the paraffin wax coating, resistance of the type of solid friction is brought into play in addition, so that the effect of both fluid friction and solid friction on the vibrating body has to be considered. Jenkins and Thomas[4] have given a spiral construction to represent this kind of motion, extending that given by Rowell[5] for the case of solid friction only. It will be assumed that the bulk of the liquid in which the float moves is at rest so that the relative velocity between the float and the liquid at a distance can be considered to be the velocity of the float $\dot{x}$ itself and the fluid friction to be $c\dot{x}$, where c is a constant. The equation of motion may be written to be

$$M\dot{x} = \pm f - Rx - c\dot{x}, \qquad \dots \quad (1)$$

R being the restoring force per unit displacement from the position of equilibrium between the weight of the float and the upward thrust, and f the limiting kinetic frictional resistance. R is evidently equal to $a\rho g$ where a is the area of cross-section of the stem, ρ the density of the fluid, and g the acceleration due to gravity. M is the virtual[1] mass of the float.

Writing $p = \sqrt{\frac{R}{M}}$ and $n = \sqrt{p^2 - \frac{c^2}{4M^2}}$, we find that when the fluid damping is not excessive so that $p^2 > \frac{c^2}{4M^2}$ or $R > \frac{c^2}{4M^2}$, the solution is

$$x = \pm \frac{f}{R} + Ae^{-\frac{ct}{2M}} \cos(nt + \epsilon) \qquad \dots \quad (2)$$

$$\text{and} \quad \dot{x} = -Ae^{-\frac{ct}{2M}} \left\{ n \sin(nt+\epsilon) + \frac{c}{2M} \cos(nt+\epsilon) \right\} \qquad \dots \quad (3)$$

$$= -pAe^{-\frac{ct}{2M}} \sin(nt + \epsilon + \phi) \qquad \dots \quad (4)$$

where $\cos\phi = \frac{n}{p}$ and $\sin\phi = \frac{c}{2Mp}$.

It should be noted that the sign of f is the same as $-\dot{x}$. Also f is a limiting value and equation (1) ceases to apply when $\dot{x}$ is zero. The constants A and ϵ in equation (2) depend upon the initial conditions.

The motion is represented diagramatically in the figure. Starting the

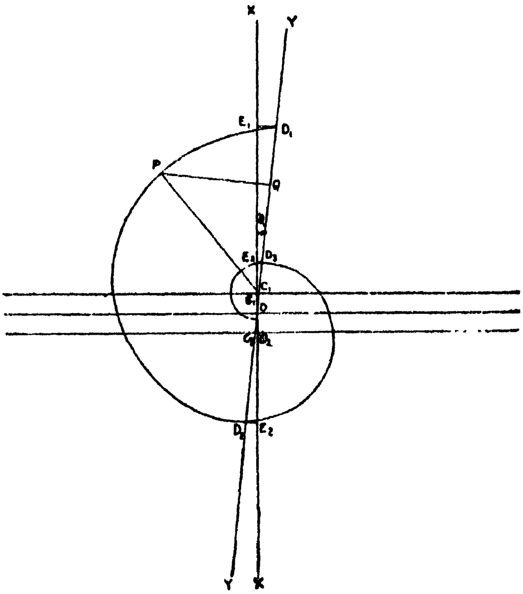

reckoning of time when the vibrating body is about to start from one extreme position, we have, if d_1 is the displacement at this instant,

$$d_1 = \frac{f}{R} + A_1 \cos \epsilon_1 \qquad \ldots \quad (5)$$

and since the velocity $\dot{x}$ is zero

$$o = -pA_1 e^{-\frac{ct}{2M}} \sin(\epsilon_1 + \phi) \qquad \ldots \quad (6)$$

from which it is seen that

$$\epsilon_1 = -\phi \qquad \ldots \quad (7)$$

$$\therefore \quad d_1 = \frac{f}{R} + A_1 \cos \phi. \qquad \ldots \quad (8)$$

If YY be drawn making an angle $-\phi$ with XX, a point c_1 taken on it so that $oc_1 \cos \phi = \frac{f}{R}$ and a point D_1 so that $c_1 D_1 = A_1$, it is seen that the displacement d_1 is given by the vertical projection oE_1 of oD_1 upon XX. At any subsequent moment in the next half oscillation

$$x = \frac{f}{R} + A_1 . e^{-\frac{ct}{2M}} \cos (nt - \phi) \qquad \ldots \quad (9)$$

so that the displacement at the time t may be derived from the vertical projection of the rotating arm $A_1 e^{-\frac{ct}{2M}}$ which revolves at angular velocity n about the centre c_1, the extremity of the arm describing an equiangular spiral. And

$$-\frac{\dot{x}}{p} = A_1 . e^{-\frac{ct}{2M}} . \sin nt. \qquad \ldots \quad (10)$$

Thus values of $\left(-\frac{\dot{x}}{p} \right)$ are given by the lengths of the perpendicular projectors such as PQ from the extremity of the rotating arm OP on to YY. When the spiral curve intersects YY, the velocity of the vibrating mass is zero, the tangent to the spiral curve is horizontal and the vertical projection of the point of intersection gives the extreme displacement of the vibrating body. Thus $\frac{f}{R}$ next reverses sign at D_2 when $\dot{x} = o$, that is, when $t = \frac{\pi}{n}$, so that for the next half oscillation, changing the constants to meet the altered conditions, we have

$$x = -\frac{f}{R} + A_2 . e^{-\frac{ct}{2M}} . \cos (nt + \epsilon_2) \qquad \ldots \quad (11)$$

$$\dot{x} = -p.A_2.e^{-\frac{ct}{2M}}.\sin(nt+\epsilon_2+\phi). \qquad \ldots \quad (12)$$

Commencing anew at the point of discontinuity for this half oscillation again, we have $t=0$ at the instant represented by the point D_2, so that, since both sets of equations (9) and (10), and (11) and (12) must be satisfied for this point

$$\dot{x} = -p.A_2\sin(\epsilon_2+\phi) = 0 = \mp p.A_1 e^{-\frac{c\pi}{2Mn}} \sin\pi \qquad \ldots \quad (13)$$

or

$$\epsilon_2 = (\pi - \phi) \qquad \ldots \quad (14)$$

and

$$d_2 = x = -\frac{f}{R} + A_2\cos(\pi-\phi) = \frac{f}{R} + A_1 e^{-\frac{c\pi}{2Mn}}\cos(\pi-\phi) \qquad \ldots \quad (15)$$

or

$$A_2\cos(\pi-\phi) = \frac{2f}{R} + A_1.e^{-\frac{c\pi}{2Mn}}\cos(\pi-\phi)$$

i.e.

$$-A_2\cos\phi = \frac{2f}{R} - A_1 e^{-\frac{c\pi}{2Mn}}.\cos\phi$$

or

$$A_2 = -\frac{2f}{R\cos\phi} + A_1 e^{-\frac{c\pi}{2Mn}}. \qquad \ldots \quad (16)$$

If we take a point c_2 now on the other side of YY, so that, $c_2 0 = \frac{f}{R\cos\phi}$, it is seen that $c_1D_2 = A_1 e^{-\frac{c\pi}{2Mn}}$, and $c_1c_2 = \frac{2f}{R\cos\phi}$, so that $A_2 = c_2D_2$. Thus c_2 now represents the centre of the oscillation and $A_2 e^{-\frac{ct}{2M}}$ will be the rotating arm of the spiral for the next half oscillation. In this way the construction may be continued, the centres of the spiral shifting from c_1 to c_2 and *vice versa* until the spiral cuts the line YY at a point between c_1 and c_2, when the body will come to rest, the restoring force now acting being balanced by the force of friction. For this to happen, $A_n e^{-\frac{c\pi}{2Mn}}$ must be less than $\frac{2f}{R\cos\phi}$ or more strictly speaking $\frac{f+f_s}{R\cos\phi}$, where f_s is the limiting value of statical friction and A_n is the value of the rotating radius at the beginning of the last half oscillation.

The above investigation may now be extended to determine the positions corresponding to the centres of oscillation c_1 and c_2 from the turning points of the vibrating body. The value of the frictional force f can then be obtained. If E_1, E_2,... are the positions of the turning points, $OE_1 = d_1$, $OE_2 = d_2$,.... Draw

c_1b_1 and c_2b_2 horizontal through c_1 and c_2 cutting the vertical through o in b_1 and b_2 respectively.

Then
$$ob_1 = oc_1 \cos\phi = \frac{f}{R}. \qquad \dots \quad (17)$$

Similarly
$$ob_2 = oc_2 \cos\phi = \frac{f}{R} \qquad \dots \quad (18)$$

so that
$$b_1b_2 = \frac{2f}{R}. \qquad (19)$$

Again
$$b_1E_1 = c_1D_1 \cos\phi = A_1 \cos\phi \qquad (20)$$

and
$$b_1E_2 = C_1D_2 \cos\phi. \qquad (21)$$

But
$$c_1D_2 = A_1 e^{-\frac{c\pi}{2Mn}}. \qquad (22)$$

$$\therefore \quad b_1E_2 = A_1 \cos\phi \; e^{\frac{c\pi}{2Mn}} = b_1E_1 . e^{\frac{c\pi}{2Mn}} \text{ [from (10)]} \qquad \dots \quad (23)$$

$$\therefore \quad E_1E_2 = (b_1E_1 + b_1E_2) = b_1E_1(1 + e^{-\frac{c\pi}{2Mn}}). \qquad \dots \quad (24)$$

If the same oscillating system can be studied without solid friction and if a_1, a_2, a_3,...... be the magnitudes of the successive swings from one turning point to the next obtained, then we have the case of damped simple harmonic motion for which it is known that

$$\frac{a_1}{a_2} = \frac{a_2}{a_3} = \frac{a_3}{a_4} = \quad \dots \quad \dots \quad \dots \quad = k = e^{\frac{c\pi}{2Mn}} = e^{\lambda} \qquad \dots \quad (25)$$

where λ is the logarithmic decrement of the system. If λ be known, k can be calculated and

$$e^{-\frac{c\pi}{2Mn}} = \frac{1}{k} \qquad \dots \quad (26)$$

so that substituting in (24), $E_1E_2 = b_1E_1(1 + \frac{1}{k}) = b_1E_1 \frac{(k+1)}{k}$

or
$$b_1E_1 = E_1E_2 \cdot \frac{k}{(k+1)}. \qquad \dots \quad (27)$$

When the turning points E_1 and E_2 are known, the value of b_1E_1 can be calculated from the above equation and the position of b_1 determined. Similarly if E_2, E_3 are the turning points for the next half oscillation, it follows that

$$b_2E_2 = E_2E_3 \cdot \frac{k}{(k+1)} \qquad \dots \quad (28)$$

and the position of b_2 can be determined. In this way the centre of oscillation for each half oscillation can be calculated, b_1 and b_2 being obtained from alternate half oscillations. When the value of b_1b_2 is thus obtained, the value of the frictional force f is easily calculated from (19) : $\frac{2f}{R}=b_1b_2$.

APPLICATION TO THE OSCILLATING FLOAT

The value of k corresponding to the value of $\lambda=0.0566$ to base 10 as recorded in table 1 is 1.140. Applying the above method of obtaining b_1 and b_2 to the observations recorded in Table 2, we get the following results :—

TABLE 3

Turning Points	Extent of Swing E_1E_2 etc.	E_1C_1 etc.	C_1 $(E_1+E_1C_1)$	C_2 $(E_2-E_2b_2)$
12.62 cm.	6.04 cm.	3.22 cm	15.84 cm	
18.66	4.29	2.29		16.37 cm.
14.37	2.78	1.48	15.85	
17.15	1.49	0.79		16.36
15.66				
16.05	Mean Values:	C_1	15.845 cm.	
		C_2	16.365 cm.	
		C_1C_2	0.52 cm.	

The last half oscillation of the series is not included in the above calculations as the small oscillations that commence then introduce some uncertainty in the position of the last turning point. If the observed turning point 16.05 is accepted, the corresponding value obtained for C_1 will be 15.87 cm. The results obtained are of great significance. They show that the damping of the large oscillations is not an irregular phenomenon but it is the consequence of a systematic frictional force operating on the vibrating body. The experiment is repeated, varying the initial position of start. The following mean values are obtained for C_1C_2 :

0.52 cm. ; 0.52 cm. ; 0.50 cm. ; 0.50 cm. ; 0.51 cm. ; 0.50 cm. ; 0.52 cm. ; 0.52 cm. ; 0.49 cm. ; 0.49 cm. ; 0.50 cm. ; 0.52 cm.

It should be noted that a millimetre scale is read through the telescope in the experiment so that the second decimal place recorded in the observations is an estimated value. The values of C_1C_2 may therefore be taken to be constant. The mean of all the above values is 0.51 cm.

Now if we put $\frac{f}{R}$ equal to h,

$$h=\frac{b_1 b_2}{2}$$

and

$$f=R.h.$$

But

$$R=a\rho g$$

$$=\pi r^2\rho g,$$

where r is the radius of cross-section of the stem.

$$\therefore \quad f=\pi r^2\rho gh \qquad \ldots \quad (29)$$

A simple assumption that we may make in regard to f is that it acts along the line of contact of the liquid surface and the stem and that it is proportional to the length of the line along which it acts. Then if F is the force per unit length

$$f=2\pi r.F$$

or

$$F=\frac{f}{2\pi r}$$

$$=\frac{r.\rho gh}{2} \quad \text{[from (29)].} \qquad \ldots \quad (30)$$

(I) In the above experiment

$$r=0.123 \text{ cm.}$$

$$\rho=1 \text{ gm. per c.c.}$$

$$g=979 \text{ cm. per sec. per sec.}$$

and

$$h=\frac{0.51}{2}=0.255 \text{ cm.}$$

$$\therefore \quad F=\frac{0.123\times 1\times 979\times 0.255}{2}=15.36 \text{ dynes/cm.}$$

∴ The limiting value of the kinetic frictional force per / cm. between paraffin wax and water is 15·36 dynes.

(II) The experiment is repeated with a second glass stem of mean diameter 0.296 cm. A typical set of observations is given below :

Mean value of logarithmic decrement to base 10 : 0.0532.

Corresponding value of k : 1.131 ; Period=43.2 sec.

TABLE 4

Turning Points	Extent of Swing	E_1C_1 etc.	C_1	C_2	C_1C_2
20.14 cm.	7.11 cm.	3.77 cm.		16.37 cm.	
18.03	5.47	2.90	15.93 cm.		0.44 cm.
18 50	4.06	2.15		16.35	0.42
14.44	2.84	1.50	15.94		0.41
17 28	1.77	0.94		16.34	0.40
15.51	0.89	0.47	15.98		0.36
16.40	0.20	0.11		16.29	0.31
16.20 16.23 16.20 } small oscillations.					

Mean Value of C_1C_2 (of the first four) : 0.42 cm.

Mean values of b_1b_2 or $2h$ obtained by repetition of the experiment are : 0.42 cm. ; 0.41 cm. ; 0.41 cm. ; 0.41 cm. ; 0.41 cm. ; 0.41 cm. ; 0.40 cm. ; 0.41 cm.

Mean of these values : 0.41 cm.

$$\therefore \quad h = 0.205 \text{ cm.}$$

Substituting these values in (30), we get

$$F = \frac{0.148 \times 1 \times 979 \times 0.205}{2}$$

$$= 14.86 \text{ dynes per cm.}$$

(III) Values obtained for a third stem :

Mean diameter of the stem :	0.360 cm.
Logarithmic decrement to base 10 :	0.0472
Value of k :	1.115
Period of oscillation :	35.14 sec.

TABLE 5

Turning Points	Extent of Swing	E_1C_1 etc.	C_1	C_2	C_1C_2
17.40 cm.	5.10 cm.	2.69 cm.	14.71 cm.		
12.30 cm.	3.88	2 05		14.35 cm.	0 36 cm.
16.18	2.85	1.50	14.68		0.33 cm.
13.33	1.94	1.02		14.35	0.33 cm.
15.27	1.10	0.58	14.69		0.34 cm.
14.17					
14.59					
14.51					
14.58					

Mean Value : 0.34 cm.

Mean values of b_1b_2 or $2h$ obtained by repetition are :

0.34 cm. ; 0.34 cm. ; 0.36 cm. ; 0.36 cm. ; 0.35 cm. ; 0.35 cm.

Mean of these values : 0.35 cm.

$$\therefore \quad h = 0.175 \text{ cm.}$$

$$F = \frac{0.180 \times 1 \times 979 \times 0.175}{2}$$

$$= 15.42 \text{ dynes per cm.}$$

Thus the values of the limiting kinetic frictional force obtained with the three stems respectively are 15.36 dynes per cm.,

14.86 dynes per cm.

and 15.42 dynes per cm.

The fair agreement between these values shows that the assumption made that this frictional force is proportional to the length of the line of contact is justifiable.

Kinetic and Statical Friction:—From the theory of vibrations developed above it is to be expected that the float should come to rest at end of the *n*th semi-oscillation, when $A_n e^{-\frac{c\pi}{2Mn}}$ is less than $\frac{f+f_s}{R}$, f_s being the limiting statical friction. The float, on the other hand, is found to execute small oscillations. This variance is due to the short-coming of the theory, in that no account has been taken of the disturbance in the water of the tank which is produced by the oscillations. The centre of small oscillations, however, does not generally coincide with the point of normal equilibrium, *o*, which is the mid-point of C_1C_2. From Table 3, it is seen that the position of *o* is 16.11 cm., while the centre of small oscillations is 16.03 cm. Similarly in Table 4 the centre of small oscillations is 16.22, while *o* is 16.15. It is also found that the centre of small oscillations may lie on either side of *o*. Since the float ultimately comes to rest at this centre, it is seen that the float can remain in equilibrium at any point within a small range on either side of *o*, showing thereby that there is also a statical force of friction between paraffin wax and water. *It is an interesting observation that a floating body can have more than one position of equilibrium if the liquid does not wet the surface of the float.* It has been possible, by trial, to keep the float with the 0.246 cm. stem in equilibrium at different points within a range of 2 mm. A satisfactory method has yet to be devised by which the range corresponding to statical friction can be accurately determined.

Attention may also be drawn to another point which may be illustrated from Table 4. Values of C_1C_2 obtained from the first 5 half oscillations are fairly constant or may be considered to have a very slight gradual decrease; but when we come to the 6th half oscillation, for which the extent of swing is 0.89 cm., there is a sudden and appreciable shift in the position of C_1 (15.98) towards *o* (16.15), showing thereby that the value of kinetic friction has become less. The time for this half oscillation is 21.6 sec. so that the average velocity during this motion is 0.89/21.6 cm./sec. or 0.41 mm. per sec. This appreciable reduction in the value of kinetic friction when the amplitude is reduced is a common observation in these investigations. This is another reason for omitting the last large half oscillation in the above calculations, from which the steady value of F is obtained.

Ablett's work :—These observations are in qualitative agreement with the results obtained by Ablett[6] for the receding and advancing contact angles between paraffin wax and water. From the relation $2F = \gamma_{LA} (\cos \theta_R - \cos \theta_A)$ it is possible to calculate the value of the frictional force (kinetic) from the values of θ_R and θ_A obtained by him, since γ_{LA}, the surface tension of water, is known. Ablett finds that the values of the advancing and receding angles remain practically constant for speeds of 0.44 mm. per sec. and above, while for lower speeds the difference between the two angles is less. His values are as follows :—

TABLE 6

Velocity mm./sec.	θ_A	θ_R	$\theta_A - \theta_R$
0.1273	109°−24′	99°−34′	9°−50′
0.1943	110 −31	98 −45	11 −46
0.1313	112 −8½	97 −5	15 −3½
	Mean	Values	
0.441 and above	113 −9	96 −20	16 −49

Assuming γ_{LA} to be 75 dynes per cm. the value of F corresponding to the mean values noted above is

$$2F = 75\ (\cos 96^\circ.12' - \cos 113^\circ.9')$$

or

$$F = \frac{75 \times 0.282}{2} = 10.58 \text{ dynes/cm.}$$

the value of the kinetic frictional force is therefore 10.58 dynes per cm. This is decidedly less than the values calculated from the float experiments. This may be due to the difference in the nature of the surface of paraffin wax obtained on the stem from that in Ablett's experiment. There may be also another explanation for this difference. It is not stated in his paper whether the surface of water is cleaned before making the observations. Any small contamination present on the surface of water is found to affect the value of this friction considerably (as will be seen in the next section) and the lower value obtained by Ablett may also be due to a trace of contamination that might have been present if the surface was not cleaned.

CONTAMINATION OF THE WATER SURFACE

Before the study of the effect of contamination is taken up the upper edge of the tank is given a coating of paraffin wax since it is found that reliable results with thin films of fatty acids can be obtained under those conditions. The contamination is supplied by dissolving one drop of oleic acid in 6 c. c. of benzene and adding 4 drops of the solution to the surface of water in the tank. The vigorous spreading of the last benzene drop showed that the film was not complete, for it was found previously that when the film is complete there is no vigorous spreading but the drop collects in the form of a lens and evaporates slowly. Results obtained with this amount of contamination are given below. The experiment was conducted with the stem of diameter 0.246 cm.

TABLE 7

Turning Points	Extent of Swing	E_1C_1 etc.	C_1	C_2
12.23 cm.	7.02 cm.	5.75 cm.	15.98 cm.	
19.25	5.88	3.14		16.11 cm.
13.37	4.91	2.62	15.99	
18.28	4.08	2.18		16.10
14.20	3.39	1.81	16.00	
17.59	2.76	1.47		16.12
14.83	2.19	1.17	16.00	
17.02	1.70	0.91		16.11
15.32	1.25	0.67	15.99	
16.57	0.86	0.46		16.11
15.71	0.48	0.26	15.97	
16.19		Mean Values :	15.99	16.11
16.03				

$$\therefore \quad b_1 b_2 = 0.12 \text{ cm.}$$

and

$$h = 0.06 \text{ cm.}$$

$$\therefore \quad F = \frac{0.123 \times 1 \times 979 \times 0.06}{2}$$

$$= 3.61 \text{ dynes per cm.}$$

The value of the kinetic frictional force is reduced to about one-fourth by the contamination. This shows how even a small amount of contamination has a considerable effect on the frictional force between the surface of water and paraffin wax.

Palmitic acid

The experiments were also conducted with coatings of palmitic acid and stearic acid given to the stem (of diameter 0.296 cm.) in the same manner by dissolving in benzene These have the property of spreading on water unlike paraffin wax, and conditions of the water surface as well as the stem gradually alter as the float oscillates up and down. Observations taken at the first start are given below :

TABLE 8

Turning Points	Extent of Swing	E_1C_1 etc.	C_1	C_2
13.99 cm.	5.03 cm.	2.67 cm.	16.66 cm.	
19.02	3.55	1.88		17.14 cm.
15.47	2.27	1.20	16.67	
17.74	1.16	0.61		17.13
16.58				
——				
16.87				
16.82				
		Mean Values :	16.665	17.135

These values may be taken to be fairly constant. The mean value of $b_1 b_2$ is 0.47 cm. so that F is equal to 17.02 dynes per cm. In subsequent oscillations the value of $b_1 b_2$ is found to change gradually, the consecutive values in an experiment being 0.54 cm., 0.51 cm. and 0.48 cm. respectively.

Stearic acid

Observations of the first series of oscillations with a coating of stearic acid on the same stem are as follows :

TABLE 9

Turning Points	Extent of Swing	E_1C_1 etc.	C_1	C_2
11.30 cm.	7.98 cm.	4.23 cm	15.53 cm.	
19.28	5.59	2.97		16.31 cm.
13.69	3.50	1.86	15.55	
17.19	1.64	0.87		16.32
15.55				
——				
15.81				
15.76				
		Mean values :	15.54	16.31

The mean value of b_1b_2 is 0.77 cm. from which F is calculated to be 27.90 dynes per cm. a value much higher than that for paraffin wax or palmitic acid.

ROUGH SURFACES

The experiments described above were worked on the day next to the one on which the coating was given. This time was sufficient for the coating to dry. The values obtained for kinetic friction were fairly uniform. But if the coated stem was allowed to stand exposed for some days, the nature of the surface was found to alter, it became more rough, and the friction increased. The values of b_1b_2 were, moreover, not uniform but showed an increase with increase in amplitude. Observations obtained with the stem of diameter 0.296 cm. (normal value of $b_1b_2=0.41$ cm.) a week after the first experiments were performed are given below :—

TABLE 10

Turning Points	Extent of Swing	E_1C_1 etc.	C_1	C_2	C_1C_2
11.60 cm.	6.37 cm.	3.38 cm.	14.98 cm.	—	—
17.97	4.58	2.43	—	15.54 cm.	0.56 cm.
13.39	3.12	1.66	15.05	—	0.49
16.51	1.81	0.96	—	15.55	0.50
14.70	0.77	0.41	15.11	—	0.44
15.47	—	—	—	—	—
15.35	—	—	—	—	—
15.40	—	—	—	—	—
......	—	—	—	—	—

These are the types obtained whenever the surface is rough. It is thus a common observation that for rough surfaces the kinetic friction is not only greater but shows also a rise as the amplitude (*i.e.*, the average velocity) increases.

FRICTION AND HYSTERISIS OF CONTACT ANGLE

The reasults of the experiments described here are in close agreement with the observations on the hysterisis of contact angle. The agreement with Ablett's work has already been mentioned. The reduction in the value of friction on adding contamination to the surface of water can be deduced from the following equations :

$$W_{SL} = \gamma_{LA}(1+\cos\theta), \qquad \ldots \quad (31)$$

when W_{SL} is the work of adhesion between the solid and the liquid, and

$$2F = \gamma_{LA}(\cos\theta_R - \cos\theta_A). \qquad \ldots \quad (32)$$

From equation (31) it follows that when γ_{LA} is lowered on account of the contamination, the contact angle (the receding as well as the advancing) becomes less, since W_{SL} cannot be altered by the change. These changes and the reduction in the value of γ_{LA} may be taken to be responsible for lowering the value of the friction. In the case of rough surfaces also there is agreement. It is found that roughness of surfaces increases the angle of contact and also the hysterisis.[8] The float experiments give the additional information that kinetic friction increases with increase of velocity in these cases instead of attaining a steady value as in the case of smooth surfaces. From these considerations it follows that there is a close correspondence between hysterisis of contact angle and friction.

It becomes necessary therefore, in the light of these results, to reconsider the ideas entertained in regard to hysterisis. It appears doubtful whether the explanation "that the work of adhesion between the liquid and the solid surface is actually different for a dry surface and for one that has been previously wetted even for a short time"[9] can be accepted. In the float experiments the surface of the stem which gives the receding angle as the float rises up must be considered to be one which has been wetted previously, but as soon as the float reverses its motion and begins to sink, it will have to be considered as one which is dry so as to give the advancing angle an explanation that is not convincing. Preference will therefore have to be given to the alternative hypothesis of Adam which postulates the same frictional force to be operating in both the cases and which further is amply supported by the results of these experiments.

FRICTION AND WETTING

In conclusion, the connection between friction and wetting may be pointed out. When the stem is clean, it is wetted by water and a thin layer of water adheres to it as it comes out of the surface. In subsequent movements water outside moves over this layer and there is little friction. With the paraffin wax coating, on the other hand, there may be no possibility for such a layer as the stem is not wetted and frictional force comes into play each time the water moves over the surface of paraffin wax. The absence of the adhering liquid layer next to the surface of the solid may therefore be considered to be responsible for the friction observed when the liquid moves over the solid. Friction between a solid surface and a liquid is probably a general phenomenon. If such a view is taken, it should follow that even in the case of a solid that is wetted by a liquid there is a frictional force operating when the liquid advances over the dry surface of the solid for the first time. The low values obtained for the rise of water in a capillary tube when the walls are dry may be due to this cause. While there may be some doubt in regard to this view that friction between a solid and liquid is general, there can be no uncertainty however as to its being present between a solid and a liquid that does not wet it, as is found with paraffin wax, palmitic acid and stearic acid.

It may be noted in this connection that the place where the friction comes into play is not the whole area of contact between the liquid and the solid. The friction is mainly due to the relative motion between the solid surface and the layer of liquid next to it, but in the case of liquids it is commonly understood that there is no slip between the solid and the layer of liquid next to it so long as the liquid is in contact with the solid. There can be this relative motion only at the place where the surface of the liquid is advancing or receding or over the solid, so that it may be said that the friction is between the surface of the liquid and the solid. Reduction in the value of friction when the surface of water is contaminated (which affects the surface and not the body of liquid), and the result that the force of friction is proportional to the length of the line of contact lend support to this view. The title to the paper is given accordingly.

A. C. College,
Guntur.

REFERENCES

[1] Subrahmanyam, *Ind. Journal of Physics*, **9**, 305 (1937).

[2] Adam, *Physics and Chemistry of Surfaces*, 2nd edition, 180 (1938).

[3] Adam and Jessop, *J. C. S.*, 1865 (1925).

[4] Jenkins and Thomas, *Phil. Mag.* Feb., 303 (1924).

[5] Rowell, *Phil. Mag.*, 284 (1922).

Ablett, *Phil. Mag.*, **46**, 255 (1923).

Adam, *Ibid.*, 179.

Ibid., 186.

Ibid., 181.

ON A THEORETICAL ESTIMATE OF AN UPPER LIMIT OF STELLAR DIAMETERS

By N. R. SEN

(*Received for publication, March 12, 1941*)

ABSTRACT. Considering the stellar body as a polytrope whose index varies from shell to shell, an upper bound has been obtained, from the conditions of mechanical equilibrium, for the product rT (radial distance × temperature), when the minimum value of the polytropic index and the maximum value of the ratio of radiation to gas pressure within the gas mass are known. Taking the minimum value of the index as 1.5 and 3 approximately for small and large stars respectively, and defining the " radius " as the distance where the temperature falls to about a million degrees, the value of this radius has been calculated in terms of the mass of the configuration, and also of the maximum value of the ratio of the pressures. For stars of small masses these calculated rough upper bounds are not unsatisfactory, but for large masses they are rather too high.

INTRODUCTION

Though stellar bodies generally show a small range of variation in their masses, their radii vary within wide limits. Several inequalities are known giving tolerably good estimates of some of the physical characteristics, such as the central pressure, mean temperature, etc., of stars of known masses and radii, but no purely theoretical formula has been given for an estimation of the radius. In the present note is attempted an estimate of an upper limit to the size of a stellar body, primarily in terms of the ratio of the pressures, and finally in terms of the mass. The limits indeed are quite rough, but considering the fact that they do not involve the opacity factor, the law of energy generation, etc., and depend only on the condition of mechanical equilibrium, these rough values may be of some interest as setting some limit to the arbitrariness of the dimensions of stars purely from conditions of mechanical equilibrium. In the deduction of the relation it is necessary to assume some compressibility condition, a relation between pressure and density. We have taken quite a general type of such a relation, namely that for a variable polytrope,

$$d(\log P)=\left(1+\frac{1}{n}\right)d(\log \rho) \qquad \dots \quad (1)$$

where the polytropic index n is variable from point to point of the star. Candler[1] has recently investigated the physical properties of such a polytrope. The estimates of upper limits made in this paper are dependent on Candler's[1] results. The next paragraph recapitulates the relevant results of Candler.

If P be the pressure, $\rho(r)$ the density, and $\bar{\rho}(r)$ the mean density within a sphere of radius r, two variables X and Y can be defined thus

$$X=\left(\frac{2\pi G}{3}\right)^{\frac{1}{2}}\frac{r\bar{\rho}(r)}{P^{\frac{1}{2}}},\ Y=\left(\frac{2\pi G}{3}\right)^{\frac{1}{2}}\frac{r\rho(r)}{P^{\frac{1}{2}}} \qquad (2)$$

Taken in conjunction with

$$\frac{dP}{dr}=-\frac{GM(r)}{r^2}\rho(r) \qquad \ldots \quad (3)$$

and

$$\frac{dM(r)}{dr}=4\pi\rho(r)r^2,\quad M(r)=\frac{4\pi}{3}\bar{\rho}(r)r^3 \qquad \ldots \quad (4)$$

and (1), it may be shown that X and Y satisfy a differential equation of the first order as follows :

$$\frac{dY}{dX}=\frac{Y-\frac{n-1}{n+1}XY^2}{(3+X^2)Y-2X}. \qquad \ldots \quad (5)$$

The solution curves of this equation have a very important characteristic. They all emerge from the origin and have unit slope there. The solution curves for $n=1$, $n=5$ are shown in the figure, as well as those for $n_1=$const., $n_2=$const. If $-1<n_1<n_2<5$, the solution curve for $n_1=$const. lies entirely above that for $n_2=$const., and both above that for $n=5$.

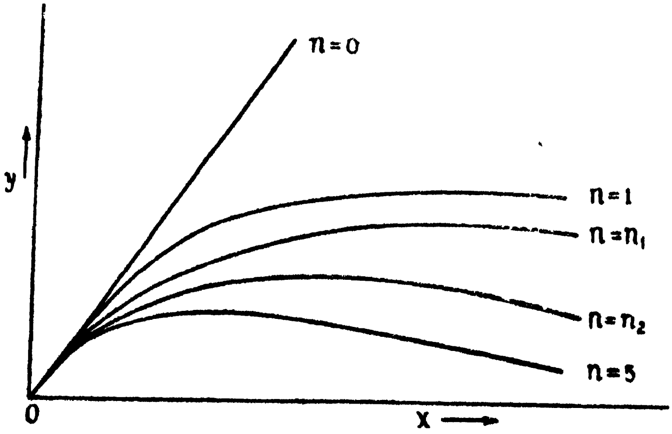

FIGURE

Now, if in a certain stellar configuration n is variable, and lies between n_1 and n_2, then the solution curve for the star in X, Y plane will lie entirely between the curves for $n_1=$const. and $n_2=$const. From this important characteristic of the solution curves it can be concluded that many of the characteristics of the variable polytrope are intermediate between the corresponding characteristics of the polytropes $n_1=$const. and $n_2=$const. at corresponding points (points with same value of X). For instance, if β_c be the ratio of gas pressure to total pressure at the centre of a star whose polytropic indices lie between n_1 and n_2, then

$$D(n_2)\frac{\pi a G^3 H^4}{18\kappa^4}\mu_c{}^4 M^2 < \frac{1-\beta_c}{\beta_c{}^4} < D(n_1)\frac{\pi a G^3 H^4}{18\kappa^4}\mu_c{}^4 M^2 \qquad \ldots \quad (6)$$

where $D(n_1)$ and $D(n_2)$ are constants whose values have been tabulated by Candler[1], and all other symbols have their usual meanings.

DEDUCTION OF AN UPPER BOUND

It is to be noticed first of all that, for a uniform polytrope ($n=$constant throughout), the variables X and Y are the two invariants of the Emden equation involving the Emden function and its first derivative, with respect to a Lane-transformation. It may thus be expected that in terms of these two variables the usual second-order equation will reduce to a first-order one. In fact, if we transform X and Y to usual polytropic variables for $n=$constant, we obtain

$$Y=\sqrt{\frac{n+1}{6}}\,I_1, \quad X=\sqrt{\frac{3(n+1)}{2}}\cdot\frac{I_2}{I_1^{\frac{n+1}{n-1}}} \qquad \ldots \quad (7)$$

where I_1, I_2 are the two invairants

$$I_1=\xi u^{\frac{n-1}{2}}, \qquad I_2=-\xi^{\frac{n+1}{n-2}}\frac{du}{d\xi}, \qquad \ldots \quad (8)$$

ξ and u being the variables of the normalised Emden equation.[2] The property which is important in the present discussion is that of I_1. It possesses *a single maximum for given n*.[2] The values of these maxima for different n are taken from the Tables of Emden functions[3] and shown in Table 1.

TABLE 1

n	$\sqrt{6}\,Y_{max}$
1.5	3.02
2	2.65
3	2.34
4	2.20
4.5	2.46

We can easily construct a function involving radius, temperature, and the ratio of the radiation to gas pressure, which is a function of Y only.

Putting

$$p_g = \beta P = \frac{\kappa}{\mu H}\rho T, \quad p_r = \tfrac{1}{3}aT^4 \qquad \dots \quad (9)$$

we get

$$q = \frac{1-\beta}{\beta} = \frac{a}{3}\,\frac{\mu H}{\kappa}\,\frac{T^3}{\rho}$$

and

$$\frac{q^{\frac{1}{2}}}{T} = \left(\frac{a}{3}\,\frac{\mu H}{\kappa}\right)^{\frac{1}{2}} \frac{T^{\frac{1}{2}}}{\rho^{\frac{1}{2}}} = \left(\frac{a}{3}\right)^{\frac{1}{2}} \frac{\mu H}{\kappa}\,\frac{\beta^{\frac{1}{2}} P^{\frac{1}{2}}}{\rho}.$$

Thus

$$\left(\frac{q}{\beta}\right)^{\frac{1}{2}} \frac{1}{rT} = \left(\frac{a}{3}\right)^{\frac{1}{2}} \frac{\mu H}{\kappa} \left(\frac{2\pi G}{3}\right)^{\frac{1}{2}} Y^{-1}.$$

or

$$\frac{rT}{\sqrt{q(1+q)}} = \frac{rT}{(1-\beta)^{\frac{1}{2}}/\beta} = \left(\frac{9}{2\pi a G}\right)^{\frac{1}{2}} \frac{\kappa}{\mu H} Y. \qquad \dots \quad (10)$$

Regarding the stellar body as a variable polytrope, let us suppose that its polytropic index n lies between two limits n_1 and n_2, so that $n_1 \leq n \leq n_2$. In case of central degeneracy (non-relativistic), or of stars whose masses are not large we may take $n_1 = 1.5$, while n_2 may be taken to be less than 5. Thus, if the complicated pressure-density relation within a star be represented by a variable n [defined by (1)] with 1.5 as its lowest value, then by Candler's theorem the value of Y at any point within the star will be less than that for the curve $n = 1.5$ at the corresponding point. In the general case $n_1 \leq n \leq n_2$, this value will be less than that for the curve n_1 at the corresponding point. But we have seen that for a fixed n_1, the relation between Y and I is given by (7), and then Y has a single maximum whose value is shown in Table I. Hence the value of Y anywhere within the star will be less than this maximum value of Y for the said fixed value of n_1 (which is the minimum value of n within the star). Hence from (10) we obtain

$$\frac{rT}{\sqrt{q(1+q)}} = \frac{rT}{(1-\beta)^{\frac{1}{2}}/\beta} < \frac{\kappa}{\mu H}\left(\frac{3}{4\pi a G}\right)^{\frac{1}{2}} \left[(n_1+1)^{\frac{1}{2}} \xi u^{(n-1)/2}\right. \equiv A. \quad \dots \quad (11)$$

For stars of small and moderate masses, we take $n_1 = 1.5$, for which we get

$$A = 5.4 \times 10^{18} \mu^{-1} (cm.)(deg.). \qquad \dots \quad (12)$$

For most small stars, the ratio of the radiation to gas pressure increases inwards, and may be taken to be maximum at the centre. This is always true if n does not exceed 3.[4] For stars of small masses, n does not probably exceed 3.25. We then write (11) and (12) as

$$rT<\gamma\,\frac{(1-\beta_c)^{\frac{1}{2}}}{\beta_c}\cdot\frac{1}{\mu}\cdot 5.4\times 10^{18}\equiv B \qquad \dots \quad (13)$$

where γ is a numerical constant introduced as a compensating factor for the contingency that the ratio of radiation to gas pressure may not be maximum at the centre. This factor, however, we put equal to 1 for stars of not large masses, which is not far from truth.

For stars in which the radiation pressure is not small compared to gas pressure, n_1 (the minimum value of n) can probably be put much higher than 1.5. For instance, for stars whose masses are such that $\mu^2(M/\odot)$ is greater than 5.7, no complete degeneracy is possible, and the radiation pressure will also be considerable. For such wholly gaseous stars calculations have been made with $n_1=3$ (figures for $n_1=1.5$ are also given). If there are convection zones near the centre where adiabatic equilibrium may be assumed, then for stars of the main sequence $n_1 \sim 1.5$ will be quite good, while for more massive stars with higher radiation pressure an intermediate value between 1.5 and 3 will be probably nearer the mark. In case of $n_1=3$, (13) should be replaced by

$$rT<\gamma\,\frac{(1-\beta_c^{\frac{1}{2}})}{\beta_c}\cdot\frac{1}{\mu}\cdot 4.2\times 10^{18}\equiv B'. \qquad \dots \quad (13)'$$

Now as n may generally exceed 3, the maximum value of q may not occur exactly at the centre, so γ is expected to exceed the value unity. But the variation of q in the *interior* is not considerable (the outer portion of the star is left out of consideration), and γ will always remain of the order of unity. But if by q_c we mean *for the present* the *maximum* value of the ratio of radiation to gas pressure within the star, we may always put $\gamma=1$. According to the recent theory of energy generation due to Atkinson, Gamow and Bethe, the energy of the main sequence stars is generated in the extreme central region, so that the stars have mostly approximately point sources of energy. In such cases, as the numerical integrations by Eddington and Biermann show the ratio of radiation to gas pressure has the maximum value near the centre, and this characteristic is expected to be retained in most stars where energy is generated by the process suggested by Atkinson, Gamow and Bethe, and the radiative gradient is replaced by an adiabatic one.

The following Table gives an upper bound of the product rT against the value of $q_c=(1-\beta_c)/\beta_c$, the ratio of the two pressures within the star at the centre. We shall rather put $\gamma = 1$, and, for the present, mean by q_c the maximum value of q in the stellar interior.

TABLE 2

q_c	$B\mu$ (cm.) (deg.)	q_c	$B.\mu.$ (cm.) (deg.)
4	25×10^{18}	$\frac{1}{4}$	3.1×10^{18}
2	13×10^{18}	$\frac{1}{9}$	1.9×10^{18}
1	7.8×10^{18}	$\frac{1}{24}$	1.2×10^{18}
$\frac{1}{2}$	4.8×10^{18}	$\frac{1}{99}$	0.56×10^{18}

We may generally put $\mu = 1$ for stars in which hydrogen is abundant.

INTRODUCTION OF MASS IN THE UPPER BOUND

Under certain circumstances we can put the upper bounds in (13) and (13′) in terms of the masses of the stars instead of the maximum value of the ratio of radiation to gas pressure.

The inequality (6) gives an upper bound for $(1-\beta_c)/\beta_c^4$ in terms of the mass M of the star, strictly speaking in terms of $\mu_c^2 M$. Both $(1-\beta_c)/\beta_c^4$ and $(1-\beta_c)^{\frac{1}{2}}/\beta_c$ being monotone increasing functions of $(1-\beta_c)$, we can calculate from (6) an upper bound for $(1-\beta_c)^{\frac{1}{2}}/\beta_c$ as well. Calling this upper bound F(M), we write

$$(1-\beta_c)^{\frac{1}{2}}/\beta_c < F(M). \qquad \dots \quad (14)$$

This, taken with the two equations (13), gives

$$rT < \gamma . \frac{1}{\mu} F(M) . \left(\begin{matrix} 5.2 \\ 4.4 \end{matrix} \right) \times 10^{18} \text{ (cm.) (deg.)}. \qquad \dots \quad (15)$$

For main sequence stars with small and moderate masses we take the figure 5.4, and put $\gamma = 1$; for more massive stars we take 4.2, and γ to be of the order of unity.

From Table 2, as also from equation (15) an idea about the size of the configuration can generally be made, if by "radius" r' we mean a central distance where the temperature has fallen to a value which is a suitable (otherwise arbitrarily chosen) fraction of the central value. This step is rather delicate and difficult. As nearly the whole of the mass of the configuration will be included within a spherical surface on which the temperature is a fraction (say one-tenth) of the central value, the application of (14) does not produce any difficulty. For stars of small and moderate masses within which the radiation pressure is either very small, or not considerable, a variation limit for n between 1.5 and 3.25 will be quite appropriate. Let us now call that value of r' the "radius" of the configuration where the temperature has fallen to, say, *one million degrees*. There are certain difficulties in fixing this limit too low. Firstly, though stellar conditions in the inside are roughly of uniform character, they diverge widely in the exterior, where the approximations will be faulty to a great extent. Secondly, as the surface is approached, the gas pressure decreases very rapidly, and generally the ratio of radiation to gas pressure will increase. An adjustment of this by the γ factor may involve the use of such high values of γ as to render the approximations useless. It may be expected that for stars of small and moderate masses a temperature of about a million degrees will generally provide against this contingency. For this reason in Table 3 up to the value 5 in the first column, the factor γ has been put equal to 1. There will, of course, remain an outer envelope whose thickness is to be added to r' for the total radius R of the star (which is connected with the effective temperature). For non-massive stars, as Chandrashekhar's[5] investigation of stellar envelopes shows, the increase of the pressure ratio within the whole of the outer envelope up to about a million degrees does not at the utmost exceed 60% of its value at the bottom of the envelope, a consideration which suggests that it is not necessary to seriously modify our approximation $\gamma = 1$ up to about a million degrees temperature. For stars of small and moderate masses the addition to r' for the outer part of the envelope is also expected to be small, probably not above 20 to 25 per cent.

For stars of comparatively larger masses with larger radii, the results are much more uncertain. Firstly, the value of γ may be comparatively large; secondly, larger values of the polytropic index n will tend to make the envelope more extensive. But there may be one fact in favour of the approximation. If the recent theory of energy generation be applicable also within stars of larger masses (it does not certainly apply to all large masses), the stars will have nearly point sources of energy, for which, as we have remarked, the pressure ratio increases inside near the centre and γ will have a value not very much differing from 1. If the arbitrary limit of the temperature of 1 million degrees be inadequate, larger errors may arise. However, the question of the thickness of the outer part of the envelope will remain here uncertain.

CALCULATIONS

Corresponding to the definition of the radius r', we shall have

$$r'(M) < \gamma \frac{1}{\mu} F(M) \begin{pmatrix} 5.4 \\ 4.2 \end{pmatrix} \times 10^{12} \text{ cms.}, \quad \ldots \quad (16)$$

Table 3 gives the maximum values of $\mu r'(M) = U$, corresponding to the values of μ_e^2M (in solar units) in the first column. $(1-\beta_c)_u$ in the second column is the upper bound of $1-\beta_c$ for corresponding values in the first column taken from Candler's Table[1]; the third column gives F(M), *i.e.*, the upper bound of $(1-\beta_c)^{\frac{1}{2}}/\beta_c$, calculated from the second column. The last column gives U the calculated upper bound of $\mu r'$ (r' in solar units) by (16). For values in the first column greater than 5, calculations have been made both for $n_1 = 1.5$, and $n_1 = 3$, and those for $n = 1.5$ have been put within brackets.

For large masses n_1 is certainly greater than 1.5 but the values corresponding to $n_1 = 1.5$ are shown to give an idea of the unattainable extreme value. γ has been put equal to 1 in the Table. It appears the bounds corresponding to $n_1 = 3$ are all sufficiently high to cover the cases of very large stars. As these approximations have been made without taking into account the flow of radiation, the opacity factor, ionisation, etc., these rough upper bounds, for stars of small and moderate masses at least, may not be considered unsatisfactory.

TABLE 3

μ_c^2M (M in ⊙ units)	$(1-\beta_c)_u$	F(M)	U (in ⊙ units)
0.5	0.0017	0.04	3
1	0.0068	0.08	6
2	0.025	0.16	12
5	0.109	0.37	29
10	(0.24) 0.16	(0.6) 0.48	(47) 29
20	(0.39) 0.30	(1.0) 0.77	(79) 46
50	(0.57) 0.50	(1.7) 0.70	(134) 84
100	(0.68) 0.62	(2.5) 2.0	(200) 120

The first column gives the values of μ_c^2 (mass of the star in solar units), and the last column the upper limit of the radius in solar units. The figures within ( ) for large masses give the values of the upper limits on the supposition that the lowest polytropic index of such star is 1.5, while the figures not within ( ) are the values for lowest polytropic index 3.

The Table 3 shows that for small masses there is a linear rise in U for varying μ_c^2M, which is approximately at the rate of 6 per unit increase in μ_c^2M. For stars of small masses we may put $\mu_c \rightarrow 1$.

We have collected the values of the masses and radii of some stars in Table 4. They are taken from Tables given by Stromgren, and in Russel, Dugan, Stewart's Astronomy, and are arranged into groups according to their masses.

TABLE 4

Name of the star	Mass	Radius
S. Ant.	0.75 0.42	1.66 1.29
W. U. Ma	0.69 0.40	0.78 0.78
Z. Hercules	1.63 1.3	1.77 3.29
ζ. Hercules	0.95	1.9
R. T. Lac br	1	4.0
R. T. Lac f	1.9	4.0
T. X. Her br	2.06	1.6
Sirius A	2.34	1.8
Capella A	4.18	15.8
Capella B	3.32	6.6
μ_1 Scorpii	12	5.5
S Auriga (B. Comp)	8.1	5.1
(K. Comp)	14.8	200
V. V. Cephei (M.Comp)	40 102	2130 2630
A. O. Cassiopiae	40	19
29 Canis Majoris A	46	20

A comparison with Table 3 shows that except for small masses the calculated upper bounds are rather too high. They indeed correspond to only one steller parameter M, whereas by Vogt-Russel theorem a complete description is possible only in terms of two parameters. Hence values much higher than the maximum values in Table 4 are not altogether unexpected in our calculations. In this respect the cases of S. Ant., R. T. Lac, Capella A are interesting. Their values nearly touch, or are within hundred per cent. of the corresponding upper bounds. The calculated bounds appear to be exceeded by E-Auriga (infra-red component), V. V. Cephei which are distinguished by their exceptionally large radii. Chandrasekhar's investigation of their envelopes shows that the masses of these stars are very probably contained within 5 to 10 per cent. of their huge radii. Our approximations will not evidently apply to such deep atmospheres.

REFERENCES

[1] *M.N.R.A.S.*, **100**, 14 (1939).

[2] British Association Tables of Emden Functions; also proved analytically *Bull. Cal. Math. Soc.*, **30**, 11 (1938).

[3] Taken from British Association Tables of Emden Functions.

[4] This is discussed in a different paper by the author.

[5] An Introduction to the Study of Stellar Structure, Chap VIII.

ON SOME THERMODYNAMIC PROPERTIES OF A MIXTURE OF GAS AND RADIATION

By N. R. SEN

(*Received for publication, March 12, 1931*)

ABSTRACT. Emden's theorem on the expansion or contraction of a polytropic gas mass with conservation of polytropic index has been extended to the case of a variable polytrope, which under similar conditions is shown to have the distribution of polytropic index unchanged. A relation is worked out between N and n, the polytropic indices for (P, ρ) and (p, ρ) relations, P being the total pressure, and p, the gas pressure. From this, a method has been given for estimating the temperature distribution in a variable polytrope when its maximum and minimum polytropic indices are known.

INTRODUCTION

In the current astrophysical theories, stellar bodies are studied as configurations of hot gas masses in equilibrium, the radiation pressure playing in general an important role in the interior. Polytropic configurations with constant indices have been investigated very thoroughly as stellar models from this point of view. But every stellar mass may be accurately conceived as made up of shells of matter in polytropic equilibrium with the polytropic index varying continuously within the mass from shell to shell. Some attempts have been made to study such configurations recently. Eddington[1] set the problem of finding those properties of such a variable polytrope, which lie intermediate between the properties of the two polytropes whose indices are constant, and identical with the upper and lower limits of the index of the variable polytrope. In this paper two simple thermodynamic properties of such variable polytropes have been discussed. The first is an extension of Emden's theorem[2] on the property of four intersecting (p, V) curves, representing two pairs of polytropes of two different indices. It is shown that under similar conditions the distribution of polytropic index within a gas mass remains unchanged. Secondly, the relation between two polytropic indices corresponding to (i) gas pressure, and (ii) the total pressure has been investigated. Writing the gas law as

$$\frac{dp_g}{p_g} = \frac{d\rho}{\rho} + \frac{dT}{T}$$

we define a polytropic index n by

$$\frac{dp_g}{p_g} = \Big(1 + \qquad d\rho \qquad \ldots \quad (1)$$

with
$$n = \frac{d(\log \rho)}{d(\log T)}$$

where n in general is variable. But the actual stellar material is a mixture of gas and radiation, and if P be the total pressure of gas and radiation, a polytropic relation of the type

$$\frac{dP}{P} = \left(1 + \frac{1}{N}\right)\frac{d\rho}{\rho} \qquad (2)$$

will subsist, where N is the effective polytropic index for the mixture of gas and radiation. We shall study the relation between N and n from purely thermodynamic considerations. Candler's[5] discussion of variable polytropes is based on the (P, ρ) relation, as the total pressure P appears in the equation of hydrostatic equilibrium, and so his results involve N. A relation between N and n enables one to show that *in a sense* the temperature of a variable polytrope is intermediate between the temperatures of two polytropes with constant limiting indices, when the corresponding points are suitably defined.

EXTENSION OF EMDEN'S THEOREM TO VARIABLE POLYTROPE

Let us take the different parts of a purely gas sphere to be in polytropic conditions characterised by different indices, and let the index n be varying continuously with the radial distance r (fig. 1).

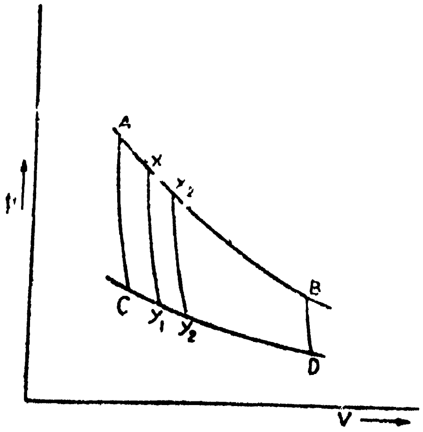

FIGURE 1

Let p be the pressure and V the specific volume at a point, and the (p,V) relation of any part of the gas sphere be represented by the continuous curve AB on the (p,V) plane (fig. 1). As the polytropic index is supposed to vary along AB, the heat capacity c will also vary along the curve, since $n=(c_v-c)/(c_p-c_v)$. We now prove the following theorem.

Theorem. If the gas-sphere undergoes some slow change (e.g., *general expansion or contraction) such that every gas element undergoes a change along a polytrope of definite index n_0, and the temperatures (or pressures, or specific volumes) of the corresponding gas elements are in a constant ratio, then the distribution of polytropic index in the gas mass after the change will remain the same as before the change.* This is a purely thermodynamic property not connected with the mechanical equilibrium of the gas mass.

Let the points A, X_1, X_2, ...B, of the (p,V) curve move along the curves AC, X_1Y_1, X_2Y_2, ...BD, all representing polytropes of a definite index n_0, such that $T_A/T_C = T_{X_1}/T_{Y_1} = T_{X_2}/T_{Y_2} = \ldots\ldots = T_B/T_D$, then we have to prove that the distribution of polytropic index, *i.e.*, of heat capacity c along CD, will be the same as that along AB.

Take a point X_1 so close to A that along AX_1 we can take the heat capacity c_1 to remain unaltered (or strictly speaking to lie within c_1 and c_1+dc_1). Let X_1 move along a polytrope n_0, to a position Y_1 such that

$$T_A/T_C = T_{X_1}/T_{Y_1}. \tag{3}$$

Putting $T_{X_1}=T_A+dT_A$, and $T_{Y_1}=T_C+dT_C$, we obtain the relation

$$\frac{dT_A}{T_A}=\frac{dT_C}{T_C}. \tag{3'}$$

Now consider an infinitely slow quasistatic cycle round ACY_1X_1. The closed integral $\int dQ/T$ round this cycle will vanish. The contribution of the side AC is $c_{n_0}\,log(T_C/T_A)$, that of CY_1 is $c'_1 dT_C/T_C$, where $(c'_1, c'_1+dc'_1)$ is the heat capacity for the element CY_1; the contributions of Y_1X_1 and X_1A are $c_{n_0}\,log(T_{X_1}/T_{Y_1})$, and $-c_1 dT_A/T_A$ respectively. Hence we must have

$$c_{n_0}\,log(T_C/T_A)+c'_1 dT_C/T_C+c_{n_0}\,log(T_{X_1}/T_{Y_1})-c_1\,dT_A/T_A=0 \tag{4}$$

But by the above relations (3) the sum of the first and the third terms disappears, and so we have by (3')

$$(c'_1-c_1)dT_C/T_C=0,$$

that is

$$c'_1=c_1. \quad \cdots \tag{5}$$

By dividing the curve AB into infinitesimal elements and considering similar circuits, we prove that the distribution of c, *i.e.*, of n along CD, is the same as that along AB.

Since (A,C) and (X_1,Y_1) are on polytropes n_0, we have from the gas law and the polytropic condition

$$\frac{RT_A}{RT_C}=\left(\frac{V_C}{V_A}\right)^{1+\frac{1}{n_0}}.\quad \frac{V_A}{V_C}=\left(\frac{V_C}{V_A}\right)^{\frac{1}{n_0}},\quad \frac{RTx_1}{RTy_1}=\left(\frac{Vy_1}{Vx_1}\right)^{\frac{1}{n}}$$

whence by (3)

$$V_C/V_A=Vy_1/Vx_1 \qquad \dots \quad (6)$$

Similarly $$\frac{p_C}{p_A}=\frac{py_1}{px_1}.$$

Hence the condition "temperatures of the corresponding gas elements being in the same ratio" in the above theorem can be replaced by "specific volumes or pressures of the corresponding gas elements being in the same ratio." The proof of the theorem can also be based on properties (5) and (6) of polytropes of constant index. This theorem is a generalisation of the well-known theorem due to Emden in which AB and CD represent two uniform polytropes.

It is known that for uniform expansion or contraction of a gas-sphere every element undergoes a polytropic change belonging to the index 3, and further the temperatures and pressures at corresponding points are proportional. Applying the theorem proved above to uniform expansion or contraction, we obtain the result that when a gas sphere with variable polytropic index expands or contracts uniformly, the distribution of polytropic index along the radius remains unaltered. This indeed may also be proved directly.

A RELATION BETWEEN N AND *n*

We shall now obtain a relation between N and n for a mixture of gas and radiation. Let us start with the gas law in the form

$$p_g V=RT \qquad \dots \quad (7)$$

where V is the specific volume, so that (2) may be written as

$$\frac{dP}{P}+\left(1+\frac{1}{N}\right)\frac{dV}{V}=0. \qquad \dots \quad (2')$$

Now $dP=d(p_r+p_g)=d\left(\frac{1}{3}aT^4+\frac{RT}{V}\right)=(4p_r+p_g)\frac{dT}{T}-p_g.\frac{dV}{V}$,

whence, putting $p_g/p_r=\beta/(1-\beta)$, we obtain

$$\frac{dP}{P}+\left[1+(\beta-1)-(4-3\beta)\frac{d(\log T)}{d(\log V)}\right]\frac{dV}{V}=0. \qquad \dots \quad (8)$$

Comparing (8) with (2′) we have

$$\frac{1}{N}=(\beta-1)-(4-3\beta)\frac{d(\log T)}{d(\log V)}=(\beta-1)+\frac{4-3\beta}{n}. \qquad \ldots \quad (9)$$

This equation can also be put as

$$N=\frac{n}{(4-3\beta)-n(1-\beta)}. \qquad \ldots \quad (9')$$

For a fixed β, corresponding to one value of n there is one value of N and *vice versa*. Also as (for fixed n)

$$\frac{dN}{d\beta}=-\frac{n(n-3)}{[(4-3\beta)-n(1-\beta)]^2},$$

with increasing β, N increases if $n<3$, and decreases if $n>3$. For $n=3$, $N=3$; also as $\beta\rightarrow 1$, $N\rightarrow n$. We cannot calculate N as $\beta\rightarrow 0$ from (9′), as for $\beta=0$, $p_g=0$. In case of pure radiation pressure we know $N=3$ [though (9)′ gives $N\rightarrow n/(4-n)$, as $\beta\rightarrow 0$]. We can now plot on the (β, N) plane the curves *for fixed values of n.*

From (9) and (9)′, the following points may be easily seen :

(*a*) through every point of the (β, N) plane there passes one and only one curve of the family $n=\text{const.}$, so that the curves $n=\text{const.}$ do not intersect (as for given N and β there is only one value of n) ;

(*b*) a curve $n=\text{const.}$ for $N>3$, continually approaches the line $N=n$ from above, so that for every value of $\beta\neq 1$, if $N>3$, then n also is >3, but less than N ; at $\beta=1$, $N=n$; the curves for constant n rapidly rise as the N-axis is approached, and in fact the curve $n=4$ is asymptotic to the N-axis ; for $n>4$, the line $\beta=(n-4)/(n-3)$ is an asymptote ; a smaller value of β would make N negative, and for a time numerically very large ;

(*c*) any curve $n=\text{const.}$ for $0<N<3$ starts from the N-axis, continuously rises and asymptotically approaches the line $N=n$ from below ; at every point on this curve (except for $\beta=1$) $N<n$, so that for every value of $\beta\neq 1$, if N be positive and <3, then $n>N$, but less than 3 ; at $\beta=1$, $N=n$;

(*d*) on a line $\beta=\text{const.}\neq 0$, the n values increase continuously upwards with increasing positive values of N ; if on this line $0<N_1<N_2$, then $n_1<n_2$.

(*e*) the line $N=3$ is singular in this respect that on this line $N=n=3$ for every value of β.

The curves drawn in fig. 2 show these properties clearly. In a stellar body, let N lie between two values, say $N_2(<3)$ and $N_1(>0)$, and in the figure let the lines AB and CD represent $N=N_2$ and N_1 respectively, and let the range of β

values, within which the pressure ratio varies within the stellar body (excluding the extreme outer portion), be marked as in the figure by the lines AC and BD. Draw the curve n_1=const. through the point D ; we have proved that $n_1 > N_1$. Similarly if A lies on the curve n_2=const., $n_2 > N_2$.

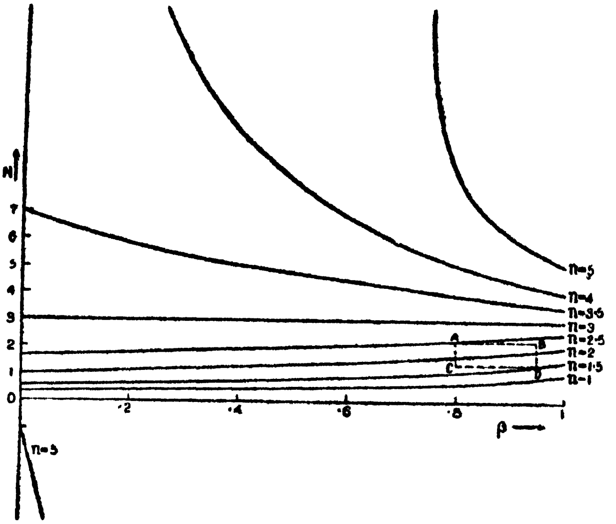

FIGURE 2

Then for any point within the stellar body the index n shall lie between n_1 and n_2, so that

$$n_1 < \frac{d(\log \rho)}{d(\log T)} < n_2, \qquad (1$$

whence

$$\frac{T}{T_0} \quad < \qquad < \quad \frac{T}{T_0}$$

T_0, ρ_0 being the temperature and density at the centre. Hence the density increases at a rate intermediate between the n_1- and n_2-th power of T. Relations (10) and (10′) evidently subsist also for values of N > 3.

LIMITS OF TEMPERATURE IN A VARIABLE POLYTROPE

We can also use the above considerations to find a pair of limits within which the temperature of a gas configuration will lie. For this purpose we shall call points within different gas masses with the same value of β (otherwise the ratio of radiation to gas pressure) *corresponding points*. Any two such masses need not have corresponding points, but for the purpose of the arguments which follow, the different gas masses will be supposed to have corresponding points.

Suppose we have a stellar body whose polytropic index N varies from N_1 to N_2, and first suppose $0<N_1<N_2<3$. If the range of β values within the gas mass be known, we can find in the manner of the previous article two index-numbers n_1 and n_2 $(n_1<n_2)$ such that all n values of the configuration lie between n_1 and n_2. When both N_1 and N_2 are less than 3, we have seen that $n_1>N_1$, $n_2>N_2$, but n_1, n_2 are also both less than 3. We now compare the given gas configuration with two polytropes of constant indices n_1 and n_2. Such a polytrope will have *two* disposable parameters, one, say, the central temperature, and the second the factor of proportionality between the pressure and, say, the $\left(1+\frac{1}{n_1}\right)$th power of the density (for the first polytrope) in the pressure-density relation. Thus we can choose the first polytrope n_1 as one whose central values of β will be the same as that of the given gas configuration, and also the central temperature of the two identical. It can easily be shown that these two conditions determine the polytrope n_1 completely. Similarly, with the same conditions we determine the polytrope n_2. We may, for the sake of generality, drop the condition of the equality of central temperatures, and have a single infinity of polytropic configurations for n_1 or n_2. The following arguments will apply to this general case. With these adjustments we shall have a series of triplets of corresponding points starting from the centre for the given configuration and the two polytropes n_1, n_2, since in the polytropes $(n_1, n_2)<3$, β will increase outwards and tend towards 1 near the surface and in the given gas configuration $(n<3)$, β will also do so. Consider a triplet of corresponding points on the configurations characterised by n_1, n and n_2. At these points we have

$$\frac{\rho_1}{\mu_1 T_1^3} = \frac{\rho}{\mu T^3} = \frac{\rho_2}{\mu_2 T_2^3}$$

so that (μ being supposed uniform throughout any one configuration and for simplicity may be taken to be the same in all of them)

$$\frac{d\rho_1}{\rho_1} - 3\frac{dT_1}{T_1} = \frac{d\rho}{\rho} - 3\frac{dT}{T} = \frac{d\rho_2}{\rho_2} - 3\frac{dT_2}{T_2}. \qquad \dots (11)$$

We have further

$$\frac{d\rho_1}{\rho_1} = n_1\frac{dT_1}{T_1}, \quad \frac{d\rho}{\rho} = n\frac{dT}{T}, \quad \frac{d\rho_2}{\rho_2} = n_2\frac{dT_2}{T_2} \qquad \dots (12)$$

From these two sets of equations follows

$$(3-n_1)\frac{dT_1}{T_1} = (3-n)\frac{dT}{T} = (3-n_2)\frac{dT_2}{T_2} \qquad \dots (13)$$

as a relation between the temperature increments at corresponding points. Since $0<n_1<n<n_2<3$, for positive increments of temperature we must have

$$\frac{dT_2}{T_2} > \frac{dT}{T} > \frac{dT_1}{T_1},$$

whence integrating we obtain

$$\frac{T_2}{T_2'} < \frac{T}{T'} < \frac{T_1}{T_1'} \qquad \ldots \quad (14)$$

where (T_1', T', T_2') are the temperatures at a triplet of corresponding points on the (n_1, n, n_2) configurations, which are respectively *interior* to the corresponding points where the temperatures are T_1, T, T_2. (14) shows that the relative temperature decrease in the given configuration is intermediate between the relative decreases in the two polytropes n_1 and n_2 at corresponding points This relation will apply as long as triplets of corresponding points are available in the three gas masses, and so for the entire given gas configuration.

If we take $T_2'=T'=T_1'=$ the central temperature of the given configuration, then $T_2<T<T_1$. The three masses have then also the same central densities and temperatures. *Hence if $N<3$, the temperature of the given configuration at any point is intermediate between the temperatures at corresponding points of the polytropes n_1 and n_2 with the same central density and temperature as the given gas mass.*

In a similar manner, it can be shown that if N lies between N_1 and N_2 both of which exceed 3, then in the same manner as before two indices $n_1(<N_1)$ and $n_2(<N_2)$ both >3 can be obtained such that any n corresponding to N lies between n_1 and n_2. In this case we obtain by comparing with polytropes n_1 and n_2 as above the inequality (14) reversed thus

$$\frac{T_1}{T_1'} < \frac{T}{T'} < \frac{T_2}{T_2'} \; ; \qquad \ldots \quad (14a)$$

and for polytropes of the same central density and temperature, $T_1<T<T_2$.

The important case, however, is when n_1 is less than 3, but N_2 greater than 3. In such a case β should increase outwards for some parts of the gas mass (so long as $N<3$), and decrease for others (when $N>3$). An estimate like (14) or (14*a*) is then possible only if the β value corresponding to the point where N attains the value 3 (then n also is 3) is known. A rough guess can sometimes be made for known stellar mass when it is considered to conform to an Eddington model for which β is connected with the mass. We can then find $n_1(<3)$ and $n_2(>3)$ such that for values of N from N_1 to 3 (β increasing outward) the n values corresponding to N are greater than n_1, and between the values of N from 3 to N_2 the corresponding n values are less than n_2. n_1 and n_2 are indeed the n values on the lines $N_1=$const. and $N_2=$const. respectively of the points where they are cut by the line $\beta_{(3)}=$const, this $\beta_{(3)}$ being the point where the N curve of the given gas mass cuts the line $N=3$. Knowing n_1 and n_2, equations like (14) and (14*a*) can be obtained easily for the two parts of the gass mass.

All these results depend only on the thermodynamic properties of the gas mass and not on its mechanical property of equilibrium. They may be useful in guessing rough values in the construction of stellar models.

BEHAVIOURS OF N AND n FOR LARGE AND SMALL VALUES

As the n value approaches and exceeds 4, the thermodynamically allowable values of N may increase to any positive value up to ∞, and may even become negative. The infinite value of N occurs as we have seen for $\beta=(n-4)/(n-3)$, *i.e.*, for $\beta/(1-\beta)=n-4$. Thus, if n be near to, say, 4.5, large values of N will occur when the radiation pressure is nearly double the gas pressure ; on the other hand, if n be near 5, large values of N will occur if these two pressures be nearly equal. For smaller values of $\beta/(1-\beta)$, even negative values of N are thermodynamically permissible On the other hand n may be negative, if N be negative and $|N|$ less than $(1-\beta)^{-1}$.

It may be noted that N and n vanish together in the ratio of 1 to $4-3\beta$. This fact will be of importance in a later investigation. Moreover as $N\rightarrow\infty$, *i.e.*, the gas mass is approximately isothermal, n will tend to the value $3-(1-\beta)^{-1}$. Lastly, as $n\rightarrow\infty$, $N\rightarrow-(1-\beta)^{-1}$.

REFERENCES

[1] *M.N.R.A.S.*, **99**, 4 (1938).
[2] *Gaskugeln*, 25.
[3] *M.N.R.A.S*, **100**, 14 (1939).

THE CALCULATION OF arg $\Gamma(ia+1)$

By JAMES G. BECKERLEY

(Received for publication, March 16, 1941)

ABSTRACT. A convenient, rapidly-converging finite sum formula is derived for the numerical evaluation of arg $\Gamma(ia+1)$. This formula is then employed to construct a four-place table of arg $\Gamma(ia+1)$ for $a=.1, .2, .3, \ldots, 2.0$. The asymptotic formula is shown to be satisfactory for computing the function when $a>2.0$

$\Gamma(z)$ for complex values of z has been tabulated to a limited extent[1,2,3]. Nevertheless, in the use of these tables the physicist must spend considerable time in understanding an author's notation (see reference 2) or considerable effort in securing interpolated values (see reference 1). Besides, the periodicals in which some of the tables appear are not always available (*e.g.*, reference 3). So it is convenient to have a simple closed formula with which any desired $\Gamma(z)$ may be calculated, a formula whose element may be obtained from commonly available tables.

The purpose of this paper is to present such formulas for the function $\Gamma(ia+1)=(ia)$. This function occurs frequently in problems involving positive energy hydrogen functions.[4]

It is unnecessary to discuss the calculation of the absolute value[5] of this function, as the exact formula for the absolute value is quite convenient for numerical calculation. $\Gamma(ia+1)=\sqrt{(\pi a)/(\sinh \pi a)}$. However, the exact formula[6] for the argument (or angle) is an infinite sum whose terms diminish so slowly as to make addition impractical.

$$\arg\Gamma(ia+1)=-Ca+\sum_{n=1}^{\infty}\left(\frac{a}{n}-\operatorname{arctg}\frac{a}{n}\right)$$

where $C=$ Euler's constant $=.5772156665\ldots$

The obvious solution to this difficulty is to break the series off at the Nth term, substitute the power series for arctg (a/n), sum the resulting series analytically, leaving only a finite sum to be evaluated. This is done in the following procedure.

$$\arg\Gamma(ia+1)=-Ca+\sum_{n=1}^{N}\left(\frac{a}{n}-\operatorname{arctg}\frac{a}{n}\right)+\sum_{n=N+1}^{\infty}\left[\frac{1}{3}\left(\frac{a}{n}\right)^{3}-\frac{1}{5}\left(\frac{a}{n}\right)^{5}\cdots\right]$$

---

* Communicated by the Indian Physical Society.

$$= -\sum_{n=1}^{N} \operatorname{arctg}\frac{a}{n} + \left(S_1^N - C\right)a + \left\{ \sum_{n=1}^{\infty}\left[\frac{1}{3}\left(\frac{a}{n}\right)^3 - \frac{1}{5}\left(\frac{a}{n}\right)^5 \ldots\right] - \sum_{n=1}^{N}\left[\frac{1}{3}\left(\frac{a}{n}\right)^3 - \frac{1}{5}\left(\frac{a}{n}\right)^5 \ldots\right]\right\}.$$

Thus,

$$(1) \quad \arg \Gamma(ia+1) = -\sum_{n=1}^{N} \operatorname{arctg}\frac{a}{n} + \left(S_1^N - C\right)a - \sum_{n=1}^{\infty} \frac{(-1)^n a^{2n+1}}{2n+1} \Delta S^N_{2n+1}$$

where $S_\mu^\nu = \sum_{n=1}^{n=\nu}\left(\frac{1}{n}\right)^\mu$; $\Delta S_\mu^\nu = S_\mu^\infty - S_\mu^\nu$.

The series S_μ^ν are the well-known numerical series whose values can be obtained analytically and which have been tabulated[7] for a reasonable range of values of μ. Now one convenient feature of formula (1) is that *the* ΔS^N_{2n+1} *diminishes very rapidly with increasing n*. This is shown in Table I, where ΔS^N_{2n+1} is tabulated for $n = 1, 2, \ldots, 5$ and $N = 1, 2, \ldots, 5$. It is apparent that the convergence becomes even better with increasing N. (Also included in Table I are values of S_1^N for $N = 1, 2, \ldots, 5$.)

TABLE I. Values of $\Delta S^N_{2n+1} = \sum_{\mu=1}^{\infty}\left(\frac{1}{\mu}\right)^{2n+1} - \sum_{\mu=1}^{N}\left(\frac{1}{\mu}\right)^{2n+1}$

n	ΔS^1_{2n+}	ΔS^2_{2n+1}	ΔS^3_{2n+1}	ΔS^4_{2n+1}	ΔS^5_{2n+1}	N	S_1^N
		$\times 10^{-4}$	$\times 10^{-4}$	$\times 10^{-6}$	$\times 10^{-6}$		
1	.202057	770.569	400.199	24394.9	16394.9	1	1.0000
2	.036928	56.777	15.6253	585.97	265.97	2	1.5000
3	008349	5.3078	7053	18.405	5.695	3	1.8333
4	.002008	.55268	.0446	.648	.136	4	2.0833
5	000494	.05908	.0263	.025	.005	5	2.2833

An even more convenient feature of formula (1) is the *alternating* character of the infinite series. This makes it possible to rewrite (1) as a finite series with a remainder term :

$$(2) \quad \arg \Gamma(ia+1) = -\sum_{n=1}^{N} \operatorname{arctg}\frac{a}{n} + (S_1^N - C)a - \sum_{n=1}^{P} \frac{(-1)^n \Delta S^N_{2n+1}}{2n+1} a^{2n+1} + R_P$$

$$|R_{.} \qquad \frac{\Delta S^{N}_{2P+3}}{(2P+3)} \times a^{2P+3}$$

where the infinite series of (1) has been terminated with the Pth term.

To illustrate the usefulness of formula (2), let us choose values of N and P such that $|R_P| < 10^{-5}$ for $0 \leq a \leq 2$. Inspection of Table I shows that we can choose either N=4, P=4 or N=5, P=3.

If we take the latter values for N and P, then the resulting finite series will be suitable for calculating a four-place table of arg $\Gamma(ia+1)$ in the range $0 \leq a \leq 2$. Substituting the values for the coefficients from Table I, we obtain the desired formula :

$$(3) \quad \arg\Gamma(ia+1) = -\sum_{n=1}^{5} \operatorname{arctg}\frac{a}{n} + \sum_{n=1}^{4} \alpha_{2n-1} a^{2n-1} - R$$

$$\alpha_1 = +1.706118\,; \qquad \alpha_5 = -5.32 \times 10^{-5}$$

$$|R| < 15 \times 10^{-9} a^{9}$$

$$\alpha_3 = +.005465\,; \qquad \alpha_7 = +8.14 \times 10^{-7}$$

The rapidly diminishing coefficients indicate the extreme usefulness of the general formula (2) in numerical calculations of arg $\Gamma(ia+1)$. So far as the five-term arctangent sum is concerned, this is not an inconvenience, since many accurate tables of this function exist.

To complete the present paper, Table II is presented. In this are listed the values of arg $\Gamma(ia+1)$ for $a = .1, .2, \ldots, 2.0$. The values have been calculated from formula (3) above. It is hoped that this table will be of use to physicists who are engaged in numerical calculations involving the "Coulomb phase factors" which occur in the continuous spectrum wave functions of hydrogenic atoms ; and it is further hoped that the table might be of use to mathematicians working in those branches of analysis which involve gamma functions of purely imaginary argument. *

As the table is restricted to values of $|a| \leq 2$ (negative values simply yield complex conjugates, which multiply the arguments by -1), it is necessary to consider the method of calculating arg $\Gamma(ia+1)$ when $|a| > 2$. For these higher values of a, the asymptotic formula[9]

$$(4) \qquad \arg\Gamma(ia+1) \approx (\pi/4) + a(\ln a - 1) - (1/12a)$$

is applicable with diminishing error for increasing values of a. This is illustrated in Table II, where for $1.5 \leq a \leq 2.0$ the values obtained from the asymptotic formula (4) have been placed in a column parallel to the values obtained from (3).

---

* Strictly speaking, $\Gamma(ia+1)$ is not a "gamma function of purely imaginary argument" but is related to such a function by the simple identity : $\Gamma(ia) = [\Gamma(ia+1)]/(ia)$. $\Gamma(ia+1)$ is, however, a factorial function of purely imaginary argument : $\Gamma(ia+1) = (ia)!$.

Comparison of the exact and asymptotic values shows that, at least as far as the physicist is concerned, formula (4) is quite adequate even for values of $a \geq 1.5$. However, for more accurate numerical work it is necessary to extend calculation to higher values of a before using the asymptotic formula.

TABLE II. Four-place Table of arg $\Gamma(ia+1)$ for $a = 0.0, 0.1, 0.2, \ldots, 2.0$ including Comparison with Asymptotic Formula [Equation (4)]

a	arg $\Gamma(ia+1)$	a	arg $\Gamma(ia+1)$	Asymptotic arg $\Gamma(ia+1)$
0.0	.0000	1.1	−.2883	...
.1	−.0572	1.2	−.2673	...
.2	−.1122	1.3	−.2392	...
.3	−.1634	1.4	−.2043	...
.4	−.2072	1.5	−.1620	−.1620
.5	−.2441			
.6	−.2727	1.6	−.1155	−.1147
.7	−.2928	1.7	−.0622	−.0616
.8	−.3042	1.8	−.0034	−.0030
.9	−.3071	1.9	+.0606	+.0611
1.0	−.3016	2.0	+.1297	+.1300

In conclusion, it is seen that the formulas derived minimize the labour necessary in numerical calculation of arg $\Gamma(ia+1)$ — or arg (ia) ! — and that the construction of a complete table of this function for an extended range of the variable is quite possible. That such a generally useful function, the factorial function, has never been completely tabulated for imaginary values of its argument, is rather a curious fact. It illustrates well the axiom that a computer's field is unbounded.

JUDSON COLLEGE,
UNIVERSITY OF RANGOON.

REFERENCES

[1] H. T. Davis: " Table of Higher Mathematical Functions," Vol. I.

[2] I. Ginzel: " Conformal Representation of the Gamma Function," *Acta Math*, **56**, 273 (1931).

[3] W. Meissner: " Table of ln Γ for Complex Arguments," *Deutsche Math.*, **4**, 537 (1939).

[4] A. Sommerfeld: " Wave Mechanics," Appendix 1; G. Gamow: " Atomic Nuclei etc.," Chapter IX, equation 15; E. C. Kemble: "Fundamental Principles of Quantum Mechanics," 177.

[5] Jahnke-Emde: " Tables of Functions " (3rd Ed.), **3**(b), 11.

[6] Jahnke-Emde: *l. c.*, 10.

[7] Adams: " Smithsonian Mathematical Formulae, etc.," 140, formulas 6.900.

[8] Jahnke-Emde: *l. c.*, 11,

ALLOTROPES OF TELLURIUM BY X-RAY DIFFRACTION METHOD*

By H. BOSE
AND
B. B. RAY

(*Received for publication, March 27, 1931*)

Plate IV

ABSTRACT. The structure of tellurium prepared by different methods was analysed by X-ray. The precipitated tellurium was so long known to be amorphous but X-ray examination revealed that it is nothing but the hexagonal variety only in a finely divided state. The diffraction patterns of tellurium were taken at different temperatures and the results obtained therein go against the hypothesis of the existence of two dynamic allotropes in ordinary tellurium. These experiments agree with the view put forward by Damiens who based his conclusions upon his own works on tellurium by chemical methods.

On chilling molten tellurium, it falls to fine powder but even this sample is not amorphous.

It was generally believed that a beam of X-rays changes the crystal structure of ordinary tellurium affecting its specific heat by about 8%, but no such change in the structure could be detected by our experiments. The diffraction pattern of liquefied tellurium was also photographed.

INTRODUCTION

Tellurium is placed in the Periodic Table along with sulphur and selenium in the 6th Group. But unlike sulphur and selenium the allotropism of tellurium is much less marked. Tellurium is known to exist in two forms—one is crystalline (hexagonal) and the other is amorphous.

Amorphous tellurium is a brownish black powder usually obtained by precipitation method, *viz.*, by reducing a solution of tellurium dioxide with sulphurous acid. It is transformed into the crystalline variety on heating with an evolution of heat.

$$\text{Te} = \text{Te cryst.} + 2630 \text{ Cal.}$$

The density of the amorphous form ranges from 5.86 to 5.87. The specific heat is 0.052.

Molten tellurium solidifies to a brittle silvery crystalline mass, which can be easily powdered ; when obtained in appreciable size, the crystals are prismatic of the trigonal system and are isomorphous with metallic selenium.

The density of crystalline tellurium is curiously variable and depends upon the method of preparation. According to Cohen and Kromer, the density also changes under the influence of heat ; and this is attributed to the presence of two dynamical allotropes in ordinary tellurium ; the density as well as other properties depends on their relative proportions. This view is however contradicted by Damiens who contends that it is the impurities which cause all these inconsistencies, the correct value is 6.310.

---

* Communicated by the Indian Physical Society.

Like density, specific heat is also variable and it ranges between 0.0475 for the distilled element to 0.6624 for the precipitated amorphous element, X-ray exposure is said to increase the specific heat by 8 p.c.

Tellurium may also be obtained in the colloidal state by a number of methods. Dilute solutions of tellurium dioxide or telluric acid on reduction, say, by hydrazine sulphurous acid etc. yield colloidal tellurium. It can also be produced by cathodic pulverisation of tellurium under water.

EXPERIMENTAL ARRANGEMENTS

As only identification rather than structure analysis was all that was necessary in the present work, only the powder method was resorted to throughout the experiment. The X-ray tube was used directly in series with the high-tension transformer without any further rectifying device. Copper K-radiation was used all along the experiment. The tube was run at 35-40 K.V. with 4-6 m.a.

The widely divergent X-ray beam coming out of the windows covered by aluminium foil of thickness 00.01 c.m. before impinging on the material became almost parallel by its passage, through a slit system.

Two types of plate-holders—cylindrical and rectangular—were used in the present work. But due to the several obvious disadvantages of the rectangular camera over the cylindrical one the preference was always given to the latter type whenever possible. Provision was made for changing the sample during the exposure without in any way disturbing the setting. For work at temperatures other than that of the laboratory, the plate camera was used with slight modifications. In the high-temperature camera, the sample was heated electrically and the double-walled film-holder is cooled by passing a cold stream of water. There was also an arrangement in which the pattern of the sample could be taken at low temperature.

The powdered material was pressed against a thin zig-zag paper which could be gummed to the slit cap with little secotine. Though the optimum thickness of the material is known to be given by $t=\frac{1}{\mu}$ (μ=mass-absorption coefficient) but trial and experiences are more reliable in this respect. Above 150°C when paper begins to char, the cells were prepared in an extremely thin walled glass tube ; capillareis were filled with the powdered mass and placed in position with both ends sealed in a groove in the cap made for this purpose. Blank exposures were given with empty glass tube for a period longer than that necessary for powder photographs but no sign of glass band could be detected. The cell to plate distance " *r* " could be obtained from a reference plate of sodium chloride, photographed at the same distance.

X-Ray Examination :—According to Groth, tellurium crystallises in the hexagonal prism. It is trigonal being isomorphous with metallic selenium. The angle between the rhombohedral axis $\alpha = 56^\circ\ 47'$, which corresponds with an axis ratio $a{:}c = 1{:}1.33$.

The structure of metallic tellurium was first determined by A. J. Bradley. It may be regarded as simple rhombohedral structures, with inter-axial angles of almost 90°, in which each atom is slightly displaced towards two of the six adjacent atoms. The resulting structure is a threefold spiral composed of three interpenetrating simple triangular lattices

$a = 4.445$ (A) for Tellurium.

The diffraction photographs of metallic tellurium was taken in a hemi-cylindrical camera (of radius 2.88 c.m.) with a 0.4 mm. slit. A large number of sharp rings was obtained (plate I).

These rings agree within experimental results with those calculated for hexagonal teilurium. The experiment was repeated in different camera-plate and hemi-cylindrical with different samples of tellurium and the same results was obtained (Table I).

TABLE I

Metallic Tellurium				Precipitated Tellurium		
" *d* " in A.U.	Sin θ	Intensity		Intensity	Sin θ	" *d* " in A.U.
3.67	0.2099	W	1	W	0.2068	3.72
3.05	0.2521	V.S.	2	V.S.	0.2507	3.07
2.86	0.2689	V.V W	3	V.V.W.		
2.24	0.3437	S	4	S	0.3467	2.22
2.12	0.3636	W	5	W	0.3592	2.14
1.99	0.3878	V.V W.	6	V.V W	0.3840	2.00
1.87	0.4115	V.V.W.	7	V.V.W.	0.4131	1.86
1.76	0.4368	V.V.W.	8	V.V.W.	0.4300	1.79
			9	V.V.W.	0.4517	1.70
1.55	0.4968	V.V.W.	10	V.V W.	0.4990	1.54
1.41	0.5461	V.V.W.	11	V.V.W.	0.5396	1.43

Precipitated tellurium (so-called amorphous variety):—Precipitated tellurium was prepared by passing slow stream of SO_2 through a solution of tellurous acid in water at the room temperature. Tellurium so obtained in finely divided state is supposed to be amorphous. A cell of the precipitated tellurium was prepared on a zig-zag paper and exposed to X-rays for a diffraction pattern in a hemicylindrical camera. The cell was changed every half an hour to avoid crystallisation during exposure. The pattern, that was obtained, was obviously that due to metallic tellurium (Plate IV). The spacings calculated from measurements of the diameters are given in Table I.

The same experiment was next carried out at lower temperatures—the preparation as well as the exposure was carried nearly at 0°C by using ice as the cooling (agent) substance.

But the sample was used throughout the exposure, as there was no arrangement for changing sample in this camera. But even then the pattern consisted of rings corresponding only to metallic tellurium.

TABLE II

Specimen	Rings	Intensities	Sin θ	d in A U.
Te at room temperature	1	W	0.2085	3.69
r=4.2 c.m.	2	S	0.2498	3.08
Te at 120° C	1	W	0.2059	3.74
r=4.2 c.m.	2	S	0.2496	3.08
Te at 150° C	1	W	0.2014	3.82
r=4.2 c.m.	2	S	0.2496	3.08
Te at 160° C	1	W	0.2014	3.82
r=4.2 c.m.	2	S	0.2493	3.08
Te obtained on chilling molten Te and cooled during exposure	1	W	0.2491	3.08
r=1.94 c.m	2	W	0.3409	2.26
Liquified Te at about 470° C	one band		0.2476	3.11
r=2.15 c.m.				

High temperature :—To test the hypothesis of two allotropes of tellurium in dynamical equilibrium, diffraction pattern of tellurium was photographed at temperatures 120°C, 150°C and 160°C. The cell used in the experiment was prepared on a zig-zag paper. Though the paper chars above 150°C, the sample together with the charred paper sticks to the cap, if undisturbed, and can be used

Fig. 1.

Fig. 2.

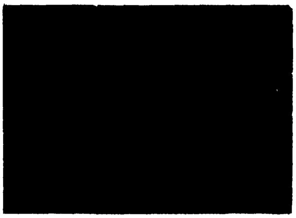

Fig. 3.

Fig. 4.

Fig. 1. Pattern due to ordinary hexagonal variety of Tellurium.

Fig. 2. Pattern of precipitated Tellurium.

Fig. 3. Liquefied Tellurium.

Fig. 4. Chilled Tellurium.

at temperatures higher than this. The high-temperature camera was used and the film kept cooled throughout the exposure by passing a stream of water through the jacket. The cell was heated by passing current through a calibrated heater fitted on the cap. The results are given in Table II. No change either in intensity distribution or in the number of rings could be detected.

With a view to investigating the effect of X-ray on the crystal structure of tellurium, a diffraction photograph of tellurium was taken with cells changed every half an hour. The pattern so obtained could be compared with another due to a sample which has been exposed to X-rays for almost 24 hours. The two patterns were completely identical.

Vitreous tellurium :—In accordance with the general method of preparing vitreous substance, *viz.*, method of sudden chilling, we tried to prepare tellurium in the vitreous state by pouring molten tellurium into cold water. Tellurium so treated falls to fine powder which, on X-ray analysis, shows itself to be purely hexagonal crystal.

The experiment was next repeated in the following way—

Molten tellurium was heated nearly to its boiling temperature and then suddenly poured into a freezing mixture. The diffraction pattern of the substance thus obtained in the finely divided state was next photographed in our low-temperature camera and the sample was kept cooled near about 0°C throughout the exposure. The pattern was almost identical with that of hexagonal tellurium and was different from the latter in the following two respects :

1. The number of rings present was fewer in this case, the weaker ones are found to be absent.
2. The background scattering is more pronounced than before.

DISCUSSION OF THE RESULTS

It was so long supposed that the precipitated tellurium (*i.e.*, the variety obtained by the method of precipitation) is amorphous. But X-ray examination has revealed its true identity ; it is crystalline and has the same structure as the metallic variety.

In order to explain certain anomalies in the properties of tellurium, the possibility of two allotropes, in temperature equilibrium, is proposed by some authors. If now a sample of tellurium be heated to a higher temperature the relative proportions of the two allotropes must change, which is sure to tell on the diffraction pattern of the sample. Hence it is natural to expect that at higher temperature either fresh rings will appear in the diffraction pattern of tellurium or at least the intensity distribution will change certain rings growing weaker while others grow stronger.

Now that no such change is noticeable in the pattern at higher temperatures we are forced to the conclusion that the hypothesis is untenable. The cause of above anomalies should be searched somewhere else, *viz.*, presence of impurities, etc.

X ray exposure is said to increase the specific heat of tellurium by about 8 p.c. This increment is attributed to a change of the crystal structure, which the substance was supposed to undergo on X-ray exposure. But the pattern obtained with cells changed every half an hour showed no difference from that due to a sample exposed for 24 hours. Therefore either X-ray has very little effect on the crystal structure of tellurium or it must have produced an instantaneous effect, the crystal structure changing completely within a very short time.

Tellurium could not be prepared in the vitreous state. In this respect it differs from sulphur and selenium. Molten selenium on sudden cooling easily passes into the vitreous state. Similar method, tried in the case of tellurium. proves a failure. According to Randall a strong directive force must be present if the vitreous state is to be obtained on chilling : "In case of selenium when the crystal melts, first the spirals will break away from each other. The complete breakdown of the spiral, if it occurs at all, will take place at a higher temperature. Now in the reverse process of rapid solidification of molten selenium the atoms of a solid body always tends to arrange themselves in such positions that the crystal potential energy is a minimum for the prevailing conditions. Since in case of selenium the main energy terms lie as it were in the spirals themselves, these will try to grow immediately on solidification It is not nearly so important for the chains to line up in full lattice arrangement. By the time the chains have grown a little the substance is too viscous to allow of any further marshaling. It is suggested therefore that strongly directional forces are necessary for the formation of glasses."*

Thus although metallic tellurium has the same crystal structure as metallic selenium, it lacks in a strong directive force while in the latter such force is present. This is to be made responsible for the difference in behaviour of tellurium and selenium as regards their production of vitreous state.

In the pattern due to chilled tellurium certain rings are absent. This cannot be attributed to any change in the crystalline nature of the substance, since it is found that it is only the weak rings which are absent. This must be due to under exposure and greater general blackening. The continuity of the rings as well as greater general blackening suggests that the operation of chilling molten tellurium must have caused a decrease in particle size of the sample. This in reality amounts to the assumption that the particle size of the chilled mass is a decreasing function of the rate of cooling, the greater the rate the smaller being the size of the individual particle.

In short, we find that tellurium whatever be its source or method of preparation is always crystalline and hexagonal in structure. The variety which had been known as amorphous is but metallic tellurium in finely divided state. It does not pass into the vitreous state on sudden cooling like selenium.

---

* Quoted from "Diffraction of X-rays, etc.," by Randall, p. 183.

Although the method of cooling diminishes the particle size, the crystals are not still small enough to yield bands. The more metallic character of tellurium is probably responsible for this high stability of ordinary hexagonal variety and the absence of vitreous state.

Amorphous and a new variety of tellurium :

We have seen that the process above referred to is not capable of causing diminution in particle size to the extent necessary for the production of a diffraction band. This, however, could be effected in the process of preparing a colloidal tellurium sol. where the existence of particles of the order 10^{-7} to 10^{-5} c.m. is possible.

By precipitating a colloidal solution by an electrolyte a sample of tellurium was obtained which yielded a band on X-ray exposure which corresponds in position to a strong group of rings in the hexagonal pattern. It suggests, therefore, that by this method the particle size can be made smaller than is obtainable by other methods. This will be more dilated upon in connection with colloidal tellurium solution. It is also found that certain results obtained suggest the existence of another variety of tellurium, details of which will be published in a separate paper.

LIQUID TELLURIUM

In general the diffraction pattern produced by X-rays passing through liquid is a complicated result of the structure of the actual molecules and the temporary arrangement of the molecules. Various theories have been put forward but none of them have been in any sense complete. This is but what can be expected since so little is known about the structural aspects of the liquid state.

For a practical working model, however, Stewart's ideas of cybotaxis is preferable. The following is an extract from Stewart's article in *Rev. Mod. Phys.* (2, 116, 1938):

" If X-rays give evidence of periodic molecular grouping, it must not be supposed that these groups are large or that the molecules in any one well-defined group remain permanently members of the group. At any instant these small groups might exist at numerous points in the liquid, the regions between them being not so orderly."

Stewart argues that it is quite unlikely that catastrophic changes in atomic and molecular arrangements take place just at the melting point. Stewart's cybotactic hypothesis suggests that the kinetic energy of the molecules (in the liquid state) is of the same order as that of the binding forces among the molecules in that state.

The experimental results suggest that in a liquid there is a general tendency towards arrangements similar to those in a solid state just below the melting point. The exceptions, for which this similarity between the two states (*i.e.*, solid and liquid) do not hold, are oxygen, nitrogen and bismuth. The case of alkali metals, lead, aluminium, appear to lie between the two extremes, while mercury fits in with the close-packing theory.

Tellurium was examined in the liquid state to test Stewart's ideas.

EXPERIMENTAL ARRANGEMENTS

Tellurium melts at 450° C, so the high-temperature camera was utilised for the investigations of the band patterns of liquid tellurium. The cell was prepared in capillary glass tube, drawn from very thin Jena glass tube. The heating could be effected by an electric heater just fitting the cap to the slit system. The heater is, in reality, a syndanio bobin wound round with nichrome wire. The heating current was produced by a step-down transformer from which steady current as high as 20 amperes could be drawn at 30 volts. The heater was calibrated so that the temperature within 2°C could be known from the current in the heating coil.

With these arrangements, exposure was given for a period of 20 hours. The pattern consisted of a single diffuse band (Plate IV). The spacings corresponding to the most intense position of the band is 3.11 (A.U.).

DISCUSSION

The value of "*d*" corresponding to the band obtained for amorphous tellurium is 3.09 (A.U.) Thus it is seen that the two "*d*" values, for liquid and amorphous are nearly equal. The slightly greater value of the former may be due to temperature effect. For hexagonal tellurium there is an intense ring of spacing 2.94 (A.U.). Thus it may be summarised that liquid tellurium also shows a similarity to the solid state.

Khaira Laboratory of Physics,
University College of Science,
92, Upper Circular Road,
Calcutta.

REFERENCES

1 Newton Friend, "*Inorganic Chemistry,*" Vol. VII, Part II.
2 ,, ,, ,, ,, ,, ,,
3 ,, ,, ,, ,, ,, ,,
4 Cohen and Kroner, *Zeits Physical Chem*, **82**, 587 (1913).
5 Damiens, *Compt. Rend*, **174**, 1344 (1922).
6 Newton Friend, "*Inorganic Chemistry,*" Vol. VII, Part II.
7 Groth, "*Chemische Krystallographie,*" Teil I, p. 32
8 Bradley, *Phil. Mag.*, **48**, 477 (1924).

A RAPID METHOD FOR CALCULATING THE LEAST SQUARES SOLUTION OF A POLYNOMIAL OF DEGREE NOT EXCEEDING THE FIFTH*

BY S. M. KERAWALA

(Received for publication, March 1, 1941)

ABSTRACT. The ordinary method for finding the least squares solution of a polynomial is very laborious. If, however, the values of the independent variable form an arithmetic series, a method can be devised to give the solution very rapidly. The method given in this paper is an improvement on the method of Birge and Shea. The process of calculating the solution has been divided into three distinct parts :

(1) Calculating the solution corresponding to the standard n values, $x_r = r - \frac{1}{2}(n+1)$ of the independent variable. Tables are given for $n \leq 30$ to facilitate rapid calculation, and a powerful method has been shown for $n > 30$.

(2) Testing the suitability of the selected polynomial.

(3) Calculating the true from the standard solution

The tables here given are more extensive than those of Birge and Shea, but every figure has been carefully tested on a calculating machine.

INTRODUCTION

The problem of fitting a number of observations to polynomials occurs frequently in physical sciences. An ideal illustration of the case is found in band spectra where it is known that most band series can be accurately represented by polynomials. Birge and Shea[1] have developed formulæ for fitting polynomials up to the fifth degree to data given for equally spaced values of the independent variable. But the methods by which they obtain the results are tentative throughout. A general and mathematically very elegant basis has been given to Birge and Shea's results by Condon.[2] But the general formula obtained by Condon for the coefficient of the highest power of the variable in the least squares solution for a polynomial is completely different from the value of the general coefficient obtained by Birge and Shea in its mathematical form. The transformation of the one general expression into the other has not yet been carried out. In the following pages I have obtained most of the equations of Birge and Shea by using Cramer's[3] rule for solving the normal equations, and have constructed tables which give the least squares solutions a little more rapidly than the corresponding tables given by Birge and Shea. Although the tables given here permit rapid caculations only if the number of observations does not exceed thirty, the general formulæ obtained here could be applied to a larger number of observations without very much increasing the labour.

---

* Communicated by the Indian Physical Society

§1. DERIVATION OF THE MAIN FORMULAE

It is supposed that n values of an observed quantity y are known corresponding to the n values of the independent variable x. It is assumed that the precision of measurement of x is large enough for the error in x to be negligible compared to the error in y. The individual x's and y's may be denoted by x_i, y $(i=1, 2, \ldots, n)$. The problem is to find constants $a_{\sigma p}$ such that if $f_p(x) = \sum_{\sigma=0}^{p} a_{\sigma p} x^{\sigma}$, the sum of the squares of the residuals between the values of y calculated from this representation and the corresponding observed values of y is a minimum. The quantity M_p to be minimised is

$$M_p = \sum_{i=1}^{n} [y_i - f_p(x_i)]^2.$$

The conditions for a minimum are

$$\frac{\partial M_p}{\partial a_{\sigma p}} = 0, \qquad \sigma = 0, 1, 2, \ldots p.$$

These $(p+1)$ equations are the normal equations for the $(p+1)$ unknowns $a_{\sigma p}$. Written out more fully, the normal equations assume the form

$$\sum_{i=1}^{n} \left\{ y_i x_i^{\sigma} - a_{0p} x_i^{\sigma} - a_{1p} x_i^{(\sigma+1)} - \ldots\ldots\ldots - a_{\sigma p} x_i^{(\sigma+p)} \right\} = 0$$

$$\sigma = 0, 1, 2, \ldots\ldots\ldots\ldots, p.$$

Writing

$$\xi_\nu = \sum_{i=1}^{n} x_i^{\nu}.$$

and

$$\eta_\nu = \sum_{i=1}^{n} y_i x_i^{\nu},$$

the normal equations can be put into the simpler form :

$$a_{0p}\xi_{\sigma} + a_{1p}\xi_{\sigma+1} + \ldots\ldots\ldots + a_{\sigma p}\xi_{(\sigma+p)} = \eta_{\sigma}$$

$$(\sigma = 0, 1, 2, \ldots p)$$

It is now assumed that the n values of x form an arithmetic series. The series assumed for the purposes of calculation is the one in which

$$x_i = i - \frac{n+1}{2}.$$

This series is preferred to any other because it yields comparatively simple values for the sums ξ_ν. And once the coefficients $a_{\sigma p}$ are calculated with the standard series, the calculation of the corresponding coefficients for any other arithmetic series does not present any difficulty. With the values of x given by the standard arithmetic series,

$$\xi_\nu = \left(-\frac{n-1}{2}\right)^\nu + \left(-\frac{n-3}{2}\right)^\nu + \ldots\ldots\ldots + \left(\frac{n-3}{2}\right)^\nu + \left(\frac{n-1}{2}\right)^\nu.$$

It follows that for odd values of ν, ξ_ν vanishes, while for even values of ν, ξ_ν can be expressed in terms of Bernoulli polynomials* thus :

$$\xi_\nu = \frac{2}{\nu+1} B_{(\nu+1)}\left(\frac{n+1}{2}\right).$$

If these considerations are to apply to polynomials of degree not exceeding the fifth, the maximum value ν can take is 10. The highest Bernoulli polynomial required is the eleventh. The first six odd Bernoulli polynomials are therefore sufficient for the purpose. They are :

$$B_1(x) = x - \tfrac{1}{2}$$
$$B_3(x) = x(x-1)(x-\tfrac{1}{2})$$
$$B_5(x) = x(x-1)(x-\tfrac{1}{2})(x^2 - x - \tfrac{1}{3})$$
$$B_7(x) = x(x-1)(x-\tfrac{1}{2})(x^4 - 2x^3 + x + \tfrac{1}{3})$$
$$B_9(x) = x(x-1)(x-\tfrac{1}{2})(x^6 - 3x^5 + x^4 + 3x^3 - \tfrac{1}{5}x^2 - \tfrac{9}{5}x - \tfrac{3}{5})$$
$$B_{11}(x) = x(x-1)(x-\tfrac{1}{2})(x^8 - 4x^7 + \tfrac{8}{3}x^6 + 6x^5 - \tfrac{10}{3}x^4 - 8x^3 + \tfrac{2}{3}x^2 + 5x + \tfrac{5}{3}).$$

The values of ξ_ν calculated from the above are :

$$\xi_0 = n, \qquad \xi_1 = 0$$

$$\xi_2 = \frac{n(n^2-1)}{}. \qquad \xi_3 = 0$$

$$\xi_4 = \frac{n(n^2-1)(3n^2-7)}{240}, \qquad \xi_5 = 0,$$

$$\xi_6 = \frac{n(n^2-1)(3n^4-18n^2+31)}{1344}, \qquad \xi_7 = 0,$$

$$\xi_8 = \frac{n(n^2-1)(5n^6-55n^4+239n^2-381)}{11520}, \qquad \xi_9 = 0,$$

$$\xi_{10} = \frac{n(n^2-1)(3n^8-52n^6+410n^4-1636n^2+2555)}{33792}.$$

A. *The polynomial is of degree 0 :* $f_0(x)=a_{00}$.

The normal equation is

$$a_{00}\xi_0=\eta_0$$

$$a_{00}=\frac{\eta_0}{n} \qquad \ldots \quad (1)$$

B. *The polynomial is of degree 1 :* $f_1(x)=a_{01}+a_{11}x$.

The two normal equations are:

$$a_{01}\xi_0=\eta_0$$

and

$$a_{11}\xi_2=\eta_1$$

$$a_{01}=\frac{\eta_0}{n}=a_{00} \qquad \ldots \quad 2(a)$$

and

$$a_{11}=\frac{\eta_1}{\xi_2}=\frac{12\eta_1}{n(n^2-1)}. \qquad \ldots \quad 2(b)$$

C. *The polynomial is of degree 2 :* $f_2(x)=a_{02}+a_{12}x+a_{22}x^2$.

$$a_{02}\xi_0+a_{22}\xi_2=\eta_0$$

$$a_{12}\xi_2=\eta_1$$

and

$$a_{02}\xi_2+a_{22}\xi_4=\eta_2.$$

Writing

$$\Delta_2=\begin{vmatrix}\xi_0 & \xi_2\\ \xi_2 & \xi_4\end{vmatrix}$$

the solutions can be written in the form

$$\frac{a_{02}}{\xi_2\eta_2-\xi_4\eta_0}=\frac{a_{22}}{\xi_2\eta_0-\xi_0\eta_2}=-\frac{1}{\Delta_2}$$

and

$$a_{12}=\frac{\eta_1}{\xi_2}.$$

But Δ_2 can be easily shown to be equal to $\frac{n^2(n^2-1)(n^2-4)}{180}$ as the ξ's have already been worked out.

$$\therefore \quad a_{02}=\frac{\xi_4}{\Delta_2}\eta_0-\frac{\xi_2}{\Delta_2}\eta_2=\frac{3(3n^2-7)}{4n(n^2-4)}\eta_0-\frac{15}{n(n^2-4)}\eta_2 \qquad \ldots \quad 3(a)$$

$$a_{12}=\frac{\eta_1}{\xi_2}=\frac{12}{n(n^2-1)}\eta_1=a_{11} \qquad \ldots \quad 3(b)$$

and

$$a_{22}=-\frac{\xi_2}{\Delta_2}\eta_0+\frac{\xi_0}{\Delta_2}\eta_2=-\frac{15}{n(n^2-4)}\eta_0+\frac{180}{n(n^2-1)(n^2-4)}\eta_2 \ldots \quad 3(c)$$

D. *The polynomial is of degree 3 :* $f_3(x) = a_{03} + a_{13}x + a_{23}x^2 + a_{33}x^3$.

The four normal equations can be separated into two pairs thus :

$$\left.\begin{aligned} a_{03}\xi_0 + a_{23}\xi_2 &= \eta_0, \\ a_{03}\xi_2 + a_{23}\xi_4 &= \eta_2, \end{aligned}\right\} \text{ and } \left.\begin{aligned} a_{13}\xi_2 + a_{33}\xi_4 &= \eta_1, \\ a_{13}\xi_4 + a_{33}\xi_6 &= \eta_3. \end{aligned}\right\}$$

The solution is :

$$a_{03} = a_{02} \qquad \ldots \quad 4(a)$$

$$a_{23} = a_{22} \qquad \ldots \quad 4(c)$$

$$a_{13} = \frac{\xi}{\Delta}\eta_1 - \frac{\xi_4}{\Delta_3}\eta_3$$

and

$$a_{33} = -\frac{\xi_4}{\Delta_3}\eta_1 + \frac{\xi_2}{\Delta_3}\eta_3$$

where Δ_3 denotes $\left|\begin{matrix} \xi_2 & \xi_4 \\ \xi_4 & \xi_6 \end{matrix}\right|$ and can be shown to be equal to

$$\frac{n^2(n^2-1)^2(n^2-4)(n^2-9)}{33600};$$

so that finally

$$a_{\;3} = \frac{25(3n^4 - 18n^2 + 31)}{n(n^2-1)(n^2-4)(n^2-9)}\eta_1 - \frac{140(3n^2-7)}{n(n^2-1)(n^2-4)(n^2-9)}\eta_3 \qquad \ldots \quad 4(b)$$

and

$$a_{33} = -\frac{140(3n^2-7)}{n(n^2-1)(n^2-4)(n^2-9)}\eta_1 + \frac{2800}{n(n^2-1)(n^2-4)(n^2-9)}\eta_3 \qquad 4(d)$$

E. *The polynomial is of degree 4 :* $f_4(x) = a_{04} + a_{14}x + a_{24}x^2 + a_{34}x^3 + a_{44}x^4$.

(δ) The five normal equations can be separated into two groups of three and two equations:

$$\left.\begin{aligned} a_{04}\xi_0 + a_{24}\xi_2 + a_{44}\xi_4 &= \eta_0 \\ a_{04}\xi_2 + a_{24}\xi_4 + a_{44}\xi_6 &= \eta_2 \\ a_{04}\xi_4 + a_{24}\xi_6 + a_{44}\xi_8 &= \eta_4 \end{aligned}\right\}$$

and

$$\left.\begin{aligned} a_{14}\xi_2 + a_{34}\xi_4 &= \eta_1 \\ a_{14}\xi_4 + a_{34}\xi_6 &= \eta_3 \end{aligned}\right\}$$

The solution is :

$$a_{14} = a_{13} \qquad 5(b)$$

$$a_{34} = a_{33} \qquad 5(d)$$

$$a_{04} = \frac{(\xi_4\xi_8 - \xi_6^2)\eta_0 - (\xi_2\xi_8 - \xi_4\xi_6)\eta_2 + (\xi_2\xi_6 - \xi_4^2)\eta_4}{}$$

$$a_{24} = \frac{-(\xi_2\xi_8 - \xi_4\xi_6)\eta_0 + (\xi_0\xi_8 - \xi_4^2)\eta_2 - (\xi_0\xi_6 - \xi_2\xi_4)\eta_4}{\Delta_4}$$

and $$a_{44} = \frac{(\xi_2\xi_6 - \xi_4^2)\eta_0 - (\xi_0\xi_6 - \xi_2\xi_4)\eta_2 + (\xi_0\xi_4 - \xi_2^2)\eta_4}{\Delta_4}$$

where Δ_4 denotes $$\begin{vmatrix} \xi_0 & \xi_2 & \xi_4 \\ \xi_2 & \xi_4 & \xi_6 \\ \xi_4 & \xi_6 & \xi_8 \end{vmatrix}$$

and can be shown to be equal in value to

$$\frac{n^3(n^2-1)^2(n^2-4)^2(n^2-9)(n^2-16)}{7938000}.$$

Now with some simple manipulations with their rows and columns the values of the following determinants can be worked out to be :

$$(\xi_4\xi_8 - \xi_6^2) = \begin{vmatrix} \xi_4 & \xi_6 \\ \xi_6 & \xi_8 \end{vmatrix} = \frac{n^2(n^2-1)^2(n^2-4)(n^2-9)(15n^4-230n^2+407)}{33868800}$$

$$(\xi_2\xi_8 - \xi_4\xi_6) = \begin{vmatrix} \xi_2 & \xi_4 \\ \xi_6 & \xi_8 \end{vmatrix} = \frac{n^2(n^2-1)^2(n^2-4)(n^2-9)(n^2-7)}{120960}$$

$$(\xi_2\xi_6 - \xi_4^2) = \Delta_3 = \frac{n^2(n^2-1)^2(n^2-4)(n^2-9)}{33600}$$

$$(\xi_0\xi_8 - \xi_4^2) = \begin{vmatrix} \xi_0 & \xi_4 \\ \xi_4 & \xi_8 \end{vmatrix} = \frac{n^2(n^2-1)(n^2-4)(n^4-10n^2+29)}{3600}$$

$$(\xi_0\xi_6 - \xi_2\xi_4) = \begin{vmatrix} \xi_0 & \xi_2 \\ \xi_4 & \xi_6 \end{vmatrix} = \frac{n^2(n^2-1)(n^2-4)(3n^2-13)}{2520}$$

and $$(\xi_0\xi_4 - \xi_2^2) = \Delta_2 = \frac{n^2(n^2-1)(n^2-4)}{180}.$$

These provide all the necessary material for completing the solution as follows:

$$a_{04} = \frac{15(15n^4-230n^2+407)}{64n(n^2-4)(n^2-16)}\eta_0 - \frac{525(n^2-7)}{8n(n^2-4)(n^2-16)}\eta_2 + \frac{945}{4n(n^2-4)(n^2-16)}\eta_4 \qquad 5(a)$$

$$a_{\ 4} = \frac{-525(n^2-7)}{8n(n^2-4)(n^2-16)}\eta_0 + \frac{2205(n^4-10n^2+29)}{n(n^2-1)(n^2-4)(n^2-9)(n^2-16)}\eta_2 - \frac{3150(3n^2-13)}{n(n^2-1)(n^2-4)(n^2-9)(n^2-16)}\eta_4 \quad \cdots \quad 5(c)$$

$$a_{44}: \frac{945}{4n(n^2-4)(n^2-16)}\eta_0 - \frac{3150(3n^2-13)}{n(n^2-1)(n^2-4)(n^2-9)(n^2-16)}\eta_2$$

$$+ \frac{44100}{n(n^2-1)(n^2-4)(n^2-9)(n^2-16)}\eta_4 \quad \ldots \quad 5(e)$$

F. *The polynomial is of degree* 5: $f_5(x) = a_{05} + a_{15}x + a_{25}x^2 + a_{35}x^3 + a_{45}x^4 + a_{55}x_5$.

The six normal equations split into two equal groups.

$$a_{05}\xi_0 + a_{25}\xi_2 + a_{45}\xi_4 = \eta_0$$

$$a_{05}\xi_2 + a_{25}\xi_4 + a_{45}\xi_6 = \eta_2$$

$$a_{05}\xi_4 + a_{25}\xi_6 + a_{45}\xi_8 = \eta_4$$

and

$$a_{15}\xi_2 + a_{35}\xi_4 + a_{55}\xi_6 = \eta_1$$

$$a_{15}\xi_4 + a_{35}\xi_6 + a_{55}\xi_8 = \eta_3$$

$$a_{15}\xi_6 + a_{35}\xi_8 + a_{55}\xi_{10} = \eta_5$$

On solving the equations

$$a_{05} = a_{04} \qquad 6(a)$$

$$a_{25} = a_{24} \qquad 6(c)$$

$$a_{45} = a_{44} \qquad 6(e)$$

$$a_{15} = \frac{(\xi_6\xi_{10} - \xi_8^2)\eta_1 - (\xi_4\xi_{10} - \xi_6\xi_8)\eta_3 + (\xi_4\xi_8 - \xi_6^2)\eta_5}{\Delta_5}$$

$$a_{35} = \frac{-(\xi_4\xi_{10} - \xi_6\xi_8)\eta_1 + (\xi_2\xi_{10} - \xi_6^2)\eta_3 - (\xi_2\xi_8 - \xi_4\xi_6)\eta_5}{\Delta_5}$$

$$a_{55} = \frac{(\xi_4\xi_8 - \xi_6^2)\eta_1 - (\xi_2\xi_8 - \xi_4\xi_6)\eta_3 + (\xi_2\xi_6 - \xi_4^2)\eta_5}{\Delta_5}$$

where Δ_5 denotes

$$\begin{vmatrix} \xi_2 & \xi_4 & \xi_6 \\ \xi_4 & \xi_6 & \xi_8 \\ \xi_6 & \xi_8 & \xi_{10} \end{vmatrix}$$

and can be shown to be equal to

$$\frac{n^3(n^2-1)^3(n^2-4)^2(n^2-9)^2(n^2-16)(n^2-25)}{234710784000}$$

Further it can similarly be shown that

$$(\xi_6\xi_{10} - \xi_8^2) = \begin{vmatrix} \xi_6 & \xi_8 \\ & \xi_{10} \end{vmatrix}$$

$$= \frac{n^2(n^2-1)^2(n^2-4)(n^2-9)(25n^8 - 900n^6 + 10230n^4 - 37060n^2 + 46137)}{2554675200}$$

$$(\xi_4\xi_{10}-\xi_6\xi_8)=\begin{vmatrix}\xi_4 & \xi_6\\ \xi_8 & \xi_{10}\end{vmatrix}=\frac{n^2(n^2-1)^2(n^2-4)(n^2-9)(3n^6-75n^4+541n^2-853)}{21288960}$$

$(\xi_4\xi_8-\xi_6^2)$ from previous work

$$=\frac{n^2(n^2-1)^2(n^2-4)(n^2-9)(15n^4-230n^2+407)}{33868800}$$

$$(\xi_2\xi_{10}-\xi_6^2)=\begin{vmatrix}\xi_2 & \xi_6\\ \xi_6 & \xi_{10}\end{vmatrix}=\frac{n^2(n^2-1)^2(n^2-4)(n^2-9)(3n^4-46n^2+199)}{1241856}$$

$(\xi_2\xi_8-\xi_4\xi_6)$ from previous work $=\dfrac{n^2(n^2-1)^2(n^2-4)(n^2-9)(n^2-7)}{120960}$

and $(\xi_2\xi_6-\xi_4^2)=\Delta_3=\dfrac{n^2(n^2-1)^2(n^2-4)(n^2-9)}{33600}$.

The solution may now be completed :

$$a_{15}=\frac{147(25n^8-900n^6+10230n^4-37060n^2+46137)}{16\,n(n^2-1)(n^2-4)(n^2-9)(n^2-16)(n^2-25)}\eta_1$$

$$-\frac{2205(3n^6-75n^4+541n^2-853)}{2n(n^2-1)(n^2-4)(n^2-9)(n^2-16)(n^2-25)}\eta_3$$

$$+\frac{693(15n^4-230n^2+407)}{n(n^2-1)(n^2-4)(n^2-9)(n^2-16)(n^2-25)}\eta_5 \tag{6(b)}$$

$$a_{35}=\frac{-2205(3n^6-75n^4+541n^2-853)}{2n(n^2-1)(n^2-4)(n^2-9)(n^2-16)(n^2-25)}\eta_1$$

$$+\frac{18900(3n^4-46n^2+199)}{n(n^2-1)(n^2-4)(n^2-9)(n^2-16)(n^2-25)}\eta_3$$

$$-\frac{194040(n^2-7)}{n(n^2-1)(n^2-4)(n^2-9)(n^2-16)(n^2-25)}\eta_5 \tag{6(c)}$$

$$a_{55}=\frac{693(15n^4-230n^2+407)}{n(n^2-1)(n^2-4)(n^2-9)(n^2-16)(n^2-25)}\eta_1$$

$$\frac{194040(n^2-7)}{n(n^2-1)(n^2-4)(n^2-9)(n^2-16)(n^2-25)}\eta_3$$

$$-\frac{698544}{n(n^2-1)(n^2-4)(n^2-9)(n^2-16)(n^2-25)}\eta_5. \tag{6(f)}$$

The coefficients $a_{\sigma\rho}$ $(0\leq\sigma\leq\rho\leq5)$ have been all expressed in terms of n and the sums η_ν $(\nu\leq\rho)$. Thus tables could be constructed to give the values of the various factors multiplying η_ν for different values of n. All that would be necessary for a rapid calculation of $a_{\sigma\rho}$ would be the evaluation of the η_ν from the n observed values y_i. However, from the form of η_ν, *viz.* $\eta_\nu = \sum_{i=1}^{n} y_i x_i^\nu$, and from the symmetrical spacing of x_i, it is at once evident that when ν is odd the factor multiplying y_{r+1} is the negative of the factor multiplying y_{n-r}; and when ν is even the two factors are identical. Further the values of $a_{\sigma\rho}$ obtained above in terms of n and η_ν are seen to involve η_ν *either* with odd values alone of ν *or* with even values alone of ν. These two facts permit the transformation of the values of $a_{\sigma\rho}$ into the one or the other of the following two forms : $a_{\sigma\rho} =$

either $\quad \delta_1(y_n + y_1) + \delta_2(y_{n-1} + y_2) + \ldots\ldots$to $[\frac{n+1}{2}]$ terms

or $\quad \delta_1(y_n - y_1) + \delta_2(y_{n-1} - y_2) + \ldots\ldots$to $[\frac{n}{2}]$ terms

where the pair factors δ_1, δ_2,... are functions of n and $[\frac{n+1}{2}]$ represents the integral part of $\frac{n+1}{2}$.

Tables could, therefore, also be constructed to give the values of the various pair-factors occurring in the new expression for $a_{\sigma\rho}$ for different values of n. The tables at the end are such tables valid for values of n up to 30. For larger values of n, use of formulæ (1) to (6) and computation of η's is recommended. The main formulae have been collected together on the last page of the tables. The tables given here have been calculated by the method mentioned above and have been tested by at least one of the polynomials $y = 1 + x^p$ $(p \leq 5)$. It is, therefore, believed that the tables are free from all errors of calculation. The tables given by Birge and Shea for $a_{\rho\rho}$ form only one half of the tables given here. After the figures were calculated and tested, they were compared with the tables of Birge and Shea. The figures were found to agree in every case.

Before proceeding further, it would be interesting to see how the results of Birge and Shea could be shown to be identical with those of Condon, at least as far as they hold for polynomials of degree up to the fifth.

Consider the equations 1, 2(b), 3(c), 4(d), 5(e) and 6(f). If $a_{\rho\rho}$ be supposed known, the six values of η_ν can be calculated in terms of $a_{\rho\rho}$ as follows from the six equations :

$$\eta_0 = n a_{00}$$

$$\eta_1 = \frac{n(n^2-1)}{12} a_{11}$$

$$\eta_2 = \frac{n(n^2-1)}{12} a_{00} + \frac{n(n^2-1)(n^2-4)}{180} a_{22}$$

$$\eta_3 = \frac{n(n^2-1)(3n^2-7)}{240} a_{11} + \frac{n(n^2-1)(n^2-4)(n^2-9)}{2800} a_{33}$$

$$\eta_4 = \frac{n(n^2-1)(3n^2-7)}{240} a_{00} + \frac{n(n^2-1)(n^2-4)(3n^2-13)}{2520} a_{22}$$
$$+ \frac{n(n^2-1)(n^2-4)(n^2-9)(n^2-16)}{44100} a_{44}$$

$$\eta_5 = \frac{n(n^2-1)(3n^4-18n^2+31)}{1344}a_{11} + \frac{n(n^2-1)(n^2-4)(n^2-9)(n^2-7)}{10080}a_{33}$$
$$+\frac{n(n^2-1)(n^2-4)(n^2-9)(n^2-16)(n^2-25)}{698544}a_{55}.$$

Substituting these values of η_ν in the formulæ for $a_{\sigma\rho}(\sigma<\rho)$ the results obtained are:

$$a_{01}=a_{00}$$

$$a_{12}=a_{11}\;;\quad a_{02}=a_{00}-\frac{n^2-1}{12}a_{22}$$

$$a_{23}=a_{22}\;;\quad a_{03}=a_{00}-\frac{n^2-1}{12}a_{22}\;;\quad a_{13}=a_{11}-\frac{3n^2-7}{20}a_{33}$$

$$a_{34}=a_{33}\;;\; a_{14}=a_{13}\;;\; a_{04}=a_{00}-\frac{n^2-1}{12}a_{22}+\frac{3(n^2-1)(n^2-9)}{560}a_{44};$$

$$a_{24}=a_{22}-\frac{3n^2-13}{14}a_{44}$$

$$a_{05}=a_{04}\;;\; a_{25}=a_{24}\;;\; a_{45}=a_{44}\;;\; a_{15}=a_{11}-\frac{3n^2-7}{20}a_{33}+\frac{15n^4-230n^2+407}{1008}a_{55};$$

$$a_{35}=a_{33}-\frac{5(n^2-7)}{18}a_{55}.$$

These results sum up in brief most of the results of Birge and Shea. Now the orthogonal polynomials defined by Condon are:

$\phi_1(x)=1$

$\phi_2(x)=x$

$$x)=x^2-\frac{\xi_2'}{\xi_0}=x^2-\frac{n^2-1}{12}$$

$$\phi_4(x)=x^3-\frac{\xi_4}{\xi_2}x=x^3-\frac{3n^2-7}{20}x$$

$$\phi_5(x)=x^4+\frac{\xi_0\xi_6-\xi_2\xi_4}{\xi_2^2-\xi_0\xi_4}x^2+\frac{\xi_4^2-\xi_2\xi_6}{\xi_2^2-\xi_0\xi_4}=x^4-\frac{(3n^2-13)}{14}x^2+\frac{3(n^2-1)(n^2-9)}{560}$$

$$\phi_6(x)=x^5+\frac{\xi_2\xi_8-\xi_4\xi_6}{\xi_4^2-\xi_2\xi_6}x^3+\frac{\xi_6^2-\xi_4\xi_8}{\xi_4^2-\xi_2\xi_6}=x^5-\frac{5(n^2-7)}{18}x^3+\frac{15n^4-230n^2+407}{1008}x$$

If use be now made of the coefficients R_{kl} defined by Birge and Shea,

$$\phi_1(x)=R_{00}$$
$$\phi_2(x)=R_{11}x$$
$$\phi_3(x)=R_{22}x^2+R_{02}$$

$$\phi_4(x) = R_{33}x^3 + R_{13}x$$
$$\phi_5(x) = R_{44}x^4 + R_{24}x^2 + R_{04}$$
$$\phi_6(x) = R_{55}x^5 + R_{35}x^3 + R_{15}x.$$

The identification is thus complete.

§II. DIRECTIONS FOR FINDING THE LEAST SQUARES SOLUTION

Subtract from each observation any convenient constant quantity. Arrange the resulting observations as indicated in model form 1 modified to suit the problem in view. To find any coefficient of the polynomial multiply the numbers in the column (A − B) or (A + B) as shown in the tables by the corresponding pair-factors and divide the algebraic sum of the products by the denominator written against the pair-factors. If finally the quantity subtracted from all the observed y's be added on to the constant term of the polynomial, the least squares solution is completed except as regards transformation of the coefficients into values corresponding to the true arithmetic series of values taken by the argument x.

If, however, it be necessary to test whether the polynomial chosen is suitable, the calculations necessary for the transformation could be postponed with advantage till the trend of the residuals between the observed and the calculated values of y has been examined. This can be done as in model form 2(a) or 2(b) according as n is odd or even. Starting from the central differences calculated by means of the formulae given in the model forms, the values of all the desired calculated values of y could be rapidly built up by successive addition or subtraction in the various columns in order from left to right.

If the fit is found suitable, the final transformation to the true values of the variable may be carried out now. Let the true set of n values of the independent variable be given by $x'_r = x'_1 + (r-1)d$ whereas the standard values x_r are given by $x_r = {}^{-(n-1)} + (r-1)$. On eliminating $(r-1)$ and writing m for $x_1 + \frac{n-1}{2}d$, which is the centre of the true set, $x_r d = x'_r - m$ is obtained. The two following transformations could now be successively applied

$$x'' = xd$$

and
$$x' = x'' + m.$$

If $b_{\sigma p}$ be the coefficients with x'' as the variable and $c_{\sigma p}$ be the coefficients with x' as the variable, the calculation of $b_{\sigma p}$ from $a_{\sigma p}$ is indicated in model form 3(a), and the calculation of $c_{\sigma p}$ from $b_{\sigma p}$ is indicated in model form $3b$. However, the calculations performed under model form 3(b) can be more conveniently carried out by Horner's scheme.[5]

§III. MODEL FORMS AND TABLES

MODEL FORM I

a_{55}	a_{35}	a_{15}	A−B	A	B	A+B	a_{05}	a_{25}	a_{45}
Pair-factors			$y_{21}-y_1$	y_{21}	y_1	$y_{21}+y_1$	Pair-factors		
,,	,,	,,	$y_{20}-y_2$	y_{20}	y_2	$y_{20}+y_2$	,,	,,	,,
,,	,,	,,	$y_{19}-y_3$	y_{19}	y_3	$y_{19}+y_3$	,,	,,	,,
,,	,,	,,	$y_{18}-y_4$	y_{18}	y_4	$y_{18}+y_4$	,,	,,	,,
,,	,,	,,	$y_{17}-y_5$	y_{17}	y_5	$y_{17}+y_5$	,,	,,	,,
,,	,,	,,	$y_{16}-y_6$	y_{16}	y_6	$y_{16}+y_6$	,,	,,	,,
,,	,,	,,	$y_{15}-y_7$	y_{15}	y_7	$y_{15}+y_7$	,,	,,	,,
,,	,,	,,	$y_{14}-y_8$	y_{14}	y_8	$y_{14}+y_8$	,,	,,	,,
,,	,,	,,	$y_{13}-y_9$	y_{13}	y_9	$y_{13}+y_9$	,,	,,	,,
,,	,,	,,	$y_{12}-y_{10}$	y_{12}	y_{10}	$y_{12}+y_{10}$	,,	,,	,,
—	—	,,	—	—	y_{11}	y_{11}	,,	,,	,,
Algebraic sum of products							Algebraic sum of products		
Denominators							Denominators		
a_{55}	a_{35}	a_{15}					a_{05}	a_{25}	a_{45}

Valid for 21 observations for the fifth degree polynomial.

MODEL FORM 3(a)

Transformation to $x''(=xd)$

b_{0p}	b_{1p}	b_{2p}	b_{3p}	b_{4p}	b_{5p} ↑
a_{0p}	$\frac{a_{1p}}{d}$	$\frac{a_{2p}}{d^2}$	$\frac{a_{3p}}{d^3}$	$\frac{a_{4p}}{d^4}$	$\frac{a_{5p}}{d^5}$

MODEL FORM 3(b)

Transformation to $x' \; (=x''+m)$

b_5	$-5mb_5$	$+10m^2b_5$	$-10m^3b_5$	$+5m^4b_5$	$-m^5b_5$
	b_4	$-4mb_4$	$+6m^2b_4$	$-4m^3b_4$	$+m^4b_4$
		b_3	$-3mb_3$	$+3m^2b_3$	$-m^3b_3$
			b_2	$-2mb_2$	$+m^2b_2$
				b_1	$-mb_1$
					b_0
c_5	c_4	c_3	c_2	c_1	c_0

The suffix denoting the degree of the polynomial is left out in $c_{\sigma p}$ and is written c_σ valid for a polynomial of degree 5.

Omit the first row and the first column for a polynomial of degree 4. Similar modifications may be introduced for polynomials of still lower degrees.

MODEL FORM 2(a) *n is odd*

x_i	Δ^5	Δ^4	Δ^3	Δ^2	Δ	$y_{calc.}$	$y_{obs.}$	$y_{calc.}-y_{obs.}$
$\frac{n-1}{2}$								
1		↑	↑	↑	↑	↑	↑	↑
	$120a_5$		$30a_5+12a_4+6a_3$		$a_5+a_4+a_3+a_2+a_1$			
0		$24a_4$		$2a_4+2a_2$		a_0	$\frac{y_{n+1}}{2}$	$\frac{y_{n+1}}{2}-a_0$
			↓		↓	↓	↓	↓
−1		↓		↓				
$\frac{1-n}{2}$								

MODEL FORM 2(b) *n is even*

x_i	Δ^5	Δ^4	Δ^3	Δ^2	Δ	$y_{calc.}$	$y_{obs.}$	$y_{calc.}-y_{obs.}$
$\frac{n-1}{2}$								
$\frac{3}{2}$		↑		↑		↑	↑	↑
			↑		↑			
$\frac{1}{2}$		$60a_5+24a_4$		$\frac{15}{2}a_5+5a_4+3a_3+2a_2$		$\frac{a_5}{32}+\frac{a_4}{16}+\frac{a_3}{8}+\frac{a_2}{4}+\frac{a_1}{2}+a_0$	$\frac{y_{n+2}}{2}$	$\frac{y_{n+2}}{2}-\left(\frac{a_5}{32}+\frac{a_4}{16}+\frac{a_3}{8}+\frac{a_2}{4}+\frac{a_1}{2}+a_0\right)$
	$120a_5$		$15a_5+6a_3$		$\frac{a_5}{16}+\frac{a_3}{4}+a_1$			
$-\frac{1}{2}$			↓	↓	↓	↓	↓	↓
		↓						
$\frac{1-n}{2}$								

a_σ is written for $a_{\sigma p}$ in the expressions for the central differences. The tables are valid for fifth degree polynomials, but by omitting the column or columns containing the higher differences, the tables can be modified for lower degree polynomials.

$n=1$

	y_1	Denominator
a_{00}	1	1

$n=2$

	y_1+y_2	Denominator	
a_0	1	2	a_{01}

$n=3$

	y_3+y_1	y_2	Denominator	
a_{00}	1	1	3	a_{01}
a_{02}	0	1	1	—
a_{22}	1	-2	2	—

$n=4$

	y_4+y_1	y_3+y_2	Denominator	
a_{00}	1	1	4	a_{01}
a_{02}	-1	9	16	a_{03}
a_{22}	1	-1	4	a_{23}

	y_2-y_1	Denominator
a_{11}	1	1

	y_3-y_1	Denominator	
a_{11}	1	2	a_{12}

	y_4-y_1	y_3-y_2	Denominator	
a_{11}	3	1	10	a_{12}
a_{13}	-1	27	24	—
a_{33}	1	-3	6	—

$n=5$

	y_5+y_1	y_4+y_2	y_3	Denominator	
a_{00}	1	1	1	5	a_{01}
a_{02}	−3	12	17	35	a_{03}
a_{22}	2	−1	−2	14	a_{23}
a_{04}	0	0	1	1	—
a_{24}	−1	16	−30	24	—
a_{44}	1	−4	6	24	—

	y_5-y_1	y_4-y_2	Denominator	
a_{11}	2	1	10	a_{12}
a_{13}	−1	8	12	a_{14}
a_{33}	1	−2	12	a_{34}

$n=6$

	y_6+y_1	y_5+y_2	y_4+y_3	Denominator	
a_{00}	1	1	1	6	a_{01}
a_{02}	−3	7	12	32	a_{03}
a_{22}	[illegible]	−1	−4	56	a_{23}
a_{04}	3	−25	150	256	a_{05}
a_{24}	−5	39	−34	96	a_{25}
a_{44}	1	−3	2	48	a_{45}

	y_6-y_1	y_5-y_2	y_4-y_3	Denominator	
a_{11}	5	3	1	35	a_{12}
a_{13}	−275	1249	652	3024	a_{14}
a_{33}	5	−7	−4	108	a_{34}
a_{15}	9	−125	2250	1920	—
a_{35}	−1	13	−34	48	—
a_{55}	1	−5	10	120	—

$n=7$

	y_7+y_1	y_6+y_2	y_5+y_3	y_4	Denominator	
a_{00}	1	1	1	1	7	a_{01}
a_{02}	−2	3	6	7	21	a_{03}
a_{22}	5	0	−3	−4	84	a_{23}
a_{04}	5	−30	75	131	231	a_{05}
a_{24}	−13	67	−10	−70	264	a_{25}
a_{44}	−3	−7	1	6	264	a_{45}

	y_7-y_1	y_6+y_2	y_5-y_3	Denominator	
a_{11}	3	2	1	28	a_{12}
a_{13}	−22	67	58	252	a_{14}
a_{33}	1	−1	−1	36	a_{34}
a_{15}	1	−9	45	60	—
a_{35}	−1	8	−13	48	—
a_{55}	1	−4	5	240	—

$n=8$

	y_8+y_1	y_7+y_2	y_6+y_3	y_5+y_4	Denominator	
a_{00}	1	1	1	1	8	a_{01}
a_{02}	−3	3	7	9	32	a_{03}
a_{22}	7	1	−3	−5	168	a_{23}
a_{04}	15	−69	85	225	512	a_{05}
a_{24}	−91	345	39	−293	2112	a_{25}
a_{44}	7	−13	−3	9	1056	a_{45}

$n=9$

	y_9+y_1	y_8+y_2	y_7+y_3	y_6+y_4	y_5	Denominator	
a_{00}	1	1	1	1	1	9	a_{01}
a_{02}	−21	14	39	54	59	231	a_{03}
a_{22}	28	7	−8	−17	−20	924	a_{23}
a_{04}	15	−55	30	135	179	429	a_{05}
a_{24}	−126	371	151	−211	−370	3432	a_{25}
a_{44}	14	−21	−11	9	18	3432	a_{45}

	y_8-y_1	y_7-y_2	y_6-y_3	y_5-y_4	Denominator	
a_{11}	7	5	3	1	84	a_{12}
a_{13}	−889	1955	2209	909	11088	a_{14}
a_{33}	7	−5	−7	−3	396	a_{34}
a_{15}	13573	−92437	249283	168445	549120	—
a_{35}	−245	1429	−1427	−1149	13728	—
a_{55}	7	−23	17	15	3120	—

	y_9-y_1	y_8-y_2	y_7-y_3	y_6-y_4	Denominator	
a_{11}	4	3	2	1	60	a_{12}
a_{13}	−86	142	193	126	1188	a_{14}
a_{33}	14	−7	−13	−9	1188	a_{34}
a_{15}	254	−1381	2269	2879	8580	—
a_{35}	−100	457	−256	−459	6864	—
a_{55}	4	−11	4	9	3120	—

$n = 10$

	$y_{10}+y_1$	y_9+y_2	y_8+y_3	y_7+y_4	y_6+y_5	Denominator	
a_{00}	1	1	1	1	1	10	a_{01}
a_{02}	−14	6	21	31	36	160	a_{03}
a_{22}	6	2	−1	−3	−4	264	a_{23}
a_{04}	10	−30	3	55	90	256	a_{05}
a_{24}	−426	1006	645	−279	−946	13728	a_{25}
a_{44}	18	−22	−17	3	18	6864	a_{45}

	$y_{10}-y_1$	y_9-y_2	y_8-y_3	y_7-y_4	y_6-y_5	Denominator	
a_{11}	9	7	5	3	1	165	a_{12}
a_{13}	−1338	1694	2675	2191	828	20592	a_{14}
a_{33}	42	−14	−35	−31	−12	5148	a_{34}
a_{15}	44274	−198506	200579	390769	188674	1372800	—
a_{35}	−402	1498	−347	−1457	−762	34320	—
a_{55}	6	−14	1	11	6	7800	—

$n = 11$

	$y_{11}+y_1$	$y_{10}+y_2$	y_9+y_3	y_8+y_4	y_7+y_5	y_6	Denominator	
a_{00}	1	1	1	1	1	1	11	a_{01}
a_{02}	−36	9	44	69	84	89	429	a_{03}
a_{22}	15	6	−1	−6	−9	−10	858	a_{23}
a_{04}	18	−45	−10	60	120	143	429	a_{05}
a_{24}	−90	174	146	1	−136	−190	3432	a_{25}
a_{44}	6	−6	−6	−1	4	6	3432	a_{45}

	$y_{11}-y_1$	$y_{10}-y_2$	y_9-y_3	y_8-y_4	y_7-y_5	Denominator	
a_{11}	5	4	3	2	1	110	a_{12}
a_{13}	−300	294	532	503	296	5148	a_{14}
a_{33}	30	−6	−22	−23	−14	5148	a_{34}
a_{15}	573	−2166	1249	3774	3084	17160	—
a_{35}	−129	402	11	−340	−316	13728	—
a_{55}	3	−6	−1	4	4	6240	—

$n=12$

	$y_{12}+y_1$	$y_{11}+y_2$	$y_{10}+y_3$	y_9+y_4	y_8+y_5	y_7+y_6	Denominator	
a_{00}	1	1	1	1	1	1	12	a_{01}
a_{02}	−9	1	9	15	19	21	112	a_{03}
a_{22}	55	25	1	−17	−29	−35	4004	a_{23}
a_{04}	45	−95	−45	87	220	300	1024	a_{05}
a_{24}	−1221	1959	1989	545	−1116	−2156	54912	a_{25}
a_{44}	33	−27	−33	−13	12	28	27456	a_{45}

	$y_{12}-y_1$	$y_{11}-y_2$	$y_{10}-y_3$	y_9-y_4	y_8-y_5	y_7-y_6	Denominator	
a_{11}	11	9	7	5	3	1	286	a_{12}
a_{13}	−1617	1227	2541	2665	1939	703	30888	a_{14}
a_{33}	33	−3	−21	−25	−19	−7	7722	a_{34}
a_{15}	626307	−2028363	515361	3020151	3310276	1396860	18670080	—
a_{35}	−3531	9363	2247	−6367	−8516	−3772	466752	—
a_{55}	33	−57	−21	29	41	20	106080	—

$n=13$

	$y_{13}+y_1$	$y_{12}+y_2$	$y_{11}+y_3$	$y_{10}+y_4$	y_9+y_5	y_8+y_6	y_7	Denominator	
a_{00}	1	1	1	1	1	1	1	13	a_{01}
a_{02}	−11	0	9	16	21	24	25	143	a_{03}
a_{22}	22	11	2	−5	−10	−13	−14	2002	a_{23}
a_{04}	110	−198	−135	110	390	600	677	2431	a_{05}
a_{24}	−2211	2970	3504	1614	−971	−016	−3780	116688	a_{25}
a_{44}	99	−66	−76	−54	11	64	84	116688	a_{45}

	$y_{13}-y_1$	$y_{12}-y_2$	$y_{11}-y_3$	$y_{10}-y_4$	y_8-y_5	y_8-y_6	Denominator	
a_{11}	6	5	4	3	2	1	182	a_{12}
a_{13}	−1133	660	1578	1796	1489	832	24024	a_{14}
a_{33}	11	0	−6	−8	−7	−4	3432	a_{34}
a_{15}	9647	−27093	12	33511	45741	31380	291720	—
a_{35}	−1430	3267	1374	−1633	−3050	−2252	233376	—
a_{55}	22	−33	−18	11	26	20	106080	—

$n = 14$

	$y_{14}+y_1$	$y_{13}+y_2$	$y_{12}+y_3$	$y_{11}+y_4$	$y_{10}+y_5$	y_9+y_6	y_8+y_7	Denominator	
a_{00}	1	1	1	1	1	1	1	14	a_{01}
a_{02}	−33	−3	22	42	57	67	72	448	a_{03}
a_{22}	13	7	2	−2	−5	−7	−8	1456	a_{23}
a_{04}	165	−255	−210	60	417	725	900	3584	a_{05}
a_{24}	−7579	8560	11484	6916	−535	−7419	−11436	466752	a_{25}
a_{44}	143	−77	−132	−92	−13	63	108	233376	a_{45}

	$y_{14}-y_1$	$y_{13}-y_2$	$y_{12}-y_3$	$y_{11}-y_4$	$y_{10}-y_5$	y_9-y_6	y_8-y_7	Denominator	
a_{11}	13	11	9	7	5	3	1	455	a_{12}
e_{13}	−69641	30547	85998	104846	95225	65260	23112	1633632	a_{14}
a_{33}	143	11	−66	−98	−95	−67	−24	58344	a_{34}
a_{15}	5711277	−14039553	−2914428	13082052	23239761	20544275	8078100	177365760	—
a_{35}	−22165	44033	25476	−13916	−39329	−38587	−15684	1434144	—
a_{55}	143	−187	−132	28	139	115	60	1007760	—

$n = 15$

	$y_{15}+y_1$	$y_{14}+y_2$	$y_{13}+y_3$	$y_{12}+y_4$	$y_{11}+y_5$	$y_{10}+y_6$	y_9+y_7	y_8	Denominator	
a_{00}	1	1	1	1	1	1	1	1	15	a_{01}
a_{02}	−78	−13	42	87	122	147	162	167	1105	a_{03}
a_{22}	91	52	19	−8	−29	−44	−53	−56	12376	a_{23}
a_{04}	2145	−2860	−2937	−165	3755	7500	10125	11063	46189	a_{05}
a_{24}	−31031	29601	44495	31856	6579	−19751	−38859	−45780	2217072	a_{25}
a_{44}	1001	−429	−869	−704	−249	251	621	756	2217072	a_{45}

	$y_{15}-y_1$	$y_{14}-y_2$	$y_{13}-y_3$	$y_{12}-y_4$	$y_{11}-y_5$	$y_{10}-y_6$	y_9-y_7	Denominator	
a_{11}	7	6	5	4	3	2	1	280	a_{12}
a_{13}	−12922	4121	14150	18334	17842	13843	7506	334152	a_{14}
a_{33}	91	13	−35	−58	−61	−49	−27	47736	a_{34}
a_{15}	78351	−169819	−65229	130506	266401	279975	175425	2519400	—
a_{35}	−8281	14404	10379	−1916	−11671	−14180	−9315	2015520	—
a_{55}	1001	−1144	−979	−44	751	1000	675	10077600	—

$n=19$

	$y_{19}+y_1$	$y_{18}+y_2$	$y_{17}+y_3$	$y_{16}+y_4$	$y_{15}+y_5$	$y_{14}+y_6$	$y_{13}+y_7$	$y_{12}+y_8$	$y_{11}+y_9$	y_{10}	Denominator	
a_{00}	1	1	1	1	1	1	1	1	1	1	19	a_{01}
a_{02}	−136	−51	24	89	144	189	224	249	264	209	2261	a_{03}
a_{22}	51	34	19	6	−5	−14	−21	−26	−29	−30	13566	a_{23}
a_{04}	340	−255	−420	−290	18	405	790	1110	1320	1393	7429	a_{05}
a_{24}	−32028	15028	35148	36357	25610	8792	−9282	−24867	−35288	−38940	3922512	a_{25}
a_{44}	612	−68	−388	−453	−354	−168	42	227	352	396	3922512	a_{15}

	$y_{19}-y_1$	$y_{18}-y_2$	$y_{17}-y_3$	$y_{16}-y_4$	$y_{15}-y_5$	$y_{14}-y_6$	$y_{13}-y_7$	$y_{12}-y_8$	$y_{11}-y_9$	Denominator	
a_{11}	9	8	7	6	5	4	3	2	1	570	a_{12}
a_{13}	−6936	−68	4648	7481	8700	8574	7372	5363	2816	255816	a_{14}
a_{33}	204	68	−28	−89	−120	−126	−112	−83	−44	255816	a_{34}
a_{15}	255102	−349928	−322378	−9473	348823	604481	680099	583549	332684	9806280	—
a_{35}	−15810	16796	20342	9818	−4329	−15546	−20525	−18554	−10368	7845024	—
a_{55}	102	−68	−98	−38	3	54	79	74	44	3505920	—

$n = 20$

	$y_{20}+y_1$	$y_{19}+y_2$	$y_{18}+y_3$	$y_{17}+y_4$	$y_{16}+y_5$	$y_{15}+y_6$	$y_{14}+y_7$	$y_{13}+y_8$	$y_{12}+y_9$	$y_{11}+y_{10}$	Denominator	
a_{00}	1	1	1	1	1	1	1	1	1	1	20	a_{01}
a_{02}	−153	−63	17	87	147	197	237	267	287	297	2640	a_{03}
a_{22}	57	39	23	9	−3	−13	−21	−27	−31	−33	17556	a_{23}
a_{04}	1530	−990	−1802	−1410	−255	2285	2895	4323	5380	5940	33792	a_{05}
a_{24}	−226746	87006	231370	253826	195919	93259	−24179	−133555	−216064	−260436	31380096	a_{25}
a_{44}	1938	−102	−1122	−1402	−1187	−687	−77	503	948	1188	15690048	a_{35}

	$y_{20}-y_1$	$y_{19}-y_2$	$y_{18}-y_3$	$y_{17}-y_4$	$y_{16}-y_5$	$y_{15}-y_6$	$y_{14}-y_7$	$y_{13}-y_8$	$y_{12}-y_9$	$y_{11}-y_{10}$	Denominator	
a_{11}	19	17	15	13	11	9	7	5	3	1	1330	a_{12}
a_{13}	−1030047	−69819	606475	1032239	1240877	1265793	1140391	898075	572249	196317	41186376	a_{14}
a_{33}	969	357	−85	−377	−539	−591	−553	−445	−287	−99	1470942	a_{34}
a_{15}	388722102	−478825638	−495267358	−99299538	397343727	792062409	978962229	922926339	651687004	234397284	15690048000	—
a_{35}	−672486	634134	842894	486434	−53911	−527937	−796397	−810827	−593372	−216612	392251200	—
a_{55}	1938	−1122	−1802	−1222	−187	771	1351	1441	1076	396	89148000	—

$n=21$

	$y_{21}+y_1$	$y_{20}+y_2$	$y_{19}+y_3$	$y_{18}+y_4$	$y_{17}+y_5$	$y_{16}+y_6$	$y_{15}+y_7$	$y_{14}+y_8$	$y_{13}+y_9$	$y_{12}+y_{10}$	y_{11}	Denominator	
a_{00}	1	1	1	1	1	1	1	1	1	1	1	21	a_{01}
a_{02}	−171	−76	9	84	149	204	249	284	309	324	329	3059	a_{03}
a_{22}	190	133	82	37	−2	−35	−62	−83	−98	−107	−110	67298	a_{23}
a_{04}	11628	−6460	−13005	−11220	−3940	6378	17655	28190	36660	42120	44003	260015	a_{05}
a_{24}	−12597	3876	11934	13804	11451	6578	626	−5226	−10061	−13224	−14322	1961256	a_{25}
a_{44}	969	0	−510	−680	−615	−406	−130	150	385	540	594	9806280	a_{45}

	$y_{21}-y_1$	$y_{20}-y_2$	$y_{19}-y_3$	$y_{18}-y_4$	$y_{17}-y_5$	$y_{16}-y_6$	$y_{15}-y_7$	$y_{14}-y_8$	$y_{13}-y_9$	$y_{12}-y_{10}$	Denominator	
a_{11}	10	9	8	7	6	5	4	3	2	1	770	a_{12}
a_{13}	−84075	−10032	43284	78176	96947	101900	95338	79564	56881	29592	3634092	a_{14}
a_{33}	285	114	−12	−98	−149	−170	−166	−142	−103	−54	519156	a_{34}
a_{15}	15033066	−16649358	−19052988	−6402438	10949042	26040033	34807914	35613829	28754154	15977364	637408200	—
a_{35}	−748068	625974	908004	598094	62644	−448909	−787382	−887137	−749372	−425412	509926560	—
a_{55}	3876	−1938	−3468	−2618	−788	1063	2354	2819	2444	1404	231784800	—

$n=22$

	$y_{22}+y_1$	$y_{21}+y_2$	$y_{20}+y_3$	$y_{19}+y_4$	$y_{18}+y_5$	$y_{17}+y_6$	$y_{16}+y_7$	$y_{15}+y_8$	$y_{14}+y_9$	$y_{13}+y_{10}$	$y_{12}+y_{11}$	Denominator	
a_{00}	1	1	1	1	1	1	1	1	1	1	1	22	a_{01}
a_{02}	−19	−9	0	8	15	21	26	30	33	35	36	352	a_{03}
a_{22}	35	25	16	8	1	−5	−10	−14	−17	−19	−20	14168	a_{23}
a_{04}	1615	−765	−1710	−1598	−765	495	1930	3330	4527	5395	5850	36608	a_{05}
a_{24}	−171969	41211	151050	183450	161435	105151	31866	−44030	−111025	−160485	−186654	29995680	a_{25}
a_{44}	1197	57	−570	−810	−775	−563	−258	70	365	585	702	14997840	a_{45}

	$y_{22}-y_1$	$y_{21}-y_2$	$y_{20}-y_3$	$y_{19}-y_4$	$y_{18}-y_5$	$y_{17}-y_6$	$y_{16}-y_7$	$y_{15}-y_8$	$y_{14}-y_9$	$y_{13}-y_{10}$	$y_{12}-y_{11}$	Denominator	
a_{11}	21	19	17	15	13	11	9	7	5	3	1	1771	a_{12}
a_{13}	−173299	−28671	77520	149320	190775	205931	198834	173530	134065	84485	28836	8075760	a_{14}
a_{33}	133	57	0	−40	−65	−77	−78	−70	−55	−35	−12	288420	a_{34}
a_{15}	686844319	−684364971	−857795622	−383761162	328835403	995865057	1441336242	1580758326	1404505071	961178101	340970370	30595593600	—
a_{35}	−965447	716091	1129854	825554	214149	−415833	−881970	−1091622	−1025607	−721877	−259194	764889840	—
a_{55}	2261	−969	−1938	−1598	−663	363	1158	1554	1509	1079	390	173838600	—

$n=23$

	$y_{23}+y_1$	$y_{22}+y_2$	$y_{21}+y_3$	$y_{20}+y_4$	$y_{19}+y_5$	$y_{18}+y_6$	$y_{17}+y_7$	$y_{16}+y_8$	$y_{15}+y_9$	$y_{14}+y_{10}$	$y_{13}+y_{11}$	y_{12}	Denominator	
a_{00}	1	1	1	1	1	1	1	1	1	1	1	1	23	a_{01}
a_{02}	−42	−21	−2	15	30	43	54	63	70	75	78	79	805	a_{03}
a_{22}	77	56	37	20	5	−8	−19	−28	−35	−40	−43	−44	35420	a_{23}
a_{04}	95	−38	−95	−95	−55	10	87	165	235	290	325	337	2185	a_{05}
a_{24}	−115577	20615	93993	119510	110545	78903	34815	−13062	−57645	−93425	−116467	−124410	22496760	a_{25}
a_{44}	1463	133	−627	−950	−955	−747	−417	−42	315	605	793	858	22496760	a_{45}

	$y_{23}-y_1$	$y_{22}-y_2$	$y_{21}-y_3$	$y_{20}-y_4$	$y_{19}-y_5$	$y_{18}-y_6$	$y_{17}-y_7$	$y_{16}-y_8$	$y_{15}-y_9$	$y_{14}-y_{10}$	$y_{13}-y_{11}$	Denominator	
a_{11}	11	10	9	8	7	6	5	4	3	2	1	1012	a_{12}
a_{13}	−3938	−815	1518	3140	4130	4567	4530	4098	3350	2365	1222	197340	a_{14}
a_{33}	77	35	3	−20	−35	−43	−45	−42	−35	−25	−13	197340	a_{34}
a_{15}	400653	−359157	−489687	−265164	106911	478349	752859	878634	840937	654687	357045	18747300	—
a_{35}	−49115	32224	55233	43928	16583	−13632	−38013	−51684	−52959	−42704	−23699	44993520	—
a_{55}	209	−76	−171	−152	−77	12	87	132	141	116	65	20451600	—

$n=24$

	$y_{24}+y_1$	$y_{23}+y_2$	$y_{22}+y_3$	$y_{21}+y_4$	$y_{20}+y_5$	$y_{19}+y_6$	$y_{18}+y_7$	$y_{17}+y_8$	$y_{16}+y_9$	$y_{15}+y_{10}$	$y_{14}+y_{11}$	$y_{13}+y_{12}$	Denominator	
a_{00}	1	1	1	1	1	1	1	1	1	1	1	1	24	a_{01}
a_{02}	−231	−121	−21	69	149	219	279	329	369	399	419	429	4576	a_{03}
a_{22}	253	187	127	73	25	−17	−53	−83	−107	−125	−137	−143	131560	a_{23}
a_{04}	3135	−1045	−2955	−3135	−2071	−195	2115	4535	6795	8679	10025	10725	73216	a_{05}
a_{24}	−43769	5379	32909	43721	42225	32341	17499	639	−15789	−29825	−39999	−45331	9472320	a_{25}
a_{44}	253	33	−97	−157	−165	−137	−87	−27	33	85	123	143	4736160	a_{45}

	$y_{24}-y_1$	$y_{23}-y_2$	$y_{22}-y_3$	$y_{21}-y_4$	$y_{20}-y_5$	$y_{19}-y_6$	$y_{18}-y_7$	$y_{17}-y_8$	$y_{16}-y_9$	$y_{15}-y_{10}$	$y_{14}-y_{11}$	$y_{13}-y_{12}$	Denominator	
a_{11}	23	21	19	17	15	13	11	9	7	5	3	1	2300	a_{12}
a_{13}	−396451	−96943	130283	292111	395425	447109	454047	423123	361221	275225	172019	58487	21312720	a_{14}
a_{33}	1771	847	133	−391	−745	−949	−1023	−987	−861	−665	−419	−143	5328180	a_{34}
a_{15}	2124400773	−1712322097	−2529019597	−1574705427	184892071	2016887349	3585776189	4373998139	4451455449	3795112407	2538493775	891256225	104384966400	—
a_{35}	−2475605	1432277	2668189	2279411	1075381	−347269	−1579677	−2375715	−2626953	−2337623	−1599583	−567281	2609624160	—
a_{55}	4807	−1463	−3743	−3553	−2071	−169	1551	2721	3171	2893	2005	715	593096400	—

$n=25$

	$y_{25}+y_1$	$y_{24}+y_2$	$y_{23}+y_3$	$y_{22}+y_4$	$y_{21}+y_5$	$y_{20}+y_6$	$y_{19}+y_7$	$y_{18}+y_8$	$y_{17}+y_9$	$y_{16}+y_{10}$	$y_{15}+y_{11}$	$y_{14}+y_{12}$	y_{13}	Denominator	
a_{00}	1	1	1	1	1	1	1	1	1	1	1	1	1	25	a_{01}
a_{02}	−253	−138	−33	62	147	222	287	342	387	422	447	462	467	5175	a_{03}
a_{22}	92	69	48	29	12	−3	−16	−27	−36	−43	−48	−51	−52	53820	a_{23}
a_{04}	1265	−345	−1122	−1255	−915	−255	590	1503	2385	3155	3750	4125	4253	30015	a_{05}
a_{24}	−143198	10373	99385	137803	138262	112067	69193	18285	−33342	−79703	−116143	−139337	−147290	34337160	a_{25}
a_{44}	1518	253	−517	−897	−982	−857	−597	−267	78	393	643	803	858	34337160	a_{45}

	$y_{25}-y_1$	$y_{24}-y_2$	$y_{23}-y_3$	$y_{22}-y_4$	$y_{21}-y_5$	$y_{20}-y_6$	$y_{19}-y_7$	$y_{18}-y_8$	$y_{17}-y_9$	$y_{16}-y_{10}$	$y_{15}-y_{11}$	$y_{14}-y_{12}$	Denominator	
a_{11}	12	11	10	9	8	7	6	5	4	3	2	1	1300	a_{12}
a_{13}	−30866	−8602	8525	20982	29236	33754	35003	33450	29562	23806	16649	8558	1776060	a_{14}
a_{33}	506	253	55	−93	−196	−259	−287	−285	−258	−211	−149	−77	1776060	a_{34}
a_{15}	8322182	−6024183	−9604353	−6671883	−544668	6301491	12139321	15896511	17062146	15593141	11820675	6356625	429214500	–
a_{35}	−284372	144463	293128	266403	146408	−5131	−144616	−244311	−290076	−279101	−217640	−118745	343371600	–
a_{55}	1012	−253	−748	−753	−488	−119	236	501	636	631	500	275	156078000	–

$n=26$

	$y_{26}+y_1$	$y_{25}+y_2$	$y_{24}+y_3$	$y_{23}+y_4$	$y_{22}+y_5$	$y_{21}+y_6$	$y_{20}+y_7$	$y_{19}+y_8$	$y_{18}+y_9$	$y_{17}+y_{10}$	$y_{16}+y_{11}$	$y_{15}+y_{12}$	$y_{14}+y_{13}$	Denominator	
a_{00}	1	1	1	1	1	1	1	1	1	1	1	1	1	26	a_{01}
a_{02}	−138	−78	−23	27	72	112	147	177	202	222	237	247	252	2912	a_{03}
a_{22}	50	38	27	17	8	0	−7	−13	−18	−22	−25	−27	−28	32760	a_{23}
a_{04}	1518	−330	−1265	−1485	−1170	−482	435	1455	2470	3390	4143	4675	4950	36608	a_{05}
a_{24}	−518650	13662	331683	479743	498142	423150	287007	117923	−59922	−226378	−365325	−464673	−516362	137348640	a_{25}
a_{44}	2530	506	−759	−1419	−1614	−1470	−1099	−599	−54	466	905	1221	1386	68674320	a_{45}

	$y_{26}-y_1$	$y_{25}-y_2$	$y_{24}-y_3$	$y_{23}-y_4$	$y_{22}-y_5$	$y_{21}-y_6$	$y_{20}-y_7$	$y_{19}-y_8$	$y_{18}-y_9$	$y_{17}-y_{10}$	$y_{16}-y_{11}$	$y_{15}-y_{12}$	$y_{14}-y_{13}$	Denominator	
a_{11}	25	23	21	19	17	15	13	11	9	7	5	3	1	2925	a_{12}
a_{13}	−304750	−94438	69391	190779	273768	322400	340717	332761	302574	254198	191675	119047	40356	18729360	a_{14}
a_{33}	1150	598	161	−171	−408	−560	−637	−649	−606	−518	−395	−247	−84	4682340	a_{34}
a_{15}	−143088770	−92843591	−159650659	−121174600	−27852494	82001662	180920753	251008183	282663258	273302078	226084429	148636175	51773150	7741168800	—
a_{35}	−140530	62330	138299	132753	81702	12682	−54353	−106139	−135210	−139006	−118981	−79711	−28002	193536720	—
a_{55}	2530	−506	−1771	−1881	−1326	−482	377	1067	1482	1582	1381	935	330	483841800	—

$n=27$

	$y_{27}+y_1$	$y_{26}+y_2$	$y_{25}+y_3$	$y_{24}+y_4$	$y_{23}+y_5$	$y_{22}+y_6$	$y_{21}+y_7$	$y_{20}+y_8$	$y_{19}+y_9$	$y_{18}+y_{10}$	$y_{17}+y_{11}$	$y_{16}+y_{12}$	$y_{15}+y_{13}$	y_{14}	Denominator	
a_{00}	1	1	1	1	1	1	1	1	1	1	1	1	1	1	27	a_{01}
a_{02}	−60	−35	−12	9	28	45	60	73	84	93	100	105	108	109	1305	a_{03}
a_{22}	325	250	181	118	61	10	−35	−74	−107	−134	−155	−170	−179	−182	237510	a_{23}
a_{04}	37950	−6325	−29670	−36432	−30580	−15705	4980	28640	52818	75435	94790	109560	118800	121943	930465	a_{05}
a_{24}	−331890	−5290	195178	294515	315548	278930	203140	104483	−2910	−107082	−198250	−268805	−313312	−328510	96768360	a_{25}
a_{44}	2990	690	−782	−1587	−1872	−1770	−1400	−867	−262	338	870	1285	1548	1638	96768360	a_{45}

	$y_{27}-y_1$	$y_{26}-y_2$	$y_{25}-y_3$	$y_{24}-y_4$	$y_{23}-y_5$	$y_{22}-y_6$	$y_{21}-y_7$	$y_{20}-y_8$	$y_{19}-y_9$	$y_{18}-y_{10}$	$y_{17}-y_{11}$	$y_{16}-y_{12}$	$y_{15}-y_{13}$	Denominator	
a_{11}	13	12	11	10	9	8	7	6	5	4	3	2	1	1638	a_{12}
a_{13}	65260	22090	−11924	−37545	−55536	−66660	−71680	−71359	−66460	−57746	−45980	−31925	−16344	4275180	a_{14}
a_{33}	130	70	22	−15	−42	−60	−70	−73	−70	−62	−50	−35	−18	610740	a_{34}
a_{15}	17059445	−9897130	−18358439	−15007684	−5186694	6982132	18473882	27239188	32082283	32539058	28755119	21363844	11364440	967683600	—
a_{35}	−494845	190210	464255	468096	314742	91932	−135338	−322288	−441827	−482026	−443591	−337336	−181656	774146880	—
a_{55}	16445	−2530	−10879	−12144	−9174	−4188	1162	5728	8803	10058	9479	7304	3960	3870734400	—

$n=28$

	$y_{28}+y_1$	$y_{27}+y_2$	$y_{26}+y_3$	$y_{25}+y_4$	$y_{24}+y_5$	$y_{23}+y_6$	$y_{22}+y_7$	$y_{21}+y_8$	$y_{20}+y_9$	$y_{19}+y_{10}$	$y_{18}+y_{11}$	$y_{17}+y_{12}$	$y_{16}+y_{13}$	$y_{15}+y_{14}$	Denominator	
a_{00}	1	1	1	1	1	1	1	1	1	1	1	1	1	1	28	a_{01}
a_{02}	−65	−39	−15	7	27	45	61	75	87	97	105	111	115	117	1456	a_{03}
a_{22}	117	91	67	45	25	7	−9	−23	−35	−45	−53	−59	−63	−65	95004	a_{23}
a_{04}	7475	−897	−5475	−7015	−6210	−3690	−22	4290	8805	13145	16995	20103	22280	23400	186368	a_{05}
a_{24}	−420615	−23075	226935	357483	394298	360770	277950	164550	36943	−90837	−207095	−302475	−369960	−404872	134634240	a_{25}
a_{44}	1755	455	−395	−879	−1074	−1050	−870	−590	−259	81	395	655	840	936	67317120	a_{45}

	$y_{28}-y_1$	$y_{27}-y_2$	$y_{26}-y_3$	$y_{25}-y_4$	$y_{24}-y_5$	$y_{23}-y_6$	$y_{22}-y_7$	$y_{21}-y_8$	$y_{20}-y_9$	$y_{19}-y_{10}$	$y_{18}-y_{11}$	$y_{17}-y_{12}$	$y_{16}-y_{13}$	$y_{15}-y_{14}$	Denominator	
a_{11}	27	25	23	21	19	17	15	13	11	9	7	5	3	1	3654	a_{12}
a_{13}	−1267695	−462475	178595	668647	1020813	1248225	1364015	1381315	1313257	1172973	973595	728255	450085	152217	88353720	a_{14}
a_{33}	585	325	115	−49	−171	−255	−305	−325	−319	−291	−245	−185	−115	−39	3155490	a_{34}
a_{15}	1042076295	−538691655	−1079419555	−240534469	−413158154	274867322	952952762	1501735222	1847051393	1953910984	1820470099	1472004629	951883621	350542680	61931750400	—
a_{35}	−874575	288535	781195	823837	595194	235926	−147754	−480454	−713977	−823695	−804923	−669293	−141128	−153816	1548293760	—
a_{55}	13455	−1495	−8395	−9821	−7866	−4182	−22	3718	6457	7887	7931	6701	4456	1560	3870734400	—

$n = 29$

	$y_{29}+y_1$	$y_{28}+y_2$	$y_{27}+y_3$	$y_{26}+y_4$	$y_{25}+y_5$	$y_{24}+y_6$	$y_{23}+y_7$	$y_{22}+y_8$	$y_{21}+y_9$	$y_{20}+y_{10}$	$y_{19}+y_{11}$	$y_{18}+y_{12}$	$y_{17}+y_{13}$	$y_{16}+y_{14}$	y_{15}	Denominator	
a_{00}	1	1	1	1	1	1	1	1	1	1	1	1	1	1	1	29	a_{01}
a_{02}	−351	−216	−91	24	129	224	309	384	449	504	549	584	609	624	629	8091	a_{03}
a_{22}	126	99	74	51	30	11	−6	−21	−34	−45	−54	−61	−66	−69	−70	113274	a_{23}
a_{04}	17550	−1350	−12025	−16050	−14874	−9820	−2085	7260	17270	27126	36135	43730	49470	53040	54251	445005	a_{05}
a_{24}	−105651	−9594	52156	85874	97333	91804	74056	48356	18469	−12342	−41316	−66194	−85219	−97136	−101192	37024416	a_{25}
a_{44}	4095	1170	−780	−1930	−2441	−2460	−2120	−1540	−825	−66	660	1200	1775	2080	2184	185122080	a_{45}

	$y_{29}-y_1$	$y_{28}-y_2$	$y_{27}-y_3$	$y_{26}-y_4$	$y_{25}-y_5$	$y_{24}-y_6$	$y_{23}-y_7$	$y_{22}-y_8$	$y_{21}-y_9$	$y_{20}-y_{10}$	$y_{19}-y_{11}$	$y_{18}-y_{12}$	$y_{17}-y_{13}$	$y_{16}-y_{14}$	Denominator	
a_{11}	14	13	12	11	10	9	8	7	6	5	4	3	2	1	2030	a_{12}
a_{13}	477477	−185796	48646	230252	363425	452568	502084	516376	499847	456900	391938	309364	213581	108992	35341488	a_{14}
a_{33}	819	468	182	−44	−215	−336	−412	−448	−449	−420	−366	−292	−203	−104	5048784	a_{34}
a_{15}	11494665	−5271435	−11441560	−10543335	−5453373	1548474	8724864	14826714	19038949	20926251	20378808	17558063	12842463	6773208	715244400	—
a_{35}	−286650	80145	243490	267685	205354	98418	−20932	−129262	−210922	−257073	−264714	−235709	−175814	−93704	572195520	
a_{55}	8190	−585	−4810	−5885	−4958	−2946	−556	1694	3454	4521	4818	4373	3298	1768	2860977600	—

$n = 30$

	$y_{30}+y_1$	$y_{29}+y_2$	$y_{28}+y_3$	$y_{27}+y_4$	$y_{26}+y_5$	$y_{25}+y_6$	$y_{24}+y_7$	$y_{23}+y_8$	$y_{22}+y_9$	$y_{21}+y_{10}$	$y_{20}+y_{11}$	$y_{19}+y_{12}$	$y_{18}+y_{13}$	$y_{17}+y_{14}$	$y_{16}+y_{15}$	Denominator	
a_{00}	1	1	1	1	1	1	1	1	1	1	1	1	1	1	1	30	a_{01}
a_{02}	−189	−119	−54	6	61	111	156	196	231	261	286	306	321	331	336	4480	a_{03}
a_{22}	203	161	122	86	53	23	−4	−28	−49	−67	−82	−94	−103	−109	−112	201376	a_{23}
a_{04}	8775	−325	−5616	−7800	−7525	−5385	−1920	2384	7095	11835	16280	20160	23259	25415	26520	226304	a_{05}
a_{24}	−6579027	−816543	2962440	5107232	5940273	5757133	4826512	3390240	1663277	−166287	−1937232	−3515208	−4792735	−5689203	−6150872	2517660288	a_{25}
a_{44}	23751	7371	−3744	−10504	−13749	−14249	−12704	−9744	−5929	−1749	2376	6096	9131	11271	12376	1258830144	a_{45}

	$y_{30}-y_1$	$y_{29}-y_2$	$y_{28}-y_3$	$y_{27}-y_4$	$y_{26}-y_5$	$y_{25}-y_6$	$y_{24}-y_7$	$y_{23}-y_8$	$y_{22}-y_9$	$y_{21}-y_{10}$	$y_{20}-y_{11}$	$y_{19}-y_{12}$	$y_{18}-y_{13}$	$y_{17}-y_{14}$	$y_{16}-y_{15}$	Denominator	
a_{11}	29	27	25	23	21	19	17	15	13	11	9	7	5	3	1	4495	a_{12}
a_{13}	−653283	−268911	42750	287086	469483	595327	670004	698900	687401	640893	564762	464394	345175	212491	71728	51264576	a_{14}
a_{33}	1827	1071	450	−46	−427	−703	−884	−980	−1001	−957	−858	−714	−535	−331	−112	12816144	a_{34}
a_{15}	19336350735	−7823192715	−18469189440	−17891310840	−10440817765	394366641	11914584096	22133368336	29702372271	33836295141	34237809672	31022499232	24643734987	15817703057	5448231679	1258830144000	—
a_{35}	−14080055	3268895	11320920	12040720	10449845	5718487	241272	−5008448	−9160303	−11822613	−12768096	−12021576	−9775691	−6360601	−2204696	31470758600	—
a_{55}	16965	−585	−9360	−11960	−10535	−6821	−2176	2384	6149	8679	9768	9408	7753	5083	1768	7152444000	—

$n > 30$

$$\eta_0 = \left[(y_n + y_1) + (y_{n-1} + y_2) + \quad \ldots \right] \qquad a_{00} = \frac{1}{n}\eta_0 = a_{01}$$

$$\eta_1 = \left[\left(\frac{n-1}{2}\right)(y_n - y_1) + \left(\frac{n-3}{2}\right)(y_{n-1} - y_2) + \quad \ldots \right] \qquad a_{11} = \frac{12}{n(n^2-1)}\eta_1 = a_{12}$$

$$\eta_2 = \left[\left(\frac{n-1}{2}\right)^2 (y_n + y_1) + \left(\frac{n-3}{2}\right)^2 (y_{n-1} + y_2) + \quad \ldots \right] \qquad a_{02} = \frac{3(3n^2-7)}{4n(n^2-4)}\eta_0 - \frac{15}{n(n^2-4)}\eta_2 = a_{03}$$

$$\eta_3 = \left[\left(\frac{n-1}{2}\right)^3 (y_n - y_1) + \left(\frac{n-3}{2}\right)^3 (y_{n-1} - y_2) + \quad \ldots \right] \qquad a_{22} = \frac{-15}{n(n^2-4)}\eta_0 + \frac{180}{n(n^2-1)(n^2-4)}\eta_2 = a_{23}$$

$$\eta_4 = \left[\left(\frac{n-1}{2}\right)^4 (y_n + y_1) + \left(\frac{n-3}{2}\right)^4 (y_{n-1} + y_2) + \quad \ldots \right] \qquad a_{13} = \frac{25(3n^4 - 18n^2 + 31)}{n(n^2-1)(n^2-4)(n^2-9)}\eta_1 - \frac{140(3n^2-7)}{n(n^2-1)(n^2-4)(n^2-9)}\eta_3 = a_{14}$$

$$\eta_5 = \left[\left(\frac{n-1}{2}\right)^5 (y_n - y_1) + \left(\frac{n-3}{2}\right)^5 (y_{n-1} - y_2) + \quad \ldots \right] \qquad a_{33} = \frac{-140(3n^2-7)}{n(n^2-1)(n^2-4)(n^2-9)}\eta_1 + \frac{2800}{n(n^2-1)(n^2-4)(n^2-9)}\eta_3 = a_{34}$$

$$a_{04}=\frac{15(15n^4-230n^2+407)}{64n(n^2-4)(n^2-16)}\eta_0-\frac{525(n^2-7)}{8n(n^2-4)(n^2-16)}\eta_2-\frac{945}{4n(n^2-4)(n^2-16)}\eta_4=a_{05}$$

$$a_{24}=\frac{-525(n^2-7)}{8n(n^2-4)(n^2-16)}\eta_0+\frac{2205(n^4-10n^2+29)}{n(n^2-1)(n^2-4)(n^2-9)(n^2-16)}\eta_2-\frac{3150(3n^2-13)}{n(n^2-1)(n^2-4)(n^2-16)}\eta_4=a_{25}$$

$$a_{44}=\frac{945}{4n(n^2-4)(n^2-16)}\eta_0-\frac{3150(3n^2-13)}{n(n^2-1)(n^2-4)(n^2-9)(n^2-16)}\eta_2+\frac{44100}{n(n^2-1)(n^2-4)(n^2-9)(n^2-16)}\eta_4=a_{45}$$

$$a_{15}=\frac{147(25n^8-900n^6+10230n^4-37060n^2+46137)}{16n(n^2-1)(n^2-4)(n^2-9)(n^2-16)(n^2-25)}\eta_1-\frac{(3n^6-75n^4+541n^2-853)2205}{2n(n^2-1)(n^2-4)(n^2-9)(n^2-16)(n^2=25)}\eta_3$$
$$+\frac{693(15n^4-230n^2+407)}{n(n^2-1)(n^2-4)(n^2-9)(n^2-16)(n^2-25)}\eta_5$$

$$a_{35}=\frac{-2205(3n^6-75n^4+541n^2-853)}{2n(n^2-1)(n^2-4)(n^2-9)(n^2-16)(n^2-25)}\eta_1+\frac{18900(3n^4-46n^2+199)}{n(n^2-1)(n^2-4)(n^2-9)(n^2-16)(n^2-25)}\eta_3$$
$$-\frac{194040(n^2-7)}{n(n^2-1)(n^2-4)(n^2-9)(n^2-16)(n^2-25)}\eta_5$$

$$a_{55}=\frac{693(15n^4-230n^2+407)}{n(n^2-1)(n^2-4)(n^2-9)(n^2-16)(n^2-25)}\eta_1-\frac{194040(n^2-7)}{n(n^2-1)(n^2-4)(n^2-9)(n^2-16)(n^2-25)}\eta_3$$
$$+\frac{698544}{n(n^2-1)(n^2-4)(n^2-9)(n^2-16)(n^2-25)}\eta_5$$

DEPARTMENT OF MATHEMATICS,
MUSLIM UNIVERSITY,
ALIGARH.

REFERENCES

[1] Birge, R. T., and Shea, J. D., *Physical Review*, **24**, 206 (1924).

[2] Condon, E. U., *University of California Publications in Mathematics*, **2**, No. 4, 55-66 (1927).

[3] Bôcher, M., *Introduction to Higher Algebra*, 43 (1929).

[4] Nörlund, N. E., *Differenzenrechnung*, Chap. II (1924).

[5] von Sanden, H., *Praktische Analysis*, 44-45 (1923).

INVESTIGATION OF TELLURIUM AND ARSENIC SULPHIDE IN THE COLLOIDAL STATE*

By H. BOSE

(Received for publication, March 27, 1941)

Plate V

ABSTRACT. With a view to obtain informations regarding the nature of colloidal particles with special attention to their changes due to slow coagulation in ageing, the following samples of tellurium were examined by X-rays: (a) Coagulum by HNO_3 from a fresh tellurium sol, (b) Coagulum by HNO_3 from a heated sol, (c) Dried up gummy mass, (d) electrolytic precipitate from aged sol, (e) electrolytic precipitate from aged heated sol, (f) Thin film of tellurium that settles on the surface of the sol on allowing it to dry up in a basin. The coagulum from a freshly prepared tellurium sol by HNO_3 was found to be amorphous, while the diffraction pattern of the coagulum of aged sol (specially the pattern of the sample mentioned in (f)) gives scope for suspecting the existence of a new variety of tellurium in it.

Similar experiments with arsenic sulphide sol shows that the natural peptisable precipitate and the electrolytic precipitate (by HCl) from a fresh sol yield amorphous bands while that from heated sol or obtained by drying the sol gives crystalline pattern.

INTRODUCTION

A colloidal solution is a two-phase heterogenous system one of which, usually a solid, is dispersed in a finely divided state throughout the other phase, generally a liquid. The diameters of the dispersed particles are generally of the order of 10^{-5} to 10^{-7} cm.

Thus instead of a single molecule separately existing in a true solution in the colloidal state, we have a large number of aggregate of a few hundreds of thousands of molecules disseminated throughout a liquid medium. The essential difference between colloidal solution and true solution or coarse suspension is of degree only rather than that of kind and there can be no sharp line of demarcation between them. The most interesting fact about colloids is that the colloidal particles are all charged with similar electricity. Though there is much difference of opinion as to the origin of this charge, there is this unanimity that the particles in the colloidal solution are enclosed by an electric double layer.

On adding suitable electrolytes, neutralisation of the charge of the colloids by the oppositely charged ions of the added electrolytes takes place causing agglomeration of the particles.

---

* Communicated by the Indian Physical Society

The present investigation was undertaken to study the nature of coagulum obtained from the solution by different ways with a view to form an idea as to the nature and particle size of the substance in the colloidal state.

EXPERIMENTAL ARRANGEMENTS

As only identification, rather than structure analysis, was all that was necessary in the present investigation, only the powder method was resorted to throughout the experiment. The X-ray bulb was a demountable porcelain Hadding tube which was used directly in series with the high-tension transformer without any further rectifying device. Cu K-radiations were used all along the experiment. The tube was run at 35 to 40 K.V. with 5-7 m.a. The widely divergent radiations coming out of the window of the tube became almost parallel by its passage through a slit system, the final slit through which the X-ray emerged before impinging on the diffracting material, being .4 mm. in diameter. The slit system was made of detachable parts and there was provision for change of sample during the same exposure without in any way disturbing the setting. All photographs were taken in either of the two hemi-cylindrical cameras of radii 2.88 cm. and 2.06 cm.

A. TELLURIUM SOL

Like Selenium sol the colloidal solution of tellurium was prepared by reducing its oxide in aqueous solution by glucose in presence of ammonia though the difficulty arose because of tellurium dioxide being sparingly soluble in water.

0.71 gm. of TeO_2 was weighed and taken in a basin and a small quantity of conductivity water added ; equimolecular (0.8 gm. in this case) quantity of extra pure glucose was next added to it. The basin containing the resulting solution was then placed on a water bath. In about 5 minutes reduction began as can be seen by the change in colour. On addition of a drop of liquor ammonia, the frothing was noticed. Next at intervals of 1 minute, a drop of NH_4OH was added, keeping the solution well stirred all the while for 20—25 minutes. To maintain the solution always in the syrupy condition drops of water were added intermittently. The reddish black paste-like solution is then diluted to ten times its volume with cold conductivity water. The reddish black solution, so obtained, was thrice filtered through double filter paper and a stable colloidal solution of tellurium was obtained.

Properties of tellurium sol.—Unlike selenium sol a fraction of which settles down without any external application, Tellurium sol is very stable and does not produce any natural precipitate even on long standing (the sol has a slightly reddish tint).

A quantity of the tellurium sol was taken in a test tube and was boiled but no coagulation occurred even when the boiling was continued for an hour.

Suspensions of tellurium are anionic and show attraction to the +ve electrode, *i.e.*, they are charged with the -ve electricity. On adding a drop of HNO_3 (strong) precipitation starts but proceeds very slowly and cannot separate the two phases completly even in 2-3 hours whereas if HNO_3 be added in excess of what is necessary, coagulation does not take place at all but this latter solution can be used to precipitate fresh sample of tellurium sol. X-ray exposure was found to have no coagulating effect on the tellurium sol.

A solution of colloidal tellurium was allowed to evaporate at the room temperature. After a few days a dark red gummy mass of tellurium was observed. This gummy mass, when shaken with water, passes into colloidal state. This gummy state persists even after a long time and is never completely dried up even when it is placed in a dessicator.

X-RAY INVESTIGATION OF COLLOIDAL TELLURIUM

The tellurium content of the sol is so weak that the diffraction pattern of a colloidal solution of tellurium does not reveal the presence of tellurium particles in it.

The following samples were examined with X-rays :—

A. Forced precipitate by HNO_3 from freshly prepared sol.

B. Forced precipitate by HNO_3 from heated sol.

C. Dried-up gummy mass.

D. Forced precipitate from aged sol.

E. Forced precipitate of heated aged sol.

F. Thin film that settles over the concentrated sol obtained on allowing a fresh sol to dry up in a basin.

A. A cell was prepared on a zig-zag paper with the precipitate obtained by adding strong HNO_3 to the freshly prepared sol and the X-ray diffraction pattern shows only one sharp band (Plate V). The value of the spacing is 3·09 (A.U.). The hexagonal pattern consists of a prominent group of rings having spacings 2.86 (V.W.), 3.05 (V.V.S.), 3.39(W), in (A.U.).

B. The addition of HNO_3 to a heated sol brings about the precipitation much more easily and in a much shorter time than is required for unheated sol. The X-ray exposure yields a pattern consisting of a large number of sharp rings. The spacings and intensity distribution of these rings correspond exactly to those due to hexagonal tellurium (Plate V).

C. The gummy mass, when exposed to X-rays, gave very faint rings as well as bands ; but the rings do not exactly correspond to those of hexagonal pattern nor to the bands of amorphous tellurium.

D. Tellurium sol, one month after its preparation, was precipitated with HNO_3. This precipitate yielded to diffused rings (Plate V) but none of them agrees with the band obtained from amorphous tellurium.

E. The effect is exactly similar to that described in B.

F. On allowing tellurium sol to dry up in a basin a thin film was found to form on the surface of the sol. The same thing also happens with sulphur sol. The thin film from latter sol is found to be a new crystalline variety of sulphur. Thin film of tellurium sol is crystalline and its intensity distribution is quite dissimilar to that of hexagonal pattern (Plate V). The spacings as well as the relative intensities of the rings of hexagonal tellurium and this thin film are given for comparison in table I and II.

DISCUSSION OF THE RESULTS

Let us first make a brief survey of the general properties and experimental methods of preparing the colloidal solution and see what can be inferred as to the nature of the colloidal particles in a very general and qualitative way before proceeding to discuss the results obtained above.

The methods of preparation of colloids in general may be classified under two headings :—

(1) The method of condensation :—

In this method, *viz.*, the chemical method, we start with atoms of the substance. These atoms, due to thermal motion, collide with each other and as a result form bigger masses. These particles as they grow up get charged in some unknown way, which perhaps increases with the increase in size of particles until the mutual repulsion between similar charges prevent the particle from coming in actual contact with each other, *i.e.*, prevents the growth of size.

(2) The method of dispersion :—

In this method the substance is taken in bulk and then dispersed in the liquid medium, *viz.*, mechanical method, etc., *i.e.*, the size of individual particles is gradually diminished until the state of equilibrium, same as described above, is reached. It is natural to suppose that the colloidal particles prepared by this method have retained the atomic arrangement peculiar to the substance in bulk, since in this method we simply dispersed the sample by gradual diminution of particle size and did not break up the substance to its atomic state ; of course it is not impossible that other factors are also to be considered. For, in this fine state of matter, where the individual particles are only few hundreds of atoms deep, energy consideration may permit of a different atomic arrangement. Besides, there may be other factors with which we are not yet familiar ; in fact, our knowledge of this fine state of matter at this stage is very limited.

In the first method, the substance is produced in the atomic state and these atoms next grow to form small masses which in their turn may coalesce with atoms or with similar groups and thus may form still bigger particles. In natural process of crystal growth, say from a solution, growth takes place from atoms

Fig. 1.

Fig. 2.

Fig. 3.

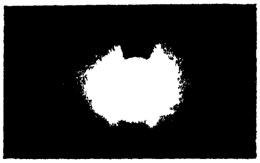

Fig. 4.

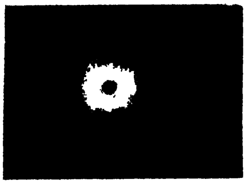

Fig. 5

Fig. 1 :- Pattern of the electrolytic Coagulum of a heated Te Sol.

Fig. 2 :- Amorphous pattern of the Coagulum from a fresh Te Sol

Fig. 3 :- Pattern of the thin film from the Surface of a Te Sol. allowing it to dry up in a basin (Suspected new variety).

Fig. 4 :- Two diffuse rings of the Coagulum from an aged Sol.

Fig. 5 :- Amorphous band of the Coagulum from a fresh AS_2 S_3 Sol.

TABLE I

Metallic tellurium (New suspected variety) : $r = 2.88$ cm.

Rings	Intensity	Sin θ	d in (A. U.)	Intensity	Sin θ	d in (A. U.)
1	W (α)	0.2080	3.070	W (α)	0.1091	7.05
2	W (β)	0.2276	3.05	W (α)	0.1436	5.36
3	V. S (α)	0.2523	3.05	W (β)	0.1754	3.96
4	V. V. W (α)	0.2689	2.86	W (α)	0.1938	3.97
5	V. V. W (β)	0.3913	2.23	S (β)	0.2098	3.31
6	V. V. W (β)	0.3256	2.13	S (α)	0.2531	3.04
7	S (α)	0.3437	2.24	W (α)	0.2948	2.61
8	W (α)	0.3636	2.12	V. W (α)	0.3193	2.41
9	V. V. W (α)	0.3878	1.99	V. W (α)	0.3482	2.21

TABLE II

Specimen	Nature of the pattern	Intensity	Sin θ	d in (A. U.)
Te sol	1 ring	W (α)	0.2099	3.67
Precipitate by HNO_3	2 rings	W (β)	0.2267	3.06
Precipitate by HNO_3 from heated Te sol	3 do.	V. S (α)	0.2541	3.05
	4 do.	S (α)	0.3458	2.23
	5 do.	V. W (α)	0.3619	2.63
	6 do.	V.V.W(α)	0.4399	1.75
Precipitate by HNO_3 from fresh Te sol	one sharp band		0.2490	3.09
Gummy mass of Te obtained on drying a Te sol	1 diffuse ring or band		0.1253	6.13
	2 rings	W (β)	0.1769	3.93
	3 rings	W (α)	0.1953	3.94
	4 diffuse rings or band		0.2405	3.20
Electrolytic Precipitate from aged Te sol	1 diffuse ring or band		0.1253	6.13
	do.		0.1854	4.15
	do.		0.2369	3.26

placing themselves in the position of minimum energy. When atoms coalesce to form small masses in this method, they may be expected to arrange themselves in agreement with the energy condition within a very short time. But in the process of growth to form a bigger mass, complete rearrangement amongst the smaller particles probably does take place instantaneously. In a freshly prepared sol, therefore, the individual colloidal particles may not be single crystals but may consist of still smaller crystallites. The crystalline nature of these crystallites should be determined by the energy consideration prevailing in that fine state of matter ; thus these crystallites may retain a structure similar to that of the stable variety (ordinary variety at room temperature) or a new variety or a mixture of both all depending upon energy difference of the different types.

On heating the sol two effects may be expected ; firstly, the individual colloidal particles tend to become single crystals due to the greater freedom of the atoms for rearrangement. Secondly, due to greater thermal energy, the particles collide in spite of their similar charges and grow in size which may ultimately cause coagulation. Also, if the charges be due to adsorption of ions by the particles, as is held by one school, the heating may also lead to partial removal of charges due to the escape of adsorped ions. Besides these, changes of specific inductive capacity due to thermal effect causes an alteration in the repulsive force between the charged particles.

On adding an electrolyte, the dielectric constant is increased, thereby decreasing the repulsive force between similarly charged particles. Besides, the charge of the colloidal particles is neutralised by oppositely charged ions of the added electrolyte and so coagulation begins.

X-ray diffraction pattern of the forced precipitate by HNO_3 consists of a single band, approximately in the positions of a group of rings of hexagonal variety. This clearly indicates that the size of the single crystallite particles present in fresh sol must be less than 10^{-5}cm. (particles lying between 10^{-3} and 10^{-5}cm. yield sharp line pattern). On adding the electrolyte, the agglomeration of the colloidal particles occurs so rapidly that they settle down (under gravity) before the crystallites can orient themselves to form bigger crystals. In other words, during the actual process of coagulation of tellurium sol by HNO_3, the sizes of the single crystallites present in the colloidal particles do not increase appreciably.

On heating the sol, each colloidal particle becomes a single crystal, and, besides this, they also grow in size. The precipitate by HNO_3 yields sharp continuous rings characteristic of the hexagonal tellurium. Supposing now that in this case, too, the process of electrolytic coagulation does not influence the size of the crystallites to any great extent, the particle size of precipitate gives a rough idea of the size of the particles in the colloidal state. This is not unlikely, for the colloidal sol may contain particles big enough to be of the order of 10^{-5} cm. and be still stable and the particles of this order are able to produce sharp and continuous rings pattern.

In general, colloidal solutions (*viz.*, sulphur, selenium, etc.) are found to coagulate (at least certain appreciable percentage of it) on heating, the reason is that the colloidal particles have grown too large to remain in suspension. In the case of tellurium we are led to the conclusion that the particle size grow up on heating but only to the order of 10^{-5} cm. so that they are still able to remain in suspension. An alternative to the above supposition may also be suggested. In case of a fresh sol where the individual colloidal particles consist of crystallites at random when the coagulation is occurring, the tendency of crystal growth is not sufficient to cause increase in the size of the crystallites to an appreciable extent. But, in case of heated sol, the individual particles being single crystals, the tendency of crystal growth is possibly larger, so that, during coagulation, the increase in crystal size by orientation of the smaller crystallites is possible; thus the presence of crystals of size 10^{-5} to 10^{-3} cm. in the coagulum becomes possible.

As the sol is heated and kept for a considerable period at a temperature much higher than the room temperature, it is likely that any other form of tellurium, even if present, should be converted into the ordinary metallic variety and in the coagulum it is only the hexagonal variety that can be expected.

The pattern of this precipitate from the heated sol also shows that the added electrolyte has no effect on the pattern due to the precipitate although the precipitate may quite justly be suspected of containing a portion of the added electrolyte.

AGEING

The effect of the orientating tendency of the colloidal particles, *i.e.*, of slow coagulation, is manifested clearly in the pattern of the coagulum from aged sol. In the pattern of the coagulum obtained from the aged tellurium sol two bands (diffuse rings) make their appearance; their spacings do not exactly correspond to that of amorphous tellurium. The strong rings in the pattern of the thin film that settles on the sol on allowing it to dry up, however, agrees closely with the position of these diffuse rings. This clearly indicate that, on ageing, growth of crystallites have taken place but still they are not large enough to yield to sharp pattern.

Tellurium sol on allowing to dry up on a basin becomes a paste-like mass. This is probably due to water molecules being strongly bound to the colloidal particles of tellurium. Two effects are superposed here. As the sol dries up, the colloidal particles come closer and the chance of collision increases. The second effect is due to ageing. Both the effects, however, may be regarded as due to ageing—only difference will be that this will behave as a sol which has been aged for a very long time. In the pattern of the gummy mass, we therefore find the continuation of the effects of ageing only to a greater extent, and rings do appear though still accompanied by a band. This also explains the line-band correspondence in the pattern due to this gummy mass and that due to precipitate from aged sol; the slight discrepancy must be ascribed to smaller particle size in case of the latter. For, it is well known that spacings depend on the particle size, the spacings decreasing with the increase in particle size.

The film formed on the surface shows crystallinity and we are thus led to the conclusion that, whatever may be the cause, it is the particles at the surface of the sol that are affected most on ageing; the scum "devitrefying" almost completely while the devitrefication of the mass inside is still incomplete.

The diffraction pattern of this film differs widely from that of hexagonal variety; besides, the intensity distribution being completely different, there are also certain rings which do not agree tolerably with any of the hexagonal rings (*cf.* B and D). Here two explanations may be suggested. Either (*a*) we are to believe in the existence of a new type of tellurium (other than the one known) which has been isolated in this way, the corresponding crystallites being present in the colloidal sol; or (*b*) we may assume that the crystallites of metallic tellurium, present in the fresh sol, cannot under the circumstances described above grow up equally on all of their faces. This unequal development in different directions may be responsible for such dissimilar pattern. The thin film in case of sulphur and selenium sol comes out to be entirely different from the ordinary stable variety, as has already been found in this laboratory. Led by this analogy and similarity between the elements—sulphur, selenium and tellurium, we believe that a new variety of tellurium (monoclinic perhaps) has been isolated in this way.

B. ARSENIOUS SULPHIDE SOL

Preparation :—A saturated solution of As_2O_3 in conductivity water was prepared by boiling the oxide with water for about two hours. The solution was next cooled and diluted to double its volume. A slow stream of H_2S gas was then passed till the solution was saturated with H_2S and a strong colloidal solution of As_2S_3 was obtained. H_2S gas was then removed completely by passing H_2 in slow stream until complete removal occurred. It was next filtered thrice through double filter paper when stable colloidal solution of As_2S_3 in water was obtained.

Properties :—The transparent yellow solution, so obtained, is very stable. When allowed to stand for days a fraction precipitate down.

Most of this precipitate is easily peptisable. So far as heating is concerned, As_2S_3 sol is very stable. It does not precipitate even on boiling for a long time.

The sol is anionic. It can be precipitated even with a small quantity of ordinary tap water. The addition of a drop of HCl bring about a complete and immediate precipitation of a large quantity of the sol.

On allowing to dry up in a basin, the sol completely dries up and falls to powder ; while under similar condition tellurium as well as selenium sol never completely dries up but forms a pasty mass.

X-ray was found to have no coagulating effect on As_2S_3 sol

X-ray investigations :—

The precipitate obtained on addition of an electrolyte to freshly prepared As_2S_3 sol was exposed on a zig-zag paper and two bands were obtained (Plate V). The bands correspond in position to two prominent groups of rings in the powder pattern of ordinary As_2S_3.

The As_2S_3 sol was taken in a flask and kept for a few days when a certain amount of precipitate was found to accumulate at the bottom. The supernatant colloidal sol was taken out with the help of a pipette without disturbing the precipitate. The sample of As_2S_3, so obtained yielded one band on X-ray exposure. This band corresponds to that at the smaller angle of scattering in the preceding case. The second band was also present but was found to be very weak.

The solution was heated in a water bath for a few hours and the stable sol was precipitated by HCl. On X-ray exposure, the precipitate yields two or three rings which agree in spacings with corresponding rings in the powder pattern of ordinary arsenic sulphide within experimental error.

A solution of colloidal arsenic sulphide was allowed to evaporate at the room temperature. The sol completely dried up and fell to powder. The pattern of this sample was exactly similar to that of the ordinary variety both in spacings and in intensity distribution. The measurements are given in table III.

TABLE III

Specimen	No.	Intensity	Sin θ	d in (A. U.)
Ordinary arsenic sulphide powder in a hemi-cylindrical camera	1	S (α)	0.1103	6.68
	2	V.S. (α)	0.1210	6.36
	3	S (α)	0.1288	5.98
$r=2.06$ cm.	4	V.V.W. (α)	0.1774	4.34
	5	S (α)	0.2391	3.21
	6	S (α)	0.2473	3.11
	7	V.W. (α)	0.3113	2.47
Precipitate by HCl	1	Band	0.134	5.74
$r=2.88$ cm.	2	"	0.1931	3 99
Natural Precipitate	1	"	0.1332	5.8
$r=2.06$ cm.	2	Too weak	0	0

The results can be summarised as follows :—

Name of the sample	Nature of the pattern	Remark
(1) Natural peptisable precipitate that settles on standing	Bands	Amorphous
(2) Forced precipitate by strong hydrochloric acid	Ring pattern similar to that of the ordinary As_2S_3 powder	Crystalline
(3) Forced precipitate by hydrochloric acid from heated sol		
(4) Dried-up sol		

DISCUSSIONS

The general considerations that were made in connection with tellurium sol are also applicable to the present case. The precipitate by an electrolyte from a fresh sol yields bands as in the case of the tellurium sol. Hence the size of the crystallites that are responsible for the pattern must be less than 10^{-5} cm., which is the limiting size for a sharp ring. The band also corresponds in position to a strong group of rings in the powder pattern of As_2S_3. On heating, it is expected that growth of size of the individual colloidal particles takes place and individual particles become single crystals and therefore show rings on X-ray analysis.

With regard to (1) and (4) the present sol behaves quite differently to tellurium sol ; arsenic sulphide sol dries up completely and falls to powder whereas tellurium sol forms a gummy mass It suggests therefore that the force of attraction between the charged colloidal particles and the electrically bound water molecules is not strong enough to resist evaporation. The high sensitiveness of the sol towards electrolytes is probably due to this small force of attraction between the charged particles and the electrically bound water molecules.

Another point of difference between the present sol and the former lies in its formation of natural peptisable precipitate. That a certain amount of As_2S_3 settles down is a clear indication of growth of size of the colloidal particles. X-ray analysis, however, reveals that the sizes of the individual crystallites are not large enough to produce a sharp ring pattern. So we are led to the conclusion that the colloidal particles collide with each other inspite of their charge and some of them get agglomerated. These agglomerates settle down before they can array themselves in a crystalline arrangement. This precipitate consists of crystallites grouped almost at random—the force of binding is simply that of cohesion ; so by shaking they may be expected to disperse easily. That is exactly what we find in this case ; this precipitate can be easily peptised. Had they been arrayed in a crystalline pattern, simple shaking could not have dispersed the crystalline particles to the colloidal state.

The work was carried out in the Khaira Laboratory of Physics, University College of Science, Calcutta. The author takes this opportunity of acknowledging his indebtedness to Prof. B. B. Ray, D.Sc., for suggesting the problem and kind guidance throughout.

Khaira Laboratory of Physics,
University College of Science,
92, Upper Circular Road,
Calcutta.

MEASUREMENT OF THE ANGLE OF INCIDENCE AT THE GROUND OF DOWNCOMING SHORT-WAVES FROM THE IONOSPHERE

By CHAMAN LAL, M.Sc.

(Received for publication, March 30, 1941)

Plates VI and VII

ABSTRACT. Measurement of downcoming angles for a number of European short-wave stations have been made. The apparatus consists of two commercial superheterodyne receivers with two parallel horizontal dipole aerials for picking up energy. Downcoming angle is inferred from the phase difference between the voltages on the two aerials.

Average values of the downcoming angles for the B.B.C. transmitters during the months of May, June, September and November, 1940, came out to be 16°; 20°.6; 15°.2 and 14°.2 respectively.

The average values obtained for the German stations for the months of May, June and November, 1940, came out to be 20°.8; 19° and 15°.

INTRODUCTION

A knowledge of the angle of incidence at the ground of short-waves propagated *via* the ionosphere is essential for the efficient design of both the receiving and the transmitting aerials, for point-to-point working in particular and broadcasting in general.

For most efficient operation the transmitting aerial, besides being orientated to radiate maximum energy along the great circle path joining the transmitter and the receiver, should also concentrate the energy so that the angle of elevation above the horizontal of the radiated beam is most favourable for reception at the receiving point. Energy radiated at other than the correct angle is wasted in so far as the receiving point is concerned. A consideration of the reciprocity theorem will show that the optimum angle of transmission will be the same as the downcoming angle measured at the receiving point. Likewise the receiving aerial should also be orientated in the correct horizontal direction and designed to receive maximum energy from the correct angle in the vertical plane. This will help to discriminate against atmospherics and other kinds of interfering signals, besides building a strong signal to overcome receiver noises, etc.

Determination of the downcoming angles is important to the physicist engaged in the study of the ionosphere. This information provides him a means of experimentally verifying his theories of electromagnetic wave propagation *via* the ionosphere. Determination of the height of the ionosphere can also be made from a knowledge of these angles of incidence at the ground.

The set-up described in this article is what is usually termed the "phase measurement method," and differs from conventional methods[1] in that it makes use of two ordinary commercial superheterodyne receivers (having R. F. sensitivity control) adopted for the experiment with the following modifications:

(1) The internal oscillators of the two receivers are made inactive.

(2) A common external local oscillator is used as a heterodyning oscillator for either.

No great care is exercised to have exact phase symmetry between the two receivers. The individual tuning control adjusts the tuning of the R. F. stages and thus controls the phase. This control can be used for phase compensation. The local oscillator is used for tuning in the required signal.

Such an arrangement is relatively easy to set up and requires no elaborate components and instruments for making special receivers, exactly matched for phase and gain.

THEORY

The basic principle underlying the method is that when radio waves from a certain direction arrive at two receiving aerials separated by a known distance the phase angle ϕ between the induced voltages is :

$$\phi = \frac{2\pi}{\lambda} d \sin\theta \sin\Delta \quad \text{radians,}$$

where d = the spacing in metres between the two receiving aerials set up parallel to each other ;

λ = the wavelength in metres of the waves under investigation ;

θ = the angle of incidence (measured from the vertical) of the downcoming waves ; and

Δ = the angle between the Azimuth of the transmitting station and the direction of the receiving aerials.

The signals from the two receiving aerials are amplified independently after being heterodyned with a common heterodyne oscillator (to ensure that proper phase relationships are maintained) and are then applied to the plates of a cathode-ray oscillograph tube where they give rise, in general, to an elliptical trace. It is possible from this pattern to calculate the relative phase difference between the two E.M.F's applied to the C.R.O. plates. Knowing this value of phase difference and granting that no extra phase difference has been introduced by the associated circuits, it is a simple matter to calculate the angle of incidence to the ground of the downcoming waves. A mathematical note, showing that when two E.M F's with a phase difference are heterodyned with a common heterodyning oscillator, they retain their original phase difference, is given in Appendix I. Appendix II presents complete mathematical discussion for the interpretation of the ellipse.

EXPERIMENTAL SET-UP

An idea of the experimental set-up can be obtained from photographs Nos. 1 and 2 (Plates VI and VII) and the lay-out diagram shown in Fig. 1.

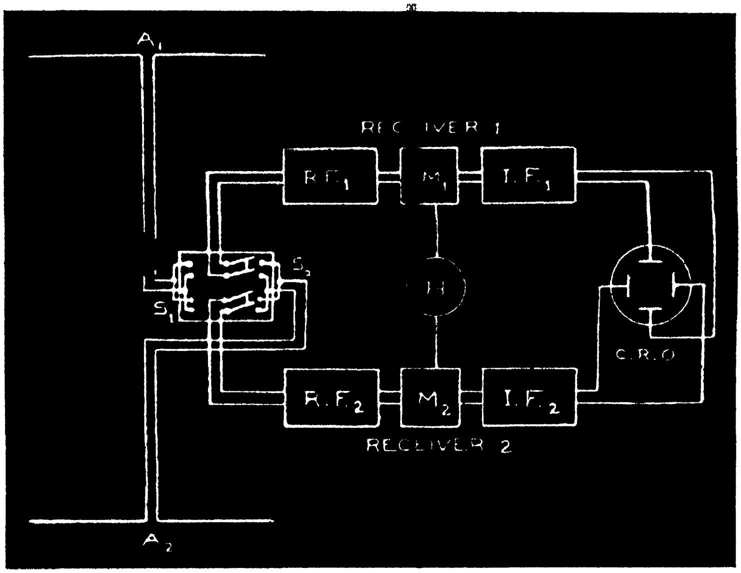

Fig. 1

A_1 and A_2 are 12 ft. high horizontal receiving dipole aerials separated by a distance '*d*' metres (approximately 1.2λ) and cut for approximately half wave operation on 19 metres band. Care is taken that the two receiving aerials are exactly symmetrical. The aerials are joined to the apparatus located in a nearby wooden hut by means of two equal lengths of twisted flex. S_1 and S_2 are D.P.D.T. knife switches (suitably shielded to avoid spurious pick-up). RF_1 and RF_2 are R.F. stages of the two commercial receivers, local oscillators of which have been made inactive. Their mixers stages M_1 and M_2 are fed in parallel from a common heterodyne oscillator H. In this arrangement the two receivers were Hammerlund Super-pro model SP-110S which have a sensitivity of 5 to 2 μv. for 601BS signal to noise ratio and the common heterodyne oscillator was the oscillator section of an R.C.A. receiver type 8T, its mixer stage having been disconnected. IF_1 and IF_2 are I.F. amplifiers working at the intermediate frequency (456 kc/s) in order to amplify the signals to a level high enough to give a suitable deflection on the cathode-ray oscillograph marked C.R.O.

PROCEDURE

Preliminary Experiments and Adjustment :—

The D.P.D.T. switches S_1 and S_2 are used to enable any one of the two receivers to be connected to any of the aerials separately or together.

With any one of the aerials connected to both the receivers in parallel, the common heterodyne oscillator H and the ganged R.F. stages of the receivers could be tuned to receive any desired transmission. The tuning and the R.F. gain-control of the receivers are then manipulated such that the trace on the C.R.O. screen becomes a line inclined at 45° to the horizontal and the vertical axes. Under these conditions the two receivers have been adjusted so that the phase retardation in one compared to that in the other receiver is a whole number of complete cycles or is zero. All that is then necessary is to put the two receivers on independent aerials and record the resultant ellipse appearing on the C.R.O. screen, either photographically or by making a tracing, though the latter will be only approximate unless the signals are very steady and no fading is present. For preliminary observations ordinary bromide photo-printing paper can be exposed directly on the C.R.O. screen when a contact print of the desired ellipse pattern will appear on the paper after development, or the pattern can be recorded by the help of an ordinary camera using rapid negative material. The ellipse pattern is then used for calculating the required phase difference. Under proper working conditions the ellipse will have its major axis inclined at 45° to the oscillograph axes and will maintain its axis and eccentricity even if the aerials are changed over by operating switches S_1 and S_2. Under such conditions the angle subtended by the minor axis at the ends of the major axis will give the desired phase angle between the two component e.m.f's which produced the ellipse (see Appendix II). Under improper conditions both the major axis at which the ellipse appears on the C.R.O. screen and its eccentricity may change on reversing the switches S_1 and S_2.

Such an improper condition when it exists is found to be mainly due to the coupled impedance thrown back by the tuned secondaries of the input transformers into their primaries being different in the two cases, with the result that when the receivers are put in parallel to work from the same aerial in order to be aligned for zero phase difference in the two limbs the impedances alter and become unsymmetrical as soon as the receivers are put on the two aerials independently. In the arrangement set up this effect was made negligible by connecting two very low resistances (about 1 ohm each) across the input of the two receivers. This helped to keep the input impedance in both the cases steady and resistive. The reduced gain of the receivers was compensated for by additional I.F. amplifiers IF_1 and IF_2.

For any measurement two successive photographs were taken by interchanging the aerials connected to the two receivers. The mean of two such measurements was taken as the final result. This procedure helped to further reduce the error introduced by the changes in the receiver input impedance

BEHAVIOUR OF THE PATTERNS APPEARING ON THE C.R.O. SCREEN

Under actual working conditions it was observed that during the day signals from long distance broadcasting stations such as B.B.C., Berlin, Moscow, etc., rarely give ellipses which are steady and useful for downcoming angle measurements. The ellipses are often seen to rotate, change their size, shape and eccentricity in a random manner, the rapidity of rotation and the agitation of the ellipses being greatest on the magnetically disturbed days. Ellipse patterns were in general found to be steady in the nights and before dawn in the mornings, when the ionisation levels in the F and the E layers are relatively low. Long distance transmitters towards the east of Delhi were generally observed to show a tendency to give steadier ellipses soon after sunset, and those to the west of Delhi in the early morning up to sunrise. Ellipse patterns from short distance short-wave stations at Delhi, Bombay, Madras and Calcutta were seldom observed to be steady either in the mornings or in the evenings up to 11 P.M. The ellipse patterns from these stations were generally more highly agitated than those obtained from long distance short-wave stations, with the result that measurements on the Indian short wave stations were not always possible.

A study of the mathematical note (Appendix II) will show that this behaviour of the ellipse patterns is to be ascribed to simultaneous arrival of energy along more than one path, with the result that the resultant direction of arrival is changing with the fading of the signals and interference between the multiple rays arriving at the receiving aerials. An experimental verification of this theory to some extent was obtained by observing the ellipse patterns by using two special diamond aerials directed towards B.B.C. which are highly directional both in the horizontal and in the vertical planes. Since the angular spread from which energy can be received in this case was considerably limited as compared to the ordinary dipole aerials the ellipse patterns from B.B.C. transmitters were seen to be relatively steadier in the case of B.B.C. diamond aerials. The limited angular spread from which energy could be received in the case of B.B.C. diamond aerials helped to cut out some of the energy arriving in multiple paths with the result that effects due to interference became less acute.

RESULTS

The apparatus was ready for making angle measurements on the 20th May, 1940, when a direct exposure was made on the C.R.O. for obtaining an ellipse pattern for GSF signals at 10 P.M. The angle of arrival of GSF waves as obtained from this photograph came out to be 16° to the horizontal. This result has been more or less confirmed by later observations and measurements. A typical direct photograph is shown in Fig. 1 (Plate VI), from which it will be observed that the ellipse pattern is a dark patch on a white background. This is because of the fading of the signal which causes the pattern to vary from zero amplitude to the maximum marked by the contour of the dark ellipse.

It must be remarked here that, with such a crude method as the one used in the earlier period of experimentation, successful photographs as the one shown in Fig. 1 (Plate VI) are subject to a certain amount of practical skill and the conditions prevailing at the time the recordings were made. In case the signals are suffering from bad fading and the exposure is made during the time that the ellipse is going through its worst agitation, a very disappointing result may be obtained, which will be utterly useless from the point of view of any measurements. Subsequent measurements were therefore made by taking instantaneous recordings with the help of an ordinary camera. A typical set of such camera recordings is shown in Figs. 2, 3, 4, 5 and 6 (Plate VI).

Preliminary adjustment for no phase difference in each of these six cases was a straight line making an angle of 135° with the positive direction of X-axis. The phase difference as shown below the photograph is the angle subtended by the minor axis at the end of the major axis. Actual phase difference will, however, be given by the following consideration :—

If the ellipse lies in the 2nd and the 4th quadrant, the phase difference can be ϕ, $360 \pm \phi$, $2 \times 360 \pm \phi$, etc., where ϕ is less than 90°.

On the other hand, for the ellipse to lie in the 1st and 3rd quadrant the phase can be $180 \pm \phi$, $540 \pm \phi$, etc.

By looking at the photograph and knowing the value of the maximum possible phase difference $(2\pi d/\lambda)$, the most probable value of the additional figure can be easily picked out. Thus, having found out the actual phase difference, the value of θ can be calculated.

It may be further added that the major axis of the ellipse in Figure 1 was actually at an angle of 135° with the positive direction of X-axis. It has been rotated through an angle of 45°, thus making the major axis appear vertical.

At this stage it was considered advisable to devise methods for experimentally checking up the behaviour of the apparatus. One of the easiest and the most reliable mothods that lent itself for this purpose was the use of the ground wave signals from the Delhi short-wave transmitters at a time when the ionisation levels in the ionosphere were low enough not to return any energy incident vertically. Under such conditions, which were mostly confined to the night after 11 P.M. or the early morning before 8 A.M., in the months of June-July, 1940, ellipses were found to be sufficiently steady to permit of good photographic records or tracings to be made. As the tall Delhi masts supporting the short-wave transmitting aerials were visible at the Todapur Receiving Centre of A.I.R. (where these experiments were conducted), the angle between the direction of the receiving aerial and that of the Delhi short-wave transmitting aerial could be measured with a high degree of accuracy with the help of a theodolite. Knowing the wavelength of the Delhi transmission used to develop any ellipse patterns, and the fact that wave propagation is horizontal, together with the angle measured between the direction of the receiving aerials and the Delhi transmitting aerial, the expected phase difference could be calculated and then checked with the phase difference obtained from the ellipse pattern appearing on the C.R.O. screen.

A typical ellipse pattern obtained with the use of the Delhi transmissions in the 19 metre band is shown in Fig. 2 (Plate VI), from which the measured phase difference comes out to be 74°. Phase difference calculated from the geometry of the set-up was found to be 77°.3 which is considered to be a fairly close agreement.

It was found that the average value for the downcoming angle in the case of B.B.C. transmitters during the months of May, June, September and November, 1940, came out to be 16°, 20°.6, 15°.2, and 14°.2 respectively.

The average values obtained for the German stations for the months of May, June and November, 1940, came out to be 20°.8, 19° and 15°.

The results, as will be apparent, indicate a general lowering of the F_2 layer height during the winter evenings as compared to the summer evenings.

Variation in the measured values :—

During the course of these observations it was noted that the results varied by as much as ±20% even on the same evening. This variation has to be ascribed partly to the well-known fact that the rays from any particular station do not come as single rays but have a certain spread in the horizontal and the vertical planes, the angular spread being more in the latter case. Results are further affected by fading, which is considered to be the chief factor contributing to such a wide variation as ±20%.

CONCLUSION

As the photographs were made by exposure of the film at the moment that the ellipse reached its maximum size they represent the main ray, and the direction inferred from that ellipse refers to the direction of the principal ray. This is particularly true in the case of the contact photographs in which measurements can only be made from the contour of the dark patch. Hence under conditions of measurement the subsidiary ray must have either faded out completely or so changed in polarization as to give no effect on the aerials. The direction of arrival of the subsidiary rays cannot be inferred from these experiments, For finding out the direction of arrival of other rays than the principal, it will be necessary to have a series of photographs of the changing ellipse at small known intervals and to analyse them so as to find out what combination of rays can give the kind of change observed.

This method, however, on the face of it is very complex and may not give very definite or easily interpretted results.

If, however, the transmitter gives short-duration pulses, each subsidiary ray will arrive at an interval of time different from that of others and will give a separate ellipse of its own. There will then appear ellipses equal in number to the number of rays present. These ellipses will represent the directions of arrival and intensity of the rays by their eccentricity and size respectively. The pulse method of observation is therefore more promising for yielding useful results relating to the more complex propagation conditions in the ionosphere.

ACKNOWLEDGMENTS

The author wishes to express his sincere thanks to Mr. C. W. Goyder, Chief Engineer, All India Radio, for permission to publish this paper and for his guidance and many useful suggestions. Many thanks are also due to Messrs. N. L. Sahdev and M. R. Rao, Assistant Engineers, and Mr. A. S. Narayanaswamy, Technical Assistant, Research Department, All India Radio. Mr. N. L. Sahdev carried out the mathematical investigation presented in Schedule II, thus paving the way for a better understanding of the patterns appearing on the Cathode-Ray Oscillograph screen. Mr. M. R. Rao carried out a considerable amount of work on setting up the experiment and obtaining useful information during many hot afternoons and sultry evenings in the wooden hut at Todapur. Mr. A. S. Narayanaswamy was responsible for constructing the additional I.F. amplifiers and modifying the Hammerlund receivers used for the experiment at Todapur.

APPENDIX I

Let $A_1 \sin \omega t$ and $A_2 \sin (\omega t + \varphi)$ be the signals applied to the two mixers, respectively in the two receivers.

Suppose further that the signal introduced by the local oscillator is :

$$B \sin (\gamma t + \xi).$$

Now, the mixer characteristic may be taken of the general form :

$$i = a_0 + a_1 e + a_2 e^2$$

where i = output current ;

e = input voltage ;

and a_0, a_1 and a_2 are constants.

PLATE VI.

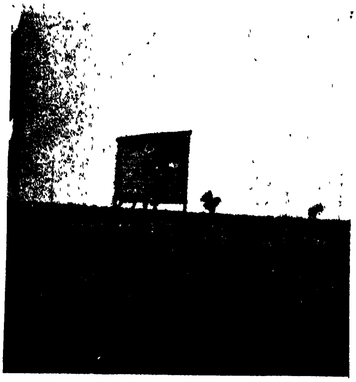

(1)

Aerial system and receiving hut
at
Toda-Pur

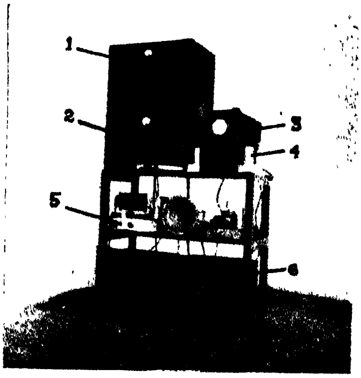

(2)

1. Receiver No. 1
2. Receiver No. 2
3. Cathode Ray Oscillograph
4. Additional I F. Amplifier
5. Common Hetrodyning Oscillator
6. Power supplies.

For mixer No. 1, the output current i_1 may therefore be written as :

$$i_1 = a_0 + a_1 \ (A_1 \sin \omega t + B \sin \overline{\gamma t + \xi}) + a_2(A_1 \sin \omega t + B \sin \overline{\gamma t + \xi})^2.$$

This after simplification may be written as :

$$\begin{aligned} i_1 = a_0 + a_2/2(A_1^2 + B^2) + a_1 A_1 \sin \omega t + a_1 B \sin \overline{\gamma t + \xi} \\ - a_2 A_1/2 \cos 2\omega t - a_2 B/2 \cos 2(\gamma t + \xi) \\ + a_2 A_1 B \cos \{(\gamma - \omega)t + \xi\} - a_2 A_1 B \cos \{(\gamma + \omega)t + \xi\}. \end{aligned}$$

This expression shows that the output of the mixer contains (1) the fundamental frequencies; (2) frequencies of twice the value of the fundamentals; (3) sum and difference of the fundamentals. As the output of the mixer is tuned to the intermediate frequency which is equal to the difference of the fundamental frequencies then the only term of importance (and which is further amplified) is:

$$a_2 A_1 B \cos \{(\gamma - \omega)t + \xi\}. \qquad \ldots \quad (1)$$

Similarly it may be shown that the I.F. output of the 2nd mixer is:

$$a_2 A_2 B \cos \{(\gamma - \omega)t + \xi + \phi\}. \qquad \ldots \quad (2)$$

It will be seen from (1) and (2) that the phase difference of the intermediate frequencies produced is ϕ, which is the phase difference between the original R.F. signals.

APPENDIX II

Intrepretation of the Ellipse forms appearing on the CRO in the experiment of " Measurement of the Angles of Down-coming Rays."

SUMMARY

It is shown that for $E_h = E_v$, the ellipse will not precess but only change its ellipticity with changing values of the phase difference ϕ. If, however, E_v does not remain equal to E_h, the ellipse will rotate. It will rotate continuously for variable E_v/E_h, and changing ϕ. Further the ellipse may not precess in case of a single ray but will do so when rays more than one are present simultaneously.

(I)—Ellipse formation and its interpretation.

Let us confine ourselves, in this section, only to what happens in the CRO itself.

A sinusoidal voltage $E = E_h' \sin \omega t$ is applied to the plates, which produces deflection in the horizontal (X-axis) direction. The deflection produced is proportional to E. Hence at any time (t) displacement (x) of the beam from the centre is given by

$$x \propto E_h' \sin \omega t$$

or

$$x = kE_h' \sin \omega t = E_h \sin \omega t \qquad \ldots \quad (1)$$

where k is a constant of the CRO and its working voltages and $kE_h' \equiv E_h$.

A voltage of the same frequency $(\omega/2\pi)$ is also applied to the vertically deflecting plates. This second voltage may have a different amplitude E_v' and phase ϕ; hence the vertical deflection

$$y = k'E_v' \sin(\omega t + \phi) = E_v \sin(\omega t + \phi) \qquad \ldots \quad (2)$$

where k' may be different from k of (1) and $k'E_v' \equiv E_v$.

Actual path traced by the spot will be determined by the combined action of (1) and (2).

Eliminating (ωt) from relations (1) and (2), we have

$$y = \frac{xE_v}{E_h}\cos\phi + E_v \sin\phi \sqrt{1 - x^2/E_h^2}$$

Transposing, squaring and simplifying, we get

$$\frac{x^2}{E_h^2 \sin^2\phi} + \frac{y^2}{E_v^2 \sin^2\phi} - 2\,\frac{xy\cos\phi}{E_v E_h \sin^2\phi} = 1. \qquad \ldots \quad (3)$$

Comparing (3) with the standard equation of the ellipse

$$ax^2 + by^2 + 2hxy = 1,$$

we find that the curve appearing on the CRO will be an ellipse. If ψ is the angle made by the direction of the major axis with the X axis, then

$$\tan 2\psi = \frac{2h}{a-b}\ *$$

which for equation (3) after simplification becomes

$$\tan 2\psi = 2\Big/\left(\frac{E_h}{E_v} - \frac{E_v}{E_h}\right) \times \cos\phi. \qquad \ldots \quad (4)$$

If α and β are the semi-major and the semi-minor axes respectively, then

$$\alpha/\beta + \beta/\alpha = \frac{a+b}{\sqrt{ab-h^2}},\ \dagger$$

$$= \left(\frac{E_h}{E_v} + \frac{E_v}{E_h}\right) \times \frac{1}{\sin\phi}. \qquad \ldots \quad (5)$$

Case I. Let $E_v = E_h$; *i.e.*, amplitudes of the horizontal and vertical deflections be equal. From equation (4) we get

$$\tan 2\psi = \infty \text{ or } \psi = 45^\circ.$$

And equation (5) gives

$$\alpha/\beta + \beta/\alpha = 2/\sin\phi.$$

---

* 'Conic Section' by C. Smith, p. 227

† 'Conic Section' by C. Smith, p. 240

Solving this quadratic equation for α/β, we get

$$\frac{\alpha}{\beta} = \tan \phi/2 \text{ or } \cot \phi/2$$

or ϕ is the angle subtended at the end of one axis by the other axis.

Thus the direction of the axes is fixed to be along 45° and 135° lines but the ellipticity depends upon the phase difference ϕ of the component oscillations.

If $\phi = 0$, the ellipse reduces to a st. line along the 45° axis [$x = y$ from (3)].

If $0 < \phi < 90°$, the ellipse lies in 1st and 3rd quadrants and changes from a st. line to a circle.

For $\phi = 90°$, the ellipse becomes a circle.

For $90° < \phi < 180°$, the major axis lies along the 135° axis and the ellipse collapses from a circle to a st. line [$x + y = 0$ from equation (3)].

To change the major axis from the 45° axis to 135° axis, and for the ellipse to have the same shape, ϕ should change to $180 \pm \phi$.

It will be observed that to deduce the value of ϕ from the shape of the ellipse ϕ is always the angle subtended by the axis of the ellipse along 135° at the end of the axis along 45°, provided the adjustment for $\phi = 0$ was a st. line along 45° (as assumed already).

Also, it is to be seen that the ellipse for $E_v = E_h$ does not rotate but passes through a circle to the other axis, direction of the axes being always confined to 45° and 135° lines.

Case II. E_v and E_h are unequal, E_v/E_h being supposed to be constant, then

$$\tan 2\psi = 2\cos\phi \Big/ \frac{E_h}{E_v} - \frac{E_v}{E_h} \tag{4}$$

and
$$\alpha/\beta + \beta/\alpha = \left(\frac{E_h}{E_v} + \frac{E_v}{E_h} \right) \times \frac{1}{\sin\phi} \tag{5}$$

and the ellipse will rotate as well as change shape with changing values of ϕ.

Let $\phi = 0$,

then $\tan 2\psi = \dfrac{2E_v E_h}{E_h^2 - E_v^2}$ or $\tan \psi = E_v/E_h$.

and $\alpha/\beta + \beta/\alpha = \infty$ $\therefore$ $\beta = 0$ and α finite,

showing that the ellipse is a st. line ; the line is inclined at an angle $\tan^{-1}(E_v/E_h)$ to the X-axis. As ϕ increases from 0 to 90°, $\cos\phi$ decreases from 1 to 0, ψ decreases from the value $\tan^{-1}(E_v/E_h)$ to 0, and the ratio of β/α increases to a maximum, *i.e.*, to E_v/E_h from 0. Thus with the phase difference ϕ increasing from 0 to 90° the ellipse rotates from the direction $\tan^{-1}(E_v/E_h)$ to the direction of X-axis, at the same time changing in shape from a st. line to ellipse with maximum β/α. As ϕ increases from 90° to 180°, $\cos\phi$ is negative and changes from 0 to -1. ψ will also be negative and change to $(-\tan^{-1}\overline{E_v/E_h})$ from 0. Thus for constant value of E_v/E_h the ellipse rocks about the X-axis through the limits $\pm\tan^{-1}(E_v/E_h)$ and at the same time changes shape so as to be st. line in the extreme positions and fattest ellipse (maximum β/α) in the position $\psi=0$.

Case III. E_h/E_v variable, but ϕ constant.

For E_h/E_v changing from ∞ to 1, $\tan 2\psi$ changes from 0 to ∞, or ψ changes from 0 to 45°.

For E_h/E_v changing from 1 to 0, ψ changes from 45° to 90°. If then ϕ changes by 180° and the change in E_h/E_v continues, the ellipse will undergo a complete rotation.

To recapitulate we have arrived at the following results:—

(1) If the ellipse has the directions of its axes fixed to 45°-135° axes, but it changes shape from a circle to a st. line along 45° or 135° axes, or *vice versa*, the amplitudes of the component oscillations must be equal but the relative phase changes and can be deduced by measuring the angle at the end of the axis along 45° subtended by the axis along 135°.

(2) If the direction of the major axis rocks about the X-axis, the ellipse becoming fattest when the major axis is coincident with X-axis and is a st. line at the maximum deviations from X-axis direction, then E_v/E_h is constant but ϕ is changing values.

If the ellipse rotates continuously, say, in the anti-clock wise direction, then E_h/E_v is constantly decreasing when the ellipse is in the 1st and 3rd quadrant; the phase difference ϕ may also be changing. Holding ϕ constant, however, E_h/E_v, changing from ∞ to 0, makes the ellipse to rotate from the X-axis to Y-axis, change in ϕ may help or retard the rotation according as the $\cos\phi$ happens to decrease or increase with E_h/E_v. From a rotating ellipse which also changes shape it is rather difficult to infer as to what is changing, E_h/E_v, ϕ or both. In all likelihood, both may be varying under a certain set of practical conditions. It is, however, possible to understand the changes from a study of a number of instantaneous forms succeeding each other under experimental conditions.

Interpretation of a particular form follows:—

Let OX and OY (Fig 1, Plate VII) be the coordinate axes along which deflections take place. Let the ellipse meet the axes of X in points X and X′ and Y in points Y and Y′. Draw a rectangle ABCD circumscribing the ellipse and having its sides parallel (Fig. 2) to the coordinate axes. Let it touch the ellipse in points A′, B′, C′ and D′. It cuts the axes of X and Y in points A″, B″, C″ and D″ as shown in Fig. 2.

PLATE VII.

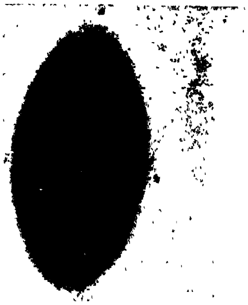

Fig : 1
GSF on 21 5.'40, at 21-30 I.S.T.
λ – 19 82 M d = 57 6 FT :
ϕ 49 2° Δ 90°
θ 77°

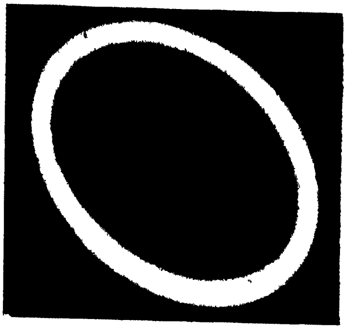

Fig : 2.
Delhi VUD3 on 16.11'40 at 23-00 I.S.T.
λ – 19·62 M d – 81·1 FT ·
experimental ϕ 74° Δ 9·81°
calculated ϕ 77·3°

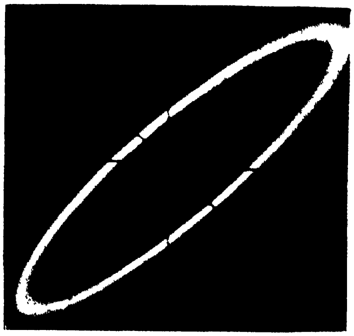

Fig . 3
GSG on 17.11.'40 at 19-00 I.S.T.
λ 16·86 M d 81·1 FT :
ϕ – 26·8° Δ – 90°
θ 70·5°

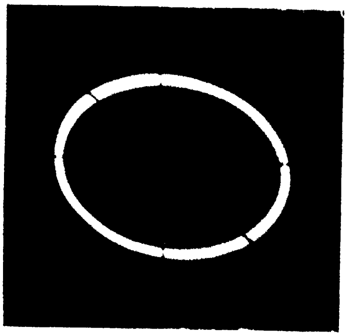

Fig · 4
GSF on 17.11.'40 at 21-30 I.S.T.
λ 19 82 M d – 81·1 FT .
ϕ – 75·3° Δ – 90°
θ – 75·8

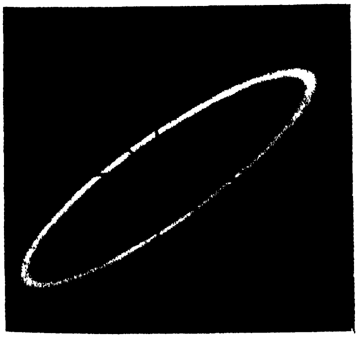

Fig 5
DJH on 17.11.'40 at 19-00 I.S.T.
λ – 16·81 M d = 81·1 FT :
ϕ – 27·8° Δ 89·4°
θ 75·4°

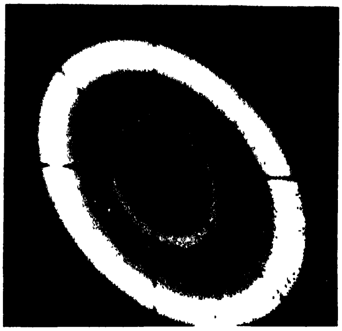

Fig : 6.
Moscow on 26.11'40 at 21-00 I.S.T.
λ – 19·47 M d – 81·1 FT :
ϕ – 70° Δ – 80·3°
θ = 72·7°

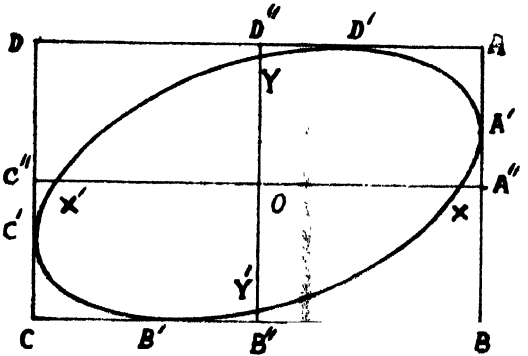

FIG. 2

(*a*) To determine E_v/E_h :

$$\left.\begin{array}{lll}\text{In equation (3) put} & x=o, & \text{then } OY=E_v \sin \phi \\ \text{next} & y=o, & \text{then } OX=E_h \sin \phi.\end{array}\right\} \quad \cdots \quad (6)$$

From (6) we have : $E_v/E_h = OY/OX$.

$$= \frac{\text{Intercept on Y-axis}}{\text{Intercept on X-axis}}$$

also $$E_v/E_h = OD''/OA''$$

$$= \frac{\text{Maximum deflection along Y-axis}}{\text{Maximum deflection along X-axis}}$$

As we know, that maximum deflections (OD'' and OA'') are proportional to E_v and E_h.

(*b*) $$\frac{OY}{OD''} = \frac{E_v \sin \phi}{E_v} = \sin \phi$$

similarly $$OX/OA'' = \sin \phi$$

thus ϕ can be inferred.

(*c*) In equation (3) put $x = E_h$: solving for y, we get $y = E_v \cos \phi$.

$$\frac{A'A''}{A''A} = \frac{\text{Ordinate of the pt. where } x \text{ is maximum}}{\text{Maximum ordinate of the ellipse}}$$

$$= \cos \phi$$

similarly $D'D''/D''A = \cos \phi$.

Knowing ϕ and E_v/E_h for a number of succeeding ellipses, we may be able to infer as to what changes and in what way.

II—Study of the case when a single incident ray is present.

Let A and B (Fig. 3) represent sections of the two parallel horizontal aerials through their middle points. A uniform wave-front of any kind of polarization is proceeding downwards, in the plane of the paper,

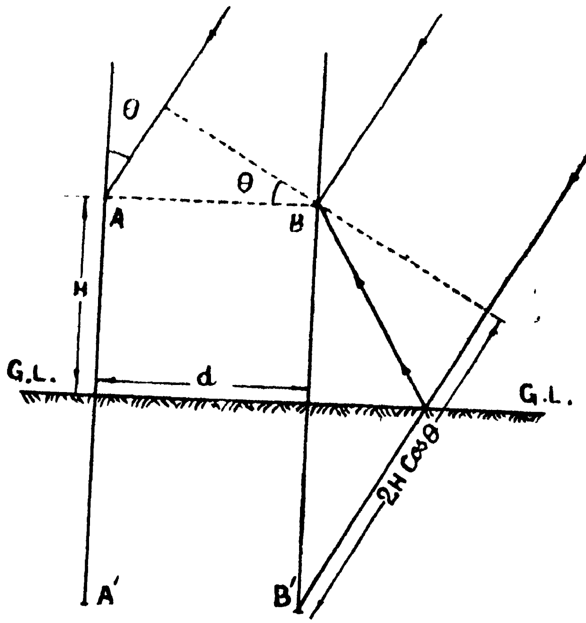

Fig. 3

the direction of propagation making an angle θ with the vertical. A part is incident on B, and induces a voltage E proportional to $E_H \sin \omega t$ where E_H is the horizontal component of the electric vector. The component of the vector perpendicular to E_H does not affect the aerial ; consequently the nature of polarization is immaterial so long as extraneous conductors and the vertical feeders do not play an important part in the pick-up. A change in polarization or rotation of the plane of polarization will only show up along with fading of the signal.

A second ray reaches B, after reflection from the ground. It has undergone the following changes :—

(1) The amplitude of the horizontal component has changed in the ratio 1 : A, where A is the coefficient of reflection.

(2) A sudden phase change ξ occurred on reflection. A and ξ depend on the nature of the reflecting soil.

(3) A phase retardation ($=4\pi$ H $\cos \theta/\lambda$) due to path difference has taken place. H is the height of the aerial above earth.

The effect of the reflected ray at B can therefore be represented to be proportional to :

$$A\, E_H \sin\left(\omega t + \frac{4\pi H \cos\theta}{\lambda} + \xi \right)$$

$$= A E_H \sin(\omega t + \chi)$$

where

$$\chi \equiv \frac{4\pi H \cos\theta}{\lambda} + \xi.$$

The resultant voltage induced in B is therefore proportional to

$$E_H \sin \omega t + AE_H \sin(\omega t + \chi)$$

$$= E_H \sqrt{1 + A^2 + 2A\cos\chi}\;\sin\left(\omega t + \tan^{-1}\frac{A\sin\chi}{1 + A\cos\chi}\right). \quad \ldots \quad (7)$$

Now consider the aerial A. It is similarly affected except that the influence takes place a little later than that on B.

Path difference between the direct ray reaching A and that reaching B $= AB \sin\theta = d\sin\theta$, where $AB = d$. Hence the directly incident ray induces a a voltage proportional to

$$E_H \sin\left(wt + \frac{2\pi d \sin\theta}{\lambda}\right).$$

Similarly, for the reflected ray, the induced voltage is proportional to

$$AE_H \sin\left(\omega t + \frac{2\pi d\sin\theta}{\lambda} + \chi\right).$$

The resultant is :

$$E_H \sqrt{1 + A^2 + 2A\cos\chi}\;\sin\left(\omega t + \frac{2\pi d\sin\theta}{\lambda} + \tan^{-1}\frac{A\sin\chi}{1 + A\cos\chi}\right). \quad \ldots \quad (8)$$

Comparing (7) and (8), we see that, provided the nature of the ground is uniform in the vicinity of the apparatus and it is level, phase difference between the voltages induced in the two aerials depends only on the path inclination θ and the distance apart of the aerials. The amplitudes of voltages in both depend only on the horizontal component E_H and upon the nature of the ground. Thus the amplitude of the induced voltage in either of the aerials should be equal. Hence $E_h = E_v$ always, if the gains are once adjusted to be equal. The ellipse should be with its axes along 45°-135° axes and should change only its shape for changing ϕ but should not rotate The phase difference $\phi = \frac{2\pi d \sin\theta}{\lambda}$ can be measured straight away by the angle subtended at the end of the major axis by the minor axis.

We can have a single ray at a particular moment by transmitting short duration pulses from the transmitter, so that each component ray reaches the receiver at a different moment from the others. A multiplicity of ellipses will then be obtained, each ellipse corresponding to a definite angle of arrival θ.

It may be noted that change in the nature of polarisation or a sudden phase discontinuity or a gradual phase or amplitude change in the single incident ray will not make the ellipse to change its shape as the phase difference in the voltages induced depend only on the path inclination, In one experiment 7″ square condenser plates, 7″ apart, were used, and the plate current of the oscillating valves was 100 milliamperes, and the plate voltage 3000 volts.

RESULTS

Any object (metal, dielectric or electrolyte) produces a deformation of the field, and the nature of the deformation depends on the material. Low resistance materials attract the lines of flow to themselves, thereby, either strengthening the field through a given space, or weakening it, depending on how they are oriented with respect to the given space. If a needle is introduced into the field, the lines of electric displacement are concentrated near the pointed portion ; this causes considerable heating of the material surrounding the needle. This introduces a source of error when thermocouples are used for measurements in such fields.

An elongated ellipsoid, of dielectric constant 80, is placed in the field. If it is placed with its longer axis perpendicular to the plates of the condenser, the intensity within it was nearly that of the field. If it is placed at right angles to its previous position, it is found that the intensity within the ellipsoid is only $\frac{1}{40}$-th of what it was before. This shows clearly the important factor of the position and orientation of the object with respect to the field.

Lines of force, that enter a dielectric surface perpendicularly, go straight through. But, if they strike at another angle, they are refracted. In the case of a glass tube filled with the white of egg the way the lines of force are deviated is shown in the figure. In Fig. 1, for purposes of better comparison only the upper half of the glass tube is supposed to be filled with the dielectric, the lower half being empty. The lower half shows the normal lines of force while the upper half shows the effect of the dielectric. Coagulation of the egg albumen begins at A [Fig. 2(a)], then spreads quickly

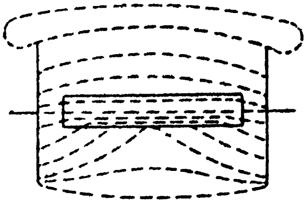

FIG. 1

FIG. 2(*a*)

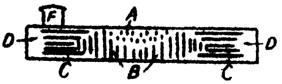

FIG. 2(*b*)

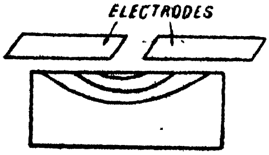

to B, then slowly to C while the ends of the tube remain cool. F is the funnel for filling and expansion. The explanation lies in the fact that additional lines of force from the total area of the electrode surfaces enter the tube along its whole length, from all sides, and so, increase the density of the lines of force at the centre. Removal of one electrode to a greater distance, or a change of size of one electrode, produces only a slight change in the site of the primary coagulation. Change of wave-length or of the intensity does not produce other behaviour except with respect to the time of coagulation, owing to the different intensities of the energy. This experiment shows the tendency of dielectrics to attract the lines of force, to refract and to conduct them, to produce different densities of energy at different distances from the electrodes. If the two plate-electrodes are placed in one plane, as shown in Fig. 2(b), coagulation of egg albumen in a flat dish occurs within 2 centimetres under or above the electrodes, starting between the electrodes. The coagulation forms quickly, but only near the electrodes' interspace ; there is no deep effect.

If the condenser plates are small enough, heat bands can be obtained in the interposed material. The field strength E is distributed in a fairly uniform manner under the electrodes, but outside them, its value falls off quickly. The production of heat at any point is proportional to the square of the field strength at the point, and the actual formation of a heat band depends on this relation. Now, since a longer time of heating will equalise a temperature gradient more readily than a shorter one, the production of local heat bands is associated with a rapid supply of energy, and this is supported by the fact that relatively long waves should always be used for the production of heat bands.

The efficiency of the supply of energy to a body in the field may be said to be equal to

$$\frac{\text{the energy absorbed by the body}}{\text{the total energy input}} \times 100.$$

The denominator is measured by a wattmeter in the input circuit. To measure the heat delivered to the substance, a calorimeter filled with an electrolyte of known specific resistance is used in the field. A preliminary test on the empty calorimeter is also made, in order to determine the amount of heating caused by its exposure to the field. A thermometer is not inserted into the solution until after the high frequency has been shut off, for the field will considerably affect the thermometer. It is found that roughly 20% of the available oscillatory energy enters the object between the plates.

EXPERIMENTS TO SHOW THE SELECTIVE HEATING EFFECTS IN A CONDENSER FIELD

In the following experiments, two six-inch condenser plates were used. An 8-metre wave with about 200 watts output was the source of energy.

(*a*) The condenser plates were placed ½″ from the sides of two concentrically placed beakers separated from each other by an air space, and kept in position by corks. The waves penetrated the glass of the beakers and lighted up a neon bulb in the interior of the inner beaker. If now the annular space between the beakers was filled with tap water, the neon bulb did not light up. The water gets heated, and appears to act as a shield to the waves.

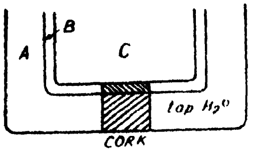

FIG. 3

(*b*) Three beakers are mounted concentrically as shown in figure 3. The space A contains 8½ ounces of tap-water, B contains air while C contains 2 ounces of tap-water. The space A is $\frac{9}{8}''$ broad, B is $\frac{1}{8}''$ broad, and the diameter of the beaker is $1\frac{7}{8}''$. The temperature of the water at the beginning of the experiment is 25°C. After exposure in the condenser field for 10 minutes, the temperature of the water in A rose to 28°·5 C., that in C remained at 25° C. Now the experiment was repeated with C filled with a three percent solution of potassium permanganate. The following results were observed :

Time in minutes	A_{H_2O}	C_{KMNO_4}
0	24°.5 C	23°.5 C
5	26°.0 C.	23°.5 C.
10	28°.0 C.	23°.8 C.

The slow rise in the temperature of C may be due to radiation from A.

Next, B was also filled with tap-water, and the experiment was repeated, with the following results :

Time in minutes	A_{H_2O}	B_{H_2O}	C_{KMNO_4}
0	25°.0 C.	25°.0 C.	24°.5 C.
2	25°.3 C.	25°.6 C.	27°.2 C.
5	25°.9 C.	26°.5 C.	31°.5 C.

The water in B heated up more than the water in A due to radiation and conduction from C. The solution in C is seen to be selectively heated.

(*c*) In this experiment the beaker C has 1¾ ounces of the solution, the test-tube B has a diameter of ¾″ and is 6″ long; the test-tube D has a diameter $\frac{9}{10}$″ and is 2″ long. Both the test tubes have the solution of permanganate. The height of the solution in B was 4½″, and that in D, 2″, the levels of the solutions in C, B and D, were below the level of the water in A. The beaker A was 4½″ in diameter, and the test-tubes will be ¼″ away from the wall of the beaker A distance of half an inch separated the beaker A from the condenser plates which were placed directly opposite the test-tubes. One would expect D to heat up most; actually it heated up least. One would also expect C to heat up least and B to heat up more than C, since it has a smaller quantity of liquid. The following were the results obtained.

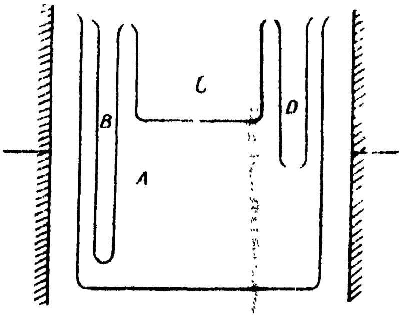

FIG. 4

Time in minutes	A	B	C	D
0	22°.5 C	22°.5 C.	22° 5 C.	22°.5 C.
5	23°.5 C	28°.0 C.	30°.0 C.	26°.5 C.
10	25°.5 C.	30°.0 C.	33°.0 C.	27°.0 C.

These unexpected results show the effect of cross-section on the heating values. C heats up most because it has a diameter greater than B or D.

(*d*) A capillary tube running parallel to the plates is attached at the middle of a larger tube placed perpendicular to the plates, and both are filled with solution. The contents of the capillary do not heat up at all. If, however, the same capillary tube be attached to the end of the larger tube, the contents of the capillary tube boil.

(*e*) Two tubes of different diameters are arranged concentrically and the middle tube has 0·2% solution of sodium chloride, while the outer tube has wax of low melting point. On applying a condenser field, and choosing a suitable wave-length, we can heat the middle tube with its solution without heating the wax. Thus this experiment shows that we have a means of producing heat under controlled circumstances, from within to the exterior of a body.

(*f*) In this experiment, 12 sheets of unglazed cardboard, each 1 mm. thick, 9″ long and 6″ broad, are in the condenser field as shown in Fig. 5. The condenser plates were ½″ away from each side of the bundle. A meter reading gave 5000 milliamperes as a measure of the floating energy in the homogeneous field between the plates. The cardboard sheets get heated all the way through. The diagram 5(b) shows the same bundle as in 5(a), but with the four central sheets moistened with 0·7% sodium chloride solution. The meter reading was now 3600 m.a. only. This shows that the rest of the energy has been absorbed in the better conducting part of the non-homogeneous medium. The waves used had a wavelength of 9.5 metres.

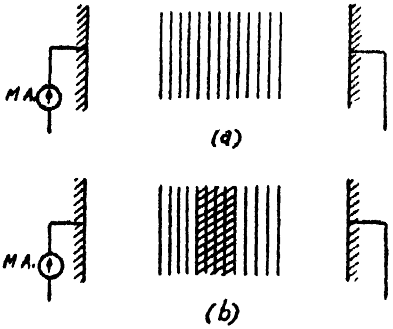

FIG. 5

SOME SPECIFIC EFFECTS OF A SHORT WAVE CONDENSER FIELD

(*a*) An emulsion of potassium hydroxide and paraffin oil, when exposed to a field, gives off steam after a time, while the temperature of the paraffin is only between 50 and 70° C. Carbon particles in the form of graphite heat up to the glowing point even when suspended in a liquid. These experiments show that the condenser field is capable of acting on the smallest particles in the field in preference to the surrounding medium.

(*b*) To an emulsion of animal charcoal and water, a small quantity of ether is added. In a condenser field one observes minute sparks in the emulsion. The ether adsorbed on the coal particles forms an insulating layer around them, between which are created strong tensions. This results in the sparking observed. This experiment shows that strong tensions may be developed in the interior of substances by the action of a short wave condenser field.

(*c*) Similar effects appear with colloidal particles. Electric charges on colloidal particles may sustain displacements through the forces of the condenser field. As the characteristics of colloids, especially the hydration of hydrophile colloids, depend to a great extent on the strength and distribution of the charges, changes in these peculiarities may be produced. These manifest themselves as changes of the electrical peculiarities, especially the capacity for conduction for high frequencies and the dielectric constant.

(*d*) Some chemical effects, such as the decolorisation of Pinocyanol, are also observed. Among other specific effects may be mentioned change of surface tension of solutions, and change in the structure of a membrane which may form on the surfaces of suspensions. The influence of the field depends on whether the field is normal to or runs parallel to the surface.

THE OPTIMAL HEATING EFFECT

If an electrolyte, say, a solution of salt is placed in a short wave condenser field, it is found that the amount of heat produced in it depends on the wave-length. The heating effect is a maximum for a particular wave-length, and decreases for longer or shorter wave-lengths. This optimal heating effect is connected with the specific resistance of the electrolyte and its dielectric constant. The relation is given by the formula $\lambda_m = \frac{dP}{6 \times 10^3}$, where λ_m is the wave-length in metres for maximum heating, *d* is the dielectric constant and P the specific resistance of the solution.

The following experimental results give an approximate verification of the above formula.

With a 7- metre wave, the maximum of heat was produced in the following solutions at the concentrations indicated.

Copper sulphate	0.35% solution
Zinc sulphate	0.35% ,,
Magnesium sulphate	0.3 % ,,
Sodium chloride	0.1 % ,,
Potassium iodide	0.25% ,,
Hydrochloric acid	0.02% ,,

With a 15- metre wave, the following results were obtained :—

Copper sulphate	0.15% solution
Zinc sulphate	0.15% ,,
Sodium chloride	0.05% ,,
Potassium iodide	0.1 % ,,
Hydrochloric acid	0.01% ,,

In each case, the rate of heating falls off abruptly with diminishing concentrations, and more gradually with increasing concentrations of the salt.

In order to study the heating of substances under identical physical conditions, the following was designed. The vertical metal rod of a kymograph was extended by a rod of hard rubber and, on the upper end, a cardboard disc with

6 holes was fastened in which 6 tubes were held. These tubes contained many different electrolytes. An alcohol thermometer graduated to $\frac{1}{5}$ degree was used. This apparatus was rotated between two condenser plates 5″ × 7″, at a speed low enough to enable readings of temperature to be taken for 10-30 minutes. The temperature-time curves appeared straight for a certain range but the steeper curves showed a tendency to flatten out after several minutes indicating heat loss by convection and radiation. The flatter curves tend to bend up suggesting indirect heating from the hotter tubes. Only points from the straight part of the curve were used for the evaluation of the subsequent results.

The table gives the values of the specific resistance, for the substances used in the 6 tubes :—

Substance	Specific Resistance in ohm/cm.
Distilled water	220,000
Colloidal gold, dialysed	10,300
Colloidal gold, undialysed	1,240
Gelatin	250
½ physiological saline	180
Physiological saline	71

Fig. 6 shows the curves discussed above.

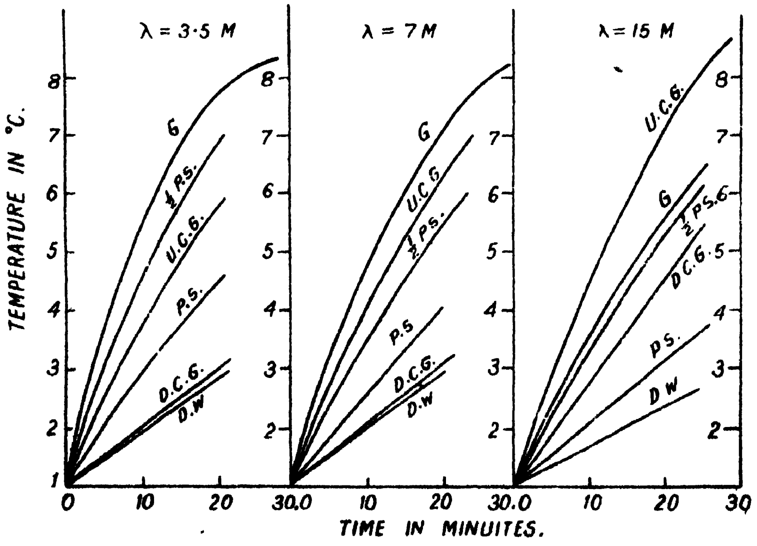

FIG. 6

Equal volumes of the above substances were exposed to the field of 3.5, 7, and 15 metres, in turn. The intensities were regulated so as to produce similar heating on an average. In order to eliminate as far as possible, the influence of the variations in the energy output in the field from one wave-length to another wave-length, all the figures can be referred to one standard, for example the heating of distilled water. In Fig. 7, the heat values at five-minute exposures have been selected as representing the part of the curve which is not influenced by the heat conductivity. The ordinate represents the ratio of the heating of each substance to that of the water. Therefore the water figure is always unity. It is evident from the graph that for gelatin and undialysed colloidal gold, a wave-length of 7 metres is optimal.

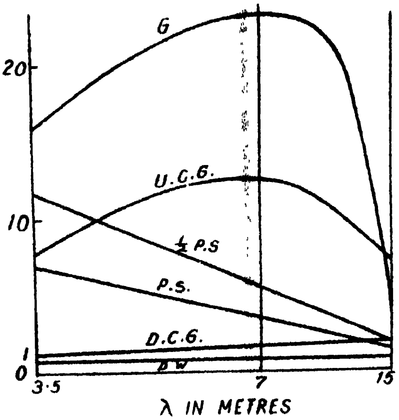

FIG. 7

Thus the heating rate of solutions of widely different salts under the same conditions is always identical when the electrical resistances were made the same by suitable selection of concentrations. Also, for any wave-length there is certain concentration for maximum heating. As the wave-length decreases, this maximum shifts to more concentrated solutions.

The heating depends on the electrolytic ions of the salts in the solution. Let us explain how this heating has maxima varying with concentration, and with orientation in space, of the substance. We picture solutions and suspensions as having electrically controllable particles. These migrate under the influence of a steady potential difference. They may be ions, molecules, colloids and even suspended matter. Undissociated salt molecules, and those colloidal particles whose natural charges are neutralised by adsorption of ions or of oppositely charged colloids are the exception to the general rule of electromigration and ionophoresis. By applying the static field at a given alternating frequency, we periodically induce electric charges which should call forth their counterparts at the extremities of the conductors in the vicinity. The point is that, in any case, this polarisation may be produced by either many ions moving a little or fewer ions moving more. When the e.m.f. is applied, as in the condenser field, the static state of equilibrium should be reached in a time proportional to the concentration of the ions. The heating effect is a measure of the work done in the solution in answer to the induced charges, and this work is a movement of the ions or the mobilised particles. For maximum heating, this work must be carried on during the whole of the half-cycle. If the frequency is so low that the induced charges build up equilibrium in a small part of each cycle, then there will be idle time within the cycle without heating. If, on the other hand, the resistance is too high (too few ions', the ions cannot build up the equivalent induced charge within a half-cycle and the energy used or the heating will be less than the maximum. Finally there will be one concentration for any given frequency in which the time period will be just sufficient to cause the ionic motion to be continuous during the entire period, and this will correspond to the maximum heat for that frequency.

THEORY OF THE VARIATION OF THE RESISTANCE OF A THERMIONIC VALVE WITH FREQUENCY

By S. R. KHASTGIR, D.Sc. (Edin.), Mem.I.R.E.

(Received for publication, April 21, 1941)

ABSTRACT Experiments of Mitra and Sil, performed some years ago, on the variation of internal resistance of a thermionic valve with frequency, showed that the internal resistance *decreased* gradually with the *decrease* of frequency in the high frequency range. With further *decrease* of frequency, however, they found that the internal resistance of the valve was *practically* constant. These measurements were recently extended to the lower frequency range by Kameswar Rao in this laboratory. Starting from a high frequency it was found, in substantial agreement with Mitra and Sil's results, that the internal resistance *decreased* steadily with the *decrease* of frequency, and that with further *decrease* of frequency, the internal resistance of the valve *increased* quite perceptively and steadily.

Mitra and Sil's theory of the variation of the resistance of a thermionic valve with frequency could very well explain the experimental results in the high frequency range but it cannot explain the observed *increase* of internal resistance of a valve with the *decrease* of frequency in the low frequency range.

In this paper an attempt is made to explain the observed variation of the internal resistance of a thermionic valve with frequency over a *wide* range of frequencies. While accepting Mitra and Sil's fundamental ideas as regards the conductivity of the valve due to the convection current, we have taken into account the conductivity arising from the displacement currents in interpreting the experimental results on the internal resistance of a thermionic valve.

An approximate mathematical theory of the variation of the internal resistance of a thermionic valve with the frequency of the field had been attempted by Hartshorn[1] some years ago. He showed that the internal resistance of a valve at very high frequencies when the displacement current would contribute almost entirely to the conductivity of the valve, should be slightly smaller than the value at very low frequencies, when the displacement current would be negligible and the voltage-gradient across the valve would be determined solely by the thermionic convection current. Later, Mitra and Sil[2] worked out a theory of the variation of the internal resistance of a thermionic valve with frequency and showed that their experimental results on the internal resistance of a valve were entirely at variance with Hartshorn's theory. Assuming a Maxwellian distribution of velocity of the electrons inside the valve they calculated

Communicated by the Indian Physical Society.

the time of flight of the electrons making certain simplifying assumptions and approximately obtained the values of the conductivity of the valve for different frequencies. These values calculated on their theory agreed well with those obtained by them experimentally in the high frequency range. Some measurements of the internal resistance of a valve were subsequently carried out by Kameswar Rao[3] in this laboratory over a wide range of frequencies. Starting from a high frequency it was found, in substantial agreement with Mitra and Sil's results, that the internal resistance of a valve decreased gradually with the decrease of frequency. With further decrease of frequency, however, the internal resistance of the valve was found to increase gradually. This latter result of Rao which has also been recently confirmed by a different method cannot be explained according to Mitra and Sil's theory.

The object of the present paper is to explain the observed variation of the internal resistance of a thermionic valve with frequency over a wide range. While accepting Mitra and Sil's fundamental ideas as regards the conductivity of the valve due to the convection current, we have taken into account the conductivity arising from the displacement currents in interpreting the experimental results on the internal resistance of a thermionic valve.

Mitra and Sil assumed that the electrons emitted from the cathode have a Maxwellian distribution of velocity. On applying an alternating field, the electrons are set into oscillatory motion which is super-imposed on their original Maxwellian velocity. It is possible that under the influence of this field, for one half of the alternation, the electrons will be able to strike the anode of the valve giving up both their kinetic energy and charges. For just reaching the anode under the applied field of frequency $\left(\frac{1}{2T}\right)$ at the end of the interval T, there must be a critical velocity v_0 with which the electrons must be moving initially. All the electrons which have been moving with velocities greater than this critical velocity v_0 at the instant when the field has begun to act would also reach the anode within the interval T. The conductivity for a particular frequency $f=\frac{1}{2T}$ would then be proportional to $\left(\frac{n.T}{T}\right)$ where n is the number of electrons having velocities within the range v_0 to ∞ and reaching the anode surface within the time interval T.

Now with a Maxwellian velocity distribution, the number dN of electrons per unit volume having normal velocity components between v and $v+dv$ is given by

$$dN=N.\sqrt{\frac{m}{2\pi kT}}\,.\,e^{-\frac{mv^2}{2kT}},$$

where N is the number of electrons per c.c., T the temperature of the emitting cathode, k = Boltzmann's const. and m = the mass of an electron. Thus the number of electrons that escape from unit surface in unit time is

$$n=\int_{v=v_0}^{v=\infty} v.\,dN \quad = N\sqrt{\frac{m}{2\pi kT}}\int^{\infty} e^{-\frac{mv^2}{2kT}}\,dv$$

$$=N\sqrt{\frac{kT}{2\pi m}}\,.\,e^{-\frac{mv_0^2}{2kT}} \qquad (1)$$

If x is the distance between the anode and the cathode and f the frequency of the applied field, then the initial velocity v_0 with which the electrons would move to reach the anode (after an interval of time corresponding to the frequency) would be given by

$$v_0=2xf.$$

Thus (1) can be written as

$$n=N\sqrt{\frac{kT}{2\pi}}\,,\,e^{-\frac{2x^2f^2}{kT}} \qquad (2)$$

It is therefore evident from (2) that the conductivity of the valve would decrease gradually with the increase of frequency. This conclusion is based on the supposition that the electrons in the inter-electrode space move *only in the positive direction, i.e., towards the anode surface*. Considering the electrons which move inward towards the cathode and which may reach the anode under the influence of the positive field developed between the grid and the cathode due to the impressed *e.m.f.*, between the grid and the plate, Mitra and Sil found on *calculation* that for time-intervals greater than that corresponding to 36 metres, the number of electrons reaching the anode under the action of applied E.M.F. remained unaltered. Thus according to their calculation the conductivity should be independent of frequency for frequencies lower than that corresponding to 36 metres and it would decrease gradually with the increase of frequency *only in the range of the higher frequencies.*

This latter part of the calculation does not, however, apply to the experiments, where the anode is given a high voltage with respect to the cathode so that practically *all* the electrons move towards the anode. Theoretically, therefore, we would expect a continuous decrease of conductivity with the increase of frequency even for the lower frequencies. There is, however, an important factor which should be taken into consideration. In the Maxwellian distribution of velocity, there must be a lower limit u_0 which is the velocity component normal to the surface necessary for the electrons to escape from the cathode. In that case it is evident that the number of electrons reaching the anode will assume a constant value, when the frequency ($1/2T$) is reduced to such an extent that the initial velocity of the electrons which would carry them to the anode in time

T becomes the same as u_0. According to this idea, therefore, the conductivity of the valve would remain constant for frequencies lower than a certain value corresponding to the limiting velocity u_0 of the electrons. This limiting velocity u_0 would be given by

$$\frac{e\phi}{300} = \tfrac{1}{2} m u_0^2$$

where ϕ is the work function (in volts) of the material of the cathode and e and m are the charge and mass of an electron. The frequency corresponding to the limiting velocity u_0 would then be given by

$$f_0 = \frac{1}{10x} \cdot \sqrt{\frac{e\phi}{6m}} \qquad \dots \quad (3)$$

where the inter-electrode distance x is equal to $\left(u_0 \times \frac{1}{2f_0} \right)$.

The conductivity arising from the convection current only has been considered so far. We shall now determine the conductivity due to the displacement currents which can only be neglected for extremely low frequencies. If v is the sinusoidal potential difference across the anode and the cathode, and E the electric field intensity at a point in the electronic medium of dielectric constant ϵ inside the valve then the displacement current-density would be given by

$$i_d = \frac{\epsilon}{4\pi} \frac{dE}{dt} = -\frac{\epsilon}{4\pi} \frac{d}{dt} \left(\frac{dv}{dx} \right).$$

For low frequencies when all the electrons having velocities from u_0 to ∞ would reach the anode, there would be no space charge, so that the voltage-gradient at any instant would remain constant. We can therefore write

$$\frac{dv}{dx} = a.\sin \omega t,$$

where a is a constant and ω the angular frequency of the voltage.
Thus

$$i_d = \frac{\epsilon}{4\pi} \omega a \cos \omega t = A \cos \omega t \text{ where } A = \frac{\epsilon\omega.a}{4\pi}$$

Consider now a small cylindrical element of the current-path between the anode and the cathode. Let the length of the element parallel to the direction of the current be dl and the cross-section perpendicular to the current path be da. If σ_d is the specific conductivity due to the displacement currents, the power dissipation in this small element is given by

$$(i_d.\, da)^2. \left(\frac{1}{\sigma_d} . \frac{dl}{da} \right) = \frac{i_d^2}{\sigma_d} (dl.\, da)$$

when averaged over one cycle, the power dissipation in the element is

$$dP = \bar{i_d^2} \cdot \frac{dl.\, da}{\sigma_d} = \frac{A^2}{2\sigma_d} \cdot (dl.\, da). \qquad \ldots \quad (4)$$

The power dissipation can also be written as

$$dP = \sigma_d \cdot \bar{E^2} \cdot dl.\, da = \sigma_d \cdot \frac{a^2}{2} \cdot (dl.\, da) \qquad \ldots \quad (5)$$

since $$E = -\frac{dv}{dx} = -a \sin \omega t.$$

Hence from (4) and (5)

$$\sigma_d = \frac{A}{a} = \frac{\epsilon \cdot \omega}{4\pi}. \qquad \ldots \quad (6)$$

We know, however, that the dielectric constant ϵ of the electronic medium increases with the increase of frequency. It was shown by Khastgir and Chowdhury[4] that the value of $(1-\epsilon)$ varied inversely as the square of frequency. Even if ϵ were regarded as constant, the conductivity σ_d due to the displacement currents would steadily increase with the increase of frequency. When the frequency exceeds the limit defined by (3), it should be remembered that the conductivity due to the convection current would no longer remain constant but would begin to decrease steadily with further increase of frequency. The experimental results on the conductivity of a valve for a wide range of frequencies can therefore be explained.

It will be interesting to obtain from (3) an approximate estimate of the frequency which corresponds to the limiting velocity u_0 of the electrons from the cathode. Let us take $\phi = 1$ volt for the oxide-coated tungsten cathode. If now the inter-electrode distance x be .3 cm, the frequency f_0 will be about .3 megacycles, *i.e.*, the wavelength will be about 30 metres. If $x = .5$ cm. the wavelength will be about 45 metres. Rao's experiments with a Telefunken valve showed that the turning point in the conductivity curve occurred at about 1600 *kc.*, *i.e.*, when the wavelength was about 180 metres. The observed turning point therefore appeared definitely at a lower frequency than what would be expected from (3). The equation $e\phi = \frac{1}{2} m u_0^2$ from which (3) is derived is, however, based on classical ideas. The results should be reviewed in the light of modern views of electron emission from metals.

DACCA UNIVERSITY

REFERENCES

1 L. Hartshorn, *Experimental Wireless and Wireless Engineer*, VIII Aug, 413 (1931).

2 Mitra and Sil, *Phil. Mag.*, xiii, 1081 (1932).

3 Kameswar Rao, *Ind. Jour. Physics*, June (1940).

4 Khastgir and Chowdhury, *Ind. Jour. Physics*, June (1940)

PROPAGATION OF SUPERSONIC WAVES IN LIQUID MIXTURES AND INTERMOLECULAR FORCES*

I. ALCOHOLS IN WATER

By RAM PARSHAD, M.Sc.

(*Received for publication, April 24, 1941*)

ABSTRACT. In this paper is reported measurements on supersonic velocities, and compressibilities of mixtures of alcohols and water. Some quite new results are obtained. The velocity concentration curves show maxima and compressibility concentration curves show minima.

For the first time the theory of molecular force fields has been applied to sound problems and is first shown why the compressibilities are always lower than expected in ideal cases and later quantitative treatment is given whereby the percentage of the mixtures for minima of compressibilities is calculated.

In the case of methyl and ethyl alcohols in water the agreement between theory and experiment is good, whereas in propyl alcohol-water mixture there is a signifiaant divergence between the two values. This divergence has also been explained.

The basic idea employed in the above treatment is that though both the alcohols and water are associated liquids, but when they are mixed, they destory each other's associations and a random motion and distribution of molecules prevail.

INTRODUCTION

The case of liquid mixtures is an important study in theory of liquids. Much work has been and is being done in various branches, *e.g.*, dielectric polarisation, heat of mixing, solubility, partial pressures, infra-red absorption spectra, but as yet we are far from any final solution of the problem. The determination of velocities and hence the compressibilities of the mixtures is expected to throw appreciable light on the state of cohesion as a function of molecular fields of liquids and also the structure of molecules as derived from the resulting intermolecular action.

Wilson and Richards[1] and Parthasarathy[2] have reported some observations on supersonic velocities and compressibilities of mixtures, without, however, any basic attempts at an explanation of their results.

We report, in this paper and in the following ones, investigations on various classes of mixtures. Some very new and interesting results have been found. In mixtures of alcohols and water there are maxima of velocity and minima of compressibility. In other mixtures have been found minima of velocity and points of inflection.

---

* Communicated by Indian Physical Society.

In this paper and the succeeding, attempt is made to explain and discuss the results obtained by the author as well as those obtained by other workers.

EXPERIMENTAL

The well-known Debye-Sears method of diffraction of light by supersonics which has been set up in this laboratory by Dr. A. K Dutta was employed to find the velocities. The green light of 5460 Å of mercury was used and the supersonic vibrations as obtained by means of a quartz crystal of frequency 3×10^6 cycles connected to the output of a suitable valve-transmitting circuit were used to produce the diffraction pattern. The quartz was always immersed in a constant liquid (xylol) and the vibrations to the liquid under investigation were transmitted through a mica window.

Great care was taken in temperature control. Round the vessel containing the liquid-mixtures and the oscillating quartz immersed in the xylol bath, was a water-bath, which was stirred continuously by a motor-driven stirrer and this bath contained a thermostat to keep the temperature at any constant value above the room temperature. The temperature was read by means of a mercury thermometer graduated to tenth of a degree. The maximum departure in rare cases from the constant value might be taken as .05°C, which however is far below the value which might in any way tend to vitiate the results. In general the maximum departure was .02°C. The spectra were photographed and measurements were made by means of Hilger comparator, reading accurately to 10^{-4} cms, of as many orders as possible and then the length of separation of the first order was deduced.

Two independent observations were taken for each mixture and in each observation three photographs were taken. The absolute velocities in the mixtures were found by comparing with the velocity in water. The velocity in water at the paticular temperature was taken from a graph plotted from the values of velocities at different temperatures for water taken from Handbuch des Experimental-physik, Vol XVII.

The velocity in any mixture was then found very simply by

$$\frac{V_m}{V_w} = \frac{d_w}{d_m}$$

where V_w is velocity in water,

V_m ,, any mixture,

d_w is length of separation of 1st order spectrum in water,

d_m is length of separation of 1st order spectrum in the mixture.

The adiabatic compressibilities of the mixtures were found from the relation,

$$V = \sqrt{\frac{1}{\beta\rho}}$$

where V is velocity in centimeteres per second,

ρ is density in gms. per c.cm..,

β is adiabatic compressibility in absolute units.

EXPERIMENTAL RESULTS

TABLE I

Liquid Ethyl Alcohol and Water

Temperature 32°.60C

No.	Volume % of alcohol in total of mixture	Density (gm./cc.)	Velocity (metre per sec.)	Adiabatic compressibility × 10^{-6}
1	0	.995	1508	44.2
2	10	.987	1557	41.8
3	25	.968	1606	40.1
4	50	.9235	1508	47.6
5	75	.862	1334	65.2
6	90	.819	1225	81.4
7	100	.782	1138	98.8

TABLE II

Liquid Methyl Alcohol and Water

Temperature 26°.00C

No.	Volume % of alcohol in total of mixture	Density (gm./cc.)	Velocity (metre per sec.)	Adiabatic compressibility × 10^{-6}
1	0	.9968	1500	44.59
2	18.6	.9700	1563	42.25
3	32.55	.9508	1573	42.47
4	46.5	.9263	1531	46.10
5	65.1	.8879	1423	55.58
6	80.55	.8496	1305	69.11
7	93	.8021	1153	93.65

TABLE III

Liquid Propyl Alcohol and Water

Temperature 26°.00C

No.	Volume % of water in total of mixture	Density (in gms./cc.)	Velocity (metre per sec.)	Adiabatic compressibility × 10^{-6}
1	50	.9241	1459	50.86
2	60	.9417	1502	47.11
3	70	.9588	1552	43.28
4	80	.9749	1592	40.46
5	90	.9855	1558	41.82
6	100	.9968	1500	44.50

atom, that this second electron begins to move in phase with the first, and as result attraction ensues.

The specific formulae for this mutual interaction energy, giving its numerical value, have been calculated for a very small number of only simple atoms or molecules, notably helium. The formula in its simplified and approximate form is

$$E = -\frac{3}{4} \cdot \frac{\alpha^2 V}{R^6}$$

where E is interaction energy,
α is polarisability,
R is distance between two interacting molecules,
V is excitation potential and may be taken as the ionisation potential.

For two different molecules

$$E = -\frac{3}{4} \cdot \frac{\alpha_1 \alpha_2 V}{R^6} \, .$$

Induction forces:—If one molecule is unsymmetrically charged, *i.e.*, is a permanent dipole, then the field produced by it on another molecule or part of it so deforms its electronic configuration that it becomes an 'induced' dipole of magnitude $M = -\alpha F$ where F is the field of the inducing molecule and α (a constant) is the polarisability of the induced molecule. The approximate formula for interaction is

$$E = -\frac{2\alpha\mu^2}{R^6}$$

where μ is permanent dipole moment of the molecules.

If the two molecules are dissimilar of moments μ_1 and μ_2 and polarisabilities α_1 and α_2 then

$$E = -\frac{1}{R^6}\left[\alpha_1 \mu_2^2 + \alpha_2 \mu_1^2\right].$$

Orientation or Keesom forces:—Two molecules having permanent dipoles are so orientated under their mutual action that their potential energy becomes negative, *i.e.*, they tend to attract each other. The formula for the potential energy is

$$E = -\frac{2}{3}\,\frac{\mu^2}{R^6} \cdot \frac{1}{RT} \quad \text{for } kT >> \frac{\mu^2}{R^3}$$

and

$$E = -\frac{2\mu^2}{R^3} \quad \text{for } \frac{\mu^2}{R^3} >> kT$$

where K is Boltzmann's constant and T absolute temperature. For unlike molecules of moments μ_1 and μ_2 the corresponding formulae become

$$E = -\frac{2}{3} \cdot \frac{\mu^2 \mu_2^2}{R^6} \cdot \frac{1}{kT} \quad \text{and} \quad E = -\frac{2\mu_1\mu_2}{R^3}.$$

Now it is clear from the above formulae that all the type of forces are extremely short-range ones. In liquids, therefore, where the distance among the atoms of different molecules are comparable to the length of dipoles, it is misleading to think of Keesom forces in terms of the total dipole moment of a molecule or molecules. It is imperative to consider the individual dipoles of a molecule, their moments and their positions with respect to the whole molecule. For example in *p*-dichlorobenzene, the net dipole moment is zero but actually there are two strong dipoles *c*−*d* which will play an important part in intermolecular forces.

Again, ethers, esters, nitrobenzene are all polar having quite large moments but still have not much Keesom energy due to the dipoles being effectively screened. In alcohols the O—H dipole has a dipole moment of 1 >D (much less than of nitrobenzene 4 D) and is on the surface of the molecule. Due to these reasons alcohols have large Keesom or orientation energy and in fact their pronounced association is due to the great activity of their dipoles.

In water, the dipole energy contributes nearly the whole of energy due to the special structure of its molecule. The molecule has two dipoles, open on both the sides for strong intermolecular action.

Cohesive energy and compressibility.—It can be seen from simple considerations that cohesive energy and compressibility are inversely related.

The kinetic energy of molecules due to temperature tend to make the molecules fly apart, while the cohesive energy tend to knit them as close as possible.

(*Note*.—We will neglect the repulsive energy which has also been recognised, due to it being an extremely short-range one, *i.e.*, falling off with about 11th or 12th power of the distance.)

The molecules will come in a dynamic equilibrium position where the potential energy is minimum. The greater the cohesive energy the nearer the molecules will be in their equilibrium position. Since the cohesive energy falls off inversely as the distance, in fact with inverse sixth power of the distance, the nearer the molecules in equilibrium the more rapid will the energy change on either side of this position. This indicates that the higher the cohesive energy the more difficult it will be to move a molecule from its equilibrium position and accordingly the compressibility will be low. To put it in other words, the higher the cohesive energy, the higher the internal pressure, and from this view point the compressibility naturally becomes small.

In fact, Bridgman [6] has actually found that liquids of high cohesive energy, *e.g.*, for glycols, and glycerols (due to their independent OH dipoles) the compressibility is extremely small.

COMPRESSIBILITY AND NATURE OF MIXTURES

If the two unlike molecules are otherwise similar in shape and structure, the compressibility change with change in the composition is expected to fall along the graph for the ideal law for mixtures, *i.e.*, all the points on the graph representing the compressibilities of the different compositions of a mixture will lie on the straight line joining the two points corresponding to the compressibilities of the two pure liquids.

The departure from the ideal case can occur in the following cases:

(1) The molecules have very different shapes, so that the forces between them cannot be taken as the average or geometrical mean of the forces between like molecules.

(2) The two unlike molecules break up the associations that were present in the pure liquid, or form associations of their own.

(3) The two liquids have different magnitudes of contributions to the different kinds of energies making up the total cohesive energy, *e.g.*, in a mixture of polar and non-polar liquid.

In the present state of knowledge of molecular forces which is very approximate, it is not possible to treat our problems quantitatively except in a few special cases, *e.g.*, the case of alcohols and water in this paper.

MIXTURE OF ALCOHOLS AND WATER

As has already been mentioned, both alcohol and water molecules have O—H dipoles and their positions with respect to the shape of the molecules is such that their field is very great for intermolecular action. Due to their active dipoles, the two liquids in their pure forms are highly associated. It is more so in water than in alcohol due evidently to there being no chain as in the latter. The existence of association has been directly shown by infra-red absorption spectra, [7,8,9,10] by dielectric polarisation measurements[11] and by X-ray measurements.[12]

Now any associated group will have its component molecules so orientated relatively, that their net dipole moment for outside field is very small, tending to zero. The associated group will be well knit up in itself, difficult to break up, and there will not be much interaction energy among the different associated groups. In sound wave propagation it is the associated groups as a whole that move to and fro, and so the compressibility measured in our case is that related to cohesive forces among the associated groups as a whole and also among those molecules which are free. If the associated groups are broken up by some means, the individual dipoles wlll be free creating a strong intermolecular field and low compressibility.

Now as water and an alcohol are mixed, the associations in both the liquids are broken up and there prevails random distribution. The evidence for this has been deduced from the following cases:

(1) The partial vapour pressures of the components of water-alcohol mixtures were determined by Martin and Brown.[13] Raolt's Law for ideal mixtures (*i.e.*, where there is random motion and distribution of the molecules) was found to hold for nearly the whole range of concentrations, the divergence being in very dilute aqueous solutions. At this extreme end, water was supposed to have the sub-crystalline structure, but otherwise there was evidence of complete random distribution.

(2) *Dielectric polarisation.*—Wyman [14] investigated the dielectric polarisation of ethyl alcohol-water mixture and found that the additivity rule held throughout all ranges of concentration. Now this can be so if the constituent dipoles contribute to the total polarisation, independently of the presence of other dipoles. Hence in these mixtures there is completely random distribution of molecules.

(3) *Spectroscopic evidence.*—It has been established that in associated polar liquids like water depolymerisation is produced by heating the liquid. On depolymerisation the infra-red or Raman frequencies of the O-H bands are shifted to a higher value. For water-alcohol mixtures the evidence is meagre. However, Bars and Cranen[15] have shown in rather a rough way that the water band is shifted to a higher frequency on mixing it with alcohol. They took two percentages 50% and 25% of alcohol by volume in water and found that the shift is maximum for 25% mixture. The exact interpretation of this result may not be forthcoming yet but it shows in a qualitative way that depolymerisation is produced.

(4) Butler, Thomson and Maclennan[16] measured the partial vapour pressures of aqueous solutions of homologous aliphatic alcohols and attempted to account for the main features of the behaviour in terms of the cohesive energy between the molecules. Langmuir, by using his postulate of "principle of independent surface action,"[17] has shown how the intermolecular energy in a liquid can be obtained by summing the interfacial energies of the various surfaces of contact of the molecules.

On the assumption that the molecules are distributed entirely at random, he obtained for a binary solution of two substances A and B an equation for activities:

$$\log f_A = \frac{\beta^2 S_A \phi}{kT} \quad \text{and} \quad \log f_B = \frac{\alpha^2 S_B \phi}{kT}$$

where S_A and S_B are the surface areas of molecules A and B respectively, α and β their surface fractions in the solution, f_A, f_B their activities, and ϕ the "mixture energy." By the mixture energy ϕ is meant the work done to bring a molecule A from its pure liquid into the pure liquid of B, or to bring the molecule B from its pure liquid state into the pure liquid of A.

The above equation accounted for not only the main difference between one alcohol and another, but also for the variation of the activity coefficients over the greater part of the range of concentrations. The divergence from the equation which occur in very dilute aqueous solutions may be due to the failure of the assumption of an entirely random distribution and orientation of molecules in these solutions. Hence we can consider that in a mixture of alcohols (particularly lower alcohols) and water, the molecules are all randomly distributed, that is, there is no grouping in any of the constituents.

Now Butler[18] in connection with a paper on entropies and heats of hydration of alcohols has obtained the energy of binding of a water molecule to another water molecule as also to OH or CH_2 groups, etc. of an alcohol molecule. As this energy relationship is required in later work, this is given here in some detail. Starting from Langmuir's[17] principle of independent surface action in solutions and Bernal and Fowler's[19] thesis of pseudo-tetrahedral structure of water molecules, he considers that when a solute molecule has to be introduced in water, a cavity has to be made large enough to hold the water molecule and then the solute molecule can be introduced in that cavity. Considering only the forces between adjacent molecules the energy ϕ required for introduction may be put as

$$\phi = \frac{n}{2}\, \gamma_{W-W} - \Sigma\, a\, \gamma_{A-W}$$

where γ_{W-W} is the energy required to separate a single pair of water molecules and n is the total number of water molecules thus separated, γ_{A-W} is the energy of interaction of the group A in the solute molecule with an adjacent water molecule and '*a*' is the number of water molecules adjacent to the group.

Thus one can write

(1) $\phi_{CH_4} = 2\gamma_{W-W} - 4\gamma_{CH-W}$

(2) $\phi_{C_2H_6} = 3\gamma_{W-W} - 6\gamma_{CH-W}$.

From these one obtains

(3) $\phi_{CH_2} = \phi_{C_2H_6} - \phi_{CH_4} = \gamma_{W-W} = 2\gamma_{CH-W}$

where ϕ_{CH_2} represents the energy of solution for the CH_2 group only. Knowing the experimental value for the heat of hydration of methane and ethane this was obtained by Butler as $\phi_{CH_2} = -1.58$ k.cal. The value of γ_{W-W} can be easily obtained from the heat of vaporisation of water. This is 10.5 k.cal. at 25°C. Since the removal of a water molecule from its surroundings means the breaking up of 4W—W bonds (water having a tetrahedral structure), and since these four broken water linkages will reunite in 2W—W bonds again, the heat of vaporisation being the difference of energy in the two cases is equal to $2\gamma_{W-W}$. Thus the value of γ_{W-W} is obtained as 5.25 k.cal. Putting this value of γ_{W-W} in equation (2) or (3) and considering the experimental values of $\phi_{C_2H_6}$ and ϕ_{CH_2} one obtains the value of $\gamma_{CH-W}=3.36$ or 3.42 which agree fairly well. The agreement shows that this method of calculation of the bond energy is tenable.

Butler then obtained the energy values of γ_{OH-W} by considering the case of ethyl alcohol. One can consider

$$\phi_{C_2H_5OH}=4\gamma_{W-W}-5\gamma_{CH-W}-3\gamma_{OH-W}\,.$$

Putting the values of γ_{W-W} and γ_{CH-W} obtained before and the experimental value of $\phi_{C_2H_5OH}=12.88$ k.cal., one finds $\gamma_{OH-W}=5.6$ k.cal.

Thus the value of γ_{OH-W} is greater than that of γ_{W-W}.

This leads to the conclusion that the OH group of alcohols have got greater attraction for water molecule than the mutual attraction between two water molecules themselves. The alcohol molecules can therefore break up the water associations. Consequently the cohesive energy increases by the addition of water to alcohol. Hence the compressibility curve should always lie below the straight line corresponding to the linear law.

Considering the equation

$$\phi_{CH_3OH}=3\gamma_{W-W}-3\gamma_{CH-W}-3\gamma_{OH-W}$$

we find

$$3\gamma_{W-W}=5.25\times 3=15.75 \text{ k.cal.}$$

$$3\gamma_{CH-W}+3\gamma_{OH-W}=3(3.36)+3(5.6)=26.88 \text{ k.cal.}$$

This shows that cohesive energy is increased when a molecule of methyl alcohol is introduced in water and gets surrounded by 6 molecules of the latter. From the molecular weights of CH_3OH and H_2O and their densities at the required temperature, the volume percentage of methyl alcohol required for the least compressibility of water-alcohol mixture can be calculated. In this case we require six molecules of water for each molecule of $CH_3.OH$.

Similar calculations can be made for ethyl and propyl alcohols. A comparison of the calculated and experimental values is shown in the next table.

Alcohol	Ratio of molecules of alcohol to those of H_2O	Weight percentage of alcohol	Volume percentage of alcohol calculated	Volume of alcohol observed
Methyl		22·9	27 3	26-27
Ethyl		24·2	29·3	28-29
Propyl		25	28·8	19

The results show that for methyl and ethyl alcohols, there is close agreement between the calculated and the observed values, while for propyl alcohol there is an appreciable departure to the extent of about 10%.

The agreement in the case of the first two alcohols shows that the basic postulates (*viz.*, Langmuir's principle of independent surface action and Bernal and Fowler's thesis about structure of water) for the energy equation are sound and that the reason for the departure in propyl alcohol-water solution must be looked for in some other direction.

Now the volume computation from the energy equation

$$\phi_{C_3H_7OH} = 5\gamma_{W-W} - 7\gamma_{CH-W} - 3\gamma_{OH-W}$$

is based upon the obvious assumption that each molecule of the alcohol is surrounded by ten molecules of water, that there are no other molecules of water which do not surround any of the alcohol molecules, and that the alcohol molecules do not aggregate.

If there is some sort of aggregation of alcohol molecules the volume computation must fail. The following is meant to show how far we can depend upon the assumption of non-aggregation of alcohol molecules. Considering pure alcohols we find that as the chain length increases, their viscosities increase and solubilities in water decrease. This has been recognised as due to increasing chain to chain aggregation of alcohol molecules with increasing chain length for it leads to lowering of potential energy. When these alcohols are added to water, the tendency of chain to chain contact will detract from the degree of solubility. Also as has been seen $\gamma_{CH-W} = 3.25$, $\gamma_{W-W} = 5.2$ k.cals, showing that CH groups tend to remain away from water, *i.e.*, are hydrophobic. This property of CH groups is well known in the investigation of behaviour of layers on water of insoluble alcohols. In the smaller chain alcohols the hydrophilic power (water-attracting powers) of OH groups predominates and they are therefore highly soluble and in the higher chain alcohols, the hydrophobic powers of the CH groups predominates, leading to aggregation of the alcohols in water, with consequential decrease of solubility. We can expect on these grounds that as the chain length increases, the departure in our calculations and in others (*e.g.*, on solubility) will be comparatively sudden, for by the addition of a single CH_2 group the alcohol as a whole may be changed from hydrophilic to hydrophobic, the non-aggregation giving place to aggregation. Bury and Hartley [20] have investigated the phenomena of micellar aggregates in aqueous solutions. Their results indicate that clustering of fatty acids and alcohols seems to begin at butyric acid and alcohol. In our case it seems to begin even at propyl alcohol.

Again the halogen alkyl amines $Cl{\cdot}CH_2{\text -}(CH_2)_{n-2}-CH_2-NH_2$ are liquids miscible with water. The lower members of this series are completely miscible. Solomon [21] has found that whereas for $n=5$ the solubility certainly exceeds 1 mol/litre, it drops by more than two hundredfold (solubility .005 mol/lit.), when $n=6$. The author tries to interpret this observation by the aid of Langmuir's principle. For $n=5$, the hydrophilic power of the amino group preponderates as opposed to the hydrophobic power of the alkyl residue but when $n=6$, this is no longer the case.

Hence it is not surprising (on the other hand expected) that we have a parallel sort of date in compressibilities. Up to ethyl alcohol the energy equation used gives accurate results, but in the next higher (*i.e.*, propyl) alcohol, the calculated percentage of alcohol for minimum compressibility is too high.

We can reason out the difference in behaviour of methyl and ethyl alcohols from the propyl, by also considering their molecular structures.

Methyl alcohol (CH_3OH) cannot be taken as a chain compound at all. It may be thought of as derived from methane CH_4 by the substitution of one H by OH. Now CH_4 is tetrahedral in shape due to the tetrahedral character of the carbon valencies and CH_3OH may be taken on the whole to be of the same structure. Due to the tetrahedral sort of structure of water, any foreign molecule or ion tetrahedral in shape will fit in better in the structure of water than that of any other shape. Frank [22] has shown from entropy considerations that ions NH_4^+, SO_4^- fit in the structure of water while NO_3^-, Cl^-, Br^-, etc., do not.

So, although the CH groups are hydrophobic, but due to the tetrahedral shape of the molecules, they will nevertheless interact with water efficiently and due to this and the fact that the hydrophilic power of OH group is comparatively strong, and that there is little or no chain character, there will be no tendency for chain-to-chain aggregation. In this case energy equation will yield the correct percentage of alcohol.

In ethyl alcohol $CH_3.CH_2.OH$, a chain has been formed but the CH_3 group as a whole may be taken tetrahedral in character and so able to interact with water. The two CH's of CH_2OH will interact with water due to the following reason :—

The group CH_2OH as a whole may be taken as conforming to the tetrahedral sort of shape, being derived from CH_3.

Due to the above and also because the chain length is not big after all, there will be no tendency for aggregation and the energy equation will give the right percentage.

With propyl alcohol the picture is different. In $CH_3.CH_2.CH_2OH$, the CH_3 and CH_2OH will behave as before but the middle group CH_2 isolated as it is from the influence of OH and not tetrahedral in shape, will show little tendency to react with water due to its inherent hydrophilic nature. Due to this significant reason, and that the chain length has increased, there will be a suddenly increased tendency to self-aggregation.

This sudden difference of behaviour of propyl alcohol from that of lower alcohols has been reflected in our compressibility data by the abrupt deviation between the ideal calculation and observation.

The energy equation shows, as has been said somewhere before, that the cohesive energy increases as a molecule of alcohol is introduced and gets surrounded by water molecules. So, we have the conclusion that the cohesive energy will be the greatest, when there are the greatest number of alcohol molecules such that each molecule of alcohol is completely surrounded by 10 water molecules, at the same time the distance between the alcohol molecules being sufficient so that they may not be expected to stick together in aggregation. The ideal computation, *i.e.*, 30% of alcohol, corresponds to the case when the alcohol molecules, are just separated from each other by these surrounding water molecules, and that there are no excess molecules of water not occupied in surrounding alcohol molecules. Since this behaviour (*i.e.*, non-aggregation) is not expected to hold for this high percentage, on the grounds presented above, the percentage volume of alcohol must be reduced till it is just sufficient to keep the molecules of the alcohol in non-aggregation. At this lower percentage then (*i.e.*, 19% in the actual case) one will have the minimum compressibility.

After the results had been obtained, the author came across two papers, [23,24] where velocities in ethyl alcohol water mixtures are measured. The results, however, were given without any attempt at theoretical treatment.

In conclusion, I tender my grateful thanks to Dr. A. K. Dutta for discussions and valuable suggestions.

I am obliged to Prof. D. M. Bose for his allowing the facilities and for the favour of very useful discussions and suggestions.

BOSE RESEARCH INSTITUTE,
CALCUTTA

REFERENCES

[1] Wilson and Richards, *J. Phy. Chem.*, **36**, 1268 (1932)
[2] Parthasarathy, *Proc. Ind. Acad. Sci.*, **3**, 297 (1936).
[3] London, *Trans. Farad. Soc.*, **1**, 8 (1937).
[4] Margenan, *Rev. of Mod. Phys.* (1938)
[5] Lennard Jones, *Proc. Phys. Soc.*, **43**, 461 (1931).
[6] Bridgman, *Rev. of Mod. Phys.* (1935).
[7] Errera, *Physica*, **1**, 1097 (1937).
[8] Errera and Mollet, *Nature*, **138**, 882 (1936).
[9] Fox Errera, Sack and Gaspart, *J. Chem. Phys*, **8**, 63 (1940).
[10] Errera, Bosschletez and Gaspart, *Physica*, **5**, 115 (1938).
[11] Wolf, *Trans. Farad. Soc.*, **33**, 179 (1937).
[12] Stewart and Morrow, *Phys. Revs.*, **30**, 232 (1927)
[13] Martin and Brown, *Trans. of Farad. Soc.*, **34**, 742 (1938)
[14] Wymann Jr., *Journ. Am. Chem. Soc.*, **53**, 3292 (1931).
[15] Bars and Cranen, *J. Chem. Phys.*, **7**, 8 (1939)
[16] Butler, Thomson and Madennan, *J. Am. Chem. Soc.*, **56**, 674 (1933).
[17] Langmuir, *Call, Symp. Monographs*, **3**, 48 (1925)
[18] Butler, *Trans. of Farad. Soc.*, **33**, 229 (1937).
[19] Bernal and Former, *J. Chem. Phys.*, **1**, 515 (1933).
[20] Bury and Hartley. Aqueous solutions of paraffin chain salts by G. S. Hartley No. 387 of the *Actualities scientifiques et industrielles* published by Hermann and *cie* Paris.
[21] Solomon, *Trans. Farad. Soc.*, **32**, 161 (1936).
[22] Frank, *J. Chem. Phys.*, **8**, 933 (1940).
[23] Salvanu, *Comptes. Rendus.*, **208**, 83 *Jam.* (1939).
[24] Mikhailov, *Comptes. Rendus.*, **26**, 145 (1940).

FORMULAE CONNECTING SELF-RECIPROCAL FUNCTIONS

By BRIJ MOHAN

(Received for publication, April 24, 1941)

1. In 1931 Hardy[1] and Titchmarsh[2] started the question as to how functions, which were self-reciprocal for Hankel Transforms of different orders, were connected with one another. They gave certain rules for deriving self-reciprocal functions for transforms of different orders from those which were self-reciprocal for transforms of a given order. In 1932 and 1934, I [3] [4] gave some more rules of a similar nature. The object of this note is to add a few more to the list of these rules. In the end I use these rules to derive some new self-reciprocal functions.

I will say that a function is R_ν if it is self-reciprocal for J_ν transforms. For $R_{\frac12}$ and $R_{-\frac12}$ I will write R_s and R_c respectively.

I will make use of the following result given by me elsewhere (3: §8) :—

If $f(x)$ is R_μ, the function

$$g(x)=\int_0^\infty P(xy)f(y)dy$$

is R_ν, provided that

$$P(x)=\frac{1}{2\pi i}\int_{k-i\infty}^{k+i\infty}2^s\Gamma(\tfrac14+\tfrac12\mu+\tfrac12 s)\Gamma(\tfrac14+\tfrac12\nu+\tfrac12 s)\lambda(s)x^{-s}ds, \qquad \ldots \quad (1.1)$$

where $$0<k<1,$$

and $$\lambda(s)=\lambda(1-s). \qquad \ldots \quad (1.2)$$

2. *Rule I.*—The kernel $x^{-\frac12}$ transforms R_μ into R_ν, where $\mu>-1$, $\nu>-1$.

This is almost obvious. For, in this case,

$$g(x)=\frac{1}{\sqrt{x}}\int_0^\infty\frac{1}{\sqrt{y}}f(y)dy.$$

This is only a constant multiple of the function $x^{-\frac12}$ which is known to be R_ν.

3. *Rule II.*—The kernel $x^{\frac32-\nu}J_{\nu-\frac12}(\frac12 x)J_{\nu-\frac32}(\frac12 x)$ transforms $R_{3\nu-3}$ into R_ν where $\nu>\frac23$.

To prove this rule, I start with the Weber-Schafheitlin [6 : 13.41 (2)] integral

$$\int_0^\infty \frac{J_m(ax)J_n(ax)}{x^\lambda}dx = \frac{(\tfrac{1}{2}a)^{\lambda-1}\Gamma(\lambda)}{2\Gamma(\tfrac{1}{2}+\tfrac{1}{2}m+\tfrac{1}{2}n+\tfrac{1}{2}\lambda)} \times \frac{\Gamma(\tfrac{1}{2}+\tfrac{1}{2}m+\tfrac{1}{2}n-\tfrac{1}{2}\lambda)}{\Gamma(\tfrac{1}{2}-\tfrac{1}{2}m+\tfrac{1}{2}n-\tfrac{1}{2}\lambda)\Gamma(\tfrac{1}{2}+\tfrac{1}{2}m-\tfrac{1}{2}n+\tfrac{1}{2}\lambda)},$$

where $R(m+n+1) > R(\lambda) > 0$.

This formula is the same as

$$\int_0^\infty x^{l-1}J_m(ax)J_n(ax)dx = \frac{(\tfrac{1}{2}a)^{-l}\Gamma(1-l)}{2\Gamma(1+\tfrac{1}{2}m+\tfrac{1}{2}n-\tfrac{1}{2}l)}$$

$$\times \frac{\Gamma(\tfrac{1}{2}m+\tfrac{1}{2}n+\tfrac{1}{2}l)}{\Gamma(1-\tfrac{1}{2}m+\tfrac{1}{2}n-\tfrac{1}{2}l)\Gamma(1+\tfrac{1}{2}m-\tfrac{1}{2}n-\tfrac{1}{2}l)}$$

$$= \frac{a^{-l}\Gamma(\tfrac{1}{2}-\tfrac{1}{2}l)\Gamma(1-\tfrac{1}{2}l)\Gamma(\tfrac{1}{2}m+\tfrac{1}{2}n+\tfrac{1}{2}l)}{2\sqrt{\pi}\Gamma(1+\tfrac{1}{2}m+\tfrac{1}{2}n-\tfrac{1}{2}l)\Gamma(1-\tfrac{1}{2}m+\tfrac{1}{2}n-\tfrac{1}{2}l)\Gamma(1+\tfrac{1}{2}m-\tfrac{1}{2}n-\tfrac{1}{2}l)},$$

where $R(m+n) > R(-l) > -1$.

By Mellin's Inversion Formula (1) we have

$$J_m(ax)J_n(ax) = \frac{1}{2\sqrt{\pi}} \cdot \frac{1}{2\pi i}\int_{b-i\infty}^{b+i\infty} \frac{\Gamma(\tfrac{1}{2}-\tfrac{1}{2}l)}{\Gamma(1+\tfrac{1}{2}m+\tfrac{1}{2}n-\tfrac{1}{2}l)}$$

$$\times \frac{\Gamma(1-\tfrac{1}{2}l)\Gamma(\tfrac{1}{2}m+\tfrac{1}{2}n+\tfrac{1}{2}l)}{\Gamma(1-\tfrac{1}{2}m+\tfrac{1}{2}n-\tfrac{1}{2}l)\Gamma(1+\tfrac{1}{2}m-\tfrac{1}{2}n-\tfrac{1}{2}l)}(ax)^{-l}dl,$$

so that

$$x^a J_m(\tfrac{1}{2}x)J_n(\tfrac{1}{2}x) = \frac{1}{2\sqrt{\pi}} \cdot \frac{1}{2\pi i}\int_{b-i\infty}^{b+i\infty} 2^l \frac{\Gamma(\tfrac{1}{2}-\tfrac{1}{2}l)}{\Gamma(1+\tfrac{1}{2}m+\tfrac{1}{2}n-\tfrac{1}{2}l)}$$

$$\times \frac{\Gamma(1-\tfrac{1}{2}l)\Gamma(\tfrac{1}{2}m+\tfrac{1}{2}n+\tfrac{1}{2}l)}{\Gamma(1-\tfrac{1}{2}m+\tfrac{1}{2}n-\tfrac{1}{2}l)\Gamma(1+\tfrac{1}{2}m-\tfrac{1}{2}n-\tfrac{1}{2}l)}x^{a-l}dl$$

$$= \frac{2^{a-1}}{\sqrt{\pi}} \cdot \frac{1}{2\pi i}\int_{b-a-i\infty}^{b-a+i\infty} 2^s \frac{\Gamma(\tfrac{1}{2}-\tfrac{1}{2}a-\tfrac{1}{2}s)\Gamma(1-\tfrac{1}{2}a-\tfrac{1}{2}s)}{\Gamma(1+\tfrac{1}{2}m+\tfrac{1}{2}n-\tfrac{1}{2}a-\tfrac{1}{2}s)}$$

$$\times \frac{\Gamma(\tfrac{1}{2}m+\tfrac{1}{2}n+\tfrac{1}{2}a+\tfrac{1}{2}s)}{\Gamma(1-\tfrac{1}{2}m+\tfrac{1}{2}n-\tfrac{1}{2}a-\tfrac{1}{2}s)\Gamma(1+\tfrac{1}{2}m-\tfrac{1}{2}n-\tfrac{1}{2}a-\tfrac{1}{2}s)}x^{-s}ds, \qquad (3.1)$$

where $-R(m+n) < b < 1$.

Putting $m-1=n=-a=\nu-\frac{3}{2}$, we get

$$x^{\frac{3}{2}-\nu}J_{\nu-\frac{1}{2}}(\tfrac{1}{2}x)\,J_{\nu-\frac{3}{2}}(\tfrac{1}{2}x)=\frac{2^{\frac{1}{2}-\nu}}{\sqrt{\pi}}\cdot\frac{1}{2\pi i}\int_{b-\frac{3}{2}+\nu-i\infty}^{b-\frac{3}{2}+\nu+i\infty}2^{s}$$

$$\times\frac{\Gamma(\frac{1}{4}+\frac{1}{2}\nu-\frac{1}{2}s)\Gamma(-\frac{1}{4}+\frac{1}{2}\nu+\frac{1}{2}s)}{\Gamma(-\frac{3}{4}+\frac{3}{2}\nu-\frac{1}{2}s)\Gamma(\frac{3}{4}+\frac{1}{2}\nu-\frac{1}{2}s)}x^{-s}\,ds,$$

where $$2-2\nu<b<1.$$

This integral is of the same form as (1.1) with $\mu=3\nu-3$,

$$x(s)=\frac{2^{\frac{1}{2}-\nu}}{\sqrt{\pi}}\frac{\Gamma(\frac{1}{4}+\frac{1}{2}\nu-\frac{1}{2}s)\Gamma(-\frac{1}{4}+\frac{1}{2}\nu+\frac{1}{2}s)}{\Gamma(-\frac{5}{4}+\frac{3}{2}\nu+\frac{1}{2}s)\Gamma(-\frac{3}{4}+\frac{3}{2}\nu-\frac{1}{2}s)\Gamma(\frac{1}{4}+\frac{1}{2}\nu+\frac{1}{2}s)\Gamma(\frac{3}{4}+\frac{1}{2}\nu-\frac{1}{2}s)},$$

which evidently satisfies (1.2).

Hence follows the result.

Putting $\nu=1$ we get

Rule III.—The kernel $\frac{\sin x}{\sqrt{x}}$ transforms R_0 into R_1.

In 1934, I (4 : §3) gave the rule that

The kernel $x^{-\frac{1}{2}\nu}H_{\frac{1}{2}\nu-\frac{1}{2}}(x)$ transforms R_1 into R_ν, where $H_n(x)$ is Struve's function [6 : 10.4(2)] of order ν.

As μ and ν are inter-changeable in (1.1), this rule may also be written thus :

The kernel $x^{-\frac{1}{2}\nu}H_{\frac{1}{2}\nu-\frac{1}{2}}(x)$ transforms R_ν into R_1.

As $H_{-\frac{1}{2}}(x)=\sqrt{\frac{2}{\pi x}}\sin x$,

it follows that Rule III is a particular case of this rule for $\nu=0$.

If, in (3.1), we take $m=n=-d=\nu-\frac{1}{2}$ and proceed as before, we obtain

Rule IV.—The kernel $x^{\frac{1}{2}-\nu}J_{\nu-\frac{1}{2}}(\frac{1}{2}x)\,J_{\nu-\frac{1}{2}}(\frac{1}{2}x)$ transforms $R_{3\nu-1}$ into R_1 for $\nu>\frac{1}{2}$.

If here we take $\nu=1$, we get

Rule V.—The kernel $x^{-\frac{3}{2}}(1-\cos x)$ transforms R_2 into R_1.

If, in (3.1), we take $m=-n=\frac{1}{2}\nu-\frac{1}{4}$, $d=0$, and proceed as above, we derive

Rule VI.—The kernel $J_{\frac{1}{2}\nu-\frac{1}{4}}(\frac{1}{2}x)\,J_{\frac{1}{4}-\frac{1}{2}\nu}(\frac{1}{2}x)$ transforms $R_{\nu-1}$ into R_{ν} for $\nu>0$.

For the particular case $\nu=\frac{3}{2}$, we have

Rule VII.—The kernel $\frac{\sin x}{x}$ transforms R_1 into $R_{\frac{3}{2}}$.

4. Titchmarsh (5 : 7.10.4) has given the pair of Mellin Transforms

$$J_n(x)\gamma_n(x),\ -\frac{1}{2\sqrt{\pi}}\frac{\Gamma(\frac{1}{2}s)\Gamma(\frac{1}{2}s+n)}{\Gamma(\frac{1}{2}+\frac{1}{2}s)\Gamma(1+n-\frac{1}{2}s)}.$$

If we start with the integral formula for this pair, and proceed as above, we arrive at

Rule VIII.—The kernel $x^{\frac{1}{3}\nu+\frac{1}{6}}J_{\frac{1}{3}\nu+\frac{1}{6}}(\frac{1}{2}x)\,\gamma_{\frac{1}{3}\nu+\frac{1}{6}}(\frac{1}{2}x)$ transforms $R_{\frac{1}{3}\nu-\frac{1}{3}}$ into R_{ν}, where $\nu>-\frac{1}{2}$.

As
$$\gamma_{\frac{1}{2}}(x)=-\sqrt{\frac{2}{\pi x}}\cos x,$$
if we put $\nu=1$ in Rule VIII, we arrive at Rule III again.

If we use the pair

$$e^{x}k_n(x),\quad \Pi^{-\frac{1}{2}}\cos n\pi.2^{-s}\Gamma(\tfrac{1}{2}-s)\Gamma(s+n)\Gamma(s-n)$$

given by Titchmarsh (5 : 7.10.9) and proceed in the same way, we obtain

Rule IX.—The kernel $x^{\frac{1}{3}\nu-\frac{1}{3}}e^{\frac{1}{2}x}k_{\frac{1}{3}\nu-\frac{1}{6}}(\frac{1}{2}x)$ transforms $R_{\nu-1}$ into R_{ν} for $\nu>\frac{1}{4}$.

When $\nu=1$, we obtain the rule that the kernel $x^{-\frac{1}{2}}$ transforms R_0 into R_1. This is already contained in Rule I.

5. I now proceed to derive certain self-reciprocal functions with the help of the above rules.

We know that the function

$$x^{\mu+\frac{1}{2}}e^{-\frac{1}{2}x^2} \qquad \ldots \quad (5.1)$$

is R_{μ}; in other words, that the function

$$x^{3\nu-\frac{5}{2}}e^{-\frac{1}{2}x^2}$$

is $R_{3\nu-1}$

Applying Rule II to this function, we arrive at the R_ν function $g(x)$ given by

$$g(x)=\int_0^\infty (xt)^{\frac{3}{2}-\nu} J_{\nu-\frac{1}{2}}(\tfrac{1}{2}xt)\, J_{\nu-\frac{3}{2}}(\tfrac{1}{2}xt)t^{3\nu-\frac{5}{2}} e^{-\frac{1}{2}t^2}\, dt$$

$$=x^{\frac{3}{2}-\nu}\int_0^\infty t^{2\nu-1} e^{-\frac{1}{2}t^2} J_{\nu-\frac{1}{2}}(\tfrac{1}{2}xt)J_{\nu-\frac{3}{2}}(\tfrac{1}{2}xt)dt.$$

This integral may be evaluated by a formula given by Macdonald (6 : 13.32) for $\nu > \frac{1}{2}$. We thus find that $g(x)$ is a constant multiple of

$$x^{\frac{3}{2}-\nu}.x^{2\nu-2}\,{}_3F_3\begin{pmatrix}\nu-\frac{1}{2}.\ \nu,\ 2\nu-1 & \\ & ;\ -\frac{1}{2}x^2\\ \nu+\frac{1}{2},\ \nu-\frac{1}{2},\ 2\nu-1 & \end{pmatrix}$$

which is the same as

$$x^{\nu-\frac{1}{2}}\ {}_1F_1(\nu\ ;\ \nu+\tfrac{1}{2}\ ;\ -\tfrac{1}{2}x^2).$$

Using Kummer's Transformation Formula

$${}_1F_1(a\ ;\ \rho\ ;\ z)=e^z\ {}_1F_1(\rho-d\ ;\ \rho\ ;\ -z),$$

we find that the function

$$x^{\nu-\frac{1}{2}}e^{-\frac{1}{2}x^2}\,{}_1F_1(\tfrac{1}{2}\ ;\ \nu+\tfrac{1}{2}\ ;\ \tfrac{1}{2}x^2)$$

is R_ν for $\nu > \frac{2}{3}$.

If we apply Rule IV to the function (5.1) we arrive at the same function again.

If we apply Rule VI to the function we find that the function

$${}_1F_1(\tfrac{1}{2}\ ;\ \tfrac{5}{4}-\tfrac{1}{2}\nu\ ;\ -\tfrac{1}{2}x^2)$$

is R_ν for $\nu > 0$.

BENARES HINDU UNIVERSITY.

REFERENCES

[1] G. H. Hardy, *Messenger of Math.*, **47**, 178-184 (1918).

[2] G. H. Hardy and E. C. Titchmarsh, *Proc. London Math. Soc.*, II, **33**, 225-232 (1931).

[3] Brij Mohan, *ibid.*, II, **34**, 231-240 (1932).

[4] Brij Mohan, *Proc. Edin. Math. Soc.*, II, **4**, 53-56 (1934).

[5] E. C. Titchmarsh, *The Theory of the Fourier Integral—Oxford* (1937).

[6] G. N. Watson, *The Theory of Bessel Functions—Cambridge* (1922).

ON THE HIGH-FREQUENCY CONDUCTIVITY AND EFFECTIVE DIELECTRIC CONSTANT OF ELECTRONIC MEDIUM IN A (HIGH-VACUUM) THERMIONIC VALVE

By R. G. BASAK, M.Sc.

(Received for publication, May 9, 1941)

ABSTRACT. In this investigation, the H. F. conductivity of the anode = screen-grid space in a thermionic valve (Philips B 442) was measured under various conditions. Willans' method of measuring H. F. resistance was adopted for the purpose and the double-heterodyne technique was followed in carrying out these measurements. The theory of the method and the experimental procedure are fully described. The conductivity experiments were made in three sections.

(1) Measurements of the conductivity of the inter-electrode space of the thermionic valve for various values of the thermionic current keeping the frequency of the field and time of stay of the electrons constant.

A linear relation was obtained between the conductivity value and the thermionic current.

(2) Measurements of the conductivity of the same electronic medium for different frequencies in the *medium frequency band* for definite values of the electron concentration and time of stay of the electrons

The conductivity was found to increase with the increase of frequency in this lower range of frequencies.

(3) Measurements of the conductivity of the same electronic medium for different transit-times of the electrons keeping electron concentration and the frequency of the field constant.

The conductivity was found to increase very rapidly with the increase of the time of stay of the electrons.

Measurements were also made of the effective dielectric constant of the inter-electrode space of the same valve to study its variation with the time of stay of the electrons. For a fixed frequency of the field and a definite electron concentration, the effective dielectric constant of the electronic medium was found to decrease very rapidly with the increase in the value of the transit-time of the electrons. Accepting Lorentz's expression for the dielectric constant of a frictionless electronic medium and introducing a multiplying factor it is concluded that this multiplying factor increases with the increase in the time of stay of the electrons in the inter-electrode space of the valve.

INTRODUCTION

The expressions for the dielectric constant and the conductivity of an atmosphere of ions and electrons are now well-known. The corresponding expressions in the case of an electronic medium inside a high-vacuum thermionic valve have not, however, been established with any certainty. Since the time of stay of the electrons in the inter-electrode space is only a small fraction of the period corresponding to the radio-frequency of the alternating field, the contribution of electrons towards the reduction of the dielectric constant should, therefore, be correspondingly small. Benner[1] had considered this effect of the finite time of transit of the electrons on the value of the dielectric constant and also on that of the conductivity of the electronic medium inside a thermionic valve. Recently, however, Hollmann and Thoma[2] deduced from their theory of the inversion of electrons substantially different formulae for the dielectric constant and conductivity of such a medium. Mitra and Sil[3] had also proposed a theory of the conductivity (or resistance) of a thermionic valve. Assuming a Maxwellian distribution of velocity of the electrons inside the valve they calculated the time of flight of the electrons making certain simplifying assumptions and approximately obtained the values of the conductivity of the valve for different frequencies. These values calculated on their hypothesis agreed well with the values found experimentally in the high frequency range. In view of these different theories, it was considered desirable to undertake accurate measurements of the dielectric constant and conductivity of the electronic medium inside a screen-grid valve under different controlled conditions. Some work[4] performed in this laboratory on the effective dielectric constant of such a medium both for medium and ultra-high frequency alternating fields had, however, been previously reported. The present investigation is *primarily* concerned with the experimental determinations of the H. F. conductivity of the anode=screen-grid space of a thermionic valve on *medium* radio-frequencies. The conductivity experiments were made in three sections:

(1) Variation of the H. F. conductivity of the anode=screen-grid space of a screen-grid valve with the thermionic current through the valve, keeping the frequency of the alternating field and the time of stay of the electrons constant.

(2) Variation of the H. F. conductivity of the similar electronic medium with the frequency of the alternating field for definite values of the electron concentration and the time of stay.

(3) Variation of the H. F. conductivity of the similar medium with the time of stay of the electrons keeping the electron concentration and the frequency of the field constant.

The variation of the effective dielectric constant of the electronic medium inside the screen-grid valve with the time of stay of the electrons in the inter-electrode space has also formed a part of this investigation. The experimental results on the H. F. conductivity and the effective dielectric constant of the electronic medium inside the screen-grid valve have been examined and theoretical interpretations given.

METHOD OF CONDUCTIVITY MEASUREMENTS

(a) *Theory of Willans' method of H. F. resistance measurement*

Willans'[5] method of H. F. measurement of resistance was employed in this investigation. The principle involved in the method is the well-known principle of transformer action.

Let us take a secondary circuit containing inductance L_1, resistance R_1 and capacity C_1 in the neighbourhood of an *oscillating* primary circuit containing inductance L, resistance R and capacity C. When a current flows in the secondary circuit, the resistance and reactance of the primary circuit would change (and *vice versa*). The change in the reactance of the oscillator (primary) coil would mean a change of the effective inductance of the same coil, which in turn would cause a change in the emitted frequency of the oscillator. This change in the frequency of the oscillator would be directly proportional to the change of reactance. The frequency-change would be:

$$\Delta f \propto \frac{\omega^2 M^2}{R_1^2 + X_1^2} . X \qquad \dots \quad (1)$$

where X is the reactance of the primary (oscillatory) circuit,
X_1 and R_1 the reactance and resistance of the secondary,
M the mutual conductance between primary and secondary coils,
and ω the angular frequency of the current.

Now it can be easily proved that for ωM=constant, the change of frequency would be maximum, when

$$R_1^2 = X_1^2$$

or

$$R_1 = \pm X_1$$

i.e.

$$\left. \begin{aligned} R_1 &= \left(\omega L_1 - \frac{1}{\omega C_1'} \right) \\ \text{and} \quad R_1 &= \left(\frac{1}{\omega C_1''} - \omega L_1 \right) \end{aligned} \right\} \qquad \dots \quad (2)$$

Hence C_1' and C_1'' are the values of the secondary capacity for the two conditions for maximum change of frequency as given in (2). Combining the two conditions, we get

$$R_1 = \frac{1}{2\omega} \left(\frac{1}{C_1''} - \frac{1}{C_1'} \right). \qquad \dots \quad (3)$$

The change in the emitted frequency due to the change in the effective reactance of the oscillatory circuit can be discerned as an alteration of the beat-note in the telephones connected to an oscillating receiver.

(b) Experimental procedure

The experimental procedure is briefly stated here. With the switch of the measurement circuit (L_1 C_1 R_1) open, the frequency of the oscillating receiver is adjusted to the desired value and the frequency of the oscillator is then adjusted by varying its tuning condenser C till no-beat is heard. When the measurement circuit is closed, its condenser C_1 is varied till the beat-note again disappears. This gives the resonance value of C_1. Next displacing C_1 by a small amount, the beat-note is again heard due to the change in the frequency of the oscillator. The tuning condenser C of the latter is now changed till the beat-note again disappears. If the process is repeated for other positions of the condenser C_1 of the measurement circuit, it will be found that the variation of C required to balance the effect of variation of C_1 is of a form with two peaks on both sides of the C_1-value which corresponds to the original frequency. These peaks appear for two different values of C_1, *viz.* C_1' and C_1''. The H. F. resistance R_1 of the measurement circuit can then be calculated from relation (3).

Experimental arrangements and the working formula for the conductivity measurements

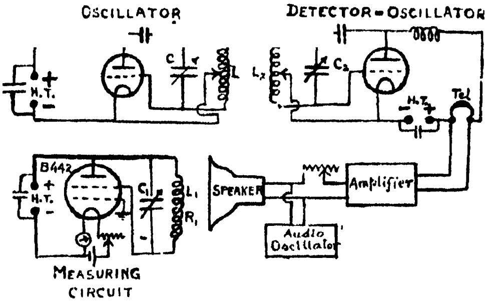

FIG. 1

The complete arrangement of the apparatus is shown in fig. 1. The oscillators were of the Hartley type. A pair of telephones was inserted in the anode circuit of the detector-oscillating valve. When the frequency of each was adjusted, it was possible to hear the heterodyne whistle. The L. F. e. m. f. developed across the telephone was then fed into amplifier of the conventional type. A loudspeaker was connected to the output of the amplifier. Through this loudspeaker was passed an audio-frequency current from the secondary circuit of an audio-oscillator of a suitable constant frequency. A variable resistance was inserted to adjust the amplitude of this audio-frequency current so that the heterodyne whistle and the sound due to the audio-frequency current from the audio-oscillator could be made of the same order of intensity. As a result of the superposition of these two audio-frequency currents through the loud-speaker, beats could be heard. The tuning condenser (C or C_2) of either oscillator could be adjusted till no beats were heard. All the condensers were properly shielded and carefully calibrated. Usually more than one condenser fitted with slow-motion dials were used in parallel with C & C_1.

To determine the H. F. conductivity (or the resistance) of the anode-screen-grid space of the experimental valve, the anode and the screen-grid were then connected to the plates of the condenser C_1 so that C_1 and the inter-electrode capacity C_1 were placed in parallel. A suitable high voltage was applied across the anode and the filament of the valve. Measurements of the H. F. resistance of the measurement circuit with the filament current on and off were then made successively by following the double-beat procedure of Willans' method as previously described. The H. F. resistance R_1' of the circuit when the filament current was switched on was found greater than the corresponding resistance R_1 when the filament current was off. The increase in the resistance $(R_1'-R_1)$ or r was the effect of a leakage across the inter-electrode space due to the conductivity of the electrons in that space. From the value of r obtained experimentally, the corresponding shunt resistance ρ was then calculated from the relation

$$\rho=\frac{1}{\omega^2 r[(C_1)_r+C_v]^2}\simeq\frac{1}{\omega^2 r(C_1)_r^2}. \qquad \ldots \quad (4)$$

Here $(C_1)_r$ is the resonance value of the condenser C_1 when the inter-electrode capacity C_v was put in parallel with C_1. C_v was very much smaller than $(C_1)_r$.

The H. F. conductivity of the electronic medium in the inter-electrode space as expressed in terms of the leakage shunt-resistance ρ across it was given by

$$\sigma=\frac{1}{4\pi(C_1)_r\rho}. \qquad \ldots \quad (5)$$

In view of (4), the conductivity of the electronic medium as expressed in terms of the increase in series resistance r would then be given by

$$\sigma=\frac{\pi C^2}{\lambda^2}\cdot(C_1)_r\cdot r$$

$$=\frac{28.27\times 10^{20}\times r}{\lambda^2}\cdot(C_1)_r \qquad \ldots \quad (6)$$

Calculations of the conductivity of the medium were made from (6)

EXPERIMENTAL RESULTS

Variation of the H.F. conductivity of the inter-electrode space of the thermionic valve with the thermionic current through it, keeping the frequency of the alternating field and the time of stay of the electrons constant

Measurements of the H. F. conductivity of the anode=screen-grid space of a Philips B 442 valve were made for two different frequencies. For each frequency

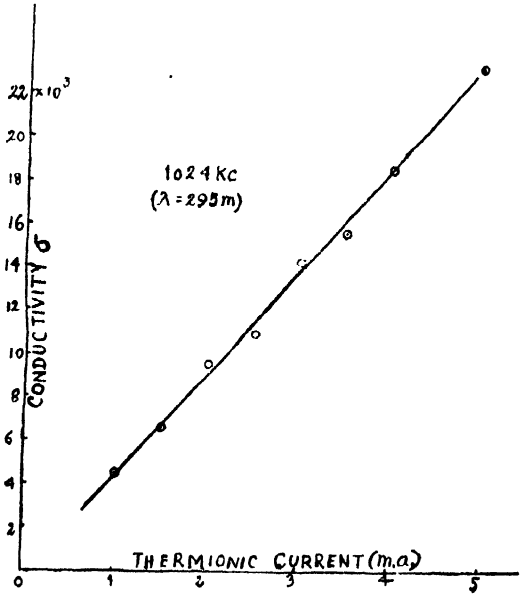

FIG. 2(*a*)

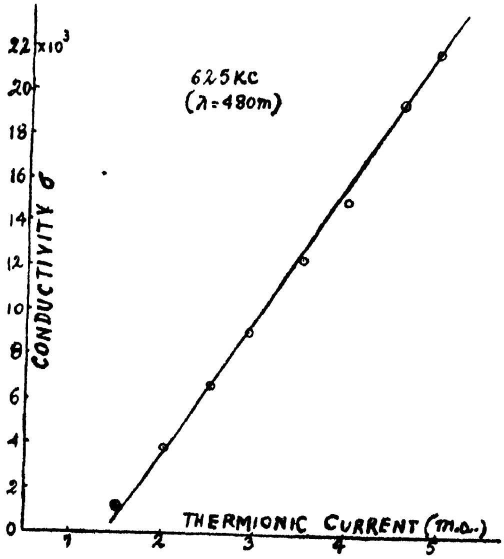

FIG. 2(*b*)

the thermionic current through the valve was varied from 0 to 5 m.a. The results for frequencies: 1024 kc. ($\lambda = 293$ m.) and 625 kc. ($\lambda = 480$ m.) are shown graphically in figs. 2 (a) & 2 (b). A pair of curves drawn from a representative set of observations for the evaluation of the H.F. resistances R_1' & R_1 of the measurement circuit by the method of Willans (when the filament of the experimental valve was switched on and off respectively) are shown in fig. 3.

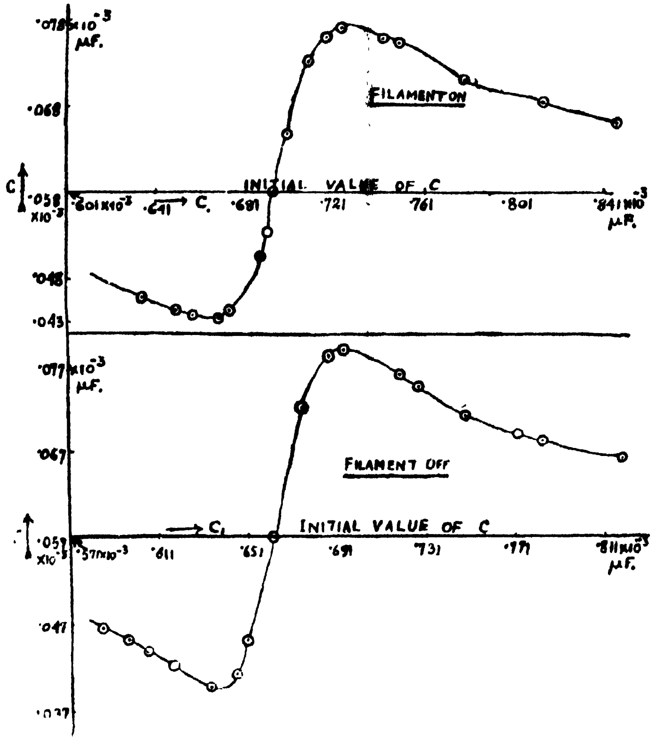

FIG. 3

The curves in fig. 2 show that a linear relation was found in these experiments to hold between the conductivity of the electronic medium and the electron concentration (which could be taken proportionate to the thermionic current since the anode voltage and the filament current were both kept fixed during each set of observations). This linear relationship is expected from any theory of the conductivity of the electronic medium inside a thermionic valve.

Variation of the H.F. conductivity of the inter-electrode space of the thermionic valve with the frequency of the alternating field for definite values of electron-concentration and time of stay of the electrons

In fig. 4 are shown the results of a typical set of experimental results showing the variation of the H.F. conductivity of the anode=screen-grid space of the same thermionic value with the frequency of the alternating field. The thermionic current was fixed at 3.5 m. a. and the frequency was varied from

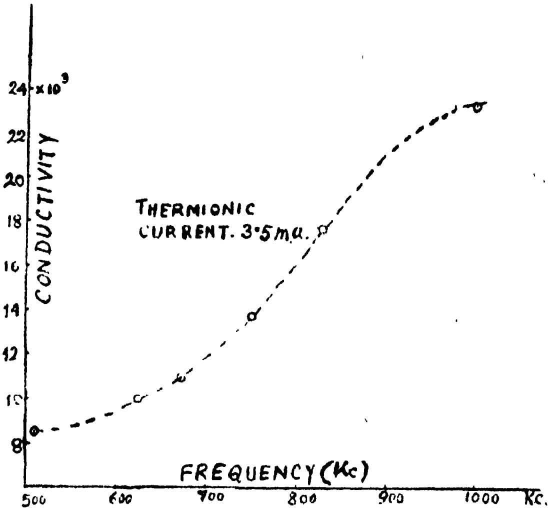

FIG. 4

512 kc. to 1000 kc. ($\lambda = 585$ m. to 300 m.). The conductivity values were calculated with the help of equation (6). It can be seen from fig. 4 that the conductivity *increased as the frequency was increased* within the experimental range, *viz.*, 512 kc. to 1000 kc. It should be mentioned here that the experiments of M. Kameswar Rao[6] performed in this laboratory on the internal resistance of a thermionic valve over a wide range of radio-frequencies revealed the same feature in the lower range of frequencies. He found that the internal resistance of the experimental valve at first decreased with the increase of frequency (till about 1600 kc. in the case of Telefunken RE134 valve and till about 2000 kc. in the case of Philips B406 valve) and that it increased again steadily with the increase of frequency.

Variation of the conductivity of electronic medium inside the valve with the time of flight of the electrons for a definite electron concentration and frequency of the field

In these sets of experiments the anode voltage was varied and *the thermionic current was maintained at a definite value by adjusting the filament current.* Measurements of the H.F. conductivity of the anode-screen-grid space for a definite frequency were then made for different anode voltages. The time of flight of the electrons could be taken as proportional to $\frac{1}{\sqrt{V}}$ where V = anode voltage. In fig. 5 are shown the results of a typical set of experiments for a definite frequency of the field. It is significant that the value of the conductivity

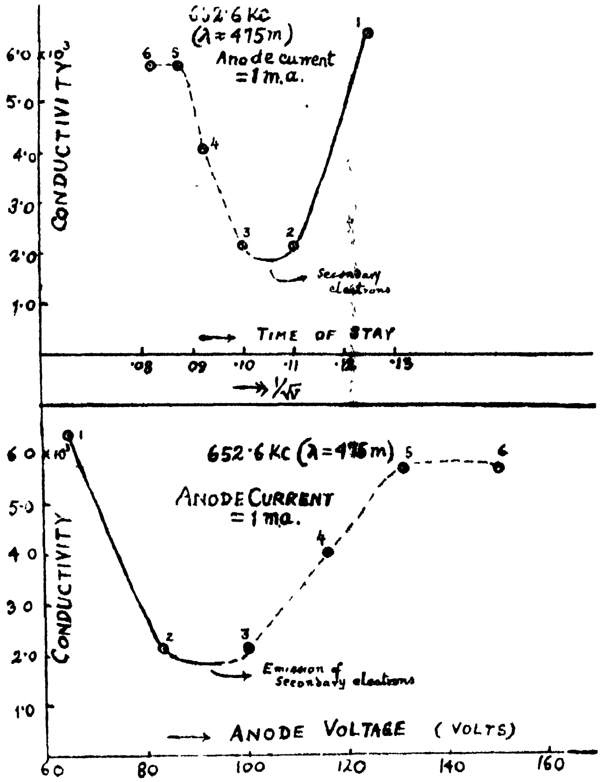

FIG. 5

decreased very rapidly with the increase of the anode voltage up to about 90 volts and then increased steadily tending to approach a limiting value. The increase of conductivity at about 90 volts must be due to the secondary electrons emitted at the anode and screen-grid surfaces. Before the emission of the secondary electrons, the experiments indicated a very rapid increase of the conductivity with the time of stay of the electrons.

DISCUSSION OF THE EXPERIMENTAL RESULTS ON THE CONDUCTIVITY OF THE ANODE-SCREEN-GRID SPACE OF THE THERMIONIC VALVE

We shall write below the expressions for the conductivity term as given by Benner and Hollmann & Thoma :

$$\text{Benner}: \quad \sigma = \frac{Nc^2}{m\omega^2 T}(1 - \cos \omega T) \qquad \ldots (7)$$

$$\text{Hollmann \& Thoma}: \quad \sigma = \frac{Ne^2T}{m}\left[\frac{\sin\frac{\omega T}{2} - \frac{\omega T}{2}\cdot\cos\frac{\omega T}{2}}{\left(\frac{\omega T}{2}\right)^2}\cdot\sin\frac{\omega T}{2}\right] \qquad \ldots (8)$$

where N = electron concentration,
T = time of stay of the electrons in the inter-electrode space,
ω = angular frequency of the field,
and e, m are charge and mass of an electron.

When ωT is sufficiently small, these equations will reduce to :—

$$\text{Benner}: \quad \sigma = \frac{Ne^2T}{m} \qquad \ldots (9)$$

$$\text{Hollmann \& Thoma}: \quad \sigma = \frac{Ne^2T}{m}\left(\frac{\omega T}{6}\right)\cdot\sin\left(\frac{\omega T}{2}\right)$$

$$= \frac{Ne^2\omega T^2}{6m}\left[\frac{\omega T}{2} - \frac{\omega^2T^3}{48}\right]$$

$$\simeq \frac{Ne^2\omega^2T^3}{12m}. \qquad \ldots (10)$$

Let us now consider our experimental results on the conductivity of the electronic medium inside the valve.

(a) Relation between the conductivity σ and the electron concentration N for fixed values of frequency and time of stay of the electrons

The observed linear relation between the conductivity of the anode = screen-grid space and the thermionic current (which could be taken as proportional to the electron concentration since the anode voltage and filament current were kept fixed) can be explained on either formula. Exact quantitative comparison between the experimental values and the values expected from either formula is not, however, possible since the time of stay of the electrons from the filament in the inter-electrode space is not accurately known. Accepting, however, an approximate estimate of T equal to 10^{-9} sec., we can find out the order of magnitude of the electron concentration N in the inter-electrode space. Taking the experimental value of the conductivity σ to be 10^4, N comes out to be 4×10^8 according to Benner's formula, whereas according to Hollmann & Thoma, N is of the order of 10^{10}. The former value is incredibly small and the latter is again too large under the conditions of our experiments.

(b) *Relation between the conductivity and the frequency of the field for fixed values of electron concentration and time of stay of the electrons*

According to Benner σ is independent of the frequency of the field. Benner's formula, therefore, cannot explain the observed variation of conductivity of the electronic medium inside the valve with the frequency of the field. A little inspection of Hollmann & Thoma's formula will show that the conductivity should increase with the increase of frequency for values of ωT from 0 to $\frac{\pi}{2}$. For very small values of ωT, however, σ should vary as the square of the frequency as is evident from (10). It should be noted that for 100 megacycles frequency ($\lambda = 3$ metres), $\omega T = .4 \times \frac{\pi}{2}$ . . assuming $T = 10^{-9}$ sec. For lower frequencies, ωT is still less. In the medium frequency range, ωT is only a very minute fraction of $\pi/2$. Thus, according to Hollmann & Thoma, the conductivity term should increase with frequency from very low to very high frequencies. Our experiments *on the medium frequency band* showed this increase of conductivity with frequency but experiments with higher frequencies performed in this laboratory and elsewhere had definitely shown a steady diminution of conductivity of the inter-electrode space of a thermionic valve with frequency. We have already referred to Rao's work in this laboratory showing a gradual decrease and then a steady increase of the internal resistance of a thermionic valve with the increase of frequency of the measuring field. Hollmann & Thoma's formula can, therefore, be regarded as untenable. Khastgir[7] has recently explained the observed variation of the resistance of a thermionic valve over a wide range of frequencies. Accepting the fundamental ideas of Mitra & Sil about the conductivity of a valve arising from the convection current and considering also the conductivity due to the displacement currents, it has been shown that the experimental results on the variation of the conductivity of the valve with frequency can be interpreted.

(c) *Effect of the time of stay of the electrons on the value of the conductivity*

Our experiments showed that for the larger values of the time of stay of the electrons, the conductivity increased very rapidly with the time of stay. Both Benner's and Hollmann & Thoma's formulae, however, demand that the conductivity of the valve should increase with the time of stay of the electrons. The observed increase was rather much too rapid.

Measurements of effective dielectric constant of the inter-electrode space in the valve and its variation with the time of stay of the electron

(a) *Theoretical considerations*

We shall write below the expressions for the change in the dielectric constant of the electronic medium inside a valve as given by Benner and Hollmann & Thoma.

Benner :

$$\Delta\epsilon = -\frac{4\pi N e^2}{m\omega^2}\left(1 - \frac{\sin \omega T}{\omega T}\right) \qquad \ldots \quad (11)$$

Hollmann & Thoma :

$$\Delta\epsilon = \frac{2\pi N e^2 T^2}{m} \cdot \frac{\sin\frac{\omega T}{2} - \frac{\omega T}{2} \cdot \cos\frac{\omega T}{2}}{\left(\frac{\omega T}{2}\right)^3} \cos\frac{\omega T}{} \qquad (12)$$

When $\omega.T$ is sufficiently small, both these expressions are reduced to

Benner :

$$\Delta\epsilon = -\left(\frac{2\pi N}{3m}\right)T^2 \qquad \ldots \quad (13)$$

Hollmann & Thoma :

$$\Delta\epsilon = \frac{2\pi N e^2 T^2}{m} \cdot \frac{\omega T}{6} = (\tfrac{1}{3}\,\pi N e^2 \omega).T^2. \qquad \ldots \quad (14)$$

The experiments[8] performed in this laboratory had previously shown that both the above expressions for the dielectric constant of electronic medium were untenable. A multiplying factor was introduced in the Lorentz formula for the dielectric constant of a frictionless electronic medium to obtain the effect of the time of stay of the electrons in the inter-electrode space. Expressing this multiplying factor in the form

$$\mu = \frac{A}{\lambda} \cdot f(T),$$

where A is a constant, T the transit-time, and λ the wavelength of the field, it was shown that μ was independent of $\left(\frac{A}{\lambda}\right)$ and depended *only* on the time of transit of the electrons. The experiments described in this section were undertaken to find the nature of this dependence.

(b) *Experimental arrangement and procedure*

The experimental technique was essentially that of the double-beat method adopted in the previous work on the subject (*vide* fig. 6.)

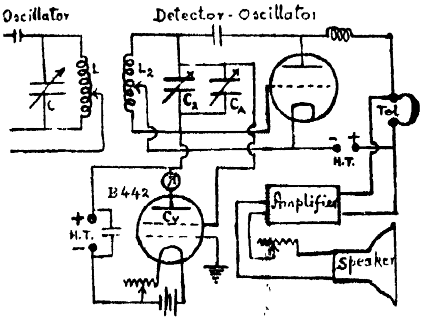

Fig. 6.

The anode = screen-grid capacity C_v of the same valve (Philips B442) was placed in parallel with the tuning condenser C_2 of a detector-oscillator circuit. The change in the capacity of C_v when the inter-electrode space was filled with electrons was balanced by changing the capacity of an accurately calibrated small variable vernier air condenser C_A in parallel with C_v and C_2, so that the total capacity $(C_v + C_2 + C_A)$ remained constant. The high frequency signal from an oscillator was received by the oscillator-detector valve-circuit which was exactly similar to the oscillator circuit. When the detector circuit was nearly in tune with the oscillator, the familiar heterodyne whistle was heard in the telephone placed in the anode circuit of the receiver. The audio-frequency voltage developed across the telephones was then amplified by a suitable amplifier and fed into a loudspeaker which gave a loud musical note. On introducing into the same loudspeaker an audio-frequency current from a specially constructed audio-oscillator capable of producing an intense note of fixed frequency, beats were heard by suitably adjusting the heterodyne frequency. (A variable resistance was placed in series with the secondary coil of the audio-oscillator to match the intensity of the heterodyne whistle with that of the audio-frequency note). Adjustments of the variable vernier condenser C_A in the oscillator to produce no beats were then made successively *first* when the inter-electrode space was devoid of electrons and *next* when the same space was filled with the electrons. In other words, the change in the capacity of C_A was noted with the filament of the experimental valve off and on after having given suitable high voltages to the anode and the screen grid. In this observed change in capacity ΔC was added a correction $(\Delta C)_\sigma$ to allow for the effect of the conductivity of the medium. The change in the capacity due to the dielectric constant change *alone* would then be given by

$$(\Delta C)_\epsilon = \Delta C + (\Delta C)_\sigma .$$

The dielectric constant was thus calculated from

$$\epsilon = 1 - \frac{(\Delta C)_\epsilon}{C_v} . \qquad \dots (15)$$

It was, therefore, necessary to determine *first* the observed change in capacity ΔC for different anode and screen-grid voltages (with suitable values of filament current to keep the thermionic current constant) and then to find the correction term $(\Delta C)_\sigma$.

(c) *Correction for the conductivity of the electronic medium*

After determining the observed decrease in the capacity ΔC for each different anode voltage in the way described before, the correction term for the conductivity effect was obtained in the following way :

The H. F. series-resistance of the electronic medium was measured by Willans' method for each different anode voltage, keeping the thermionic current constant. The corresponding shunt resistance ρ was then calculated by the standard formula. A graph was then drawn showing ρ against the anode voltage. Next in a separate experiment the inter-electrode capacity was shunted by different non-inductive metal film high resistances and the corresponding increase in the effective capacity of the oscillating system necessary to restore resonance condition was accurately measured by following the double-beat method already described. Another graph was then constructed from the observed data showing the increase in the capacity against the value of the metallised shunt resistance employed. From these two graphs the correction terms $(\Delta C)_\sigma$ (for the different values of the shunt resistance ρ corresponding to the H. F. series-resistances γ of the electronic medium) were obtained for different anode voltages and a correction graph constructed showing correction $(\Delta C)_\sigma$ for the different anode voltages. To each value of the observed decrease in capacity obtained in the main experiment for each different anode voltage, the requisite value of $(\Delta C)_\sigma$ obtained from the correction graph was then added. This gave the change in the capacity $(\Delta C)_\epsilon$ due to the dielectric constant change alone.

(d) *Experimental results*

The results of a typical set of experiment are shown in fig. 7 and the data are entered in the table below :

Serial No.	V Anode Voltage (volts)	$t \propto \frac{1}{\sqrt{V}}$ $\frac{1}{\sqrt{V}}$	ΔC (μμf)	$(\Delta C)_\sigma$ (μμf)	$(\Delta C)_\epsilon = \Delta C + (\Delta C)_\sigma$ (μμf)	$\epsilon = 1 - \frac{(\Delta C)_\epsilon}{C_\nu}$
1	65	.125	2.8	1.99	4.79	·52
2	83	.110	1.65	1.00	2.65	·735
3	100	.100	1.55	1.00	2.55	·745
4	118	.093	1.9	1.99	2.89	·71
5	135	.087	2.2	2.8	5.0	·50
6	150	.082	2.5	2.9	5.4	·46

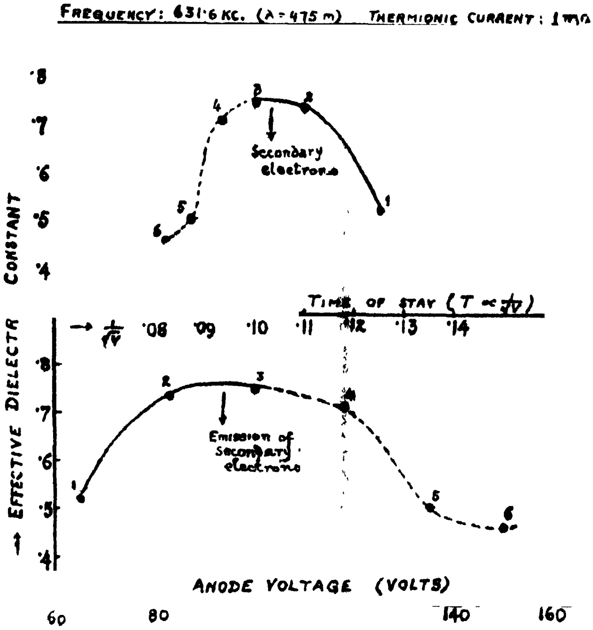

FIG. 7

It can therefore be said that, before the emission of the secondary electrons, the effective dielectric constant of the electronic medium increased with the anode voltage, *i.e.*, it *decreased* with the time of stay of the electrons.

(e) Discussion of the experimental results and conclusion therefrom

From Benner's and Hollmann and Thoma's expressions for the dielectric constant of electronic medium in a thermionic valve, we find that the dielectric constant in the former case would *decrease* with the increase of the time of stay T and that in the latter case it would *increase* with the transit time of the electrons. According to Hollmann and Thoma, however, the dielectric constant would be greater than unity for the given value of ωT. In view of the results of experiments performed in this laboratory and already referred to, we consider both formulae untenable. Accepting, however, Lorentz's formula for the dielectric constant of a frictionless electronic medium with a multiplying factor μ in it and neglecting the Lorentz term, *viz.*,

$$\epsilon = 1 - \frac{4\pi(N\mu)e^2}{m\omega^2} \qquad \ldots \quad (16)$$

we conclude that as the effective dielectric constant was found to decrease with the increase of the time of stay of the electrons, the factor μ, would *increase* with the increase of the transit-time T.

ACKNOWLEDGMENTS

I must express my sincere thanks to Dr. S. R. Khastgir under whose direction and guidance the above investigations were carried out. Our thanks are also due to Prof. S. N. Bose, Head of the Physics Dept., for all the facilities given during the progress of the work.

DACCA UNIVERSITY

REFERENCES

[1] Benner, *Ann. d. Phys.*, **5**, 993 (1929).
[2] Hollmann & Thoma, *Ann. d. Phys* , **5**, 32 (1938).
[3] Mitra & Sil., *Phil. Mag.*, **13**, 1081 (1932).
[4] Khastgir & Serajuddin, *Phil. Mag.*, Ser. 7, **28**, 532 (1939); Khastgir & Choudhury *Ind. Jour. Phy.*, July (1940).
[5] *Vide* Turner's paper in *Experimental Wireless and Wireless Engineer*, 348, March (1925)
[6] M. Kameswar Rao, *Ind. Jour. Phys.*, June (1940).
[7] Khastgir, *Science and Culture*, May, (1941).
[8] Khastgir and Serajuddin, *Phil. Mag.*, Ser. 7, **28**, 532, Nov. (1939) Khastgir and Choudhury, *Ind. Jour. Phys.*, June (1941).

RAMAN EFFECT IN DEUTERO-NITRIC ACID

By Dr. G. B. BANERJI, M.Sc., Ph.D. (Lond.)

AND

B. MISHRA, M.Sc.

(Received for publication, May, 14, 1941)

Plate XVIII.

ABSTRACT. Deutero-nitric acid has been prepared by the action of nitrogen pentoxide on heavy water. The Raman spectra of the acid have been photographed and consist of frequencies 166, 589, 667, 790, 905, 1017, 1293, 1536, 1640, 1849, 1972 and 2455 (band). By comparison with HNO_3 it has been found possible to calculate the isotope shifts and also to explain the origin of the vibrations in DNO_3.

INTRODUCTION

Since the isolation of heavy water, a large number of experimenters have studied the Raman frequencies of various compounds in which hydrogen is replaced by deuteronium. The results have led to measurable isotope shifts and have served as a check to theoretical developments in this connection. Leckie[1] prepared Deutero-sulphuric acid and photographed the Raman spectra of the 100% acid and also of the acid in various dilutions of heavy water. Small but definite isotope shifts have been recorded. Nitric acid has a number of Raman frequencies and it was thought desirable to prepare Deutero-nitric acid and study the Raman effect in 100% acid.

EXPERIMENTAL ARRANGEMENTS

After various trials, DNO_3 was prepared by the action of N_2O_5 on heavy water. In order to prepare N_2O_5, a mixture of strong nitric and sulphuric acid was first distilled. The nitric acid thus obtained was mixed with phosphorus pentoxide and distilled. The distillate was cooled by freezing mixture and consisted of solid N_2O_5. This was purified and a small weighed quantity of the solid was taken and to it a definite quantity of heavy water(100%) was added as required by the reaction $D_2O+N_2O_5=2DNO_3$. For this work only 5 c.c. of the acid was prepared. The acid thus obtained looked slightly brown due to the presence of nitrous fumes. To make it transparent a small current of perfectly dry air was passed through it for about an hour, care being taken to avoid contamination with moisture. After the completion of the work, the strength of DNO_2 was tested and found to be 98%.

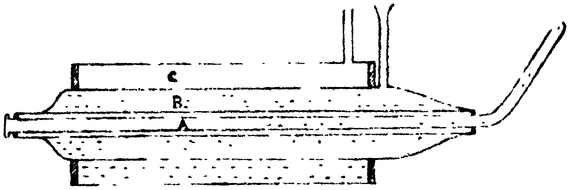

FIG. 1

The acid was transferred to a glass tube A (Fig. I) with one end blown flat and the other end was quickly sealed off. The tube was about 25 cm. long and had a bore of 4 mm. only. Some 3 c.c. of liquid was sufficient for investigation.

To avoid complications, Raman spectra was produced by filtering out all lines of the mercury arc other than the 4358 group. With this view, a simple piece of pyrex glass apparatus (Fig. I) was blown. The experimental tube was surrounded by two jackets B and C containing a very dilute solution of iodine in carbon tetrachloride and a concentrated solution of sodium nitrite in water respectively. The former solution absorbed the wave-lengths longer than 4358 Å, while the latter absorbed shorter wave-lengths. The whole arrangement was quite handy.

A bent mercury arc of pyrex glass, like the one devised by Ananthakrishnan [2] was employed. This surrounded the central part of the apparatus.

Two card-boards were slipped over the jacket C at its two ends and these allowed the light from the mercury arc to fall only over the middle part of the experimental tube.

The mercury arc was run at 4 amperes and the exposure lasted for 80 hours in the case of DNO_3. For photographing a Hilger spectrograph with a very dense flint glass prism was employed.

RESULTS

The wave-lengths of all the Raman lines were measured with the help of Hartmann's formula, taking known lines of copper arc as standard. Nearly all the lines are rather broad and there may be a maximum error of 5 in the reported frequencies.

Plate XVIII is a reproduction of the spectrum obtained, in which the stronger Raman lines of DNO_3 can be seen. All the Raman lines for DNO_3 are listed in the following table :—

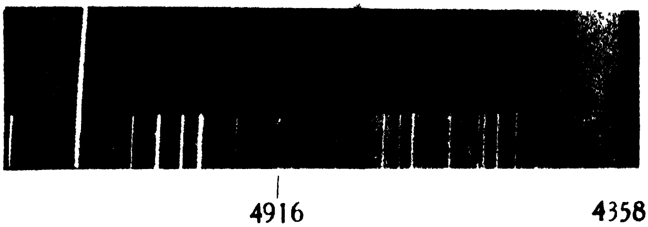
4916
4358

TABLE I

Raman shifts for DNO_3 (98%)

Wave-lengths of Raman lines	Frequencies	Shift in cm.$^{-}$
4391.41 (2d)	22772	166
4474.48 (0)	22349	589
4480.20 (2)	22281	667
4515.01 (0)	22148	790
4538.73 (4)	22033	905
4561·76 (1)	21921	1017
4619.92 (10)	21645	1293
4672.47 (2)	21402	1536
4695.17 (2b)	21298	1640
4741.80 (0)	21089	1849
4769.53 (0)	20966	1972
4882.1 (Band)	20483	2455

For correlating the Raman spectra of DNO_3 with HNO_3, we have taken a few photrgraphs with a sample of 80% HNO_3. In table II, the Raman frequencies obtained by us are listed as also those by other workers working with 100% acid. It will be seen that a new broad line with a shift of 1779 cm.$^{-1}$ has been obtained by us.

TABLE II

Raman Frequencies for 100% Nitric acid

Angus and Leckie [3]	Dadieu and Kohlrausch [4]	Medard and Volkringer [5]	Aderhold and Weiss [6]	Present Authors (80% acid)	Mean
608 (3)	607	613	607	627 (2)	613 (2)
679 (4)	667	675	667	682 (2b)	674 (2b)
924 (6)	916	923	—	935 (5)	924 (5)
1064 (2)	—	1048	—	1041 (2)	1051 (2)
1126 (0)	—	1103	—	—	1115 (0)
1297 (8b)	1292	1295	1291	1302 (10b)	1296 (10)
1407 (1)	—	—	—	—	1407 (1)
1516 (1)	—	1537	—	—	1527 (1)
1611 (0)	—	—	—	—	1611 (0)
—	1665	1670	1665	1674 (2)	1679 (2)
1699 (4)	1687	—	1687	—	—
—	—	—	—	1779 (2b)	1779 (2b)
—	3420 (Band)	—	—	-	3420 (Band)

From the intensities and natures of the lines for HNO_3 and DNO_3 acids it is easy to find out the wave-numbers for similar modes of vibrations. This is done in table III.

TABLE III

Raman frequencies for HNO_3	Raman frequencies for DNO_3	Isotope shift in cm.$^{-1}$	Origin of vibration
—	166 (2d)	—	—
613 (2)	589 (0)	26	p_1
674 (2b)	667 (2)	7	p_2
—	790 (0)	—	—
924 (5)	905 (4)	19	ω_1
1051 (2)	1017 (1)	34	ionic
1115 (0)	—	—	p_3
1296 (10)	1293 (10)	3	ω_2
1407 (1)	—	—	ionic
1527 (1)	—	—	—
1647 (0)	—	-	—
1685 (2)	1536 (2)	149	p_4
1779 (2b)	1640 (2b)	139	—
—	1849 (0)	—	—
—	1972 (0)	—	—
3420 (Band)	2455 (Band)	935	OH. OD bands

DISCUSSIONS

Let us first consider the modes of vibrations in HNO_3. In dilute solutions, the only line which gains in intensity is 1051 cm.$^{-1}$ and hence this line is regarded as due to the dissociated molecule of nitric acid. The NO_3 ion has probably a plano-symmetric structure and the frequency 1051 represents the symmetric and parallel vibrations of the nitrogen atom.

Venkateswaran[7] has attributed the formula 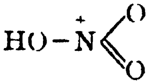 $HO-\overset{+}{N}\langle{}^{O}_{O}$ to nitric acid and taking the configuration AB_3, where all the B atoms are different and the atom A at the apex of the pyramid, the Raman frequencies of Nitric acid can be adequately explained. The two strong frequencies 924 and 1296 are to be attributed to the two parallel vibrations of the AB_3 group in nitric acid. These two vibrations are represented by ω_1 and ω_2 in table III. The four perpendicular vibration frequencies are 613, 674, 1115 and 1685. These are represented by p_1, p_2, p_3 and p_4 in table III. In Deutero-nitric acid the two corresponding parallel vibrations are 905 and 1293. In DNO_3 three of the four perpendicular vibrations have appeared, namely 589, 667 and 1536.

Venkateswaran has pointed out that the excitation of the line with an apparent shift of 1685 cm.$^{-1}$ is due to 4046 line of mercury arc. The authors took a number of photographs by avoiding the 4046 group of lines with a concentrated sodium nitrite solution and confirmed that the line is actually excited by 4358 line of mercury arc. There is also a similar type of line in DNO_3 at 1536 with an isotopic shift of 149 cm^{-1}.

The band at 2455 with DNO_3 extends over 150 wave-numbers and is due to the OD bond. The double lines, recorded as 167 in DNO_3 are probably to be attributed to lattice structure.

REFERENCES

[1] A H. Leckie, *Trans. Far. Soc.*, **32**, 1700 (1936).
[2] R. Ananthakrishnan, *Proc. Ind. Soc.*, **5**, 76 (1936).
[3] Angus and Leckie, *Proc. Roy. Soc. A*, **149**, 327 (1935).
[4] Dadieu and Kohlrausch, *Naturwissenschaften*, **19**, 690 (1931).
[5] Medard and Volkringer, *Compt. Rend.*, **197**, 83 (1934).
[6] Aderhold and Weiss, *Zeit für Phys.*, **83**, 83 (1934).
[7] C. S. Venkateswaran, *Proc. Ind Acad. Sci.*, **4**, 174 (1936).

ELECTRICAL INTERFERENCE TO RADIO BROADCAST RECEPTION

By S. P. CHAKRAVARTI

AND

N. L. DUTT

(*Received for publication, May 17, 1941*)

ABSTRACT. The paper relates to studies of electrical interference to radio broadcast reception on short and medium wave-lengths from typical Indian sources like d. c. ceiling fan, d. c. pumping installation, d. c. operated refrigerator, d. c. operated electric tool, etc. After discussing the nature of r. f. interference signal, different methods of measurements employed elsewhere as well as the authors' method were considered in details.

The r. f. interference voltage input to the receiver (resulting from the normally polarized electric component of the direct radiation field of the source as well as that of radiation field of any wiring along which energy may have been conducted) has been measured at a typical distance on wave-lengths from 10 to 550 metres for different sources. The effect of speed regulation of ceiling fans has been studied.

Studies have been made on the state of polarization of r. f. ground wave interference signals. The ratio of abnormally polarized to normally polarised component has been measured on various wave-lengths for different sources, and its variation with speed in case of ceiling fans has been observed.

Studies have been made on the propagation of r. f. interference signal in typical surroundings. An attempt has been made to verify the view-point that the interference signal is propagated from the source to the receiving point in typical conditions both (*a*) as radiated ground wave and (*b*) as wave conducted simultaneously by the electrical wiring to the vicinity of the receiving equipment whence it may be radiated to be picked up by the same. Horizontal polar diagrams have been shown.

Studies have been made as to the frequency components in the audio-frequency band resulting from r. f. interference signal from different sources and the distribution of power in the band. The effect of speed variation of ceiling fans has also been observed in this connection.

The equivalent normally polarized and abnormally polarized components of the electrical field intensity (in mv/m) of the interference on different metre-bands at typical distance have been obtained for various sources. The ratio of broadcast signal strength to total noise strength has been estimated in a few cases.

1. INTRODUCTION

Electrical Interference to radio broadcast reception is direct consequence of electrification for domestic, industrial, traction and other utilization purposes.

Direct-current equipments and systems are much greater offenders than alternating-current ones. Ceiling and table fans, pumping installations, refrigerators, vacuum cleaners, lifts, high-voltage transmission systems, converting plants, tramways, trolley-buses, automobile and aircraft systems, neon signs and electro-medical apparatus are known to have sources of interference associated with them.

The usual locations of interference source in some of the electrical machines and systems are (*a*) commutators in d.c. fan motors; (*b*) commutators, switches, contactors, etc., in large d. c. pumping installations; (*c*) commutators, switches and relay circuits in d. c. operated refrigerators; (*d*) high-voltage switchgears, contactors, mercury-arc rectifiers, etc., in power systems; (*e*) spark plugs, magnetos and electric horns in automobiles; and (*f*) collectors, brake-magnet coils, etc, in tramway systems.

Investigations on electrical interference from traction systems,[8] trolley buses,[11] high-voltage transmission lines,[1] electro-medical equipments,[11] automobiles and air-crafts,[1] have been undertaken by various bodies and solo workers in Great Britain, the United States and on the Continent. The methods of suppression and the legistations, [2,3,5,9] relating to them have also received adequate attention.

The conditions are much different in India and other tropical countries which, though much less industrially developed, need fans, pumps and refrigerators as household necessities. The direct-current supply systems still hold the field in majority of town areas in these regions. The chief interfering sources are therefore located in d. c. operated domestic equipments like fans, pumps and refrigerators out of which the d. c. fans may be called the worst type of offenders. Also it is evident that in majority of cases the sources of interference are situated either within the very premises of radio listener or in premises adjacent to his.

With the rapid expansion of radio broadcasting (specially of the short-wave type) in India during last five years, the demand for study of electrical interference on various wave-lengths from typical sources found here has considerably increased. The present paper has been an attempt to meet with the same and to obtain data suitable for broadcast designers.

2. NATURE OF R. F. INTERFERENCE SIGNAL

The interference signal can be considered to be made up of signal components at various frequencies arising out of any variation in the electrical condition of circuit or circuits associated with the interference source under consideration. The more abrupt the variation in the condition, the higher will be the frequencies of the interference signal components. The frequencies of the signal components will vary with different types of electrical equipment as well as with speed and other conditions at which they are worked.

Difference has also been found to exist between similarly designed equipments of the same type but of different makes and even between individual equipments of same design and same make. Moreover, the type of maintenance applied to equipment makes lot of difference to the interference caused by it. A badly maintained equipment causes much severe interference than a well-maintained one of the same design and make.

The analysis of the audio output (in Section 7) as well as the observation of oscillograph patterns (in Section 5) indicate that the interference signal spectrum for fans, pumping installation and refrigerator is more or less continuous.

Taking the specific case of commutator of a d. c. motor it will be noted that deviation from linear commutation takes place due to 'reactance voltage' (*i.e.*, self-induced e. m. f. in the coil due to change of current in it). This results in sparking between the brush and the receding commutator segment whose duration is prolonged due to self-induction. During this small duration of sparking, the circuit conditions undergo rapid change. A steady spark condition giving a limited number of frequency components is rapidly being altered to unsteady spark conditions giving rise to larger number of frequency components more or less as in a continuous spectrum. The greater the speed of the motor, the greater becomes the reactance voltage and consequently the greater the liability for sparking.

The electric equipment thus regarded as a source of radio-frequency energy (almost of the continuous spectrum type) radiates wave-components of various frequencies in all direction. The receiver picks up the portion of the radio-frequency interference spectrum lying in the band accepted by it and reproduces it as audio noise in the loud-speaker. It is likely that some radio-frequency energy is simultaneously conducted along the electrical wiring and re-radiated from a point to be also picked up by the same receiving equipment.

The plane of polarization of the radiated ground-wave interference signal from fans, pump and refrigerator has not been found to be vertical as it was observed by workers elsewhere for other electrical equipments. The interference signal is elliptically polarized. Measurement of normally and abnormally polarized components of the electric vector at a receiving point (outside the influence of induction field) has shown that the strength of the latter component is about 70 to 80 per cent of the former component. The ratio between the components has been found to vary with wave-length as well as with speed of the motor incorporated in the equipments.

On tuning a receiver connected to an aerial designed to pick up, say, the vertical component of the electric vector for a modulated broadcast signal of angular carrier frequency 'ω', the voltage input to the receiver due to broadcast signal will be

$$V_s = A(1 + m \cos pt) \cos \omega t \qquad \ldots \quad (1)$$

and that due to the integral of the radio-frequency (vertically or normally polarized) interference spectrum lying in the band accepted by the receiver will in general be

$$V_{RF} = a_0 \cos[\omega t + \theta_0] + a_1 \cos[(\omega + p_1)t + \theta_1] + a_2 \cos[(\omega + p_2)t + \theta_2] + \;\ldots \quad (2)$$

where $\omega/2\pi$ = broadcast carrier frequency; $p/2\pi$ = modulating frequency; $p_1/2\pi$, $p_2/2\pi$, $p_3/2\pi$...are *frequency differences* between interfering voltage frequencies and carrier frequency; θ_0, θ_1, θ_2,...are phase differences between interfering voltage components and signal voltage; A = carrier amplitude (vertically polarized component), m = modulation factor; a_0, a_1, a_2, are amplitudes of (vertically polarized) interference voltage components.

3. MEASUREMENT OF INTERFERENCE VOLTAGE

If the input to a receiver consists of modulated carrier and interference voltages, say, due to normally polarized (vertically) components represented as follows:

$$V'_{RF} = A(1 + m \cos pt) \cos \omega t + \Sigma a_n \cos[(\omega + p_n)t + \theta_n], \quad \ldots \quad (3)$$

then the audio-frequency output of the receiver (which selects a band of frequencies, rectifies the resultant linearly, rejects all except a certain band of audio frequencies and introduces constant amplification to the frequencies selected) will be given by

$$V' = K' \times [Am \cos pt + \Sigma a_n \cos(p_n t + \theta_n)] \quad \ldots \quad (4)$$

where K′ is a constant. Signal/Noise at the output $= \frac{Am}{\text{[illegible]}}$ (4a)

It will be seen that the interfering voltages appear undisturbed in the output, only their frequencies are changed to the difference between the original r. f. value and the carrier frequency.

If the modulated carrier be regarded to be absent and only the integral of the radio-frequency interference spectrum in equation (2) when it tends to be continuous be the incoming signal, then it can be shewn [11] that the audio-frequency electrical output of the receiver is approximately given by

$$V = k \times \Sigma a_n \cos(p_n t + \theta_n - \phi) \quad (5)$$

where $\phi = \tan^{-1}[\Sigma \tan(p_k t + \theta_k)]$

and k = a constant.

It will be seen that noise amplitude still remains proportional to Σa_n, but the character of the noise is slightly altered from that of the previous case.

Three distinct methods of measurement [6,7,11] of electrical interference (depending upon the above calculations) have been employed elsewhere. In one method (used by Siemens and Halske), in addition to the interference voltage, a modulated carrier of frequency same as that of the broadcast carrier is introduced to the input of the measuring set and the audio frequency noise output due to interference is measured by a specially designed peak voltmeter. In another method adopted by the British Post Office and Electrical Research Association, the interference voltage is measured by means of a special valve voltmeter associated with a suitably selective (superheterodyne) amplifier system. In the third method used in U S.A., the audio-frequency noise output due to interference voltage alone (without introduction of carrier) is measured by a calibrated radio receiver provided with an output voltmeter.

If the characteristic of the measuring equipment be quite linear and the interference has continuous and fairly uniform spectrum, the introduction of carrier does not produce much difference. The same measurements carried out by both first and third methods have yielded results almost agreeing with each other.

The method of measurement developed here is similar to the third method with the important difference that, instead of measuring directly the audio-frequency electrical output, the audio-frequency acoustic output has been measured by a directional microphone connected to an amplifier system.

The loudspeaker as well as the directional microphone-amplifier system have almost uniform response as well as negligible distortion over the audio-band involved. The overall characteristic of the entire measuring equipment (*i.e.*, 'radio-frequency interference input' *vs.* 'audio-frequency noise output of the microphone-amplifier') has been obtained fairly linear.

The advan'ages of the method are as follows :—

(*a*) The use of acoustic output enables an aural estimation of the intensity and character of the disturbance more or less as they would be in the actual reception to be simultaneously made, and

(*b*) the use of acoustic output is further helpful in distinguishing aurally the 'electrical noise' from the 'atmospheric noise' (which may happen to be picked up) and ensuring measurement of the desired disturbance only at all times in a tropical country (where the atmospheric disturbance is prevalent throughout the year).

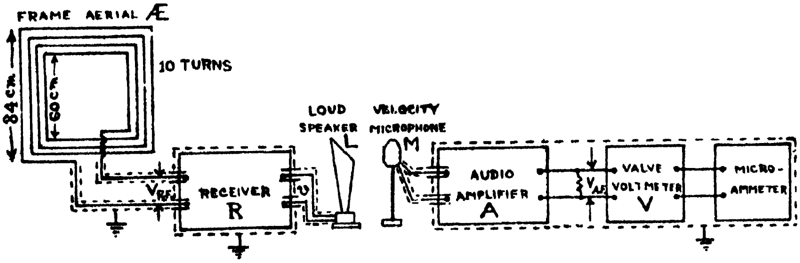

FIG. 1

Fig. 1 shows the block schematic diagram of the measuring equipment. Æ is a square frame aerial with 10 turns of 7/34 copper conductor (outer dimensions=84 cms. × 84 cms. and spacing between turns=1.2 cms) all in the same vertical plane rotatable about vertical axis and has been rendered free of "antenna effects" both in normal (aligned) and cross positions. This aerial shown in Fig. 1 has been used for measurement of vertically or normally polarized component of the electric field intensity for which the frame is placed with its plane in the direction of the source and observations taken at hours when other sources in the same or other directions are not in action. A horizontal aerial (rotatable about horizontal axis) has been used for horizontally or abnormally polarized component.

R is high-class superheterodyne receiving unit designed for medium and short wave bands in which A. V. C. can be switched on and off. The internal noise output (electrical) of the unit is about 100 to 110 micro-volts over the audio-frequency band which is about 100 db below the minimum electrical interference output. L is a high-quality loud-speaker of moving-coil type incorporated in the receiver unit and has uniform response and negligible distortion over the audio-band involved.

M is a velocity ribbon microphone of uniform response and negligible distortion over range 30-10,000 c.p.s. fixed at a distance of 4″ from the loud-speaker for all measurements. The velocity ribbon microphone has been selected for picking up the acoustic output for the following reasons :—(*a*) Its internal noise level is about the lowest ; (*b*) its response characteristic on the low-frequency side extends uniformly up to 30 c.p.s. and it has therefore been deemed suitable for picking up acoustic output of interference consisting of very low frequencies as well ; (*c*) it is a directional microphone most suitable for these measurements since it is undesirable for it to pick up sound from directions other than from the loudspeaker of the receiving equipment ; and (*d*) there is no harmonic distortion in such a microphone.

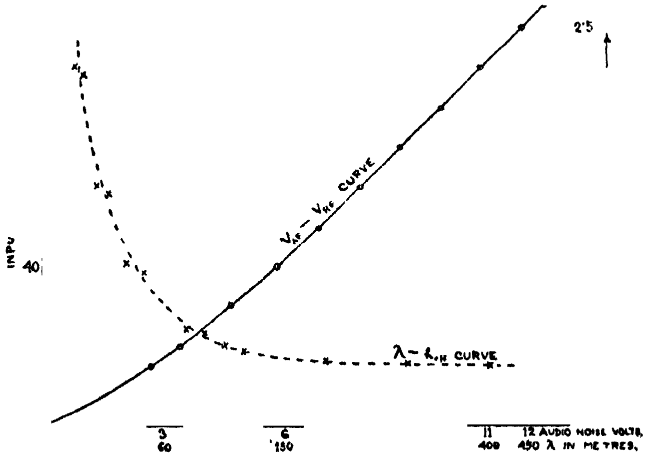

FIG. 2

A is an audio-voltage amplifier unit which is linear and has uniform amplification characteristic over the range 30-9000 c.p.s. V is a special valve voltmeter for measuring audio voltage across a non-reactive impedance connected across the amplifier output.

The measured overall characteristic of the entire equipment showing r.f. receiver input (V_{RF}) against audio noise voltage output (V_{AF}) of the microphone-amplifier is shown in Fig. 2. The variation of the effective height of the frame aerial shown in Fig. 1 with wave-length is also given in Fig. 2.

4. R. F. INTERFERENCE VOLTAGE DEVELOPED FOR DIFFERENT SOURCES

Measurement has been made by equipment in Fig. 1 on the r. f. interference voltage input to the receiver resulting from the vertically polarized electric component of the direct radiation field of source as well as that of radiation field of any wiring along which energy may have been conducted.

I. D. C. Ceiling Fan

The d. c. ceiling fan is generally regarded to be the worst offender. The site of interference source in the fan is the commutator.

(*a*) *Ceiling fans of same design and horse-power but of different makes*

Four ceiling fans (Walter Lock, Dayton, India Electric and Bengal) each of about 1/10 H.P. with same service age and same degree of maintenance applied to them have been examined.

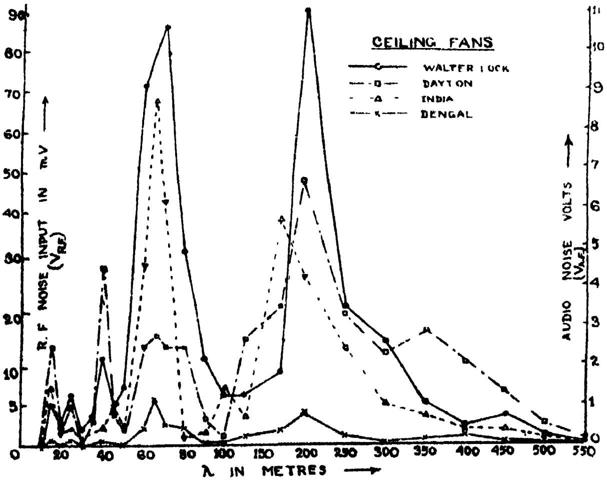

FIG. 3

Fig. 3 shows the radio-frequency noise voltage input (V_{RF}) into the receiver at various short and medium wave-lengths (the band-width associated with each wave-length being about 16 kc/s) measured at 50 feet from the source which is outside the influence of the induction field of the source. The distance over which the effect of induction field can be reasonably expected to exist depends upon the frequency (or wave-length) as well as upon the strength of commutator sparking current component at the frequency. The speed regulator in all cases is adjusted for 300 r.p.m.

It will be seen on comparison of the experimental curves that (*a*) the "Bengal Fan" gives in general the lowest noise voltage level for wave-lengths in short and medium wave bands, (*b*) all the four fans examined give very high noise voltage on the wave-length ranges 55-80 metres and 150-250 metres, (*c*) all the fans (except the Bengal fan) give high noise voltage on the wave-length range 13-15 metres, 26-28 metres, 35-45 metres, 130-150 metres and 250-350 metres and (*d*) all the fans give low noise voltage on the wave-length range 16-22 metres, 28-32 metres, 45-50 metres, 90-110 metres and 400-545 metres.

(*b*) *Effect of speed regulation*

Four ceiling fans (Walter Lock, India Electric, Siemens and Bengal) have been examined for the effect of speed regulation. Investigation has been carried on three speeds—"full," "medium" and "slow." Full, medium and slow speeds were respectively 520, 300 and 120 r.m.p. for Bengal Fan ; 380, 250 and 100 r.p.m. for India Fan; 350, 220 and 100 r.p.m. for Siemens Fan and 250, 150 and 80 for Walter Lock Fans fitted with our regulators.

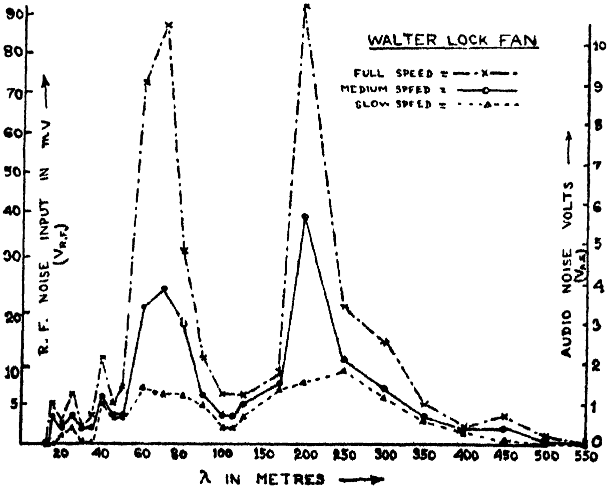

FIG. 4(*a*)

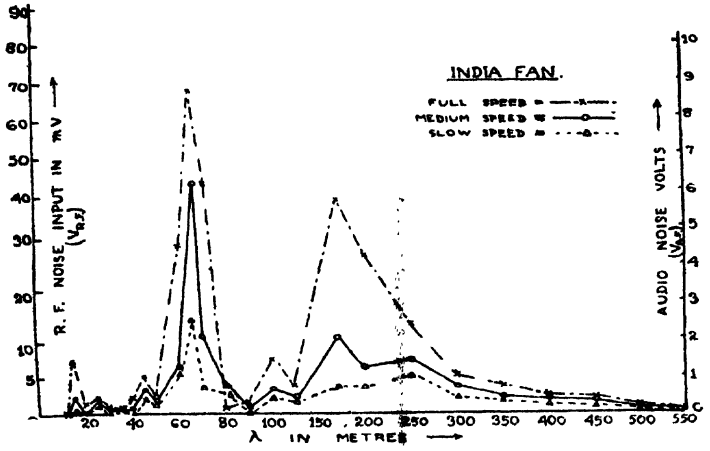

FIG. 4(*b*)

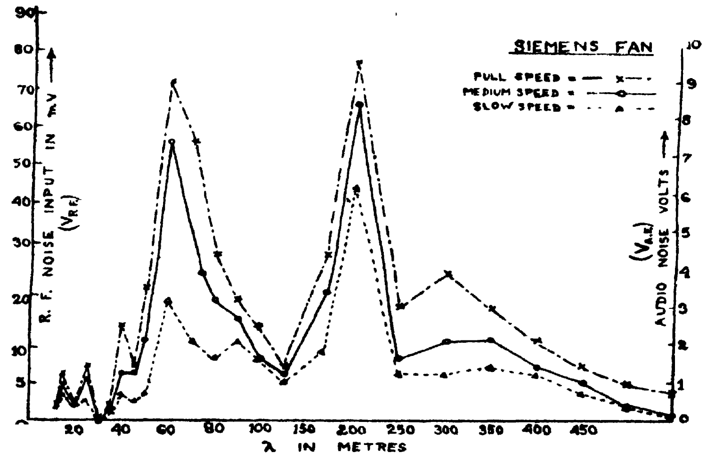

FIG 4(*c*)

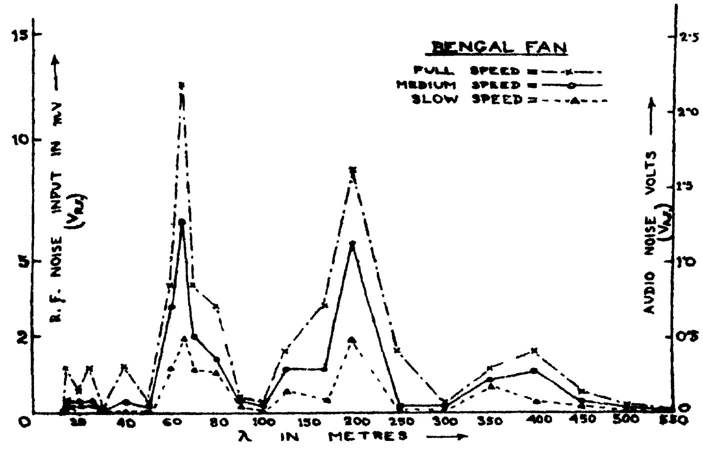

FIG. 4(*d*)

Fig. 4(*a*), 4(*b*), 4(*c*) and 4(*d*) show the radio-frequency noise voltage input (V_{RF}) into the receiver at various short and medium wave-lengths measured at 50 feet from the sources under different speed conditions.

It will be seen from the figures that, on decreasing the speed, the radio-frequency noise voltage (V_{RF}) at the various short and medium wave-lengths decreases. It will be noticed that the peaks (obtained at full speed) on certain wave-length ranges in case of Walter Lock and India Electric fans get reduced or disappear when the speed is reduced to 'slow' and thus the effect of speed reduction is to decrease or eliminate completely the interference on certain wave-lengths.

Table I shows the reduction of noise level in decibels on speed reduction on typical wave-lengths.

TABLE I

Fan Make	Wave-length (metres)	Reduction of noise voltage in *db* on changing from	
		Full to medium speed	Full to slow-speed
Walter Lock	70	8.7 *db*	19.1 *db*
	200	6.1 ,,	17·3 ,,
India Electric	66	3.0 ,,	11.0 ,,
	170	9.0 ,,	18.1 ,,
Siemens	60	2.0 ,,	9.0 ,,
	200	2.0 ,,	4.0 ,,
Bengal	66	5.0 ,,	13.0 ,,
	200	3.0 ,,	10.4 ,,

II. D. C. Pumping Installation

The d. c. pumping installation (whether for domestic or other purpose) interferes severely with the broadcast reception. The sites of interference sources in the installation are commutator, switchgear, contactor, etc.

Measurements have been taken on a d. c. pumping installation with 2 H.P. G.E.C. motor at 200 feet from it, the motor running at about the full speed (28,000 r.p.m.),

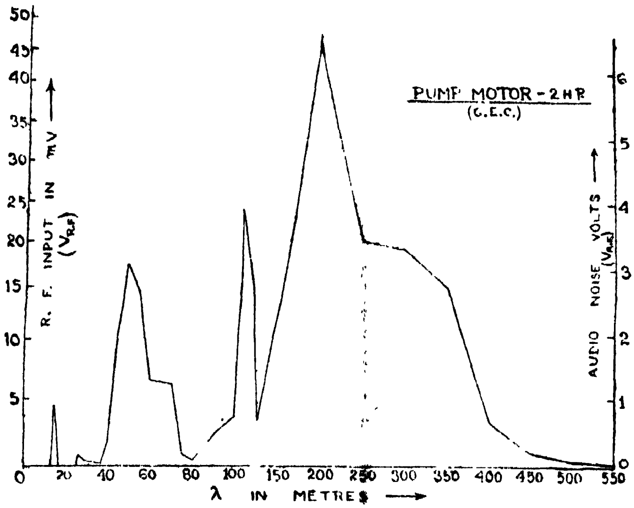

FIG. 5

Fig. 5 shows the radio-frequency noise voltage input (V_{RF}) at various short and medium wave-lengths measured at 200 feet from the source.

It will be seen therefrom that the noise voltage is (*a*) considerably high on the wave-length range 175-240 metres, (*b*) quite high on about 14 metres and on wave-length ranges 42-72 metres, 92-175 metres and 240-400 metres and (*c*) low on other wave-lengths.

It would also appear that a d. c. pumping installation of the type would not, in general, interfere with short wave-lengths from 12 to 40 metres (except on 14 metres).

III. D. C. Operated Refrigerator

The refrigerator operated from the d c. mains causes interference on a comparatively larger number of wave-lengths in short and medium wave bands. The sites of interference sources in the refrigerator are commutator, switch and relay circuit.

Measurements have been taken on a typical refrigerator manufactured by Frigidaire Co. (U.S.A.) and fitted with ¼-H.P. motor at 50 feet from it, the motor running at about the full speed (1200 r.p.m.).

Fig. 6 shows the radio-frequency noise voltage input (V_{RF}) at various short and medium wave-lengths measured at 50 feet from the source.

It will be seen therefrom that unlike other sources (previously discussed) the refrigerator causes disturbance over larger number of wave-length ranges. The noise voltage is (*a*) very high on range 38-46 metres and on 120 metres, (*b*) high on ranges 36-38 metres, 46-88 metres, 110-120 metres, 130-150 metres

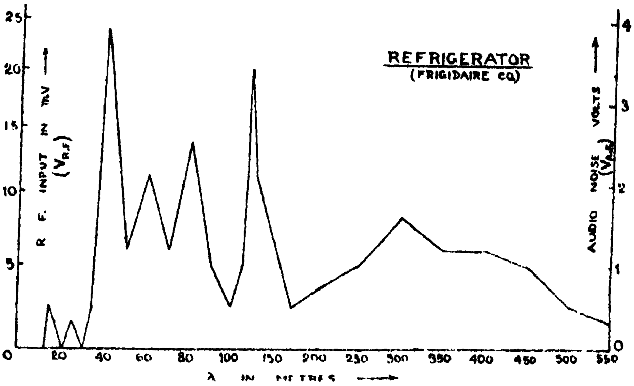

FIG. 6

and 250-450 metres and (*c*) low on other wave-lengths specially on the range 12-36 metres.

5. POLARIZATION OF GROUND-WAVE INTERFERENCE SIGNALS

To examine the state of polarization of the ground-wave interference signals, a receiving point outside the influence of induction field has been so chosen that there are no radiating wirings in the vicinity of the point to modify the receiver input voltage developed from the electric component (vertically polarized or horizontally polarized) of the direct-ray field. The consideration of sky ray does not come in at all for distance involved here.

For obtaining r. f input voltages due to vertically polarized and horizontally polarized components of the electric vector, aerials of the type discussed in section 3 have been employed. Knowing the voltages developed in the aerials and their effective heights, the ratio of horizontally polarized component (E_H) to vertically polarized component (E_V) has been estimated at various wave-lengths.

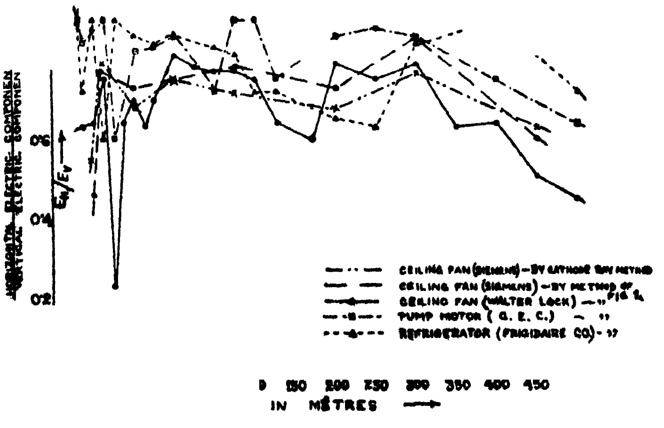

FIG. 7

Fig. 7 shows the ratio plotted against wave-length for ceiling fan (1/10 H.P.), pumping installation (2 H.P.) and refrigerator (¼ H.P.) situated at 50, 200 and 50 feet respectively from the receiving point. It will be seen that the ratio (E_H/E_V) decreases on wave-lengths above 400 metres and also below 40 metres and that the average ratio for equipments examined varies from 0.7 to 0.8 over the range 40-400 metres.

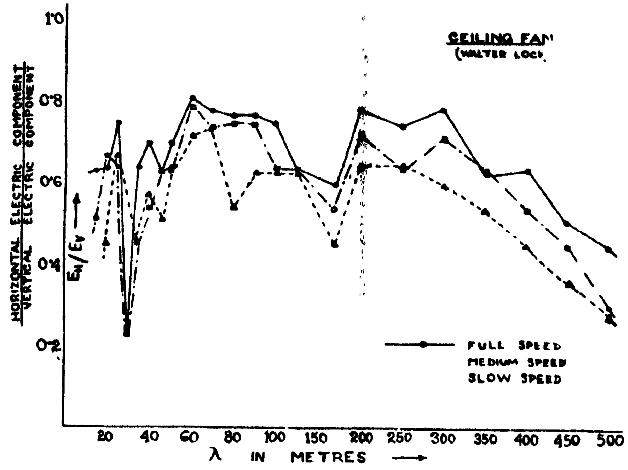

FIG. 8

Fig. 8 shows the ratio plotted against wave-length for ceiling fan at three different speeds. It will be seen that the ratio decreases in general as the speed is reduced.

The ratio of the components as well as the elliptical patterns have also been obtained by an alternative method—by connecting up the vertical and horizontal aerials of almost same effective height to two exactly similar superheterodyne receiving units (loud-speakers disconnected) with same beating oscillator and applying their electrical outputs to two pairs of plates of a cathode-ray oscillograph tube. Fig. 7 shows that ratio E_H/E_V for "Siemens fan" obtained by cathode-ray oscillograph and previous method is more or less in agreement. Patterns observed at various wave-lengths from 19 to 450 metres show a number of ellipses (due to various interference signal components accepted by receiver) superimposed on one another, some of them being more agitated than others.

6. PROPAGATION OF R. F. INTERFERENCE SIGNAL IN TYPICAL SURROUNDINGS

The mode of propagation of r. f. interference signal from the source to the receiving point (in typical surroundings) is more complex than that of either atmospheric disturbance or broadcast signal. In majority of cases the sources of interference are situated either within the very premises of the listener or in premises adjacent to his. It is only in exceptional cases that badly maintained electrical equipments interfere with radio reception at distant receiving points.

Taking the common case, it will be realized that a number of electrical wirings of various types invariably run vertically or horizontally or both ways between the position of interfering equipment and proximity of the receiving point. It is more or less impossible to ignore the part played by them in modern premises. It may therefore be said that the interference signal is likely to be propagated from the source to the receiving point (situated outside the influence of induction field of the source) simultaneously (*a*) as radiated ground wave and (*b*) as wave conducted by the electrical wiring to the vicinity of the receiving aerial whence it is either radiated to be picked up by the receiving equipment or transferred to it by induction depending upon separation between wiring and receiving aerial, wave-length, power, etc. The consideration of sky ray for distances involved here does not arise at all.

The propagation of signal along the electrical wiring can take place either as that of potential difference between the two conductors themselves or of potential difference between the mean potential of conductors and earth known in subsequent paragraghs as 'symmetrical' and 'asymmetrical' propagations respectively.

It will be seen in the following portions of the present section how far the mode of propagation suggested above holds good in an actual case. Table II shows the measured values of r. f. interference voltage input resulting from the vertically polarized electric component of the radiation field of the source as well as of any wiring radiating the conducted energy.

TABLE II

Distance from source (yds.)	Ceiling Fan—Walter Lock		Electric Tool—Electromag. Tool Co.	
	R. F. Voltage input (mv.) on		R. F. Voltage input (mv.) on	
	$\lambda = 15$ m.	$\lambda = 450$ m.	$\lambda = 15$ m.	$\lambda = 400$ m.
10	14	4·5	160	42
15	7	3·5	82	31
20	4·5	2.0	29	28
25	3	1.0	14	24·5
30	1	0.5	10.05	23·5
50	0.4	0.2	6	21.6

Calculation of r. f. noise voltage input

The r. f. noise voltage input due to vertically polarized electric component of the direct radiation field of the source as well as of wiring radiating the condut-ed energy has been calculated for ceiling fan and electric tool.

I. *Ceiling fan—Walter Lock (1/10 H. P.).*

The necessary design data for motor in the above ceiling fan are as follows :—

Armature diameter $= D_A = 9$ cms. ;
Commutator diameter $= D_c = 4$ cms. ;
Effective embedded length of loop of commutated coil $= l_e = 12$ cms. ;
Effective free portions of loop of commutated coil $= l_f = \frac{3\pi D_A}{n}$;
Number of turns/slot $= M = 70$;
Number of poles $= n = 2$;
Armature current $= I_A = 0.4$ amperes ;
Brush contact resistance $= r_b = 5$ ohms ;
R. P. M. (at full speed) $= 250$;
Brush thickness $= 6$ mms. ; and mica insulation thickness $= 1$ mm.

Then, by calculation,

Current in commutated coil $I_c = I_A / n = 0.2$ amperes.

$t_c =$ time of commutation (during which current change take place) $= .01$ sec.

$L_c = 8M^2 (l_e + 0.1 l_f) \times 10^{-8}$ Henries $= 128 \times 49 \times 10^{-6}$ Henries.

$E_s =$ Reactance voltage (sparking voltage)

$$= L_c . \frac{I_c - (-I_c)}{t_c} \times 10^{-8} \text{ volts} = L_c . \frac{2I_c}{t_c} \times 10^{-8} \text{ volts.}$$

$= 250$ mv.

$I_s =$ sparking current $= 50$ m.a. (max.).

The sparking current for this fan may be regarded to consist of current components of various frequencies (almost as in continuous spectrum from 0.5 Mc/s to 30 Mc/s. The representative current strength (I) (for vertical component) over a band-width of 16 Kc/s (*i.e.*, 8 Kc/s on either side of the frequency under consideration) associated with 0.66 Mc/s (*i.e.*, 450 metres) component may be estimated to 2 m.a. and over the same band-width associated with 20 Mc/s (*i.e.*, 15 metres) about 0.5 m.a.

The *euqivalent* effective height of the fan aerial at 0.66 and 20 Mc/S has been arrived at to be 58.5 metres and 6.5 metres respectively. Taking appropriate absorption factor A_1 for medium and short wave-lengths, the vertical component of electric intensity of the direct (radiation) field in the two cases has been obtained from the equation

$$E_\nu = 377 \cdot \frac{h\,I}{\lambda D} A_1 \text{ mv/m} \tag{6}$$

where h and λ are in metres, D in Kms. and I in amperes. The voltage developed in the receiving aerial of effective height h_r is given by

$$V_a = E_\nu \;.\; h_r \qquad \ldots \tag{7}$$

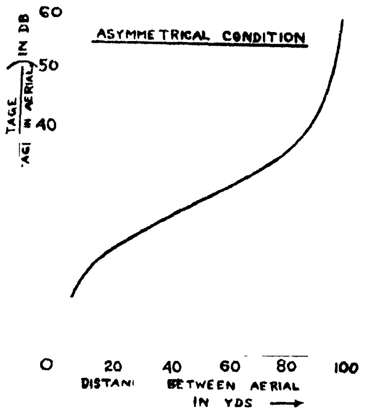

Fig. 9(*a*)

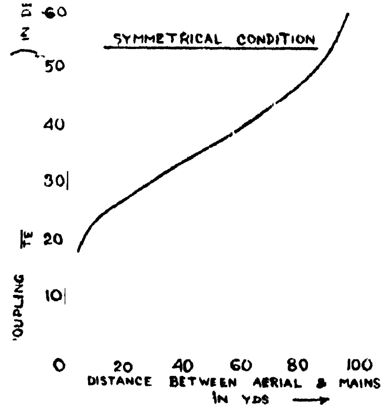

Fig. 9(*b*)

To calculate the voltage developed in the aerial (V_a') on account of the vertical component of radiation field of electric wiring along which the interference voltage has been conducted from the source to the vicinity of the receiving aerial, use has been made of experimental curves (Figs. 9) showing coupling factor (R. F. voltage on the mains wiring at the point divided by interferenee voltage in aerial) for different separations between the wiring and the aerial. Transmission over mains has been considered both for symmetrical and asymmetrical conditions which give results not much different from each other in this particular case. The total r.f. noise voltage input $= V_{RF} = V_r + V_c$ since individual voltages V_r and V_c due to pure radiation and conduction – radiation respectively are in the same phase.

Table III shows the voltages arrived at by calculations.

Table III

Distance from source (yds.)	λ = 15 metres			λ = 450 metres		
	V_r (mv.)	V_c (mv.)	V_{RF} (mv.)	V_r (mv.)	V_c (mv.)	V_{RF} (mv.)
10	12.96	0.28	13.24	3.78	.37	4.15
20	4.05	0.17	4.22	1.89	.22	2.11
30	1.8	0.11	1.91	1.26	.15	1.41
50	1.08	0.07	1.15	0.76	.14	0.90

II. Electric Tool—(Electro-magnetic Tool Co.) (1/4 H. P.).

The necessary design data for motor in the above tool are as follows :—

Armature diameter $= D_A = 5$ cms. ;

Commutator diameter $= D_c = 2.5$ cms. ;

Effective embedded length of loop of commutated coil $= l_e = 10$ cms. ;

Effective free portions of loop of commutated coil $= l_f = \frac{3\pi D_A}{n}$;

No. of turns/slot $= M = 200$;

No. of poles $= n = 2$;

Armature current $= I_A = 0.9$ ampere ;

Brush contact resistance $= r_b = 5$ ohms ; Brush thickness $= 4$ mm. ;

Mica insulation thickness $= 1$ mm. ;

R. P. M. (when at full speed) $= 500$.

Then, by similar calculations as before, $I_c = 0.45$A ; $t_c =$ time of commutation $= .005$ sec. ; $L = 384 \times 10^{-4}$H ; sparking voltage $E_s = 6.9$V and sparking current $I_s = 1.4$A.

With similar consideration as in the previous case, the representative current strength (I) (for vertical component) over a band-width of 16 Kc/s associated with 0.75 Mc/s (*i.e.*, 400 metres) component may be estimated to about 31 m.a. and over the same band-width associated with 20 Mc/s (*i.e.*, 15 metres) to about 11 m.a. The equivalent effective height of the tool (placed at 7 feet above ground on an insulating stand) at 0.75 and 20 Mc/s has been obtained to be 34 and 3 metres respectively. The voltage developed in the receiving aerial due to vertical electric component of direct radiation field in two cases has been similarly calculated. The voltages developed in the receiving aerial due to radiation from wiring under symmetrical (S) and asymmetrical (A) conditions are much different in this case.

The r.f. noise voltage input to receiving equipment is shown in Table IV.

TABLE IV

Distance from source (yds.)	λ = 15 metres V_r (mv.)	V_i (mv.) S	V_i (mv.) A	V_{ri} (mv.) S	V_{ri} (mv.) A	λ = 400 metres V_r (mv.)	V_i (mv.) S	V_i (mv.) A	V_{ri} (mv.) S	V_{ri} (mv.) A
10	125	.25	.07	125.25	125.07	41.13	.32	.08	41.45	41.21
20	39	.8	.14	39.8	39.14	20.14	1.0	.18	21.14	20.32
30	18	.3	.8	18.3	18.8	14.0	.4	.11	14.4	14.11
50	15.4	.24	.6	15.64	16.0	10.5	1.5	.50	12.0	11.0

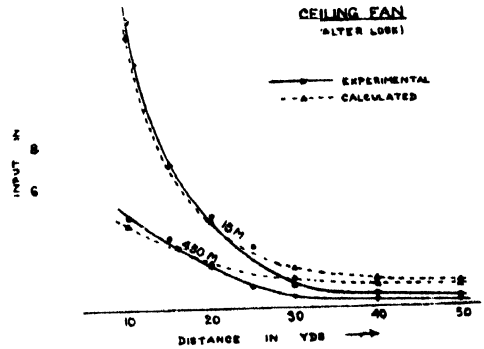

FIG. 10(*a*)

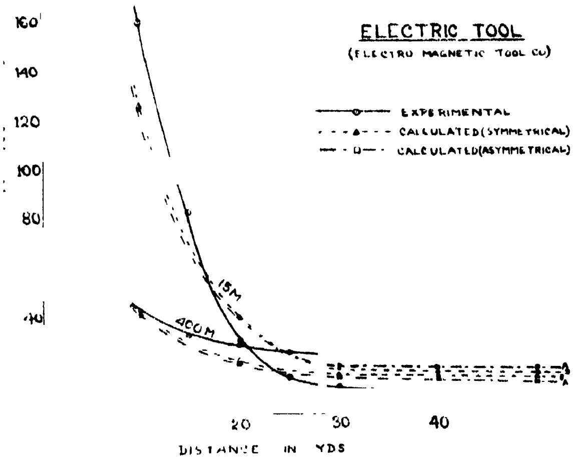

FIG. 10(*b*)

Fig. 10(*a*) and 10(*b*) show the measured and calculated variations of r.f. noise voltage input with distance. It will be seen that complete agreement between theoretical and experimental curves has not been obtained due to certain uncertain factors involved in calculations which cannot be eliminated. It is likely that in actual case more than one electrical wiring has been taking part in conducting the signal and radiating it from various points.

Horizontal polar diagram of sources

The horizontal polar diagrams of sources installed in typical surroundings on representative wave-lengths in medium and short wave bands have been obtained. The variation of r.f. noise voltage with distance in different directions depends upon (*a*) the nature of structural construction and fittings at various distances in different directions and their conductive properties, (*b*) the distance, (*c*) the frequency or wave-length, and (*d*) the proximity or presence of electrical wirings at various distances in different directions. Diagrams obtained for (*a*) Dayton ceiling fan and (*b*) G.E.C. pump motor are shown in Figs. 11(*a*) and 11(*b*) respectively.

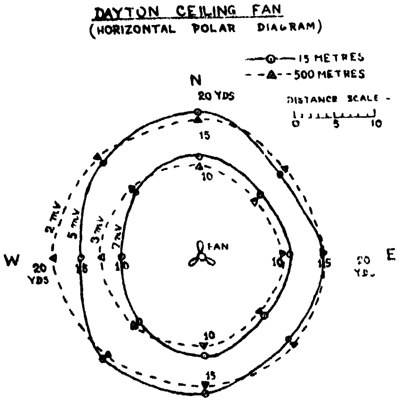

FIG. 11(*a*)

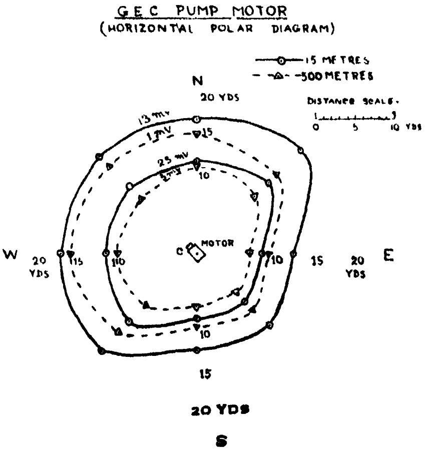

FIG. 11(*b*)

It will be seen therefrom that (*a*) Dayton ceiling fan gives on 15 metres almost the same r.f. noise voltage at the same distance on all sides and on 500 metres greater noise voltage at the same distance on the western side, and (*b*) pump motor gives on both wave-lengths the lowest r.f. noise voltage at the same distance on the south-eastern side.

For the ceiling fan the greater noise voltage on the western side may be due to the presence of wiring on that side and for pump motor the lowest noise voltage on the south-eastern side may be due to the screening effect of the rest of the motor behind the commutator C, the other factors remaining the same.

7 ANALYSIS OF AUDIO NOISE

The section relates to study as to the frequency components in the audio-frequency band resulting from r.f. noise voltage input and the distribution of power in the same.

It has been discussed in section 2 that an electrical equipment is more or less an interference source of continuous spectrum type and further the receiver picks up the r.f. interference spectrum lying in band accepted by it.

The frequency components in the audio noise band shall depend upon (*a*) the r.f. interference spectrum about the r.f. frequency under consideration and the degree to which it could be regarded as continuous and (*b*) the band-width accepted by the receiver employed; whereas the distribution of power in the band shall depend upon (*a*) the amplitudes of the radio frequency components in the portion of spectrum accepted by the receiver, (*b*) the degree to which the interference spectrum could be regarded as continuous, and (*c*) the performance of the receiver with regard to the various components in the band accepted.

For analysis and estimation of power in different portions of the band, the output of the microphone amplifier in Fig. 1 has been arranged to pass through each of the several narrow band-pass filters of negligible attenuation at a time. From measurement of the total output voltage as well as of output voltages of the several filters (the voltages being measured across the same impedance), the distribution of power in different portion of the band has been ascertained.

Table V shows the results of analysis on the pick-ups of r.f. interference spectrum (vertical component) from ceiling fans running at different speeds on short and medium wave-lengths.

It will be seen therefrom that (*a*) the frequencies in the audio noise band roughly lie between 30 and 8000 c.p.s. and (*b*) over 80 to 90% of the power is within the range 30 to 800 c.p.s. and over 42 to 53% of the power is in the range 30-150 c.p.s. Further it will be observed that the effect of motor speed variation on the distribution of power in the audio band is complex. It can only be said that the effect of reducing speed is to lower the power percentage in the frequency range above 400 c.p.s. (except over portion of band 1200-2000 c.p.s. in certain cases) but the frequency limits of the audio band remain the same.

TABLE V

Sub-bands of the audio band (c.p.s.)	G. E. C. FAN						BENGAL FAN					
	Percentage noise voltage						Percentage noise voltage					
	λ = 25 m.			λ = 300 m.			λ = 25 m.			λ = 350 m.		
	Full	Medium	Slow	Full	Medium	Slow	Full	Medium	Slow	Full	Medium	Slow
	%	%	%	%	%	%	%	%	%	%	%	%
30-60	23.1	29.6	29.6	29.6	29.6	35.8	36	36	40	36	40	40
60-150	19.4	19.4	19.4	12.9	19.4	13.2	16.5	19.6	15.6	19.6	15.6	20.9
150-250	12.5	12.0	12.0	16.4	9.9	9.9	14.8	16.7	16.7	16.7	16.7	15.5
250-400	8.8	8.1	11.9	4.9	10.2	10.2	16.7	14.0	11.7	11.7	14.0	9.9
400-800	16.6	14.9	14.1	9.1	7.8	7.8	6.2	5.5	6.2	7.8	5.5	5.5
800-1200	9.4	5.8	2.8	11.1	7.1	10.1	4.6	2.9	4.5	1.7	2.9	2.9
1200-2000	2.5	3.5	4.4	8.3	9.3	6.3	1.2	2.3	2.3	3.5	2.3	2.3
2000-4000	6.2	5.7	4.8	6.2	5.7	5.7	2.7	2.0	1.7	2.1	1.7	2.1
4000-8000	1.5	1.0	1.0	1.5	1.0	1.0	1.3	2.0	1.3	0.9	1.3	0.9

Table VI shows the results of analysis on similar pick-ups from pump and refrigerator. It will be seen therefrom that about 90% of the power is within the range 30-1200 c.p.s. for noises both from pump and refrigerator.

TABLE VI

Sub-bands of the audio band (c.p.s.)	PUMP		REFRIGERATOR	
	Percentage noise voltage		Percentage noise voltage	
	λ = 15 m	λ = 300 m.	λ = 15 m.	λ = 300 m.
	%	%	%	%
30-60	35.9	12.0	19.4	15.3
60-150	17.8	16.9	13.5	17.6
150-250	5.7	5.3	10.1	16.1
250-400	9.7	8.7	16.7	10.0
400 800	7.8	8.1	17.0	14.7
800-1200	10.3	6.3	11.2	13.5
1200-2000	2.6	4.8	7.5	6.2
2000-4000	8.7	6.4	3.7	5.0
4000-8000	1.5	1.5	1.6	1.6

8. ESTIMATION OF SIGNAL/TOTAL NOISE ON VARIOUS METRE-BANDS

The section relates to the representative values of (equivalent) interference field-strength on various wave-length bands (accommodating the broadcasting stations) at the receiving aerial situated at given distance from the source outside its induction field as well as the estimation of the ratio of signal to total noise (including "atmospheric" and "man-made static") and is meant for direct application to the actual problem.

The estimated equivalent field-strength values shown here for short wave-length bands can be taken as representative figures for the whole of the wave-band associated with the various wave-lengths as follows:—11-metre band (25.6-26.6 Mc/s); 13-metre band (21.45-21.75 Mc/s); 16-metre band (17.75-17.85 Mc/s); 19-metre band (15.1-15.35 Mc/s): 25-metre band (11.7-11.9 Mc/s); 31-metre band (9.5-9.7 Mc/s); 41-metre band (7.2-7.3 Mc/s); 49-metre band (6.0-6.2 Mc/s); 60-metre band (4.9-5.1 Mc/s); 80-metre band (3.65-3.85 Mc/s); and 90-metre band (3.43-3.23 Mc/s).

Those shown for medium wave-lengths are representatives for smaller band-width of about 18 kc/s associated with each of them.

Table VII gives the *equivalent* normally polarized component of the electrical field intensity (in milli-volts/metre) on different wave-length bands. The distance of the source from receiving aerial has been 50 feet for ceiling fan and refrigerator with wiring running in a normal way and 200 feet for pumping installation without much wiring nearby. The *equivalent* abnormally polarized component of the electrical field intensity can be obtained by multiplying the figures in Table VII by the ratios of E_H/E_V shown in Figs. 7 and 8.

TABLE VII

Source	Milli-volts/metre on metre-bands													
	11	13	16	19	25	31	41	49	60	80	90	250	350	450
(1) India Electric Ceiling Fan (1/10 H.P.)	1.2	2.8	2.4	1.0	1.03	1.0	1.67	4.0	40	8.2	3.0	33.3	9.2	5.4
(2) Frigidaire and Co. Refrigerator (motor horse power = 1/4 H.P.)	0	0.4	0.8	0.25	0.86	0.67	8.3	14	14.7	23.6	12	13	15.9	16.2
(3) G.E.C. Pumping Installation (motor horse power = 2 H.P.).	0	0.7	0.3	0	0.22	0.25	1.25	10.5	9	0.9	4	52	41	8.1

TABLE VIII

Electrical source	Signal/Total Noise Ratio											
	19-metre DELHI				25-metre DELHI				370-metre CALCUTTA			
	Signal Strength (quasi-max)	Atmospheric strength	Man-made strength	Ratio	Signal strength (quasi-max)	Atmospheric strength	Man-made strength	Ratio	Signal strength	Atmospheric strength	Man-made strength	Ratio
	mv/m	mv/m	mv/m	db	mv/m	mv/m	mv/m	db	mv/m	mv/m	mv/m	db
(1) India Electric Ceiling Fan (at 50 ft. distance).	3.0	0.2	1.0	8	4.0	0.3	1.03	9.6	120	3	5.4	23.1
(2) Frigidaire & Co. Refrigerator (at 50 ft. distance).	3.0	0.2	0.25	16.4	4.0	0.3	0.86	10.8	120	3	16.2	16.0
(3) G. E. C. pumping installation (at 200 ft. distance).	3.0	0.2	0	23.5	4.0	0.3	0.22	17.8	120	3	8.1	20.8

It will be seen that by taking all the sources examined (*a*) the 11, 16, 19, 25, and 31-metre bands appear to be the best for use and (*b*) the 13, 41, 90 and 400-metre bands are better than others.

The ratio of signal/total noise has been estimated for three cases, namely, (*a*) Delhi 19-metre day transmission, (*b*) Delhi 25-metre night transmission and (*c*) Calcutta 370-metre medium wave transmission as shown in Table VIII. Normally polarized components for both signal and noise were taken. Signal strength as measured at the Communication Engineering Laboratories (Calcutta) during March-April, 1941, atmospheric peak strength as measured[12] during summer (non-thundery days) and man-made static strength as obtained above have been taken to estimate the ratio.

9. ACKNOWLEDGMENT

The whole of the experimental work was carried out at the Kanodia Electrical Communication Engineering Laboratories of the Department of Applied Physics, University of Calcutta. The authors desire to thank very heartily Prof. P. N. Ghosh, M.A., Ph.D., Sc.D., F.Inst.P., Head of the Department of Applied Physics, for his kind interest and encouragement throughout.

REFERENCES

[1] Curtis, *Proc. I.R.E.*, **20**, 674 (1932).

[2] Morris, *J.I.E.E.*, **74**, 245 (1934).

[3] *Report to I.E.E. Council*—"Electrical Interference with broadcasting," *J.I.E.E.*, **74**, 801 (1934).

[4] Langton and Bradshaw, *J.I.E.E.*, **75**, 643 (1934).

[5] Neale, *Electrical Power Engineer*, **17**, 510 (1935).

[6] Subra, *Annales des Postes, Telegraphes, et Telephones*, **24**, 368 (1935)..

[7] Mumford and Barker, *J.P.O.E.E.*, 40 (1935).

[8] Schumacher, *Proc. I.R.E.*, **23**, 779 (1935).

[9] Warren, *J.P.O.E.E.*, **28**, 23 (1935-36).

[10] *Report on "Electrical Interference with Broadcasting,"* *J.I.E.E.*, July-Dec., 206 (1936).

[11] Gill and Whitehead, *J.I.E.E.*, **83**, July-Dec., 345 (1938).

[12] Chakravarti, *L'Onde Electrique*, 99-110, March (1939).

A STUDY OF ALLOTROPES OF SELENIUM BY THE X-RAY DIFFRACTION METHOD *

By K. DAS GUPTA, S. R. DAS

AND

B. B. RAY

(*Received for publication, May 17, 1941*)

Plate IX

ABSTRACT. The transformation of monoclinic selenium into metallic (hexagonal) form has been studied by the X-ray diffraction method and it has been found that the period of transformation depends on the temperature, *e.g.*, at 120°C it takes one hour, at 80°C, 15 days, and at 65°C more than 17 days are required for complete transformation. The transition is monotropic.

The amorphous varieties soften even at 38°C (the melting point of metallic selenium being 217°C) and on X-ray diffraction analysis three broad bands coinciding in position and intensity with the three distinct groups of lines of the crystalline varieties are obtained. It has been found that the vitreous selenium devitrifies even at 28°C and the devitrified mass gives crystalline pattern. The rate of devitrification and the transformation into the crystalline modification depends very much on the temperature. The surface of the sample of vitreous selenium supplied by Dr. Grippenberg preserved in his laboratory in Finland for seven years (the maximum temperature throughout the year being below 27°C) when examined was found to be crystalline, while the internal portion of the sample gave diffuse broad bands.

It has also been shown that at a very low temperature the devitrified product is purely monoclinic and at a high temperature it is purely hexagonal. There are intermediate temperatures at which both monoclinic and hexagonal varieties are produced.

Accurate measurements of the spacings corresponding to the bands obtained with samples of vitreous selenium heated for different periods at 38°C show that the band spacing is a continuous function of the period of heating. Now as there is a regular growth of size of the crystallites present in vitreous selenium with the period of heating, it is clear that the band-spacing is a function of the size of the crystallite. Our experimental results thus satisfy the theoretical work of Lenard Jones, *viz.*, that the lattice constant should be a function of the particle size. The band spacing corresponding to the sample of amorphous selenium coagulated from the colloidal solution is 3.8 A.U. while that of the vitreous selenium heated for 60 hours at 38°C is 3.4 A.U. only.

INTRODUCTION

Vitreous selenium, the most well-known amorphous variety, obtainable in the form of black sticks, can be easily prepared by rapidly cooling molten selenium. Selenium thus obtained is a brittle black substance having average density of 4.28 gms./c.c. On heating, gradual softening commences at 50°C. The red precipitated selenium or red amorphous selenium is prepared by the reduction of selenious acid with sulphurous acid, glucose, etc. Its behaviour on heating is the same as that of the vitreous selenium. The density of this variety is 4.26 gms./c.c. Both of the foregoing varieties are partially soluble in carbon disulphide.

---

* Communicated by the Indian Physical Society.

Red monoclinic selenium is obtained when CS_2 solution of amorphous selenium is allowed to crystallise by evaporation at the room temperature. The density of this variety is 4.44 gms./c.c. at 0°C. It melts at 170°C and the transformation into metallic or hexagonal form begins slowly at 120°C. Metallic selenium, the hexagonal variety, is the most stable form and is obtained by the transformation of the above-mentioned forms of selenium. The density is 4.78 gms./c.c. at 0°C and melts at 217°C. The boiling point is 690°C. The electrical conductivity of metallic selenium is exceedingly small in the dark but on exposure to light the resistance deminishes in a remarkable manner. Selenium can also be obtained in colloidal state by the reduction of aqueous solution of SeO_2 by means of requisite quantity of SO_2 or glucose.

Bradley[1] has determined the structure of the hexagonal selenium (the metallic variety). The structure of the monoclinic selenium has been determined by Klug.[2] Prins and Dekeyser[3] studied by X-ray diffraction method the crystallisation of vitreous selenium. Their conclusions may be summarised as follows : (*a*) The transformation of the vitreous selenium into the hexagonal variety may take place at 60°C if a thread of vitreous selenium be kept under tension at that temperature. (*b*) In the absence of any tension the crystallisation does not take place below 73°C.

The representation made in this paper comprises the results obtained during the course of a systematic study of the various modifications of selenium, under different physical conditions by X-ray diffraction method.

Experimental method.—The usual "powder photograph" method was adopted in our investigation. The tube was operated at 35-40 K.V. with a current of 5-6 M.A. Hemicylindrical cameras were used since the usual method of comparison of intensities of different rings are tenable only when the rays travel the same distance before falling on the X-ray film. Two hemicylindrical cameras, having radii 2.888 cms. and 1.814 cms. respectively, were used. In order to heat the sample during X-ray exposure, the sample was pressed against the slit cap or introduced within a thin-walled capillary which was surrounded by an electric heater. The electric heater consists of a syndanio bobbin, wound with a nichrome wire resistance, tightly fitting the slit tube. The temperature of the sample was measured by a calibrated copper-constantan thermocouple. For high temperature work, the film was cooled by circulating water through a metallic jacket pressing the film.

Allotropes of selenium.—Black vitreous selenium was prepared by rapidly quenching boiling liquid selenium in ice-cold water. Selenium thus obtained formed a hard shining black vitreous mass showing conchoidal fracture. The powdered vitreous selenium softens even at 38°C (melting point of the most stable hexagonal variety being 217°C) and the powdered mass coalesce. Vitreous selenium is partly soluble in CS_2 which on evaporation gives red monoclinic crystals. *Red precipitated selenium* was prepared by passing pure SO_2 gas through aqueous solution of SeO_2. In order to avoid the transformation of the red precipitated selenium into the metallic variety due to heat evolved in the process, the cylinder containing the aqueous solution of SeO_2 was kept cooled by surrounding it with a cold water jacket. It was found that at 40°C the red amorphous selenium turns black within half an hour. Its behaviour with CS_2 is the same as that of vitreous selenium.

Metallic (hexagonal) selenium can be prepared by heating any variety of selenium at 130°C for 12 hours. It can also be prepared by the following sublimation process. Vitreous selenium was taken in long glass tube which was carefully evacuated and sealed. The lower part of the tube was maintained at 73°C by means of an electric heater. After several days crystals appeared in the cooler part. It is insoluble in CS_2 and melts at 217°C.

X-ray diffraction photographs of these allotropes were taken. The interplanar spacings calculated for the rings obtained with the metallic variety correspond to that obtained by Bradley, in the case of hexagonal selenium. (Table I). The spacings obtained with the monoclinic variety is also given in Table I.

TABLE I

Hexagonal Selenium			Monoclinic Selenium		
Intensity	Bragg angle θ	Spacings in A.U.	Intensity	Bragg angle θ	Spacings in A.U.
W.	10 35′	3·781	W.	10 25′	4·256
S.	11 50′	3·753	W.	11 34′	3·837
W.	13 30′	2·976	S.	12 30′	3·555
V.S.	15 0′	2·973	W.	13 34′	3·281
V.W.	19 44′	2·057	S.	14 32′	3·066
W.	20 41′	2·178	S	16 4′	2·781
M.S.	21 53′	2·065	W.	18 20′	2·446
W.	22 54′	1·977	V.W.	19 9′	2·346
M.S.	25 59′	1·756	V.W.	20 8′	2·236
M S.	28 2′	1·637	V.W.	21 21′	2·115
M.S.	30 48′	1·503	W.	22 49′	1·985
M.S	32 46′	1·422	W.	23 56′	1·897
V.W.	34 2′	1·375	V.W.	25 28′	1·785
			V.W.	30 0′	1 583
			V.V.W.	30 47′	1·56

The vitreous and the red amorphous selenium give three broad bands. The ring system of the crystalline (hexagonal) variety of selenium can also be broadly divided into three groups, each group containing several lines of fair intensity. The pattern obtained with the monoclinic selenium contains only one such group which approximately corresponds in position with the first group of the hexagonal variety. The bands obtained with the amorphous varieties correspond approximately in position and intensity with the *groups* mentioned in the hexagonal variety. This ' line-band ' correspondence suggests that there is some relation existing between the crystalline and the corresponding amorphous state. In Table II the band spacings of the vitreous and red amorphous selenium are given. It will be seen from the table that the band spacing of the vitreous and the red amorphous selenium are somewhat different. The cause of the discrepancy will be discussed later on.

TABLE II

Black Vitreous Selenium			Red Amorphous Selenium		
Intensity	Bragg angle	Spacings in A.U.	Intensity	Bragg angle	Spacings in A.U.
S.	12 31′	3·551	S.	12 14′	3·633
W.	25 59′	1·757	W.	24 54′	1·828
V.W.	36 43′	1·406	V.W.	36 55′	1·281

Conversion of Monoclinic Selenium into the Hexagonal Modification :—From the thermo-chemical data [7] a quantity of heat (about 2.2 Cal. per gm.) is evolved when monoclinic selenium converts into the hexagonal form at higher temperature. Again the heat of formation of SeO_2 from the monoclinic selenium is greater than that of the same from the hexagonal variety.

This suggests that the monoclinic selenium has got a greater energy content than the hexagonal form and thus the former will have a tendency to pass into the hexagonal state.

It has been found that heated for 12 hours at 120°C, monoclinic selenium is completely converted into the hexagonal form. The conversion was then studied at 80°C. With the sample, heated for 12 hours at 80°C, no sign of transformation, from the monoclinic to the hexagonal form, was detected. The sample of monoclinic selenium was then maintained at 80°C and photographs were taken with the sample heated for 168, 200, 300 hours. In the photograph of the sample heated for 200 hours at 80°C, faint lines corresponding to the hexagonal pattern were indicated. The sample was then maintained at 80°C continuously for 15 days and on X-ray analysis it was found that complete conversion into the hexagonal form has occurred (Plate IX). With the sample of monoclinic selenium heated at 65°C for 17 days a photograph was obtained in which the rings corresponding to both monoclinic and hexagonal selenium are present. The interplanar spacing corresponding to above-mentioned photographs are given in Table III.

TABLE III.

Monoclinic selenium converted at 80°C			Monoclinic selenium partially converted at 65°C		
Intensity	Bragg angle θ	Spacings in structure*	Intensity	Bragg angle θ	Spacings in structure*
W	10 34′	3.782 H	W	10 22′	4.276 M
S	11 39′	3.81 H/M	M. S.	11 45′	3·779 H
V. W.	12 30′	3·555 M	M. S.	12 32′	3·546 M
W	13 23′	3·325 H	W	13 37′	3·270 M
V. S	14 52′	2.995 H/M	V. S.	14 51′	3.004 H
W	15 55′	2.805 M	M. S.	16 5′	2.778 M
V. W.	19 39′	2.289 H	—	—	—
W	20 41′	2.179 H	—	—	—
S	21 57′	2.062 H	—	—	—
W	22 49′	1.985 H	—	—	—
V. W.	23 49′	1 905 H	—	—	—
M. S.	25 54′	1.762 H	—	—	—
M. S.	28 8′	1.632 H	—	—	—
M. S.	30 51′	1.501 H	—	—	—
M. S.	32 38′	1.427 H	—	—	—

We should mention in this connection that transition of monoclinic selenium into the hexagonal variety is monotropic. The case is similar to that of S_ω which passes into S_α even at the ordinary temperature, and more quickly at higher temperatures. Again, we see that in these cases of monotropic transition, apparently there is no sharply defined transition temperature. The transformation takes place practically at all temperatures but the rate depends on the temperature at which the transformation takes place. Monoclinic selenium converts into the hexagonal form and the reverse process cannot occur, since the hexagonal variety has got the minimum crystal potential energy. But it will be seen, later on, that in the case of crystallites or minute crystals of the hexagonal type, its conversion into the bigger monoclinic variety is quite possible.

VITREOUS SELENIUM

Devitrification of Selenium :—Powders of vitreous selenium were heated at temperatures 55°, 70°, 120°, 170°C with the help of an electric heater.

---

* H=Hexagonal, M=Monoclinic, H/M=Both H and M superposed.

At any temperature as the heating was continued and sample specimens were taken out of the heated mass at suitable intervals of time and the corresponding X-ray powder-diagrams were taken. The results of the X-ray study are summarised in the chart presented below.

Period of heating	55°C	70°C	120°C	170°C
0 hr.	3 amorphous bands.	3 amorphous bands.	3 amorphous bands.	3 amorphous bands.
12 hrs.	amorphous band with some indication of structure in the band.	A pure crystalline pattern with no indication of bands. The pattern corresponding to that of hexagonal selenium.		
24 hrs.	amorphous band and two faint rings superimposed on the 1st band.	,,		
36 hrs.	amorphous band and four rings superimposed on the 1st band.	,		
72 hrs.	weak amorphous bands, four rings on the 1st band and several other rings in the position of the 2nd band.			

From the above chart it is evident that the gradual devitrification of vitreous selenium is due to its gradual crystallisation and the rate of crystallisation is found to be slower at low temperature.

The question naturally arises whether such crystallisation of vitreous selenium is at all possible at a still lower temperature. To investigate this point we analysed specimens of vitreous selenium heated at 43°C for 36, 60, 84, 182, and 200 hours. It was found that the diffraction patterns of the specimens heated for less than 182 hours showed only the amorphous bands. The patterns obtained with specimens heated for longer periods showed indications of rings, corresponding to the hexagonal form, but two faint rings of the system correspond to the two strong lines of the monoclinic pattern. After 20 days of continuous heating the pattern (plate IX) obtained with the specimen consisted only of sharp rings showing complete crystallisation. The next experiment was conducted with a specimen heated at 38°C. In this case the first indication of crystallisation was observed in the specimen heated for 200 hours and even when the sample was kept at that temperature for 1100 hours we obtained (plate IX) both rings and amorphous bands in the diffraction pattern. It is peculiar that in this case the spacings of the rings suggest transformation both to the hexagonal and monoclinic form.

It has been mentioned before that vitreous selenium converts itself only to the hexagonal form above 43°C. But at 43°C two faint rings corresponding to the monoclinic form is just observed along with the strong lines of the hexagonal variety. But when the vitreous selenium is heated at 38°C for 1100 hours a different picture appears on the plate. In this transformation the percentage of monoclinic selenium in the transformed product is much greater than that obtained at 43°C. This is clearly evident not only from the number of rings of the monoclinic variety but also from the relative intensities of the rings of the two crystalline types.

Dr. Grippenberg of Masaby, Finland, supplied us with a stick of vitreous selenium which had been preserved in his laboratory for seven years. The temperature of his laboratory does not rise on an average above 28°C throughout the whole year. The stick was analysed on the very day it was received here in Calcutta ; the temperature of our laboratory was 30°C ; a quantity of fine powder was scraped from the surface of the stick and the diffraction photograph was taken. Sharp Debye pattern was obtained showing sign of complete crystallisation into the monoclinic form. It is peculiar that at 28°C vitreous selenium converts only into the monoclinic form (plate IX).

TABLE IV

Vitreous Selenium devitrified below 28°C

Specimen	Intensity	Bragg angle θ	Spacings in A.U.	Structure
Grippenberg's sample of vitreous selenium scraped from the surface of the stick, 7 years after its preparation (temp. below 28°C).	V.W.	10 24′	4.264	M
	V.W.	11 39′	3.810	M
	S	12 39′	3.514	M
	W	13 30′	3.298	M
	S	14 32′	3.066	M
	S	16 5′	3.778	M

To examine the nature of selenium in the body of the stick, the stick was broken and a sample was taken from its central portion. On X-ray analysis three broad bands were observed and their spacings correspond to that of the vitreous or amorphous selenium.

Dependence of the Band Spacings on the period of heating :— From the powdered vitreous selenium maintained at 38°C, samples were taken at intervals of 12 hours and X-ray photographs were taken with these samples. The diameters of the bands of different photographs were accurately measured and corresponding band spacings calculated. Table V shows that the value of the spacings of the first band gradually increases with the period of heating. The intensities of the second and third band are very weak and it is difficult to measure accurately the diameter of the outer bands and further experiments with the microphotometer records will be taken up to investigate the mode of their change with the period of heating.

TABLE V

BAND SPACINGS OF VARIOUS FORMS OF SELENIUM

Specimen	Bragg angle θ	Spacings in A.U
Red selenium coagulated naturally from colloidal selenium solution.	11 41′	3·80
Red selenium coagulated naturally from another sample of colloidal solution.	11 50′	3·753
Red precipitated selenium prepared in the Laboratory.	12 14′	3·633
Black vitreous selenium.	12 21′	3·551
Black vitreous selenium heated for 12 hours at 37°-39°C.	12 38′	3·519
Black vitreous selenium heated for 24 hours at 37°-39°C.	12 48′	3·474
Black vitreous selenium heated for 36 hours at 37°-39°C.	12 50′	3·465
Black vitreous selenium heated for 60 hours at 37°-39°C.	13 4′	3·404

Photographs of Red selenium coagulated naturally from colloidal solution and of Black Vitreous Selenium heated for 60 hours at 37°-39°C are reproduced in Plate IX. The differences in the diameters of the band in the photographs (a & b) can be easily seen.

Generally we know that the diffraction pattern of liquids and amorphous substances consists only of broad diffuse bands but the investigations of Laue[4] and others proved that considerable broadening of the diffraction lines may take place on the diminution of the size of the diffracting crystallites. If the size of the particles be sufficiently small, the line may become broad enough so as to appear as bands resembling those of the liquids and the truly amorphous

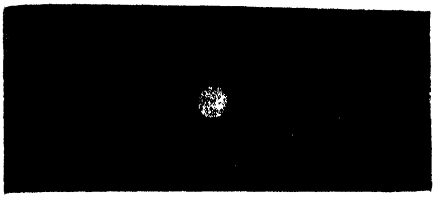

Fig. 1.

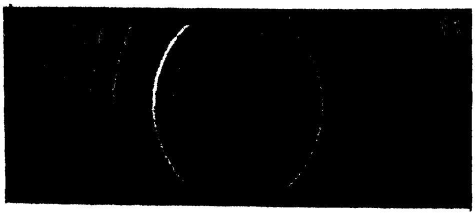

Fig. 2.

Fig. 3.

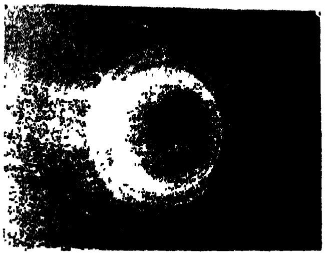

Fig. 4.

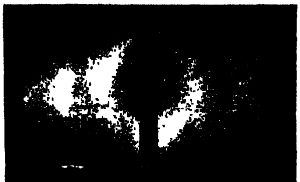

Fig. 5 (a)

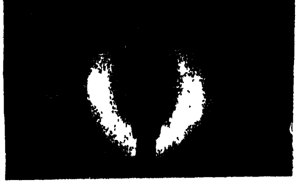

Fig. 5 (b)

1. Monoclinic selenium transformed into the hexagonal form at 80°c.
2. Black vitreous selenium transformed into the hexagonal form at 43°c.
3. Partial transformation of vitreous selenium into both monoclinic and hexagonal form at 38°c. Lines superimposed on the band.
4. Vitreous selenium transformed into the monoclinic form at 28°c.

5.(a) Spontaneous coagulum of colloidal sol of selenium on ageing.

(b) Vitreous selenium heated at 38°c for 60 hours. The difference in the diameter of the band in plate V(a) & V(b) is to be noted.

substances. The positions of the bands approximately coincide with the positions of the groups of intense lines in the pattern from crystals of larger sizes of the same substance. Generally, in order to have a sharp continuous Debye-Scherrer pattern the particle size should lie between 10^{-3}cm. to 10^{-4}cm. Thus the line-band correspondence indicate that the bands are due to the substance in an extremely subdivided state. Another effect, which is produced by the diminution in the size of diffracting crystallites, is the change in the diameter of the bands. This change may correspond either to an increase or decrease of the inter-atomic distances in the crystallites. That the lattice dimension is a function of the size of the crystallites was first theoretically investigated by Prof. Lenard Jones[5] in the case of non-ionic crystals. The order of this change may be understood from the consideration of an ideal case in ionic crystals (such as NaCl), if the size of a simple cubic crystal be reduced to 500 atoms deep only, the lattice dimension changes by about 5%, and in 3 atoms deep the change is about 14%.

Lowry and Bozorth[6] while agreeing with the general resemblance between the patterns for graphite and amorphous carbon (which is assumed to consist of small crystallites of the graphite) pointed out that the spacings of the basal planes increased as the average particle size diminished.

DISCUSSION

When the molten selenium is suddenly cooled down so as to pass into the vitreous state, the mass solidifies before it can liberate the whole amount of its latent heat. The atoms of a solid body tend to arrange themselves in such positions that the crystal potential energy is minimum. In the case of selenium such a process of formation of crystal also happens by the marshalling of atoms in liberating the latent heat ; but by the time the crystals have grown a little, the substance becomes too viscous to allow of any further marshalling or crystaliisation. Thus instead of bigger crystals of the order of 10^{-3}-10^{-4}cm. in size, we get minute crystals or crystallites of lesser dimension. If the formation of crystals would not have been thus checked, the molten selenium would easily pass into the crystalline state by giving up the whole of its latent heat, as is usual in the case of solidification of most of the substances. From the above argument, it is clear that some heat energy is actually retained by the crystallites present in the vitreous selenium, and the whole amount of the latent heat has not thus been liberated. In consequence, the crystallites present in vitreous selenium will have a greater energy content than ordinary crystals, *i.e.*, crystals of larger dimensions, in the formation of which, the whole amount of latent heat has been liberated. These crystallites, therefore, are in unstable state and will always have a tendency to liberate the heat retained in the so-called amorphous state and form bigger crystals. This can only happen if, by heating the vitreous mass, we increase the mobility of the molecules of selenium, so that marshalling or crystallisation can again begin and the size of the crystallites increase gradually. The rapidity of crystallisation will depend on the degree of mobility or softening of the mass, which again will evidently depend on the temperature at which selenium has been maintained. This explains the increase in the rate of crystallisation of vitreous selenium with the rise of temperature. A portion of the vitreous selenium is soluble in CS_2 and monoclinic selenium is the only variety of selenium which is soluble in CS_2. Thus vitreous selenium contains crystallites of both monoclinic and hexagonal selenium. From the consideration of experimental results on transformation of vitreous selenium into monoclinic at low temperature and into hexagonal at high temperatures, both with the evolution of heat it follows that both of these crystallites have got greater energy content than either of ordinary bigger monoclinic or hexagonal crystals. Also from thermochemical data[7] it will be found that the heat content of vitreous selenium (containing both hexagonal and monoclinic crystallites) is greater than that of the ordinary monoclinic crystals which again has got greater heat content than the stablest hexagonal variety. Thus, both monoclinic and hexagonal crystallites present in vitreous selenium can pass either into purely hexagonal form or purely monoclinic form. And it has been found experimentally that at temperatures below 28°C vitreous selenium converts only into the monoclinic form. At temperatures above 43°C vitreous selenium is converted only into the hexagonal form and at intermediate temperatures, *viz.*, between 28°C and 43°C both monoclinic and hexagonal crystals are found in the transformed product.

The gradual growth of the size of the crystallites with the period of heating has got two experimental evidences. The diffraction photograph of a sample of vitreous selenium heated for a certain period at a particular temperature gives sharp lines superimposed on broad bands. The broad bands, as has been explained before, are due to crystallites still present in the vitreous selenium and the sharp rings are due to ordinary crystals, formed by the gradual growth of size of the crystallites, and lines superimposed on the bands directly shows the line-band correspondence.

According to the theoretical investigation of Lenard Jones, in the case of non-ionic crystal, lattice dimension increases as the particle size diminishes. This has been verified by Lowry and Bozorth in the case of carbon. The increase in the band spacings of vitreous selenium, with the period of pre-heating of the sample suggests, therefore, a gradual growth of size of the crystallites with the period o heating.

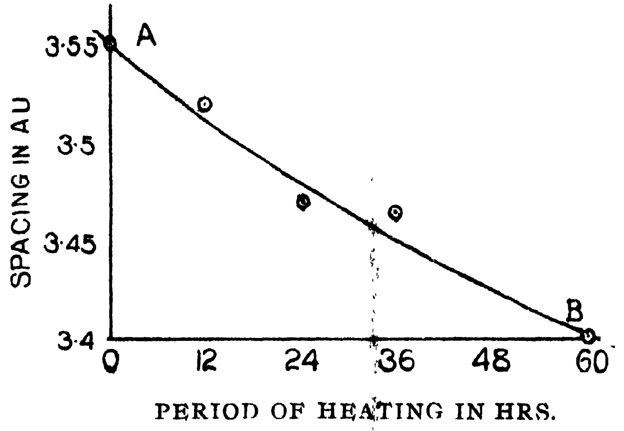

FIG. 1

The different band spacing obtained in the case of red amorphous selenium, red selenium coagulated from colloidal solution of selenium, can also be ascribed to the different sizes of the crystallites in these varieties. If these varieties of selenium are now arranged in the order of diminishing crystal sizes, based on X-ray determination, it will be observed that the same arrangement is again obtained, based on the colour of the specimen. As the grains get finer, the colour changes from black to red. Table V shows the various types of selenium arranged in order of increasing size of the crystallites against corresponding band spacings. From the smooth graph AB (Fig 1) in which abscissa represents the period of heating of vitreous selenium, in our experiment, and the ordinate being the spacings in A.U., it will be evident that there exists a relation between band spacings of vitreous selenium and the period of heating.

KHAIRA LABORATORY OF PHYSICS,
UNIVERSITY COLLEGE OF SCIENCE,
CALCUTTA.

REFERENCES

[1] Bradley, *Phil. Mag.*, **48**, 477 (1934).
[2] Klug, *Z. Krist.*, **88**, 128 (1934).
[3] Prins and Dekeyser, *Physica.*, **4**, p. 900 (1937).
[4] Laue and others, "*Diffraction of X-rays etc.*" by Randall, p. 31.
[5] Lenard Jones, *Z. f. Krist.*, **75**, 250 (1930).
[6] Lowry and Bozorth, *J. Phys. Chem.*, **32**, 1524 (1928).
[7] Newton Friend, *Inorganic Chemistry*, **7**, Part II.

X-RAY STUDY OF SELENIUM IN THE LIQUID AND COLLOIDAL STATE*

BY K. DAS GUPTA AND S. R. DAS

(Received for publication, May 17, 1941)

Plate X

ABSTRACT. Liquid selenium at various temperatures, *viz.*, from 220° to 430°C, has been studied by the X-ray diffraction method with a specially designed camera. A single broad band with a band-spacing much bigger than that of amorphous varieties was obtained. The density of liquid selenium at various temperatures was also accurately determined. It is found that with the rise of temperature the band-spacing of liquid selenium also increases. By plotting the band-spacing of liquid selenium against the corresponding temperature and the cube-root of the reciprocal of density against the temperature, two smooth curves of similar nature were obtained.

Selenium, in its colloidal state, has been studied by the X-ray diffraction method. Colloidal solution prepared was fairly stable and coagulation occurs on addition of HNO_3. The solution is stable even when heated at 100°C for several hours. Both heated and unheated solutions, when allowed to evaporate at the room temperature form a sticky mass. Coagulum obtained with unheated solutions gives sharp monoclinic pattern if the coagulation is effected at a very slow rate. On rapid coagulation, however, the precipitate gives on X-ray analysis broad bands. Similar results are also obtained with previously heated solution, the difference being that the coagulated specimen now gives pure hexagonal pattern.

The gummy mass both from the heated and unheated sol gives only one single broad band. The spacing of the band (4.07 A.U.) is the same as that obtained in the case of liquid selenium, near its melting point, but it does not correspond with that of amorphous varieties of selenium (3.5 A.U). This essential similarity in the nature of the diffraction pattern of liquid selenium and colloidal selenium suggests that the arrangement of atoms in each colloidal particle of selenium is the same as that in the groups present in the liquid selenium.

INTRODUCTION

The property of a substance in the colloidal state is peculiarly different from the same in the ordinary solid state. In the colloidal state, the substance is in a highly dispersed condition and each colloidal particle consists of several atoms or molecules of the substance closely packed to each other. The peculiarity of the property of the substance in their colloidal state can be attributed to the smallness of their particle-size and the mode in which the atoms are arranged in space, relative to each other in the small colloidal particle. Colloidal metal sols[1] in general give the diffraction pattern characteristic of the massive material, except that the sharp Debye ring is broadened in proportion as the particle size is smaller. It has also been noticed that the same substance giving crystalline pattern in the ordinary solid state gives band pattern in the colloidal state.

---

* Communicated by the Indian Physical Society.

Substances in their liquid state also give on X-ray analysis broad bands which can be ascribed to the presence of some groups of (cybotactic) atoms on molecules in the liquid state. The groups are always being formed and destroyed due to thermal disturbances.

Substances in the amorphous state also characterise themselves by band pattern which has been attributed to the presence of groups or crystallites in which atoms or molecules are arranged in some particular fashion. Now, substances (*a*) in the colloidal state, (*b*) liquid state, and (*c*) amorphous state show bands on X-ray analysis and the nature of the band pattern is characteristic of the size of the group and the mode of arrangement of atoms in the groups.

An attempt has been made here to establish some relation which might exist among the different states mentioned above of the element selenium.

Liquid selenium :—Selenium melts at 217°C and diffraction photographs were taken at different temperatures lying between 220°C and 430°C. The camera essentially consists of a collimating system and a plane plate holder. The cell containing the liquid selenium consists of very thin walled glass capillary closed at both ends. The empty glass capillary was put before the X-ray and the wall of the tube was so thin that no diffraction pattern due to glass was obtained. One such capillary containing selenium closed at both ends was put before the slit cap. The slit cap being surrounded with an electric heater wound with nichrome wire resistance. The temperature of the liquid selenium was measured by introducing a thermocouple of Cu-Constantan at the position of the cell containing the liquid. The intensity of the band to be obtained in the case of liquid selenium being too weak, the film holder is to be kept very near the cell containing the liquid. The X-ray film is to be protected from the heat radiation coming out of the electrical heater surrounding the liquid cell. A water cooling jacket, in the form of a circular disc, with a 2 mm bore at the centre, was placed vertically, in between the film holder and the slit cap, so that the major part of the heat radiation from the heater was cut off, but only the scattered cone of X-rays from the specimens to be analysed can pass unobstructed through the central hole of the water-cooling jacket. The water was being continually circulated through the jacket during the exposure. This arrangement was quite successful up to 315°C. But at higher temperatures it was necessary to cool the X-ray film. The lid of the film holder pressing the film was replaced by a double walled metallic jacket through which water was constantly being circulated. This modification enabled us to take photographs of liquid selenium even upto 430°C [Plate X(1)]. Diffraction photographs were taken at 220°, 261°, 315°, and 430°C. The time of exposure varied between 30-40 hours, Voltage: 40 K.V., current 5·10 M.A.

EXPERIMENTAL RESULTS

The pattern obtained in the case of liquid selenium consisted of one diffuse band. Table I gives the values of the band spacings at different temperatures.

TABLE I

Band spacings of liquid selenium at different temperatures

Temp. of liquid selenium	Bragg angle θ	Spacings in A.U.
220°C	10 59′	4.04
261°C	10 51′	4.09
315°C	10 41′	4.15
430°C	10 18′	4.30

From the table it will be seen that with the increase of the temperature the values of the spacings also increase.

In fig. 1(*a*) spacings have been plotted against corresponding temperatures and the smooth curve AB has been obtained. The curve AB evidently suggests that the variation of spacing with temperature is almost linear and there is no sudden change in the spacing at any temperature in the region covered by our experiment. The density of liquid selenium at different temperatures were measured very accurately.

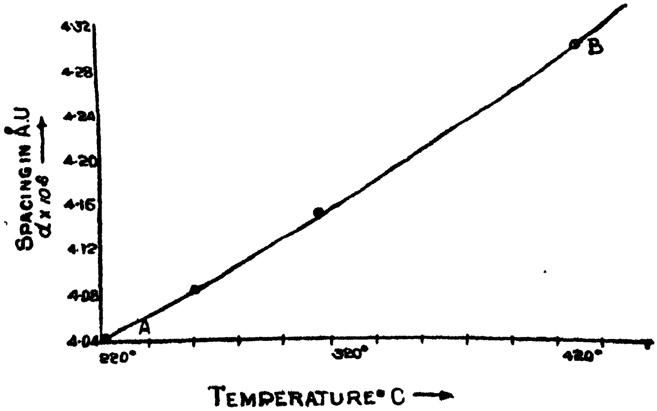

FIG. 1(*a*)

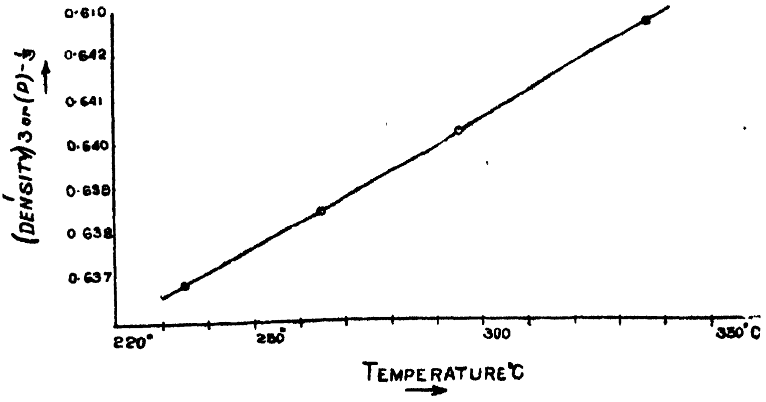

FIG. 1(*b*)

The density of liquid selenium at different temperatures were determined by using a glass tube with a narrow mouth. The tube containing the liquid selenium could be maintained at any temperature up to 400°C or more by inserting it into closely fitting holes of an electric heater the current through which could be regulated. The temperature of the bath was noted by a mercury thermometer. Two such tubes were taken and maintained at the desired temperature above the melting point of selenium and small pieces of selenium were gradually introduced which soon melted and thus the tubes were filled up with liquid selenium without any air bubble lying within it. To determine the density at some other higher temperature the current is regulated. Liquid selenium overflows through the capillary mouth. The tubes were taken out, cooled and weighed after carefully cleaning the surface of the tubes. The tubes were first filled up with distilled water and weighed, the density of water at that temperature was taken from the Physical Table. The value of the density calculated from the two tubes differed by less than one per cent. The density of liquid selenium at different temperatures are given in Table II.

TABLE II

Temperature of the liquid selenium	Density in gms/c.c.
235°C	3.8719
265°C	3.8393
295°C	3.8094
335°C	3.7741

The smooth curve A′B′ in fig. I(*b*) is obtained by plotting the reciprocal of the cube-root of density against the temperature. The similarity between the curve AB (Fig. I*a*) and curve A′B′ (fig. I*b*) evidently suggests that the mode of variation of the cube-root of specific volume with temperature and that of the spacings with the temperature are similar. The observed change in spacing is merely a natural consequence of the thermal expansion of the liquid which is also responsible for the change in density.

DISCUSSION

The band-spacing of the liquid selenium at 220°C, *i.e.*, near about the melting point is 4.04 A.U. Now the largest value of the spacings obtained in the case of amorphous varieties, is with colloidal selenium coagulated by electrolytes or coagulated on ageing, and the value is found to be 3.8 A.U.

It has been observed that the colloidal selenium left to atmosphere at the room temperature forms a gummy mass which on X-ray analysis gives one broad band and peculiarly enough the nature of the band is similar to that obtained in the case of liquid selenium.

The points of similarity lie in the fact that (1) both liquid selenium and the gummy colloidal selenium on X-ray analysis give one single broad band, whereas in the case of amorphous varieties of selenium, *viz.*, vitreous selenium, red amorphous selenium and colloidal selenium coagulated by means of electrolyte we always get three broad bands. (2) The value of the band-spacings in the case of gummy colloidal selenium is 4.07 A.U. which agrees well with the value of the spacing, 4.09 A.U., in the case of liquid selenium at 261°C. This interesting point of similarity between colloidal selenium will be dealt later on.

Colloidal selenium : preparation[2] *and properties* :—Equimolecular quantities of SeO_2 and extra pure dextrose were taken in a small basin with a little quantity of distilled water and kept over a water bath. The solution becomes reddish and syrupy. On addition of a few drops of liquor ammonia to this syrupy liquid, frothing begins. This process is continued till the solution turns deep red. The syrupy condition being always maintained by adding drops of water at intervals and finally the whole thing is stirred up with cold water and red colloidal solution of selenium is obtained. The solution containing excess of any electrolyte is dialysed by means of a cellophane paper membrane.

Colloidal solution thus prepared is fairly stable. Spontaneous coagulation occurs just after the preparation of the solution ; but the rate of such coagulation becomes imperceptible after 2 or 3 days. The colour of this natural coagulum is red. The colloidal sol was boiled at 100°C for 36 hours, but the sol was stable even after boiling. Coagulation does not take place when colloidal sol is exposed to X-rays. On addition of few drops of dilute HNO_3 coagulation takes place in the case of both heated and unheated colloidal sol. The rate of coagulation depends very much on the amount of electrolyte (HNO_3) added and also on the amount of shaking. Colloidal selenium sol when allowed to evaporate at the room temperature forms a gummy mass. This gummy mass when shaken with water, the original colloidal sol is obtained. Thus, we have the following types of samples to be examined by the X-ray diffraction method :—

(A) Coagulum formed during ageing.

(B) Precipitate obtained by *rapid coagulation* of unheated sol by addition of HNO_3.

(C) Precipitate obtained by *slow coagulation* of aged unheated sol by addition of HNO_3.

(D) Precipitate obtained by *rapid coagulation* of colloidal sol, heated at 100°C for different periods by the addition of HNO_3.

(E) Precipitate obtained by *slow coagulation* of colloidal sol heated at 100°C for different hours by the addition of HNO_3.

(F) Gummy colloidal selenium obtained by evaporating both heated and unheated colloidal sol, at the room temperature.

The samples mentioned above were all pressed against the slit cap on a thin zig-zag paper and photographs taken in a hemicylindrical camera.

EXPERIMENTAL RESULTS

(A) Three broad bands similar to those obtained in the case of red amorphous selenium and black vitreous selenium were obtained [Plate X(2)]. The band spacing of the first intense band is 3.8 A.U. which is greater than the value 3.55 A.U. in the case of black vitreous selenium. The values of the band spacings obtained in the case of colloidal selenium (A) are given in Table III.

TABLE III

Coagulum formed during Ageing

Intensity	Bragg angle θ	Band Spacing in A.U.
S	11 41′	3.80
W	24 54′	1.83

This increase in the band-spacing is attributed as due to the smallness of the particle size of colloidal selenium.

(B) Coagulum obtained by rapid coagulation of sol by addition of HNO_3 gives also three broad bands similar to (A).

(C) Slow coagulum obtained by addition of HNO_3 from aged, unheated sol showed purely crystalline pattern [Plate X(3)]. The interplanar spacings correspond to that of the monoclinic selenium but the intensity distribution of the lines are peculiarly different as can be seen from [Plate X(3)]. The table IV below shows the values of the spacings against the corresponding spacings obtained with monoclinic selenium prepared in the Laboratory.

TABLE IV

Precipitate obtained by Slow Coagulation of Aged Unheated Sol by addition of HNO_3

Intensity	Bragg angle θ	Spacing in A.U.	Monoclinic prepared in the Lab.	
			Intensity	Spacings in A.U.
W	10 18′	4 29	W	4.26
W	11 24′	3.90	W	3.84
W	12 30′	3.55	S	3 56
S	13 34′	3.28	W	3 28
W	14 29′	3.09	S	3 07
V.W.	15 55′	2.82	S	2.87
M.S.	20 9′	2 23	V.W.	2 24
W	21 27′	2.10	V.W	2.11
S	22 31′	2.00	W	1 99
W	23 56′	1 90	W	1.90
W	25 5′	1.81	V W.	1.77

(D) Precipitate obtained by rapid coagulation of colloidal sol heated previously for 36 hours at 100°C by HNO_3 gives on X-ray analysis three broad bands similar to those obtained in the case of amorphous varieties of selenium.

(E) Precipitate obtained by slow coagulation of colloidal sol heated previously at 100°C for 36 hours by the addition of HNO_3 gives on X-ray analysis purely crystalline pattern. Table V shows that the interplanar spacings correspond to the hexagonal form of selenium [Plate X(4)].

TABLE V

Intensity	Bragg angle θ	Spacings in A.U.	Spacings of the hexagonal Se prepared in the Lab. in A.U.
W	10 25′	3.84 (β)	3.781
S	11 89′	3.81	3.77
W	13 23′	2.99 (β)	2.99
S	14 53′	2.99	2.99
W	20 49′	2.16	2.17
V.W.	21 49′	2.07	2.07
V.W.	26 15′	1.74	1.75
V W.	28 8′	1.63	1.63

(F) Gummy colloidal solution both from heated and unheated solution give on X-ray analysis one single broad band the spacing of which is 4.07 A.U. [Plate X(5)].

From these experiments it is clear that if colloidal sol (either heated or unheated) is precipitated slowly the particles give crystalline pattern Whereas the sample (heated or unheated) if precipitated rapidly produces so-called broad amorphous bands. But it is evident from the experiments that heated sample precipitated slowly produces hexagonal pattern whereas the unheated sample treated in the same way produces only monoclinic pattern.

DISCUSSION

Colloidal selenium consists of groups of atoms of selenium packed together in the way as in the liquid selenium. This follows naturally, from the fact, that the band pattern obtained by X-ray analysis of liquid selenium and highly concentrated colloidal selenium (gummy colloidal selenium) are similar in every respect. The growth of size of the above-mentioned groups present in the colloidal selenium always takes place, both on ageing the solution and also on heating the samples; but generally this growth is not large enough so as to precipitate the selenium present in colloidal solution. Thus, in the case of both aged colloidal sol and heated colloidal sol, each colloidal particle although of dimension less than 10^{-5} cm is now a "colloidal crystal." On rapid coagulation the growth of size of these "colloidal crystals" takes place only by the capillary action and we get on X-ray analysis three broad bands as have been obtained in the case of so-called amorphous varieties of selenium. On slow coagulation however, the growth of size is effected not only by the capillary action but also

PLATE X.

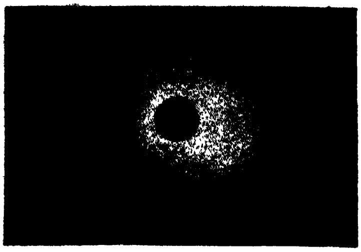

Fig. 1.

Fig. 2.

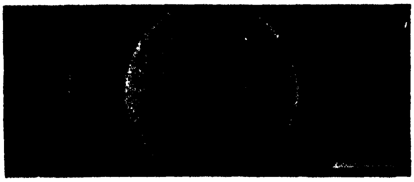

Fig. 3.

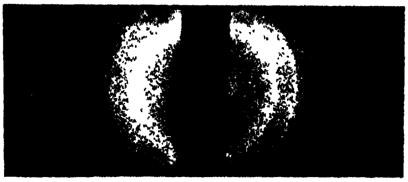

Fig. 4.

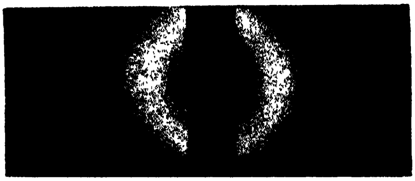

Fig. 5.

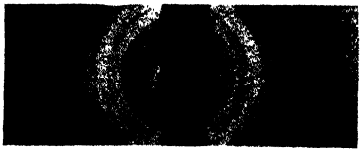

Fig. 6.

(1) Liquid selenium at 315°C.

(2) Coagulum formed during ageing.

(3) Precipitate obtained by slow coagulation of aged unheated Sol by addition of HNO_3

(4) Precipitate obtained by slow coagulation of colloidal Sol heated at 100°C for 16 hours, by the addition of HNO_3

(5) Gummy colloidal selenium.

(6) Presence of $S\omega$ in colloidal Sulphur.

some orientating field is predominant which causes a regular lattice formation so that the precipitate on X-ray analysis gives a sharp crystalline pattern. From the experimental results we have found that with the previously heated colloidal solution, the precipitate obtained by slow coagulation gives always hexagonal crystals. But, unheated aged, colloidal sol on slow coagulation gives monoclinic crystals. The conditions in which the hexagonal or monoclinic crystals are formed from so-called amorphous selenium have been discussed in another paper.[3]

Thus the experimental results show that colloidal sol of selenium may contain both hexagonal and monoclinic crystals. To determine whether colloidal particles of sulphur can also exist both in S_α and S_ω form various samples of colloidal sol of sulphur prepared under different physical conditions were examined. The presence of S_α in colloidal sulphur sol has been previously shown in this Laboratory.[4]

THE PRESENCE OF S_ω IN COLLOIDAL SULPHUR

The colloidal sol of sulphur was prepared by passing pure H_2S gas through a concentrated solution of SO_2 in water. The solution was kept in a tall cylinder completely immersed in an ice-bath. The colloidal sol thus obtained is poured on a flat basin and was allowed to evaporate at about 25°C in a moist atmosphere. A thin gummy rubber like membrane was obtained, which could be torn to pieces. X-ray diffraction photograph of these pieces was taken, samples being changed every half an hour. A good crystalline pattern was obtained and the interplanar spacings of the rings were found to correspond accurately to those of insoluble white sulphur (S_ω) [Plate X(6)]

(The work was carried in the Khaira Laboratory of Physics, University College of Science, Calcutta. The author takes this opportunity of acknowledging his indebtedness to Prof. B. B. Ray, D.Sc., for suggesting the problem and kind guidance throughout).

Khaira Laboratory of Physics,
University College of Science,
Calcutta

REFERENCES

1 G. L. Clark, "X-ray and Colloids," Colloid Symposium Monograph, Vol. IV (1926).
2 A. Gutbier, *Colloid Zeitschrift*, 33, 334 (1923).
3 *Ind. Jour. Phys.*
4 S. R. Das & K. Ghosh, *Ind. Jour. Phys.*, Vol. XIII, Part II (1939).

DIFFRACTION PATTERN OF SULPHURIC ACID AT DIFFERENT CONCENTRATIONS

BY H. N. BOSE

(Received for publication, May 17, 1941)

Plate XI

ABSTRACT. In the present investigation, X-ray diffraction of pure acid and at concentrations corresponding to the formulae H_2SO_4, H_2O; H_2SO_4, $2H_2O$; H_2SO_4, $3H_2O$; H_2SO_4, $10H_2O$; H_2SO_4, $20H_2O$, etc., were studied. Pure sulphuric acid yields two well-defined bands (spacings 4.07 and 7.98 A.U.) with very little general scattering thereby following the general behaviour of highly associated liquids, though the inner band remained undetected so long. With dilution, the main band dilated and at the same time underwent an increase in diffuseness till at high dilution the familiar band of water made its appearance and the main peak of sulphuric acid nearly coincided with the first band of water (3.24 A.U). Considering the main peak at largest angle at any dilution, the spacing of the acid was found to be intermediate between those of pure sulphuric acid (4.07 A.U.) and pure water (3.24 A.U.). The spacing underwent a violent change when the concentration was changed to H_2SO_4, H_2O and again at H_2SO_4, $20H_2O$.

At concentrations corresponding to H_2SO_4, $2H_2O$ and H_2SO_4, $3H_2O$ the spacings remained constant 3.54 A.U. This may be taken to indicate something akin to hydrate formation. Sulphuric acid, it is known, ionises in aqueous solution in two stages. But apart from making the bands a bit diffuse, this was found to have little effect on the X-ray diffraction pattern. This is but what can be expected for (SO_4), (HSO_3) and (H_2SO_4) have almost the same dimension and scattering due to H^+ is negligible. The general behaviour of sulphuric acid has been tried to be explained qualitatively by extending the ideas of Lenard Jones.

INTRODUCTION

The affinity of sulphuric acid for water naturally suggests the possible formation of definite compounds or hydrates and the existence of such hydrates has been demonstrated in various ways. The freezing point curve for mixtures of two substances is usually regarded as affording a definite evidence of the occurrence or otherwise of chemical combination between the constituents and with mixtures of sulphuric acid and water definite results are obtained. With sulphur trioxide and water as two components, maxima on the freezing curve occur at proportions corresponding to the composition of the following compounds[1]: SO_3 : H_2SO_4 ; H_2SO_4, H_2O ; H_2SO_4, $2H_2O$; H_2SO_4, $4H_2O$. Thus the existence of a mono-, di- and a tetra hydrate of sulphuric acid in the solid condition is proved but the possibilities of other hydrates, for instance, H_2SO_4, $3H_2O$; H_2SO, $5H_2O$; and H_2SO_4, $12H_2O$ are not excluded.

Sulphuric monohydrate, H_2SO_4 H_2O crystallises from the acid of the corresponding concentration, in hexagonal prisms and melts at 9°C, the di-hydrate H_2SO_4, $2H_2O$ melts at -37°C and the tetra hydrate H_2SO_4, $4H_2O$ at -24°.5C. H Shiba and T. Walnabe[2] were the first to study the diffraction of X-rays by aqueous solution of sulphuric acid at four concentrations. They reported a contraction of the halo with increase in concentration. In their experiments, the central undeflected beam of X-rays was not cut off and consequently they were not able to record any change in the diffraction pattern with change in concentration at a very small angle of scattering.

R. S. Krishnan[3] investigated the diffraction of X-rays by aqueous solution of sulphuric acid and attempted to correlate his results with those obtained from Raman effect data.

X-ray diffraction of pure acid and at concentrations corresponding to formulae H_2SO_4, H_2O ; H_2SO_4, $2H_2O$: H_2SO_4, $3H_2O$; H_2SO_4, $10H_2O$; H_2SO_4 $20H_2O$ were undertaken to investigate if any information regarding such hydrate formation could be obtained purely from diffraction photograph We could detect in the present experiment, apart from the usual strong band, another inner weak band, which was not observed by any of the previous investigators.

EXPERIMENTAL TECHNIQUE

The arrangement of apparatus in the present investigation was the same as is generally used in powder photograph. The X-ray bulb was a demountable porcelain Hadding tube with a copper anticathode without any rectifying device. A hemicylindrical camera of radius 2.85 c.m. was used with a slit system having an aperture of .8 m.m. Liquid cells were prepared in a specially prepared thin walled glass capillary tube which was filled with a freshly prepared acid of required concentration, sealed at both ends so that the concentration remained unchanged and was then fixed to the cap of the slit with a bit of wax. The central beam was cut off with a lead cap placed on the film holder. The contribution of the container tube to the diffraction pattern was almost negligible as was observed in a trial experiment. The bore of the glass capillary was approximately kept constant (about 0.8 m.m.).

Sulphuric acid labelled ' Merck ' for analytical Reagent (99.2%) was used in this experiment. The different concentrations were prepared by adding 5 c.c. of the pure acid with the help of a graduated pipette to the calculated amount of water.

RESULTS (PURE SULPHURIC ACID)

The diffraction pattern of pure sulphuric acid consists of two sharp bands. The band at larger angles is much stronger than the other. Besides these, a central corona extending almost up to the inside of the inner band could be noticed. The diameters and the corresponding values of Bragg spacings are given in the Table for all the concentrations.

PLATE XI.

Fig. 1.

Fig. 2.

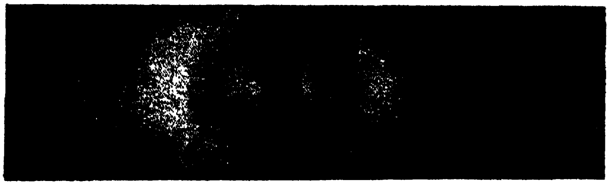

Fig. 3.

Fig. 1.—$H_2SO_4 + H_2O$

Fig. 2.—Pure H_2SO_4

Fig. 3.—$H_2SO_4 + 20H_2O$

The aqueous solution of sulphuric acid of concentration corresponding to the formula H_2SO_4, H_2O (*i.e.*, sulphuric acid and water being present in the proportion of 98 gms. to 18 gms.) was next prepared and its diffraction pattern was investigated. The conspicuous change that differentiates it from the previous one, *i.e.*, for pure acid, lies not only in the increase of diameters of the bands but also they are more diffuse, or in other words, the Bragg-spacings corresponding to the maximum intensity of the bands have decreased and at the same time they are more diffuse thus increasing the band width. The shift in the position of the maximum intensity of the band towards larger angle and the loss of sharpness are more pronounced in the case of the outer band.

TABLE

Aqueous Sulphuric Acid

Hemicylindrical Camera of radius 2.85 c.m.

Molecular proportion	Strength of sol. by weight	Approx p c. contraction of volume	No.	Angle of difiraction corresponding to maximum intensity	'd' (A U)
Pure H_2SO_4	99.2%		1	$10^\circ 54'$	4.07
			2	$5^\circ 32'$	7.98
H_2SO_4, H_2O	84.5%	8.6%	1	$12^\circ 22'$	3.6
			2	$6^\circ 2'$	7 32
H_2SO_4, $2H_2O$	73.1%	9.5%	1	$12^\circ 34'$	3.54
			2		
H_2SO_4, $3H_2O$	64.5%	9 2%	1	$12^\circ 34'$	3 54
			2	$6^\circ 2'$	7.32
H_2SO_4, $10H_2O$	35.2%	5 8%	1	$12^\circ 48'$	3.47
			2	$7^\circ 2'$	6.28
H_2SO_4. $20H_2O$	21.4%	4.4%	1	$13^\circ 34'$	3.28
			2	$7^\circ 2'$	6.28
			3	$23^\circ 43'$	1.91
			4	?	
H_2SO_4 Water	50%	6.4 %	1	$12^\circ 43'$	3 50

In the diffraction pattern at concentrations corresponding to H_2SO_4, $2H_2O$ and H_2SO_4, $3H_2O$, changes of similar nature are observed ; with concentration H_2SO_4, $10H_2O$, besides the changes stated, the pattern was remarkable by the appearance of a very weak band at still larger angles. For the concentration H_2SO_4, $20H_2O$

the third band appeared with great intensity and a fourth one could be suspected at a still larger angle. These additional bands were found to correspond to those of water.

R. S. Krishnan reported previously of the absence of any band at 50% concentration. In the present investigation, however, a diffuse band could be obtained even at this concentration.

The results are given in the table. In the first column, are given the molecular proportions of H_2SO_4 and H_2O, and in the second, the amount of H_2SO_4 present in 100 gms. of the solution. The third column contains percentage contraction corresponding to the concentration, the angle of maximum scattering and the corresponding Bragg spacing are listed in the fourth and fifth columns respectively.

All measurements, given here, were made with the help of a glass scale on the negative Generally, the bands are neither sharp nor intense, so that the order of accuracy, usually claimed in the measurement of sharp rings, is not attainable here. In the present case the first band is, in most of the concentrations, very weak and diffuse, hence the measurements on the first band are to be taken as approximate and the shift in the position of this band is likely to be less reliable.

DISCUSSION OF THE RESULTS

The presence of well-defined bands, with very little general scattering in the diffraction pattern of the pure acid is indicative of the existence of a very orderly arrangement of the molecules. Sulphuric acid is a highly associated liquid and associated liquids, in general, exhibit a secondary maximum in addition to the principal one We find that sulphuric acid is also not an exception and shows, as expected, two bands in the diffraction pattern.

P. Krishnamurti[4] has studied various liquid mixtures at different concentrations. For completely miscible liquids, he found that the diffraction pattern is different from that of either of the constituents. The main peak is invariably of intermediate spacing. With dilution, the main peak dilates and ultimately coincides with that of the major constituent. It is found that the liquids of this type are all associated. Similar results are also obtained for sulphuric acid. The main band of pure sulphuric acid and pure water have spacings 4.07 A.U. and 3.24 A.U. respectively, we find that spacings for other concentrations are intermediate between these two limits. In the first concentrations (H_2SO_4, H_2O) the spacing changes considerably (4.07 A.U. for pure H_2SO_4 to 3.6 A.U.). The change in spacing when the acid is diluted from H_2SO_4, $10H_2O$ to H_2SO_4, $20H_2O$, is also large. At concentrations H_2SO_4, $2H_2O$ and H_2SO_4, $3H_2O$ the spacings remain unaltered (3.54 A). These seem to indicate the presence of some hydrate of definite composition near about these concentrations. The presence of the inner band in all the concentrations is rather puzzling. Similar inner ring whose spacings remain almost constant in all concentrations were also noticed by P. Krishnamurthy in certain liquids like glycerine, etc. It is peculiar that the spacing of this inner band is always almost double the spacing of the main band.

For solids, Lennard Jones[5] has shown that band spacing of an ionic crystal decreases with the decrease in particle size. A very quantitative explanation of the results may also be obtained by extending his ideas for this case. In the pure state, sulphuric acid consists of groups of molecules which are responsible for the pattern. We may assume that in the process of dilution the number of molecules constituting the groups decreases which results not only in a diminution of the size of the groups but also in the band spacing. The other effect of dilution, *i.e.*, the increase in the diffuseness of the bands, is perhaps due to the fact that as dilution proceeds, the molecules forming a particular group become less and less permanent. This proceeds till the water content of the solution is sufficient to produce a pattern. This explains in general the behaviour of the solution. Before this final stage is reached it is, however, possible that there may be certain intermediate concentrations when the groups will be consisting of molecules of both kinds. Another factor which influences the nature and size of halo is the change in volume on mixing. Mixture of sulphuric acid and water is accompanied by changes in volume. This factor influences the patterns since it affects the distance between neighbouring molecules but the computation of the nature of its dependence on the spacing is evidently very difficult and is not possible at this stage.

The work was carried out in the Khaira Laboratory of Physics, University College of Science, Calcutta. The author takes this opportunity of acknowledging his indebtedness to Prof. B. B. Ray, D.Sc., for suggesting the problem and his kind guidance throughout.

KHAIRA LABORATORY OF PHYSICS,
UNIVERSITY COLLEGE OF SCIENCE,
CALCUTTA

REFERENCES

1 Newton Friend, *Inorganic Chemistry*, Vol. VII, part II, page 167.

2 H. Shiba and T. Walnabe, *Scientific papers of the Institute of Physical and Chemical Research*, **10**, 187 (1929).

3 R. S. Krishnan, *Proc. Ind. Acad. Science*, Vol. IV, Section A, page 661.

4 P. Krishnamurti, *Ind. Journ. Phys.*, Vol. III, page 331.

5 Lennard Jones, *Z. F. Krist.*,**75**. 216 (1930).

VIBROGRAPH USED AS A VISCOMETER

By T. TIRUNARAYANACHAR, M.Sc.

(Received for publication May 5, 1941)

Plates XII and XIII.

ABSTRACT. A method has been described for comparing the viscosities of highly viscous liquids by using an improved form of the vibrograph devised by the author It is essentially a damping coefficient determination method, the damping coefficients K_0 and K being calculated from the vibration curves of an oscillating sphere in air and in the liquid respectively. The method has the merit that it takes a very short time (a fraction of a second), to make an observation and that a permanent photographic record of the damped oscillations is obtained by which the visual uncertainty in noting the ends of the swing is automatically eliminated. It is suggested as an easy and quick method for comparing the viscosities of highly viscous liquids. An experiment conducted with glycerine at various temperatures shows a linear dependence of ηd (viscosity × density of the liquid) on the value of $(K-K_0)^2$.

INTRODUCTION

The coefficient of viscosity of liquids has been determined by different methods by different investigators. The capillary flow method due to Poiseuille is a very convenient and accurate method. But in the case of highly viscous liquids like glycerine, it takes hours to make even one set of observations of the flow, since the rate of flow is extremely small under ordinary experimental conditions. The method is therefore tedious and unsuitable for the determination of η, the coefficient of viscosity of liquids in such cases. A modified method of using Poiseuille's apparatus for the determination of η of highly viscous liquids is described by Bhimasenachar.[1] The essential features of the arrangement are provision for temperature control, provision for keeping the apparatus dry in the case of hygroscopic liquids and provision and the use of a reservoir into which air is pumped to a required pressure. It takes comparatively smaller time to obtain a reading with the arrangement. Another satisfactory method for the determination of η of highly vicous liquids is the coaxial cylinder method. Among the logarithmic decrement methods for measuring the η of liquids we may mention the well known Meyer's oscillating disc method which consists in finding the logarithmic decrement of an oscillating flat disc in air and in the liquid; the method of simple pendulum vibrating in the liquid (Stokes[2]); and H. Martin's[3] experimental method based on Stokes' mathematical investigation of a vibrating wire in a liquid medium. The accuracy of the method depends on the accuracy of the determination of the damping coefficient of the vibration of an electrically maintained wire in the liquid under test. The chief source of error in the method of finding η based on the determination of κ the logarithmic decrement or the damping coefficient is consequent on the uncertainty in noting the ends of the swings of the vibrating body. In the present investigation, a method has been described which is specially suited for the experimental comparison of η of highly viscous liquids like glycerine. It is essentially a damping coefficient determination method, the damping coefficient being calculated from the vibration curves of an oscillating system in air and in a liquid surrounding the body. The vibration curves are obtained by employing the improved vibrograph designed by the author.[4] The merits of the method are: (1) it takes a very short time, a fraction of a second to make an observation by this method; (2) a permanent photographic record of the damped oscillations is obtained and the visual uncertainty in noting the ends of the swing is automatically eliminated. It is suggested as an easy and quick method for comparing the viscosities of highly viscous liquids.

EXPERIMENTAL ARRANGEMENTS AND THEORETICAL CONSIDERATIONS

The experimental arrangement consists of a steel bar of uniform cross section rigidly clamped at one end so that a convenient length of the bar projects from the top of the table. A hollow brass sphere about one inch in diameter is rigidly attached to the free end of the bar through a short, stout wire, thereby constraining the sphere to vibrate only in the vertical plane in a direction perpendicular to the length of the bar. A rigid pointer, which can conveniently be a pin, attached to the free end of the bar as shown in the diagram of the experimental arrangement illuminated by the optical system and focussed on the slit of the vibrograph (*vide* Plates XII & XIII). The bar is set vibrating and the vibrations of the oscillating system are recorded on the photographic plate shot at right angles to the direction of vibrations. Vibration curves are obtained first with

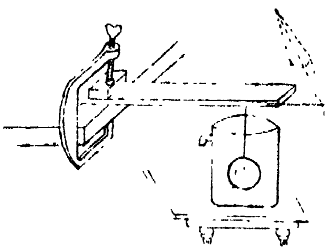

FIG. 1

the sphere oscillating in air and then in the liquid contained in a vessel placed beneath the sphere so that it is well immersed in the liquid. In working with different liquids the level of the liquid in the vessel is kept the same so that the vibration curves are obtained under identical conditions, as far as possible, the only variables being η and d the density of the liquid when working with different liquids. From the vibration curves, κ_0 the damping coefficient in air and κ the damping coefficient when the sphere is vibrating in the liquid are determined. Starting from the undisturbed position of the vibrating system, if a_0 is the amplitude of vibration at the end of a swing and a_n the amplitude at the end of n oscillations, then $a_0/a_n = e^{\kappa\tau n}$ where τ is the period of oscillation of the system.

$$\kappa = \text{the damping coefficient} = \frac{1}{n\tau} \log_e \frac{a_0}{a_n}.$$

or

$$\kappa = \frac{2.303}{n\tau} \log_{10} \frac{a_0}{a_n}.$$

$$\because \qquad \kappa \propto \frac{1}{n} \log_{10} \frac{a_0}{a_n}. \qquad \ldots \quad (1)$$

The reaction of the surrounding medium, *viz.*, the liquid in which the sphere is immersed, has two-fold effects. The first is the loss of the energy due to the viscosity of the medium and the second the diminution of energy due to the added mass, a layer of the medium moving bodily with the sphere. This added mass increases the inertia of the moving sphere without increasing its weight. Thus the added mass of the liquid affects the damping constant and not the frequency of the vibrating sphere. The irregularities attending the initial motion of the sphere inside the liquid, the eddies and the wall effect etc., do not affect the periodic time but may produce only second order effects on account of the shortness of time (about 1/5 sec.) during which the observations are recorded. The effect of the wire to which the sphere is attached on the liquid is likewise a small quantity and has a negligible effect on the motion of the sphere. The damping coefficient κ is, as in the case of Martin,[3] a function of η, d, a, the radius of the sphere, d_0 the density of the material of the sphere and N the frequency of oscillations of the vibrating system.

$$\kappa = \phi\,(\eta,\ d,\ d_0,\ a,\ \mathrm{N}).$$

Since, in using the apparatus, vibration curves are obtained with the sphere oscillating in different liquids at the same temperature or in a given liquid at different temperatures, d_0, a and N can be considered to remain constant. We are therefore interested in the investigation of the dependence of κ on η and d. From Martin's experimental verification of Stokes' formula, we are justified in assuming that $\kappa^2 \propto \eta d$ or $\kappa^2 = A\eta d$ where A is a constant. A is not dimensionless but is a function of d_0, a and n.

Thus to compare the viscosities η_1 and η_2 of two liquids having densities d_1 and d_2, we have to determine κ_1 and κ_2 the damping coefficients in the two liquids. If κ_0 is the damping coefficient in air, we have then,

$$\frac{\eta_1 d_1}{\eta_2 d_2} = \frac{(\kappa_1 - \kappa_0)^2}{(\kappa_2 - \kappa_0)^2}. \tag{2}$$

The effective damping of the liquid only is taken as in Meyer's[5] experiment, the damping due to mechanical causes and vibrations of the sphere in air being subtracted.

EXPERIMENTAL RESULTS

Bi-distilled glycerine for analysis (sp. gr. 1.23), is the liquid chosen and the vibration curves are obtained with the sphere oscillating in the liquid at various temperatures. Table I gives the analysis of the results obtained.

TABLE I

T°C Temp. of the liquid.	a_0 in cm Amplitude at the commencement.	a_n in cm. Amplitude at the end of n (=5) oscils.	Damping Constant κ of the Oscil. system in the liquid.	κ_0 Damping constant in air.	$(K-K_0)$	$(K-K_0)^2$
In air at 32°C	0.93	0.70	...	0.02468	...	...
34.0	0.75	0.35	0.06620	0.02468	0.04152	0.0017240
45.0	1.10	0.59	0.05410	0.02468	0.02942	0.0008654
55.0	0.93	0.52	0.04850	0.02468	0.02382	0.0005665
63.5	0.97	0.58	0.04468	0.02468	0.02000	0.0004000
79.0	0.85	0.54	0.03940	0.02468	0.01472	0.0002167
95.0	1.00	0.66	0.03610	0.02468	0.01232	0.0001518

Note.—In evaluating K_0 and R the constant terms (2,303 and τ) are omitted. This will not affect the final results since we are *comparing* the damping coefficients.

The vibration curves obtained at different temperatures are shown in the plate at the end of the paper. To verify the results indicated by formula (2), the relative viscosities of the same specimen of the liquid at various temperatures are determined by using a viscometer.

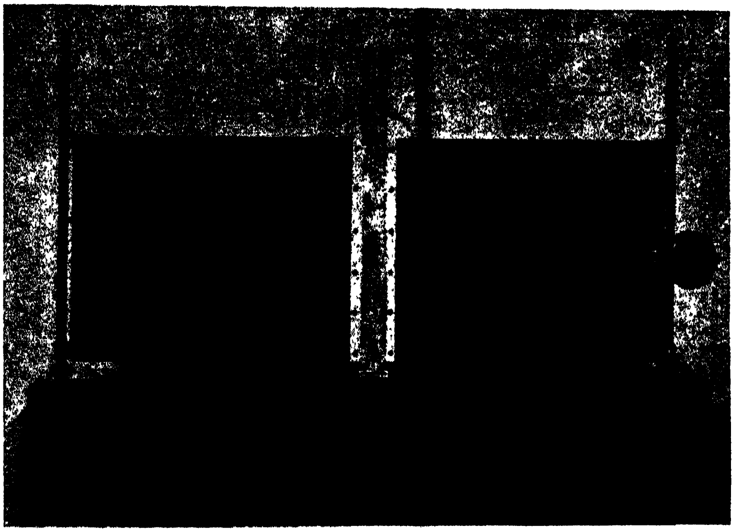

Fig. II. Front view of the vibrograph.

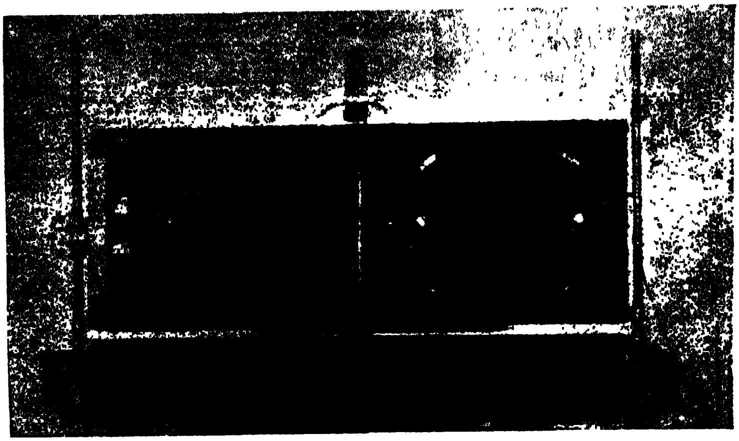

Fig. III. Back view of the vibrograph.

TABLE II.

T°C Temp. of the bath in which the viscometer is immersed.	t secs. Time taken for the liquid to flow past the two marks on the viscometer	d Density of the liquid at the Temp.	$\eta \propto td$ Relative viscosity of the liquid at the Temp.	$\eta d \propto td^2$.
32.0	4854	1.209	5869	7096
40.2	2971	1.203	3575	4300
45.5	2211	1.200	2653	3184
58.0	1271	1.192	1515	1805
69.0	890	1.185	1052	1946
80.0	612	1.177	720	847
95.0	397	1.166	463	540

Table II gives the values of relative viscosities obtained. A graph (Fig. 2) is drawn showing the relation between temperature T and ηd, and from the grahp, the values of ηd corresponding to the temperatures at which $(\kappa - k_0)^2$ are obtained by the vibrograph are computed.

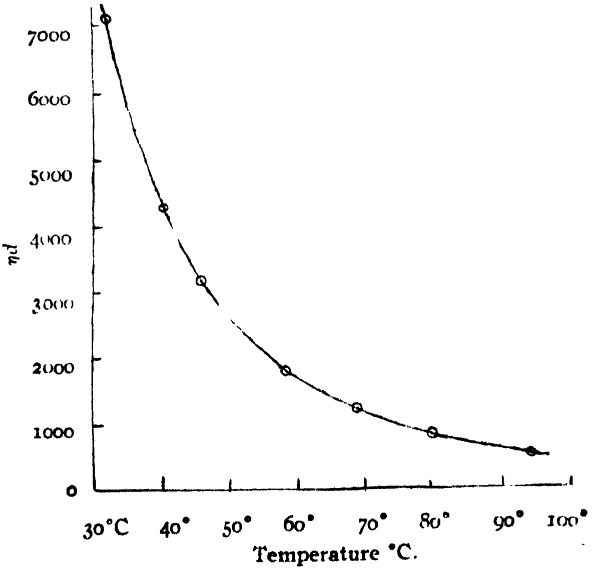

FIG. 2.

Table III gives the interpolated results.

TABLE III

T°C						
Temperature of liquid ..	34·0	45·0	55·0	63·5	79·0	95·0
Relative values of ηd at T°C got by interpolation from Fig. IV. ...	6250	3250	2050	1500	880	540
$(K-K_0)^2$ from vibration curves. ...	0.0017240	0.0008654	0.0005665	0.0004000	0.0002167	0.0001518

Fig. 3 shows the linear relation between ηd and $(\kappa-\kappa_0)^2$ both computed at the same temperature.

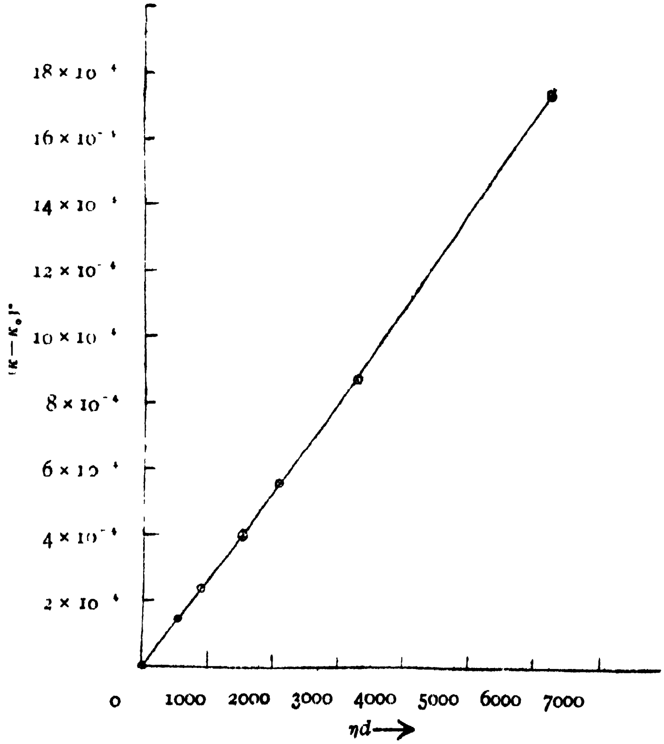

FIG. 3

The experimental results obtained with the liquid therefore support the procedure suggested for comparing the viscosities of liquids using a vibrograph. This method of comparing the viscosities of liquids using the vibrograph where for-

PLATE XIII.

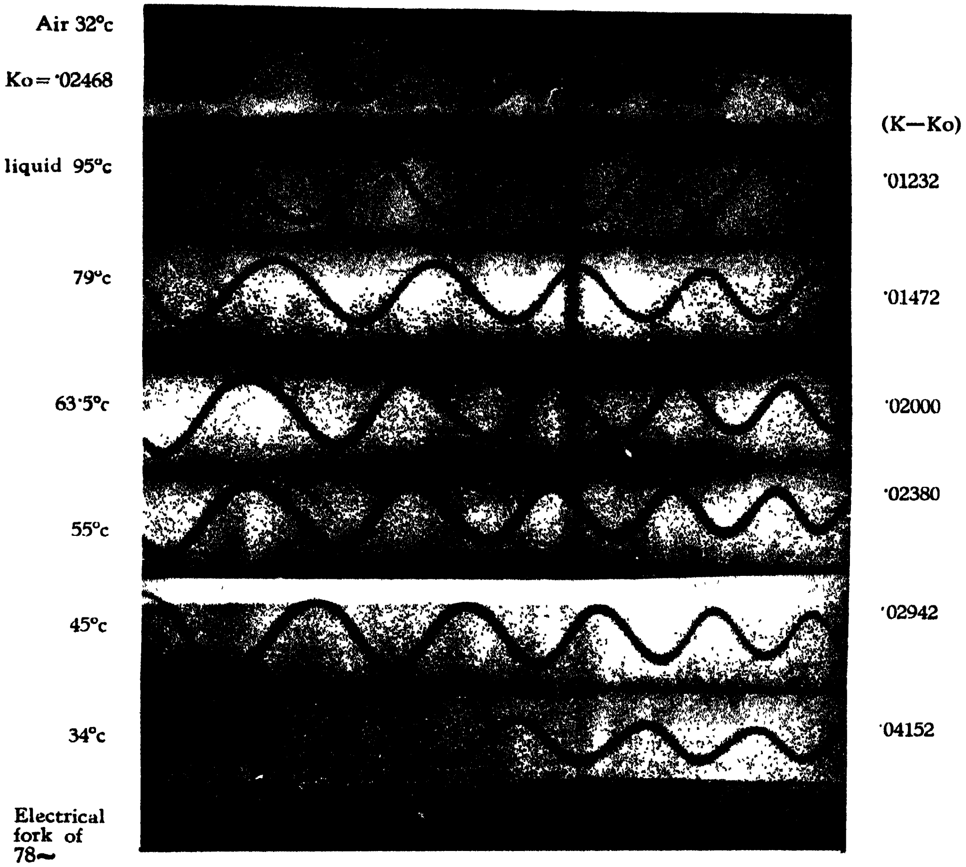
Air 32°c
Ko = ·02468
(K—Ko)
liquid 95°c
·01232
79°c
·01472
63·5°c
·02000
·02380
55°c
45°c
·02942
34°c
·04152
Electrical fork of 78~

each liquid the time required is of the order of less than a second will be found convenient in the quick determination of relative viscosities of thick oils etc., used for lubrication purposes; especially so because of the permanent photographic records of the vibrations which can be used for subsequent computation or verification.

ACKNOWLEDGMENT

The author wishes to express his grateful thanks to Dr. L. Sibaiya for the guidance and facilities afforded in carrying out this investigation.

DEPARTMENT OF PHYSICS,
UNIVERSITY OF MYSORE,
BANGALORE.

REFERENCES

[1] J Bhimasenachar, *Proc. Ind. Acad Sci.*, A. **10**, 141-44 (1939 .
[2] Stokes, " Mathematical and Physical papers, Vol III.
[3] H. Martin, *Ann. d. Physic*, **77**, 627 (1925).
[4] T. Tirunarayanachar, *Rev. Sci. Inst.*, 3 (1932).
[5] Poggendorf Annalen, No. 113, p. 55.

THE OPTICAL HYGROMETER AND ITS WORKING

By L. D. MAHAJAN, M.Sc., Ph.D., F.Inst.P. (London)

(Received for publication, June 15, 1941)

ABSTRACT. In this paper, the description of the construction of the optical hygrometer is given. It works on the principle of a balance in the form of a rod supported by two loose screws and at right angles to it there is another rod having two pans on its ends, rigidly attached with it. One pan contains the substance having high power of absorption and desorption of moisture and the other pan balancing weights. The rotation of the rod which is proportional to the change in humidity is measured by the lamp and scale arrangement.

The theory, its sensitiveness and working are discussed in detail. A few observations recorded with this instrument are compared with those of the other kinds of hygrometers.

INTRODUCTION

Various kinds of hygrometers are being used in these days for determination of the relative humidity of the air. Some of the common forms are the wet and dry bulb hygrometer, hair hygrometer, and the paper hygrometer. But all of them are such that they take a long time to adopt the conditions of the air and do not show high degree of accuracy. Moreover, the hair and the paper hygrometers do not give correct readings at very high and very low relative humidities. The small changes in the humidities of the air cannot be detected easily and correctly by any one of them.

In view of the above difficulties, a new type of hygrometer[1] has been invented in this Laboratory which works on the principle of optical instruments. By its use many practical difficulties, which one has to face for the accurate work, will be overcome.

A short note regarding it has already been published in the Current Science in its February number, 1941. But now in this paper, a detailed study of its construction, theory, sensitiveness, and use has been made. A short note regarding the selection of a suitable substance having high power of absorption and desorption of moisture is given. Besides a few observations recorded with it are compared with those of the other kinds of hygrometers commonly used in the laboratories.

CONSTRUCTION

Its construction is very simple and its line sketch is given in Fig. 1. To a zinc rod *a* (balance beam) of about 1 mm. thickness, 2 mm. depth, and 6 cm.

length, a cup of zinc of about 1 cm. square and about 2 mm. deep, is regidly attached on its each end. Another cylindrical revolving rod of copper, *b*, about 1 mm. thick and 4 cm. long passing through the middle of the beam *a* is regidly attached at right angles to it. A small galvanometer mirror *m* of about 2 metres focal length is fixed to the revolving rod, just on one side of the junction of the revolving rod and the balance beam.

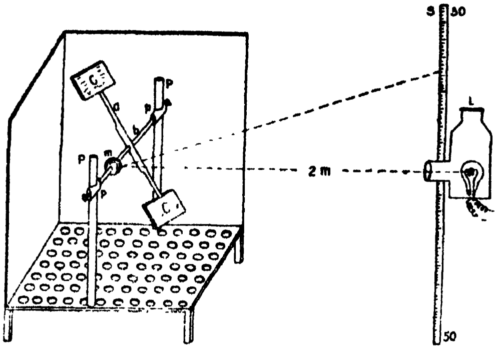

Fig. 1

The two ends of the revolving rod are made to rest on two fine well-polished and equally levelled glass plates *p*, *p* fitted on stands or they are very loosely fitted in the grooves of two hollow adjustable screws fixed in the two vertical supports P and P. The former method is more sensitive than the latter one but the latter is stabler than the former. Any one of them can be used according to the nature of the experiment and the accuracy needed.

One of the cups (*c* and *c*) is filled with the Plaster of Paris containing about two percent calcium chloride or the black cotton-soil of Poona. Both have fairly high power of absorption and desorption of moisture, being available easily and at cheaper rate and also having slightly higher power of absorption and desorption of moisture than that of the former. Suitable weights are added into the other pan till the balance beam (zinc rod *a*) becomes horizontal. Instead of the fractional weights, pure thick sand or quartz powder can be used and may prove better than the weights which sometimes move in the pan and disturb equilibrium.

The whole instrument is enclosed inside a rectangular glass cover. It fits well on its base which is perforated with holes. They help in free circulation of the external air inside it. The cover avoids any disturbance to the revolving arrangement due to any direct and strong current of air.

Then the beam of light is thrown from an electric lamp and the scale arrangement L on the galvanometer mirror and the reflected beam is thrown somewhere in the middle of a vertical scale S at a distance of about 200 cms. from the mirror. With a small change in the humidity of the air the spot of light moves through a great distance on the vertical scale.

SELECTION OF THE SUBSTANCE

In view of selecting a suitable substance having high power of absorption of moisture from the moist air and desorption of moisture to the dry air, for the pan of the balancing beam, powders of various substances were tried. Some of them which need a mention are the following :—

Plaster of Paris, calcium hydroxide, aluminium hydroxide, lycopodium powder, sodium bicarbonate, sodium nitrate, calcium chloride, black cotton-soil of Poona; Patiala soil, and various mixtures of Plaster of Paris and calcium chloride, in quantities varying from 1% to 50% of calcium chloride in Plaster of Paris.

It was observed that the calcium chloride, calcium hydroxide, and sodium bicarbonate have high power of absorption of moisture from the air and little power of desorption of moisture to the dry air. While aluminium hydroxide, stearic acid, sodium nitrate, and lycopodium powder have very little power of absorption and desorption of moisture. But it was observed that the fine powdered soil of Patiala, the black cotton-soil of Poona, and Plaster of Paris containing 2% calcium chloride work quite satisfactory for they cause a good shift of the spot of light on the scale for a small change in the humidity of the air, and the rates of absorption of moisture from the moist air and desorption of moisture to the comparatively dry air are almost the same. But the last two are far better than the first, and the black cotton-soil of Poona is undoubtedly the best.

It is a better arrangement, if a paste be made by mixing the black cotton-soil with a suitable quantity of water and one of the cups is filled with it. On drying up the paste, it works well. This process avoids the blowing away of the fine particles of the soil from the cup.

THEORY

Let the weight of the substance in one of the cups be m gms. and the standard weights in the other pans be also m gms., so that the balance beam be horizontal. When the relative humidity of the air increases, the substance in the cup absorbs some more moisture from the air and by this let the increase in weight of the substance be μ gms. This will bend the balance beam on the soil side through an angle θ and raise the other side by the same angle. The revolv-

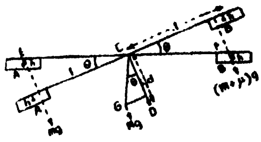

FIG. 2

ing rod which is rigidly attached to the balancing beam rotates through the same angle. The galvanometer mirror attached with the revolving rod also rotates through the same angle. But the reflected ray of light deviates through double that angle, *i.e.*, 2θ.

Now in the above fig. 2, let the weight of the balancing beam be M gms. When the beam is horizontal in the position ABC, the weight mg is acting at A, mg at B, and Mg at C. But after the adsorption of moisture, the beam takes the inclined position ECF. By imagining the vertical section taken through the centre of the beam that it cuts the beam at E, G, F. Thus the weight mg acts at E, $(m+\mu)g$ at F and Mg at G. In this case the three points where the weights of the central beam and the pans are acting are not coplanar, *i.e.*, A, B and C are not coplanar but C is slightly higher than the other two points A and B.

Let l be the length of each arm, *i.e.*, horizontal distance, $CB=CA=l$ and d the depth of centre of gravity D below C. Let h be the depth of A and B below C when the balance beam is horizontal. It is approximately the same in both cases.

When the beam is inclined :—

The horizontal distance of A from C $= l\cos\theta + h\sin\theta$.

,, ,, B ,, $= l\cos\theta - h\sin\theta$.

,, ,, C ,, $= d\sin\theta$.

When the beam is in the equilibrium position, the moments acting on both the sides are equal. Therefore,

$$(m+\mu)g\ (l\cos\theta - h\sin\theta) = Mg.d\sin\theta + (l\cos\theta + h\sin\theta)mg$$

since the angle θ is very small, so $\cos\theta = 1$ and $\sin\theta = \theta$ very approximately and the above equation can be put down in the following form :

$$(m+\mu)g\ (l-h\theta) = Mg.d\theta + (l+h\theta)mg$$
$$-\mu h\theta + ml - mh\theta + \mu l = Md\theta + ml + hm\theta.$$

By neglecting the product $\mu\theta$ which is very small and negligible, we get :

$$\theta = \frac{\mu l}{Md+2mh} \qquad \dots (1)$$

or

$$\frac{\theta}{\mu} = \frac{l}{Md+2mh} \qquad \dots (2)$$

and

$$\mu = \left(\frac{Md+2mh}{l}\right)\theta \qquad \dots (3)$$

$$= k\theta \qquad \dots (4)$$

where k is a constant equal to $\frac{Md+2mh}{l}$.

The equation (2) gives the ratio of the deflection θ to the difference μ in the loads on the two cups. This ratio is the sensitiveness of this instrument.

The equation (4) gives the value of μ, the increase in weight of the soil by adsorption of moisture from the moist air in terms of a constant k and deflection θ where k is equal to $\frac{Md+2mh}{l}$ which remains constant for any instrument and depends merely on its construction. Therefore, the increase in weight μ is proportional to θ which is the rotation of the revolving beam.

$$\mu \propto \theta.$$

But the increase in weight is proportional to the increase of the relative humidity of the air,[1] therefore

$$(H_2 - H_1) \propto \theta \quad \ldots \quad (5)$$

where H_1 and H_2 are the initial and final relative humidities of the air. When H_1 is zero, we get

$$H_2 \propto \theta \quad \ldots \quad 6)$$

The angle θ of rotation of the revolving rod is measured by means of a lamp and scale arrangement. If the distance of the scale be y cms. from the galvanometer mirror and the spot of light shifts through the distance x cms. on the vertical scale, then we get :

$$2\theta = \frac{x}{y} \text{ (angle } \theta \text{ being very small)}$$

or

$$\theta = \tfrac{1}{2}\left(\frac{x}{y}\right) \quad \ldots \quad (7)$$

therefore, by substituting this value in equation (4), we obtain :

$$\mu = k.\tfrac{1}{2}\left(\frac{x}{y}\right)$$

$$= Gx \quad \ldots \quad (8)$$

where G is another constant equal to $\tfrac{1}{2}.\frac{k}{y}$ which remains constant as long as the arrangement of the apparatus, *i.e.*, the distance of the scale from the mirror remains the same.

Let μ_1 be the increase in weight when the humidity increases from H_0 to H_1 and μ_2 be the increase in weight when the humidity increases from H_0 to H_2, and let the shifts of the spot of light in both cases on the vertical scales be x_1 and x_2 respectively, then

$$\frac{H_1-H_0}{H_2-H_0}=\frac{\mu_1}{\mu_2}$$

$$\therefore\ \frac{H_1-H_0}{H_2-H_0}=\frac{Gx_1}{Gx_2}=\frac{x_1}{x_2}. \qquad \ldots \quad (9)$$

If H_0 and H_1 are known, H_2 can be calculated. If the arrangement is so made that H_2 represents zero, relative humidity and the corresponding reading on the scale be zero cm. and R_1 and R_2 are the readings taken on the scale for the relative humidities H_1 and H_2, then

$$\frac{H_1}{H_2}=\frac{R_1}{R_2}. \qquad \ldots \quad (10)$$

If H_1 is known, we can calibrate the scale in terms of the relative humidities. Then the readings on the scale will represent directly the relative humidity of the air or any chamber where the instrument is kept for record of observation.

SENSITIVENESS OF THE INSTRUMENT

The equation (2) $\frac{\theta}{\mu}=\frac{l}{Md+2mh}$ which has already been derived above represents the ratio of the deflection θ to the difference μ in the loads on the two cups and is the sensitiveness of the instrument. But if the cups are so made that they are above the horizontal, that is, C is below A and B, then the sensitiveness of the instrument becomes :

$$\frac{\theta}{\mu'}=\frac{l}{Md-2mh}. \qquad (2.a)$$

Thus the sensitiveness can be increased in both the cases by increasing l the length of the arms of the balancing beam and by decreasing M the mass of the beam and d the depth of the centre of gravity of the beam from the point of suspension.

In the former case, the sensitiveness will also increase by decreasing m the load in either pan, and h the depths of the points A and B below the horizontal. But in the latter case the sensitiveness will increase by increasing m and h for C is below the external points.

In both the cases, the quantity $(Md \pm 2mh)$ is very small and l is fairly large for the balancing beam is made of zinc and has small dimensions and the beam is almost horizontal. The quantity $2mh$ is very small. Therefore the sensitiveness is very high.

OBSERVATIONS

The results obtained with this instrument are satisfactory. It works to a high accuracy. The small changes in humidity of the air can easily be detected with it. A few of the observations recorded with it and other kinds of hygrometers are given below in table I and indicate the comparison of results.

TABLE I

No.	Kind of Hygrometer	Change in % Humidity recorded by it	Shift of the spot of light on the vertical scale or of the needle on the dial of the instrument
1	Wet and dry bulb Hygrometer	1.2% increase	A fraction of a degree on the thermometers
2	Paper Hygrometer	1.5% ,,	1 mm. approximately on the dial
3	Hair Hygrometer	1.1% ,,	1.5 mm. approximately on its dial
4	Optical Hygrometer	1.0% ,,	2.5 cms. approximately on the vertical scale
1	Wet and dry bulb Hogrometer	1.1% decrease	A fraction of a degree on the thermometers
2	Paper Hygrometer	1.3% ,,	1.1 mm. approximately on its dial
3	Hair Hygrometer	1.0% ,,	1.4 mm. approximately on its dial
4	Optical Hygrometer	1.0% ,,	2.4 cms. approximately on the vertical scale

The above observations lead us to the conclusion that even one percent. increase or decrease of humidity of the air cannot be easily detected and accurately read from the wet and dry bulb, the hair and the paper hygrometers, as in the first instrument the size of the degree of the thermometer is very small, and in the case of the second and third instruments the shift of the pointer on the dial is hardly of the order of one millimetre. But the same change in the humidity causes a shift of the spot of light on the vertical scale of the optical hygrometer through 2.5 cms. which can be read quite easily and accurately. Thus small variations in the relative humidity of the air, even of the order of 1% or less than 1% can easily and accurately be detected by this instrument.

The sensitiveness of this instrument may be compared with that of the hair hygrometer by comparing their shifts on their corresponding scales. Thus,

$$\frac{\text{Sensitiveness of the Optical Hygrometer}}{\text{Sensitiveness of the Hair Hygrometer}}$$

$$=\frac{\text{Shift of the spot of light on the vertical scale}}{\text{Shift of the pointer on the dial}}$$

$$=\frac{2.5}{0.15}$$

$$=17 \text{ times approximately.}$$

CONCLUSIONS

Further work is being done in this laboratory to find a better substance having still higher power of absorption of moisture from the moist air and desorption of moisture to the comparatively dry air, than that of the present ones used in it. Attempts are also being made now to make it more sensitive, accurate and practicable for everyday use in the laboratories and the meteorological observatories.

The author is greatly indebted to the Government of Patiala, for having provided facilities to carry out the above work in the Research Laboratory of the Mahendra College, Patiala. The author also expresses his heartfelt thanks to Dr. L. A. Ramdas, Agricultural meteorologist of the India Meteorological Department, Poona, for having provided me with a sample of black cotton soil of Poona for the above work.

PHYSICS RESEARCH LABORATORY,
MAHENDRA COLLEGE,
PATIALA.

REFERENCES

[1] L. D. Mahajan, " An Optical Hygrometer." *The Current Science*, **9**, 100, (1941 .

[2] L. D. Mahajan, " Adsorption of Moisture from the Moist Air by the Soils," *Ind. Jour. Phys.*, **14**, 441-450, (1940).

THE SECONDARY K-ABSORPTION SPECTRA OF FERRIC OXIDE IN SOLID AND IN COLLOIDAL SOLUTION*

By S. SEN

(*Received for publication, June 30, 1941.*)

ABSTRACT. Secondary K-absorption spectra of colloidal solution of ferric oxide have been investigated and compared with those obtained in solid ferric oxide. An extended secondary structure has also been found in the colloidal solution. A comparison of the secondary structure in the solid state of ferric oxide and in the state of colloidal solution has revealed that the positions of the succeeding maxima and minima are not identical in the two cases. Marked difference has also been noticed in the position and width of the primary edge These results have given rise to important speculation as to the nature of the colloidal particles. From this experiment it has not been possible at the present moment to decide definitely whether these colloidal particles are simple molecular aggregation or crystallites of Fe_2O_3.

INTRODUCTION AND EXPERIMENT

The behaviour of substances in the colloidal state has been the subject of interesting and important study in physical chemistry. The colloidal particles, as we know, are matter in finest division having their diameter small enough to share the random motion of the molecules in accordance with the well-known gas kinetic laws and do not settle under the force of gravity, but are large enough compared to single molecules so as to be visible under ultra-microscope. The radii of the colloidal particles usually ranges from 10^{-5} to 10^{-7} cm.† Each particle is therefore formed of several molecules clustered together. Now each colloidal particle, say Fe_2O_3, may be crystalline, the oxygen and iron atoms being regularly arranged or it may be a cluster of several Fe_2O_3 molecules. We have undertaken this investigation with the view that the study of the secondary structure may throw some light on this question.

An electron type of metal X-ray tube was used for the present investigation. The slit of the spectrograph, which is adjustable, was kept constant at .1 mm. It was covered with a thin aluminium foil and the well-known Bragg focussing method was adopted. The dispersion on the photographic plate was 15.6 X.U. per mm. Each negative plate was microphotographed at several points for precision measurement and the dispersion on the microphotograph was 2.4 X.U. per mm.

---

* Communicated by the Indian Physical Society.

† The Physical Properties of Colloidal Solution (3rd Edition), E. F. Burton

The colloidal solution was prepared in the following way. Ferric hydrate $Fe(OH)_3$ precipitated from ferric chloride solution by adding ammonium hydroxide is filtered and well washed with distilled water to remove the trace of NH_4OH and Cl_2. The precipitated ferric hydroxide is then added to a saturated solution of ferric chloride and the whole was then well shaken. The colloidal solution of ferric oxide is thus obtained. On long standing, the coarse particles, formed at first, gradually break up into finer ones. One such colloidal solution having its particle size roughly of the order of 10^{-6} to 10^{-7} cm. in diameter has been investigated.

A special type of cell holder was designed for the purpose in which the colloidal solution may be contained and exposed to the path of X-ray beam. It consists of two rectangular brass plate in which similar rectangular slots were cut out. A thin piece of rubber sheet was placed between the plates and screwed at four corners. The solution is contained in the rectangular opening; the two surfaces of the plates were covered by thin pieces of celluloid film.

The results on colloidal ferric oxide as well as on solid ferric oxide are given in tables I and II. The position of the succeeding maxima and minma are given in X.U. The differences of the position of these maxima and minima from the main edge are given in X.U. and in electron volts.

The following peculiarities are noteworthy :

1. The secondary absorption edges appear on the short-wavelength side of the principal K-absorption edge of iron in colloidal solution of ferric oxide, and extend to about 200 volts from the main edge.

2. The distances of the secondary maxima and minima in volts from the principal absorption edge have not come out identical in colloidal Fe_2O_3 and in solid Fe_2O_3. The intensity distribution in the fine structure in the two cases is also different.

3. The position of the primary edge in colloidal solution has shifted to longer wavelength compared to that in the solid state.

4. The width of the edge has also increased in the colloidal solution.

TABLE I

Solid and Colloidal Ferric Oxide

		K	A	α	B	β	C	γ	D	δ	E	ε	F
Solid Fe_2O_3	λ in X.U.	1736.4	1732.8	1727.8	1722.1	1717.7	1714.0	1711.8	1703.5	1698.3	1694.7	1689.7	1687.3
	δλ	0	3.6	8.6	14.3	18.7	22.4	24.6	32.9	38.1	41.7	46.7	49.1
	δν	0	14.78	35.4	59.0	77.4	92.9	102.2	137.4	159.5	175.0	196.5	206.9
Colloidal Fe_2O_3	λ in X.U.	1737.2	1732.7	1726.6	1721.4	1719.6	1717.7	1714.7	1703.6	1696.0	1691.8	1689.9	
	δλ	0	4.52	10.62	15.82	17.6	19.5	22.5	33.6	41.2	45.4	47.3	
	δν	0	18.5	43.7	65.2	72.7	80.7	93.3	140.2	172.6	190.7	198.9	

TABLE II

Positions and Widths of Principal Absorption Edge in Solid and Colloidal Fe_2O_3

	λ in X.U.	ν/R	δλ	δν	Width in X.U.	Width in *e.v.*
Solid	1736.4	524.8	0	0	3.6	14.7
Colloidal	1737.2	524.6	8	3.3	5.0	22.9

DISCUSSION

Secondary structures extending over several hundred volts may be either due to the crystal lattice or due to the polyatomic molecules. But the secondary structure from the crystalline field is different from that which simply arises from the molecular field. Further as the particle size diminishes its crystalline property may be different from that in which the particle size is large. Hence the secondary structures may also be different owing to the diminution of the particle size.

Our experimental results on colloidal solutions indicate that the secondary structure obtained in the colloidal solutions is different from that obtained in the solid Fe_2O_3. This difference in secondary structure suggests that if the colloidal particles exist in the crystalline state, their crystalline property is different from that in which it exists in the solid Fe_2O_3. This may be due to the diminution of particle size and as such there may be a change in the secondary structure. From the diffraction experiments on colloidal precipitates done in this laboratory, we have observed that precipitates of metal sols are crystalline while non-conducting colloidal precipitates show amorphous bands coinciding in position with the strongest groups of sharp lines of the crystalline sample. This observation further complicates the problem as these diffraction bands (amorphous) may really arise from very small crystalline particles where the number of lattice planes is too small to show any perfect interference. Further the colloidal particles may also exist as simple molecular aggregation without any crystalline field. This may also account for a change in the secondary structure. At present it is however difficult to arrive at any definite conclusion as regards the two hypotheses, *viz.*, whether the colloidal particles are simple molecular aggregation or small crystallites of Fe_2O_3.

This investigation was carried out in the Laboratory of the University College of Science and the author thanks Prof. B. B. Ray for the interest he has taken during the progress of the work.

KHAIRA LABORATORY OF PHYSICS,
UNIVERSITY COLLEGE OF SCIENCE,
CALCUTTA.

STUDIES IN ANTENNA RESISTANCE AND REACTANCE*

By S. R KHASTGIR, D.Sc., Mem. I. R. E.

AND

C. CHOUDHURY, M.Sc.

(Received for publication, July 9, 1941.)

ABSTRACT: Measurements of antenna resistance and reactance were carried out by following Willans' double-beat method for a range of frequencies from about 330 kc/sec. to about 2300 kc/sec.

The theory of the method of measurements is described and the experimental results given in the paper. Measurements were made for three different types of receiving aerials *viz.*, (1) vertical aerial, (2) inverted L-aerial and (3) T-aerial, each being earthed. The effect of varying the length of the horizontal part of the last two aerials was also studied.

1. INTRODUCTION

The Antenna resistances and reactances of three different types of receiving aerials *viz.* (1) vertical aerial, (2) T-aerial and (3) inverted L-aerial were measured by Willans'[1] method for different radio frequencies within the range from about 2300 kc/sec. to about 330 kc/sec. and the results of these measurements are recorded in this paper. Willans' method had already been applied to a detailed investigation of the variation with frequency of the resistance and reactance of an earthed receiving aerial of approximate L-shape over a very wide range of frequencies by Wilmotte and Colebrook,[2] of the Radio Research Board, Great Britain. Antenna resistance measurements by other methods had also been carried out by many investigators, such as T. L. Eckersley,[3] Moullin,[4] Miller,[5] Smith-Rose and Colebrook[6] and others for different ranges of frequencies.

All the three types of receiving aerials employed in this investigation were grounded. In the case of the T-type and the L-type of aerials, measurements were also carried out to find the effect of the length of the horizontal parts of these aerials on the values of antenna resistance and reactance.

2. WILLANS' METHOD OF H. F. RESISTANCE MEASUREMENTS

The principle involved in the method of Willans is really an essential part of the method. The principle is the well known principle of transformer action

---

* Communicated by the Indian Physical Society.

e.g. when a current flows in a secondary circuit, the resistance and reactance of primary circuit apparently change.

Consider a secondary circuit having inductance L, resistance R and capacity C in the neighbourhood of an *oscillating* primary circuit having inductance L_1, resistance R_1 and capacity C_1. Let M be the mutual inductance between the primary and the secondary inductances and ω the angular frequency of the currents. If X_1, R_1 and X, R be the values of the primary and secondary reactance and resistance respectively without the secondary effect, then calling X' and R' the effective values of the primary reactance and resistance, we can write

$$R' = R + \gamma^2 R_1 \quad \ldots \quad (1)$$

and

$$X' = X - \gamma^2 X_1 \quad \ldots \quad (2)$$

where

$$\gamma^2 = \frac{\omega^2 M^2}{R^2 + X^2}$$

The change in the reactance means a change of the effective inductance of the oscillator (primary) coil which in turn causes a change in the emitted frequency of the oscillator. This change in the frequency of the oscillator is directly proportional to the change of reactance which is $\gamma^2 X_1$. The frequency-change is then given by

$$\Delta f \propto \frac{\omega^2 M^2}{R^2 + x^2} . X_1$$

Now it can be easily proved that for ωM = constant, the change in frequency is maximum, when $R^2 = X^2$ or when $R = \pm x$

i.e.

$$\left.\begin{aligned} R &= \left(\omega L - \frac{1}{\omega C'}\right) \\ \text{or} \quad R &= \left(\frac{1}{\omega C''} - \omega L\right) \end{aligned}\right\} \quad \ldots \quad (3)$$

Here C' & C'' are the values of the secondary capacity for the two alternative conditions for maximum change of frequency as given in (3). Combining now the two alternative conditions, we get

$$R = \frac{1}{2\omega}\left(\frac{1}{C''} - \frac{1}{C'}\right) \quad \ldots \quad (4)$$

3. GENERAL EXPERIMENTAL PROCEDURE IN WILLANS' METHOD

The change in the emitted frequency due to the change in the effective reactance of the oscillator circuit can be discerned as an alternation of the beat note in the telephones connected to an oscillating receiver. Let us consider three circuits (1), (2) & (3) as shown in fig. 1. Circuit (1) is the measuring

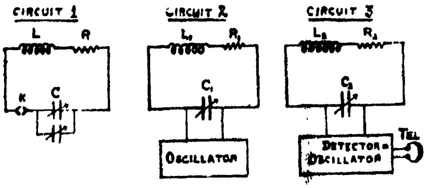

FIG. 1

circuit which comprises an inductance L, a resistance R, a suitable standardised variable condenser C and a switch K, circuit (2) is an oscillator circuit with an inductance L_1, a resistance R_1 and a suitable standardised condenser C_1. Circuit (3) is a detector-oscillator of the same type as the circuit (2) with an inductance L_2 a resistance R_2 and a variable condenser C_2. A pair of telephones is in the anode circuit of this detector oscillator. When the frequencies of the two oscillators are suitably adjusted, it is possible to hear the heterodyne beat-note in the telephones.

The experimental procedure is as follows : With the switch of circuit (1) open, the frequency of (3) is first adjusted to the desired value and the frequency of (2) is adjusted by varying C_1 till no beat-note is heard. With the circuit (1) closed, the condenser C varied till the beat-note again disappears ; *i.e.* the frequency of (2) is back to its original value. This gives C_r the resonance value of C. Next displacing C by a small amount the beat-note is again heard due to a change in the frequency of (2). C_1 is now changed till the beat-note disappears. If the process is repeated for other positions of C, it will be found that the variation of C_1 required to balance the effect of variation of C is of the same form as the variation of frequency shown in fig. 2. Here the ordinate

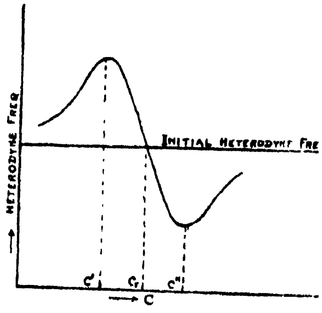

FIG. 2

represents the heterodyne frequency (which depends on the value of C_1) and abscissa, the value of C. Two peaks are observed on both sides of the C-value which corresponds to the original frequency and these peaks appear for two different values of C *viz.*, C′ & C″. The H.F. resistance R of the measuring circuit (1) can then be obtained from equation (4).

The curve cuts across the horizontal line representing the capacity of C_1 corresponding to the initial frequency of (2), at a certain value of the capacity C which is the same as the resonance capacity C_r.

4 EXPERIMENTAL TECHNIQUE IN THE PRESENT INVESTIGATION

The complete arrangement of the apparatus is shown in fig. 3. The oscillators were of the Hartley type. A pair of telephones was inserted in the anode circuit of the detector-oscillating valve. When the frequency of each was adjusted, it was possible to hear the heterodyne whistle The L.F. e.m.f. developed across the telephone was then fed into a 3-valve amplifier of the conventional type. A loudspeaker was connected to the output of the amplifier. Through this loudspeaker was passed an audio-frequency current from the secondary circuit of an audio oscillator of a suitable constant frequency. A variable resistance was inserted to adjust the amplitude of this audio-frequency current so that the heterodyne whistle and the sound due to the audio-frequency current from the audio-oscillator could be made of the same order of intensity. As a result of the superposition of these two audio-frequency currents through the loudspeaker, beats could be heard. The tuning condenser C_1 or C_2 of either oscillator could be adjusted till no beats were heard. This double-beat technique increased the accuracy of the condenser settings to a considerable extent.

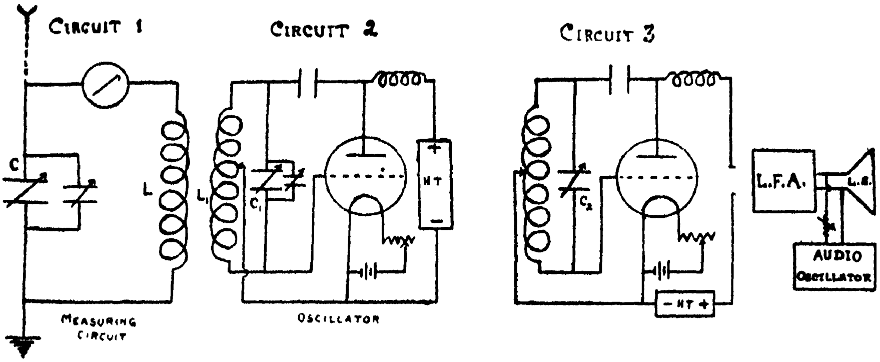

FIG. 3

All the condensers were properly shielded and calibrated very accurately. A mercury-link was included in the measuring circuit. Usually more than one condensers fitted with slow-motion dials were used in parallel both for C and C_1. Long glass rods fixed to the condenser knobs were employed for turning the condensers.

5. MEASUREMENT OF THE ANTENNA RESISTANCE AND REACTANCE AND THE THEORY OF THE METHOD

First, the measuring circuit consisted of an inductance L and a standardised variable capacity C. The H.F. resistance R of this circuit was measured by the method of Willans. The resonance value of C was C_r. Next, the aerial under investigation was connected to one end of the inductance and the other end was put to the earth. Similar procedure was followed to measure the equivalent resistance R′ of the complex circuit. The resonance capacity of the variable condenser in this case was C'_r which was different from C_r.

Measurements of R and R′ were made successively and the coupling between the coil of the oscillator and the coil of the measuring circuit was kept fixed for each frequency.

The theory of the method is indicated below. If R_e be the effective antenna resistance, it can be shown that

$$R' = R_e + \frac{R}{\omega^2 L C'_r}, \quad \text{since } \omega R C'_r << (1 - \omega^2 L C'_r).$$

Therefore $$R_e = R' - \frac{R}{1 - \omega^2 L C'_r} = R' \quad \frac{R}{1 - \omega^2 L C_r \left(\frac{C'_r}{C_r} \right)} .$$

Since $\omega^2 L C_r = 1$, we can write

$$R_e = R' - R . \frac{C_r}{C_r - C'_r} \qquad \dots \quad (5)$$

The effective reactance X_e of the antenna can be obtained in the following manner. If X′ be the reactance of the complex circuit when the antenna is connected in the manner shown in fig. 3, the condition of resonance is given by $X_e + X' = 0$. Under the conditions of the experiment, it can be shown

$$X' \approx \frac{\omega L}{1 - \omega^2 L C'_r} \approx \omega L . \frac{C_r}{C_r - C'_r} ,$$

so that the antenna reactance will be given by

$$X_e = - \omega L . \frac{C_r}{C_r - C'_r} \qquad \dots \quad (6)$$

The values of the antenna resistance and reactance were obtained with the help of (5) and (6).

6. EXPERIMENTAL RESULTS—VARIATION OF ANTENNA RESISTANCE AND REACTANCE WITH FREQUENCY

The results of measurements for the earthed vertical aerial, the inverted L-aerial and the T-aerial are given in figs. 4, 4(*a*), 5, 5(*a*) and 6, 6(*a*).

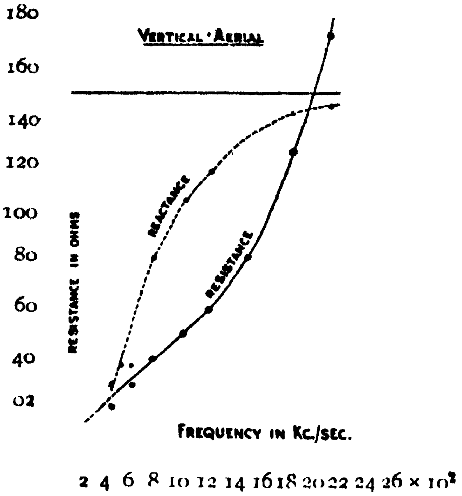

Fig. 4

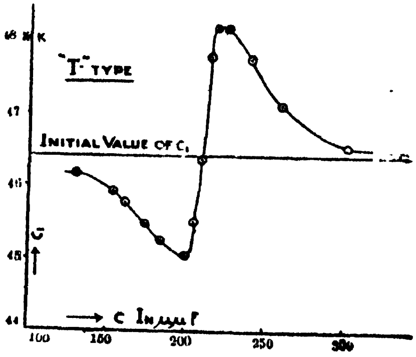

Fig. 5(a)

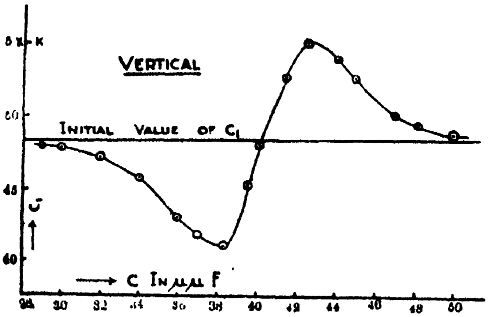

Fig. 4(a)

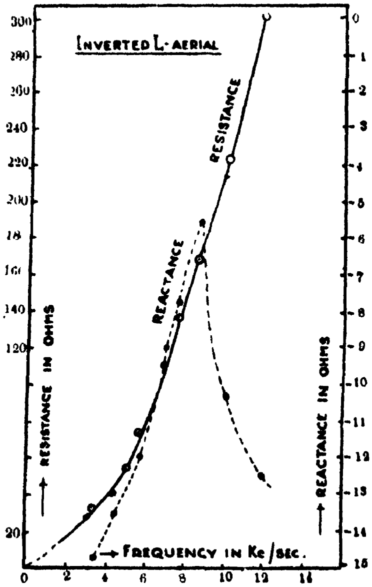

Fig 6

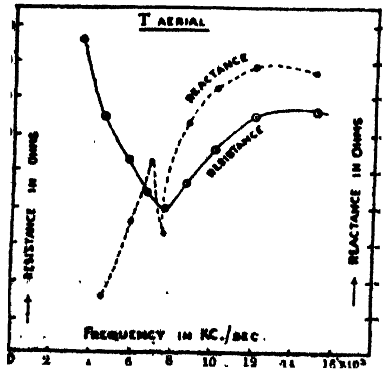

Fig. 5

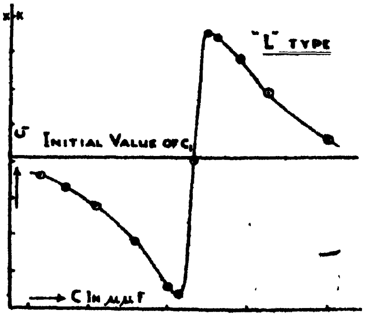

Fig. 6(a)

7. VARIATION OF ANTENNA RESISTANCE AND REACTANCE WITH THE LENGTH OF THE HORIZONTAL PART OF THE T-AERIAL AND THE L-AERIAL

The experiments on the variation of the antenna resistance and reactance with the horizontal top length were carried with freq : 845 kc/sec. ($\lambda = 355m$). The results of measurements with a "T"-aerial are given in table IV.

TABLE IV

Earthed T-aerial: Frequency : 845 kc/sec. ($\lambda = 355m$).

Top length (metres)	Without aerial				With aerial					
	C' $(\mu\mu f)$	C'' $(\mu\mu f)$	C_a $(\mu\mu f)$	R (ohms)	C' $(\mu\mu f)$	C'' $(\mu\mu f)$	C'_a $(\mu\mu f)$	R' (ohms)	R_a (ohms)	X_a (ohms)
11.0					292	350	319	54.2	41.8	-7.01×10^2
10.5					305	365	332	50.46	37.4	-7.36 ,,
10.0	579	600	589	5.7	312	370	339	46.9	33.5	-7.57 ,,
9.5					312	366	344	43.45	29.7	-7.72 ,,
8.5					328	382	354	39.8	25.5	-8.05 ,,

Similar experiments were performed with an L-aerial of different horizontal top-lengths for a definite frequency. The results of measurements are given in table V. These are illustrated in fig. 7.

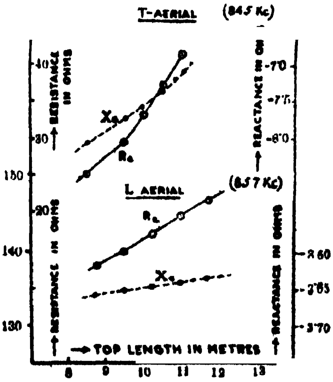

FIG 7

TABLE V

Earthed L-aerial (inverted). Frequency : 857 kc/sec. ($\lambda = 350 m$).

Top length (metres)	Without aerial				With aerial				R_e (ohms)	X_e (ohms)
	C' ($\mu\mu f$)	C'' ($\mu\mu f$)	C_r ($\mu\mu f$)	R (ohms)	C' ($\mu\mu f$)	C'' ($\mu\mu f$)	C'_r ($\mu\mu f$)	R' (ohms)		
11.75	778	788	783	3.0	123	150	137	150.2	146.6	-2.885×10^3
11.0					124	151	138	148.2	144.6	-2.888 ,,
10.25					125	152	139	145.9	142.25	-2.893 ,,
9.5					126	153	140	143.5	139.85	-2.897 ,,
8.75					127	154	141	141.7	138.0	-2.902 ,,

8. DISCUSSION OF THE EXPERIMENTAL RESULTS

In the case of the earthed vertical aerial and the earthed inverted L-aerial, the effective antenna resistance R_e was found to increase steadily with frequency as can be seen from figs. 4 & 6. The smallest wavelength in the investigation was however larger than the natural fundamental wavelength of the antenna.) In the case of the T-aerial, on the other hand, the resistance at first decreased steadily with the increase of frequency and attained a minimum value but subsequently it increased with further increase of frequency. The minimum value of the antenna resistance appeared at 750 kc/sec. The existence of such a minimum in the value of antenna resistance had also been previously observed by earlier investigators.

There had been attempts also to explain the nature of the variation of the antenna resistance with frequency. An approximate theory for the case of a perfectly conducting straight vertical wire connected to homogeneous earth with a horizontal surface, had been worked out by Eccles.[7] It had been shown that if R is the antenna resistance at any wavelength λ, then

$$\frac{R_0 - R}{R_0} = \frac{3\lambda_0(\lambda - \lambda_0)}{\lambda^2},$$

where λ_0 is the natural wavelength (fundamental) of the antenna and R_0 is the antenna resistance at that wavelength. The equation shows that if the resistance R be plotted against frequency, the curve is a parabola. It can be seen that the minimum resistance is $R_0/4$ and occurs at $\lambda = 2\lambda_0$ and that when $\lambda = 3\lambda_0$, the curve is straight and directed through the origin. The resistance is $R_0/3$ for $\lambda = 3\lambda_0$. This ideal curve was, of course, departed in many practical cases. According to Colebrook's[8] theory, the antenna resistance of a vertical or an L-aerial should vary much in the same way as in our experiments. The observed variation of the antenna resistance of a T-aerial resembled Eccle's theoretical curve to a certain extent.

Referring to the antenna reactance of a vertical earthed aerial, it can be seen from fig. 4 that its value was negative and that it increased steadily with frequency, tending to pass through the zero value. In the case of the earthed inverted L aerial, the antenna reactance (which was also negative) increased with frequency and in the region of 900 kc/sec., it suddenly began to decrease with the increase of frequency, as is evident from fig. 6. In the case of the T-aerial, the antenna reactance was found to fall suddenly in the frequency region of minimum antenna resistance; otherwise, *on the whole*, the antenna reactance showed an increase with the increase of frequency. (See fig. 5)

Regarding the variation of the antenna resistance and reactance with the horizontal top-length of the T-aerial or that of the inverted L-aerial for a definite frequency, the experimental results showed that both resistance and reactance increased steadily with the length of the horizontal part. (See fig. 7.)

9 SUMMARY

Experiments to study the variation of the total-loss-resistance and reactance of receiving aerials with frequency were carried out following Willans' double-beat method of measuring H.F. resistance. Three different types of aerials were employed *viz.* the vertical aerial, T-aerial and the inverted L-aerial each being grounded. It appears that in the case of the vertical aerial and the inverted L-aerial, the antenna resistance steadily increased with frequency. The range of frequencies did not however include the natural fundamental frequency of the aerial or its harmonics. In the case of the T-aerial a definite minimum for the antenna resistance appeared to exist within the range of frequencies employed in these measurements.

The antenna reactance was found, in general, to increase with the increase of frequency. In the case of the inverted L-aerial the rise was followed by a sudden decrease with the increase of frequency at a certain frequency. In the case of the T-aerial, there appeared a sudden diminution in the value of the antenna reactance in the region where the minimum antenna resistance was observed.

The experiments also showed that the antenna resistance and reactance of a T-aerial and an inverted L-aerial increased with the increase of the top-length of the horizontal part of each aerial.

PHYSICS LABORATORY,
DACCA UNIVERSITY

REFERENCES

[1] Willans *vide* Turner's paper, Experimental Wireless & Wireless Engineer, p. 348, March, 1925.

[2] Wilmotte & Colebrook *Jour Inst*, " Elec. Engineers *vide* Exp. Wireless & W E." p. 83 (1931).

[3] T. L. Eckersley, *Jour. I.E.E.*, **9**, 58 (1922).

[4] Moulin, High Frequency Measurements, p. 406 (1931).

[5] Miller, Bureau of Standards, **13**, 1916-17.

[6] Smith-Rose & Colebrook, Exp. Wireless & W.E. **2**, 207 (1925).

[7] Eccles, Handbook of Wireless Telegraphy & Telephony, 2nd edition, p. 129.

[8] Colebrook, Experimental Wireless and Wireless Engineer, p. 657, Nov. 1927.

APPLICATION OF THE THEORY OF RANDOM SCATTERING ON THE INTENSITY VARIATIONS OF THE DOWN-COMING WIRELESS WAVES OVER LONG TRANSMISSION PATHS

By M. M. SEN GUPTA

AND

S. K. DUTT

(Received for publication, May 20, 1941)

ABSTRACT. Pawsey's theory of random scattering to explain the variation of the amplitude of down-coming radio waves was applied in the case of transmission over moderately great distances in the medium wave band Results indicate that while random scattering is a predominant factor in determining the strength of the down-coming waves, the observational data cannot be fully accounted for by this theory alone. It is suggested that for long transmission paths the presence of other factors must also be taken into consideration.

INTRODUCTION

Pawsey[1] has shown that a single reflected ray from ionosphere does not consist of a single ray but is built up of elementary contributions from a series of diffracting centres distributed more or less at random in the ionosphere. Working with a wavelength in the medium band (200 m. to 500 m.), he found that the variation of the amplitude of the down-coming wave is consistent with the probability formula given by Lord Rayleigh. The result of his experiments, was obtained with a transmission path of 56 Kms. (London Regional Transmitter —Sydney Sussex College Receiving Station); it was thought desirable to test whether the theory of random scattering as given by Pawsey is applicable even when the transmission path is made considerably great. The present communication gives an account of the study of variation of intensity of down-coming waves in the medium band (wavelengths 370.4 m. and 257.1 m.) from two Indian Broadcasting stations, *viz.*, Calcutta and Dacca, at distances as great as 480 and 610 Kms.* All the data for measurements were obtained in our case from automatic photographic records of received signals taken between the hours 6 P.M. and 10-30 P.M. over a period of about two years.

---

* Recently a paper has been published by Khastgir and Ray (*Indian Journal of Physics*, **14**, 283, 1940), but here also the distance was not more than 245 Kms Moreover, the data were secured from visual observation of galvanometer deflections

AUTOMATIC RECORDING

The automatic recording was made as follows :—A bromide paper was fixed on a drum rotated by a clockwork, the whole system being put inside a light-tight box. On one side of the box there was a fine horizontal slit which could be opened or closed. The vertical image of the straight filament of a lamp formed by reflection from the galvanometer mirror was allowed to fall on the slit. The deflection of the spot of light at any instant was thus automatically recorded. The vertical lines in the photographic records of Fig. 4 were obtained by means of another clockwork making contacts of an electric circuit containing a 4-volt lamp every 4 minutes.

RECEIVING SYSTEM

The receiver was a battery set of the superheterodyne type consisting of two stages of H. F. amplification preceding an octode frequency-changer with a separate oscillator and one stage of I. F. amplification followed by a second detector which was a double-diode-triode giving a linear detection. The relation between the input voltage and the deflection in the galvanometer is shown in Fig. 1. It will be observed that it is practically linear within the working range except for field strengths below 70 $\mu v/m$. We had also used a square-law detector in some of our measurements. The circuit diagrams of both types of detection are shown in Figs. 2 and 3.

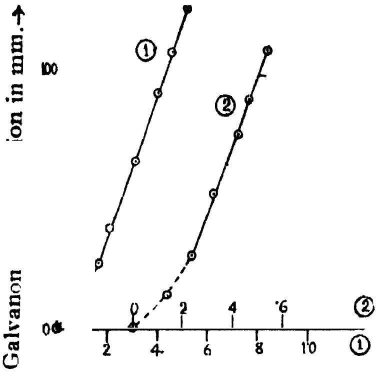

Calibrating H. F. current in the coil of 2 turns.

(1) Diode bias ... 0 volt.

(2) Diode bias ... 0.5 volt.

FIG. 1

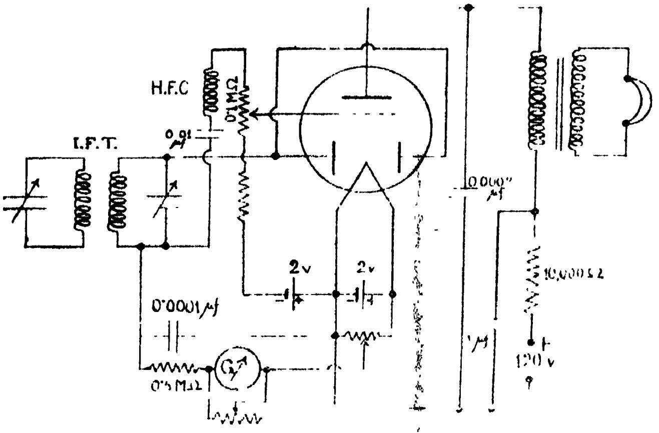

Linear Detector

FIG. 2

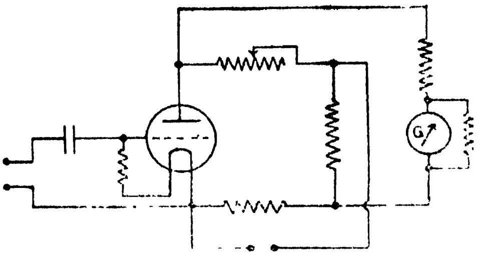

Square law Detector.

FIG. 3

The calibration of the receiving set (photographically) and calculation of the field strengths.—The calibration of the receiving set was done by the method adopted by the Standardization Committee of Radio Engineers (Hund's High Frequency Measurements, page 346). A small coil of 2 turns was placed along the axis of the loop aerial. The deflections d_1, d_2, d_3 [Fig. 4(*b*)] in the output galvanometer (G) corresponding to known H. F. currents in milliamps. of the same frequency as that of the signal in suitable steps were photographed. This was done both in the beginning and at the end of each observation with the loop set in the minimum position. The line joining the spots in the beginning and end of each observation for a particular H. F. current thus gave the strength level when reduced to micro-volts per metre. A graph was plotted with galvanometer deflection against calibrated field strength, from which the desired field strength corresponding to any deflection could be easily evaluated.

It will be observed from photographic records that the zero setting remained almost undisturbed throughout the period of observation which was 2 hours generally and about 30 minutes in some cases. In some of the records of the spots, changes of deflection could be noticed in the beginning but this invariably settled down to constant values. The variations noticed were due to the movement of the spot while setting the loop from maximum to minimum position or due to fluctuation of H. F. current while adjusting to a particular value [Fig. 4(*b*)]. The beam of light giving the spot when switched off while bringing the loop to minimum position or adjusting the H. F. current and switched on again after a minute or so, the variations disappear. The level line in each case was drawn along horizontal portion of the path traced by the spot.

The frequency of the calibrating H. F. currents was set by adjusting the local oscillator to exact no beat condition with the help of a very slow motion vernier dial of ratio 1 : 80 operated by a long earthed handle outside the shielded cover of the oscillator. The strength of the H. F. current (I mA) passing through the inducing coil of N turns and radius r was measured by Cambridge Vacuum Junction of 5 mA range which had been previously calibrated by comparison with Moullin's Multi-range Thermal Milliammeter. The voltage E induced in the loop at a perpendicular distance d from the coil was then calculated from the formula[*]

$$E = k\,\frac{18840\,I\,r^2 N}{(d^2+r^2)^{3/2}}\ \mu v/m.$$

The deflections due to the calibrating fields in the case of the diode detector were found to be linear except for very low field strengths. All our observations excepting a few in the beginning were, therefore, taken with the diode detector. This facilitated evaluation with greater accuracy of results than was possible with the square-law detector.

GROUND WAVE SUPPRESSION

For reliable results due consideration must be paid to the ground wave effect as well as the antenna effect. In our experiments the magnitude of the ground wave was found to be negligible relative to that of the sky wave. This is quite in accordance with the experimental results given by Sommerfield and Eckersley. The distances of the two broadcasting stations Calcutta ($\lambda = 370.4$ m.) and Dacca ($\lambda = 257.1$ m.) are 480 Km. and 610 Km. respectively. Corresponding to these distances and wavelengths the strength of the ground wave field intensities given are 40$\mu v/m$ for good ground and 1.4 $\mu v/m$ for poor ground assuming power output in the transmitter to be 2 kilowatts for Calcutta; for Dacca these are zero for distances over 500 Km. for good ground and also zero for distances over 350 Km. for poor ground. These values are obtained from unmodified Sommerfield curves and if diffraction corrections are applied according to Eckersley,[2]

[*] As d was not very large in comparison with the dimensions of the loop, the correction factor k was introduced in the actual calculation.

these become still less. The length of the horizontal slit in front of the bromide paper was 130 mms. only and so the output galvanometer G had to be adjusted in our case for 130 mm. deflection for the maximum field intensity in any setting. This maximum field intensity recorded was of the order of 300 $\mu v/m$ for Dacca and 600 $\mu v/m$ for Calcutta. Thus even assuming the ground wave intensity for good conducting grounds, the deflection that will be recorded will not be more than 1 mm. for Calcutta, while for Dacca it would be still less. In Pawsey's experiments the ground wave component was as much as 20 times stronger than the sky wave component* and hence the ground wave suppression was absolutely necessary in his case. From the above considerations it will be seen that at the transmission distances with which we worked, the ground wave component being practically negligible compared to the sky wave component no special arrangement was necessary for its suppression.

In order to minimise the antenna effect as much as possible, the dimensions of the loop were made purposely small. The loop was nearly 86 cm. square and had 6 to 8 turns of wire. The effective height was about 100 cms. The following procedure was adopted to test the magnitudes of both the ground wave effect and the antenna effect relative to the maximum sky wave component :—During daytime the zero position of the galvanometer was noted with all the high tensions of the set switched on except that of the oscillator valve. The reading in the galvanometer (G) gave the actual zero of the graph, *i.e.*, the real zero signal strength level [B in Fig. 4(*a*)]. The H. T. of the oscillator valve was then switched on with the loop set both in the maximum and minimum positions. It was seen that there was absolutely no change recorded in the zero reading B in Fig. 4(*a*) for the whole period of observation which was not less than half an hour indicating that both the ground and antenna effects were practically negligible. The readings for different strength levels were then taken in steps in the way explained before (under the heading 'Calibration of the Set'). Without disturbing the adjustments made during the daytime, the above procedure was repeated during the night-time reception period 6.00 to 10.30 P.M., but now with the loop in the minimum position only. The records showed again the absence of any appreciable change either in the zero level or in those for the different strength levels both in the beginning as well as at the end of the period of observation (Fig. 4). Thus it will be seen that in our arrangements the antenna effect was negligible even during the night time.

Some typical records giving the variation of galvanometer deflection with time are shown in Plate XIV.

The ordinate r representing the galvanometer deflection was divided into a large number of small parts each representing equal change of field intensity by utilising the calibration graph plotted with field intensity against galvanometer deflection. The abscissa representing time was also divided into half-minute intervals. The number of a particular amplitude between r and $r+dr$ that occurred during the period was counted, the amplitude within the range occurring for half a minute being counted as one. From this the fraction of the total time during which the amplitude lay between r and $r+dr$ was determined. As mentioned before, all our records were taken for periods varying from half an hour to two hours.* Distribution curves were then drawn with values of fractions so obtained against average amplitudes of r and $r+dr$. From these curves the value of the most probable amplitude r_m was obtained; this value of r_m was used in drawing the theoretical probability curves in accordance with Rayleigh's expression

---

* In Khastgir and Ray's work the ground wave component was 3 to 4 times stronger than the sky wave component.

$$P' = \frac{2r}{R^2} \qquad \overline{R}^2$$

(where R^2 ... the sum of the squares of the components
$P'dr$ ... the probability of a resultant amplitude between r and $r+dr$)

for the probability of occurrence of any resultant amplitude on the assumption of a large number of components of random phases. The maximum value of P' corresponds to $R^2 = 2r_m^2$ where r_m is the most probable value of r in the experi-

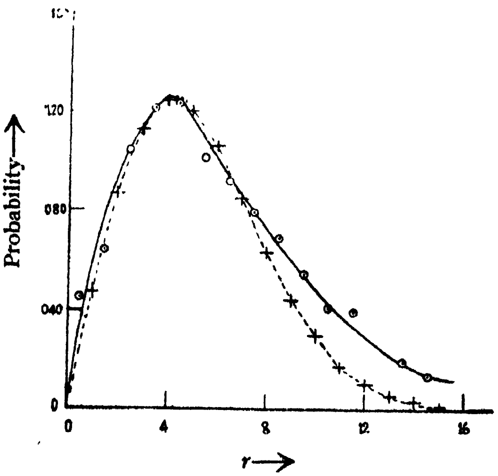

for (a) Calcutta
2-12-37

FIG. 5(a)

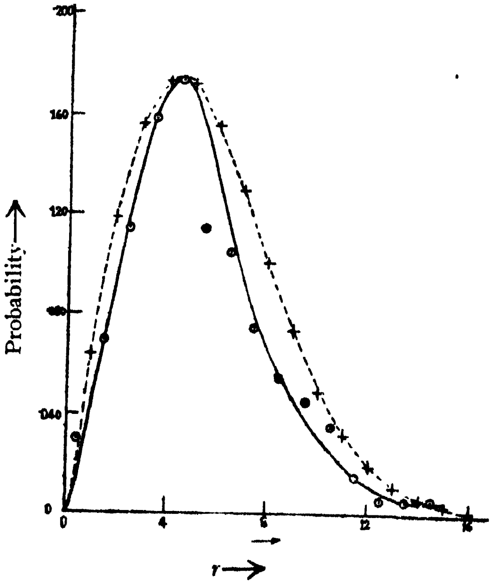

for (b) Dacca
16-1-40

FIG. 5(b)

---

* The chief considerations being practical convenience and sufficient number of readings, we made the total period of observation half an hour and more.

Fig. 4(a)—Calcutta, 18. 1. 39.

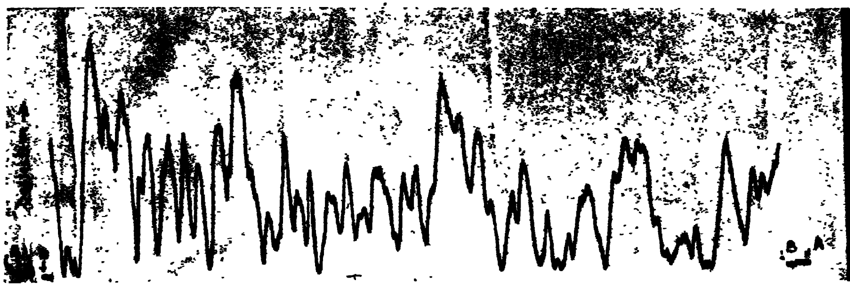

Fig. 4(b)—Dacca, 12. 2. 40.

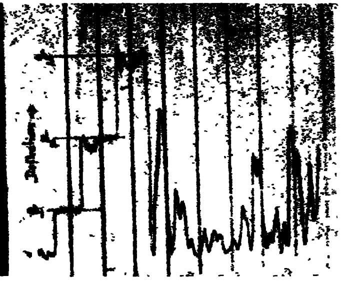

Fig. 4(c)—Calcutta, 7. 12. 37.

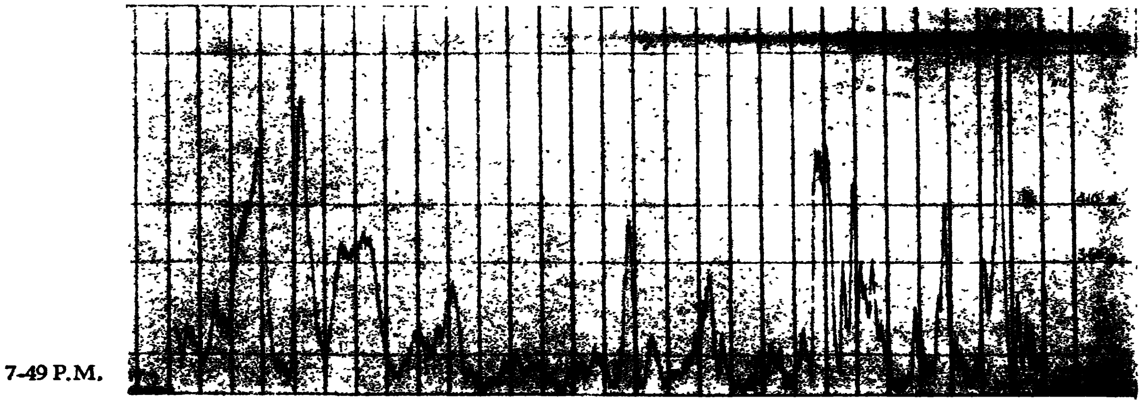

mental distribution curves. The scales in the figures have been adjusted to give the best fit. Figs. 5 and 6 give the typical results in which the experimental curves are shown as full-line curves and the theoretical ones as dotted. It will be seen from the experimental results that the agreement between the theoretical and experimental curves are not as good as in cases of experiments* with smaller transmission distances. We have, therefore, shown the results in two broad representative types, *viz.*, those with fair agreement (Fig. 5) and those showing great divergence (Fig. 6). It may, therefore, be concluded on the basis of our observations that for long transmission paths the intensity of the down-coming waves is not determined only by irregular scattering at the ionosphere but also by

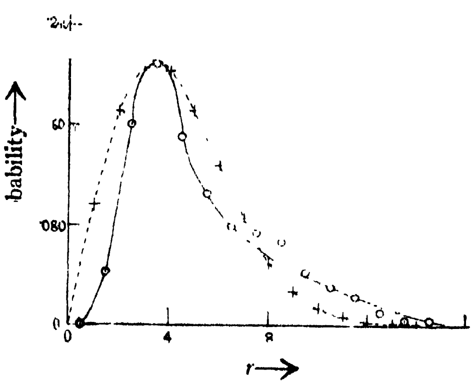

for (*a*) Calcutta
7-12-37

Fig. 6(*a*)

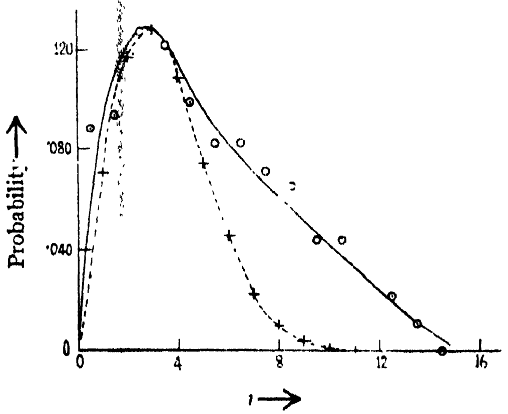

for (*b*) Dacca
12-2-40

Fig. 6(*b*)

the existence of other factors ; the effect of the latter sometimes becomes quite appreciable as may be found in the 2nd type of curves (Fig. 6). Observations are being continued to study fully the nature of these factors.

In conclusion, the authors take this opportunity to thank Principal K. Prosad, I.E.S , who has taken much interest in our work. One of us (S. K. D.) is grateful to the Government of Bihar for the grant of a research scholarship which has enabled him to take part in this work.

Physical Laboratory,
Patna Science College.

---

* Experiments by Pawsey[1] and by Khastgir and Ray.[3]

REFERENCES

Pawsey, *Proc. Camb. Phil. Soc.*, **31**, 125 (1935).
Eckersley, *Proc I.R.E.*, **20**, 1555 (1932).
Khastgir and Ray, *Indian Jour. of Phys.*, **14**, 283 (1940)

STRUCTURE OF THE ELECTRONIC BANDS OF THE OD MOLECULE. PART III

By M. G. SASTRY

(*Received for publication, July 18, 1941*)

Plate XV

ABSTRACT. Between λ3105 and λ3295 about 360 lines due to the (1, 1), (2, 2) and (3, 3) bands of the OD molecule have been measured. The six main branches of each of the bands have been identified. The combination term-differences have enabled the calculation of the rotational constants. These agree respectively with those previously determined by the author for the states $v'=1, 2, 3$ and $v''=1, 2$. The constants for $v''=3$ are newly determined.

In Parts I and II of this series of papers[1] the rotational structure of the bands (1, 0), (2, 1) and (3, 2) in the region λ2900 and of the (3, 0) band at λ2570 was reported. The present part gives the structure of some of the bands at λ3065, which form the sequence $\Delta v=0$. Of these the (0, 0) band was analysed by Ishaq[2] and while the present work was in progress, Ishaq[3] reported also the constants of the (1, 1) band. It was intended therefore to confine this work to the study of the (2, 2) and (3, 3) bands.* However, as the overlapping of these bands with the structure of (1, 1) is so very great that the analysis of these would not be quite clear unless the structure of all of these is shown, it is considered necessary to include in this paper the details of the assignments relating to the (1, 1) band as well, which has been worked out by the author independently.

The experimental work on the OD bands forming the basis of these papers was described in Part I. The instrument used for photographing the bands was a Hilger Littrow Quartz Spectrograph of the E_1 type giving an average dispersion of 5.6 A per mm. in the region under consideration. Although this dispersion is small, the use of a very narrow slit and the high resolution ensured sufficient accuracy in measurement. On the other hand, as the (2, 2) and (3, 3) bands lie in the tail end of the sequence where the structure is more widely open, an advantage is gained by using a comparatively smaller dispersion instrument, the fainter lines being thereby obtained more easily. In fact, the analysis of the (3, 3) band, which occurs very faintly, is made possible on this account. The exposures varied from ten minutes to four hours and the measurements are averages of three independent sets, made on different plates. The wave-lengths are considered to be correct to about 0.03 Å.U.

---

* A letter by Dr. Narayan also has since appeared in Current Science, Feb., 1941, on the (2, 2) band. But no data or constants have been reported. The work, it is learnt, is aimed at the correlation of the OD bands with the yet unidentified Solar Wave-lengths.

RESULTS

The Table at the end contains a complete list of all the observed lines, extending from λ3105 towards the long wave-length end of the band. The measurements of the other lines (towards the short wave-length end) are omitted as they were previously reported by Ishaq. The intensities are visual estimates. The last columns give the classification of the lines into the several branches of the bands. The six main branches only of each band have been identified; the satellite branches are presumed to be mostly unresolved. Some of the lines are very broad and are believed to be certainly blends of two or more lines. In measuring these, the cross-wire of the micrometer is set at the centre and the outer edges and an arbitrary division is made into two or three lines. Such lines are indicated in the Table by asterisks. This procedure has facilitated the working out of the analysis. The (0, 0) and (1, 1) bands are developed particularly well and the branches of the latter are identified to such high rotation quantum number as K=34. The (3, 3) band is relatively faint and poorly developed; only about a dozen members of each of its branches could be detected with certainty.

The correctness of the identification is shown in each case by the application of the combination principle. Tables (1) and (2) give the values of $\Delta_2F_1'(K)$ and $\Delta_2F_2''(K)$ for the upper state $^2\Sigma^+$ in the three bands. There is close agreement between these and the corresponding values for the (1, 0), (2, 1) and (3, 2) bands respectively which are quoted here from Part I. The spin doubling in the upper state, expected to be small, is ignored.

TABLE I

$$R_1(K)-P_1(K)=\Delta_2F_1'(K)$$

K	λ 3105 (1, 1)	3149 (2, 2)	3195 (3, 3)	2872 (1, 0)	2916 (2, 1)	2963 (3, 2)
1	52.7	—	—	52.6	51.1	47.9
2	88.5	85.3	—	87.6	83.5	81.4
3	121.5	119.0	114.0	121.4	117.1	114.2
4	156.3	152.8	144.4	156.1	150.8	144.5
5	190.2	186.1	179.4	191.1	184.4	177.4

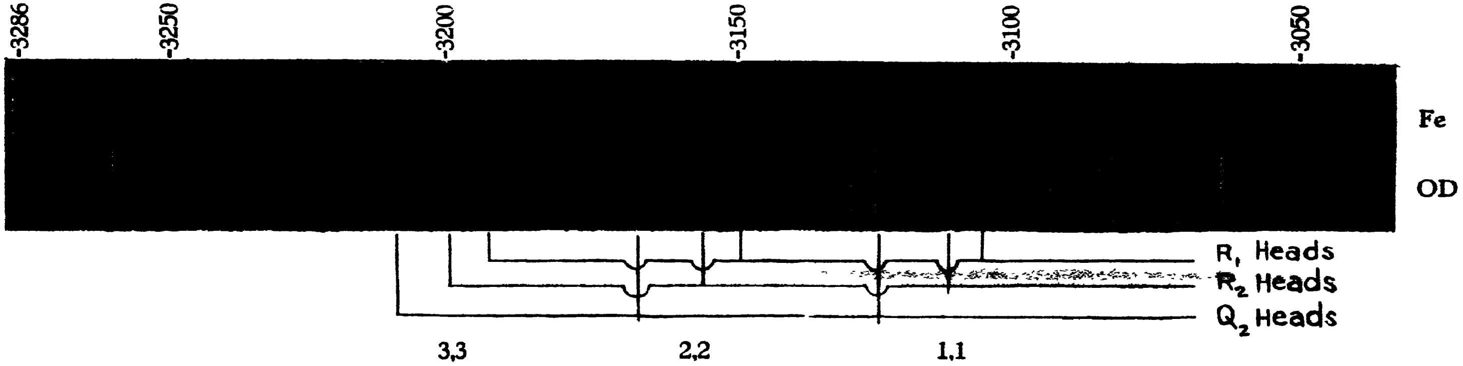

OD Bands of $\Delta\nu=O$ Sequence.

TABLE I (*contd.*)

K	λ 3105 (1, 1)	3149 (2, 2)	3195 (3, 3)	2872 (1, 0)	2916 (2, 1)	2963 (3, 2)
6	225.3	215.4	208.6	225.7	215.9	208.8
7	258.4	247.4	240.5	259.8	249.1	240.1
8	293.6	283.1	273.5	293.4	282.1	272.2
9	327.2	314.9	302.5	327.4	315.2	302.8
10	360.0	347.8	333.1	360.8	347.5	333.6
11	392.9	380.8	364.2	394.0	379.3	364.9
12	427.7	412.7	—	427.2	411.0	394.1
13	460.2	441.5	-	459.8	442.5	424.0
14	492.5	474.8	—	492.4	474.1	—
15	524.6	503.2	—	523.7	504.2	—
16	551.4	534.9	—	556.0	534.3	—
17	586.0	562.0	—	586.8	563.0	-
18	615.5	592.1		616.6	591.1	—
19	648.5	619.4		647.5		
20	676.2	648.3		676.0		
21	704.6	676.6		706.1		
22	733.1	704.1	-	734.0		—
23	762.8	730.2	—	762.5	-	—
24	792.4	762.1	—	790.1	—	
25	817.5	—	—	816.4	—	—
26	841.3	—	—	841.8	—	—
27	864.4	—	—	—	—	—
28	890.4	—	—	—	—	—
29	916.6	—	—	—	—	—
30	942.6	—	—	—		
31	965.6	—	—	—	—	—
32	989.5	—	—	—	—	—
33	1014.1	—	—	—	—	—
34	1043.2	—	—	—	—	—

TABLE II

$R_2(K) - P_2(K) = \Delta_2F_2'(K)$

K	λ 3105 (1, 1)	3149 (2, 2)	3195 (3, 3)	2872 (1, 0)	2916 (2, 1)	2963 (3, 2)
1	54.1	—	—	52.3	—	52.6
2	88.4	—	—	85.8	83.3	81.9
3	122.7	115.5	116.9	121.4	119.4	114.7
4	156.5	152.3	145.5	156.8	150.3	144.5
5	189.5	182.0	177.5	190.7	183.1	176.4
6	224.4	216.1	208.9	224.9	216.7	208.1
7	259.2	248.3	238.3	259.2	249.2	239.2
8	294.0	280.9	268.0	293.2	282.6	271.3
9	328.1	313.1	300.4	327.4	315.1	302.6
10	359.9	346.7	329.4	360.6	346.4	333.4
11	393.0	379.3	359.9	393.8	378.2	363.1
12	427.8	411.4	—	426.8	—	—
13	459.6	438.3	—	459.9	—	—
14	495.5	473.4	—	491.9	—	—
15	523.4	503.6	—	—	—	—
16	556.5	534.8	—	—		—
17	586.2	565.9	—	—	—	—
18	616.2	592.7	—	—	—	
19	648.7	623.6	—	—	—	—
20	677.2	649.1	—	—		—
21	705.9	680.4	—	—	—	
22	734.3	705.5	—			
23	761.2	—	—	—		—
24	789.2	—		—	—	—
25	814.2	—		—		—
26	840.7		—			
27	866.0					
28	892.5	—	—		—	
29	916.5	—	—	—	—	
30	940.3	—	—	—	—	—
31	963.8	—	—	—	—	—
32	987.8	—		—	—	—

In Tables III, IV and V the values of the rotational term differences for the lower state $^2\Pi$ are shown. The combination defect is a measure of the Λ-doubling. The progressive variation of this doubling with increasing rotation quantum number is evident both in $^2\Pi_{1\frac{1}{2}}$ and $^2\Pi_{\frac{1}{2}}$ states. This variation is found to be in keeping with the theoretical prediction due to Van Vleck[4] for a band system representing an intermediate stage of coupling between Hund's Case (*a*) and Case (*b*).

Plate A is an enlargement of the OD bands in the region between λ3000 and λ3290 in which the positions of the band heads and of the branches are indicated.

TABLE III

Combination Differences for λ3105

K	R (K)− Q_1(K+1)	Q_1 (K)− P_1(K+1)	R_2 (K)− Q_2(K+1)	Q_2 (K)− P_2(K+1)
1	16.5	44.1	37.2	—
2	63.4	62.3	51.3	50.1
3	81.5	82.5	71.4	71.9
4	98.9	99.4	89.3	90.9
5	117.7	118.5	109.5	112.3
6	136.6	136.3	129.2	130.0
7	154.8	154.8	149.5	149.5
8	173.7	172.4	169.3	170.4
9	193.0	190.7	186.9	186.7
10	210.7	207.2	206.0	204.6
11	230.1	225.6	226.5	225.7
12	249.0	244.1	244.0	242.8
13	268.0	262.6	262.2	260.6
14	285.4	279.1	284.9	280.8
15	302.4	295.4	296.6	297.2
16	319.6	313.6	317.2	313.6
17	339.2	330.4	333.9	330.8
18	354.4	346.8	351.2	347.8
19	373.9	364.2	371.6	364.0
20	389.2	379.7	388.0	381.0
21	406.8	395.2	403.8	397.1
22	422.9	410.6	419.9	412.7
23	441.0	431.8	438.7	429.0
24	453.6	441.3	451.8	441.2
25	473.4	456.2	465.7	459.0
26	485.8	469.6	482.4	472.5
27	499.5	485.0	498.4	487.2
28	516.1	498.9	513.8	501.6
29	533.1	513.1	528.8	516.2
30	550.0	526.3	543.4	528.9
31	562.9	537.8	557.9	541.4
32	576.0	553.6	573.7	555.3
33	586.0?	568.7	—	568.0
34	604.0?	585.3		580.3

TABLE IV

Combination Differences for λ 3149

K	R_1 (K) − Q_1(K+1)	Q_1 (K) − P_1(K+1)	R_2 (K) − Q_2(K+1)	Q_2 (K) − P_2(K+1)
1	—	46.6	—	29.3
2	62.8	61.1	–	49.0
3	82.0	81.1	66.5	72.3
4	97.2	96.5	84.5	90.0
5	116.7	113.8	106.6	108.3
6	131.8	130.7	125.3	124.9
7	150.7	151.3	142.6	145.8
8	169.8	168.6	162.1	163.2
9	189.3	185.6	181.9	181.6
10	207.8	200.4	203.2	200.4
11	224.2	219.1	220.7	215.5
12	244.3	236.7	239.8	233.9
13	258.3	253.4	251.2	254.6
14	276.4	271.4	269.7	275.0
15	296.2	289.9	286.7	288.0
16	309.8	301.3	307.7	303.6
17	328.2	321.3	327.5	322.4
18	344.2	337.2	340.8	337.4
19	360.4	353.3	360.0	353.6
20	377.2	366.5	370.5	370.0
21	394.7	383.1	—	389.5
22	413.5	399.3	—	–
23	428.0	411.5	—	—
24	446.5	—	—	—

TABLE V

Combination Differences for λ 3195

	R_1 (K) − Q_1(K+1)	Q_1 (K) − P_1(K+1)	R_2 (K) − Q_2(K+1)	Q_2 (K) − P_2(K+1)
1	—	43.6		–
2	—	59.5		45.6
3	79.1	78.5	71.3	69.3
4	95.0	95.3	86.5	85.3
5	112.9	110.7	104.8	103.3
6	130.5	130.5	123.6	123.2
7	144.4	148.0	139.6	140.0
8	164.9	164.6	156.1	158.3
9	182.6	179.9	178.5	177.7
10	199.8	197.9	190.2	189.9
11	217.7	215.3	209.6	211.3
12	—	—	—	228.8
13	—	—	—	246.9
14	—	—	—	268.1

TABLE VI

Catalogue and Classification of Observed Lines

		3105					
Vac.	Int.	R_1	Q_1	P_1	R_2	Q_2	P_2
*32191.5	6	8	—	—	—	—	—
190.4		7, 9	—	—	—	—	—
189.3		6	—	—	—	—	—
* 187.1	10	10	—	—	—	—	—
186.0		5	—	—	—	—	—
183.1	4*d*	11	—	—	—	—	—
181.4	3*d*	4	—	—	—	—	—
178.5	10	12	—	—	—	—	—
176.7	10	3	—	—	—	—	—
171.0	5	2	—	—	—	—	—
169.1	3	13	—	—	—	—	—
166.8	8	—	—	—	—	—	—
164.0	2	1	—	—	—	—	—
* 158.5	4 *bd*	14	—	—	—	—	—
157.4							
155.4	2	—	—	—	—	—	—
153.2	8	—	—	—	—	—	—
146.6	2	15	—	—	—	—	—
* 144.2	10 *bd*	—	—	—	—	—	—
143.4							
140.6	3	—	—	—	—	—	—
* 132.1	10 *bd*	16	—	—	—	—	—
130.5		—	—	—	10, 11	—	—
129.0					9	—	—
126.6	8	—	1	—	8, 12	—	—
123.5	1	—	—	—	—	—	—

TABLE VI (*contd.*)

		3105					
Vac.	Int.	R_1	Q_1	P_1	R_2	Q_2	P_2
* 120.8	5 *bd*	—	—	—	7, 13	—	—
119.1						—	—
117.5	8	17	2	—	14	—	—
111.3	3	—	—	1	6	—	—
109.9	6	—	—	—	—	—	—
107.6	4	—	3	—	—	—	—
105.7	8	—	—	—	—	—	—
103.1	2	—	—	—	—	—	—
101.1	2	—	—	—	5, 15	—	—
097.6	3	18	—	—	—	—	—
095.2	7	—	4	—	—	—	—
091.9	3 *d*	—	—	—	16		—
088.5	3	—	—	—	4	—	—
085.1	10	—	—	—	—	—	—
082.5	7 *bd*	—	5	2	—	—	—
080.0	6	19	—	—	—	—	—
077.1	5	—	—	—	17	—	—
073.9	10	—	6	—	3	—	—
068.3	4	—	—	—	—	—	—
066.3	8	—	—	—	—	—	—
060.1	2	—	—	—	18	—	—
055.2	5	20	—	3	2	—	—
052.7	6	—	7	—	—	—	—
044.1	1	—	—	—	19	—	—
* 042.0	10	—	—	—	—	—	—
041.1							
038.5	1	—	—	—	1	—	—
035.6	10	—	8	—	—	—	—

TABLE VI (*contd.*)

		3105					
Vac.	Int.	R_1	Q_1	P_1	R_2	Q_2	P_2
031.0	1	21	—	—	—	—	—
027.3	1	—	—	—	—	—	—
025.1	10	—	—	4	—	—	—
022.1	1	—	—	—	20	—	—
019.3	1	—	—	—	—	—	—
017.8	5	—	9	—	—	—	—
014.7	5	—	—	—	—	—	—
*32003.9	10 *bd*	22	—	—	—	3	—
002.5		—	—	—	—	4	—
001.0		—	—	—	—	2	—
*31999.2	10 *bd*	—	—	—	—	5	—
997.4			10	—	21	—	—
995.8		—	—	5	—	1	—
991.6	1	—	—	—	—	6	—
988.6	5		—	—	—	—	—
984.4	2	—	—	—	—	—	1
982.1	10	—	—	—	—	7	—
979.1	2	—	—	—	—	—	—
976.4	6	23	11	—	—	—	—
971.3	5	—	—	—	22	8	—
969.8	3	—	—	—	—	—	—
966.8	3	—	—	—	—	—	2
964.0	4	—	—	6	—	—	—
960.6	3	—	—	—	—	—	—
957.3	7	—	—	—	—	9	—
953.0	8	—	12	—	—	—	—
951.2	8	—	—	—	—	—	3
942.1	8	24	—	—	23	10	—

TABLE VI (*contd.*)

Vac.	Int.	3105					
		R_1	Q_1	P_1	R_2	Q_2	P_2
939.3	1	—	—	—	—	—	—
937.1	10	—	—	—	—	—	—
934.1	1	—	—	—	—	—	—
932.0	10	—	—	7	—	—	4
928.6	7	—	13	—	—	—	—
924.5	5	—	—	—	—	11	—
911.6	8	25	—		24	—	5
908.8	8	—	—	—	—	—	—
*905.4	7 d	—	—	—	—	—	
904.0		—	—	—	—	12	—
902.3		—	—	—	—	—	—
901.1	5	—	14	—	—	—	—
897.9	5	—	—	8	—	—	—
892.3	1	—	—	—	—	—	—
890.0	10	—	—	—	—	—	—
886.9	5	—	—	—	—	—	6
882.6	5	—	—	—	—	13	—
876.4	1	—	—	—	25	—	—
873.1	5	26	15	—	—	—	—
868.7	1	—	—	—	—	—	—
866.0	6	—	—	—	—	—	—
863.2	8	—	—	9	—	—	—
861.6	2	—	—	—	—	—	7
858.5	3	—	—	—	—	14	—
855.0	10	—	—	—	—	—	—
852.3	1	—	—	—	—	—	—
846.8	3	—	—	—	—	—	—
844.2	5	—	16	—	—	—	—
841.5	10	—	—	—	26	—	—

TABLE VI (*contd.*)

		3105					
(vac.)	Int.	R_1	Q_1	P_1	R_2	Q_2	P_2
832.6	6	27	—	—	—	15	8
829.5	1	—	—	—	—	—	—
827.1	5	—	—	10	—	—	—
820.9	1	—	—	—	—	—	—
818.1	7	—	—	—	—	—	—
814.8	7	—	—	—	—	—	—
812.5	4	—	17	—	—	—	—
806.6	1	—	—	—	—	—	—
804.5	10	—	—	—	27	16	—
802.9	3	—	—	—	—	—	—
800 9		—	—	—	—	—	9
792.7	1	28	—	—	—	—	—
790.2	10	—	—	—	—	—	—
785 4	1	—	—	11	—	—	
780 7	1	—	—	—	—	—	—
778.3	6	—	18	—	—	—	—

		3105						3149					
Vac.	Int	R_1	Q_1	P_1	R_2	Q_2	P_2	R_1	Q_1	P_1	R_2	Q_2	P_2
31774.7	5	—	—	—	—	17	—	—	—	—	—	—	—
770 6	3	—	—	—	—	—	10	—	—	—	—	—	—
769.3	5	—	—	—	—	—	—	—	—	—	—	—	—
766 5	1	—	—	—	—	—	—	—	—	—	—	—	—
764 4	6	—	—	—	28	—	—	—	—	—	—	—	—
758.5	1	—	—	—	—	—	—	—	—	—	—	—	—
754.1	1	—		—	—	—	—	—	—	—	—	—	—
750.8	8	29	—	12	—	—	—	5, 6, 7,	—	—	—	—	—

TABLE VI (*contd.*)

		3105						3149					
Vac.	Int.	R_1	Q_1	P_1	R_2	Q_2	P_2	R_1	Q_1	P_1	R_2	Q_2	P_2
		—	—	—	—	—	—	8	—	—	—	—	—
746.4	4	—	—	—	—	—	—	4, 9	—	—	—	—	—
743.2	8	—	19	—	—	18	—	3, 10	—	—	—	—	—
737.5	8	—	—	—	—	—	11	2, 11	—	—	—	—	—
729.0	2	—	—	—	—	—	—	12	—	—	—	—	—
720.7	2	—	—	—	29	—	—	—	—	—	—	—	—
718.1	7	—	—	—	—	—	—	13	—	—	—	—	—
712 0	6	—	—	—	—	—	—	—	—	—	—	—	—
708.9	6	—	—	13	—	19	—	—	—	—	—	—	—
706.1	6	30	20	—	—	—	—	14	—	—	—	—	—
701 9	4	—	—	—	—	—	—	—	—	—	—	—	—
698 8	6	—	—	—	—	—	12	—	1	—	—	—	—
691.6	3	—	—	—	—	—	—	15	—	—	—	—	—
685.3	4b	—	—	—	—	—	—	—	2	—	9, 10	—	—
682.3	7	—	—	—	—	—	—	—	—	—	8, 11	—	—
680.0	3	—	—	—	—	—	—	—	—	1	—	—	—
678.0	3	—	—	—	—	—	—	—	—	—	7, 12	—	—
674.7	5	—	—	—	30	—	—	16	3	—	—	—	—
672.5	5	—	—	—	—	20	—	—	—	—	6	—	—
666 0	8	—	21	14	—	—	—	—	—	—	13	—	—
661.2	4	—	—	—	—	—	13	—	4	—	5	—	—
657.0	6	31	—	—	—	—	—	17	—	—	14	—	—
652.2	4	—	—	—	—	—	—	—	—	2	—	—	—
649.2	4	—	—	—	—	—	—	—	5	—	4	—	—
646.0	2	—	—	—	—	—	—	—	—	—	—	—	—
643.4	8	—	—	—	—	—	—	—	—	—	15	—	—
635 7	2	—	—	—	—	—	—	18	—	—	3	—	—
634.1	7	—	—	—	—	21	—	—	6	—	16	—	—

TABLE VI (*contd.*)

		3105						3149					
Vac.	Int.	R_1	Q_1	P_1	R_2	Q_2	P_2	R_1	Q_1	P_1	R_2	Q_2	P_2
626.8	2	—	—	—	31	—	—	—	—	—	—	—	—
* 624.2	8	—	22	—	—	—	—	—	—	3	—	—	—
622.0	—	—	—	15	—	—	14	—	—	—	—	—	—
619.0	2	—	—	—	—	—	—	—	7	—	17	—	—
613.6	2	—	—	—	—	—	—	—	—	—	—	—	—
611.0	8	—	—	—	—	—	—	19	—	—	—	—	—
607.8	2	32	—	—	—	—	—	—	—	—	—	—	—
600.1	6		—	—	—	—	—	—	8	—	—	—	—
596.7	2	—	—	—	—	—	—	—	—	—	18	—	—
593.6	5	—	—	—	—	22	—	—	—	4	—	—	—
588.7	2	—	—	—	—	—	—	—	—	—	—	—	—
586.5	7	—	—	—	—	—	—	20	—	—	—	—	—
581.0	5b	—	23	—	—	—	—	—	9	—	—	—	—
577.7	4	—	—	16	32	—	15	—	—	—	19	2, 3	—
569.2	5	—	—	—	—	—	—	—	—	—	—	4	—
		—	—	—	—	—	—	—	—	—	—	1, 5	—
564.7	8	—	—	—	—	—	—	—	—	5	—	—	—
560.7	2	—	—	—	—	—	—	21	—	—	—	—	—
557.1	3	—	—	—	—	—	—	—	10	—	—	—	—
554.6	6	33		—	—	—	—	—	—	—	—	6	—
551.4	5	—	—	—	—	23	—	—	—	—	20	—	1
547.2	2	—	—	—	—	—	—	—	—	—	—	7	—
541.1	6	—	—	—	—	—	—	—	—	—	—	—	—
535.4	6	—	24	—	—	—	16	—	11	6	—	8	2
530.6	3	—	—	17	—	—	—	22	—	—	—	—	—
528.1	7	—	—	—	—	—	—	—	—	—	21	—	—
520.2	4	—	—	—	—	—	—	—	—	—	—	9	3
513.3	5	—	—	—	—	—	—	—	12	—	—	—	—

TABLE VI (contd.)

		3105						3149					
Vac.	Int.	R_1	Q_1	P_1	R_2	Q_2	P_2	R_1	Q_1	P_1	R_2	Q_2	P_2
31506.3	5	34	—	—	—	—	—	—	—	—	—	—	—
503.4	6	—	—	—	—	24	—	—	—	7	—	10	—
499.7	3	—	—	—	—	—	—	—	—	—	—	—	—
496.9	8	—	—	—	—	—	—	23	—	—	22	—	4
493.2	2	—	—	—	—	—	—	—	—	—	—	—	—
490.9	5	—	—	—	—	—	17	—	—	—	—	—	—
488.0	4	—	25	—	—	—	—	—	—	—	—	—	—
484.7	5	—	—	—	—	—	—	—	—	—	—	—	—
482.1	5	—	—	18	—	—	—	—	13	—	—	11	—
479.2	6	—	—	—	—	—	—	—	—	—	—	—	5
467.7	8	—	—	—	—	—	—	24	—	8	—	—	—
464.6	2	—	—	—	—	—	—	—	—	—	—	—	—
461.6	2	—	—	—	—	—	—	—	—	—	—	12	—
459.8	5	—	—	—	—	25	—	—	14	—	—	—	—
456.4	2	—	—	—	—	—	—	—	—	—	—	—	6
443.9	4	—	—	—	—	—	18	—	—	—	—	—	—
441.5	2	—	—	—	—	—	—	—	—	—	—	—	—
438.2	8	—	26	—	—	—	—	—	—	—	—	13	—
* 431.5	7b	—	—	19	—	—	—	—	—	9	—	—	—
429.7		—	—	—	—	—	—	—	15	—	—	—	7
417.2	2	—	—	—	—	—	—	—	—	—	—	—	—
414.8	6	—	—	—	—	—	—	—	—	—	—	14	—
410.7	3	—	—	—	—	26	—	—	—	—	—	—	—
407.6	2	—	—	—	—	—	—	—	—	—	—	—	—
405.5	7	—	—	—	—	—	—	—	—	—	—	—	—
401.4	3	—	—	—	—	—	—	—	—	—	—	—	8
395.4	5	—	—	—	—	—	19	—	16	10	—	—	—
387.3	5	—	27	—	—	—	—	—	—	—	—	15	—
379.0	5	—	—	20	—	—	—	—	—	—	—	—	—

TABLE VI (*contd.*)

Vac.	Int.	3105						3149					
		R_1	Q_1	P_1	R_2	Q_2	P_2	R_1	Q_1	P_1	R_2	Q_2	P_2
375.2	6	—	—	—	—	—	—	—	—	—	—	—	—
372.2	6	—	—	—	—	—	—	—	—	—	—	—	9
364 9	5	—	—	—	—	—	—	—	17	—	—	—	—
* 359.1	5	—	—	—	—	27	—	—	—	—	—	—	—
356.7		—	—	—	—	—	—	—	—	—	—	16	—
349 3	6	—	—	—	—	—	—	—	—	11	—	—	—
344.9	3	—	—	—	—	—	—	—	—	—	—	—	—
341.8	5	—	—	—	—	—	20	—	—	—	—	—	—
338 6	3	—	—	—	—	—	—	—	—	—	—	—	10
333 1	4	—	28	—	—	—	—		—	—	—	—	—
328 8	3	—	—	—	—	—	—	—	18	—	—	—	—
326.4	5	—	—	21	—	—	—	—	—	—	—	17	—
318 3	2	—	—	—	—	—	—	—	—	—	—	—	—
316.3	2	—	—	—	—		—	—	—	—	—	—	—
314 7	2	—	—	—	—	—	—	—	—	12	—	—	—
312.4	6	—	—	—	—	—	—	—	—	—	—	—	—
305.8	5	—	—	—	—	28	—	—	—	—	—	—	—
303 0	5	—	—	—	—	—	—	—	—	—	—	—	11

Vac.	Int	3105				3149				3195			
		Q_1	P_1	Q_2	P_2	Q_1	P_1	Q_2	P_2	R_1	Q_1	P_1	R_2
31296 5	1	—	—	—	—	—	—	—	—	5, 6	—	—	—
293 6	1	—	—	—	—	—	—	—	—	4, 9	—	—	—
291 5	6	—	—	—	21	—	—	18	—	3, 8	—	—	—
287.1	1	—	—	—	—	—	—	—	—	9	—	—	—
279.8	5	—	—	—	—	—	—	—	—	10	—	—	—
276.6	5	29	—	—	—	—	13	—	—	—	—	—	—
270.8	2	—	22	—	—	—	—	—	—	11	—	—	—

TABLE VI (*contd.*)

		3105				3149				3195			
Vac.	Int.	Q_1	P_1	Q_2	P_2	Q_1	P_1	Q_2	P_2	R_1	Q_1	P_1	R_2
266.6	3	—	—	—	—	—	—	—	12	—	—	—	—
255.9	4	—	—	—	—	—	—	19	—	—	—	—	—
250.6	5	—	—	29	—	20	—	—		—	—	—	—
247.6	5	—	—	—	—	—	—	—	—	—	1	—	—
239.7	2	—	—	—	—	—	—	—	—	—	—	—	—
237.0	2	—	—		22	—	—	—	—	—	2	—	—
233.2	2	—	—	—	—	—	—	—	—	—	—	—	—
231.3	5	—	—	—	—	—	14	—	—	—	—	1	—
227.7	2	—	—	—	—	—	—	—	13	—	3	—	—
222.1	1	—	—	—	—	—	—	—	—	—	—	—	8, 9
219.6	1	—	—	—	—	—	—	—	—	—	—	—	7
217.7	5	30	—	—	—	—	—	20	—	—	—	—	6, 10
213.6	3	—	23	—	—	—	—	—	—	—	—	—	11
212.4	—	—	—	—	—	—	—	—	—	—	4	—	—
204.0	1	—	—	—	—	—	—	—	—	—	—	2	—
209.3	6	—	—	30	—	21	—	—	—	—	—	—	5
198.6	2	—	—	—	—	—	—	—	—	—	5	—	4
191.9	2	—	—	—	—	—	—	—	—	—	—	—	—
188.4	4	—	—	—	—	—	15	—	—	—	—	—	3
183.6	3	—	—	—	—	—	—	—	14	—	6	—	—
180.9	7	—	—	—	23	—	—	21	—	—	—	—	—
177.5	2	—	—	—	—	—	—	—	—	—	—	3	—
166.0	5	—	—	—	—	22	—	—	—	—	7	—	—
156.1	7	31	—	—	—	—	—	—	—	—	—	—	—
149.2	3	—	24	—	—	—	—	—	—	—	8	4	—
142.9	2	—	—	—	—	—	—	—	—	—	—	—	—
139.8	8	—	—	—	—	—	16	—	15	—	—	—	—
134.4	5	—	—	—	—	—	—	—	—	—	—	—	—
131.3	4	—	—	31	—	—	—	—	—	—	—	—	—
126.6	1	—	—	—	—	—	—	—	—	—	9	—	—

TABLE VI (*contd.*)

		3105				3149				3195			
Vac	Int.	Q_1	P_1	Q_2	P_2	Q_1	P_1	Q_2	P_2	Q_1	P_1	Q_2	P_2
31122.4	3	—	—	—	24	—	—	—	—	—	—	3	—
117.1	3	—	—	—	—	23	—	—	—	—	5	2, 4	—
112.1	6	—	—	—	—	—	—	—	—	—	—	5	—
104.5	2	—	—	—	—	—	—	—	—	10	—	6	—
099 3	5	—	—	—	—	—	—	—	16	—	—	—	1
094.1	6	32	25	—	—	—	17	—	—	—	—	7	—
087.9	2	—	—	—	—	—	—	—	—	—	6	—	2
080.0	7	—	—	—	—	—	—	—	—	11	—	8	—
071.5	2	—	—	—	—	—	—	—	—	—	—	—	3
068.9	8	—	—	32	—	24	—	—	—	—	—	—	—
066.0	4	—	—	—	—	—	—	—	—	—	—	9	—
062.2	3	—	—	—	25	—	—	—	—	—	—	—	—
058.5	5	—	—	—	—	—	—	—	—	—	—	—	—
053.1	3b	—	—	—	—	—	—	—	17	12	7	—	4
043.6	2	—	—	—	—	—	18	—	—	—	—	10	—
041.6	8	—	—	—	—	—	—	—	—	—	—	—	—
031.8	4	33	26	—	—	—	—	—	—	—	—	—	5
027.5	2	—	—	—	—	—	—	—	—	—	—	11	—
018.0	1	—	—		—	—	—	—	—	—	8	—	—
021.2	2	—	—	—	—	25	—	—	—	—	—	—	—
008.8	3b	—	—	—	—	—	—	—	—	—	—	—	6
004.0	3	—	—	33	—	—	—	—	18	—	—	12	—
000.8	4	—	—	—	26	—	—	—	—	—	—	—	—
30996.4	7	—	—	—	—	—	—	—	—	—	—	—	—
991.6	1	—	—	—	—	—	19	—	—	—	—	—	—
984.6	1	—	—	—	—	—	—	—	—	—	9	—	7
981.3	2	—	—	—	—	—	—	—	—	—	—	13	—
979.2	3	—	—	—	—	—	—	—	—	—	—	—	—
971.9	3	—	—	—	—	—	—	—	—	—	—	—	—
968.6	8	34	27	—	—	—	—	—	—	—	—	—	—

TABLE VI (*contd.*)

		3105				3149				3195			
Vac.	Int.	Q_1	P_1	Q_2	P_2	Q_1	P_1	Q_2	P_2	Q_1	P_1	Q	P_2
959·5	3	—	—	—	—	—	—	—	—	—	—	14	—
954·1	3	—	—	—	—	—	—	—	19	—	—	—	8
946.7	1	—	—	—	—	—	—	—	—	—	10	—	—
938.2	5	—	—	—	27	—	20	—	—	—	—	—	—
935·7	3	—	—	34	—	—	—	—	—	—	—	—	—
921.7	7	—	—	—	—	—	—	—	—	—	—	—	9
919.0	2	—	—	—	—	—	—	—	—	—	—	—	—
906.6	1	—	—	—	—	—		—	—	—	11	—	—
902.3	4	35	28	—	—	—	—	—	20	—	—	—	—
897.0	3	—	—	—	—	—	—		—	—	—	—	—
894·9	6	—	—	—	—	—	—	—	—	—	—	—	—
888 3	3	—	—	—	—	—	—	—	—	—	—	—	10
884·1	3	—	—	—	—	—	21	—	—		—	—	
871.9	3		—	—	28	—	—	—	—	—	—	—	—
864·7	3	—	—	—	—	—	—	—	—	—	12	—	—
853·7	1	—	—	—	—	—	—	—	—	—	—	—	11
847.7	1		—	—	—	—	—	—	21	—	—	—	—
845.1	6	—	—	—	—	—	—	—	—	—	—	—	—
834.2	5	—	29	—	—	—	—	—	—	—	—	—	—
826.2	2	—	—	—	—	—	22	—	—	—	—	—	—
818.6	6	—	—	—	—	—	—	—	—	—	—	—	—
816.2	2	—	—	—	—	—	—	—	—	—	—	—	12
812.3	3	—	—	—	—	—	—	—	—	—	—	—	—
804.2	3	—	—	—	29	—	—	—	—	—	—	—	—
791·4	3	—	—	—	—	—	—	—	22	—	—	—	—
783 3	1	—	—	—	—	—	—	—	—	—	—	—	—
775·2	1	—	—	—	—	—	—	—	—	—	—	—	13
766.7	7	—	—	—	—	—	23	—	—	—	—	—	—
763·5	2	—	30	—	—	—	—	—	—	—	—	—	—
745·6	2	—	—	—	—	—	—	—	—	—	—	—	—
739.6	5	—	—	—	—	—	—	—	—	—	—	—	—

TABLE VI (*contd.*)

		3105				3149				3195			
Vac.	Int.	Q_1	P_1	Q_2	P_2	Q_1	P_1	Q_2	P_2	Q_1	P_1	Q_2	P_2
734.4	3	—	—	—	30	—	—	—	—	—	—	—	14
725.2	3	—	—	—	—	—	—	—	—	—	—	—	—
715.6	2	—	—	—	—	—	—	—	—	—	—	—	—
705.6	2	—	—	—	—	—	24	—	—	—	—	—	—
691.4	3	—	31	—	—	—	—	—	—	—	—	—	15
685.5	5	—	—	—	—	—	—	—	—	—	—	—	—
673.1	2	—	—	—	—	—	—	—	—	—	—	—	—
663.0	3	—	—	—	31	—	—	—	—	—	—	—	—
659.2	4	—	—	—	—	—	—	—	—	—	—	—	—
654.3	3	—	—	—	—	—	—	—	—	—	—	—	—
642.7	1	—	—	—	—	—	—	—	—	—	—	—	—
634.2	3	—	—	—	—	—	—	—	—	—	—	—	—
618.3	3	—	32	—	—	—	—	—	—	—	—	—	—
602.9	4	—	—	—	—	—	—	—	—	—	—	—	—
589.9	4	—	—	—	32	—	—	—	—	—	—	—	—
577.4	5	—	—	—	—	—	—	—	—	—	—	—	—
560.4	2	—	—	—	—	—	—	—	—	—	—	—	—
553.8	2	—	—	—	—	—	—	—	—	—	—	—	—
547.0	2	—	—	—	—	—	—	—	—	—	—	—	—
540.5	3	—	33	—	—	—	—	—	—	—	—	—	—
518.0	4	—	—	—	—	—	—	—	—	—	—	—	—
513.6	3	—	—	—	33	—	—	—	—	—	—	—	—
492.0	4	—	—	—	—	—	—	—	—	—	—	—	—
463.1	3	—	34	—	—	—	—	—	—	—	—	—	—
442.3	3	—	—	—	—	—	—	—	—	—	—	—	—
436.0	3	—	—	—	34	—	—	—	—	—	—	—	—
430.2	4	—	—	—	—	—	—	—	—	—	—	—	—
404.2	4	—	—	—	—	—	—	—	—	—	—	—	—
383.3	3	—	35	—	—	—	—	—	—	—	—	—	—
361.5	2	—	—	—	—	—	—	—	—	—	—	—	—
355.4	3	—	—	—	35	—	—	—	—	—	—	—	—
340.4	3	—	—	—	—	—	—	—	—	—	—	—	—

ROTATIONAL CONSTANTS

The combination differences set forth in the above tables have led to the following rotational constants. As D_v is of the order of 10^{-4} cms^{-1}, the calculated values of these have been assumed in determining B_v. All the values in the table are expressed in cms^{-1}.

	(1, 1)	(2, 2)	(3, 3)
B′	8.73	8.42	7.96
B″	9.58	9.40	9.08
A	138.9	139.1	−140.0
Null Line ($'n_{\frac{3}{2}}$)	32124.6	31692.7	31244.5

The author desires to express his grateful thanks to Prof. K. R. Rao for his kind interest and guidance in the course of the work. He is indebted to the Andhra University for the award of a Fellowship which enabled him to carry out this work.

The author is indebted to Dr. Ishaq for a private communication to Prof. K. R. Rao in which he intimated to us the progress of his work so that overlapping and duplication might be avoided.

ANDHRA UNIVERSITY, WALTAIR.

REFERENCES

[1] *Ind. Jour. Phys.* (in the course of publication).

[2] *Proc Nat. Inst. Sci Ind* , **8**, 389 (1939).

[3] *Current Sci.*, June, 1940.

[4] *Phys. Rev.*, **33**, 467 (1929).